INTERNATIONAL COURT OF JUSTICE

DISPUTE OVER THE STATUS AND USE OF THE WATERS OF THE SILALA

(CHILE v. BOLIVIA)

REJOINDER OF THE PLURINATIONAL STATE OF BOLIVIA

ANNEX 23.5

APPENDIXES B AND C

VOLUME 4 OF 6

15 MAY 2019

LIST OF ANNEXES TO THE REJOINDER OF THE PLURINATIONAL STATE OF BOLIVIA

VOLUME 4 OF 6

Annex 23.5

Appendix b

SERGEOMIN, "Structural Geological Mapping of the Area Surrounding the Silala Springs", September 2017

(English Translation)

FINAL REPORT

INTERINSTITUTIONAL AGREEMENT
GEOLOGICAL-STRUCTURAL MAPPING PROJECT
OF THE SURROUNDING AREA TO THE SILALA SPRINGS
DEPARTMENT OF POTOSI

La Paz, September 2017

Prepared by:

GEOLOGICAL MINING SERVICE "SERGEOMIN"
Federico Zuazo Street N° 1673
P.O. Box N° 2729
Phone: (591-2) 2330981 – 2331236 – 2330895
Fax: (591-2) 2391725
E-mail www.sergeomin.gob.bo
La Paz – Bolivia

Technical Personnel:
Eng. Jorge Vega Enrriquez
Eng. Nielsen Morillas Vidangos
Eng. Efrain Apaza Poma
Eng. Limber Carlo Garcia
Grad. Maribel Urquiete Quenallata
Grad. Diego Gonzalez Herrera
Eng. Adolfo Orsolini Campana
Eng. Mario Barragan Espinoza
Eng. Jorge Bejarano Delgado
Eng. Andres Casas Saavedra
Eng. Hernan Condori Ticona
Eng. Laura Cahuana Flores

Support Personnel: (Drivers)
Mr. Bernardo Medrano Uturuncu
Mr. Vicente Coro Loayza

Mr. Hector Cusi Quispe
Mr. Juan Roque Lobaton

Management:

Eng. Roberto Perez M. EXECUTIVE DIRECTOR

Eng. Fernando Caceres J.
TECHNICAL DIRECTOR OF PROSPECTION AND EXPLORATION

Eng. Javier Rodriguez G.
HEAD OF THE EXPLORATION UNIT

For DIREMAR: Strategic Office of Strategic Office of Maritime Vindication

Management:

Lic. Emerson Calderon Guzman
SECRETARY GENERAL – SILALA AND INTERNATIONAL WATER RESOURCES

Lic. Omar Rocha
PROJECT SUPERVISOR

Eng. Phd. Fernando Urquidi Barrau, PROJECT SUPERVISOR

Index

List of figures

Picture List

Picture No. 6. a) Marker horizon corresponding to a crystal-vitreous tuff, 20 cm thick, that delimits the Silala Ignimbrite 1 (Nis 1) and Silala Ignimbrite 2 (Nis 2); b) Hand sample of the tuff level where a banded structure can be observed.

Picture No. 7. Silala Ignimbrite 2 (Nis 2) which underlies the tuff horizon and Silala Ignimbrite 1 (Nis 1); b) The Silala ignimbrite 2 (Nis 2) with pumice content, presenting a massive structure

Picture No. 8. a) brownish-reddish debris flow 2 (NFd2), sub-rounded clasts of igneous rocks can be observed; b) chaotic structure that does not present any clast structuring

Picture No. 9. Reddish Silala Ignimbrite 3 (Nis 3), presenting a splintered structure; b) Silala ignimbrite 3 (Nis 3), presenting a porphiric texture, with plagioclase, potassium feldspar and quartz

Picture No. 10. a) Silala Chico hill, Inacaliri stratovolcano in the back; b) Silala Chico lava (Nlsc), of a dacite composition, presenting a splintered structure

Picture No. 11. a) Cerro Negro with a dome-like morphology. b) Lava flow of Cerro Negro (Nlcn), it presents a reddish-brown coloration with a splintered structure

Picture No.12. Volcanic dome of Torito hill (Nlct), rock outcrops and hand-drawn samples

Picture No. 13 a) Inacaliri lava flows (Nlin1), b) basal breccia of the aforementioned flows

Picture No. 14. Pseudo-stratified lava flows (Nlsg)

Picture No. 15. Stratovolcanic lava flows (Nlin 2)

Picture No. 16. Pastos Grandes Tuff (Ntpg)

Picture No. 17. Panoramic view of the Runtujaritas dome-lava

Picture No. 18. Lava flows of Cerro Chico hill (Nlcc)

Picture No. 19. High-angle normal conjugated faulting, affecting the Silala Grande lavas

Picture No. 20. Sub-horizontal, conjugate faults, affecting the joints of the Silala ignimbrite

Picture No. 21. Fractured massif outcrop of dacite lava, Meson hill

Picture No. 22. Silala ignimbrite mantles, presenting fractures that cut the outcropping levels. South side of the Silala ravine

LIST OF TABLES

ANNEXES

GLOSSARY OF GEOLOGICAL-STRUCTURAL TERMS

Alluvial Fan: Detrital material deposited in the form of a fan, by an aqueous current, at the change of slope of a torrent, or close to its base level. Synonym: alluvial cone.

Alluvial: Term used to refer to all type of process or material related to the fluvial processes. Example: alluvial deposit, alluvial terrace, alluvial cone, etc.

Andesite: Volcanic igneous rock (intermediate) of aphanitic or porphyritic texture, generally of green color, being able to vary to reddish, violet and other colors, acquired by the alteration of the ferromagnesian minerals that it contains.

Spectral band: Each of the ranges of wavelengths that a sensor is capable of detecting.

Bofedal: In arid environments, lowlands, waterlogged or well watered and very fertile, where it is common the existence of springs and whose abundance of vegetation is due to mineralized and clayey soils, which store water all year round.

Pitch: Angle of intersection between the alignments and a horizontal plane.

Volcanic caldera: It is a large depression of volcanic origin, elliptical or circular in shape, which can reach tens of kilometers in diameter.

Cirque: Deep circular or sub-circular valley formed by erosion and glacial eruption, snow accumulation and formation of glaciers.

Colluvial: Materials weathered and transported by the action of gravity; for example, slope debris, etc.

Colluvial-Fluvial: They are materials transported and deposited by water. Its size varies from clay to thick gravel, cobbles and blocks.

Geometric correction: Correction of the distortions that occur during the process of acquiring an image due to the rotation and curvature of the Earth, the angle of vision or variations in the position of the satellite.

Radiometric correction: Any modification that alters the original values recorded by the sensor, in order to correct the possible effects produced in the image by the atmosphere, the observation geometry or the physical characteristics of the sensor itself.

Volcanic crater: Circular or elliptical depression limited by an abrupt edge.

Dacite: Igneous, volcanic, acid rock, equivalent to granodiorite, has an aphanitic texture.

Joint: Fracture without displacement.

Rose diagram: Graphic representation of fractures in two dimensions.

Dome: Emission duct characterized by a structure similar to a volcanic cone but lacking a crater. Their lava flows are usually acidic and very thick, so they do not usually get too far from the emitting center.

Radiometric age: Method of measuring the disintegration of unstable elements. Since each radioactive element has a defined half-life period.

Eluvial: Deposit of detrital material, resulting from the alteration or decomposition of parent rocks that remain in-situ.

Stress: Strength per unit area.

Stratovolcano: The stratovolcanoes are large conical buildings in which lavas and pyroclasts accumulate. For its formation a long period of eruptive activity or the repetition of numerous eruptions in a restricted area is required.

Structure: Geological or structural feature referring to the way in which rocks or fractures are related.

Reverse fault: Fracture with displacement or rise of the roof or lower block.

Right side fault: Fracture with horizontal displacement to the right.

Left side fault: Fracture with horizontal displacement to the left.

Normal fault: Fracture with displacement or fall of the roof or upper block.

Fault: Fracture with relative displacement of blocks.

Faulting: Fracking zone.

Spectral signature: Curve that represents the variation of the reflectance of an object as a function of wavelength.

Debris flow: Debris flows or so-called debris flows occur when rainwater begins to erode the material of a slope or when a landmass is saturated with water, aided by slope and gravity. Fluvial-Glacial: Abandoned after the retreat of glaciers and ice sheets.

Fracture: Any opening or fissure with or without displacement.

Geophysics: Surveying technique inside the subsoil.

Graben: Normal faulting zone with collapse of blocks.

Ignimbrite: Rock or deposit formed from a pumice pyroclastic flow, regardless of whether it is welded or not.

Merged image (Pan-Sharpened): Image product of the fusion of a panchromatic image and its multispectral equivalent by means of a series of mathematical algorithms. The resulting image has the spatial resolution of the panchromatic and the spectral bands

Multispectral image: Image captured by a sensor that measures the energy simultaneously in two or more spectral bands

Immersion or plunge: Angle that forms the line with its projection in the horizontal plane, measured in the vertical plane.

Lava: Fluid rocky material that comes out of a volcano or a crack in the Earth's crust and that flows or slides on the surface. The lava in natural fusion is in a liquid-viscous state product of the volcanic eruption.

Lineament: Structural or morphological feature that has a direction.

Spring: Continuous natural flow to the Earth's surface, from groundwater, is formed around an upwelling by physical and chemical accumulation.

Microstructure: Small-scale structure or feature.

Morphology: Natural form of rocky outcrops.

Moraines: A moraine is a mountain range or mantle of till deposited near a glacier. There are several types of moraines, which depend on their relationship with the glacier: moraine in the bottom: it is located under the ice, in contact with the bed.

Secondary permeability: The ability of a fractured material to allow the flow of liquids.

Pixel: Each of the elements that make up an image, arranged in a matrix and columns

Fault plane: Fracture plane through which the blocks move.

Porosity: System of empty spaces through which fluids can move.

Stereographic projection: Graphic representation of structural data in three dimensions.

Reflectance: Relationship between the amount of radiation reflected by a surface and the one that falls on it. It is usually expressed in % or with values between 0 and 1.

Trend or orientation: Geometric layout of the structures according to a direction.

Stress Tensioner: Vector force of compression or distension.

Tuff: Volcanic igneous rock, product of the consolidation of pyroclastic materials, pumps, lapilli, ash, with sedimentary material that favors its cementation.

EXECUTIVE SUMMARY

Within the framework of the consultancy contract between the Strategic Office for the Maritime Claim, Silala and International Water Resources (DIREMAR) and the Geological Mining Service (SERGEOMIN), the geological and structural survey of the areas surrounding the Silala springs was carried out, generating geological-structural information exposed in the following paragraphs.

The Silala Springs area is characterized by a relatively flat to undulating topography, with a slight inclination to the west, with wide depressions flanked by various volcanic structures such as domes, cones, calderas and stratovolcanoes. The morphology of the place was modeled by both endogenous and exogenous processes and has an average height of 4,000 meters above sea level, varying from 4,278 meters above sea level (Silala Ravine) to 5,701 meters above sea level (Stratovolcano of Silala Grande Hill).

The development of the study contemplates diverse phases (office and field), in the first one was collected and analyzed all the existing technical information, proceeding with the interpretation and analysis of satellite images, for example; Images Landsat 7 ETM + Bands RGB 742, Bing Maps and Fusion of images Landsat 7ETM + Y Radar Alospalsar, in order to discriminate geological features, such as lithological contacts and regional lineaments, structuring the base maps that were later corroborated with the field work, using the method of station point, transects and GPS points.

Within the geological part we must mention that, the study area is within the morpho-structural domain of the Western Mountain Range or Volcanic Belt in its southern block, it develops in the Central Volcanic Zone of the Andes and is part of the Altiplano-Puna Volcanic Complex (APVC). The volcanic activity develops from the Upper Miocene to the Lower Pleistocene, generating igneous rocks intermediate to calc-alkalic intermediates rich in potassium, related to the subduction of the Nazca plate during the Andean tectonic phase.

The intense magmatic activity of the region begins with an explosive volcanism of the Plinian type, building large volcanic calderas and chains (Guacha, Pastos Grandes, Agua de Perdiz) and extensive ignimbrite shields to which the Silala Ignimbrites of dacitic composition would correspond, (defining in this study three members). Later a gradual reduction in the volatile content of the magma causes the volcanism to change to an effusive type, placing volcanic domes such as Silala Chico and Torito hills and emitting lava flows of andesitic-dacitic composition forming Stratovolcanoes such as Inacaliri and Silala Grande.

As for the tectonic framework, the structural survey of fractures and faults was carried out, with a subsequent analysis, management and interpretation of these data and results through the use of the Dips 5.1 program, generating maps of main structures with kinematic components and field of associated stresses, fused with the existing regional lineaments.

The system of general fracturing is defined by three dominant structural trends: the first and main system is of general trend NE-SW (40° - 70°), the Uyuni-Khenayani fault system is included. The second system has longitudinal direction NW-SE (100° - 140°);

the main volcanic centers of the area coincide with this system. A third structural system with general trend N-S (340° - 10°), some volcanic cones are aligned in this direction.

In the volcanic rocks of the area the deformation is of fragile type, it is clear that by its tectonic and volcanic activity (cooling) the fracturing is potentially suitable for the transport and circulation of fluids. The most intense fracturing is located along the Silala springs, where the ignimbrites are better exposed. It is important to point out that, in an aquifer composed of volcanic rocks, the secondary porosity is more relevant than the primary one and derives from the network of fractures and discontinuities depending on their opening, continuity, persistence and infilling, these characteristics define the Silala Ignimbrites (Members 1 and 2) as the lithology with the greatest potential to become aquicludes due to the acquired secondary porosity.

STRUCTURAL GEOLOGICAL MAPPING OF THE AREA SURROUNDING THE SILALA SPRINGS

1. BACKGROUND

In accordance with Supreme Decree No. 3131, the Strategic Office for the Maritime Claim, Silala and International Water Resources (DIREMAR for its Spanish acronyms) procured the product-based counselling services of the Geological Mining Service of Bolivia (SERGEOMIN for its Spanish acronyms) under a contract dated 05/05/2017 for the performance of a geological and structural mapping of the area surrounding the Silala springs. The study is intended to acquire data on the geology and structural features of the area—which is characterized by lineaments, faults and joints—and their influence and control on the Silala springs. The study will constitute a basis to be complemented with geophysical, hydrological, hydrogeological and geomorphological studies of the area and is strategic for the State's interests.

2. OBJECTIVES

2.1. General objective

- Geological data is essential to define the textural features of volcanic rocks and their influence on the accumulation of water in the aquifers that conform the outcrops of the Silala springs.

- The structural survey is fundamental to identify the structural features of the lineaments, faults and joints present in the sectors that comprise the area as a whole. Defining the behavior of the native and non-native geological structures is essential to determine their influence on the accumulation of water in the aquifers and the emergence of water in the Silala springs.

- The geological-structural survey will be the basis for additional geophysical, hydrological, hydrogeological and geomorphological studies.

2.2. Specific objective

To perform a geological survey at scales of 1:10.000; 1:20.000 and 1:50.000 in three specific Areas in order to:

-Delimit and define the local formations and units present in the area (stratigraphy), particularly in regard to the ignimbrite found in the vicinities of the Silala springs (1st Area), their thickness and position (inclination for their reconstruction and to try identify their sources).
-Take rock samples for the performance of petrographic surveys to define their texture and composition related features.

Prepare maps, lithological columns, geological sections and a report containing a geological interpretation of the area.

To perform a semi-detailed structural survey and collect data at the scales of 1:10.000; 1:20.000 and 1:50.000 for three specific areas in order to:

- Collect data on the regional faults, joints and local fractures to prepare rose diagrams intended to better comprehend the behavior and stresses that acted in the area.

- Collect structural data on the fractures and joints of the potential recharge areas (ignimbrite) in order to determine the recharge ratio of the aquifers (density map).

- Perform a structural interpretation of the faults, joints and fractures of the geological units in order to acquire knowledge on their effect as a potential water recharge source in the aquifer that discharges waters into the Silala springs.

2.3. Methodology

2.3.1 Desk work

- Preparation of an activity time table
- Compilation and analysis of existing data
- Preparation of base maps of the three areas to be studied
- Satellite image processing and interpretation
- Preparation of spreadsheets for the data; geological and structural data collection

2.3.2 Field work

- Geological and structural mapping at different scales
- Rock sampling for petrographic analysis
- Preparation of maps at different scales
- Preparation of stratigraphic columns
- Data collection to generate structural data tables

3. GENERAL INFORMATION

3.1 Earlier works

"Chrono-stratigraphy of Ar40/Ar39 of the ignimbrite of the Altiplano-Puna Volcanic Complex Reveals the Development of an Important Magmatic Province"

This study comprised the mapping and laser dating of the sanidine and biotite of 56 points, together with the collection of magnetic data and a comparison of the ages established in earlier works to define the specific volumes and time in which the ignimbrite emplacement occurred in

Bolivia and the north of Chile so as to unveil that monotonous volcanism of intermediate composition was prodigious and episodic in the whole complex. These new results present the eruptive history of the Pastos Grandes and Guacha calderas, two big complexes of multi-cyclical lava flows located in Bolivia. These two calderas, together with the complexes of Vilama and La Pacana calderas and the small ignimbrite shields, were the main sources of ignimbrite-producing eruptions during the Miocene in the history of the Altiplano-Puna volcanic complex.

“Geological technical survey on the Silala”

This was a technical-geological survey carried out in 2016 by senior students of the Faculty and was presented by the Tomas Frias Autonomous University to the Governorate of the Potosi Department. The survey reaffirms that the waters of the Silala constitute springs located in Bolivian soil—the university, however, demanded more resources and technology to pursue the survey further.

“Study on the Geology, Hydrology and Environment of the Silala Springs area”

The Regional Integration Project (PIR, for its Spanish acronyms) of the national Geology and Mining Service (SERGEOMIN) was carried out at the instruction of the Ministry of Economic Development and the Ministry of Foreign Affairs and Worship.
The objective of this survey, completed within the PIR’s scope, was to attain data on the geological, hydrological and hydrogeological evolution of the area of the Silala Springs, the approximate extent of which is of 150 km2, with details on the formation and evolution of the Silala ravines—where the Silala springs, which comprise an extent of 79 km2, are located—together with a characterization of its waters.

“Study on the hydrographical basins of Pastos Grandes, Cuenca 16 and the North and South Lipez Provinces of the Potosi Department”

This survey was intended to identify and characterize the hydrological units that have the potential to discharge groundwater, relating the emergence of water springs, wetlands, and others, with the relative permeability of the igneous and/or sedimentary rocks. The units delimited correspond to three categories linked with the emergence of groundwater in porous, unconsolidated soils.

“Structural evolution of the Miocene-Quaternary of the Uyuni-Atacama region, Chilean–Bolivian Andes”

This survey was intended to describe the Miocene-Quaternary geological-structural evolution of the Uyuni Salt Flat and Atacama regions, found in the Chilean–Bolivian Andes.

3

Four main tectonic events were recognized on basis of the geometry and the kinetics of the faults and stratigraphic data.

"Geological Map for the Inca hill/Khara Lagoon Sheet No. 5928-6028"

The survey was performed by taking samples of the lithology of Inacaliri volcano, the volcanic domes of Torito, Negro and Chascon hills. The extent of the Silala ignimbrite and the Pastos Grandes caldera ignimbrite were also surveyed, concluding that those of Silala are younger in age.

"Geological Map for the Sanabria Sheet No. 5927-6027"

This geological sheet records the volcanic units of the area and defines a series of volcanic formations lined up with a NNW and NNE direction that present andesite-dacite related features—believed to have given origin to the Meson Negro, Linzor and Pabellon stratovolcanoes. The survey also defined the Silala tuffs (6.6. mya.) and the Silala lava, together with the tectonic framework and petrology of the area.

"Geological Map of the Silala Sheet No. 5927"

This survey presents an initial outline of the units that conform the Silala springs. The area was mapped at a scale of 1:50.000.

"Volcanoes and supervolcanoes of the Lipez region of Potosi Department"

This geological survey summarizes the volcanic structures identified in Bolivian soil and that form part of the Altiplano-Puna Volcanic Complex, with an emphasis on the significant ignimbrite eruptions of the area studied and a detail on the volumes, ages and types of eruptions.

4. GENERALITIES

4.1 Location of the area studied

The Silala springs are located in Canton Quetena Chico of the San Pablo de Lipez Municipality, of South Lipez Province, in Potosi Department (Figure No. 1).

The central coordinate of the area, in the UTM-WGS 84 system, Zone No. 19, of the South Hemisphere is: East: 601004, North: 7566389. The site is found at 4,378 MASL.

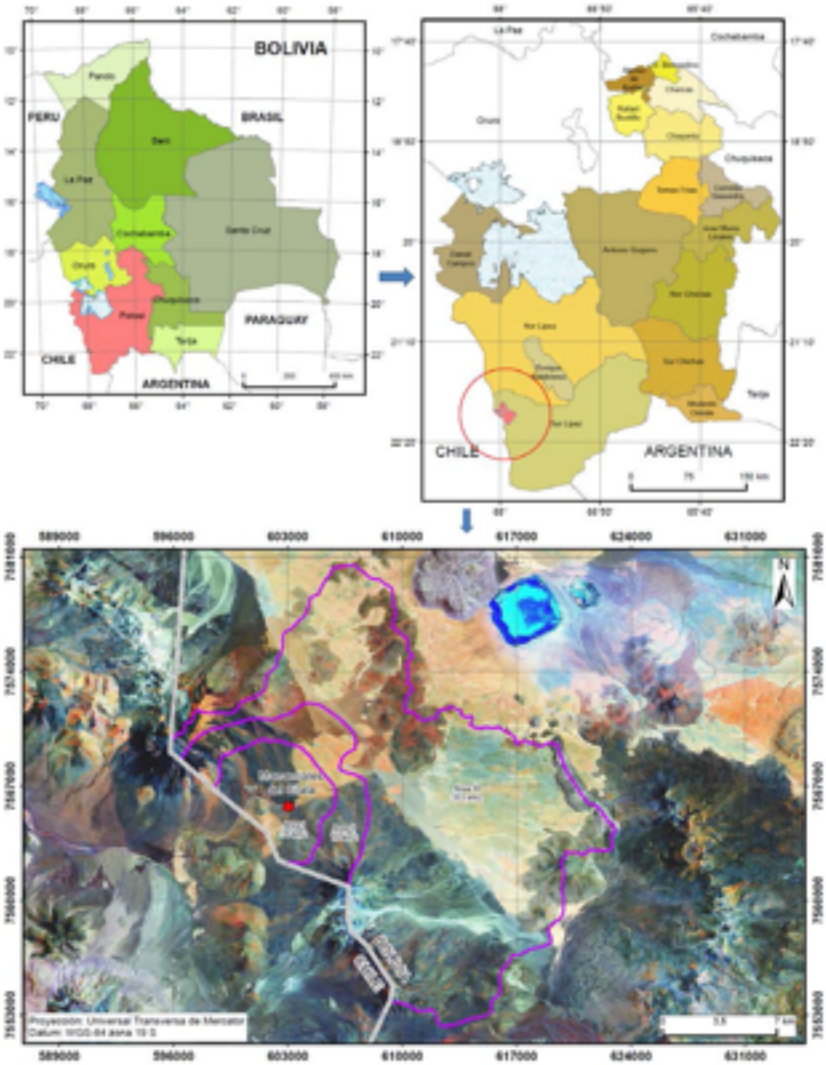

Figure No. 1. Location of the area of the Silala springs

4.2 Accessibility

The area surveyed can be accessed through the 1st order La Paz-Oruro-Challapata-Uyuni road, which is found at 560 km. Two 2nd and 3rd order routes can also be used from Uyuni to the area, i.e. the Uyuni-Culpina K-Cruce Avaroa-Silala road, found at 350 km, and the Uyuni-Villa Alota-Villa Mar-Laguna Colorada-Silala, at 290 km. (Figure No. 2).

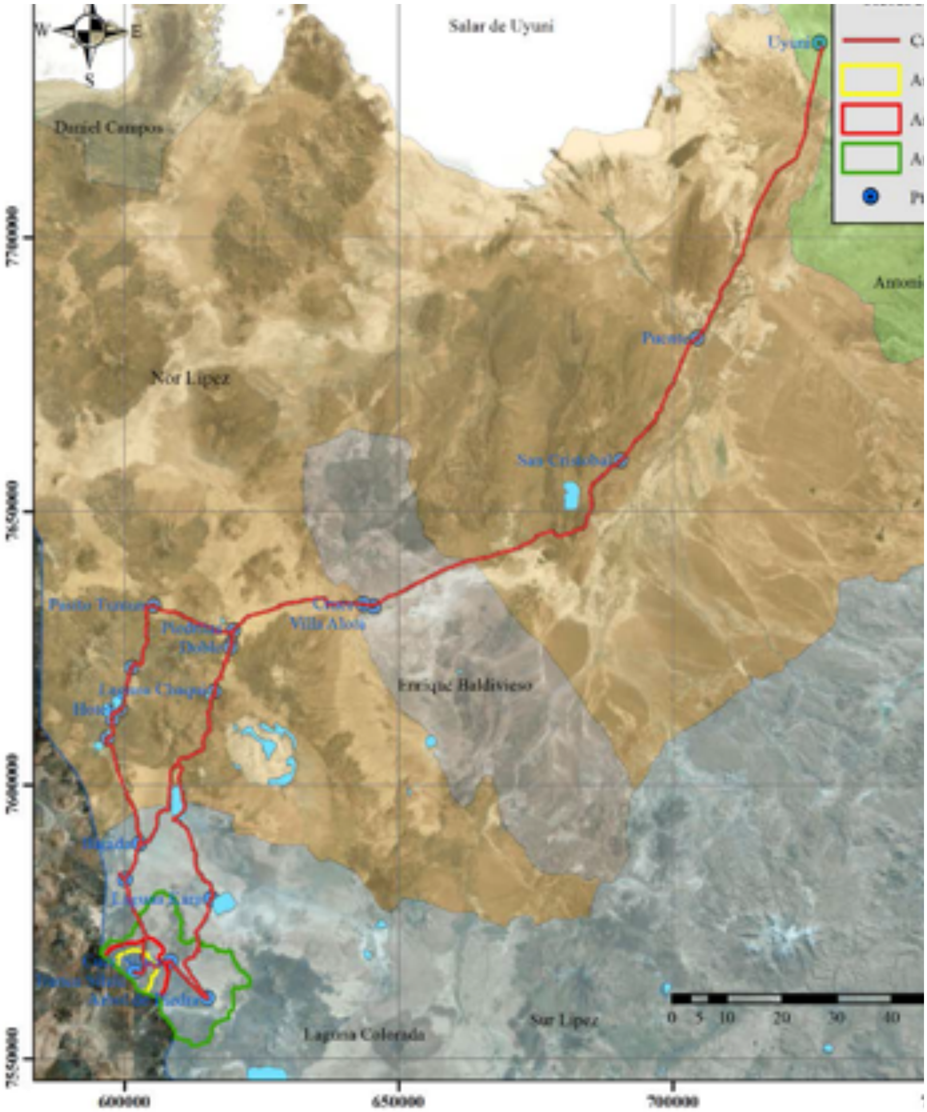

Figure No. 2. Access map of the area of the Silala springs

4.3 Relief

The relief of the Silala springs are is characterized by an undulated topography, with wide depressions and a slight inclination to the west. The area is flanked by different volcanic structures, such as domes, volcanic cones and stratovolcanoes. The average altitude of the area is of 4,000 MASL, and raises from 4,278 (at the Silala ravine) to 5,701 MASL (at the Silala Grande stratovolcano). The area also presents ample plains with wide valleys, forming a characteristic U-shaped profile, which then evolve to fluvio-glacial valleys, favoring the formation of lagoons in topographic depressions.

4.4 Climate

According to Koppen's climatic classification, adapted for the Bolivian territory by Montes de Oca (1997), "the main types of climates in Bolivia are: tropical rainy climates, dry climates, mesothermic climates and cold climates". The area is characterized by the following climates: Cold climates (E), Tundra climates (ET) in the lower flanks of the mountain ranges and part of the high plateau, associated with minor morpho-structural units (mountain ranges and intra-mountainous valleys), and high mountain climates (EB) which correspond to the high summits of the mountain ranges that are covered with snow or ice most of the year.

The climatic conditions of Bolivia's western region are essentially determined by its altitude above the sea level and local factors such as sunlight, the valleys' orientation and atmospheric currents (Montes de Oca, 1997). The major morpho-structural units of the region exert a decisive influence as a climate moderating factor, but do not reduce latitudinal dependence. The climate of the Altiplano is a direct function of its altitude above sea level.

This altitude, which reaches an average of 3,800 meters above sea level, has an influence on the atmospheric conditions, making ample insolation and irradiation possible due to the rarefied and diaphanous air, and the little humidity and absence of heat diffusion, causing temperature to be high under sunlight and cold in the shadow. The maximum temperature of the Altiplano reaches the 31.1˚C and the minimum 35˚C below zero, both of which were recorded in Laguna Colorada (in February, 1996 and September, 1992 respectively).

According to Koppen's classification, the climate of Bolivia's South Altiplano (Lipez region) is characterized by a polar high mountain climate (EB), which corresponds to the high summits of the region, and a Tundra climate (ET), which would correspond to the mountain ranges and much of the Altiplano (Potosi, Oruro and part of La Paz). The hydrological parameters that are described below correspond to the meteorological station of Laguna Colorada (considered the most representative of the basin), which recorded hydrological data for 18 years and allow having an idea of the hydrological behavior of the area.

The National Service of Hydrology and Meteorology divides the country into three categories, i.e. highlands, valleys and plains.

7

The Altiplano, with elevations between 3,500 to 6,000 m or more and cold lands that include the entire Andean region, and the high plateau, which comprises the departments of Potosi, Oruro and part of La Paz are both characterized by tundra (ET) and high mountain polar (EB) climates.

The period of fluvial precipitation begins in December and extends until March, reaching a maximum of 21.8 mm in January. The drought period extends from April to November.

The maximum temperatures are recorded from December to March, reaching the 14 ºC. From April to August, on the other hand, the minimum temperatures fluctuate between 0 to -20 ºC, with a minimum annual average of -15 ºC. The total annual precipitation is very low and presents an annual average of 59 mm, which decreases to 0.0 mm in July.

Below, historical data obtained from the Laguna Colorada weather station is presented:

Precipitation. –The monthly distribution of average rainfall is unimodal. The period of highest precipitation extends from December to March, which represents 90% of the general precipitation, with a maximum of 21.8 mm in January. The dry season extends from April to November, with a minimum precipitation of 0.0 mm., recorded in July. The average annual precipitation for the period of 1983 to 2001 is 72.1 mm/year.

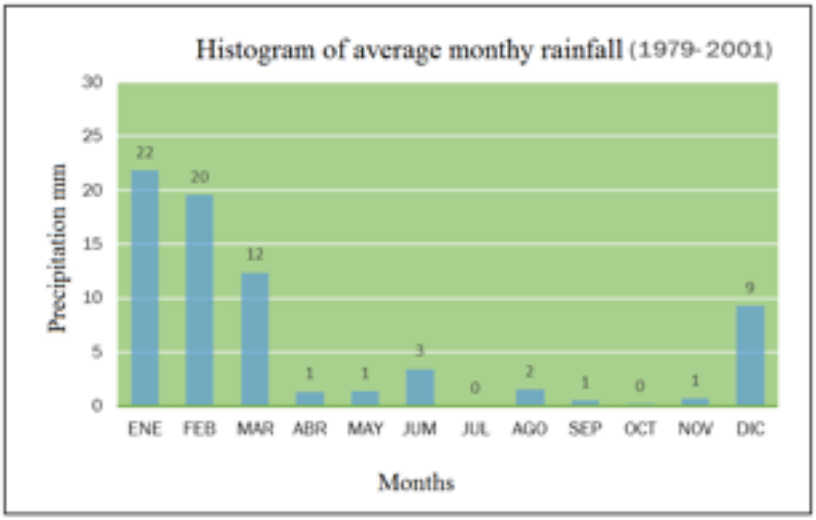

Figure No. 3. Histogram of average monthly rainfall, Laguna Colorada meteorological station

Temperature. –The distribution of average monthly temperature is also unimodal. The highest temperatures are recorded from December to March, with maximum of 7.2 °C recorded in the former. The minimum temperatures are observed from April to August, with average temperatures that fluctuate between 4.3 °C to -8.9 °C. The average annual maximum temperature is 12.9 °C and the minimum -8.7 °C, with a variation range of approximately 21 °C.

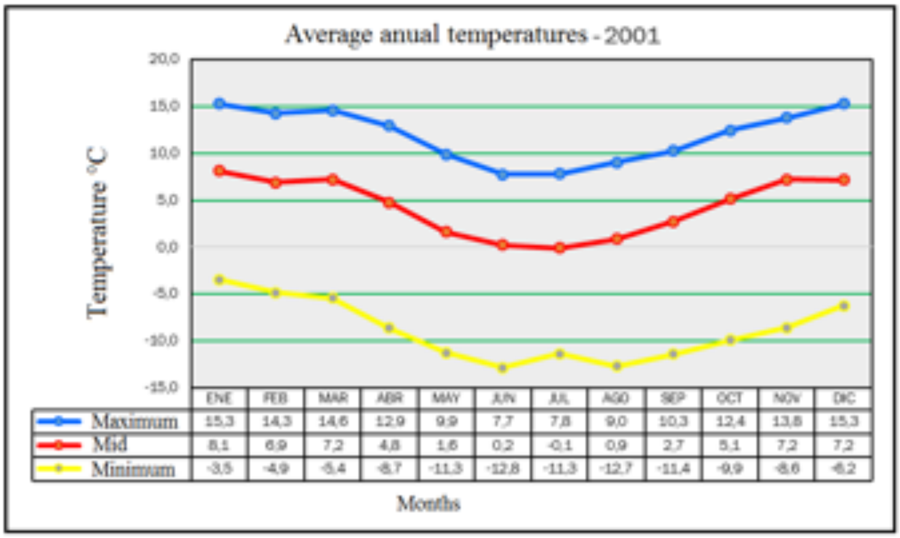

	ENE	FEB	MAR	ABR	MAY	JUN	JUL	AGO	SEP	OCT	NOV	DIC
Maximum	15,3	14,3	14,6	12,9	9,9	7,7	7,8	9,0	10,3	12,4	13,8	15,3
Mid	8,1	6,9	7,2	4,8	1,6	0,2	-0,1	0,9	2,7	5,1	7,2	7,2
Minimum	-3,5	-4,9	-5,4	-8,7	-11,3	-12,8	-11,3	-12,7	-11,4	-9,9	-8,6	-6,2

Figure No. 4. Temperature historiography, Laguna Colorada meteorological station

4.5 Vegetation and fauna

The plant life and fauna is very limited and characteristic of the western mountain range and the Bolivian Altiplano. The Silala wetlands present a flora and fauna that is characteristic of high-altitude wetlands. The flora comprises paja brava, yareta and thola and the fauna, llamas and wild animals as vizcachas, flamingoes, vicunas and foxes.

4.6 Resources and infrastructure

The most relevant infrastructures are found in Laguna Colorada, 38 km to the south of the springs. These comprise an overnight and feeding installation for tourists crossing from Uyuni to Laguna Verde (border with Chile) and vice versa, and the installations of the National Electricity Company and National Protected Areas Service. The closest towns are found in Villa Mar, Quetena Grande.

The main road network constitutes the road that connects Uyuni with Laguna Colorada. There are also several parallel (third order) alternative routes, which are used by tourism companies. Currently, the road to the Silala military post is unobstructed and in good conditions.

The San Cristobal and Uyuni towns are the main sources of fuel and food provisions. Authorization is required to purchase fuel in drums for long trips.

Most of the towns lack a potable water supply system. Water is supplied by wells, springs and/or rivers. The Silala springs are the only place where there is good quality water for human consumption.

Electricity in Silala is supplied by solar panels and by diesel electric generators in Laguna Colorada. The military post counts on an Entel satellite antenna that provides cell-phone signal.
Health centers and other services are not available in the area, since the region is quite uninhabited.

5. SATELLITE IMAGE INTERPRETATION

The desk work stage comprehended the processing and interpretation of different satellite images, using SERGEOMIN's image processing. The images were processed on basis of the needs for the geological mapping (lithological contact) and structural mapping (preliminary lineament interpretation).
Three image types were used for the interpretation:

- Landsat 7 ETM + RGB 742 images
- Bing Maps
- Combination of Landsat 7ETM + Y Radar Alospalsar images

5.1. Landsat 7 ETM + RGB 742 images

The data collected by the LANDSAT 7 satellite was consulted for this part of the survey, together with the data collected by The Enhanced Thematic Mapper Plus (ETM+) sensors. The multispectral processing and analysis was made with 7 ETM + bands, which allow for a study that comprises specter ranges from visible (0.45 μ) to far infrared (12.5 μ).

The spatial resolution is of 30 x 30, comprising seven bands that correspond to thermal infrared, with the exception of the sixth band, which is of 120 x 120 m. The spatial resolution of ETM+ images in the panchromatic is of 15 x 15 m.

The image was obtained from the United States Geological Survey's servers (http://earthexplorer.usgs.gov/). The scene used for the area was LE72330752003067COA01, acquired on 8 March 2003.

5.1.1 Methodology to process satellite images

The methodology was based on the integrated analysis of the data obtained from multispectral optical images. Visual interpretation and digital analysis were completed to obtain the needed data.

The data obtained allowed a lithological identification/classification for the area of the Silala springs. The methodology needed and digital processing used were the following:

- Geometrical corrections
- A visual improvement of the images
- Band combination

Geometrical correction. Owing to its experience, LANDSAT provides a proper correction based on the processing level of the image—which was nevertheless not completed for this part of the survey, inasmuch as the correction was performed with a geometrical adjustment only.

Visual analysis and improvement. The images' visual analysis was performed using three RGB sensor bands. Contrasts, highlights and filters were used for visual improvement.

Composition of Images. Band combination allowed for highlighting color, texture, tone variations, and identifying the different types of lithology present on the surface.

5.1.2 Results

Combination of spectral bands

- 1st, 2nd and 3rd Band (RGB): This is a natural color image, which reflects the area as seen by the human eye in a color aerial photograph.
- 4th, 5th and 7th Bands (RGB): The 4th band corresponds to the infrared for the near field; the 5th Band highlights the altered rocks and humid areas related to fracturing zones; the 7th Band is useful to highlight lithological contrasts.
- The 7th, 4th and 2nd (RGB): This combination of bands is widely used in geology. It uses the three less correlated bands; the 7th Band, presented in red, covers the segment of the electromagnetic spectrum in which the clay minerals absorb the energy, instead of reflecting it. The 4th Band, in green, covers the segment in which the vegetation strongly reflects [SIC, the energy]. The 1st Band, in blue, covers the segment in which minerals with iron oxides absorb the energy (Chuvieco E. Emilio 2002).

Of all the color compositions generated, the 742nd composition was the one that presents a better lithological discrimination and the one used most for the preliminary interpretation of lithology necessary for the geological mapping. (Figure No. 5).

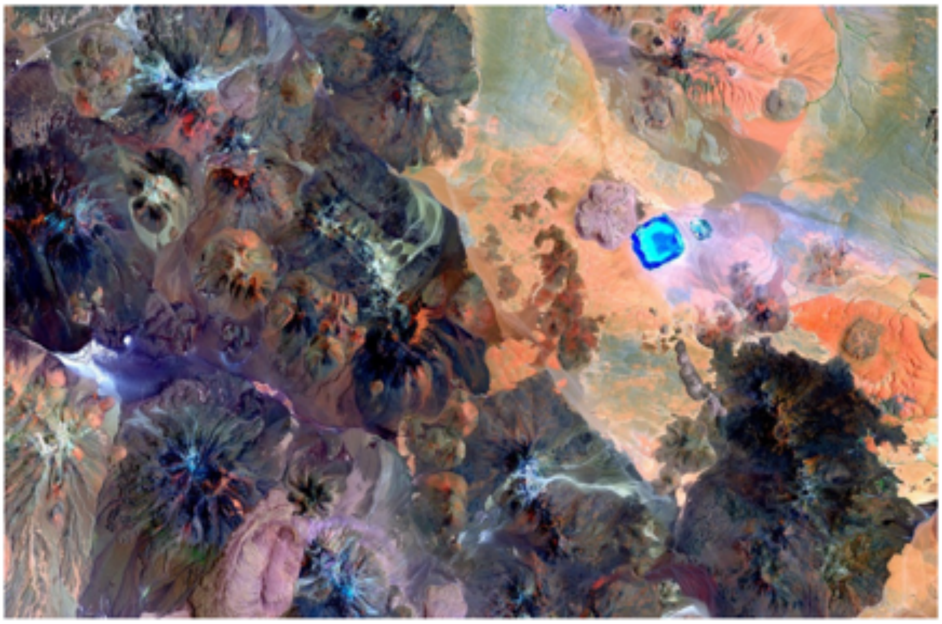

Figure No. 5. Landsat Satellite Image 7 ETM + 742 RGB bands used for lithological discrimination

5.2. Bing Maps

Bing Maps is a versatile tool that provides a determined precision and allows to position, in an almost exact manner, a specific point. The tool can be applied in Geology for geological mapping by means of a visual analysis of satellite images, due to its high spatial resolution, which is of up to 0.30 m, in some cases. In addition, with a spectral treatment of the image, it is possible to highlight the lithology on basis of the characteristic spectral patterns, which in this case is in the range of the visible spectrum, covered by the BING server.

5.2.1 Methodology to process satellite images

There are many tools that can be employed to perform spectral processing and improve the data.

Contrast improvement: One the most important quality-related factors of satellite images is contrast. Contrast is created by the difference of brightness reflected from two adjacent surfaces. If an image’s contrast is concentrated in a specific range, the information might be lost in areas that are excessive and uniformly concentrated. The idea behind contrast stretching is augmenting the dynamic range of the gray levels in which the image is processed. Contrast stretching entails an alteration of the distribution and value range of the Digital Number (Arezo Marcos, 2013).

Intensity-Hue-Saturation (HIS): Intensity is the total brightness or opacity of a specific color. Hue is related to what is perceived as the predominant color or wavelength of light. Saturation refers to color purity. In general, the transformation uses an image composed of three colors taken from the original satellite data. Original spatial data is separated in the intensity component, while spectral data is separated in the tone and saturation of the components (Arezo Marcos, 2013).

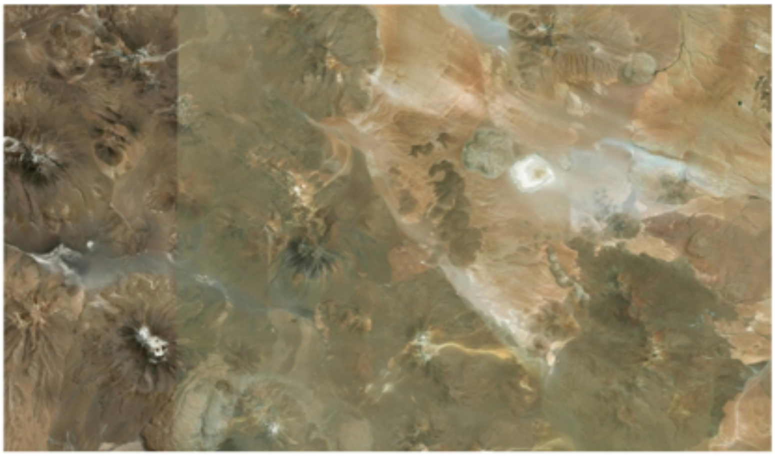

Figure No. 6. Bing Map Image used to interpret structural lineaments and to discriminate the lithological units in the Silala area

The above image was used to differentiate the lithological units, discriminate the ignimbrite, lava, and alluvial and colluvial deposits, and identify the structural lineaments.

5.3. Combination of LANSAT 7 ETM and Y Radar Alos-Palsar images

A lineament is a linear, rectilinear or slightly curvilinear physical feature on the earth's surface (O' Leary et. al. 1976). Lineaments can be either simple or composite as a function of the expression of their complexity on the soil, and thus constitute "natural structural discontinuities" of the earth's surface and generally reflect structural phenomena of the subsoil (Ohara & Flores B., 1998). A structural system categorized as a "fault" can present different dimensions, millimetric dislocations and even continental dimensions (Flores Naranjo G., 2000).

This technique demonstrates the usefulness of mapping lineaments on shaded relief maps (hill shades) for analysis of satellite images based on a combination of radar images and optical images.

5.3.1 Methodology to process satellite images

Two image types were used to perform the combination: i.e. Landsat 7 images–ETM + (optical) and ALOS-PALSAR (radar). These images were selected due to the accessibility of the data, the spatial resolution of the images (appropriate for the regional scale of the study) and the wavelengths that cover the 7 Landsat bands between 0.45 and 2.35 µm—ranging from the visible region of the electromagnetic spectrum to mid-infrared, which offers the possibility of analyzing the physical and chemical characteristics of the coverages—and the L band of the ALOS PALSAR radar image with a wavelength of 23.62 cm, which provides information on the geometry of the coverages. These wavelengths complement each other and allow analyzing the earth's surface taking into consideration its different characteristics. Rodriguez-Esparragon Dionisio et.al., 2015.

- Optics (ETM + 233/075 (08-03-2003)).
- Radar (HH - 1.5 FBS (12-31-2010)).

5.3.2 Data processing

5.3.2.1 LANDSAT 7 ETM + (Enhanced Thematic Mapper Plus)

The data comprises satellite images for which each pixel is assigned a digital level (DL) after the radiance data captured by the sensor for the different wavelengths is adjusted, which is why it does not present the direct physical dimension of the objects observed (Chuvieco, 2002). The original DL from the satellite images were converted into the actual physical dimension of the objects, resulting in corrected images represented in reflectance values (Conesa, et.al., 2004).

5.3.2.2 Alos-Palsar (Phased Array Type L-Band Synthetic Aperture Radar)

These comprise georeferenced images, with a uniform pixel size, calibrated radiometrically with the backscattering coefficient sigma (s) scaled to decibels [dB] and filtered to reduce the errors introduced by the speckle effect. (Palomino-Angel et.al. 2014).
Since each scene covers only an area of 50 x 70 km, a mosaic of radar images was generated to cover the entirety of the area of concern.

14

The processing was performed with the ENVI 5.3 (Pan Sharpering) software to then integrate the data to the ArcGis 10.4.1 software. These shaded and merged relief images were used for the visual interpretation of regional lineaments.

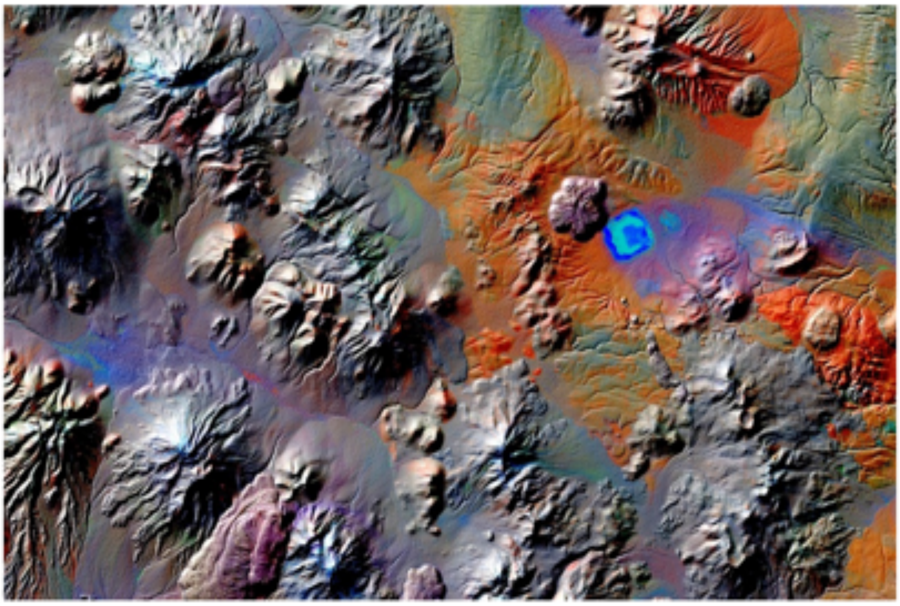

Figure No. 7. Landsat 7 ETM + 742 RGB Bands combined with the Alos Palsar L Band radar image used for the preliminary interpretation of the structural lineaments

5.3.2.3 Conclusions from image processing

There are certain advantages in the use of radar images for mapping lineaments. It allows controlling the angle of incidence of light and its azimuth (hill shade) and changing the image scale at any time, for instance. Further, as opposed to aerial photographs, radar images are not flawed by any type of deformation and the vegetation does not interfere in the interpretation.

It should be noted, however, that the lineaments obtained must be contrasted with the structural information obtained in the field. The combination of the 742 Landsat satellite images (RGB) was the one that best highlighted the lithological units, and was thus used for the geological mapping described below. The desk work carried out in regard to the different images allowed the geological mapping to determine lithological contacts that were subsequently corroborated with the field work stage.

15

6. GEOLOGICAL MAPPING

6.1 Geomorphology

The relief of the study area is characterized by a relatively flat to undulating topography, with a slight inclination to the west and wide depressions flanked by various structures such as domes, volcanic cones and stratovolcanoes.

The average altitude of the area is 4,000 MASL which increases from 4,278 MASL (at Silala ravine) to 5,701 MASL (Cerro Silala Grande Stratovolcano).

The morphology of the area was modeled by endogenous and exogenous processes; among the former, the most significant comprised volcanism followed by tectonism, which formed the predominant geoforms of the area, i.e. domes, volcanic cones, stratovolcanoes, calderas, ignimbrite shields, collapse escarpments, circular fractures and plateaus, which were then were degraded by erosion and weathering.

Among the later, the most significant for the area are glacial, eolian and gravitational processes, together with—through to a lesser degree—fluvial and physical weathering processes, particularly erosion, giving place to geoforms of accumulation and erosion such as glacial cirques, moraines, U-profile valleys, dunes, pillars or stone trees, colluvial cones, fans, plains and abrupt ravines.

The area studied does not present drainage designs of any kind, since no surface or permanent water flows were identified.

The glacial activity, together with volcanic activity and weathering, modeled the current geomorphological forms of the region, which are represented by constructional and destructive geoforms, evidenced above all in the vicinity of the Inacaliri stratovolcano. The area presents a glacial cirque, and its pre-existing valleys have deepened, lengthened and widened.

The most representative accumulation geoforms are lateral and terminal moraines and fluvioglacial deposits (at the Inacaliri hill). These products were formed during the isotope stage 4 (85,000 to 65,000 years BP) and isotope stage 3 (65,000/36,000 years BP), which had an influence on the Andes (the mountain ranges and high plateau) (Argollo et. al., 1987).
In general, the area is characterized by moraines encased in glacial valleys, the most distal of which are at an approximate altitude of 4,500 MASL and correspond to the Last Glacial Maximum, which took place in the Central Andes 14,500 years BP (Argollo, J., 1991).

Other fluvio-glacial geoforms are present as accumulations of a semi-heterogeneous granulometric composition that extend as far as the endpoints of the glacial valleys, which are surrounded by stratovolcanoes, and Silala ravines.

The colluvial deposits are found in different parts of the area studied and cover gentle slopes. These deposits have a quite incipient sedimentary structure, and are heterogeneous and often polygenic.

Alluvial activity is represented by the runoff of fluvioglacial waters, which gave rise to forms of erosion and accumulation that date back to 10,000 years BP, which are in turn represented by older and extensive fans, and plains characterized by reddish paleosols developed on the ignimbrite and lavas.

Where spring waters well up, wetlands are formed by the influence of the stagnant waters on the fine to medium sandy-loamy material, particularly in the upper part of the topographic depressions, where the slope is much softer, or inexistent—these are characteristic high-altitude wetlands (known also as Bofedales).

6.1 Regional Geology

The area of the Silala springs, the present object of the study, is found within the morpho-structural domain of the Western Mountain Range or Volcanic Belt, in its southern block, which is in turn formed in the Central Volcanic Zone of the Andes and is part of the Altiplano-Puna Volcanic Complex. The volcanic activity developed from the Upper Miocene to the Lower Pleistocene and its products were placed and deposited on a substrate of Paleozoic and Paleogenic rocks exposed in neighboring areas. Regionally, the outcropping volcanic rocks constitute large structures that form the Pastos Grandes and Capina calderas and smaller ones such as the Capina, Kheñawal and Agua de Perdiz centers and volcanic chains. The magmatic activity in the area is interconnected with the subduction of the Nazca plate, an event that occurred during the Andean tectonic phase.

The intense magmatic activity of the region began with an explosive volcanism of the Plinian type, forming large calderas (Chuhuilla, Guacha, Pastos Grandes) and extensive ignimbrite shields that correspond to extra-caldera facies (the Silala Ignimbrite). These ignimbrite deposits are monotonous, and contain dacite and calc-alkaline rhyolites rich in potassium.

Thereafter, a gradual reduction in the volatile magma content caused volcanism to change to an effusive type, forming volcanic domes, such as Cerro Silala Chico and Torito hills, discharging lava flows of andesitic-dacitic composition and creating stravolcanoes, as the Inacaliri and Silala Grande.

The most representative structural feature of the area is the transcurrent fault of Pastos Grandes-Cojina, to the east and southeast of the Khenayani-Uyuni fault system, characterized by a minor vergence. The tectonics of the zone is linked to the subduction of the Nazca plate under the South American plate and the uplift of the Cordillera, which occurred during the Andean Cycle.

Two preferred fault and fracture directions are defined in the area: NW-SE and NE-SW, the former is more evident, although both control the region's magmatism and combine in a series of dextral course faults in a transpressive tectonic environment. They also develop transtensional areas that facilitate the emission or effusion of volcanic products, such as the circular collapse structures of large calderas, which in turn is an indication of their resurgence stage.

6.3 Volcanic products and morphology

Ignimbrite

Ignimbrite is a term that is difficult to define due to its special characteristics; occasionally, the term has been used in a lithological sense, to refer to welded tuffs, in others it has been used in a generic sense, referring to pyroclastic flow deposits.

The first concept—welded tuffs—is inherently confusing, since the ignimbrites can present non-welded zones. Thus, the definition presented by Cas and Wright (1992), which provides that ignimbrite is a rock or deposit formed from a pumice pyroclastic flow, independently of whether it is welded or not, is used in this report. The fragments can vary in size, with pumice and xenolith rocks floating in a matrix composed of ash.

Picture No. 1. Ignimbrite of the Silala springs area

The regional basement is made up of partially welded tuff mantles called Silala Ignimbrite, of colors that range from light pink to violet, and of dacitic composition constituted by plagioclase, quartz, biotite and hornblende. Their matrix is composed of reddish-brownish iron oxides of the limonite type, volcanic glass and microliths of plagioclase. They correspond to the calc-alkaline series rich in K2O and their SiO2 content varies between 63 and 66%.
The ignimbrite layers, based on extrapolated radiometric data obtained from geology maps published by SERGEOMIN and/or SERGEOTECMIN, have an age of 7.8 (Myr) and correspond to the Upper Miocene (Choque, 1996, Lema & Ramos, 1996, Richter, et al., 1992).

Throughout the area studied, ignimbrite outcrops of a reddish brown color have been identified; the degree to which these are welded, as well as the matrix and lithic components that differentiate one from the others, varies.

Lava flows

These comprise lava flows that are likely to have been emitted from a volcano's upper, or secondary crater, or from a crack in its crust or flanks. Driven by gravity, these flows are distributed on the surface in proportion to the topography. In general terms, they occur in low or intermediate eruptions.

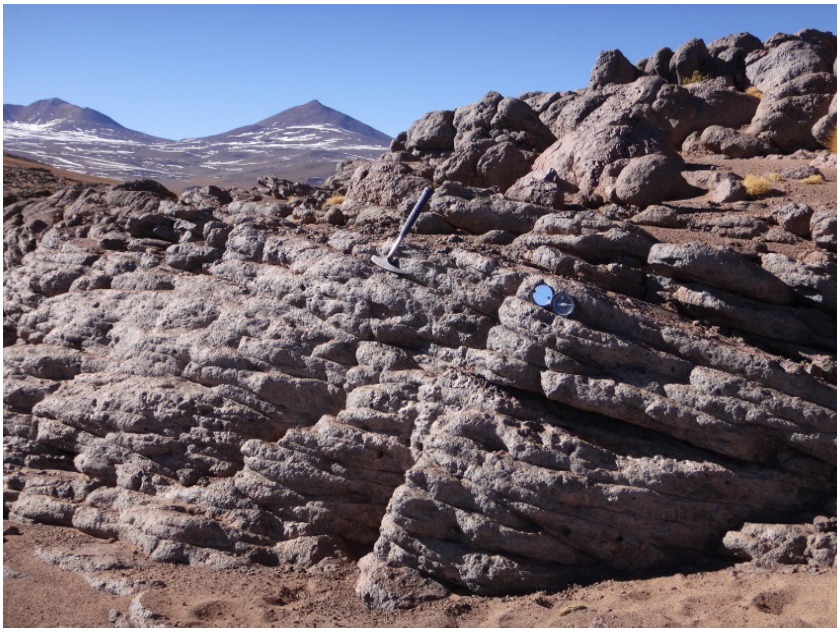

Picture No. 2. Lava flow, presenting pseudo-stratification

The different temperatures and compositions of the magma can give place to different types of lava flows. Another type of lava flow, which is very common in volcanoes that present more acidic and viscous products, are lava blocks, which appear when the flow surface solidifies and gets fragmented.

Extensive areas of lava flows have been identified in the area studied. These are characterized by forming thin pseudo-stratification layers. Their mineralogical composition indicates the presence of intermediate composition andesitic and dacitic lava, which are commonly superposed on one another.

Scoriaceous lava flows have also been observed. These present very rough surfaces that are formed by a thick layer of scoriaceous fragments and that develop autoplastically by breaking and welding the external layer that solidified during movement.

Debris flow

These debris include mud and rock particles. Debris flow occurs when rainwater, or snow that melts during eruption, erodes a slope's materials, or when a landmass is sub-saturated with water, facilitated by the gradient and gravity. This movement is faster on steep slopes and collects debris in its way. In the valley of concern for the study, loose soil and rolling rocks that have slid off the slope and moved by water have been dragged by debris flow.

When the water drags on more mud and rocks, it starts acquiring the appearance of a fast-flowing river. This debris mass can move so fast that it can drag large-size rocks and leave them on their way along the flow path. The speed and vastness of the particles dragged cause a dangerous debris circulation, wherein rocks are likely to be mixed into a viscous mass.

Stratovolcanoes or Composite Volcanoes

These constitute steep conical shapes, the top of which is truncated by a crater. These are complex structures formed by the alternating accumulation of lava flows and pyroclastic material discharged through the same outlet, which present an apparent stratification—reason why they are called stratovolcanoes.

Picture No. 3. View of Inacaliri stratovolcano

Dykes, sills, volcanic plugs, inter alia, can be observed in these areas. There are also smaller cones on the slopes—known as adventitious cones—that result from the presence of secondary emission conduits (Cepeda 1982).

These structures result from volcanic emissions characterized by alternating stages of significant explosive activities and calmer periods evidenced by different lava traces, which are the result of different eruption types, e.g. Pelean, Strombolian or Vulcanian eruptions (Vargas 1992).

In the area studied, it is possible to observe this kind of structures characterized by prominent elevations, such as the Inacaliri stratovolcano and the Silala Grande.

Domes

These are volcanic structures characterized by an accumulation of dense lava around their outlet, which, owing to its high viscosity, was unable to flow during eruption and formed steep slopes of a dome-like shape—reason why they are called volcanic domes, bulbous domes and cluster toroidal domes (Baily, 1968).

The lava that forms these domes are generally rhyolitic or andesitic and can form in the crater of an older volcano. Domes are mostly wide, and not too high, and present needle-like forms on the top and protruding vertical, abrupt walls.

In the area studied, the common domes of the sector are represented by the rock outcrops of Runtu Jaritas, Chascon (which are lined up following a NE-SW orientation) and Silala Chico (of a N-S orientation).

6.4 Local geology

The Silala springs are located in the southern block of the Western Mountain Range and are part of the Andes Central Volcanic Zone.

The weathering, erosion and deposition processes are represented by unconsolidated Quaternary and Recent sediments that cover large parts of this area. The materials deposited form glacial, fluvio-glacial, colluvial and alluvial deposits constituted by blocks, or polygenic boulders, clasts of different rocks and sizes, and fine sediments such as sand and silt.

Tectonism, manifested as the faulting and jointing of the effusive and explosive rocks in the area, had a significant influence on the location of the Silala springs.

Upper Miocene volcanic activities are of importance for the area. Several craters, volcanic centers and domes were formed during this cycle. These are manifested by the eruption and deposition of a regionally extensive ignimbrite cover—known as the Silala ignimbrite—, which is exposed on the surface of the area and is partially covered by lava flows from the stratovolcanoes of the sector.

The basal unit is constituted by ignimbrite of dacitic-andesitic composition that dates back to 6.6 and 7.8 Myr. Andesitic-dacitic lava of a porphyritic texture overlay this unit, forming the Silala Chico volcanic dome—the age of which dates back to 6.04 Ma. (Source: Andean Multinational Project–AMP).

An observation made in the springs' ignimbrite (Spring No.1) confirmed the presence of malachite (copper carbonate-supergene) on the ignimbrite surface, which is possibly an indicator of the existence of copper sulphide (hypogenic mineral) in the depth.

Sample No.7814 was taken from the rock that hosts the malachite, which, based on a petrographic analysis, corresponds to andesitic ignimbrite that contains hornblende crystals (Annex C). On the other hand, a mineralogical analysis evidenced the absence of malachite as the main rock constituent, indicating that this mineral constitutes only an impregnation on the rock.

Copper forms oxidized mineral that remains in the oxidized zone, but can also be precipitated below the groundwater level by hypogenic sulphide and form sulphide that is richer in copper—this process is efficient for copper (secondary enrichment).

A siliceous layer (opal) overlays the ignimbrite, as a nodular-shaped crust. Its formation is attributed to diagenetic processes that resulted from the chemical precipitation of continental thermal waters formed by the fast cooling of silica-containing waters.

Patches of silica crust are found surrounding the spring, corroborating the silica's origin by thermal waters. Chert was also found in the immediacies of Laguna Blanca.

6.5 Stratigraphy

Based on the geological information generated in the field through detailed geological mapping of exposed outcrops, as well as the gathering of data found in technical reports, geological and geophysical maps, inter alia, the elaboration and interpretation of a stratigraphic sequence has been achieved, allowing the elaboration of lithological profiles for the area studied. These profiles present, in a schematic and representative way, the lithological units, from base to top, that outcrop in the region.

6.5.1 Stratigraphic column for Silala

The work carried out resulted in the preparation of a stratigraphic column (Figure No. 8) for the three areas mapped in the Silala (Geological Map for Areas 1-2-3, Annex A) The dating established for the different units is presented below. The base of ignimbrite 1 (Nis1) does not appear in the Silala ravine. Geophysical studies have concluded that there is a deep lithological continuation. The description of the column will begin with the description of Debris Flow 1 (Nfd1).

Debris Flow 1 (Nfd1)

This horizon appears on both banks of the Silala ravine and has a reddish-brownish color, on altered surfaces, and reddish-salmon on fresh surfaces. It is composed of clasts of igneous rocks with a sub-angular to sub rounded morphology, and diameters that range from a few centimeters to 25 centimeters, dispersed in a rather earthy clay-sandy matrix with a low degree of compaction.

The thickness of this level fluctuates between 60 to 140 centimeters. This variation in thickness is caused by the paleorelief present at the time of deposit and the amount of material dragged by the flow. The deposits do not present any type of defined structure, resulting in a chaotic mass.

However, in the middle of this unit, fragments of rock up to 40 centimeters in diameter (monomictic blocks) were observed, stacked in a more or less continuous horizon, reflecting a high transport energy, facilitated by the slope.

Picture No. 4. a) Debris flow 1 in sub-horizontal contact with the Silala ignimbrite 1 (Nis 1). b) Debris flow 1 with sub-rounded clasts of igneous rocks of up to the 30 cm.

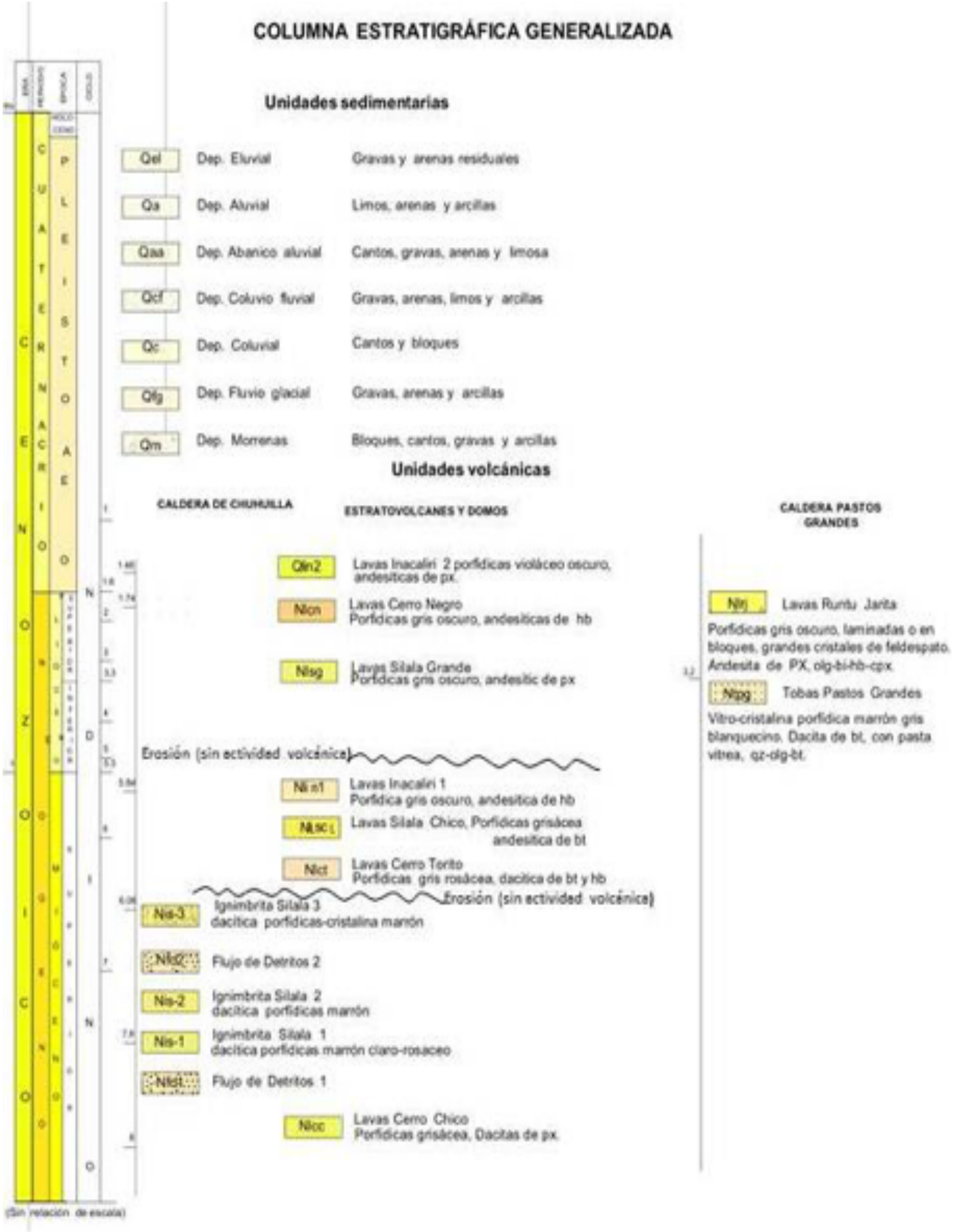

Figure No. 8. Stratigraphic column for the Silala springs

Based on the petrographic analysis carried out by SERGEOMIN's laboratory, in samples collected from this horizon, the rock clasts would correspond to pyroxene andesite and present an agglomerated structure and a mid-grain porphiric texture (> 2 mm), with abundant ferruginous paste of limonite-goethite. A very small amount of volcanic glass and pumice fragments has also been found.

Silala Ignimbrite 1 (Nis1)

The ignimbrite deposits of the Silala springs are pyroclastic flows of the Neogene. They outcrop in both Silala canals and date back to 7.8 Myr., (Upper Miocene). Their root does not outcrop, but overlays debris flow (Nfd1) in discordant contact in some parts.

The unit is composed of ignimbrite of a moderately welded flow and a pinkish-brown color, on altered surfaces, and whitish-gray to rosacea on fresh surfaces. It presents light to brown banding, with vertical parallel to subparallel fractures It has a porphyritic texture with feldspar phenocrysts, quartz, biotite and limited pyroxene (35%), lithic igneous rocks (2%), limited pumice (5%) (in fiamme sectors), and a matrix (58%) composed of microcrystals, vitreous fragments and ferruginous paste.

The exposed thickness varies from 3 to 8 meters, has a sub-horizontal arrangement with a slight inclination toward the center of the ravine. This unit is of importance because of its lithology and higher fracture index. This is the rock that hosts the Silala springs. This theory is confirmed by the amount of springs mapped along the ravine.

Picture No. 5. a) Silala ravine, where the Silala ignimbrite 1 (Nis 1) can be observed with vertical fractures. b) the Silala ignimbrite 1 (Ns1), presenting a brownish-reddish color on the surface.

A petrographic analysis carried out for a rock sample taken from the North Canal established a dacitic composition, with plagioclase crystals (oligoclase variety), smoky quartz, oxidized biotite, volcanic glass and iron oxides, agglutinated in a limonitic paste (ferruginous), volcanic glass and some microliths of plagioclase [SIC].

Microscopically, the rock has a banded, or fluidal structure and a medium-grain porphyritic texture (> 1 mm), the matrix does not present a specific structure; it is of the massive type characterized by a propagation of scattered iron oxides and pumice.

Cristal-vitreous tuff (Ntcv)

This unit overlaps the Silala ignimbrite 1 in almost all of the main ravine. It is constituted by very thin and compact tuffs, with an average thickness of 15 centimeters, an intermediate texture, and a phaneritic grain texture that ranges from fine to medium grains. In some sectors, it presents a vesicular texture. It also presents an alternation of lenticular bands of a reddish-brown color and dark gray bands—giving the rock a laminar aspect.

Due to the small size of the crystals, it is difficult to recognize them macroscopically; however, it was possible to establish the presence of feldspars, biotite, hematite and magnetite surrounded by a vitreous ferruginous matrix. To provide a better description, samples were taken (Nos. 7702 and 7706) and their results are detailed infra.

This is an intermediate composition pyroclastic rock (glassy vitreous tuff), which corresponds to andesitic ignimbrite, characterized by a fluidal to banded structure, medium-grain porphyritic texture (> 1 mm), tabular—and slightly oriented—prismatic plagioclase crystals (oligoclase), and quartz in the form of anhedral crystals, clinopyroxene (Augite) with a prismatic and tabular habit for brown tones, pumice and scattered iron oxides.

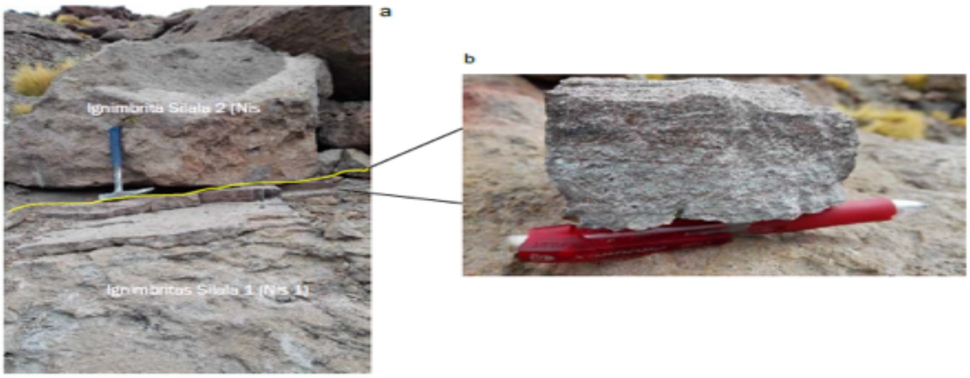

Picture No. 6. a) Marker horizon corresponding to a crystal-vitreous tuff, 20 cm thick, that delimits the Silala Ignimbrite 1 (Nis 1) and Silala Ignimbrite 2 (Nis 2); b) Hand sample of the tuff level where a banded structure can be observed.

The matrix is mainly a massive texture and is composed of reddish-brown iron oxides of the limonite (ferruginous) type, volcanic glass and microliths of plagioclase.

This tuff level is very important and constitutes a marker horizon. Due to its lithostratigraphic position, areal extension and its sub-horizontal arrangement, it allowed subdividing the Silala Ignimbrite in two members (Nis1 and Nis2) and it is also an indicator of possible vertical displacements produced by the faulting or sliding of the rock massif.

Silala Ignimbrite 2 (Nis2)

The ignimbrite deposits that correspond to this horizon (Nis2) outcrop along the Silala ravine. They concordantly overlap the level of the vitreous crystal tuff (Ntcv) at the base and are topped by Debris Flow 2 (Nfd2).

The unit is composed of welded ignimbrite (flow tuffs) of a reddish to pinkish color on altered surfaces and whitish gray, with pinkish tones, in fresh surfaces, somewhat rusty, massive structure in some sectors banded [SIC]. It has a porphyritic texture with lithic plagioclase phenocrysts, quartz, pyroxene and amphibole, with very variable diameters; it corresponds to andesite, pumice of up to 10 cm length, and are crushed, or deformed, showing the welding degree. The matrix occupies 65% of the rock and is composed of microcrystals of plagioclase and volcanic glass.

Its thickness can reach 10 meters. It is different from the underlying ignimbrite in that their lithic components have a fining or inverse gradation and a lower fracturing degree. They are more competent, or more welded and therefore are less permeable—although, due to supergene alteration, they present thin crusts of malachite in some sectors.

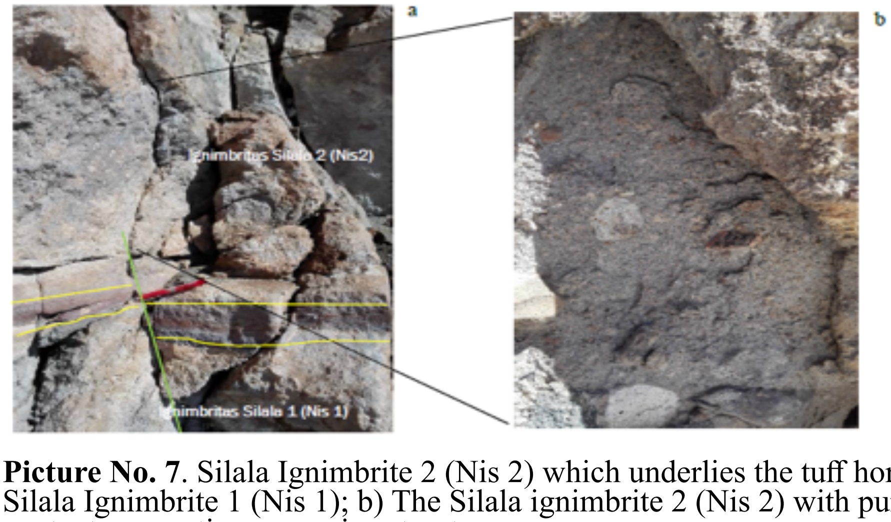

Picture No. 7. Silala Ignimbrite 2 (Nis 2) which underlies the tuff horizon and Silala Ignimbrite 1 (Nis 1); b) The Silala ignimbrite 2 (Nis 2) with pumice content, presenting a massive structure

Sample No. 7814 (Annex C) analyzed petrographically, belongs to this unit. It presents an acid-intermediate composition and corresponds to a biotite-hornblende dacite, with plagioclase crystals of the Oligoclase-Andesine variety, quartz with fractures and embayment, prismatic to tabular clinopyroxene (augite), in addition to altered hornblende; the pumice also contains splinters of volcanic glass and plagioclase microcrystals.

The matrix is the main component of the rock; it is composed of microliths of plagioclase and does not present a preferred orientation. To a lesser percentage, it has volcanic glass and very fine grain iron oxides. The whole set presents a massive structure.

Debris Flow 2 (Nfd2)

This unit outcrops in both sides of the Main Ravine, in the form of windows surrounding the south end of the Inacaliri lava. It has a brownish-reddish color on altered surfaces and grayish-brownish in fresh surfaces. It is composed of clasts of igneous rocks with a sub-angled to surrounded morphology and a chaotic distribution. It can reach diameters of up to 40 centimeters and is dispersed in a sandy-clayey, ferruginous and slightly earthy matrix, with a fair degree of compaction.

a

b

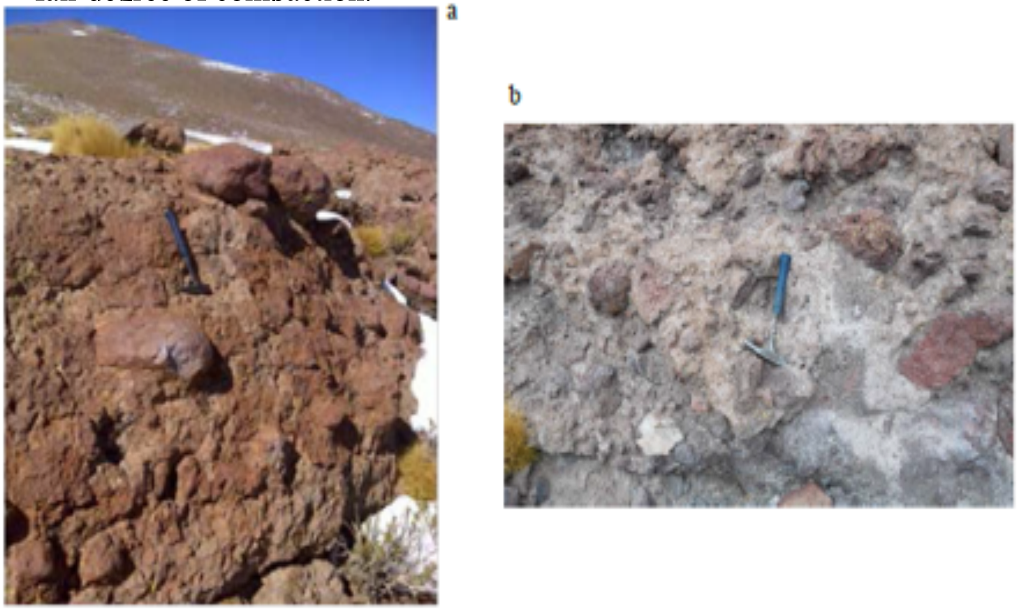

Picture No. 8. a) brownish-reddish debris flow 2 (NFd2), sub-rounded clasts of igneous rocks can be observed; b) chaotic structure that does not present any clast structuring

The thickness of Debris Flow 2 (NfD2) varies between 50 to 180 centimeters. This thickness variation is a function of the slope and instability of its base when the flow was deposited. The deposits do not present any defined structure—e.g. clast interweaving. It comprises an agglomerated mass that presents no geometrical structure. It presents a vesicular texture in some sectors.

The thickness of Debris Flow 2 (NfD2) varies between 50 to 180 centimeters. This thickness variation is a function of the slope and instability of its base when the flow was deposited. The deposits do not present any defined structure—e.g. clast interweaving. It comprises an agglomerated mass that presents no geometrical structure. It presents a vesicular texture in some sectors.

The petrographic analysis performed for this horizon presents an agglomerated structure and a porphiric structure of mid to thick grains (>2 mm), with an abundant ferruginous matrix and pumice fragments. The rock clasts correspond to dark andesite and dacite.
This flow is more widely distributed in the area than the Nfd1 flow and is thicker and more compacted. Its surface has been more polished by glacial processes, giving it a desert varnish brightness, with faceted sides and stretch marks.

Silala Ignimbrite 3 (Nis3)

The rocks of this unit constitute the major ignimbrite outcropping in the area and are found in the north-east sector of the ravines. This unit has the shape of a fan, with the apex pointing in the direction of the Silala South Ravine. This unit's base does not outcrop, but it is assumed that its basal part is similar to that of units Nfd2 and Nis2. Its contact with the unit found above it creates an angular discordance.

The Nis3 unit is constituted by moderately welded tuffs of a reddish-pinkish color in altered surfaces and whitish-pinkish in fresh surfaces. It has a splintered structure that is similar to pseudo-stratification. It is massive in some sectors, with a saccharide to porphiric texture. The rock is slightly oxidized. (Picture No. 9).

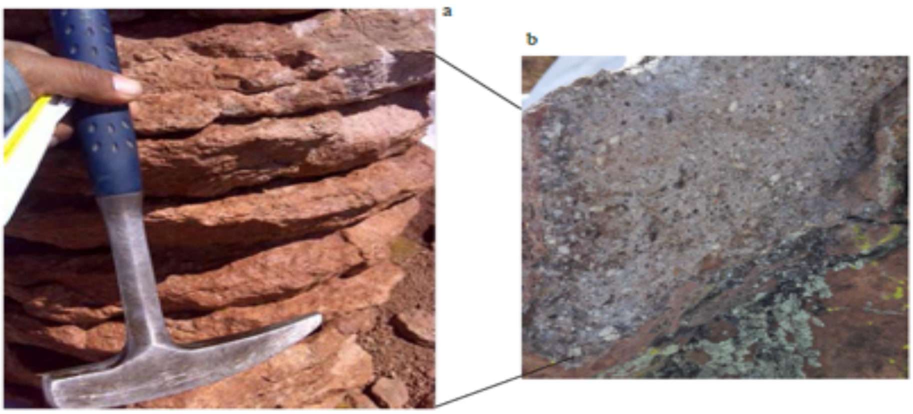

Picture No. 9. Reddish Silala Ignimbrite 3 (Nis 3), presenting a splintered structure; b) Silala ignimbrite 3 (Nis 3), presenting a porphiric texture, with plagioclase, potassium feldspar and quartz

It presents quartz phenocrysts (some are smoked), plagioclase, potassium feldspar and biotite (40-45%), andesite, dacite and tuffs (2-3 %) and pumice (5%). In some sectors, it presents fiammes that reflect the unit's welding degree. All these components are connected by a 45-47% matrix, which is constituted of glass, iron oxides and microcrystals. This unit has an approximate thickness of 12 meters. It has been differentiated from the Silala ignimbrite because of its composition, higher content and development of crystals, structure, position and ample areal distribution.

The analysis of samples Nos. 7716, 7721 and 7802 has established that this rock corresponds to welded crystalline glass, or acid-composition ignimbrite, which corresponds to biotite dacite, with fractured quartz crystals and oligoclase-andesite plagioclase, presenting a preferred direction and crystal twinning. There is a reduced proportion of potassium feldspar and biotite, forming oriented tabular crystals.

The paste or matrix is abundant. It is formed mainly by glass, limonite, hematite, and presents a massive structure. Sporadically, it presents spherulites. The pumice has inclusions of biotite and plagioclase. The lithic rocks are volcanic (andesite and dacite).

Silala Chico Lava (Nlsc)

The Nlsc unit outcrops mostly in the southern part of the ravines. Half of the rock mass is found in Chilean territory (Cerro Silala Chico), although there are also relicts in the northern sector. In both cases, the ravines flank the Silala Ignimbrite 1 and 2 in the Silala Main Ravine.

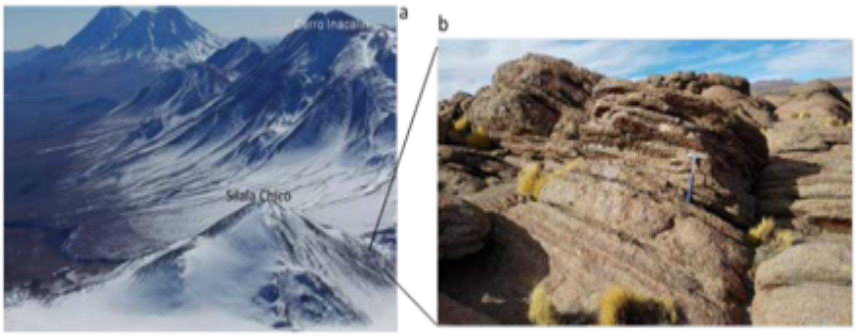

Picture No. 10. a) Silala Chico hill, Inacaliri stratovolcano in the back; b) Silala Chico lava (Nlsc), of a dacite composition, presenting a splintered structure

These rocks correspond to a volcanic dome, with a N-S orientation, approximately (it lines up with other similar bodies in Chile). The dome is constituted by brown dacite on altered surfaces and whitish gray on fresh surfaces. It has a porphiric texture, with developed quartz, feldspar, pyroxene and biotite. The crystals are rounded, and present a fine paste. They have a fluidal structure, with dark and brown bands. They form centrimetrical to decimetrical banks and present a mild-to-strong oxidation and calcite impregnations.

Samples Nos. 7712 and 7713—taken from the west of the volcanic dome—present the following petrographic features (see Annex C): acid-composition lava, corresponding to biotite dacite to quartz biotite andesite, with fractured and embayed quartz anhedral crystals, oligoclase-andesite plagioclase, as tabular and prismatic crystal twinning. Biotite is represented as subhedral tabular crystals, as clinopyroxene, hornblende and iron oxides accessories.

The lava paste, or matrix is abundant and composed of volcanic glass of a massive texture, and plagioclase microliths to a lesser degree, as well as limonite and hematite disseminations. Its microscopic structure is holocrystalline and its texture is medium-grain porphiric (> 2mm). It presents a microlitic matrix of an altered aspect.

Cerro Negro Lava (Nlcn)

This unit outcrops to the northeast of the Inacaliri stratovolcano, as a body of an isolated dome shape that intrudes the surrounding ignimbrite, since it has an age of 6.04 Myr (Regional Integration Project, 2001-2003). This volcanic body has a basal diameter of 2 km; and an approximate altitude of 5,200 MASL.

The Nlcn unit corresponds to a volcanic dome composed of violet gray lava flows on altered surfaces and dark gray on fresh surfaces. It has a massive laminar structure that shows pseudo-stratification. The porphyritic texture presents phenocrysts of plagioclase, quartz, biotite and hornblende, agglomerated in a very fine ferruginous matrix and with microcrystals of plagioclase. The rock has a high degree of hardness and conchoidal fractures.

Picture No. 11. a) Cerro Negro with a dome-like morphology. b) Lava flow of Cerro Negro (Nlcn), it presents a reddish-brown coloration with a splintered structure

31

The petrographic analysis of samples No. 7822, 7822 and 7727 (Annex C) established that these are intermediate composition lavas, that correspond to biotite to hornblende andesite, with a holocrystalline structure, a medium grain porphiric texture (> 2 mm), composed of plagioclase crystals (oligoclase) with tabular to prismatic forms, with reaction edges and crystal twinning, anhedral quartz, tabular biotite, with inclusions of plagioclase, hornblende as phenocrysts, euhedral and subhedral, asides from disseminated iron oxides.

The matrix is in a percentage of 55 to 60% and is constituted mainly by microliths of plagioclase without orientation, and a smaller amount of brown volcanic glass. The paste has a massive texture in felty sectors.

Cerro Torito lava (Nlct)

The rocks that make up this unit emerge northeast of Silala, in two contiguous sectors; the first is presented as a volcanic dome with an approximate height of 4,900 MASL in its highest part, and a basal diameter of approximately 1.6 km. The second is presented as a lava dome of an ellipsoidal shape with a length of up to the 10 km and a maximum height of 5,024 m. Because of their chronostratigraphic position, they both intrude the Silala Ignimbrite.

The Nlct unit is formed by lavas of a greenish-gray color on altered surfaces and dark gray to whitish on fresh surfaces, with well-developed crystals of plagioclase, biotite, pyroxenes and sparse quartz; it is surrounded by a very fine paste and presents a porphiric saccharide texture, with fractures of the hexagonal type; in some places, it presents pseudo-stratification and in other sectors, it becomes massive, quite competent rock; due to the weathering, some outcrops are quite crumbly.

Picture No.12. Volcanic dome of Torito hill (Nlct), rock outcrops and hand-drawn samples

32

Microscopically, the volcanic rocks of Torito hill correspond to lavas of acid to intermediate composition. They are biotite and hornblende dacite and andesite; the former mostly appear at the base. These rocks are constituted by abundant fractured plagioclase crystals (Oligoclase-Andesite) that present crystal twinning. Moderate to sparse quartz, anhedral and subhedral, they present embayment, clinopyroxene (Augite) of a prismatic to polygonal habit, biotite and hornblende as main accessories of tabular and rhombic forms, somewhat altered and with inclusions of iron oxides.

Abundant matrix, formed by microliths of plagioclase without an orientation and with a felty texture, asides from volcanic glass, hematite and limonite. All these characteristics were evidenced in the field samples Nos. 7726, 7729 and 7805, (See Annex C).
Inacaliri Lava 1 (Nlin1)

The rocks of this unit form the Inacaliri stratovolcano and emerge on its eastern flank. They correspond to the first pulses that formed this volcanic structure. They date back to 5.94 Myr (PIR Regional Integration Project, 2001-2003).

The Inacaliri Lavas 1 are constituted by lava flows of a grayish brown color on altered surfaces and dark gray on fresh surfaces. They present lamination, forming a pseudo-stratification and are massive in some sectors; they have a porphyritic to aphanitic texture, with plagioclase phenocrysts, pyroxenes, biotite and quartz, surrounded by a very fine grain paste. In some places, a fluid structure can be observed. The rock is quite hard and compact.

In various sectors, these lava flows develop basal breccia constituted by the same rock that is cooling and solidifying as it flows downhill dragging and assimilating clasts from the underlying rocks. The morphology of the clasts varies from sub-angular to sub-rounded with very variable diameters, reaching even one meter in diameter.

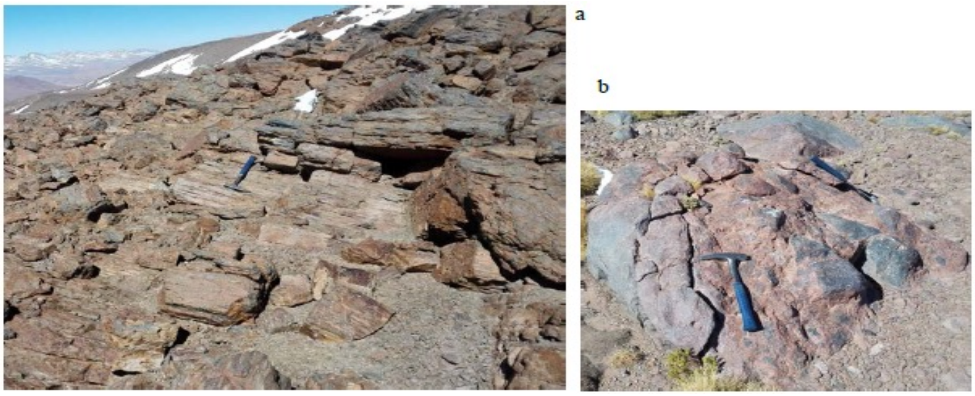

Picture No. 13 a) Inacaliri lava flows (Nlin1), b) basal breccia of the aforementioned flows

The analysis of samples Nos. 7813 and 7833 (Annex C) has established that these are lavas of intermediate composition, which correspond to a hornblende andesite, weakly oxidized, with a holocrystalline structure, constituted by plagioclase crystals of the oligoclase variety with a preferred orientation, anhedral and subhedral quartz, brown prismatic hornblende, suboptimal prismatic clinopyroxene and polygonal euhedral and tabular biotite. The matrix is constituted by plagioclase microliths.

Silala Grande Lava (Nlsg)

This unit is one of the largest in the area. Its rocks outcrop to the north and northeast of Silala, forming a Quaternary Stratovolcano (1.9 Myr, Regional Integration Project). It has a diameter of 14 km and a height of 5,700 MASL; its slope varies, from the base to the peak, from 12% to more than 40%.

The Nlsg unit is constituted of several andesitic-to-quartz andesitic lava and basal breccia. It has a brownish reddish to gray color on altered surfaces and dark gray on fresh surfaces. Its structure is very variable, ranging from massive to splintered and fluidal. It presents a porphyritic, aphanitic, trachytic and even vesicular texture, composed of phenocrysts of plagioclase, pyroxene, amphibole, biotite and quartz.

The basal breccia of the andesitic lava flows has the same composition and presents a ferruginous matrix and polymictic lithoclasts of volcanic rocks, with sub-angular to sub-rounded morphology and diameters that range from the few centimeters to the 100 centimeters in diameter. The breccia and the lava flows both have a high degree of hardness and compaction, and present bread-like or hexagonal crust fractures. Pseudo-stratification has also been established in disturbed sectors, and pseudo-folding in others.

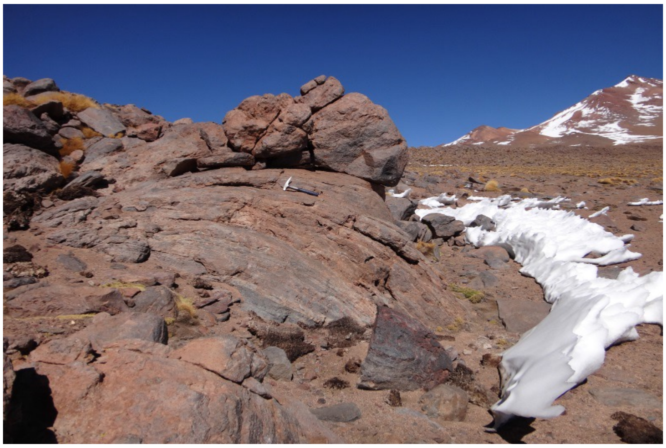

Picture No. 14. Pseudo-stratified lava flows (Nlsg)

The petrographic analyzes of these flows (samples Nos. 7816, 7820, 7818, 7830 among others, see Map No. 4) have indicated that these are lavas of intermediate exclusion, that correspond to pyroxene and hornblendic andesite with a holocrystalline structure, porphyritic rock texture, with abundant plagioclase crystals of the Oligoclase-Andesite variety, hornblende, augite and biotite in anhedral, subhedral and euhedral crystals. Texture of the trachytic and felty matrix, composed mainly of microliths of plagioclase and, to a lesser extent, volcanic glass and iron oxides [SIC].

Inacaliri Lava 2 (Nlin2)

The rocks that make up this unit were emitted in a second pulse dated back to 1.9 Myr (Lema & Ramos, 1996), covering the volcanic cone formed in the first event. A well preserved crater can be observed in the upper part of the volcano. The deposits of the Nlin 1 and Nlin2 units cover the Silala Ignimbrite.

The Inacaliri Lava 2 consists of lava flows of an andesitic composition with a basic tendency. They also develop basal breccia in several sectors; the rocks show a brown to reddish gray coloration in altered surfaces and dark gray in fresh surfaces, and develop lamination that forms a pseudo-stratification and centimetric to decimetric splinters and are massive in certain sectors. [It presents a] Porphyritic to aphanitic texture, with plagioclase phenocrysts, pyroxenes, biotite and quartz, surrounded by a very fine grain paste. Fluidal structure is observed, and the rock is quite hard and compact.

Picture No. 15. Stratovolcanic lava flows (Nlin 2)

The analyses of samples Nos. 7720, 7743, 7810 and 7811 have established that the lavas are of intermediate composition, rather basic, and correspond to pyroxene-hornblende andesite with fluidal to vesicular microstructure. The texture of the porphyritic rock with tabular to prismatic plagioclase (oligoclase-andesite) crystals that present crystal twinning and zoning [SIC]; clinopyroxene (augite) as anhedral and subhedral phenocrysts, some of which are twinned; brown prismatic and polygonal hornblende, iron oxides as inclusions and disseminated in the paste, with a minor proportion of quartz. The matrix presents a eutaxitic to felty texture composed of microliths of plagioclase and volcanic glass, limonite and hematite.

Pastos Grandes Tuffs (Ntpg)

This unit consists of fall and flow tuffs, with a brown to pinkish coloration on altered surfaces and whitish pinkish on fresh surfaces, [; it presents] a massive structure and is formed in blocks, porphyritic texture with feldspar phenocrysts, some smoky quartz and biotite, volcanic stone lithic materials ranging from millimeters to up to 50 centimeters in diameter and pumice with quartz and biotite crystals as inclusions in sectors form fiammes, agglutinated in a tuff-vitreous matrix. The rocks vary in their hardness or welding degree.

The outcrops that correspond to this unit are located northeast and southeast of the Silala springs, these tuff deposits are part of the Caldera of Pastos Grandes and date back to 3.4 Myr in their southern distribution (Lema & Ramos, 1996) and to 2.9 Myr in their northern proportion (Salisbury et al., 2010).

The analysis of samples Nos. 7722 and 7723 (Annex C) has indicated that these are vitro-crystalline tuffs of acidic composition, biotite dacite, with a hypo-crystalline structure and medium grain texture (> 1 mm), with a vitreous matrix of a massive texture.

Runtujaritas hill lava (Nlcrj)

These domes outcrop in the easternmost part of the area and present a NW direction connected with the faults. It has a horizontal elongated lobular shape, with a length of approximately 6 kilometers and an average height of 4,900 MASL.

Macroscopically, the rocks that constitute this unit are presented as lavas formed in scoriaceous blocks, of a grayish brown color on altered surfaces and whitish gray on fresh surfaces. [They present a] massive vesicular structure, a porphyritic texture with feldspar phenocrysts, biotite, pyroxenes and rare quartz, surrounded by a fine matrix apparently composed of volcanic glass. The rock presents a medium hardness and is mildly oxidized.

The microscopic analysis of sample No. 7737 has indicated that this is lava of acid-intermediate composition that corresponds to pyroxene dacite, with a holocrystalline structure and medium-grain porphyritic texture (> 2 mm), with twinned plagioclase crystals, oxidized tabular biotite, prismatic hornblende partially replaced by limonite, [and] clinopyroxene of the augite variety in clusters. The matrix is vitreous and presents a perthitic texture.

Picture No. 16. Pastos Grandes Tuff (Ntpg)

Cerro Chico hill lava (Nlcc)

This volcanic formation is located southeast of Silala Grande stratovolcano, adjacently to the Runtujaritas domes. It has an irregular lobed shape, regularly sub-horizontal—which is why it is called El Meson Negro hill.

The lavas of this unit have a brown coloration on altered surfaces and whitish gray to dark gray on fresh surfaces. The unit presents a massive structure formed in blocks, in laminated sectors, porphyritic texture with feldspar phenocrysts, biotite, pyroxenes, quartz and iron oxides, inside a fine-grained matrix. The rock displays a high hardness and compaction.

Picture No. 17. Panoramic view of the Runtujaritas dome-lava

The analysis of sample No. 7827 (see Annex C) has indicated that the lava is of acidic composition and corresponds to weakly oxidized pyroxene dacite, with a holocrystalline structure and a medium grain porphiric texture (> 2 mm), with subhedral and anhedral quartz crystals, plagioclase with crystal twining of the albite type, dark brown tabular biotite, prismatic augite and greenish polygons. The matrix is composed of microliths of plagioclase and iron oxides, showing a microlitic texture.

Picture No. 18. Lava flows of Cerro Chico hill (Nlcc)

Quaternary deposits

Glacial Deposit-Moraines (Qgm)

Glacial activity is represented by erosion and accumulation geoforms located in the vicinity of the stratovolcanoes and in the Silala Main Ravine. Within the former, glacial cirques developed in the Inacaliri and Silala Grande stratovolcanoes can be observed. Another effect of glacial erosion is the deepening, lengthening and widening of pre-existing valleys, giving them the typical U-profile.

The main accumulation geoforms are the lateral, frontal and terminal moraines. The formation of these glacial products can generally be associated to the Isotopic Stage 4 (85,000 to 65,000 BP) and Isotopic Stage 3 (65,000/36,000 BP), which occurred in Los Andes (the Mountain Ranges and Altiplano) (Argollo et al., 1987 and Argollo and Iriondo, 1991).

There are three groups of moraines encased in glacial valleys. The outermost, or most distal one is located at an approximate elevation of 4,500 MASL and corresponds to the Last Glacial Maximum, which occurred in the Central Andes 14,500 years ago BP (Argollo, J., 1991)—according to earlier studies carried out by radio-carbon methods, mainly in tuffs and shells, for both the Western and Eastern Cordillera. The second moraine is found at 4,670 MASL and the last one at 4,800 MASL, and corresponds to a tardiglacial.

Glaciation events that date back to 14,500 BP caused strong alterations in the landscape owing to the movement and thawing of ice masses, which resulted in the formation of lakes, lagoons and deep valleys.
Thawing activity was essential for the formation of the Silala ravine, which is a typical example of a ravine that was carved by meltwater, facilitated by areas of weakness (faults and fractures); the current design of the Main Ravine, however, presents a U-shaped cross section, with vertical side walls and a flat base. The water produced by the melting of the glacier mass is an important source for the current groundwater stored in the Silala ignimbrite.

Fluvioglacial deposit (Qfg)

The fluvioglacial sediments are represented by the accumulation of volcanic and pyroclastic rock fragments, of an almost heterogeneous granulometric size. They are deposited at the ends of the glacial valleys that surround the stratovolcanoes and in the Silala ravine.

These deposits are made up of sand and some silt, with clasts, boulders and cobblestones of volcanic rocks of different diameters. The larger blocks present glacial striations that reflect the movement of ice masses, while the material of a smaller granulometry reflects a fluvio-glacial transport and erosion.

Colluvial-Fluvial deposit (Qcf)

This is a deposit formed on a gentle slope, where the sediment accumulated as a result of the transport of rocky material caused by gravity, combined with the action of intermittent runoff water. They are the product of melting and snowfall.

Colluvial-Deposit (Qc)

Colluvial sediments are found in different parts of the area, forming on smooth and steep slopes as colluvial cones. These accumulations present incipient sedimentary deposits, are heterometric and frequently polygenic and are constituted of blocks, boulders, pebbles and gravel of volcanic rocks that outcrop from the Silala Chico, Silala Grande and Inacaliri, inter alia, inactive volcanoes.

Alluvial Fan Deposit (Qaa)

Alluvial activity is represented by the runoff of fluvioglacial waters that gave rise to forms of erosion and accumulation 10,000 years BP. Large alluvial fans can be observed, reflecting somewhat more temperate climatic conditions, causing ice masses to melt and, in consequence, amounts of runoff water that were completely different from the current ones. These deposits were formed by varied materials of medium to fine granulometry, (gravel, sand, silt and clays), arranged in a decreasing grain shape from top to bottom, with the apex exposed in the highest part.

Alluvial Deposits (Qa)

These deposits are located in the springs, where water deposits are found, but do not circulate and remain stagnant, forming high Andean wetlands. Fine sediments, mostly organic matter, can be observed here. Other forms of alluvial accumulation in the area studied comprise alluvial plains with red paleosols developed on ignimbrite (which dates back to 7.8 Myr) and andesite-dacite lava (which dates back to the Quaternary).

6.5.2 Cross-sections of the Silala springs area

Seven cross-sections (Figure No. 9), approximately every two hundred meters, were produced on basis of the field work with the aim of correlating the different ignimbrite and debris flow horizons of the area (Annex B). According to the cross-sections obtained, it can be assumed that the debris flow horizons are distributed at different levels, have an irregular base and reflect the instability of the valley. These horizons are syngenetic to explosive volcanic activities.

The Silala ignimbrite units are differentiated by their degree of welding, fracturing and vertical jointing, which allows the water to infiltrate through the fractures. Other parameters to differentiate the ignimbrite units comprise the content of pumice (fiammes), lithic materials and crystals.

The geological sections were produced on basis of the topographic map prepared by the Military Geographical Institute (IGM, for its Spanish acronyms), which provides more precise data, since it was elaborated with total station equipment.

6.5.3 Data Base

The field data, sampling points, and dating collected from different reports and petrographic analyzes are presented in Annex D to this report.

6.6 Generalized Geological Section of the Silala springs area

Radiometric data obtained within the framework of the Regional Integration Project (2001-2003) has indicated that the Silala ignimbrite (Nis 1) dates back to 7.8 Myr BP. This ignimbrite corresponds to explosive products and extra-caldera facies of the Chuhuilla event. This unit is widespread at the regional level and is the oldest unit of the area. At a first stage, it was subsequently intruded by the domes of Silala Chico, Cerro Negro and Cerro Torito. These intrusions date back to 5.94-6.04 Myr BP and have andesitic to dacitic compositions.

Figure: 9 Location of the cuts made in the quarry of Silala

Another explosive pulse was then recorded, which resulted in the deposition of wide ignimbrite mantles between 3.4 and 2.9 (Salisbury et al., 2010); these are assigned as the Pastos Grandes event, although they are not represented in this section due to their location in respect to the cross-section.
Following the largest intrusions, and with ages that range between (1.6-1.9) Myr, the Inacaliri stratovolcanoes (second pulse) and the Silala Grande were formed. These were events of the effusive type. These lavas that currently constitute the topography of the Silala area have andesitic and dacitic compositions.

6.7 Conclusions

The detailed geological survey works carried out for the area of the Silala springs allowed defining that the base of the area is constituted by the Silala Ignimbrite 1 (Nis 1). The salient feature of this unit is its high degree of fracturing. Debris flows were also identified in the exposed lower area. Considering the genesis of these volcanic-clastic products, however, it has been concluded that they are local. The Silala Ignimbrite 1 dates back to 7.8 Myr BP, the Upper Miocene. From the hydrogeological perspective, this unit is the most important one inasmuch as it contributes to the formation of water springs.

A crystallovitreous tuff level of 15 centimeters of power has been identified. It has an andesitic composition that forms a marker horizon and separates the first two Silala ignimbrite units (Nis1 and Nis2).
Overlaying this horizon, there is a level of flow tuffs that are semi-welded and denominated as Silala Ignimbrite 2 (Nis 2). This level presents a higher degree of welding and inverse grain-growth or gradation of lithic [materials], and is of a dacitic composition. In the area, this level culminates with quite compact debris flows (Nfd2).

A final ignimbrite level, denominated the Silala Ignimbrite 3 (Nis 3), of a greater areal exposure and exposed to the east of the Silala springs area, presents a pink coloration. Its distinctive feature is a larger development of crystals. This set of ignimbrite units are the product an event that preceded the formation of the Pastos Grandes Caldera and can be attributed as extra-caldera facies of the event known as the Chuhuilla Caldera.

Lava flows from the Silala Chico volcanic dome (Nlsc), dating back to 6.04 Myr, ejected from the first pulses (5.94 Ma) of the Inacaliri volcano (Nlin1) cover the Silala ignimbrites Nis1 and Nis2, as well as debris flow Nfd1 and Nfd2. Thereafter, the ejection of lava and dome-lava from Torito hill (Nlct), Negro hill (Nlcn) and Silala Grande stratovolcano, of a dacitic to andesitic composition, display a continuity in the volcanic activity in the sector. This set of effusive products dates back to the Late Miocene to Lower Pliocene. The volcanic activity of the sector ends with effusive products of the Pliocene in the second pulse of the Inacaliri stratovolcanoes (Nlin2), as well as the lavas of the Runtujaritas and Chascon.

During the Pliocene, the Pastos Grandes Caldera developed with the formation of explosive products of extra-caldera facies constituted by crystalline vitro tuffs that date back to 3.5 Myr and the subsequent development of their intra-caldera facies (outside the area), dating back to 2.9 Myr (Salisbury et al., 2010).

Products of the Pleistocene to Holocene constitute Glacial deposits conformed by lateral, frontal and terminal moraines, developed in the Inacaliri and Grande hills, the remains of the formation of which constitute the glacial cirques currently visible in the area. These were once of importance as recharge products for the aquifer of the Silala springs.

It is important to underline that, at that time, meltwater was the main product that gave place to the origin and recharge of the Silala springs. It has been found that the Silala Ignimbrite (Nis1), due to their degree of fracturing, permeability and secondary porosity, constitutes the host rock of the aquifers that gave rise to the Silala springs. Lava, on the other hand, behaves as semipermeable layers, allowing water to infiltrate and circulate very slowly through fractures and joints; therefore, they did not have an influence in the formation of aquifers.

Finally, it should be emphasized there are no drainage designs in the area. Further, no surface or permanent water flows were identified. This aspect is determinant to define the formation of the Silala springs and ravine that surrounds them as a product of erosion and deposition of glacial processes, which acted in areas of tectonic weakness where fluvio-glacial processes subsequently formed the current topography of the Silala.

6.8 Recommendations

- So as to determine the physical properties of the rocks of the area, particularly the Silala ignimbrite, it is recommended that permeability tests be carried out for the core samples that will be obtained from the ongoing drilling program.

- The petrological survey and geochemical analysis of whole rock samples and trace elements is also of importance, particularly in regard to ignimbrite and tuff. This analysis will allow defining, from a chemical perspective, the rock type and magma that formed the different units of volcanic rocks, differentiating their varieties and the level from which the magma emerged.

7. STRUCTURAL GEOLOGY

7.1 Introduction

A robust description and interpretation of structural data based on the cartography of the distinct deformation phases connected with the volcanic deposits are not available. Characterizing the fracture systems on basis of stress and structural control is important for the process of water movement. A geological-structural interpretation will allow establishing the variation degree of permeability as a function of the geology.

It is clear that due to the tectonic and volcanic activities, fracturing is potentially suitable for the generation and circulation of water, linked with secondary permeability.

The results and observations presented in this survey will help understand the zones that are likely to contribute with and distribute formation water.

7.2 Objectives

To analyze the fracturing and faulting of rocks at different scales, an analysis of the structural geology of the area was carried out on basis of two objectives:

- To identify the geological structures related with the fractures of the area, mainly in regard to secondary-type fractures, which are a major concern for secondary permeability. To this end, structural data on the joints, foliation and fault striation has been obtained in the field so as to conduct an analysis of weak deformation on basis of microstructural data.

- From the analysis and interpretation of structural data, maps containing the main structural features of the area were prepared and complemented with rose diagrams for the fractures, with a kinematic stereographical projection and stresses linked with the fractures, to present a view of the existing relation between fracturing and zones that are likely to contain and discharge waters. The work carried out is detailed below in the subheading entitled “Work methodology”.

7.3 Work performed

7.3.1 Clerical work

The work started with a review of existing data on the tectonics, structural geology, geophysics and volcanology of the area. It was complemented with an analysis and interpretation of Landsat 7 - ETM + optical satellite images (RGB: 3 2 1, 5 4 3, 7 4 2) and images taken from the Google Earth, Bing and Esri servers; digital elevation models (DEM SRTM V3) and radar images Alos Palsar (L band) were also analyzed.

The result of the structural interpretation was recorded in a base map and integrated into geographic information systems (ArcGis). The study was continually enriched with new structural data after each field campaign.

7.3.2 Field work

The field survey was carried out with the idea that the fracturing presents a fractal behavior, therefore, that map prepared at a metric scale (mesostructure) contains a clear representation in the whole area.
The absence of microstructural data regarding the area studied constituted the main disadvantage to perform a structural analysis of a further approximation.

The structural survey comprised 32 workdays, completed in 3 field campaigns. The places to perform the field surveys were chosen on basis of an initial discussion with the working group. The selection and routes for the survey were based on the importance of the fracturing and main structures. See Figure No. 10.

7.4 Regional structural setting

The area studied is part of Bolivia's western volcanic chain, where the tectonic setting is the result of the convergence of the Nazca and south American plates and the volcanism that occurred throughout the mountain ranges. This plate interaction is responsible for the different structural forms present in the region. The tectonic framework of the zone that comprises the area studied indicates that the latter is dominated by a set of synthetic and antithetical conjugated structures that respond to the regional stress tensor, with a $\sigma 1$ in a W-E general direction.

The volcanism of the area is characteristic of a geodynamic arc environment, regionally dominated by compressive tectonics that forms regional faults that serve as feeding channels of volcanic foci. The tectonic environment also favors the development of fractures that serve as channels for the circulation of fluids.

In their "Structural evolution of the Quaternary Miocene of the Uyuni-Atacama regions, Chilean-Bolivian Andes", Tibaldi, Corazzato and Rovida (2008), members of the Department of Geological and Geotectonic Sciences of the University and National Institute of Geophysics and Volcanology of Milan, Italy, note that the Mio-Pliocene compression is directly related with a fast convergence and apparently significant coupling of the continental and oceanic plates. The EW to WNW-ESE shortening direction of the Miocene structures and the $\sigma 1$ NW-SE of the Pliocene structures seem to be more related with an inter-Andean reorientation of structures, following an absolute WNW movement of the South American plate. The extensional deformations can be interpreted as being related with the forces of gravity that affect the highest parts of the volcanic belt, causing a somewhat asymmetrical collapse of the latter.

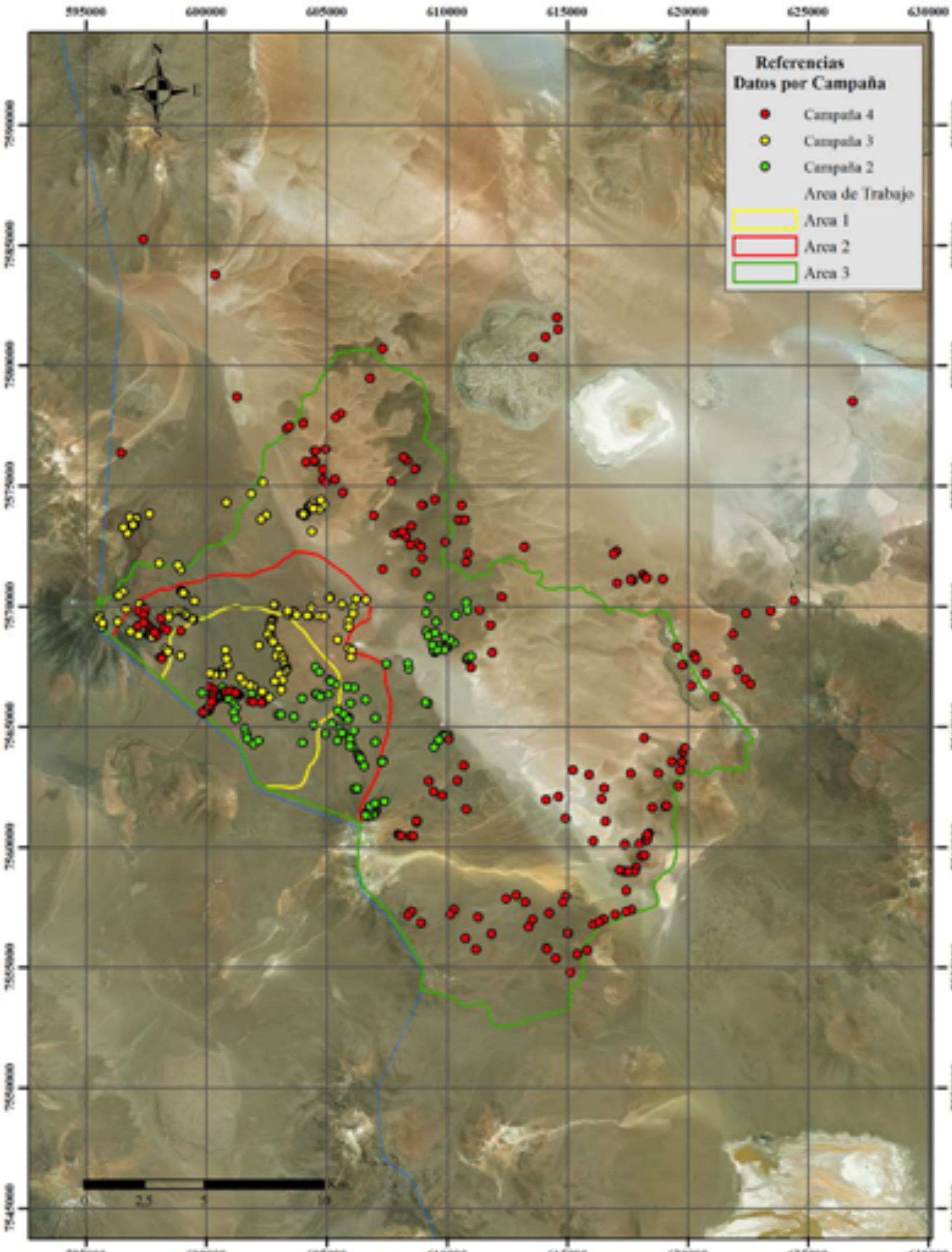

Figure No. 10. Map of the coverage of the structural data survey

46

Herail et. al. (1990), researchers of the ORSTOM-France and Bolivian Fiscal Oil Fields elaborated a cross-cutting relationship of the South of Bolivia and note that the geological and geophysical data of the Lipez basin evidence that Andean deformation began during the Late Oligocene by a sinistral wrenching, followed by landslides on its edges (Khenayani fault system in the west, San Vicente fault in the east). The shortening produced by these thrust faults is of 50 km approximately.

The Uyuni-Khenayani fault is a regional structure whose trace is found few kilometers to the south of the area studied. Mention is made of this fault by Aranibar and Martinez (1990) in their paper on the Structural Interpretation of the Bolivian Altiplano, wherein it is noted that the fault has a northeast trend and separates two provinces: i.e., the Uyuni Salt Flat province—which presents right-lateral faults and comprises flower structures and step-overs—to the west and the Lipez province—which is dominated by thin-skinned landslides—to the east.

7.5 Structural geology of the area

The structural setting of the area has been initiated on basis of the interpretation of satellite images that were addressed in the chapters above. These images present a variety of tones and hues, which highlight the rectilinear elements of the landscape and the limits of tone variations.

The rose diagram prepared on basis of the lineament and fault maps of the studied area (cf. Structural Map of Liniments and Faults, Annex) indicates that the general fracturing system presents three predominant structural trends (Figure No. 11).

The fist and main system presents a general NE-SW trend (40°-70°) and discontinuous, shorter features that are well-represented in the south and north of the area—this includes the Uyuni-Khenayani fault.

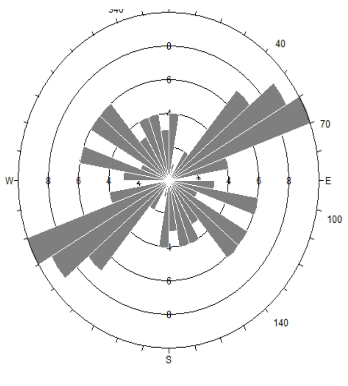

Figure 11. Rose diagram of lineaments and faults (n = 5) Silala area

47

The second system has a NW-SE longitudinal direction (100°-140°); the main volcanic centers in the area coincide with this system, which is more frequent and continuous in the northwest and northeast of the area.

The third structural system presents a general N-S trend (340°-360°) and is mainly found in the south. Some volcanic cones are lined up in this direction. An E-W to E-NE structural system, less frequent and transversal to the others, is found in the central part of the area. These cones cut and dephase some lineaments that present a N-S longitudinal trend. The table below presents a statistical table of the main structural trends of the area.

Table 1. Statistical Table of structural trends in the Silala area

Structural data	Structural trends			
Lineaments-faults	NE-SW	NW-SE	N-S	Others
Azimuth (*)	40°-70°	100°-140°	340°-360°	
Number (n)	25	20	10	20
Percentage (%)	33	27	13	27

The aeromagnetic data obtained by SERGEOMIN for the western mountain range and the Altiplano (BGM Airborne Survey, 1991) evidences that there is concordance between the structural design of the surface and the magnetic properties of the area. In the area surveyed, some magnetic anomalies reduced to the local pole and the first derivative (Map No. 6) present lineal features connected with the magnetic gradients that follow an EW to NNE-SSW direction. These lineaments are projected from the eastern limit of Pastos Grandes Caldera (4,500 MASL) transversally towards the western slope of this caldera until they reach the lower topographical end of the Silala springs (4,300 MASL). Similarly, a magnetic high in the Pastos Grandes Caldera is adjusted to the Silala-Llancor lineament (which has an ENE-WSW (70°) trend). The latter presents major anomalies in the influence sector of the Silala springs. On the other hand, it is also possible to observe gradients that separate magnetic lows and highs that coincide with the position of the volcanoes of the area. It is also possible to see that certain NW lineaments that concur with the surface of monogenetic volcanic cones have blurred out, allowing to infer their surface source.

The structural control of magnetic anomalies is evidenced by the fact that these anomalies predominantly follow an ENE to WSW direction the secondary structural trend of the area.

7.5.1 Fracturing characteristics

Most of the faults are less visible in the field, though with some morphological indications; these are characterized by almost vertical fault planes. Some of the fault planes, however, present inclinations that border the 45°. Most of the faults, owing to their cartography, are minor and shallow.

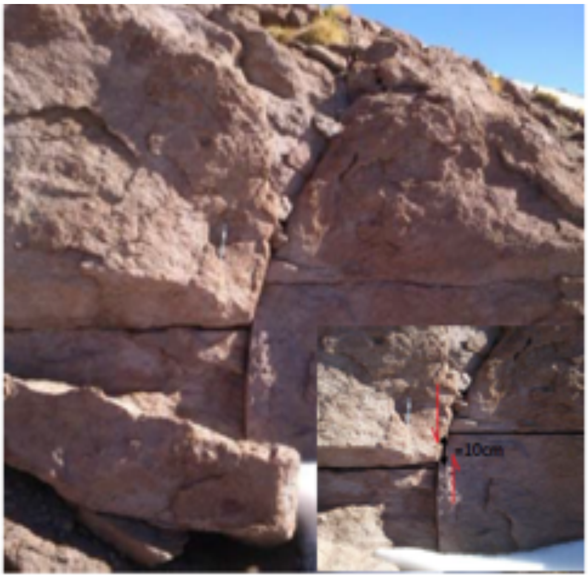

Picture No. 19. High-angle normal conjugated faulting, affecting the Silala Grande lavas

Fracturing and faulting of the dacite, andesite and ignimbrite units. These generally present a semi-vertical geometry and are represented as follows:

- In the dacite and andesite lava of the area, the fracturing commonly presents inclined and sub-horizontal planes, which are not representative for the area. The faulting caused by the current deformation is mainly semi-vertical (80°-90°) (Picture 20). Some normal faults that have NW-SE to NNW-SSE and NE-SW orientations have been identified in the ignimbrite of the Silala springs. These generally present high dips (70°-80°) and become vertical as they go deeper. These faults normally present a high angle and a slight displacement, with rebounds that do not surpass the thirty centimeters.

- Fracturing of the ignimbrite is greater, concurring with the frequencies obtained, where fracturing presents semi-vertical planes, that respond to thermal concentration processes caused by cooling; the limited sub-horizontal planes obey to a lateral faulting of slight displacement, caused more by relaxation than by lithostatic pressure. Hence, the intersection of fracture planes in the ignimbrite must be considered as a significant planar element for the movement of water, mainly as far as aquifer recharge is concerned.

Since the lithological units present a joint conjunction and faults to a lesser degree, it is possible to mention that the fracturing of the zone is conjugated, i.e. that fracturing also affects the jointing system (Picture No. 20).

Picture No. 20. Sub-horizontal, conjugate faults, affecting the joints of the Silala ignimbrite

7.5.2 Principal Structures

The Silala springs sector is dominated by NEE-SWW lineaments (60°-80°) that are transversal to those that constitute the general NW-SE trend and parallel to the Silala-Llancor lineament. To the east, the lineaments reach the limits of the western end of the Pastos Grandes Caldera.

To the north of the springs, a series of normal NW-SE orientation faults reach the limits of the Cerro Negro dome. The faults are truncated and laterally dephased to the right by the NE-SW faults of the same system as that of the Silala. To the south of the spring, the main fracturing maintains NEE-SWW trends, with some N-S to NNW-SSE variations.

7.5.2.1 Inacaliri Graben

A major normal fault system of a NW direction is present from Aguilucho hill (Chile) to Inacaliri hill (Chile-Bolivia). In this sector, two major faults present converging dips and escarpments of 150 m height, forming a symmetric graben (Tibaldi, et. al., 2008). The graben affects a series of stratovolcanoes of the Pliocene, lined up in NW-SE direction. The main fault related to the graben, to the NE, is truncated to the NE by a lava dome that dates back to 80-130 ka BP, 40Ar/39Ar (Renzulli et. al., 2006, quoted in Tibaldi et. al., 2008). Since the dome is found right on the main faults trace, its displacement was guided by the fault. A minor fault, parallel to the escarpment of the main fault, compensates the graben's base and also affects the dome with a normal predominant movement.

The structure of the graben has a NW-SE direction (300°) and a width of 3.5 km; the fault's traces that limit the structure, towards the southeast, prolong into Bolivian territory beyond the Cerro Negro hill (2 km to the north of the Silala wetlands), and are clearly visible in the satellite image that combines Landsat 7 and Alos Palsar radar images (Figure No. 9). Slightly to the northwest of Cerro Negro hill, the faults of the structure are apparently dephased dextrally by other faulting systems of a NE-SW direction (50°).

The aeromagnetic data of BGM Airborne Survey (1991), reduced to the pole and the main derivative, coincide with an anomalous low magnetic area until it reaches Negro Hill, demonstrating the deep nature of the structure. To the NW, there is a loss in the definition of the anomaly.

The distension related nature of the structures, the traces of which involve the Silala ignimbrite to the north, allow fluids to mover and circulate.

7.5.2.2 Lipez Lineaments

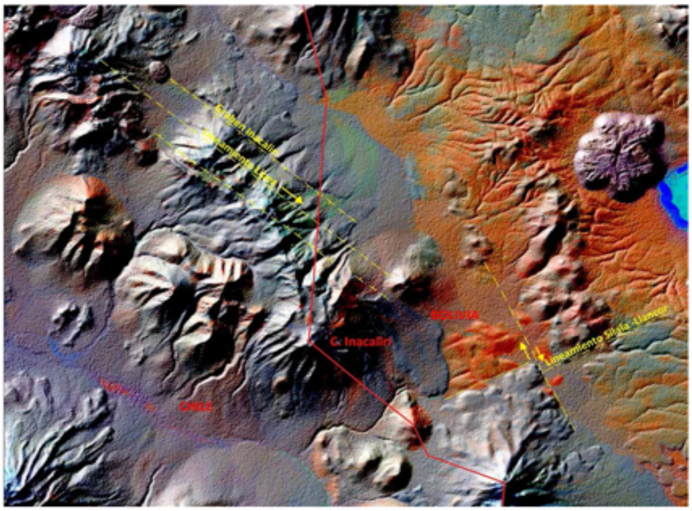

Figure No. 12. Major tectonic structures of the area surveyed

Regionally and within this graben structure, the western trace of the "Lipez Lineament" is delineated (Figure No. 12). According to Kaiser's work on the evolution of the Pastos Grandes Caldera, this structure is a sinistral movement fault with a NW-SE orientation. This lineament prolongs as far as the northern area of the Silala wetlands (Figure No. 12) and is parallel to a fault that presents a similar movement and that is marked a few kilometers to the northeast of the area. These two faults of leftward lateral movement are slightly analogous to the Khenayani fault (south of the area), although in opposed directions.

7.5.2.3 Silala-Lincor Lineament

This is an ENE-WSW (70°) lineament that crosses the central part of the area. It coincides pro parte with the Silala springs canal (cf. Map of Lineaments and Faults). This lineament is formed in between the Silala ignimbrite and the Silala Grande hill lavas. On the level of Silala Grande hill, the lavas present a somewhat lined-up morphology, in an E-W direction, with a slight inclination to the north. This lineament's trace towards the east is dephased dextrally by other transversal lineament that presents a NW-SE direction (300°) near the Cerro Torito hill lava. Further to the east, in the vicinities of the edge of the Pastos Grandes Caldera, the lineament crosses over the Runtu Jarita tuffs, ignimbrite and domes, where apparently the lineament seems to sinisterly displace the northern segment of the domes.

The aeromagnetic anomalies that are reduced to the local pole and the first derivative of the BGM Airborne Survey (Map 6) underscore a magnetic high from the Silala springs to the Pastos Grandes Caldera, with a loss in the anomaly's definition in the central part, close to Torito hill. In the area where the Silala springs bear a certain influence, the lineament reaches higher magnetic anomalies.

7.5.2.4 Runtu Jarita Lineament

This lineament crosses the eastern edge of the area surveyed, with a NW-SE orientation (335°) adjusting to the general "trend" of the area. In turn, the lineament adjusts to the occurrence of the Runtu Jarita dome, which is lined-up further to the north with the Chascon dome; apparently the lineament cuts the southern part of Chascon dome. In the map of total magnetic intensity (Map No. 6) high anomalies are observed; these coincide pro-parte with the lineament until they reach the limits of the Chascon hill dome, where they are truncated—according to the aeromantic data—with a negative anomaly.

7.6 Work methodology

The objective of this part of the survey is to identify the geological structures related with the fractures of the area. Structural data on the joints, foliation and faulting planes was obtained in the field to perform an analysis of fragile deformation on basis of microstructural data. For this analysis, faulting planes that present striations and are abundant in the area were preferably surveyed. The limited data on striations was processed to deduce the force fields that caused them, or the tension of paleo-stress linked with faulting, as well as the kinematics of the structures produced during deformation. To determine the displacing direction of the faults, kinematic indicators, such as Riedel-type structures, striated surfaces and echelons, were used.

As a result of the preliminary analysis and interpretation of structural data, and on basis of the major kinematic features maps were prepared to visualize the relation between fracturing and the presence of water sources identified in the area surveyed.

7.6.1 Data processing

The data obtained in the field was processed using a database prepared in an Excel sheet, recording the most relevant structural characteristics of the faults and joints. The processed data was thereafter further processed with the Rocscience DIPS 5.0 software (free version), which is a useful program to analyze the orientation of spatial data through rose diagrams and a stenographic network.

The input and storage data required by this program are: the dipping direction, dipping, plunge direction (azimuth) and plunge for the fault striation. The value for the dipping direction ranges from 0 to 359°, considering the correction of magnetic inclination, which is currently of 6° to the W. The dipping angle and plunge range between 0° and 89°, from the horizontal plane. Where it was possible, the relative direction of displacement (normal, inverse, dextral, sinistral) was also recorded for the faults. Additionally, data on the frequency, form, thickness, openness, continuity, infilling and presence of water was also recorded.

The ArcGis v.10.1 software was used to integrate the data on faults and fractures and correlate them with the lineaments interpreted on basis of satellite images.

To estimate the structural domains, or perform force analysis, the structural elements are discriminated taking into account similar geological events and are treated separately, projecting poles, planes and pitch directions.

7.6.2 Population analysis of fractures by sector

In order to simplify the correlation, analysis and interpretation of the fracturing systems that form the database for the structural geological survey, the area surveyed was divided into 11 sectors so that each sector groups the outcroppings that present a similar lithology and approximate origin age.

In some of these sectors, the lithological features, fracturing intensity and morphological characteristics of fractures that are similar were also correlated.

The sectors that cover the areas surveyed are presented in Table No. 2 and Figure No. 13

Geological Unit	Sector	Lithology	Age (Myr) - Source
Qlie	Inacaliri Hill	Porphiric and aphanitic dark gray lava, with fluidal banding, andesite and dacite	1.48 (PIR)
Qlie	Silala Grande	Porphiric and aphanitic dark gray lava, vesicular to massive, andesite and dacite	1.9 (PIR)
Qlie	Cahuana hill	Porphiric and aphanitic dark gray lava, andesite and dacite	1.9 (PIR)
Npst	North Pastos Grandes Ignimbrite	Dacitic ignimbrite, gray, whitish to reddish	2.9 (Salisbury et al.)
Npst	South Pastos Grandes Ignimbrite	Grey to violet dacite ignimbrite	3.4 (Sheet 5927-6027 Silala-Sanabria)
Ntol	Torito hills	Porphiric gray to violet porphiric lava, andesite	5.8 (Sheet 5928-6028 Laguna Khara)
Ninl	Inacaliri Lavas	Porphiric dark gray lava, dacite	5.94 (PIR)
Ncnd	Negro hills	Porphiric gray lava, dacite	6.04 (PIR)
Nsll	Silala Chico	Porphiric dark gray lava, dacite	6.04 (PIR)
Nslt	Silala ignimbrite	Pinkish to violet dacite ignimbrite	7.8 (PIR)
Nmse	El Meson hill	Dark gray lava, andesite, dacite and trachyandesite	7.8 (Sheet 5927-6027 Silala-Sanabria)

Table No. 2. Sectors of each of the structural data processing, presenting the ages and codes used for the structural processing

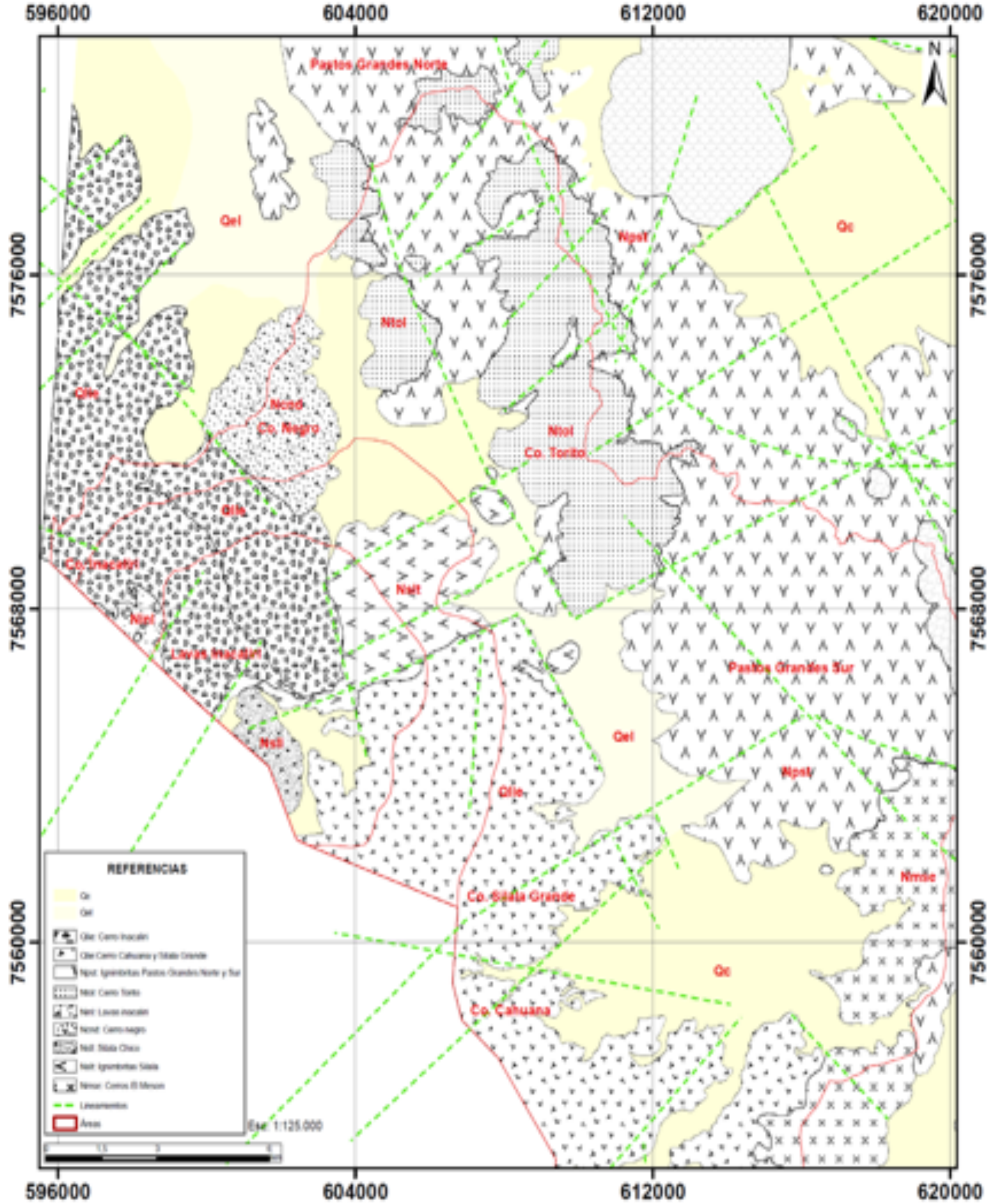

Figure No. 13. Scheme for the sectors used to process structural data

7.7 Fracture and discontinuity analysis

The relation between the fracture type and the lithological unit type defines a fissure system that also determines the secondary permeability of the sector. The morphology of the fractures presents additions factors that affect porosity and, thus, the permeability of the lithological unit. In the structural sector-based mapping, the fracture or discontinuity type were identified collecting structural data and the morphological parameters of the fractures (Table 3).

Table No. 3. Fracture parameters recorded

Discontinuity type identified	Characteristic of the fracture
Faults (normal, inverse, lateral) Joints Cooling parameters, pseudo-stratification Foliation Lithological contact	1. Continuity 2. Persistence (frequency) 3. Opening and infilling type 4. Form 5. Thickness 6. Humidity content 7. Hardness

7.7.1 Nmse Sector – El Meson hill

This sector is located to the southern end of the third area. It comprises three hills that extend from south to north, the Meson, Apacheta and Cerro Chico. These are composed of dacitic, andesitic and trachyandesitic lava, of a dark gray to brown color, a thick texture and tuffaceous enclaves of up to 5 cm.

The outcropping massifs present few fault planes that get confused between joint and pseudo-stratification planes and fractures caused by weathering. These massifs are intertwined and intersected and take the appearance of disturbed blocks (Picture No. 21.).

Picture No. 21. Fractured massif outcrop of dacite lava, Meson hill

7.7.1.1 Structures identified in Meson hill

To perform the structural analysis of this sector, 105 data grouped into three subgroups was reproduced in fault and joint rose diagrams. To prevent a limited number of fault populations, 15 inverse faults, 1 thrust fault and 1unidentified movement fault were grouped into a second subgroup; 38 normal faults and 50 joints were identified in the area.

7.7.1.1.1 Nmse Faults – El Meson hill

Most of the faults of this geological unit present a planar to undulated form, with a continuity that exceeds the 10 m, with openings of 1 to 5 cm and a rugose surface. The density for every 10 m is of 1.

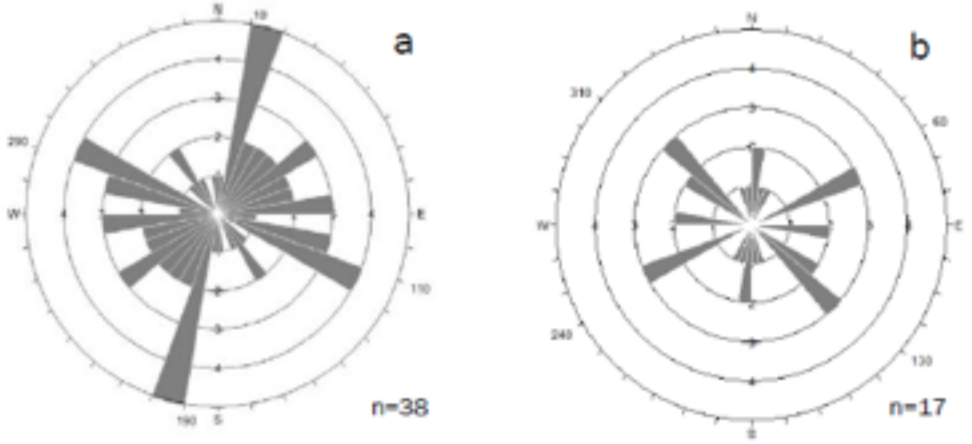

Figure No. 14. a) Rose diagram for normal fault fracturing. Meson hill. b) rose diagram for the fracturing of inverse faults

Figure No. 14 (a) presents the normal faults of the sector, which have a NNE-SSW preferred direction. This trend is close to the N-S domain, which is observed in the units located north of the area. The sector's inverse faults are represented in Figure (b). Given that this subgroup includes a thrust fault and an unidentified movement fault, it can be concluded that the number of normal structures is higher in a relation of 2 to 1 with respect to inverse faults.

7.7.1.1.2 Meson hill joints

The features of the joint planes in the outcroppings of this sector are mostly of a high-angle, discontinuous and planar to escalated. Rugosity is high owing to their crystalline texture. The joints present openings, are unfilled and do not contain humidity. Their frequency reached 1 to 2 fractures for every meter.

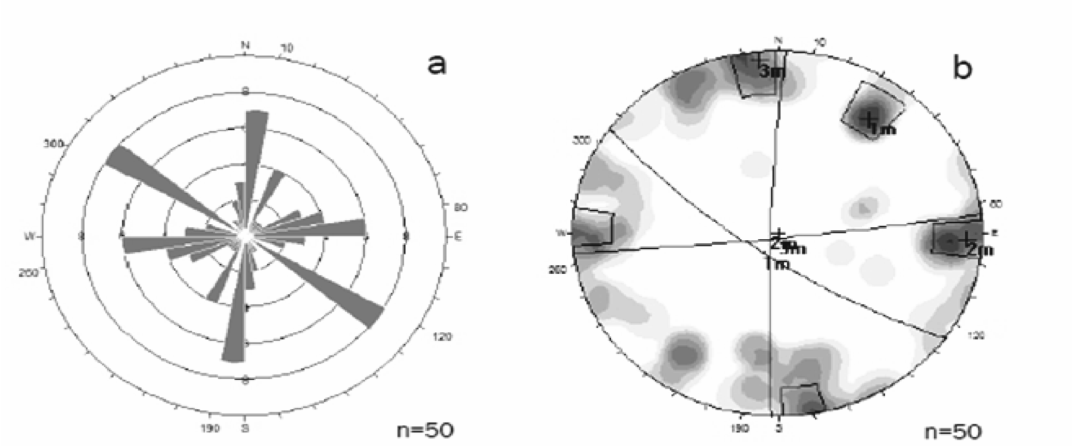

Figure No. 15. a) Rose diagram for the joints of Meson hill. b) pole diagram and preferred plane for the fractures of Meson hill

The above Figure presents three preferred directions, i.e. NW-SE (120°-300°), N-S and E-W, that coincide with the macrostructures of the region, suggesting that there is a kinematic relation at the microstructural scale similar to that of the macrostructural scale.

7.7.2 Silala ignimbrite sector (Nslt)

This sector is located in the ravine that is formed between the base of Inacaliri and Silala Chico hills. It extends towards the NE, in an elongated and narrow fashion, through the ravine upstream as far as the wetlands, from where it further broadens forming a regular surface with a positive slope towards the east. The rock outcroppings that are present in this sector correspond to pyroclastic deposits formed in a sub-horizontal form. Most of these outcrops present sub-vertical fractures that shape columnar forms with heights that reach the 5 m (Picture No. 20) and conjugate with minor discontinuous fracture sets that have greater inclinations.

To the east, these outcrops are highly weathered and present a foliation in the form of highly fractured splints. The outcroppings where data was recorded are dispersed mainly in the northern end of the sector. The ignimbrite presents a massive structure, mild hardness and fracturing. Joints and faults in varied directions can be observed in the thickness (Picture No. 22).

The fracturing density is determined by the amount of cooling joints, rearrangement fractures and limited minor faults, which extend continuously and intertwined. Generally, the fractures are closed and occasionally opened, displaying a water flow. They are rugged, their continuity is variable and their fracturing frequency ranges from 2 to 4 for every 10 m, on the side of the station cell, which is why this rock massif is characterized as moderately fractured.

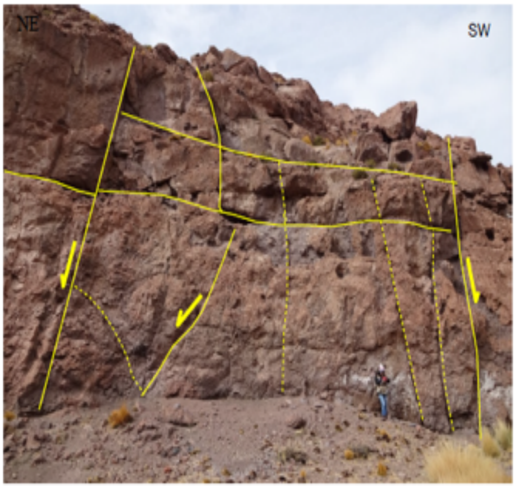

Picture No. 22. Silala ignimbrite mantles, presenting fractures that cut the outcropping levels. South side of the Silala ravine

7.7.2.1 Structures identified in the Silala ignimbrite sector

7.7.2.1.1 Faults of the Silala Ignimbrite sector

The faults identified in the Silala Ignimbrite sector, recorded in station points, reached a total amount of 185, comprising 85 normal faults, 26 inverse faults, 11 lateral faults and 63 faults that don't present kinematic displacement. The relative movement of these faults present displacements of a few centimeters that are mostly caused by gravity-triggered landslides. It is not possible to identify the direction of these striations in the fault planes to differentiate the events that occurred in the sector.

A structural analysis was carried out with additional data to process and produce a rose diagram for the fractures, ensuring that the data represents the structural domains of the unit to correlate them at a macrostructural level with faults and lineaments defined on basis of the satellite image analysis.

Figure No. 16 a) presents the rose diagram for the fracturing of normal faults (n = 85) that compose the first subgroup of fractures measured in the Silala ignimbrite sector, which have NW-SE (125°-305°), N-S (175°-355°), NE-SW (35°-215°) orientations. Figure No. 16 b) presents a stenographic projection of inverse faults (n = 26) that conform the second subgroup of fractures measured in this sector, which have NE-SW (55°-235°) and NW (325°-145°) orientations. The number recorded for this trend is to the number of normal faults, which leads to the tentative conclusion that distension forces are predominant in the area.

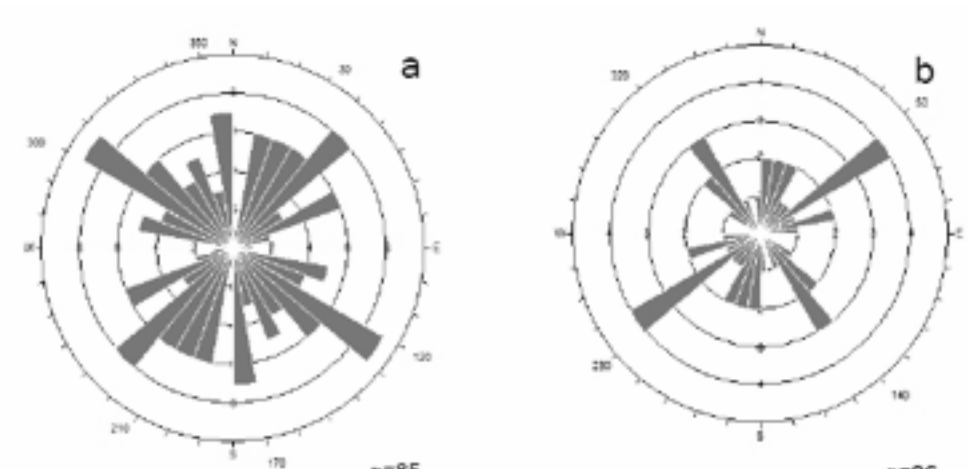

Figure No. 16. a) Rose diagram for normal fault fracturing, Silala ignimbrite; b) rose diagram representing inverse fault fractures, Silala ignimbrite

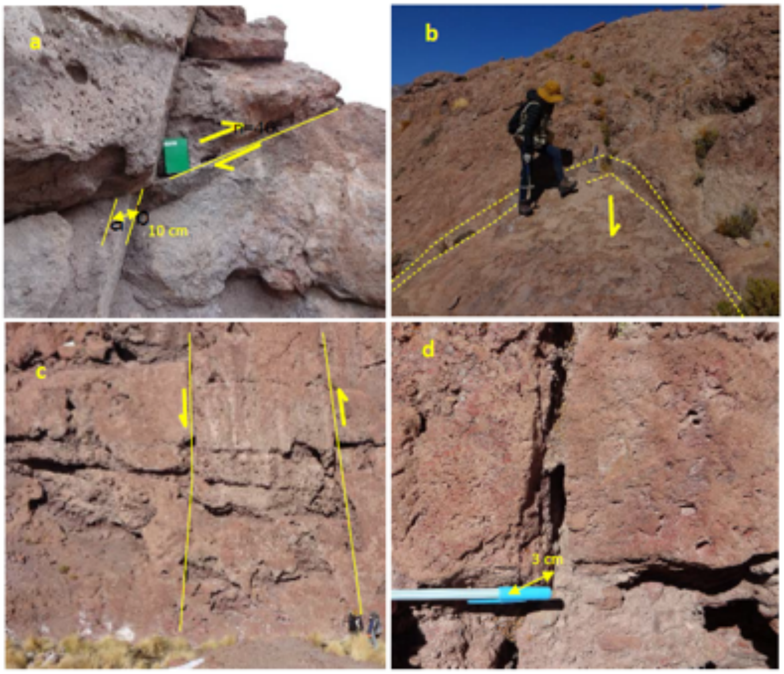

Picture No. 23. a) Lower angle inverse fault; b) Block sunken between normal faults; 15 cm displacement; c) Block found between a normal fault and an inverse fault; d) Fractured block with a regular centimetric displacement

The frequency of the normal faults of the first trend (NW-SE, 125°-305°) presents an immediate directional relation with the Inacaliri graben traces (NW-SE, 300°), which is found to the north of the area. Another trend (N-S) represented in the normal fault rose diagram is less frequent and presents a relation with the N-S lineaments that are parallel to Linzor stratovolcanoes and to others that have a shorter length to the south and center of the area.

7.7.2.1.2 Silala ignimbrite joints

These joints present the characteristics of planar forms, are continuous and surpass the 5 m, displaying a frequency of 10 to 15 joints every 10 m. They prevail in the whole ravine (Picture No. 23). The openings range from millimetric to centimetric (occasionally reaching the 20 cm).

Most of these joints do not present any type of infilling. The joints that present clay infilling millimetric separations are of a reduced percentage. Wall thickness is two-type, i.e. walls formed by cooling are smooth and those that are formed by stress present moderate rugosity. Water and humidity are only present to the north of the ravine, from the latter's forking onwards.

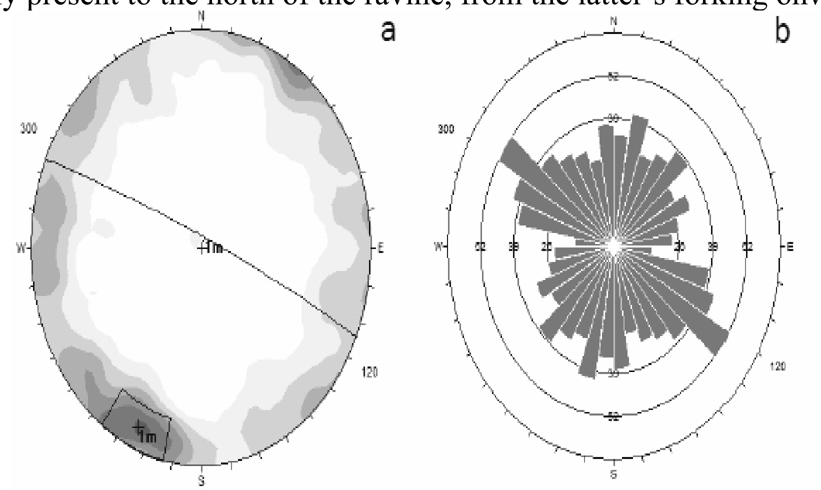

Figure No. 17. a) Rose diagram for contours; b) rose diagram for jointing planes in the Silala ignimbrite sector (n = 637)

Figure No. 17 a) represents the contour diagram produced on basis of the jointing population. A joint family of a lesser frequency, a NW-SE (125°-305°) and prevailing sub-vertical dipping have also been identified. Based on 637 planes measured in fixed points, the rose diagram for the joints of the Silala ignimbrite sector also contain joints formed by cooling and weathering, which causes the direction frequency to be chaotic.

Most of the joints formed by cooling present a predominant direction that is similar to that of normal faults (NW-SE, 305°), which was directly related with the Inacaliri Graben's structure (Tibaldi et.al. op. cit) and the regional lineaments that present similar direction.

7.7.3 Silala Chico hill sector (NsII)

This mapped sector is located on the top of Silala Chico hill and extends longitudinally towards that hill, with fixed data collection points distributed as a function of the outcroppings found. Silala Chico hill is composed of dacitic, porphiric and pseudo-stratified lava, formed in dark-gray to light brown blocks.

7.7.3.1 Structures identified in Silala Chico hill

The structures mostly observed correspond to jointing caused by cooling. These are transversal to the flow direction.

7.7.3.1.1 Silala Chico hill faults and joints

The faults found and identified for their classification are reduced in number and, thus, comprise a small percentage of the massif's total fractures; these bear little incidence on the global direction of the fracturing observed in the pole projection and contour diagram (Figure No. 18 a) and b)) constituted by: normal faults (2), inverse faults (2), lateral faults (1) and joints (79). The distribution of fixed points and amount of data collected within the area are precarious. For the analysis of structural domain, faults and joints are assumed as representing a single group of the unit's global fractures.

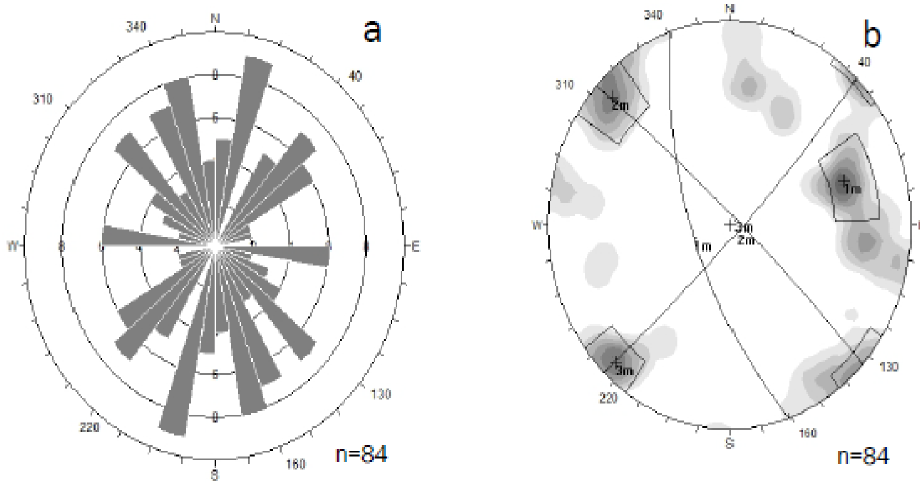

Figure No. 18. a) Rose diagram of the fractures of Silala Chico; b) pole diagram for the Silala Chico fractures

Figure No. 18 a) and b) presents the dispersion of the fault's plane poles projected in a rose diagram for the fractures, representing the varied frequency and trends without defining a clear domain. The diagram of percentage contours presents the domain planes for the fractures of the Silala Chico.

The three direction trends are:

- NE-SW (45°-225°)
- NWN-SES (160°-240°)
- NW-SE (130°-310°)

The joints generally present planar shapes. Most of them have a continuity that surpasses the 5 meters, and persist between 2 to 6 fractures every 10 meters. The opening of these fractures ranges from millimetric to centimetric (20 cm).

Most of the joints do not present infilling. The rugosity observed in the fractures' plane differs relatively between JRC from 8 to 10 (Hoek, 2007), corresponding to a moderate rugosity. Water or humidity are not present in the fractures measured. All these fractures correspond to andesite lava rock, with hardness of R4-R5 (hard to very hard rock).

7.7.4 Negro Hill sector (Ncnd)

This sector corresponds to the areas that surround Negro hill, north of the third area. It comprises lava domes to the NE of its base. Its composition is dacitic, porphiric, pseudo-stratified formed on dark gray light brown blocks.

7.7.4.1 Structures identified in Negro Hill

The majority of the structures correspond to joints formed by thermal contraction during the cooling phase and generally present a bedding that is transversal to block foliation. The tectonic joints are hard to differentiate from the fractures produced by weathering and can be recognized by the continuity in the massif.

7.7.4.1.1 Faults and Joints of Negro Hill

The faults found and identified for their classification are reduced in number and thus represent a small percentage of total fractures of the massif. They have a reduced incidence on the global fracturing direction that can be observed in the pole projection and contour diagram (Figure No. 19a and 19b). These are constituted by normal faults (9), inverse faults (0), lateral faults (1), joints (191) and unclassified faults (10).

The distribution of fixed points and amount of data collected from the area are precarious; as a result, faults and joints were assumed as a single group for the global fractures to complete the analysis of structural domains.

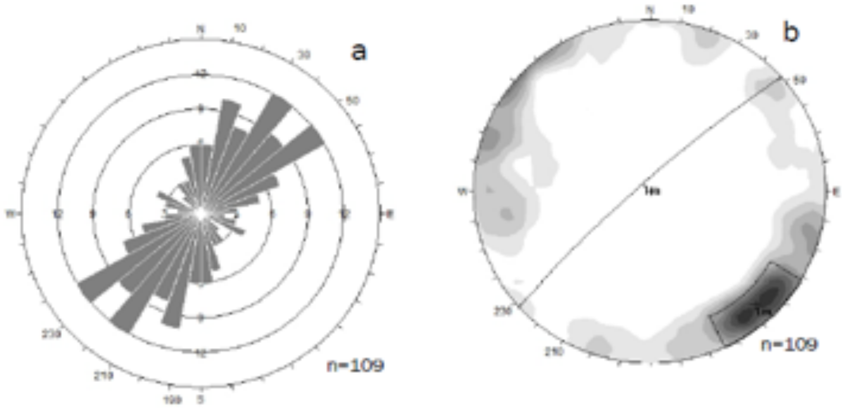

Figure No. 19. a) Rose diagram for the fractures of Negro hill; b) Pole diagram of the fractures of negro hill

The above figure represents the pole dispersion of the fault planes projected in the rose diagram of fractures, placing in evidence a high frequency of fractures that have a NE-SW trend. The diagram of percentage contours presents, in a particular way, the general direction preference in the fracture planes of Negro Hill, the domain of which is NE-SW (50°-230°).

The joints generally present planar to stepped forms. Most of them have a continuity that surpasses the 5 meters and persists between 1 and 2 fractures every 10 meters. The opening of these fractures ranges from millimetric to centimetric, reaching the 40 cm.

Most of these joints do not present infilling. The rugosity that can be observed in the fracture planes differs relatively between JRC from 4 to 8 (Hoek, 2007), which corresponds to moderate rugosity. There is no water or humidity in the fractures measured. All these fractures correspond to the dacitic lava rock-type, with a hardness that ranges between R4 to R5 (hard rock to very hard rock).

7.7.5 Inacaliri Lavas sector (Ninl)

The Inacaliri Lavas display small outcrops as lithological windows that date back to 5.84 Myr on the southern flank of the Inacaliri hill; these are composed of crystalline coarse-grain dacitic lavas, which form foliate blocks that have the appearance of small boards and present a brownish-grayish coloration.

7.7.5.1 Structures identified in the Inacaliri lavas

This sector is characteristic of pseudo-stratification planes that can be observed throughout the outcropping massif. The faults and joints are presented transversally, with a high angle and present a continuity that surpasses the 20 m. The morphometric features of the fault planes are similar in all structures.

Picture No. 24. Inacaliri lava outcrops, presenting sectioned by normal transversal faults. Southern flank of the Inacaliri hill

7.7.5.1.1 Faults and joints of the Inacaliri lavas

Owing to the reduced amount of structures in this sector, it was deemed convenient to make the global analysis of the structures (faults) without a prior classification, preparing a rose diagram for the fractures to determine the major trends of the sector. Another subgroup is composed by joint planes, which configure a field of approximate stresses.

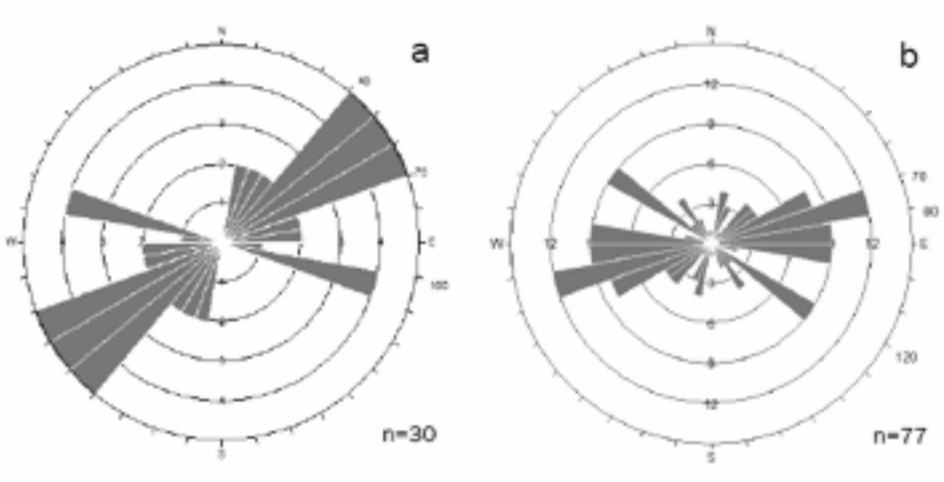

Figure No. 20. a) Rose diagram for the fractures of Inacaliri lavas; b) rose diagram of the joints of Inacaliri lava

The faults found in this sector are continuous, and have a planar to bended form, with openings of a few centimeters. Their rugosity is high and are present every 1 to 2 meters. They present no infilling and do not contain water.

Figure No. 20 a) presents the rose diagram for total fracturing, with a representation of undifferentiated faults. These fractures present a NE-SW trend (40°-70°), which has a connection with the NEE-SWW lineaments—determined in the macrostructural lineament and fault map. A second preferred direction is NWW-SEE and presents a fewer amount of relevant faults.

The joint sets (Figure No. 20 b) of this sector define a similar trend, approximating to an E-W (125°-305°) preferred direction. A second joint set with a NW-SE (125°-305°) can also be identified, reaffirming the directional control in the fault set.

7.7.6 Torito Lava Volcano (Ntol)

The Torito lava sector comprises the Meson Bayo Lomas, Torito, Colorado, Pabelloncito, Pajonal, Chanca Loma and Bayo hills, which are dispersed and lined up with the western edge of Pastos Grandes Caldera; to the north, it is found between Chascon and Negro hill. The south end, begins 1.4 km to the east of the entry to the Silala springs.

The volcanic body exposed is apparently related with the lava domes, which have a dacitic composition, with plagioclase crystals, feldspars, quartz and biotite in a dark greenish gray matrix. It forms in pseudo-stratified lavas of a massive appearance piled up by blocks.

The lava outcrops of the Torito hills present structures formed by the cooling of volcanic material, joints and some faults, which are an indication of a fragile regime. The holocrystalline-crystalline textures form continuous fractures of an undulated-to-stepped shape that present centrimetrical openings with rugose surfaces. These are occasionally infilled by coarse sands, but are generally not infilled and do not present humidity. The 10 m lineal frequency reaches 2 fractures. The pseudo-stratification planes present closed, continuous and apparently shallow junctions, the frequency of which reaches the 8 junctions per lineal meter.

Another structural element of relevance for the frequency are pseudo-stratification planes that are displaced in a localized fashion in the area. They present laminar structures that are intersected by joints (Picture No. 25). These laminations represent the lava flow direction. They present continuous and discontinuous planar forms and pronounced openings on the weathering surface, which close up a few millimeters towards the massif body and repeat 7 times per meter transversally to their planes and do not present humidity. This structural data is related with the massif’s fracturing level and secondary porosity. Thus, this data cannot be used for an analysis of the structures or stresses of the area.

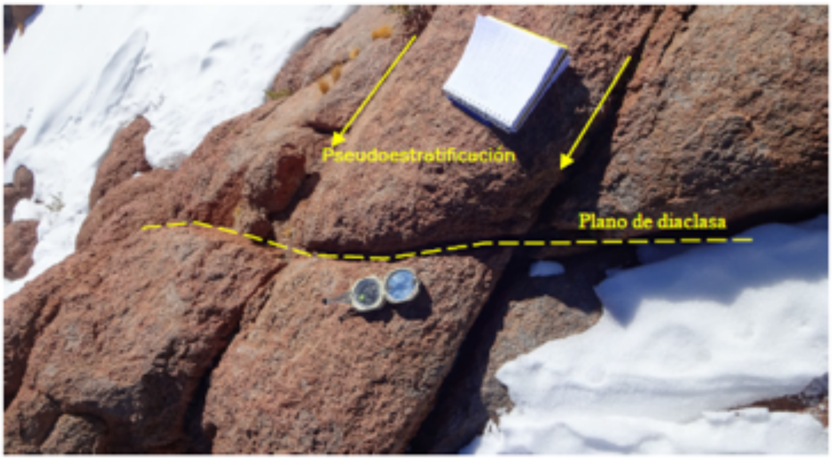

Picture No. 25. Joints that cut the pseudo-stratification planes of the Torito hill lavas

7.7.6.1 Structures identified in the Torito hill lavas

Two-hundred eighty-three structural data pieces on the lava were recorded in this area; these include 234 joints, 18 normal faults, 32 faults. Structural data of the pseudo-stratification planes was also recorded.

7.7.6.1.1 Faults of the Torito hill lava

The fractures are dry and present average 4-cm openings. This sector contains both open fractures that are not infilled and fractures infilled with coarse sand. Most structures present direction trends analyzed in the rose diagrams. The reduced number of the faults found in the outcrops of the area require that the structures be analyzed taking into account three fracture subgroups composed by:

1. Normal faults
2. Inverse faults, right-lateral faults, left-lateral faults and faults in which movement types were not identified
3. Joints

Due to the scarce amount of fault data collected for the area, the normal fault planes, inverse faults and unclassified faults are regarded sufficient for the analysis of domains, or forces, which is why the projection of poles and planes is presented in concert so the directions and dips can be better appreciated. The preferred direction of these faults, among which those that are unclassified predominate, are presented in the rose diagram prepared for the fractures (Figure No. 21).

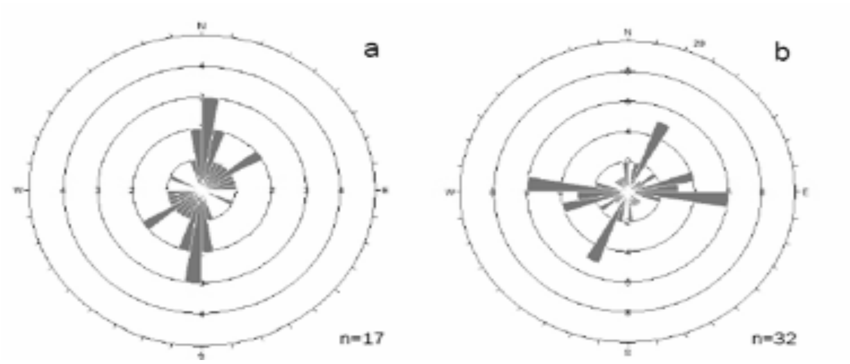

Figure No. 21. a) Rose diagram representing the fractures of normal faults of Torito hill; b) Rose diagram representing inverse faults, lateral faults and unclassified faults

7.7.6.1.2 Torito hill joints

The rock type of the sector differentiates the joints found in other sectors and present stepped and undulated, discontinuous and continuous, rugose to very rugose forms. Their openings are centimetric and are infilled by coarse sands. Their persistence is changeable. Many of these forms are caused by physical weathering, while a great number of the others correspond to joints formed by transversal cooling of lava blocks.

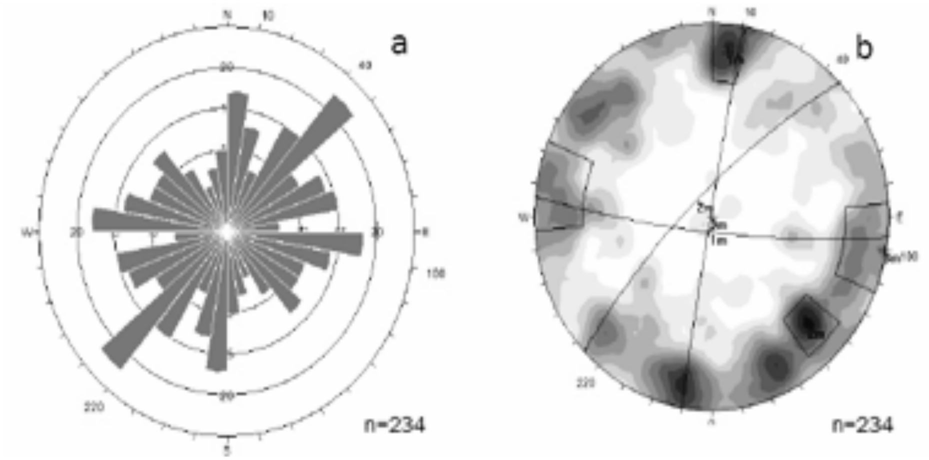

Figure No. 22. a) Rose diagram representing the Torito hill joints; b) rose diagram of poles, preferred planes and joints of Torito hill

The joints of Torito hill present a major NWW-SEE trend and a secondary NE-SW fracture trend. A great number of the joints correspond to fractures formed by the cooling of lava.

7.7.7 North and South Pastos Grandes Tuffs

This sector corresponds to an extensive area that covers the Altiplano and surrounds the edge of Pastos Grandes Caldera, from the southern limit of the 3rd area to the northern and western limit of the major area. The rock outcrops are dispersed towards the edges of this unit and the interior of the ravines. They generally present tuff columns that reach the 8m of height. These have a whitish-gray coloration (Picture No. 26 a), with brownish tones, and are formed on mantles that have sub-horizontal contact [bedding] planes. Their structure presents lithic fragments that correspond to dacite. Pumice of up to 12 cm in diameter can be observed gradually ascending towards the top.

Picture No. 26. a) Tuff outcrops in South Pastos Grandes; b) joint planes that form fractured structures and contain thrust planes

The orientation and inclination dataset obtained in these stations is reduced (n=31) owing to the repetition of planes in the cooling joints. However, normal and inverse faults, together with jointing caused by stress, have also been identified and are relevant for the interpretation carried out.

These inverse faults present a displacement of up to 10 cm and form a low angle with the horizontal, which evidences thrusting of tuff mantles at a low scale and demarcates local kinetics related with the regional structure (Picture No. 26 b).

7.7.7.1 Structures identified in the Pastos Grandes Tuff

For the analysis of fault and joint data collected at great scale, two sectors were divided, i.e. South and North, and normal and inverse faults, along with joints, are represented in rose diagrams. The data that is reduced in number is not significantly representative for the population of fractures in area, nevertheless, it is sufficient to observe the preferred directions in relation to major scale lineaments.

7.7.7.1.1 North and South Pastos Grandes Tuff

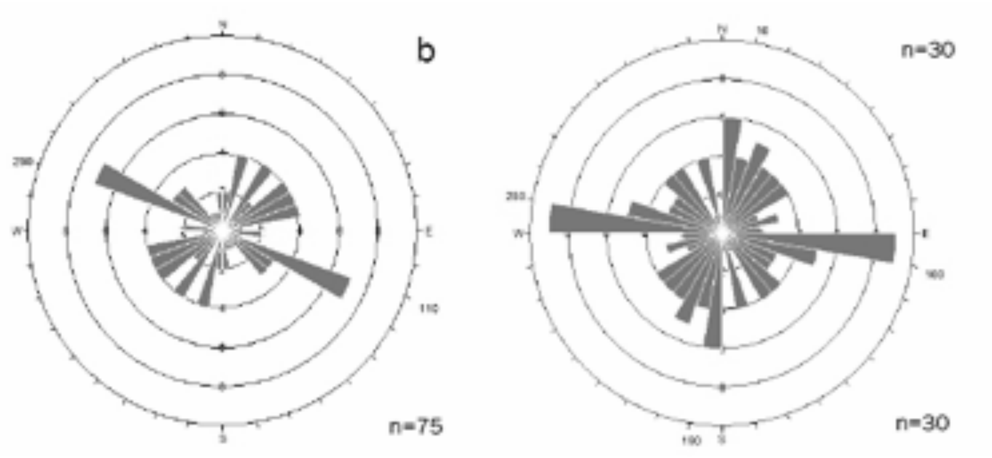

Figure No. 23. a) Rose diagram representing the normal faults of North Pastos Grandes; b) rose diagram representing the inverse faults of North Pastos Grandes

The trends of this sector are different. The normal faults present a WWN-EES preferred direction (100°-280°). The inverse faults present variable directions. A general trend for the sector has not been defined, which is why the preferred direction considered will be that obtained as a result of the normal fault plotting.

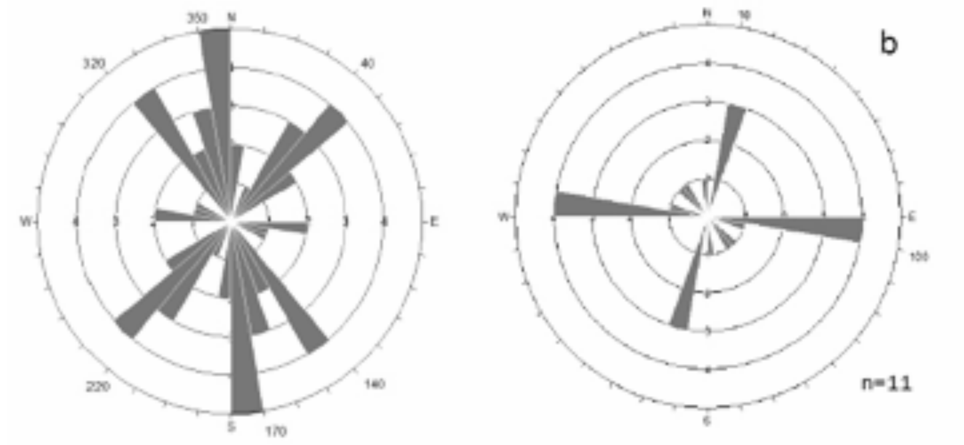

Figure No. 24. a) Rose diagram representing the normal faults of South Pastos Grandes; b) rose diagram representing the inverse faults of South Pastos Grandes

The above figure presents clear trends. The normal faults have a preferred N-S direction and the inverse faults, which are reduced in number, have a W-E preferred direction.

7.7.7.1.2 Joints of the North and South Pastos Grandes Tuff

Fracturing caused by joints in these tuffs is predominant. The joints are flat, almost smooth, continuous, contain no water and have openings that are smaller than 1 cm. They do not present any infilling, and some of the joints are even closed.

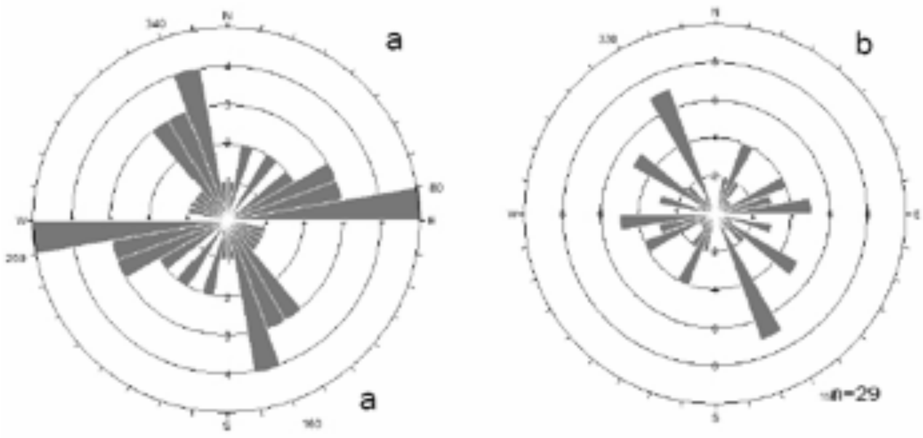

Figure No. 25. a) Rose diagram for the North Pastos Grandes joints; b) rose diagram for the jointing of South Pastos Grandes

The major trend in the south sector follows a W-E direction, while the secondary one presents a N-S to NE-SW direction. These domains are similar in the north sector, the only difference being that they have an hourly rotation of up to the 20°. The general fracture direction is, nevertheless, E-W.

7.7.8 Cahuana hill sector (Qlie)

The structural data collected in Cahuana hill also correspond to the body of the stratovolcano that conforms the hill, which is located in the prolongation of the volcanic chain to the south of Silala hill, as part of the Linzor stratovolcanoes, with a composition that is similar to that of the Silala Grande hill. It presents dacitic, andesitic and trachyandesite lavas, with massive and banded textures. They present a NE lava flow direction.

7.7.8.1 Structures identified in Cahuana hill

The structural dataset measured in Cahuana hill reaches a total of 76 particulars, i.e. 14 normal faults, 10 inverse faults, 10 unclassified faults, 1 lateral fault and 41 joints.

The reduced amount of structures requires that the structures be treated in two subgroups, the first one of which is formed by normal, inverse, strike-slip and unclassified fault planes, inasmuch as these are produced by tectonic stress. The second subgroup corresponds to joints that generally include cooling surfaces and occasionally weathering surfaces.

7.7.8.1.1 Cahuana hill faults

The faults that were generally identified present displacement of a few centimeters, without exceeding the 10 cm on flat surfaces of nearly vertical to moderate angles. Most of these faults are represented in undulated and stepped forms, with a limited continuity and centimetric openings. They do not present any infilling. The dacite and andesite present hardness that ranges from high to very high. The rugosity of the fault planes is high. Just like in other places, the fault planes do not show traces of striation directions that might help differentiate the events that took place in this sector.

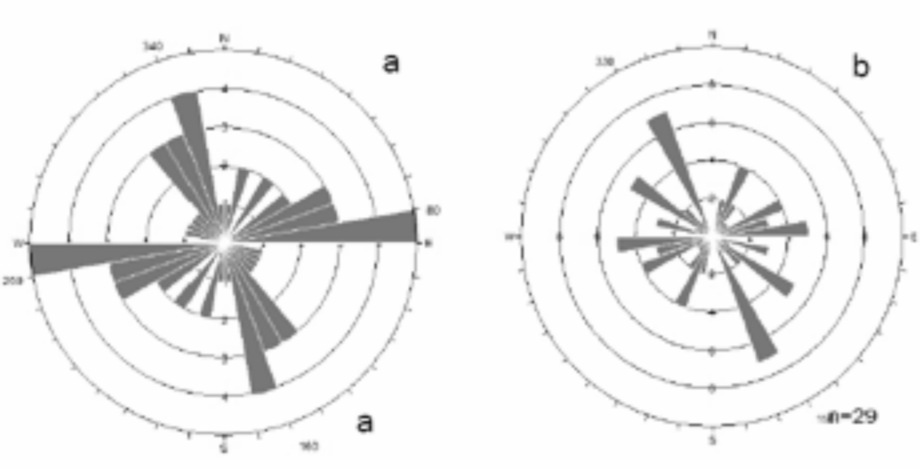

Figure No. 26. a) Rose diagram for the fracturing of Cahuana hill; b) rose diagram for the jointing of Cahuana hill

The major macrostructural trend found in this sector reaffirms the E-W direction structural domain that can be observed in other sectors. The secondary trend approximates the N-S direction, and is lined up with the occurrence of volcanic bodies.

7.7.8.1.2 Cahuana hill joints

The composition of the rock outcrops of Cahuana hill has led to the conclusion that the joints present characteristics that are similar to those of the Silala Grande hill lava, with undulated, stepped, continuous and rugose planes, mainly arranged transversally to the flow fronts, with centimetric openings that do not present infilling or humidity. These planes can be observed with a certain frequency in weathered outcrops.

The preferred jointing direction is NW-SE (155°-335°) and coincides with the second fracture trend measured in this hill. Likewise, the dip faults range from high to moderate. Fractures formed by cooling can be distinguished in a sub-vertical position transversally to the pseudo-stratified blocks.

7.7.9 Silala Grande sector (Qlie)

The structural data collected in Silala Grande hill correspond to the inactive stratovolcano found on a base of 41 km2 and composed of massive and banded dacitic and andesitic lava, brecciated on the base. These flowed to the NW-N-NE and reached a distance of up to 5.5 km.

These lavas present sub-horizontal banding, of a light gray to dark gray coloration, indicating the flow direction. These form rock outcrops composed of massive flows that conform a structure in blocks and are dispersed, occasionally presenting flow folding (Picture No. 27 b) in elongated and convex forms, corresponding to the flow front. In most of the surface, these flows are covered with colluvial deposits.
These fronts formed in blocks are mildly weathered and form fractured scarplets that reach 3 m in height. They frequently present a vertical form transversally to the block, owing to cooling effects. It is also possible to observe pseudo-stratification planes that form open discontinuities. The density of the joints is higher in relation to pseudo-stratification planes and the faults identified.

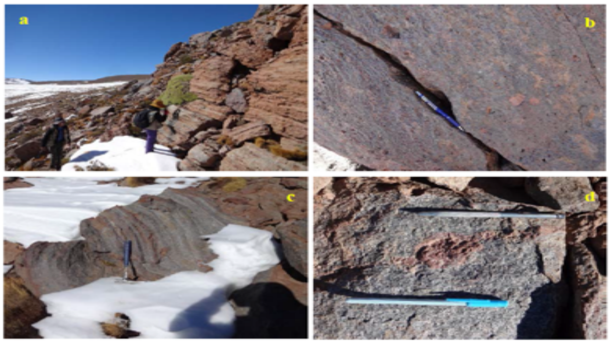

Picture No. 27. a) Flow front of outcropping lava in blocks; b) morphology of the factures in dacitic lava; c) banding folds caused by lava flow; d) porphiric tails, a kinematic indicator of dextral shear stress

Elongated tails are observable in the brownish-reddish porphyroclast. This indicator of block movement evidences that the simple sheer stress of a right-lateral direction and high deformation had an effect on the rock massif, causing rotation and dragging the porphyroclast's re-crystalized tails.

7.7.9.1 Structures identified in Silala Grande hill

7.7.9.1.1 Faults of the Silala Grande hill

Fifty-nine faults were observed in this sector, comprising 30 normal faults, 6 inverse faults, and 23 displacement faults that do not present kinematics. The normal faults identified present displacements of a few centimeters only—not exceeding the 10 cm—and have flat and discontinuous forms, with centimetric openings. They do not present infilling. The dacite and andesite have a rock hardness that ranges from high to very high. The fault planes do not show evidence of an striation direction that might help differentiate the events that took place in this sector.

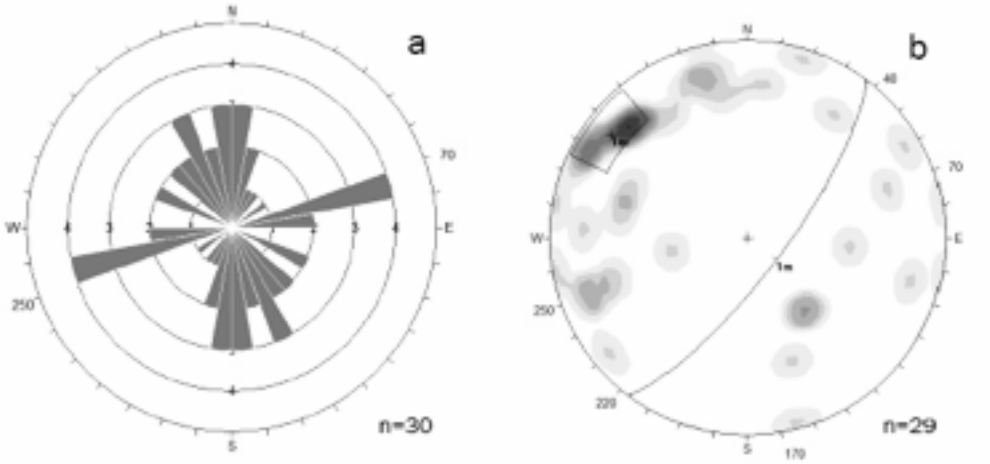

Figure No. 27. a) Rose diagram of normal fracturing faults; b) rose diagram of reverse fault fracturing, Silala Grande

The above representation of normal faults presents two preferred directions, i.e. NEE-SWW (70°-250°) and N-S. The first trend presents a slight hourly rotation (20°) with respect to the trends determined in the Silala ignimbrite sector, given that fault frequency is smaller in number. The second trend concurs with the direction determined in the Silala ignimbrite sector and the macrostructural lineaments.

The above figure presents the pole density diagram and establishes the preferential plane of faults with a predominant direction of NE-SW (40°-220°). The poles and planes plotted belong to inverse faults (6) and faults that do not present any identified movement type (26), which are grouped together owing to the absence of frequency of reverse faults.

Other discontinuities present in this unit are pseudo-stratification planes formed by the foliation of lava (Picture No. 28).

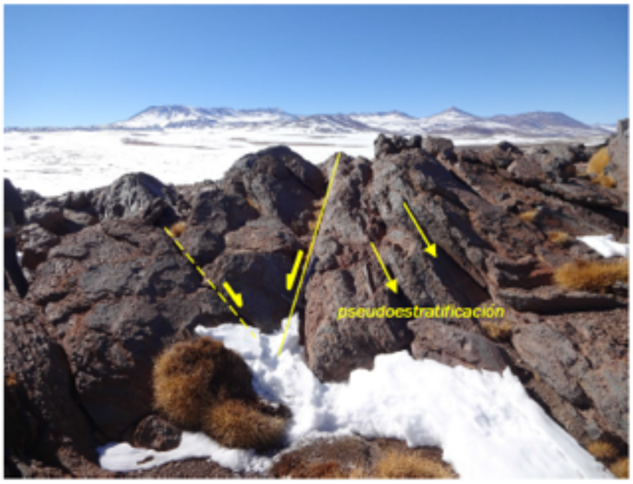

Picture No. 28. Normal fault cutting the pseudo-stratification planes of the lavas. Northern flank of Silala Grande hill

7.7.9.1.2 Joints of the Silala Grande Lavas

These joints present mostly discontinuous planar surfaces. They persist between 3 to 5 fractures every 10 meters. The openings that can be observed range from millimetric to centimetric (25 cm).

The majority of these joints don't present any type of infilling. The rugosity observed in the fracture plane differs relatively between JRC from 8 to 12 (Hoek, 2007), corresponding to moderate rugosity. It was not possible to observe water in the fractures, nevertheless, there were fractures where humidity and certain contents of water were observed, possibly owing to the presence of snow and to the fact that thawing creates an apparent humidity in the fractures.

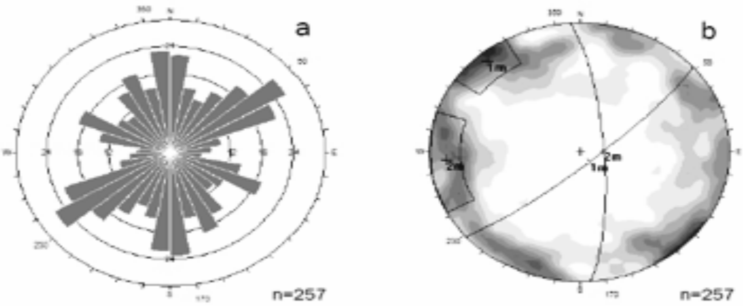

Figure No. 28. a) Rose diagram of jointing in the Silala Grande hill; b) Pole frequency diagram presenting the joints of the Silala Grande hill

Based on the 257 planes measured in each fixed station, it has been established that the joints have a N-S and NE-SW (55°-235°) predominant direction, with a general mean dip of 70°. The poles that are less frequent and present disarranged dips correspond to joints that are transversal to the lava flow direction, which are arranged in the form of blocks and have a variable direction that is a function of the slope of the stratovolcano.

7.7.10 Inacaliri hill sector (Qlie)

So as to differentiate the data collection in accordance with the lithological differences that pertain to this stratovolcano, this sector was divided into two subsectors:

• Eastern Inacaliri hill (Qlie). This sector corresponds to the lenticular lava flow body and has a NW-SE flow direction, covering a great proportion of the Silala ignimbrite towards the bottom of the valley. Its composition corresponds to porphiric dacite of vitreous texture and andesite of a trachytic texture, with dark gray vesiculated coloration and a presence of plagioclase, forming flow front structures in blocks (Picture No. 29 a).

• Western Inacaliri hill (Qlie). This sector corresponds to the highest past of Inacaliri hill. It is composed of dacite and andesite of a vitreous aphanitic texture and dark gray coloration. These are arranged on lava flow mantles and superposed volcanic breccia and extend as far as the volcano's crater (Picture No. 29 b).

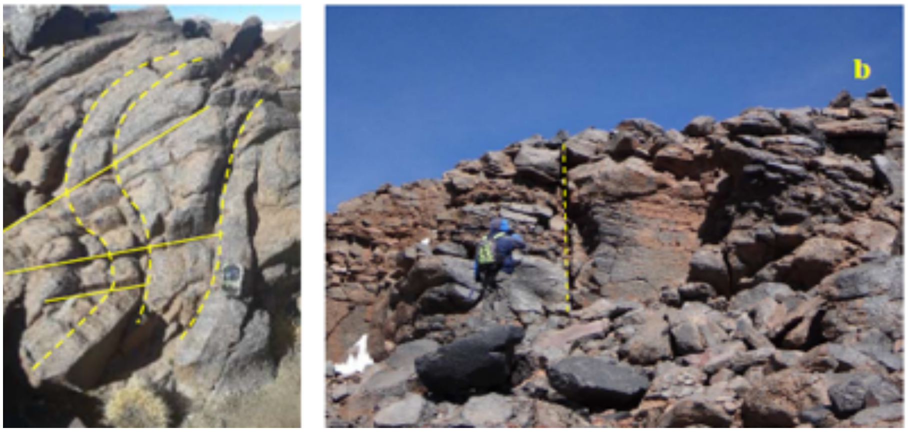

Picture No. 29. a) Sheared outcrops of Eastern Inacaliri hill (Qlie); b) Joint planes that form fractured columns in the Eastern Inacaliri hill (Qlie)

The structural dataset prepared as a result of the tectonic forces that were recorded in these stations is reduced in number. Owing to the nature of the lithological unit, the fault planes are confused with the thermic jointing planes, which are arranged in a chaotic manner—a common feature of flow front blocks.

7.7.10.1 Structures identified

• Eastern Inacaliri hill (Qlie)

The structures registered in the flow front correspond almost in their entirety to flow front blocks, where the fracturing density is the result of jointing transversal to the massif, displaying high angles. These merge with pseudo-stratification planes, forming a chaotic fracturing.

• Western Inacaliri hill (Qlie)

The few rock outcrops found in the higher part of the stratovolcano are hard to access inasmuch as they are surrounded by rocky ground [sallerios] that present a steep slope. These are also displayed as rocky peaks that can reach several meters of height. The data was collected from the face of the outcrops.

7.7.10.1.1 Inacaliri hill faults (Qlie)

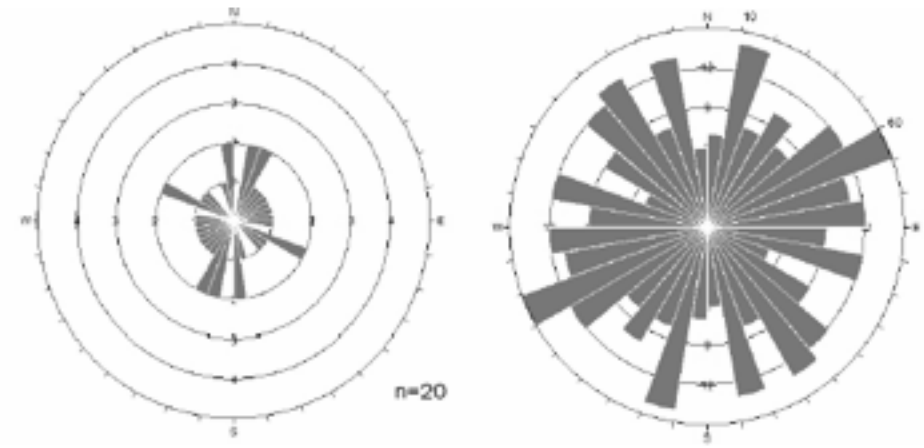

Figure No. 29. a) Rose diagram of the fractures of Eastern Inacaliri hill; b) rose diagram of the jointing of Eastern Inacaliri hill

The whole set of faults are too few to carry out a trend analysis. The joints, on the other hand, present a significant amount of fractures, though a preferential direction cannot be distinguished clearly given that their chaotic arrangement.

77

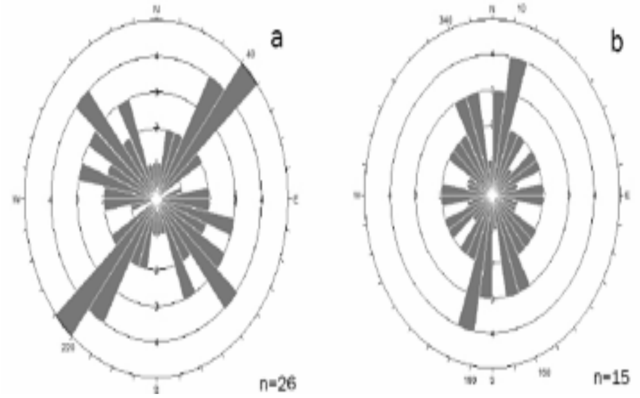

Figure No. 30. a) Rose diagram of normal fault fractures of western Inacaliri hill; b) rose diagram of inverse, unclassified and strike-slip faults of the Western Inacaliri hill

The preferential trends of this sector are different, inasmuch as the normal faults present a WWN-EES (100°-280°) preferred direction. The inverse faults in this sector display variable directions and do not define a general trend; thus, the preferred direction taken into account will be that obtained from the plotting of normal faults.

7.7.10.1.2 Western Inacaliri hill joints (Qlie)

Unlike the direction of the Eastern Inacaliri joints (Qlie), where a chaotic arrangement was observed, the joints measured in this sector display a significant proximity in its preferred direction (Figure No. 32).

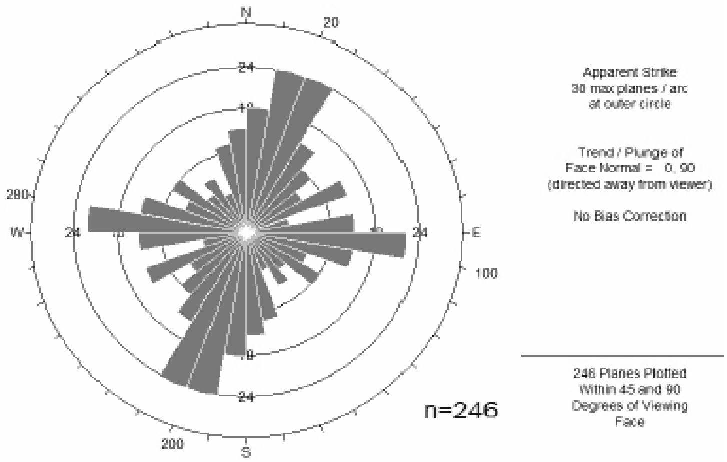

Figure No. 31. Rose diagram for the jointing of Western Inacaliri hill

The Western Inacaliri sector (Qlie C) displays a NNE-SSW (20°-200°) major trend direction. The secondary trend displays a W-E direction, which coincides with the trends defined in other sectors.

7.8 Microstructural analysis of the fault population

As a result of an assessment of the results obtained from the field and clerical works performed for the sectors covered in the project, a representative area was selected to perform a microstructural analysis that contains the data necessary for a process of stress calculation. That the sector had to contain data on the fractures of the same lithological unit and bear a close relation with the trace of specific microstructural faults was deemed important for the analysis. It was within these criteria that the area found in the southern flank of the south ravine of the Silala wetlands was selected, inasmuch as it is in this area that the ravine shifts its direction from SW to NW, following the ravine's slope (Figure No. 33). A microstructural survey at a scale of 1:250 was completed in the area chosen, using a 10 x 10 grid in orthogonal directions that coincide to the north and east of the sector. The starting point corresponds to the 601501 E and 7566222 N coordinates.

The area comprises 81 structural data, which contain:

- Six normal faults (2 striations)
- Three inverse faults (2 striations)
- Two unclassified faults
- Seventy joints

The methodology employed for this analysis was the Right Dihedral Method, which is broadly accepted and adjusts to kinematic models for fault population analyses. The area selected does not present a significant number of faults to pinpoint a pitch direction, however, owing to the pyroclastic deposits medium, this area is the one that contains the largest number of faults with kinetics that can be reconciled in relation with the surface analyzed, as compared to other sectors found within the 3 areas studied.

The paleostress tensor was derived from the abovementioned Right Dihedral Method, which bears a certain similarity with the calculation of the focal mechanisms of earthquakes; with a supplementary plane perpendicularly to the displacement striation, the region is divided into four right dihedrals around a fault. The major stress ($\sigma 1$) is contained in the compression dihedrals, while the minor one ($\sigma 3$) is contained in the extension dihedrals. The superposition of compression and extension dihedrals of all the faults of a specific population defines the most probable direction of $\sigma 1$ and $\sigma 3$, respectively. The application calculates, for each of the direction spaces, the percentage of faults included in the dihedral of extension; the maximum value corresponds to the optimal position of the extension axis and the minimal to that of the compression axis. According to "The Analysis Methods of Paleostress based on Fault Population: Systematics and Application Techniques" (Casa et. al., 1990), the rationale to use this method is that it enables a fast observation of the approximate orientation of the stress axes likely to explain the set of analyzed faults.

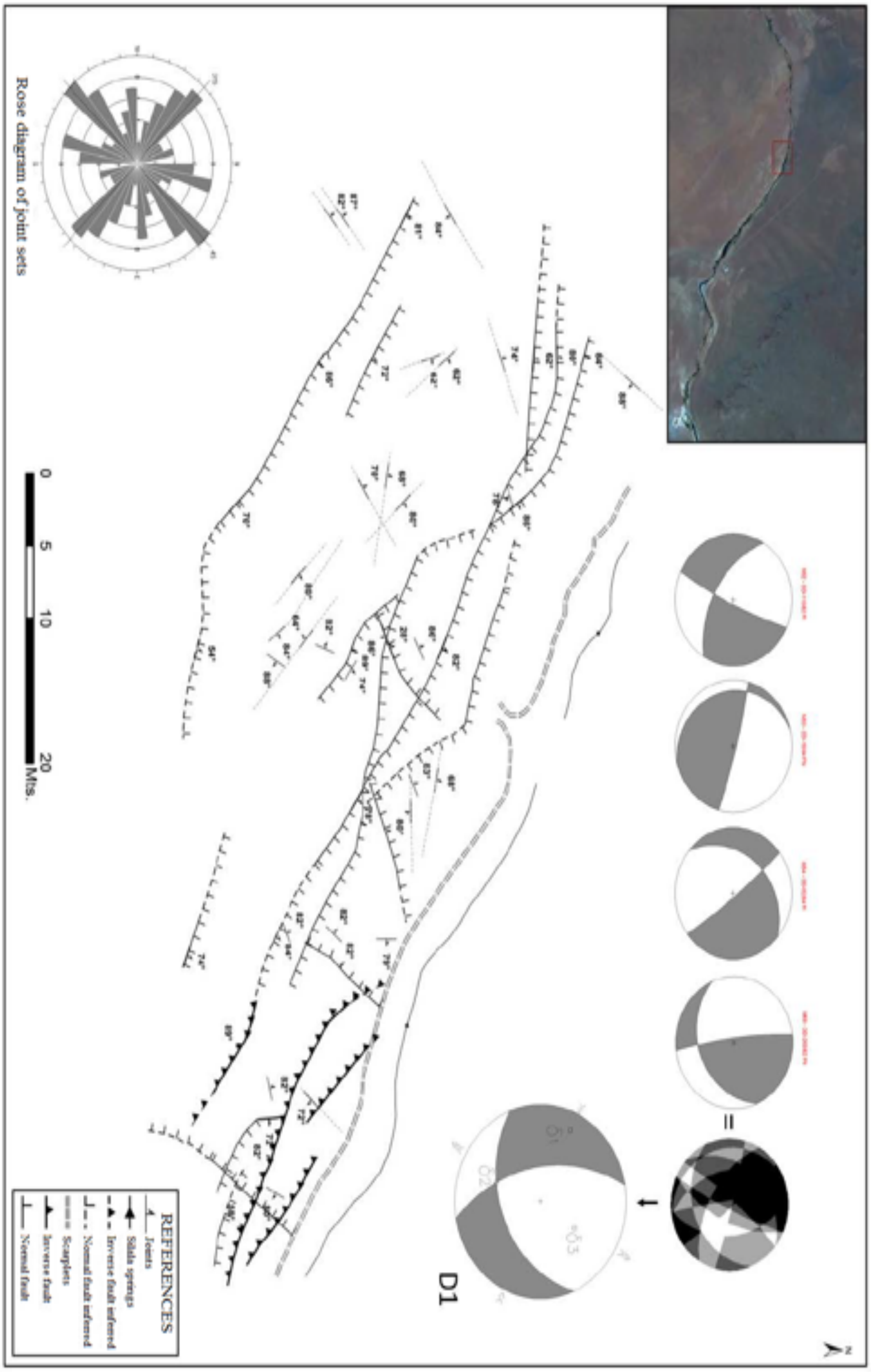

Figure No. 32. Microstructural analysis of stresses in the east flank and south sector of the Silala springs

The major problem connected with this method has to do with the impossibility of separating compatible faults from tensors of different stresses (Casa et. al. op. cit.).

The analysis of right dihedrals resulted in the finding of stress dihedral D1 (Figure 32), which marks the direction of the main stresses σ1 NW-SE (295°), σ3 NE-SE (35°); to this, the data of the area mapped, where the largest number of normal faults was found, is added, allowing the deduction of a field of distension stresses, which is coherent with the extension directions of the faults mapped. This field also lines up with the direction shift of the ravine, suggesting that there is a normal fault that extends with the depth. This distension forms vertical structures that shape the sector's relief.

Regarding the structural geological history, it is essential to state that the distention stress σ3 was activated after the compressive efforts, configuring the ground with normal small-scale faults.

7.9 Relation between faulting and volcanism

The Central Volcanic Belt is characterized by eruptive centers that are mainly lined up throughout a NW-SE corridor, which is crosswise to the major N-S orientation of this part of the Andean Volcanic Arc. Most of the stratovolcanoes from the Late Miocene are clearly lined up with a NW-SE orientation.

These fractures of a NW-SE direction are likely to have exerted tectonic control over the distribution of volcanic centers, which are crosswise to the general pattern of volcanism in this part of the Andes (de Silva et. al. 1994). The region is, thus, important to understand the structure of the Central Andean Chain, as well as the relation between tectonics and volcanism, which is in turn important inasmuch as they concern volcanoes that have a strong explosive activity. The structures that have a NW direction were created when the volcanic arc was formed. Many of the volcanoes of the Pliocene are spread throughout the area; in the central and southern parts of the area, they display a clear lined-up NW-SE direction. The stratovolcanoes of the Late Pliocene-Pleistocene concentrate in the south of the area, where they are lined up in a NE-SE direction in the north and in a N-S direction in the south.

7.10 Relation between the fracturing and the water regime

It is clear that, owing to their tectonic and volcanic activities, fracturing is potentially adequate for water-flow transport and circulation. This relation leads to the postulate that the Silala-Llancor lineament—which has an ENE-WSW (70°) orientation—behaves as a left-lateral fault, which crosses the central part of the area, coinciding pro-parte with the Silala springs' canal, passing between the Silala ignimbrite and the Silala Grande hill lavas. An analysis of the Silala hill level indicates that the lavas present a somewhat abrupt morphology, lined up with a general E-W orientation and an inclination to the north (45°). In the absence of kinematic field evidence, but bearing in mind the secondary fracturing that develops in the sectors that are adjacent to the structure, it is possible to assume that the structure presents a transtensional character (Figures Nos. 33 and 34).

The fracturing measured in the Torito hill lava has a NE-SW (15° to 35°) orientation and behaves as tension fractures arranged crosswise to a fault that has an angle inferior to 35°. The fracturing corresponds to the general jointing of the sector and the sporadic faults that present reduced displacement. In the Silala Grande hill, tension fractures are represented by short lineal segments that follow the same direction, which is clearly visible in the satellite image below and is demarcated by the rectilinear limits of tone variations that can be observed. At the level of the outcrops, the apparently dextral shears affect the lavas, sustaining the sinistral character of the structure (Picture No. 30).

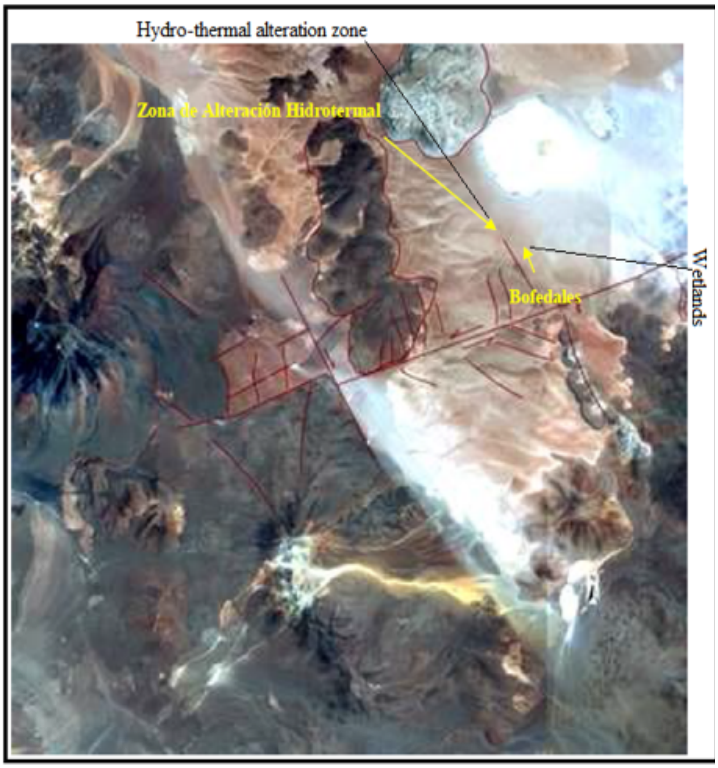

Figure No. 33. Structural scheme of the Silala-Llancor Lineament

82

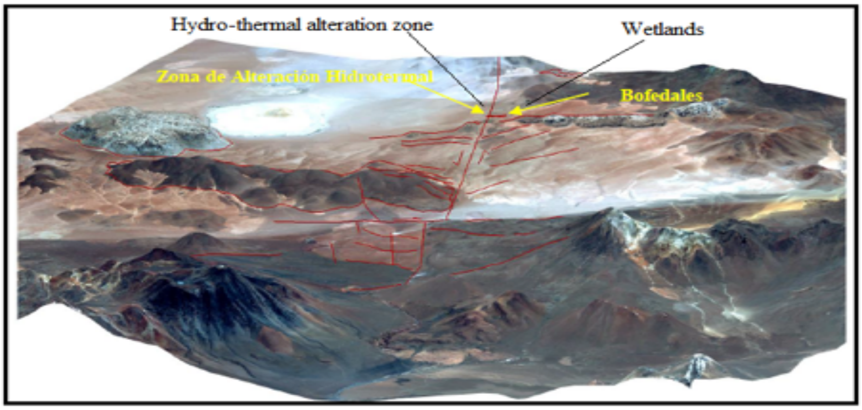

Figure No. 34. 3D Structural scheme of the Silala-Llancor Lineament

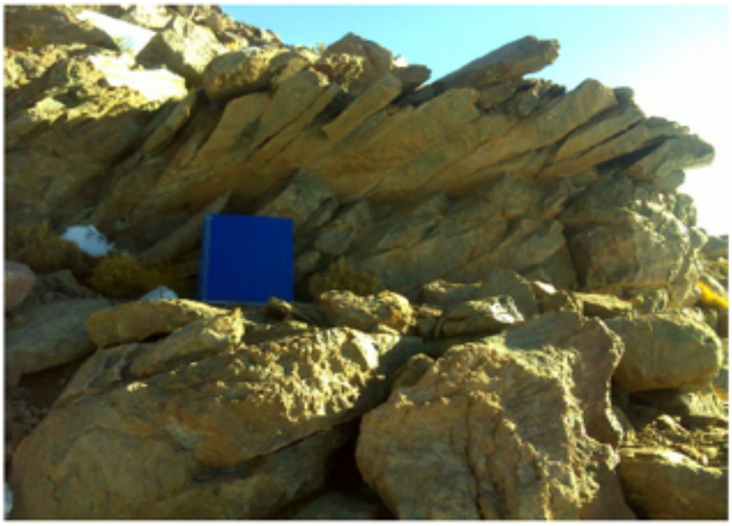

Picture No. 30. Dextral shearing in the Silala Grande hill

In general, the field observations and interpretation of structural data have led to the following considerations:
The sporadic presence of a thin film of calcite in some fractures (Picture No. 31) and the occurrence of banded chalcedony elements, with a globular habit and little transport, accumulated surrounding the Silala-Llancor fault trace, seem to indicate that an intense circulation of fluids occurs throughout deep fractures. These flows are mainly produced by a combination of deep peri-volcanic hydro-thermal fluids, which could be an indication of a recent tectonic activity.

The deep fluids move to the surface through fractured zones, mixing up on their way with weathered waters until they reach the fault, which is fit for lateral flow and serves as the preferred path for the migration of deep fluids. To the east of the area, the Silala-Llancor fault coincides with the wetlands and springs of the Pastos Grandes Caldera; the mean altitude of these springs is 4,500 MASL. To the west, the fault reaches the limits of the Silala (4,300 MASL). The unevenness of the terrain seems to contribute to the lateral migration of fluids towards the area that is topographically lower.

Finally, the interrelation between the kinematics of the reduced number of faults under the current stress field apparently causes a displacement that also affects the jointing, creating, in given sectors of the area, openings in some corners and closures in others, namely, producing compressional and dilatational syntaxes. The water sources well up in the intersection of open joints, throughout certain NW-SE transversal faults and in their intersection with semi-vertical joints.

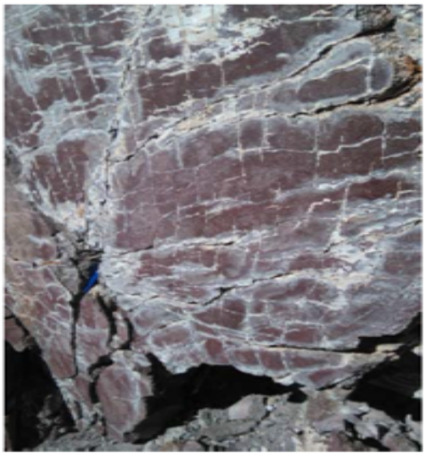

Picture No. 31. Joint plain infilled with calcite in the fractures of the Inacaliri lava

7.11 Conclusions

The fracturing system displays predominant structural trends, i.e. the first and major system presents a NE-SW

84

general trend (40°-70°) and displays discontinuous and shorter features that are well represented in the south and north sector of the area—this is where the Uyuni-Khenayani fault system is included. The second system has a NW-SE longitudinal direction (100°-400°); the main volcanic centers of the area coincide with this system, which is more frequent and continuous in the northwest and northeast sector of the area. A third structural system, presenting a N-S general trend (340°-360°) is found to the south of the area; some volcanic cones are lined up in this direction.

The most intense fracturing is found throughout the Silala springs, where ignimbrites are more exposed (up to 2 fractures per meter). It must be noted that in a complex aquifer of fractured rocks, the permeability and porosity of a lithological unit are composed of a network of fractures, discontinuities, block matrixes, open continuities and fracture infilling. These characteristics define the Silala ignimbrite as the component that generates the most secondary porosity, owing to the continuity, opening and flat-smooth form of their fractures.

The fracturing and faulting observed in the dacitic and andesitic lava of the area are not representative of the area, because they are considered discontinuous. The fracturing directions measured at the level of microstructures clearly respond to the regional fracturing, inasmuch as the same NE-SW, NW-SE and N-S trend structures, which coincide with the main reduced fault and fracture systems of the area, can be observed.

Though it is possible to observe some morphological evidence characterized by almost vertical planes and inclinations approximate to the 45°, the faults are not really visible in the field. Many of the faults, owing to their cartography, are minor and shallow. The fractures generally present a semi-vertical geometry in all their lithological units, ranging from the 70° to 90°.

The Silala-Llancor lineament—which has an ENE-WSW (75°) orientation that coincides pro-parte with the South Canal of the Silala springs—is modeled in the middle of the Silala ignimbrite and the Silala Grande hill lava. Its E-direction trace is arranged dextrally by a transversal NW-direction (300°) trace, at the level of the Torito hill lavas.

If the lineament is regarded as a lateral sinistral (strike-slip) fault, the trace of which would be located in the vicinity of the Silala springs, the fracture variation or orientation shift from NW-SE (Silala ignimbrite) to NE-SW (Silala Grande hill lavas) might be related with that structure; in theory, the former orientation would present sinistral kinematics and the latter dextral kinematics. This variation in the kinematics, which is unexplainable for the time being owing to the absence of evidence of subsequent successive tectonic events, might have some influence on the origin of the canals formed by the Silala waters.

The NW-SE (3.5 km of width) orientation graben structure would apparently prolong to 2 km to the north of the Silala wetlands; a priori, the distensive nature of the structures the traces of which involve the jointed ignimbrite of Silala with an agglomerate on its basal part, constitute a favorable environment for the transport and circulation of fluids.

A WSW-ENE distension direction stress field was determined in the field for the ignimbrite and lava. This is assumed to be related with a deformation event subsequent to the Pliocene—the Pleistocene perhaps—that is older than the Inacaliri lava.

Finally, a table-summary presenting the first and second order trends, together with rose diagrams for the fractures of the different sectors, are presented:

SECTOR	ROSE DIAGRAMS			TRENDS	
	NORMAL FAULTS	INVERSE FAULTS	JOINTS	1st ORDER	2nd ORDER
MESON HILL				NNE-SSW	NW-SE
SILALA IGNIMBRITE				NW-SE	NE-SW
SILALA CHICO HILL				NNE-SSW	NNW-SSE
NEGRO HILL				NE-SW	
TORITO HILL				NNE-SSW	NWW-SEE
PASTOS GRANDES				NNW-SSE	NWW-SEE

SECTOR	ROSE DIAGRAMS			TRENDS	
	NORMAL FAULTS	INVERSE FAULTS	JOINTS	1st ORDER	2nd ORDER
CAHUANA HILL				NNW-SSE	NWW-SEE
SILALA GRANDE HILL			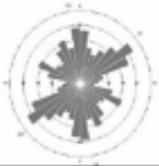	NE-SW	NNE-SSW
WESTERN INACALIRI HILL				NE-SW	NWW-SEE
EASTERN INACALIRI HILL				NE-SW	NW-SE

8. BIBLIOGRAPHY

Aranibar O. and Martinez E., 1990, Structural Interpretation of the Altiplano, Bolivia. Final work: Structure and Evolution of the Atlas Mountain System in Morocco and Structure and Evolution of the Central Andes in Northern Chile, Southern Bolivia and Northwestern Argentina. Abstract Volume, Berlin, p. 47

Arezo Marcos, 2013, (SATELLITE REMOTE SENSORS IN THE MEASUREMENT OF ENVIRONMENTAL IMPACT IN MINING, Master in Spatial Applications of Early Warning and Response to Emergencies).

Argollo J. and Iriondo, 1991, The Quaternary of Bolivia and Neighboring Regions.

Argollo J. et al., 1987, Plio-quaternary Geology of Bolivia. Unpublished.

Argollo J. and Mourguiart P., 1995, Quaternary Climates in South America, p. 360

Baby P., Sempere T., Oller J., Barrios L., Herail G., 1990, The Southern Altiplano of Bolivia: An Oligo-Miocene Intermontane Foreland Basin. Final work: Structure and Evolution of the Atlas Mountain System in Morocco and Structure and Evolution of the Central Andes in Northern Chile, Southern Bolivia and Northwestern Argentina. Abstract Volume, Berlin, p. 69

Cas R. A. F. and Wright J. V., 1992, Volcanic Successions. Modern and Ancient. Ed. Chapman & Hall, p. 528

Casa, A. M., Gil, I., and Simon, J. 1990, Analysis Methods of Paleo-Efforts based on Fault Populations: Systematics and Application Techniques. Geological studies, p. 385-398.

Cepeda, H., Acevedo A. P. 1982, The Sotara volcano: geology and geochemistry of major elements, p. 19-30.

Chuvieco E. Emilio, 2002, Fundamentals of Space Remote Sensing, Second Edition RIALP Editions. S.A. Madrid (p. 449).

Conesa, Alvarez, Martinez, 2004, Environment, Resources and Natural Risks—Analysis by Sig technologies and remote sensing Vol. II—University of Murcia, (p. 473).

Flores Naranjo Gonzalo, 2000, (Interpretation of Structural Lineaments based on Mosaic-Image Landsat/Tm and Data obtained from the Shuttle Radar Topography Mission for the Definition of Critical or Sensitive Areas—Scientific Research Journal of the Institute de Petroleum Studies (p. 218).

Jorge Davila Burga, 2011, Geological Dictionary, INGEMMET.

Jose Lugo Hubp, 2011, Geomorphological Dictionary, Institute of Geography of the UNAM.

Herail G., Baby P., Sempere T., Oller J., Barrios L., Montemurro G., Salinas R., 1990, Structural Cross Section in Southern Bolivia. Final work: Structure and Evolution of the Atlas Mountain System in Morocco and Structure and Evolution of the Central Andes in Northern Chile, Southern Bolivia and Northwestern Argentina. Abstract Volume, Berlin, p. 53

Kaiser J. F., 2014, Understanding Large Resurgent Boilers and Associated Magma Systems: The Large Pastures Caldera Complex, Southwest Bolivia. Thesis degree of Doctor of Philosophy, 192 p.

Montes de Oca Ismael, 1997, Geography and Natural Resources of Bolivia. O'Leary, D. W., Friedman, J. D., and Pohn, H. A., 1976. Lineament, linear, lineation, Some proposed new standards for old terms: Geological Society of America, v. 87, p. 1463-1469

Palomino-Angel Sebastian, - Anaya-Acevedo Jesus A., 2014, Synergy between optical and radar data to determine soil cover: preliminary results for the Uraba region, Colombia – Faculty of Engineering, University of Medellín. XVI INTERNATIONAL SYMPOSIUM SELPER (p. 21).

Peter L. Nester, Eugenia Gayo, Claudio Torre, Teresa Jordan, Nicolas Blanco, 2007, Perennial stream discharge in the hyper-arid Atacama Desert of northern Chile during the last Pleistocene. PNAS, vol. 104 No.50.

Rodriguez-Esparragon Dionisio, Garcia-Pedrero Angel, Gonzalo-Martin Consuelo, Marcello-Ruiz Javier and Eugenio-Gonzalez Francisco, 2015, Measurement of the spectral quality of images fused using the CIEDE2000 algorithm. Remote Sensing: Wetlands and Protected Areas. XVI Congress of the Spanish Association of Remote Sensing (p. 4).

Salisbury M.J., Jicha B. R., De Silva S.L., Singer B.S., Jimenez N.C., Ort M. H., 2010, Ar/Ar Chrono-stratigraphy of Altiplano-Puna volcanic complex ignimbrites reveals the development of a major magmatic province.

Geological Service of Bolivia, Report on Regional Geology of the Southwestern part of Bolivia, GEOBOL-CONAMAR, 1977 vol. 1 and vol. 2.

National Geology and Mining Service, 1996, Bolivia Geological Charter Sheet 5927-6027 Silala-Sanabria, Scale 1: 100 000.

National Geology and Mining Service, 2003, Bolivia Geological Charter Sheet 5928-6028 Cerro del Inca-Laguna Khara, Scale 1: 100 000.

National Service of Geology and Mining, 2003, Study of Pastos Grandes basin—Basin 16.

National Service of Geology and Mining, 2003, Study of the geology, hydrogeology and environment of the area of the springs of Silala (Project of Integration PIR) Study of the hydrographical basin-basin of the Silala springs–basin 20. June 2000-2001.

Tibaldi A., Corazzato C., Rovida A., 2008, Miocene-Quaternary structural evolution of the Uyuni-Atacama region, Andes of Chile and Bolivia. Tectonophysics. Ed. Elsevier, p.114-135.

Vargas E., 1992, Aerial photography and its application to geological and geomorphological studies: principles of remote perception, 436 p. 90.

Annex A

Geological and Structural Maps

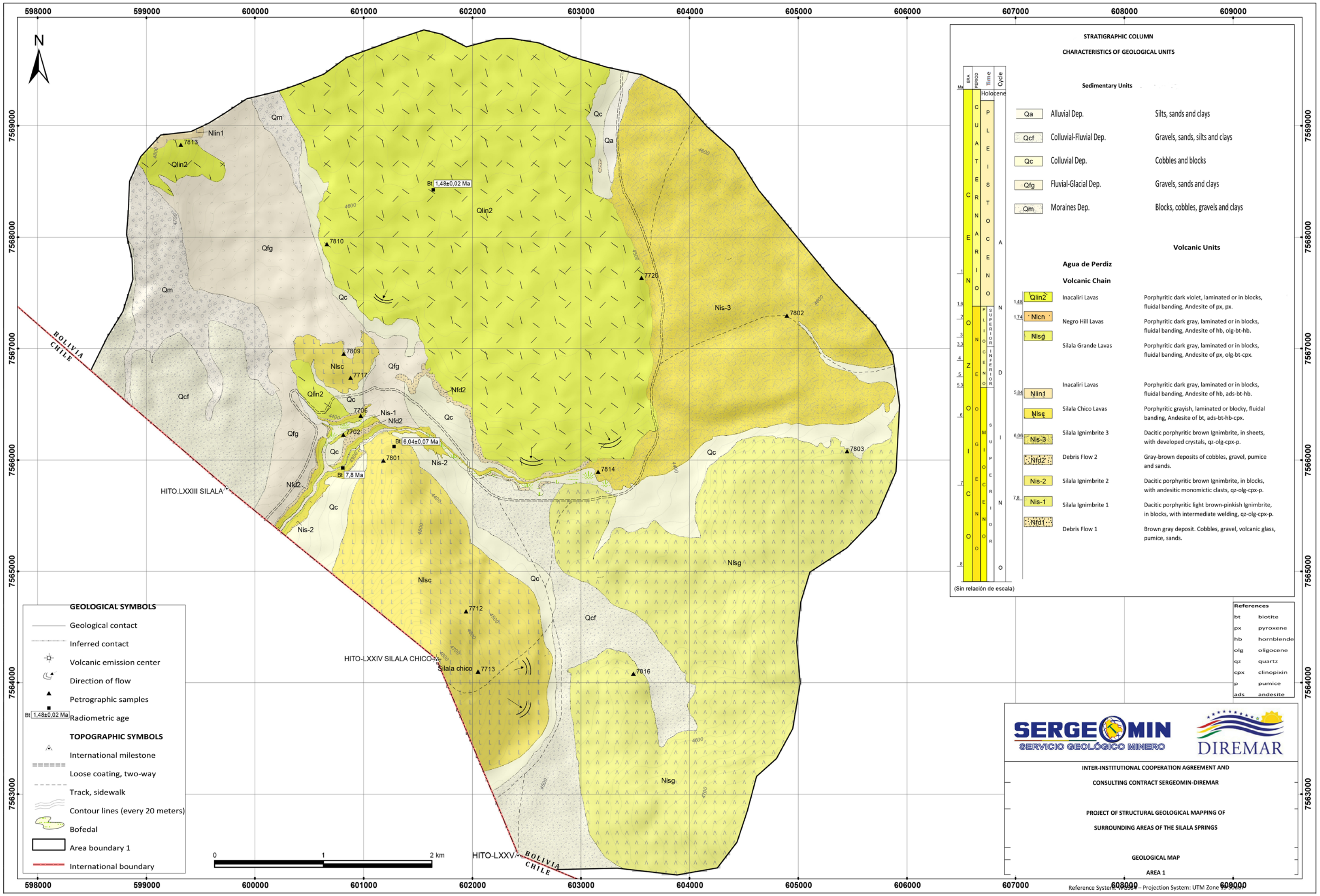
STRATIGRAPHIC COLUMN
CHARACTERISTICS OF GEOLOGICAL UNITS
Sedimentary Units
Qa Alluvial Dep. Silts, sands and clays
Qcf Colluvial-Fluvial Dep. Gravels, sands, silts and clays
Qc Colluvial Dep. Cobbles and blocks
Qfg Fluvial-Glacial Dep. Gravels, sands and clays
Qm Moraines Dep. Blocks, cobbles, gravels and clays
Volcanic Units
Agua de Perdiz
Volcanic Chain
Qlin2 Inacaliri Lavas Porphyritic dark violet, laminated or in blocks, fluidal banding, Andesite of px, px.
Nlcn Negro Hill Lavas Porphyritic dark gray, laminated or in blocks, fluidal banding, Andesite of hb, olg-bt-hb.
Nlsg Silala Grande Lavas Porphyritic dark gray, laminated or in blocks, fluidal banding, Andesite of px, olg-bt-cpx.
Nlin1 Inacaliri Lavas Porphyritic dark gray, laminated or in blocks, fluidal banding, Andesite of hb, ads-bt-hb.
Nlsc Silala Chico Lavas Porphyritic grayish, laminated or blocky, fluidal banding, Andesite of bt, ads-bt-hb-cpx.
Nis-3 Silala Ignimbrite 3 Dacitic porphyritic brown Ignimbrite, in sheets, with developed crystals, qz-olg-cpx-p.
Nfd2 Debris Flow 2 Gray-brown deposits of cobbles, gravel, pumice and sands.
Nis-2 Silala Ignimbrite 2 Dacitic porphyritic brown Ignimbrite, in blocks, with andesitic monomictic clasts, qz-olg-cpx-p.
Nis-1 Silala Ignimbrite 1 Dacitic porphyritic light brown-pinkish Ignimbrite, in blocks, with intermediate welding, qz-olg-cpx-p.
Nfd1 Debris Flow 1 Brown gray deposit. Cobbles, gravel, volcanic glass, pumice, sands.
(Sin relación de escala)
References
bt biotite
px pyroxene
hb hornblende
olg oligocene
qz quartz
cpx clinopixin
p pumice
ads andesite
GEOLOGICAL SYMBOLS
Geological contact
Inferred contact
Volcanic emission center
Direction of flow
Petrographic samples
Radiometric age
TOPOGRAPHIC SYMBOLS
International milestone
Loose coating, two-way
Track, sidewalk
Contour lines (every 20 meters)
Bofedal
Area boundary 1
International boundary
SERGEOMIN
SERVICIO GEOLÓGICO MINERO
DIREMAR
INTER-INSTITUTIONAL COOPERATION AGREEMENT AND
CONSULTING CONTRACT SERGEOMIN-DIREMAR
PROJECT OF STRUCTURAL GEOLOGICAL MAPPING OF
SURROUNDING AREAS OF THE SILALA SPRINGS
GEOLOGICAL MAP
AREA 1
HITO.LXXIII SILALA
HITO-LXXIV SILALA CHICO
HITO-LXXV
Silala chico
BOLIVIA
CHILE
Bt 1,48±0,02 Ma
Bt 6,04±0,07 Ma
Bt 7,8 Ma
0 1 2 km

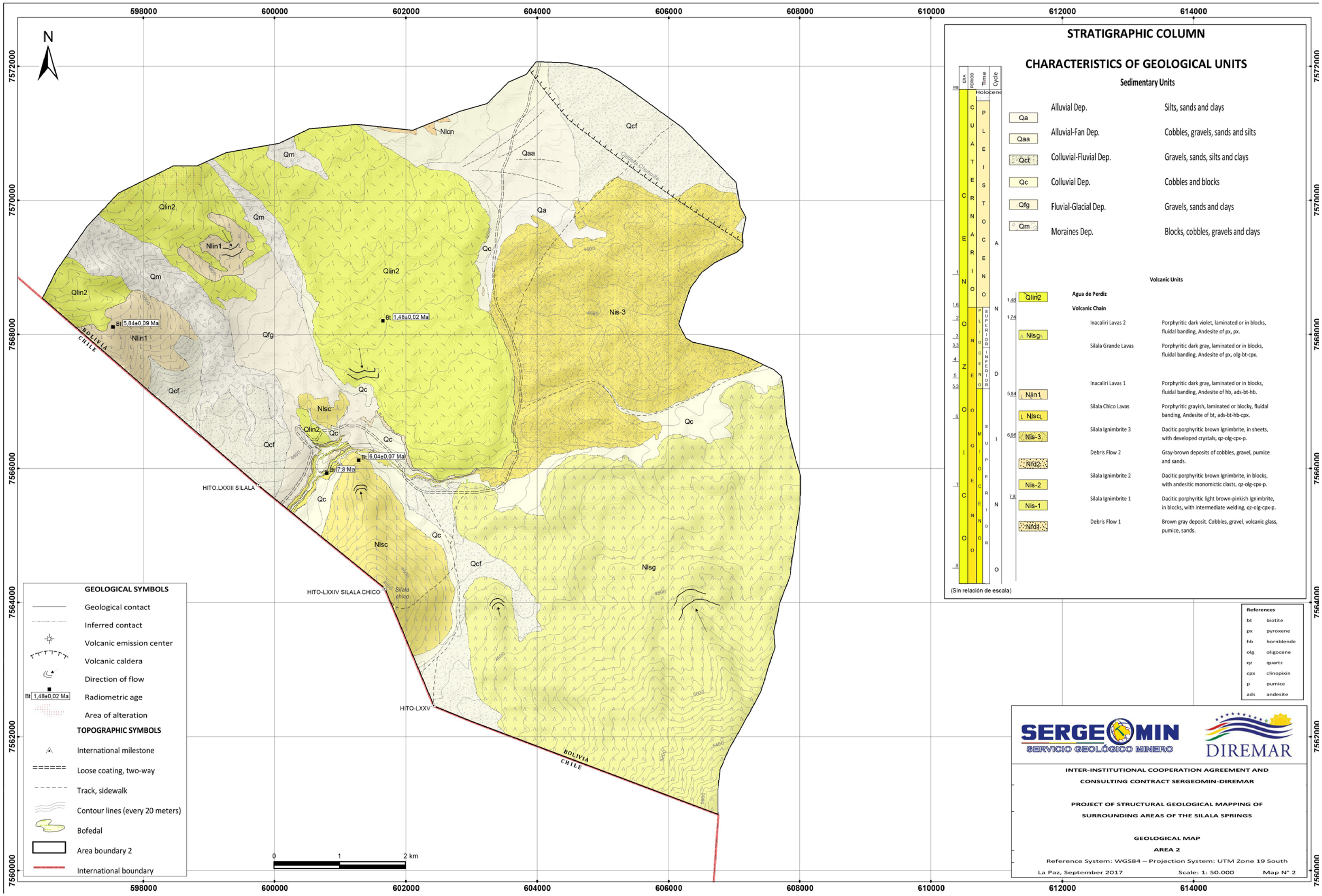
STRATIGRAPHIC COLUMN
CHARACTERISTICS OF GEOLOGICAL UNITS
Sedimentary Units
Qa Alluvial Dep. Silts, sands and clays
Qaa Alluvial-Fan Dep. Cobbles, gravels, sands and silts
Qcf Colluvial-Fluvial Dep. Gravels, sands, silts and clays
Qc Colluvial Dep. Cobbles and blocks
Qfg Fluvial-Glacial Dep. Gravels, sands and clays
Qm Moraines Dep. Blocks, cobbles, gravels and clays
Volcanic Units
Qlin2 Agua de Perdiz
Volcanic Chain
Inacaliri Lavas 2 Porphyritic dark violet, laminated or in blocks, fluidal banding, Andesite of px, px.
Nlsg Silala Grande Lavas Porphyritic dark gray, laminated or in blocks, fluidal banding, Andesite of px, olg-bt-cpx.
Nlin1 Inacaliri Lavas 1 Porphyritic dark gray, laminated or in blocks, fluidal banding, Andesite of hb, ads-bt-hb.
Nlsc Silala Chico Lavas Porphyritic grayish, laminated or blocky, fluidal banding, Andesite of bt, ads-bt-hb-cpx.
Nis-3 Silala Ignimbrite 3 Dacitic porphyritic brown Ignimbrite, in sheets, with developed crystals, qz-olg-cpx-p.
Nfd2 Debris Flow 2 Gray-brown deposits of cobbles, gravel, pumice and sands.
Nis-2 Silala Ignimbrite 2 Dacitic porphyritic brown Ignimbrite, in blocks, with andesitic monomictic clasts, qz-olg-cpx-p.
Nis-1 Silala Ignimbrite 1 Dacitic porphyritic light brown-pinkish Ignimbrite, in blocks, with intermediate welding, qz-olg-cpx-p.
Nfd1 Debris Flow 1 Brown gray deposit. Cobbles, gravel, volcanic glass, pumice, sands.
(Sin relación de escala)
References
bt biotite
px pyroxene
hb hornblende
olg oligocene
qz quartz
cpx clinopixin
p pumice
ads andesite
GEOLOGICAL SYMBOLS
Geological contact
Inferred contact
Volcanic emission center
Volcanic caldera
Direction of flow
Radiometric age
Area of alteration
TOPOGRAPHIC SYMBOLS
International milestone
Loose coating, two-way
Track, sidewalk
Contour lines (every 20 meters)
Bofedal
Area boundary 2
International boundary
HITO.LXXIII SILALA
HITO-LXXIV SILALA CHICO
HITO-LXXV
BOLIVIA
CHILE
Bt 5,84±0,09 Ma
Bt 1,48±0,02 Ma
Bt 6,04±0,07 Ma
Bt 7,8 Ma
SERGEOMIN
SERVICIO GEOLÓGICO MINERO
DIREMAR
INTER-INSTITUTIONAL COOPERATION AGREEMENT AND CONSULTING CONTRACT SERGEOMIN-DIREMAR
PROJECT OF STRUCTURAL GEOLOGICAL MAPPING OF SURROUNDING AREAS OF THE SILALA SPRINGS
GEOLOGICAL MAP
AREA 2
Reference System: WGS84 – Projection System: UTM Zone 19 South
La Paz, September 2017
Scale: 1: 50.000
Map N° 2

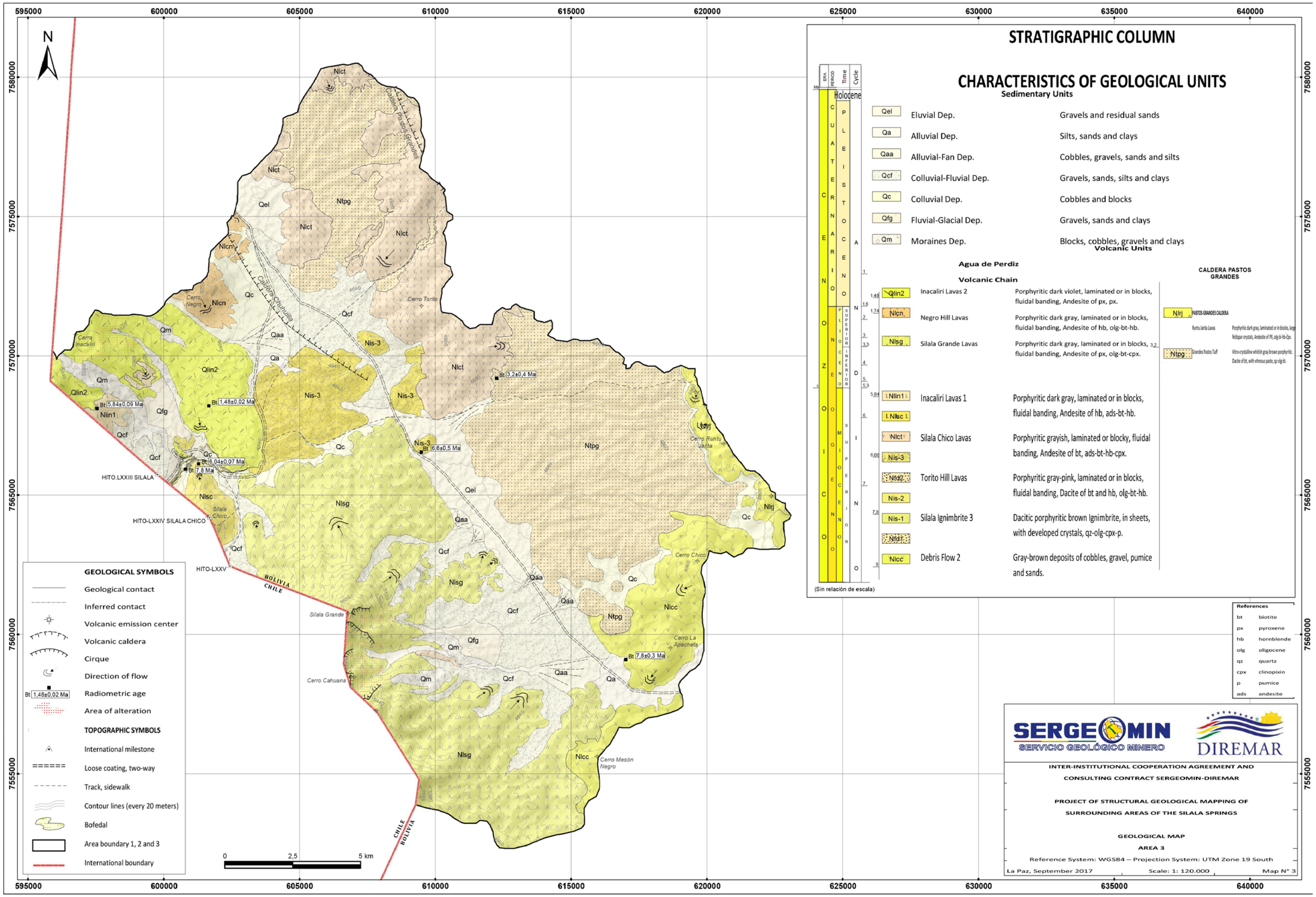

STRATIGRAPHIC COLUMN
CHARACTERISTICS OF GEOLOGICAL UNITS
Sedimentary Units
Qel Eluvial Dep. Gravels and residual sands
Qa Alluvial Dep. Silts, sands and clays
Qaa Alluvial-Fan Dep. Cobbles, gravels, sands and silts
Qcf Colluvial-Fluvial Dep. Gravels, sands, silts and clays
Qc Colluvial Dep. Cobbles and blocks
Qfg Fluvial-Glacial Dep. Gravels, sands and clays
Qm Moraines Dep. Blocks, cobbles, gravels and clays
Volcanic Units
Agua de Perdiz
Volcanic Chain
Qlin2 Inacaliri Lavas 2 Porphyritic dark violet, laminated or in blocks, fluidal banding, Andesite of px, px.
Nlcn Negro Hill Lavas Porphyritic dark gray, laminated or in blocks, fluidal banding, Andesite of hb, olg-bt-hb.
Nlsg Silala Grande Lavas Porphyritic dark gray, laminated or in blocks, fluidal banding, Andesite of px, olg-bt-cpx.
Nlin1 Inacaliri Lavas 1 Porphyritic dark gray, laminated or in blocks, fluidal banding, Andesite of hb, ads-bt-hb.
Nlct Silala Chico Lavas Porphyritic grayish, laminated or blocky, fluidal banding, Andesite of bt, ads-bt-hb-cpx.
Ntd2 Torito Hill Lavas Porphyritic gray-pink, laminated or in blocks, fluidal banding, Dacite of bt and hb, olg-bt-hb.
Nis-1 Silala Ignimbrite 3 Dacitic porphyritic brown Ignimbrite, in sheets, with developed crystals, qz-olg-cpx-p.
Nlcc Debris Flow 2 Gray-brown deposits of cobbles, gravel, pumice and sands.
CALDERA PASTOS GRANDES
Nlrj
Ntpg
(Sin relación de escala)
References
bt biotite
px pyroxene
hb hornblende
olg oligocene
qz quartz
cpx clinopixin
p pumice
ads andesite
GEOLOGICAL SYMBOLS
Geological contact
Inferred contact
Volcanic emission center
Volcanic caldera
Cirque
Direction of flow
Radiometric age
Area of alteration
TOPOGRAPHIC SYMBOLS
International milestone
Loose coating, two-way
Track, sidewalk
Contour lines (every 20 meters)
Bofedal
Area boundary 1, 2 and 3
International boundary
SERGEOMIN
SERVICIO GEOLÓGICO MINERO
DIREMAR
INTER-INSTITUTIONAL COOPERATION AGREEMENT AND CONSULTING CONTRACT SERGEOMIN-DIREMAR
PROJECT OF STRUCTURAL GEOLOGICAL MAPPING OF SURROUNDING AREAS OF THE SILALA SPRINGS
GEOLOGICAL MAP
AREA 3
Reference System: WGS84 – Projection System: UTM Zone 19 South
La Paz, September 2017
Scale: 1: 120.000
Map N° 3
HITO LXXIII SILALA
HITO-LXXIV SILALA CHICO
HITO-LXXV
BOLIVIA
CHILE
Caldera Pastos Grandes
Caldera Chuhuilla
Cerro Torito
Cerro Chico
Cerro Mesón Negro
Cerro Cahuana
Silala Grande

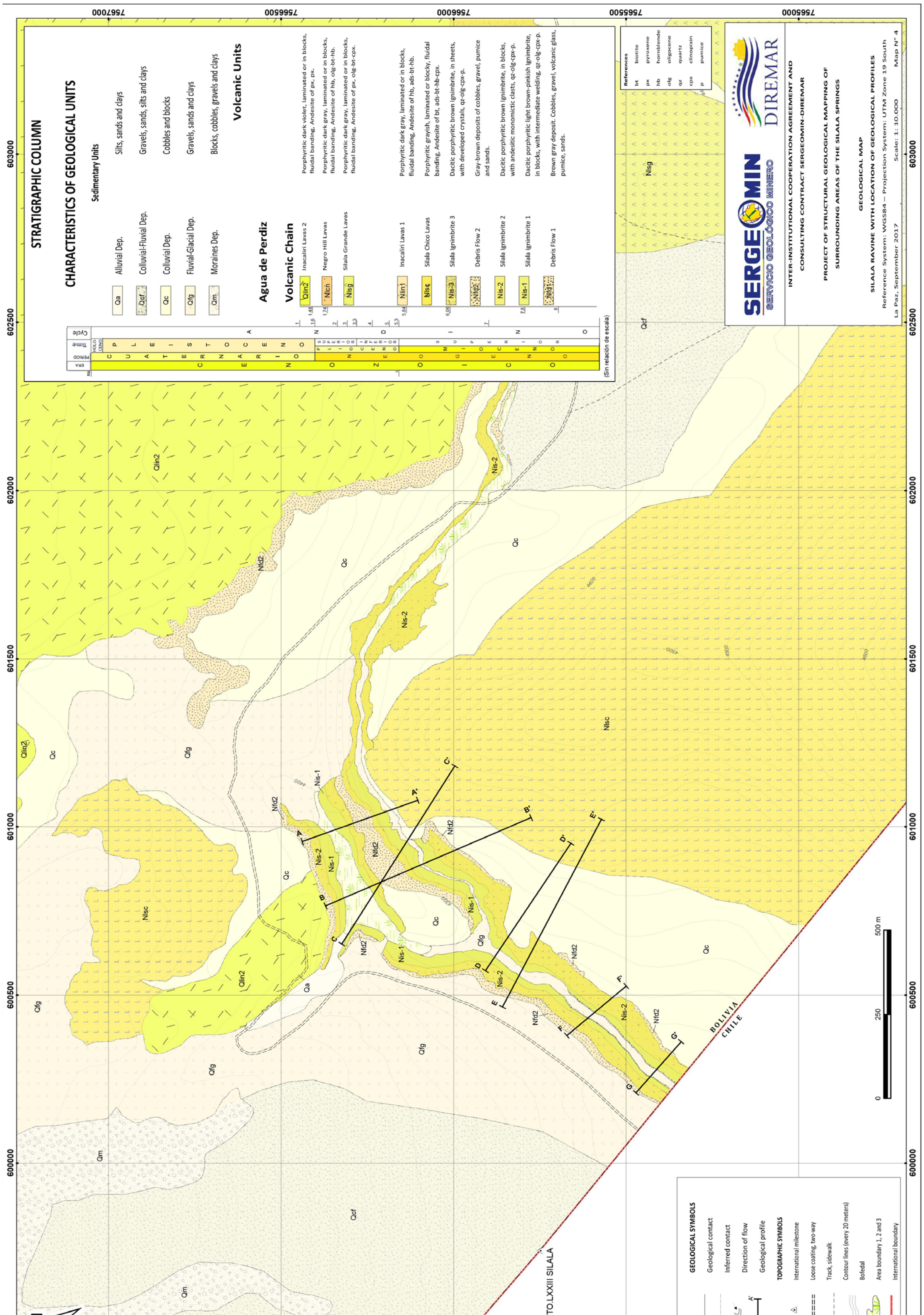
STRATIGRAPHIC COLUMN
CHARACTERISTICS OF GEOLOGICAL UNITS
Sedimentary Units
Qa Alluvial Dep. Silts, sands and clays
Qcf Colluvial-Fluvial Dep. Gravels, sands, silts and clays
Qc Colluvial Dep. Cobbles and blocks
Qfg Fluvial-Glacial Dep. Gravels, sands and clays
Qm Moraines Dep. Blocks, cobbles, gravels and clays
Volcanic Units
Agua de Perdiz
Volcanic Chain
Qlin2 Inacaliri Lavas 2 Porphyritic dark violet, laminated or in blocks, fluidal banding, Andesite of px, px.
Nlch Negro Hill Lavas Porphyritic dark gray, laminated or in blocks, fluidal banding, Andesite of hb, olg-bt-hb.
Nlsg Silala Grande Lavas Porphyritic dark gray, laminated or in blocks, fluidal banding, Andesite of px, olg-bt-cpx.
Nlin1 Inacaliri Lavas 1 Porphyritic dark gray, laminated or in blocks, fluidal banding, Andesite of hb, ads-bt-hb.
Nlsc Silala Chico Lavas Porphyritic grayish, laminated or blocky, fluidal banding, Andesite of bt, ads-bt-hb-cpx.
Nis-3 Silala Ignimbrite 3 Dacitic porphyritic brown ignimbrite, in sheets, with developed crystals, qz-olg-cpx-p.
Nfd2 Debris Flow 2 Gray-brown deposits of cobbles, gravel, pumice and sands.
Nis-2 Silala Ignimbrite 2 Dacitic porphyritic brown ignimbrite, in blocks, with andesitic monomictic clasts, qz-olg-cpx-p.
Nis-1 Silala Ignimbrite 1 Dacitic porphyritic light brown-pinkish ignimbrite, in blocks, with intermediate welding, qz-olg-cpx-p.
Nfd1 Debris Flow 1 Brown gray deposit. Cobbles, gravel, volcanic glass, pumice, sands.
(Sin relación de escala)
References
bt biotite
px pyroxene
hb hornblende
olg oligocene
qz quartz
cpx clinopiroxen
p pumice
SERGEOMIN SERVICIO GEOLÓGICO MINERO
DIREMAR
INTER-INSTITUTIONAL COOPERATION AGREEMENT AND CONSULTING CONTRACT SERGEOMIN-DIREMAR
PROJECT OF STRUCTURAL GEOLOGICAL MAPPING OF SURROUNDING AREAS OF THE SILALA SPRINGS
GEOLOGICAL MAP
SILALA RAVINE WITH LOCATION OF GEOLOGICAL PROFILES
Reference System: WGS84 – Projection System: UTM Zone 19 South
La Paz, September 2017 Scale: 1: 10.000 Map N° 4
GEOLOGICAL SYMBOLS
Geological contact
Inferred contact
Direction of flow
Geological profile
TOPOGRAPHIC SYMBOLS
International milestone
Loose coating, two-way
Track, sidewalk
Contour lines (every 20 meters)
Bofedal
Area boundary 1, 2 and 3
International boundary
HITO LXXIII SILALA
BOLIVIA
CHILE
0 250 500 m
599500 600000 600500 601000 601500 602000 602500 603000
7565000 7565500 7566000 7566500 7567000

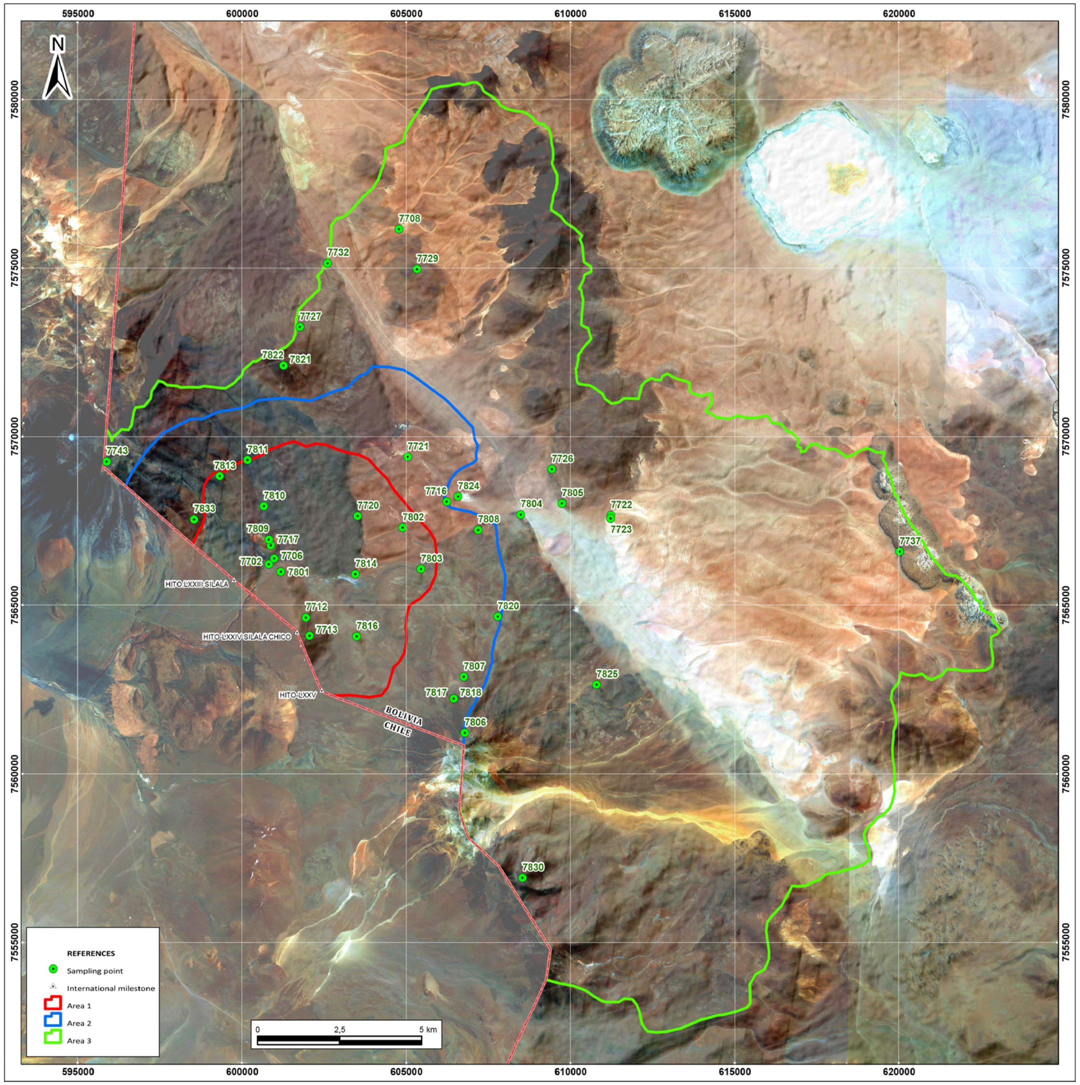

MINING GEOLOGICAL SERVICE

STRATEGIC OFFICE FOR THE MARITIME CLAIM, SILALA AND INTERNATIONAL WATER RESOURCES

GEOLOGICAL MAPPING OF THE AREA SURROUNDING THE SILALA SPRINGS

SUMMARY LABORATORY TABLE

Nº	East (UTM)	North (UTM)	Elevation (m.s.n.m.)	Sample Code	Lithology	Rock Name
1	600813	7566226	4383	7702	TOBA	IGNIMBRITA ANDESITICA
2	600973	7566397	4395	7706	IGNIMBRITA	IGNIMBRITA ANDESITICA
3	601181	7565996	4457	7801	IGNIMBRITA	ANDESITICA BIOTITICA
4	604898	7567298	4543	7802	IGNIMBRITA	DACITA BIOTITICA
5	605450	7566080	4602	7803	LAVA	ANDESITA PIROXENICA
6	608497	7567689	4583	7804	LAVA	ANDESITICA BIOTITICA
7	609739	7568018	4596	7805	LAVA	DACITA BIOTITICA
8	604787	7576158	4522	7708	TOBA	IGNIMBRITA ANDESITICA
9	601942	7564641	4606	7712	LAVA	DACITA BIOTITICA
10	606789	7561214	5649	7806	LAVA	ANDESITA PIROXENICA
11	606758	7562878	5041	7807	LAVA	IGNIMBRITA ANDESITICA
12	602052	7564099	4766	7713	LAVA	ANDESITICA BIOTITICA
13	607188	7567230	4596	7808	LAVA	IGNIMBRITA ANDESITICA
14	606242	7568071	4596	7716	TOBA	DACITA BIOTITICA
15	600871	7566783	4437	7717	LAVA	DACITA BIOTITICA
16	603511	7567642	4500	7720	LAVA	ANDESITA PIROXENICA CUARZOSA
17	605051	7569399	4580	7721	IGNIMBRITA	DACITA BIOTITICA
18	600816	7566953	4485	7809	LAVA	ANDESITICA BIOTITICA
19	600661	7567938	4547	7810	LAVA	BASALTO PIROXENICO
20	600166	7569312	4671	7811	BRECHA BASAL	ANDESITA PIROXENICA
21	599317	7568831	4759	7813	BRECHA BASAL	IGNIMBRITA ANDESITICA
22	603440	7565926	4422	7814	TOBA	ANDESITA HORNBLENDICA
23	603483	7564079	4558	7816	LAVA	ANDESITA PIROXENICA
24	606447	7562228	5165	7817	LAVA	ANDESITA PIROXENICA
25	606447	7562228	5165	7818	LAVA	ANDESITA PIROXENICA
26	611232	7567663	4626	7722	TOBA	DACITA BIOTITICA
27	607792	7564663	4802	7820	LAVA	ANDESITA PIROXENICA
28	611225	7567577	4640	7723	TOBA	ANDESITA CUARZOSA
29	609442	7569033	4653	7726	LAVA	DACITA DE BIOTITA Y HORNBLENDA
30	601256	7572117	5181	7821	LAVA	ANDESITA HORNBLENDICA
31	601256	7572117	5181	7822	LAVA	ANDESITA HORNBLENDICA
32	601757	7573261	4833	7727	LAVA	ANDESITICA BIOTITICA OXIDADA
33	602604	7575147	4607	7732	LAVA	ANDESITICA BIOTITICA OXIDADA
34	605330	7574972	4741	7729	LAVA	ANDESITICA BIOTITICA OXIDADA
35	606578	7568225	4555	7824	ARCILLITA	ARCILLITA
36	610800	7562642	4647	7825	LAVA	ANDESITA PIROXENICA
37	620023	7566597	4864	7737	LAVA	ANDESITA PIROXENICA
38	619703	756092	5107	7827	LAVA	DACITA PIROXENICA
39	608546	7556911	5420	7830	LAVA	ANDESITA HORNBLENDICA
40	595872	7569264	5631	7743	LAVA	ANDESITA HORNBLENDICA
41	598532	7567548	4609	7833	LAVA	ANDESITA HORNBLENDICA

SERGEOMIN
SERVICIO GEOLÓGICO MINERO

DIREMAR

INTER-INSTITUTIONAL COOPERATION AGREEMENT AND CONSULTING CONTRACT SERGEOMIN-DIREMAR

PROJECT OF STRUCTURAL GEOLOGICAL MAPPING OF SURROUNDING AREAS OF THE SILALA SPRINGS

SAMPLING MAP

Reference System: WGS84 – Projection System: UTM Zone 19 South

La Paz, September 2017 | Scale: 1: 120.000 | Map N° 5

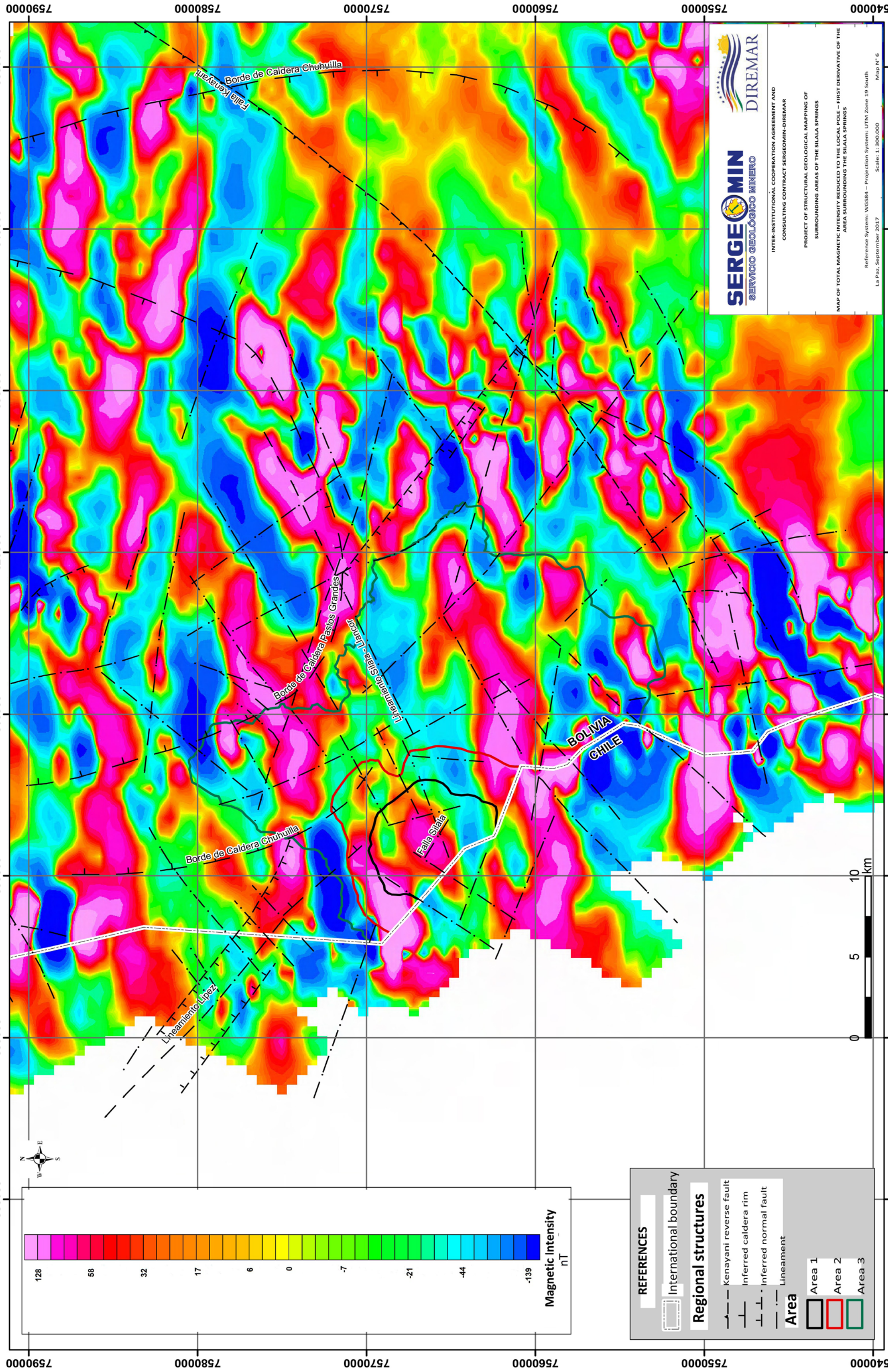
SERGEOMIN
SERVICIO GEOLÓGICO MINERO
DIREMAR
INTER-INSTITUTIONAL COOPERATION AGREEMENT AND CONSULTING CONTRACT SERGEOMIN-DIREMAR
PROJECT OF STRUCTURAL GEOLOGICAL MAPPING OF SURROUNDING AREAS OF THE SILALA SPRINGS
MAP OF TOTAL MAGNETIC INTENSITY REDUCED TO THE LOCAL POLE – FIRST DERIVATIVE OF THE AREA SURROUNDING THE SILALA SPRINGS
Reference System: WGS84 – Projection System: UTM Zone 19 South
La Paz, September 2017
Scale: 1: 300.000
Map N° 6
Borde de Caldera Chuhuilla
Falla Kenayani
Borde de Caldera Pastos Grandes
Lineamiento Silala - Llareta
Falla Silala
Lineamiento Lípez
BOLIVIA
CHILE
Magnetic Intensity
nT
128
58
32
17
6
0
-7
-21
-44
-139
REFERENCES
International boundary
Regional structures
Kenayani reverse fault
Inferred caldera rim
Inferred normal fault
Lineament
Area
Area 1
Area 2
Area 3
0
5
10
km
7590000
7580000
7570000
7560000
7550000
7540000
580000
590000
600000
610000
620000
630000
640000
650000

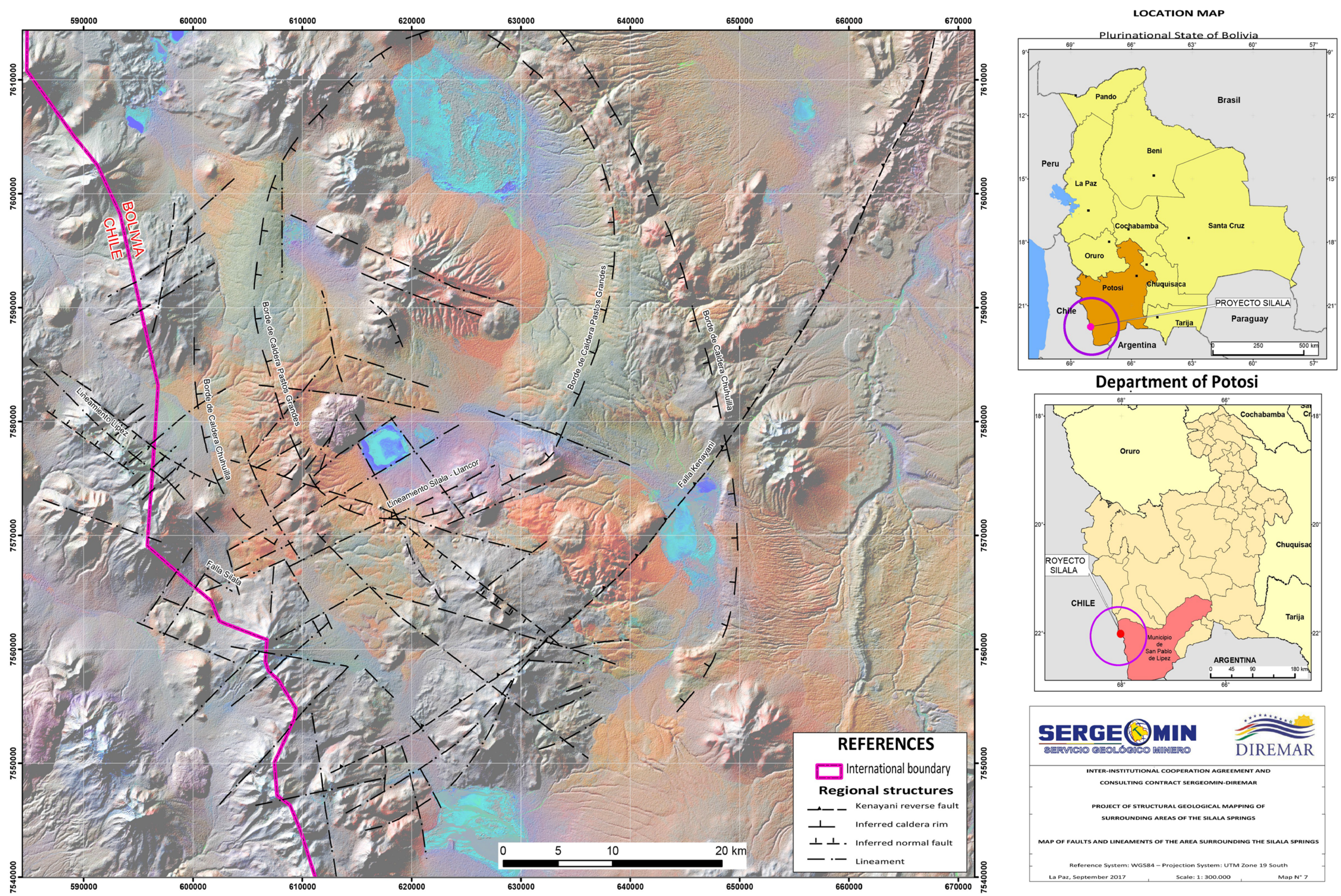
LOCATION MAP
Plurinational State of Bolivia
Pando
Brasil
Beni
Peru
La Paz
Cochabamba
Santa Cruz
Oruro
Potosi
Chuquisaca
Chile
PROYECTO SILALA
Paraguay
Tarija
Argentina
Department of Potosi
Cochabamba
Oruro
Chuquisaca
ROYECTO SILALA
CHILE
Tarija
Municipio de San Pablo de Lípez
ARGENTINA
BOLIVIA
CHILE
Borde de Caldera Pastos Grandes
Borde de Caldera Chuhuilla
Lineamiento Lípez
Lineamiento Silala - Llancor
Falla Silala
Falla Kenayani
REFERENCES
International boundary
Regional structures
Kenayani reverse fault
Inferred caldera rim
Inferred normal fault
Lineament
0 5 10 20 km
SERGEOMIN
SERVICIO GEOLÓGICO MINERO
DIREMAR
INTER-INSTITUTIONAL COOPERATION AGREEMENT AND
CONSULTING CONTRACT SERGEOMIN-DIREMAR
PROJECT OF STRUCTURAL GEOLOGICAL MAPPING OF
SURROUNDING AREAS OF THE SILALA SPRINGS
MAP OF FAULTS AND LINEAMENTS OF THE AREA SURROUNDING THE SILALA SPRINGS
Reference System: WGS84 – Projection System: UTM Zone 19 South
La Paz, September 2017
Scale: 1: 300.000
Map N° 7

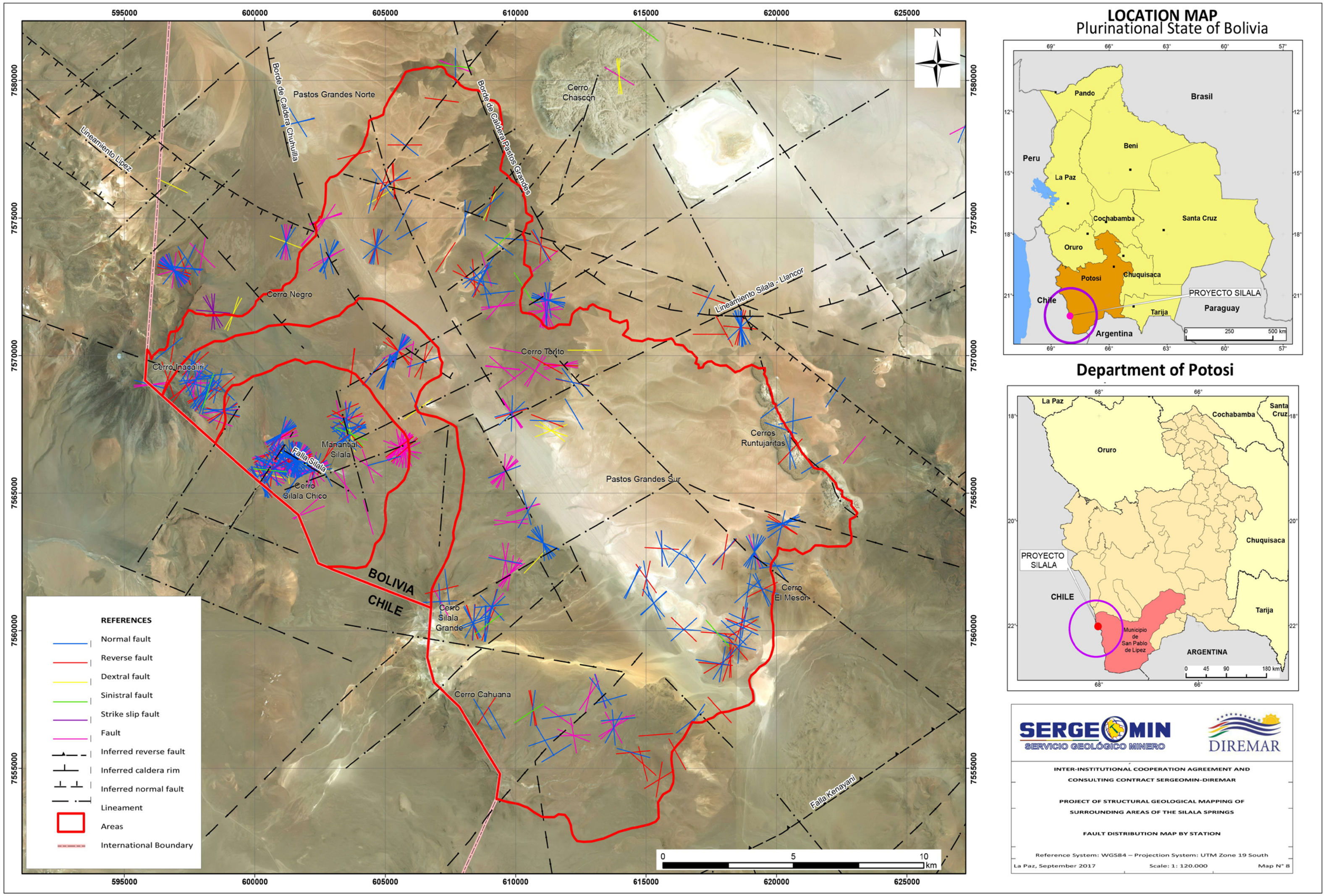
LOCATION MAP
Plurinational State of Bolivia
Pando
Brasil
Beni
Peru
La Paz
Cochabamba
Santa Cruz
Oruro
Potosi
Chuquisaca
Chile
PROYECTO SILALA
Paraguay
Tarija
Argentina
Department of Potosi
La Paz
Cochabamba
Santa Cruz
Oruro
Chuquisaca
PROYECTO SILALA
CHILE
Tarija
Municipio de San Pablo de Lípez
ARGENTINA
SERGEOMIN
SERVICIO GEOLÓGICO MINERO
DIREMAR
INTER-INSTITUTIONAL COOPERATION AGREEMENT AND CONSULTING CONTRACT SERGEOMIN-DIREMAR
PROJECT OF STRUCTURAL GEOLOGICAL MAPPING OF SURROUNDING AREAS OF THE SILALA SPRINGS
FAULT DISTRIBUTION MAP BY STATION
Reference System: WGS84 – Projection System: UTM Zone 19 South
La Paz, September 2017
Scale: 1: 120.000
Map N° 8
Pastos Grandes Norte
Borde de Caldera Chuhuilla
Borde de Caldera Pastos Grandes
Cerro Chascon
Lineamiento Lipez
Cerro Negro
Lineamiento Silala - Llancor
Cerro Inacaliri
Cerro Tojito
Manantial Silala
Falla Silala
Cerro Silala Chico
Cerros Runtujaritas
Pastos Grandes Sur
BOLIVIA
CHILE
Cerro Silala Grande
Cerro El Mesor
Cerro Cahuana
Falla Kenayani
REFERENCES
Normal fault
Reverse fault
Dextral fault
Sinistral fault
Strike slip fault
Fault
Inferred reverse fault
Inferred caldera rim
Inferred normal fault
Lineament
Areas
International Boundary
0
5
10
km

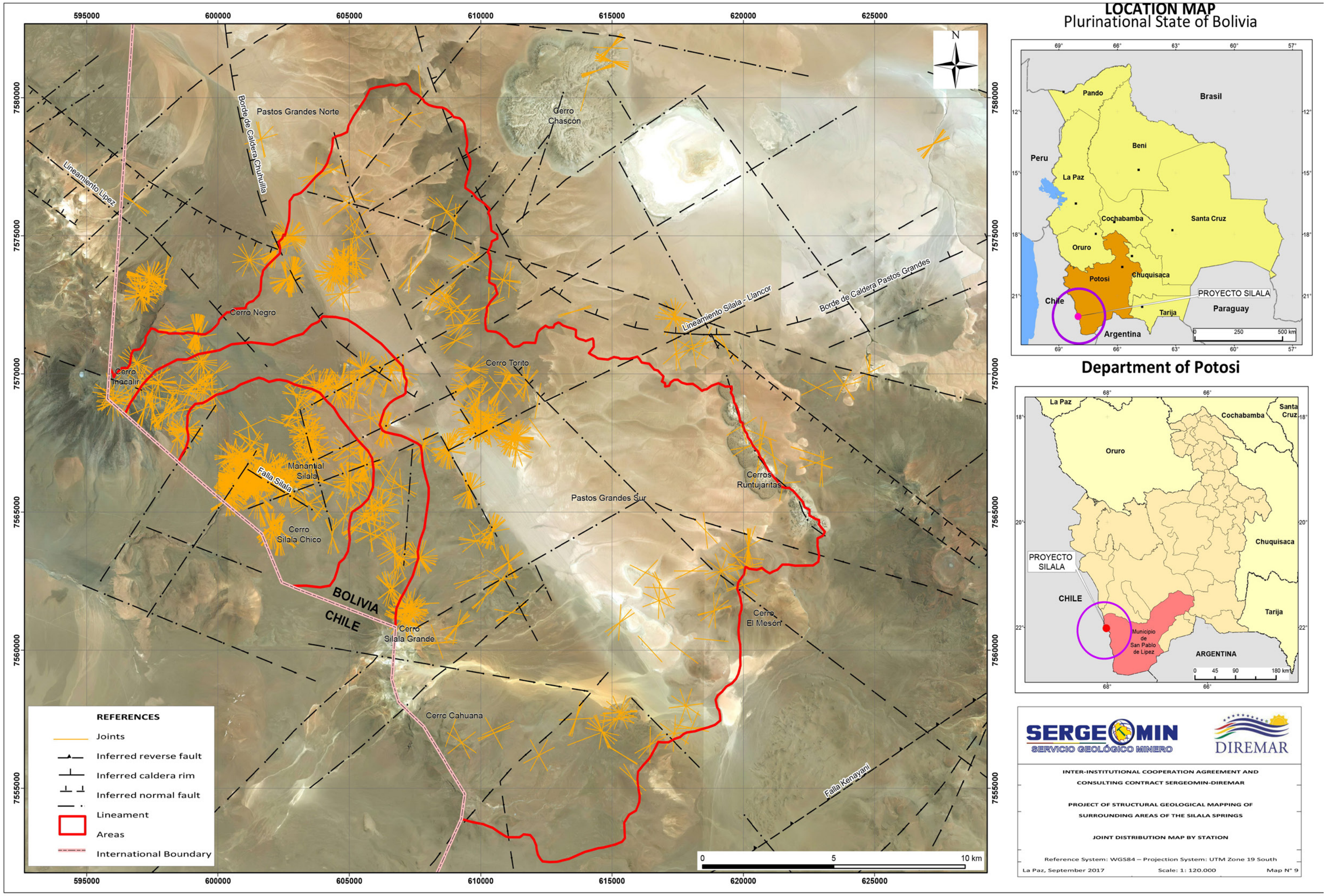
LOCATION MAP
Plurinational State of Bolivia
Department of Potosi
PROYECTO SILALA
Pando
Brasil
Beni
Peru
La Paz
Cochabamba
Santa Cruz
Oruro
Potosi
Chuquisaca
Chile
Tarija
Paraguay
Argentina
Municipio de San Pablo de Lipez
CHILE
ARGENTINA
REFERENCES
Joints
Inferred reverse fault
Inferred caldera rim
Inferred normal fault
Lineament
Areas
International Boundary
Pastos Grandes Norte
Borde de Caldera Chuhuilla
Lineamiento Lipez
Cerro Chascon
Cerro Negro
Cerro Inacaliri
Cerro Torito
Lineamiento Silala - Llancor
Borde de Caldera Pastos Grandes
Manantial Silala
Falla Silala
Cerro Silala Chico
Pastos Grandes Sur
Cerros Runtujaritas
BOLIVIA
CHILE
Cerro Silala Grande
Cerro El Meson
Cerro Cahuana
Falla Kenayani
SERGEOMIN
SERVICIO GEOLÓGICO MINERO
DIREMAR
INTER-INSTITUTIONAL COOPERATION AGREEMENT AND CONSULTING CONTRACT SERGEOMIN-DIREMAR
PROJECT OF STRUCTURAL GEOLOGICAL MAPPING OF SURROUNDING AREAS OF THE SILALA SPRINGS
JOINT DISTRIBUTION MAP BY STATION
Reference System: WGS84 – Projection System: UTM Zone 19 South
La Paz, September 2017
Scale: 1: 120.000
Map N° 9

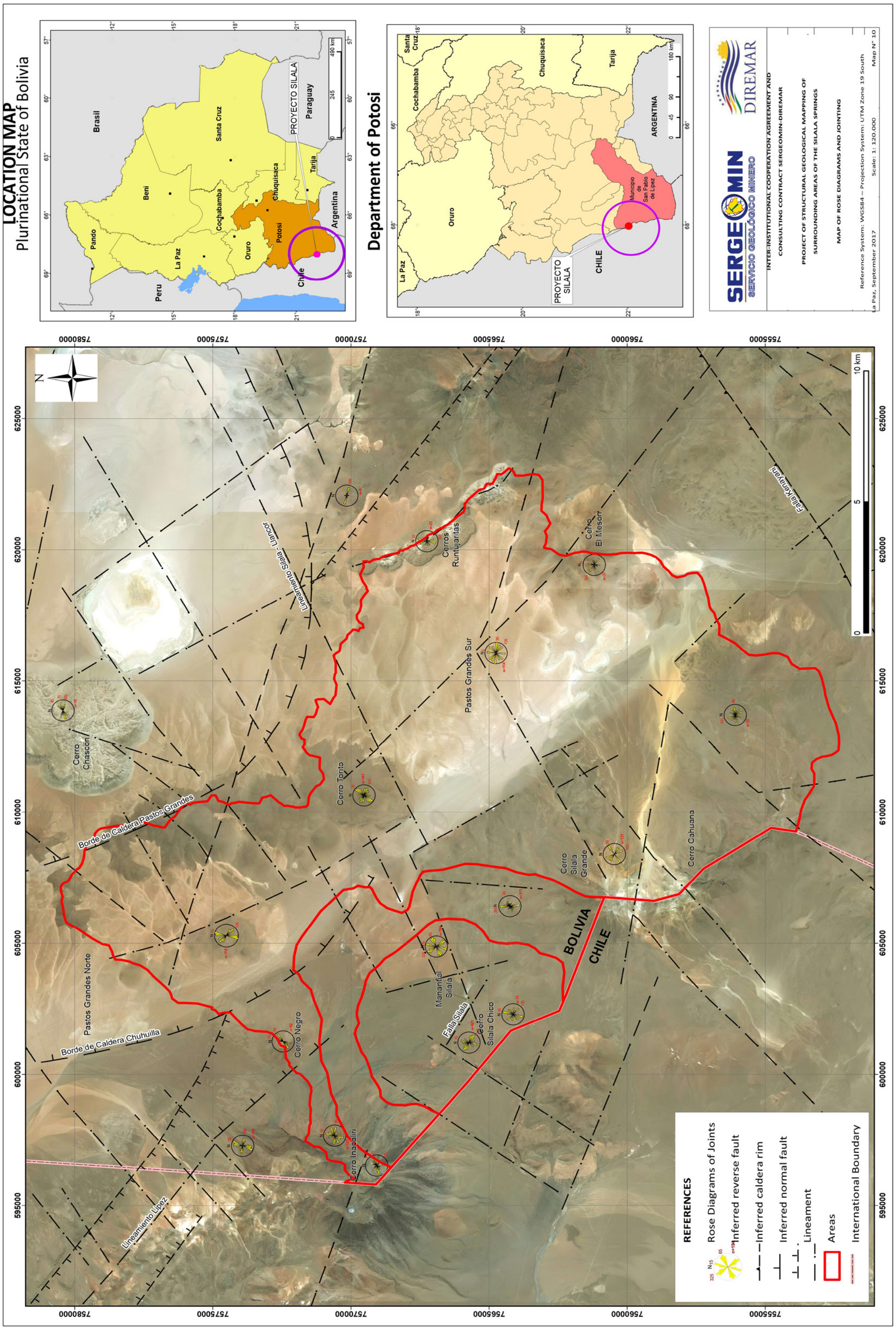
LOCATION MAP
Plurinational State of Bolivia
PROYECTO SILALA
Department of Potosi
Municipio de San Pablo de Lipez
PROYECTO SILALA
SERGEOMIN
SERVICIO GEOLÓGICO MINERO
DIREMAR
INTER-INSTITUTIONAL COOPERATION AGREEMENT AND CONSULTING CONTRACT SERGEOMIN-DIREMAR
PROJECT OF STRUCTURAL GEOLOGICAL MAPPING OF SURROUNDING AREAS OF THE SILALA SPRINGS
MAP OF ROSE DIAGRAMS AND JOINTING
Reference System: WGS84 – Projection System: UTM Zone 19 South
La Paz, September 2017
Scale: 1: 120.000
Map N° 10
REFERENCES
Rose Diagrams of Joints
Inferred reverse fault
Inferred caldera rim
Inferred normal fault
Lineament
Areas
International Boundary
BOLIVIA
CHILE
Cerro Chascon
Cerro Torito
Cerros Runtujarias
Cerro El Mesor
Pastos Grandes Sur
Pastos Grandes Norte
Cerro Negro
Cerro Inacaliri
Manantial Silala
Falla Silala
Cerro Silala Chico
Cerro Silala Grande
Cerro Cahuana
Borde de Caldera Pastos Grandes
Borde de Caldera Chuhuilla
Lineamiento Silala - Llanor
Lineamiento Lipez
Falla Khayani

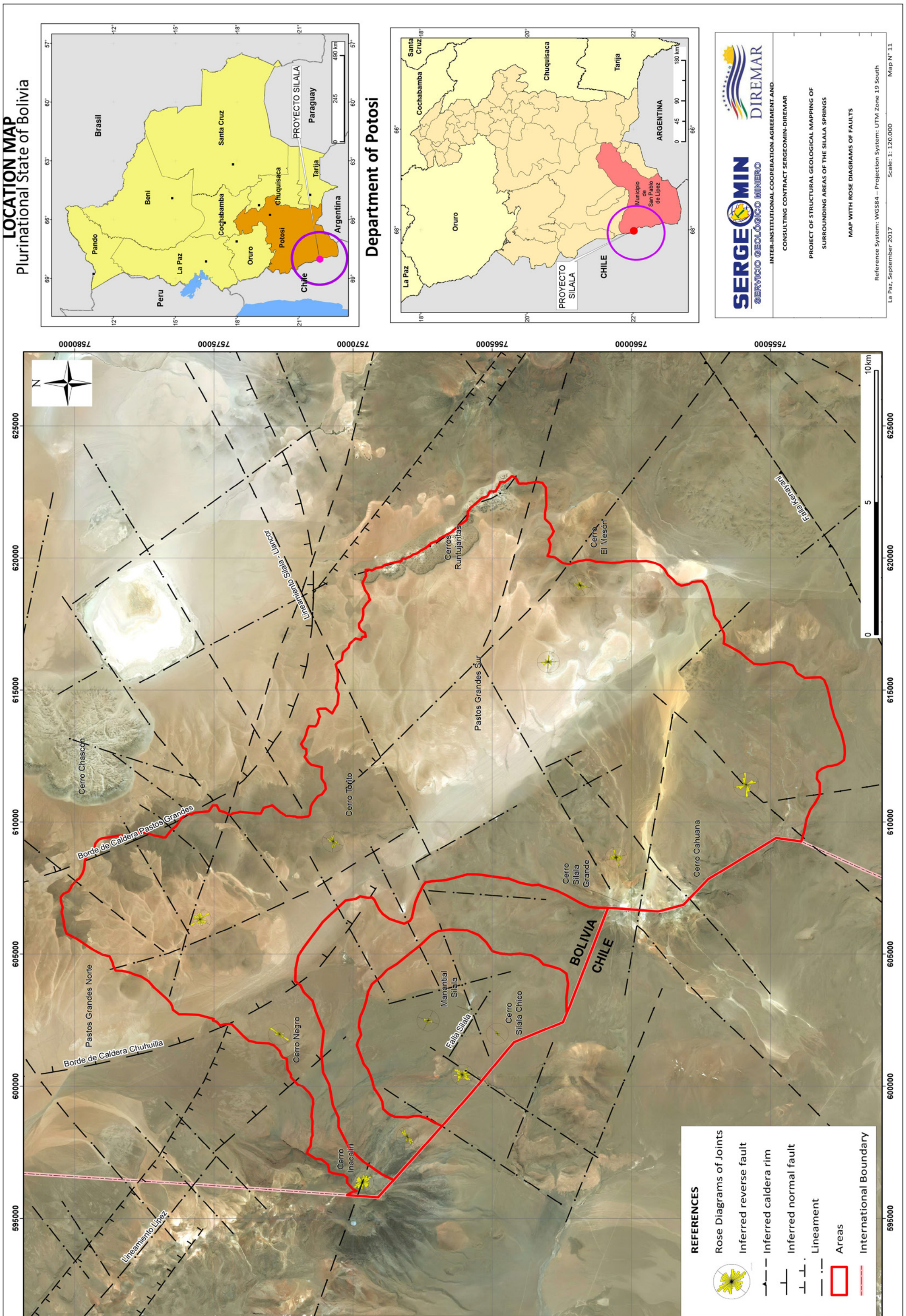

LOCATION MAP
Plurinational State of Bolivia
Department of Potosi
PROYECTO SILALA
Brasil
Pando
Beni
Santa Cruz
La Paz
Cochabamba
Oruro
Potosi
Chuquisaca
Tarija
Paraguay
Argentina
Chile
Peru
Municipio de San Pablo de Lipez
ARGENTINA
CHILE
SERGEOMIN
SERVICIO GEOLÓGICO MINERO
DIREMAR
INTER-INSTITUTIONAL COOPERATION AGREEMENT AND CONSULTING CONTRACT SERGEOMIN-DIREMAR
PROJECT OF STRUCTURAL GEOLOGICAL MAPPING OF SURROUNDING AREAS OF THE SILALA SPRINGS
MAP WITH ROSE DIAGRAMS OF FAULTS
Reference System: WGS84 – Projection System: UTM Zone 19 South
La Paz, September 2017
Scale: 1: 120,000
Map N° 11
Cerro Chascón
Borde de Caldera Pastos Grandes
Lineamiento Silala - Llajcor
Cerros Runtujantas
Cerro El Mesón
Pastos Grandes Sur
Cerro Todito
Pastos Grandes Norte
Borde de Caldera Chuhuilla
Cerro Negro
Manantial Silala
Falla Silala
Cerro Silala Chico
Cerro Silala Grande
Cerro Cahuana
Cerro Inacaliri
Lineamiento Lipez
Falla Kenyani
BOLIVIA
CHILE
REFERENCES
Rose Diagrams of Joints
Inferred reverse fault
Inferred caldera rim
Inferred normal fault
Lineament
Areas
International Boundary
0 5 10km

Annex B

Geological Profiles

GENERALIZED GEOLOGICAL SECTION OF THE SILALA SPRINGS

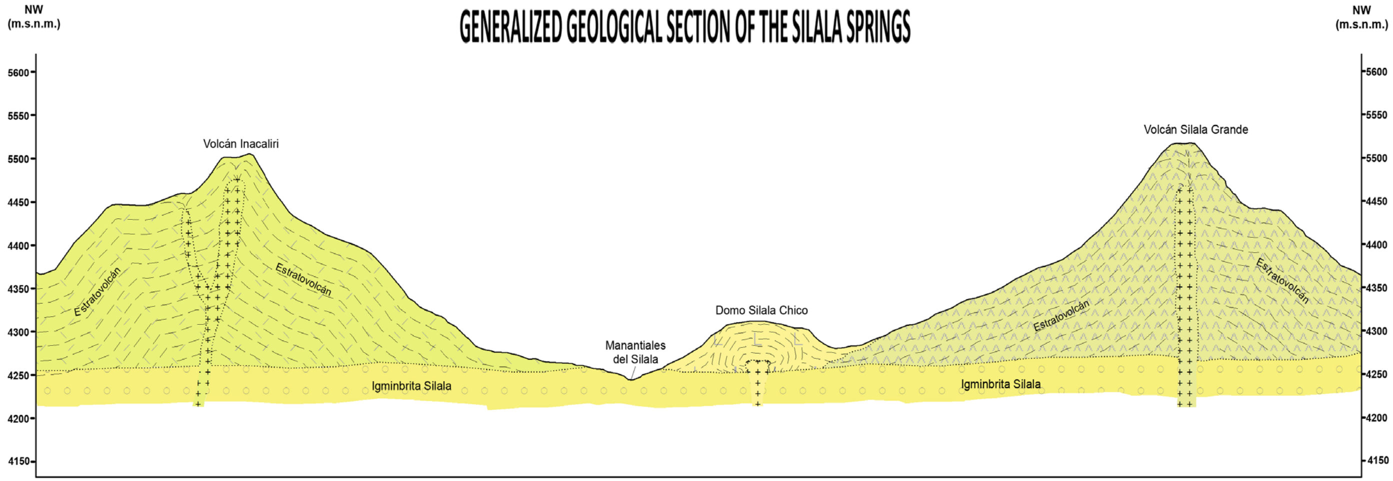

NW = NO

m.s.n.m. = m.a.s.l.

Volcán Inacaliri = Inacaliri Volcano

Estratovolcán = Stratovolcano

Ignimbrita Silala = Silala Ignimbrite

Manantiales del Silala = Silala Springs

Domo Silala Chico = Silala Chico Dome

Volcán Silala Grande = Silala Grande Volcano

SERGEOMIN
SERVICIO GEOLÓGICO MINERO

DIREMAR

INTER-INSTITUTIONAL COOPERATION AGREEMENT AND
CONSULTING CONTRACT SERGEOMIN-DIREMAR

PROJECT OF STRUCTURAL GEOLOGICAL MAPPING OF
SURROUNDING AREAS OF THE SILALA SPRINGS

GENERALIZED GEOLOGICAL SECTION

Reference System: WGS84 – Projection System: UTM Zone 19 South

La Paz, September 2017 Scale: 1: 6.000 Section N° 1

PERFIL "A"

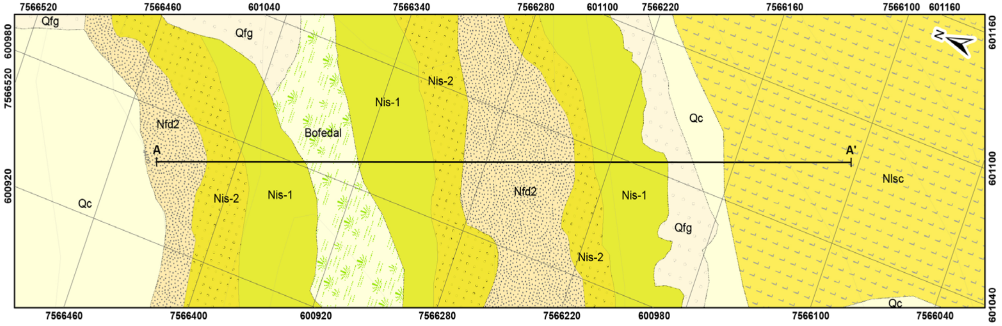

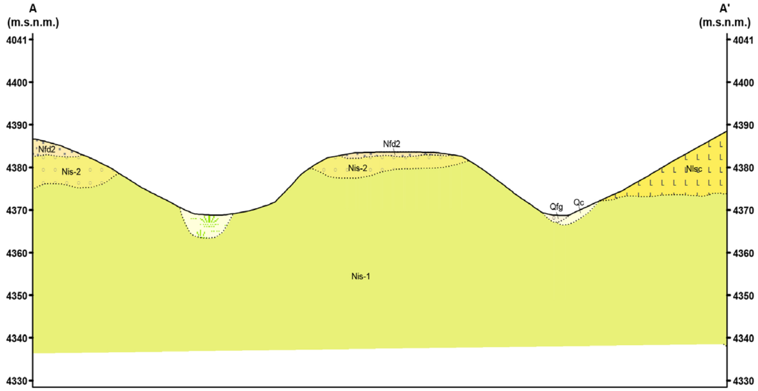

Escala horizontal y vertical 1:2.000

MAPA DE UBICACIÓN

Estado Plurinacional de Bolivia

REFERENCIAS

Qc	Dep. Coluvial	Cantos y bloques
Qfg	Dep. Fluvio glacial	Gravas, arenas y arcillas
Nlsc	Lavas Silala Chico	Porfídicas grisácea, laminadas o en bloques, bandeamiento fluidal. Andecita de bt, ads-bt-hb-cpx
Nfd2	Flujo de Detritos 2	Depósitos gris marrón de Cantos, gravas, pómez, arenas.
Nis-2	Ignimbrita Silala 2	Ignimbrita dacítica porfídicas marrón, en bloques, con clastos monomícticos andesíticos, qz-olg-cpx-p
Nis-1	Ignimbrita Silala 1	Ignimbrita dacítica porfídicas marrón claro-rosaceo, en bloques, con soldadura intermedia, qz-olg-cpx-p

SERGEOMIN SERVICIO GEOLÓGICO MINERO DIREMAR

INTER-INSTITUTIONAL COOPERATION AGREEMENT AND

CONSULTING CONTRACT SERGEOMIN-DIREMAR

PROJECT OF STRUCTURAL GEOLOGICAL MAPPING OF SURROUNDING AREAS OF THE SILALA SPRINGS

GEOLOGICAL PROFILE "A"

Reference System: WGS84 – Projection System: UTM Zone 19 South

La Paz, September 2017 Scale: 1: 2.000 Section N° 2

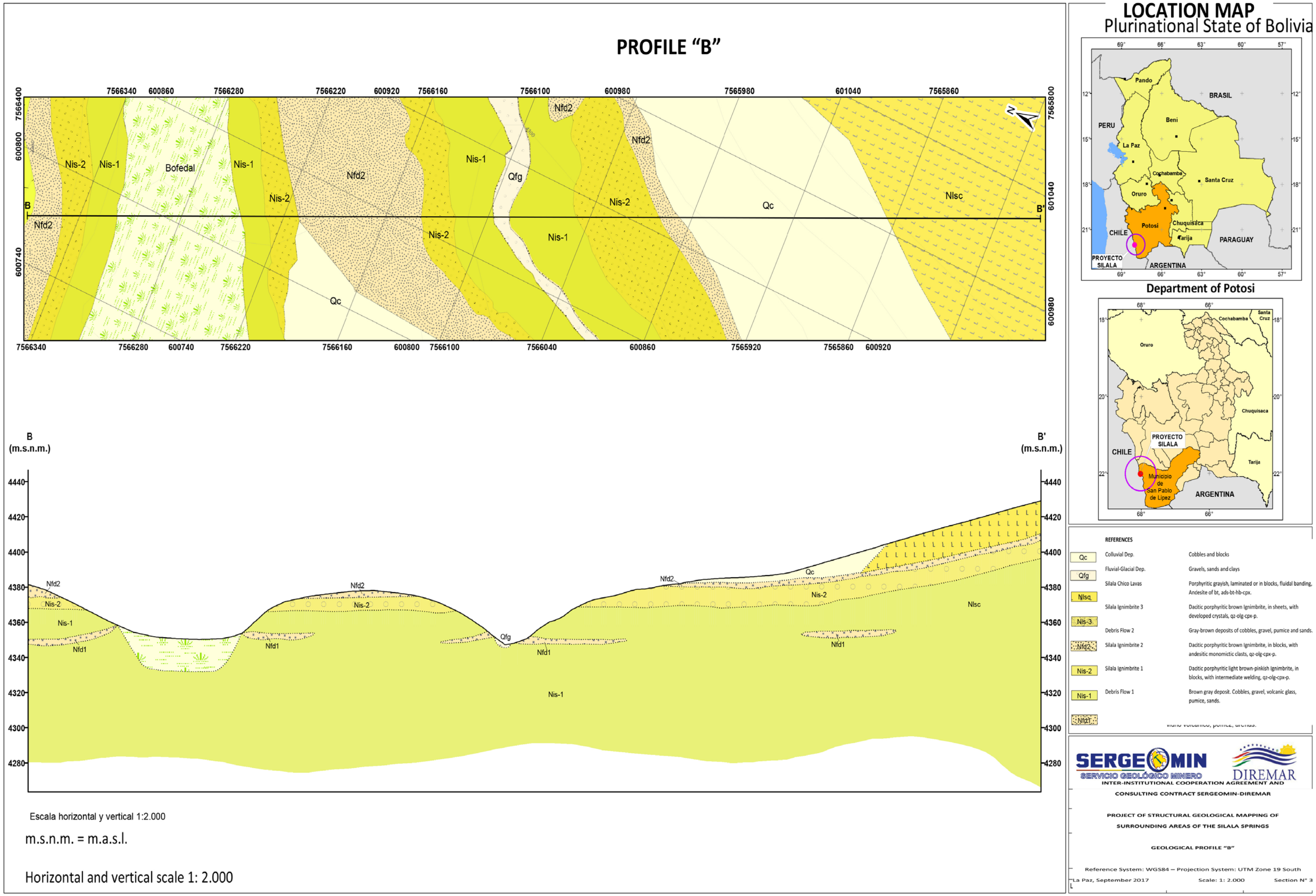
PROFILE "B"
LOCATION MAP
Plurinational State of Bolivia
Department of Potosi
PROYECTO SILALA
Municipio de San Pablo de Lipez
B
B'
(m.s.n.m.)
Qc
Qfg
Nlsc
Nis-1
Nis-2
Nfd1
Nfd2
Bofedal
Escala horizontal y vertical 1:2.000
m.s.n.m. = m.a.s.l.
Horizontal and vertical scale 1: 2.000
REFERENCES
Qc Colluvial Dep. Cobbles and blocks
Qfg Fluvial-Glacial Dep. Gravels, sands and clays
Nlsq Silala Chico Lavas Porphyritic grayish, laminated or in blocks, fluidal banding, Andesite of bt, ads-bt-hb-cpx.
Nis-3 Silala Ignimbrite 3 Dacitic porphyritic brown Ignimbrite, in sheets, with developed crystals, qz-olg-cpx-p.
Nfd2 Debris Flow 2 Gray-brown deposits of cobbles, gravel, pumice and sands.
Nis-2 Silala Ignimbrite 2 Dacitic porphyritic brown Ignimbrite, in blocks, with andesitic monomictic clasts, qz-olg-cpx-p.
Nis-1 Silala Ignimbrite 1 Dacitic porphyritic light brown-pinkish Ignimbrite, in blocks, with intermediate welding, qz-olg-cpx-p.
Nfd1 Debris Flow 1 Brown gray deposit. Cobbles, gravel, volcanic glass, pumice, sands.
SERGEOMIN
SERVICIO GEOLÓGICO MINERO
DIREMAR
INTER-INSTITUTIONAL COOPERATION AGREEMENT AND CONSULTING CONTRACT SERGEOMIN-DIREMAR
PROJECT OF STRUCTURAL GEOLOGICAL MAPPING OF SURROUNDING AREAS OF THE SILALA SPRINGS
GEOLOGICAL PROFILE "B"
Reference System: WGS84 – Projection System: UTM Zone 19 South
La Paz, September 2017
Scale: 1: 2.000
Section N° 3

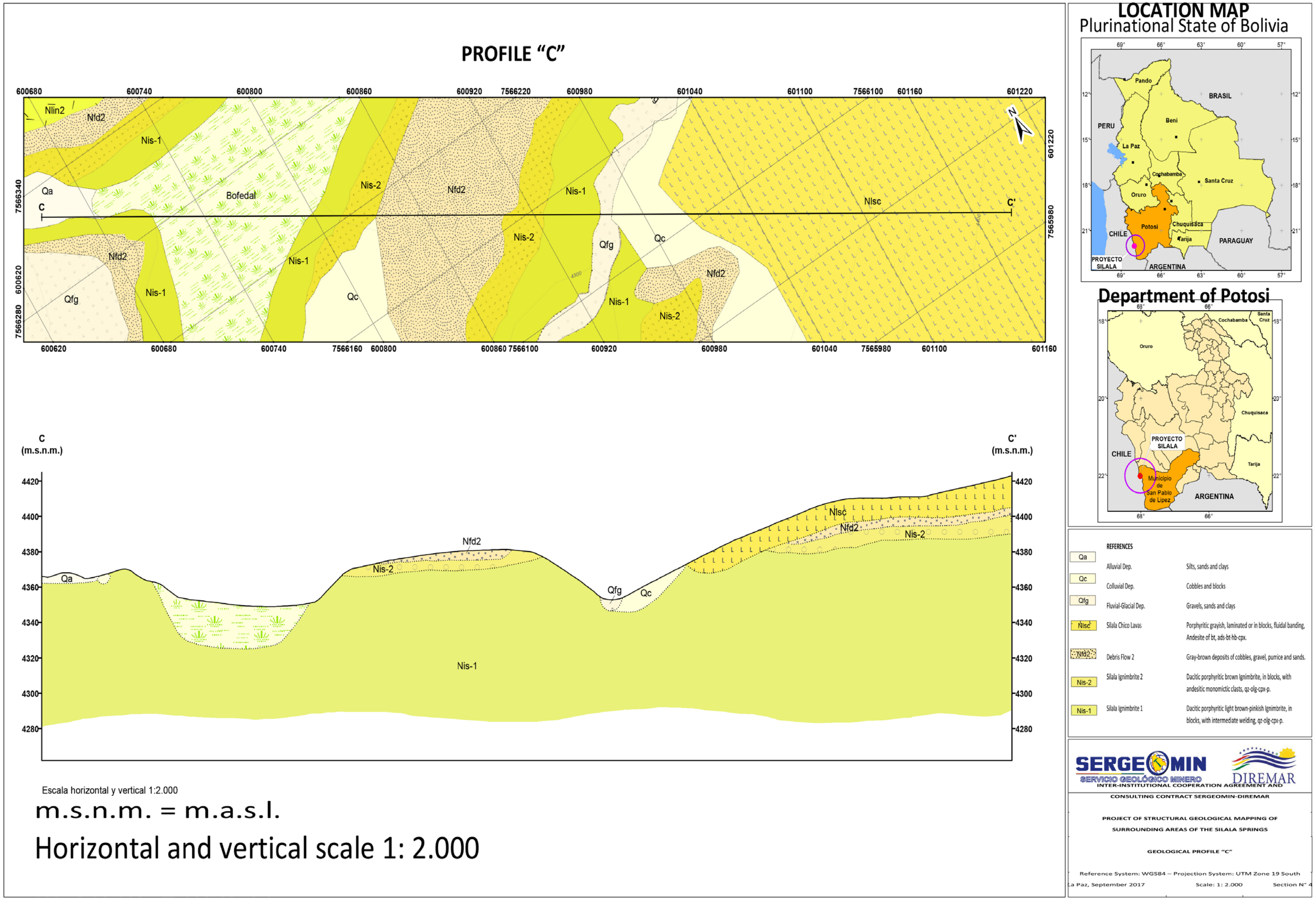
PROFILE "C"
LOCATION MAP
Plurinational State of Bolivia
Department of Potosi
REFERENCES
Qa Alluvial Dep. Silts, sands and clays
Qc Colluvial Dep. Cobbles and blocks
Qfg Fluvial-Glacial Dep. Gravels, sands and clays
Nlsc Silala Chico Lavas Porphyritic grayish, laminated or in blocks, fluidal banding, Andesite of bt, ads-bt-hb-cpx.
Nfd2 Debris Flow 2 Gray-brown deposits of cobbles, gravel, pumice and sands.
Nis-2 Silala Ignimbrite 2 Dacitic porphyritic brown Ignimbrite, in blocks, with andesitic monomictic clasts, qz-olg-cpx-p.
Nis-1 Silala Ignimbrite 1 Dacitic porphyritic light brown-pinkish Ignimbrite, in blocks, with intermediate welding, qz-olg-cpx-p.
SERGEOMIN SERVICIO GEOLÓGICO MINERO
DIREMAR
INTER-INSTITUTIONAL COOPERATION AGREEMENT AND
CONSULTING CONTRACT SERGEOMIN-DIREMAR
PROJECT OF STRUCTURAL GEOLOGICAL MAPPING OF SURROUNDING AREAS OF THE SILALA SPRINGS
GEOLOGICAL PROFILE "C"
Reference System: WGS84 – Projection System: UTM Zone 19 South
La Paz, September 2017 Scale: 1: 2.000 Section N° 4
C (m.s.n.m.)
C' (m.s.n.m.)
Nis-1
Nfd2
Nis-2
Nlsc
Qa
Qfg
Qc
Bofedal
Nlin2
Escala horizontal y vertical 1:2.000
m.s.n.m. = m.a.s.l.
Horizontal and vertical scale 1: 2.000

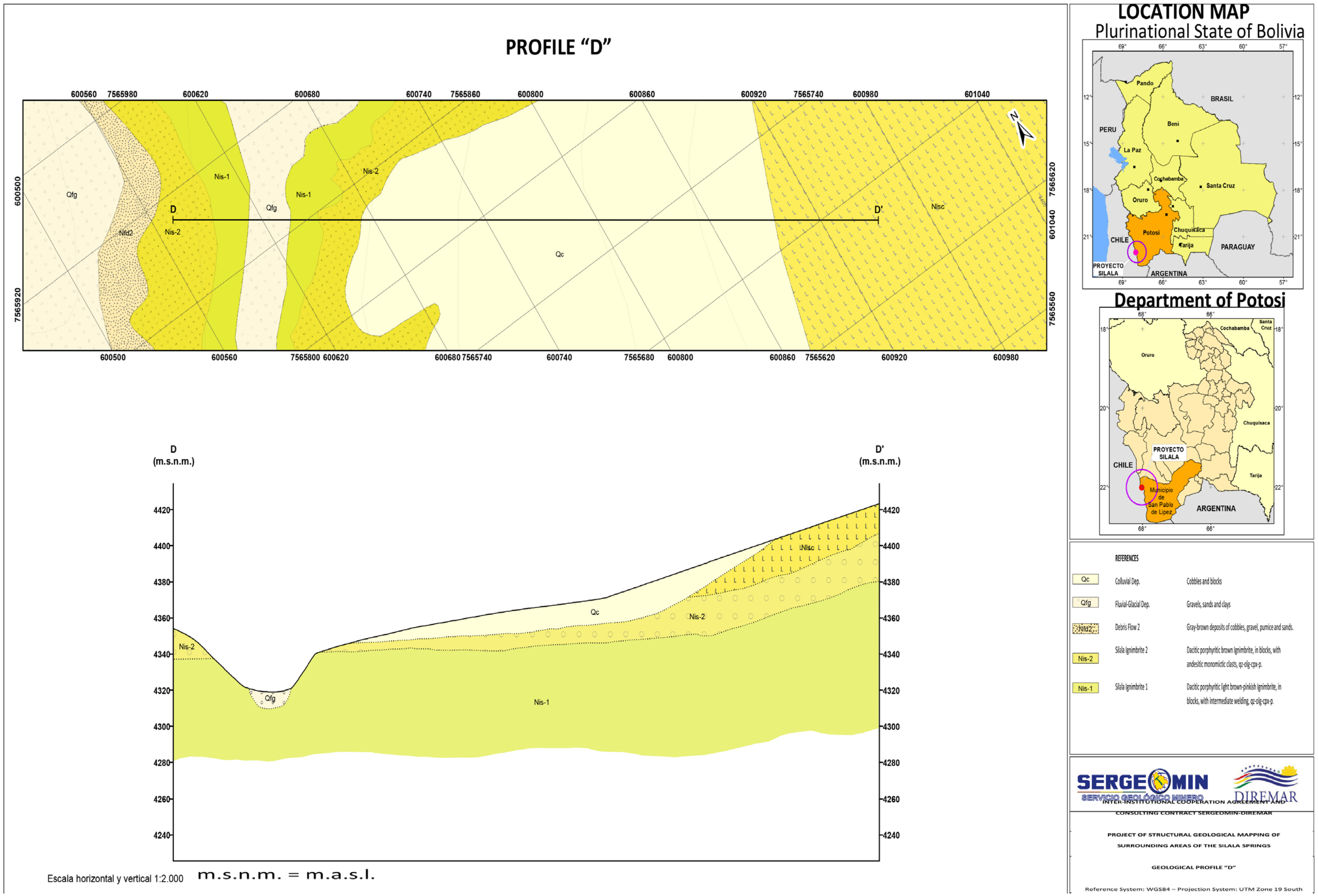
PROFILE "D"
600560
7565980
600620
600680
600740
7565860
600800
600860
600920
7565740
600980
601040
600500
7565920
601040
7565620
7565560
600500
600560
7565800 600620
600680 7565740
600740
7565680
600800
600860
7565620
600920
600980
Qfg
Nfd2
Nis-2
Nis-1
Qfg
Nis-1
Nis-2
Qc
Nlsc
D
D'
D
(m.s.n.m.)
D'
(m.s.n.m.)
4420
4400
4380
4360
4340
4320
4300
4280
4260
4240
Nis-2
Qfg
Nis-1
Qc
Nis-2
Nlsc
Escala horizontal y vertical 1:2.000
m.s.n.m. = m.a.s.l.
LOCATION MAP
Plurinational State of Bolivia
Pando
PERU
BRASIL
Beni
La Paz
Cochabamba
Santa Cruz
Oruro
Potosi
Chuquisaca
Tarija
CHILE
PARAGUAY
PROYECTO SILALA
ARGENTINA
Department of Potosi
Cochabamba
Santa Cruz
Oruro
Chuquisaca
PROYECTO SILALA
CHILE
Tarija
Municipio de San Pablo de Lipez
ARGENTINA
REFERENCES
Qc Colluvial Dep. Cobbles and blocks
Qfg Fluvial-Glacial Dep. Gravels, sands and clays
Nfd2 Debris Flow 2 Gray-brown deposits of cobbles, gravel, pumice and sands.
Nis-2 Silala Ignimbrite 2 Dacitic porphyritic brown Ignimbrite, in blocks, with andesitic monomictic clasts, qz-olg-cpx-p.
Nis-1 Silala Ignimbrite 1 Dacitic porphyritic light brown-pinkish Ignimbrite, in blocks, with intermediate welding, qz-olg-cpx-p.
SERGEOMIN
SERVICIO GEOLÓGICO MINERO
DIREMAR
INTER-INSTITUTIONAL COOPERATION AGREEMENT AND CONSULTING CONTRACT SERGEOMIN-DIREMAR
PROJECT OF STRUCTURAL GEOLOGICAL MAPPING OF SURROUNDING AREAS OF THE SILALA SPRINGS
GEOLOGICAL PROFILE "D"
Reference System: WGS84 – Projection System: UTM Zone 19 South

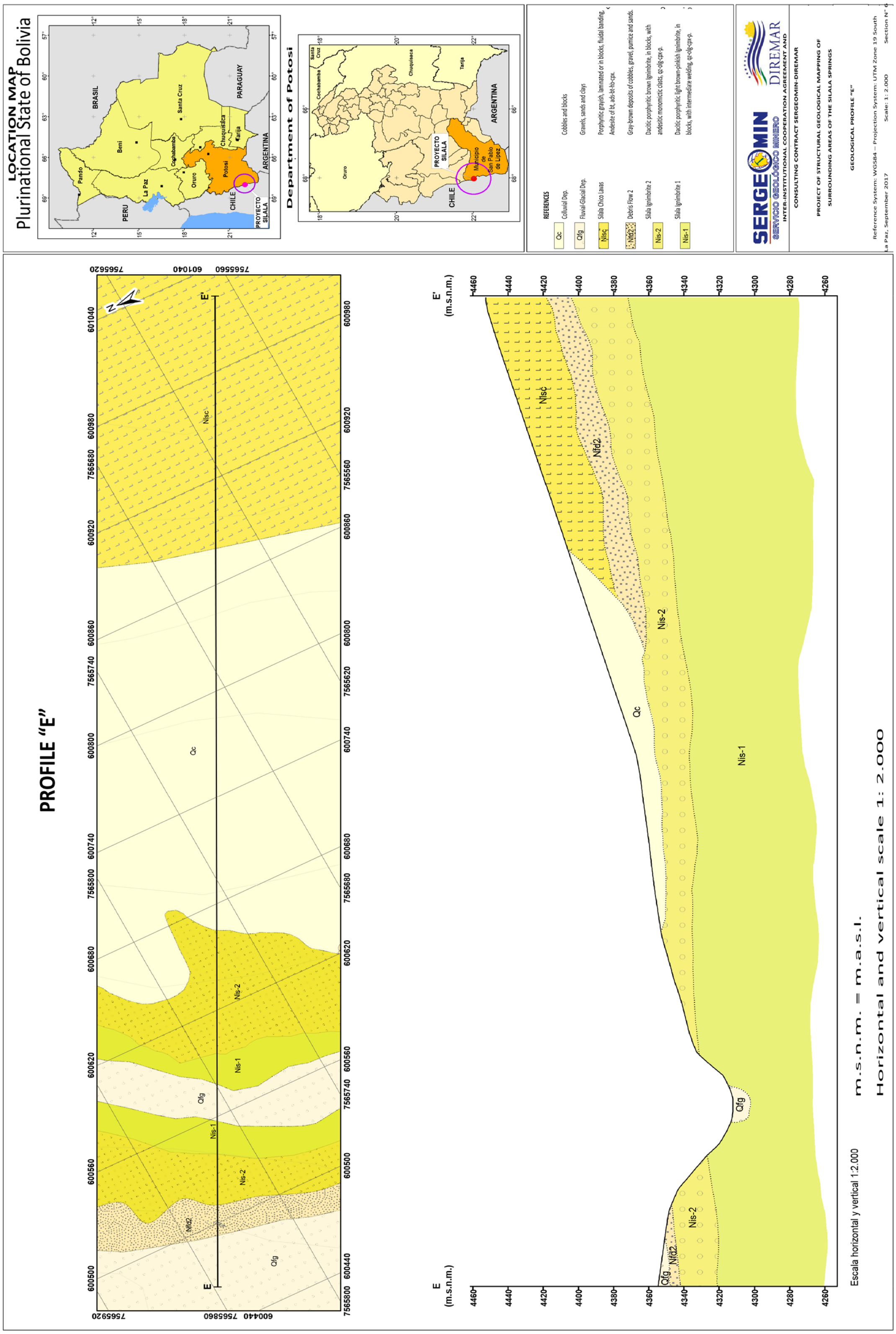
PROFILE "E"
LOCATION MAP
Plurinational State of Bolivia
Department of Potosi
PROYECTO SILALA
REFERENCES
Qc Colluvial Dep. Cobbles and blocks
Qfg Fluvial-Glacial Dep. Gravels, sands and clays
Nlsc Silala Chico Lavas
Nfd2 Debris Flow 2 Gray-brown deposits of cobbles, gravel, pumice and sands.
Nis-2 Silala Ignimbrite 2
Nis-1 Silala Ignimbrite 1
SERGEOMIN
SERVICIO GEOLÓGICO MINERO
DIREMAR
INTER-INSTITUTIONAL COOPERATION AGREEMENT AND
CONSULTING CONTRACT SERGEOMIN-DIREMAR
PROJECT OF STRUCTURAL GEOLOGICAL MAPPING OF
SURROUNDING AREAS OF THE SILALA SPRINGS
GEOLOGICAL PROFILE "E"
Reference System: WGS84 – Projection System: UTM Zone 19 South
Scale: 1: 2.000
La Paz, September 2017
E (m.s.n.m.)
E' (m.s.n.m.)
Escala horizontal y vertical 1:2.000
m.s.n.m. = m.a.s.l.
Horizontal and vertical scale 1: 2.000

PROFILE "F"

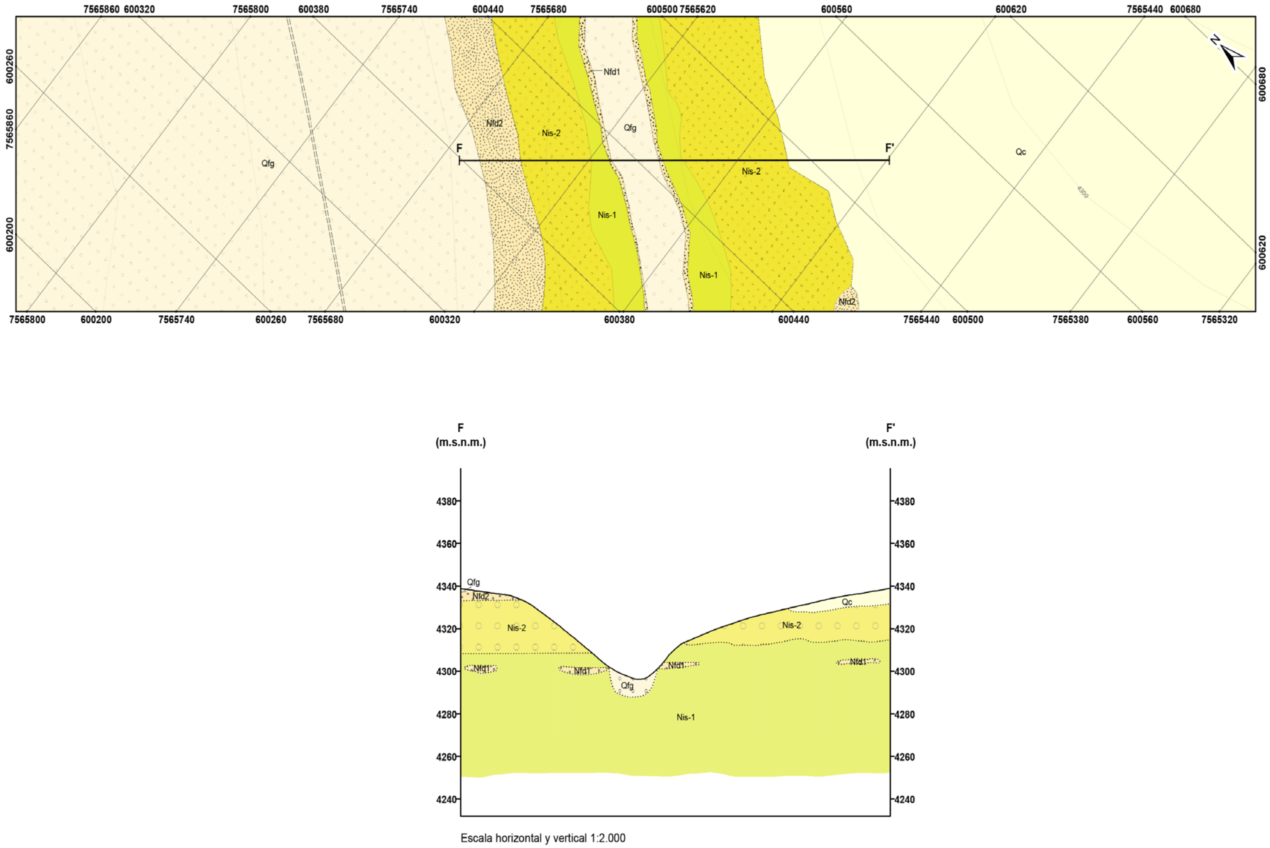

m.s.n.m. = m.a.s.l.

Horizontal and vertical scale 1: 2.000

LOCATION MAP
Plurinational State of Bolivia

Department of Potosi

REFERENCES

Qc	C	Colluvial Dep.	Cobbles and blocks
Qfg	C	Fluvial-Glacial Dep.	Gravels, sands and clays
Nfd2	F	Debris Flow 2	Gray-brown deposits of cobbles, gravel, pumice and sands.
Nis-2	Ig	Silala Ignimbrite 2	Dacitic porphyritic brown Ignimbrite, in blocks, with andesitic monomictic clasts, qz-olg-cpx-p.
Nis-1	Ig	Silala Ignimbrite 1	Dacitic porphyritic light brown-pinkish Ignimbrite, in blocks, with intermediate welding, qz-olg-cpx-p.
Nfd1	Fl	Debris Flow 1	Brown gray deposit. Cobbles, gravel, volcanic glass, pumice, sands.

SERGEOMIN
SERVICIO GEOLÓGICO MINERO
DIREMAR
INTER-INSTITUTIONAL COOPERATION AGREEMENT AND
CONSULTING CONTRACT SERGEOMIN-DIREMAR

PROJECT OF STRUCTURAL GEOLOGICAL MAPPING OF SURROUNDING AREAS OF THE SILALA SPRINGS

GEOLOGICAL PROFILE "F"

Reference System: WGS84 – Projection System: UTM Zone 19 South

La Paz, September 2017 | Scale: 1: 2.000 | Section N° 7

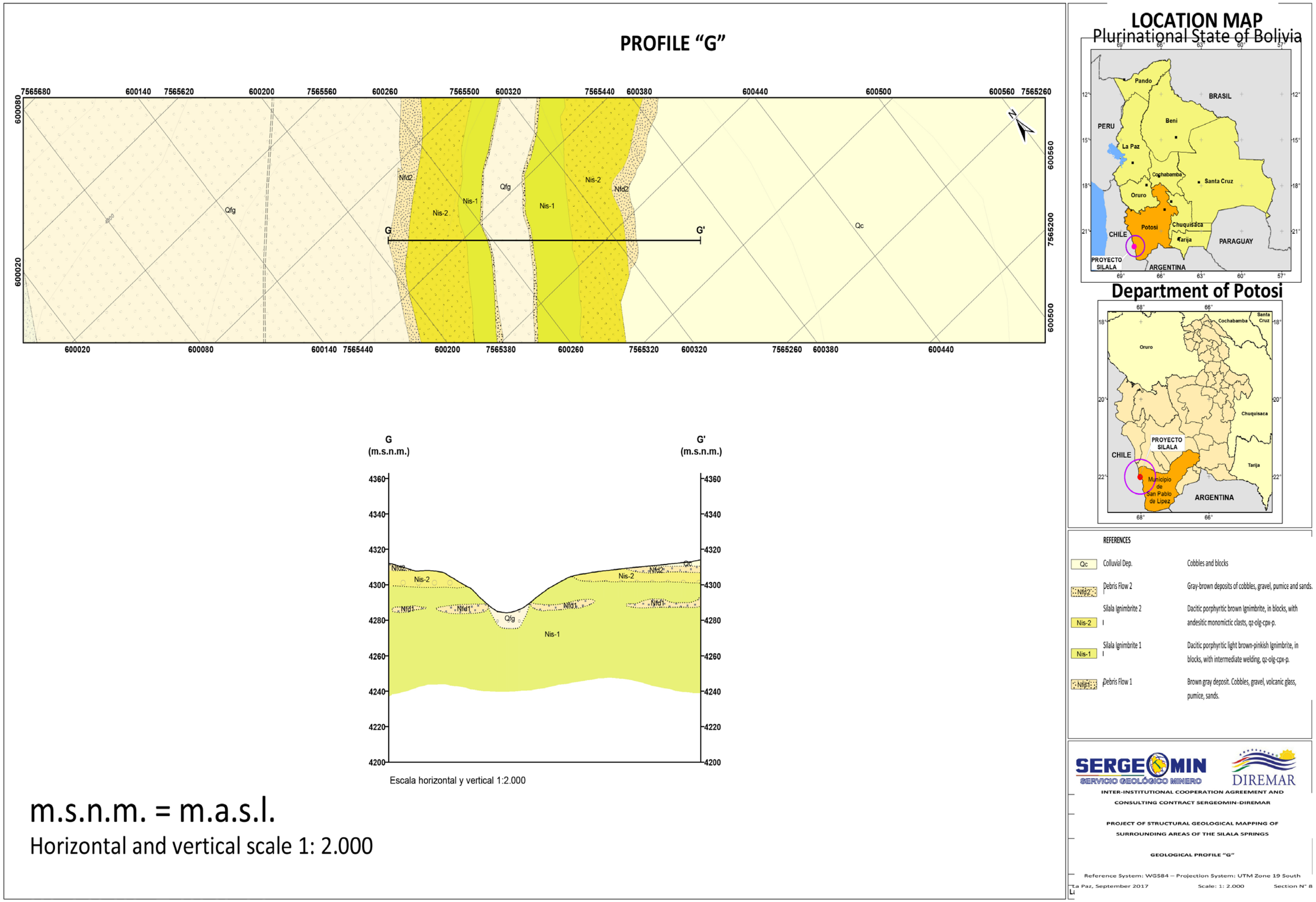
PROFILE "G"
7565680
600140
7565620
600200
7565560
600260
7565500
600320
7565440
600380
600440
600500
600560
7565260
600080
600020
600560
7565200
600500
600020
600080
600140
7565440
600200
7565380
600260
7565320
600320
7565260
600380
600440
Qfg
Nfd2
Nis-2
Nis-1
Qfg
Nis-1
Nis-2
Nfd2
Qc
G
G'
G
(m.s.n.m.)
G'
(m.s.n.m.)
4360
4340
4320
4300
4280
4260
4240
4220
4200
Nfd2
Nis-2
Nfd1
Qfg
Nis-1
Qc
Escala horizontal y vertical 1:2.000
m.s.n.m. = m.a.s.l.
Horizontal and vertical scale 1: 2.000
LOCATION MAP
Plurinational State of Bolivia
Pando
BRASIL
PERU
Beni
La Paz
Cochabamba
Santa Cruz
Oruro
Potosi
Chuquisaca
Tarija
CHILE
PARAGUAY
PROYECTO SILALA
ARGENTINA
Department of Potosi
Oruro
Cochabamba
Santa Cruz
Chuquisaca
PROYECTO SILALA
CHILE
Tarija
Municipio de San Pablo de Lipez
ARGENTINA
REFERENCES
Qc
Colluvial Dep.
Cobbles and blocks
Nfd2
Debris Flow 2
Gray-brown deposits of cobbles, gravel, pumice and sands.
Nis-2
Silala Ignimbrite 2
Dacitic porphyritic brown Ignimbrite, in blocks, with andesitic monomictic clasts, qz-olg-cpx-p.
Nis-1
Silala Ignimbrite 1
Dacitic porphyritic light brown-pinkish Ignimbrite, in blocks, with intermediate welding, qz-olg-cpx-p.
Nfd1
Debris Flow 1
Brown gray deposit. Cobbles, gravel, volcanic glass, pumice, sands.
SERGEOMIN
SERVICIO GEOLÓGICO MINERO
DIREMAR
INTER-INSTITUTIONAL COOPERATION AGREEMENT AND
CONSULTING CONTRACT SERGEOMIN-DIREMAR
PROJECT OF STRUCTURAL GEOLOGICAL MAPPING OF
SURROUNDING AREAS OF THE SILALA SPRINGS
GEOLOGICAL PROFILE "G"
Reference System: WGS84 – Projection System: UTM Zone 19 South
La Paz, September 2017
Scale: 1: 2.000
Section N° 8

Annex C

Results of laboratory analysis

STRATEGIC OFFICE FOR THE MARITIME CLAIM, SILALA AND INTERNATIONAL WATER RESOURCES
GEOLOGICAL MAPPING OF THE AREA SURROUNDING THE SILALA SPRINGS
SUMMARY LABORATORY TABLE

N°	East (UTM)	North (UTM)	Elevation (m.a.s.l.)	Elevation (m.a.s.l.)	Sent to laboratory	Rock Name	Petrographic Result	Mineralogical Result (Mineral Associations)
1	601181	7565996	4457	7801	SERGEOMIN	LAVA INTERMEDIA	ANDESITA BIOTITICA	
2	604895	7567297	4541	7802	SERGEOMIN	TOBA VITRO CRISTALINA	DACITA BIOTITICA	
3	605449	7566078	4602	7803	SERGEOMIN	LAVA INTERMEDIA	ANDESITA PIROXENICA	
4	608499	7567690	4595	7804	SERGEOMIN	LAVA INTERMEDIA	ANDESITA BIOTITICA	
5	609737	7568016	4597	7805	SERGEOMIN	LAVA ACIDA	DACITA BIOTITICA	
6	606789	7561214	5649	7806	SERGEOMIN	LAVA INTERMEDIA	ANDESITA PIROXENICA	
7	606758	7562878	5041	7807	SERGEOMIN	TOBA CRISTALO VITREA	IGNIMBRITA ANDESITICA	Magnetita-Hematita-Limonita
8	607192	7567230	4601	7808	SERGEOMIN	TOBA CRISTALO VITREA	IGNINBRITA ANDESITICA	Magnetita-Hematita-Limonita
9	600816	7566953	4485	7809	SERGEOMIN	LAVA INTERMEDIA	ANDESITA BIOTITICA	
10	600661	7567938	4547	7810	SERGEOMIN	LAVA BASICA	BASALTO PIROXENICO	
11	600166	7569312	4671	7811	SERGEOMIN	TOBA LITICA INTERMEDIA	ANDESITA PIROXENICA	
12	599317	7568831	4759	7813	SERGEOMIN	TOBA SOLDADA INTERMEDIA	IGNIMBRITA ANDESITICA	
13	603126	7565890	4422	7814	SERGEOMIN	TOBA INTERMEDIA	ANDESITA HORNBLENDICA	
14	603483	7564079	4558	7816	SERGEOMIN	LAVA INTERMEDIA	ANDESITA PIROXENICA	
15	606447	7562228	5165	7817	SERGEOMIN	LAVA INTERMEDIA	ANDESITA PIROXENICA	
16	606447	7562228	5165	7818	SERGEOMIN	LAVA INTERMEDIA	ANDESITA PIROXENICA	
17	607792	7564663	4802	7820	SERGEOMIN	LAVA INTERMEDIA	ANDESITA PIROXENICA	
18	601256	7572117	5181	7821	SERGEOMIN	LAVA INTERMEDIA	ANDESITA HORNBLENDICA	
19	601256	7572117	5181	7822	SERGEOMIN	LAVA INTERMEDIA	ANDESITA HORNBLENDICA	
20	606578	7568225	4555	7824	SERGEOMIN	VOLCANO SEDIMENTARIA	ARCILLITA	
21	600813	7566226	4367	7702	SERGEOMIN	TOBA CRISTALO VITREA	IGNINBRITA ANDESITICA	Hematita-Magnetita-Calcopirita Limonita
22	600973	7566397	4395	7706	SERGEOMIN	TOBA CRISTALO VITREA	IGNINBRITA ANDESITICA	Hematita-Magnetita-Calcopirita Limonita
23	604396	7576010	4522	7708	SERGEOMIN	TOBA	IGNIMBRITA ANDESITICA	
24	601942	7564641	4606	7712	SERGEOMIN	LAVA ACIDA	DACITA BIOTITICA	
25	602052	7564099	4756	7713	SERGEOMIN	LAVA INTERMEDIA	ANDESITA BIOTITICA CUARZOSA	
26	606242	7568071	4593	7716	SERGEOMIN	TOBA VITRO CRISTALINA	DACITA BIOTITICA	
27	600879	7566738	4437	7717	SERGEOMIN	TOBA VITRO CRISTALINA	DACITA BIOTITICA	
28	603557	7567635	4500	7720	SERGEOMIN	LAVA INTERMEDIA	ANDESITA CUARZOSA	
29	605051	7569399	4580	7721	SERGEOMIN	TOBA VITRO CRISTALINA	DACITA BIOTITICA	
N°	**ESTE (UTM)**	**NORTE (UTM)**	**ELEVACION (m.s.n.m)**	**CODIGO MUESTRA**	**ENVIADOS LABORATORIO**	**NOMBRE DE LA ROCA**	**RESULTADO PETROGRÁFICO**	**RESULTADO MINERAGRAFICO (Asociaciones Minerales)**
30	611232	7567663	4626	7722	SERGEOMIN	TOBA VITRO CRISTALINA	DACITA BIOTITICA	

31	611225	7567577	4640	7723	SERGEOMIN	TOBA VITRO CRISTALINA	DACITA BIOTITICA	
32	609442	7569033	4630	7726	SERGEOMIN	LAVA ACIDA	DACITA DE BIOTITA Y HORBLENDA	
33	601557	7573260	4834	7727	SERGEOMIN	LAVA INTERMEDIA	ANDESITA BIOTITICA OXIDADA	
34	605330	7574972	4741	7729	SERGEOMIN	LAVA INTERMEDIA	ANDESITA BIOTITICA OXIDADA	
35	602573	7575219	4607	7732	SERGEOMIN	LAVA INTERMEDIA	ANDESITA BIOTITICA OXIDADA	
36	610800	7562642	4647	7825	SERGEOMIN	LAVA INTERMEDIA	ANDESITA PIROXENICA	
37	619857	7562113	5107	7827	SERGEOMIN	LAVA ACIDA	DACITA PIROXENICA	
38	608546	7556911	5420	7830	SERGEOMIN	LAVA INTERMEDIA	ANDESITA HORNBLENDICA	
39	598653	7567307	4609	7833	SERGEOMIN	LAVA INTERMEDIA	ANDESITA HORNBLENDICA	
40	620023	7566597	4864	7737	SERGEOMIN	LAVA INTERMEDIA	ANDESITA PIROXENICA	
41	595872	7569264	5631	7743	SERGEOMIN	LAVA INTERMEDIA	ANDESITA HORNBLENDICA	

Lava intermedia = Intermediate lava
Toba vitro cristalina = Vitro crystal tuff
Lava ácida = Acidic lava
Toba cristalo vítrea = Glass crystal tuff
Lava básica = Basic lava
volcano sedimentaria = sedimentary volcano
Toba = Tuff

Andesítica Biotítica = Biotic Andesitic
Dacita Biotítica = Biotic Dacite
Andesita Piroxénica = Pyroxene Andesite
Andesítica Biotítica = Biotitic Andesitic
Ignimbrita Andesítica = Andesite Ignimbrite
Basalto Piroxénico = Pyroxene Basalt
Andesita hornbléndica = hornblende andesite
Arcillita = Arcillite
Andesita Biotítica Cuarzosa = Quartzite Biotitic Andesite
Dacita Piroxénica = Pyroxene Dacite
Dacita Biotítica y Hornbléndа = Biotic and Hornblende Dacite
Andesita Biotítica Oxidada = Oxidized Biotitic Andesite
Andesita hornbléndica = hornblende andesite
Magnetita – Hematita – Limonita = Magnetite – Hematite – Limonite

Hematita – Magnetita – Calcopirita – Limonita = Hematite – Magnetite – Chalcopyrite – Limonite

Annex 23.5

Appendix c

Tomás Frías Autonomous University (TFAU),
"Hydrogeological Characterization of the Silala
Springs", 2018

(English Translation)

[Front cover]

[Logos of the Tomas Frias Autonomous University and the Faculty of Geological Engineering]

“TOMAS FRIAS” AUTONOMOUS UNIVERSITY

OFFICE OF THE VICE-PRINCIPAL

FACULTY OF GEOLOGICAL ENGINEERING

INSTITUTE OF GEOLOGICAL – ENVIRONMENTAL RESEARCH

“HYDROGEOLOGICAL CHARACTERIZATION OF THE SILALA SPRINGS”

FINAL REPORT

(2018)

DIRECTION AND SUPERVISION BY:

Dr. Eng. Pedro Guido Lopez Cortes

VICE-PRINCIPAL

TOMAS FRIAS AUTONOMOUS UNIVERSITY

POTOSI – BOLIVIA

PRESENTATION OF THE RESEARCH WORK ENTITLED "HYDROGEOLOGICAL CHARACTERIZATION OF THE SILALA SPRINGS"

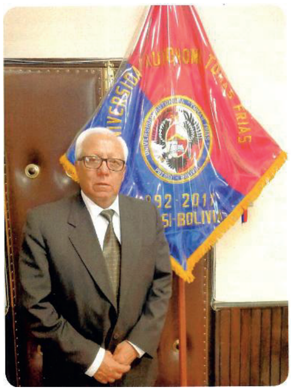

In my capacities as the chief Academic Authority of the Tomas Frias Autonomous University, I am pleased to present the research work carried out by the Faculty of Geological Engineering, with the Institute of Geological–Environmental Research and a group of professors committed to regional development.

With this perspective in mind, over this last period, the university has strengthened the Research Institutes of different Faculties, with the purpose of carrying out researches that have a social impact, reciprocating with the diligence that society demands from this House of Higher Studies and allowing their students to complete their theses to obtain their academic degree, as is the case of the Geological Engineering and Environmental Engineering careers.

One of the research works carried out by the aforementioned institute is the "**HYDROGEOLOGICAL CHARACTERIZATION OF THE SILALA SPRINGS**," as technical input for the existing issue related to these springs, the sovereignty of which, despite being found within the territory of the Potosi province, is now facing an unjustified claim filed by the Republic of Chile.

The results reported in said technical survey show that the springs are found within Bolivian territory, specifically in the Potosi Department and, in light of everything that is specified in the project, there should be absolute certainty that the technical aspects are settled by the adequate argumentation and substantiation presented in the final report, which is put to the consideration of the readers. It is up to the relevant institutions to take on the defense of this significant groundwater resource from a Historical–Legal perspective and as a State Policy.

The University hopes that the present technical study will constitute a fundamental contribution for the team of professionals that are dealing with the defense of the Silala springs as a principle of respect for the territory of our Homeland, preserving the rights of future generations.

Dr. Eng. Pedro Guido Lopez Cortes

VICE-PRINCIPAL OF THE TOMAS FRIAS AUTONOMOUS UNIVERSITY

TEAM OF TECHNICIANS

Dr. Eng. Pedro Guido Lopez Cortes	Vice-Principal of the Tomas Frias Autonomous University
M.Sc. Eng. Juan Carlos Erquicia Landeau	Director of the Geological – Environmental Research Institute
M. Sc. Eng. Jorge Diaz Zelada	Professor of the Geological Engineering Faculty
Eng. Yerko Wilber Lopez Velasquez	Professor of the Geological Engineering Faculty

LOGISTICS SUPPORT

INSTITUTE OF GEOLOGICAL – ENVIRONMENTAL RESEARCH

University Student Issabo Miranda Zamudio	Researcher of the Geological Engineering Faculty
University Student Gabriela Isabel Mealla Barrera	Researcher of the Geological Engineering Faculty
University Student Erice Loma Andia	Researcher of the Geological Engineering Faculty
University Student Salomon Medinaceli Terrazas	Researcher of the Geological Engineering Faculty

LOGISTICS SUPPORT IN THE FIELD

Field Geology students – GLG 831 S
Geophysics students 11- GLG 625
Hydrogeology students – GLG 834
Candidates to the Bachelor Degree

DIRECTION AND SUPERVISION

Dr. Eng. Pedro Guido Lopez Cortes

VICE-PRINCIPAL OF AUTONOMOUS THE TOMAS FRIAS UNIVERSITY

INDEX

FIGURES

PHOTOGRAPHS

ANNEXES

HYDROLOGICAL CHARACTERIZATION OF THE SILALA SPRINGS

ABSTRACT

We are honored to present the research work completed by the TOMAS FRIAS AUTONOMOUS UNIVERSITY, with the help of the Geological Engineering Faculty, as a response to the mandate of society as a whole in the face of the issue that arose in relation to the utilization of the waters of Silala Springs.

Said problem arose in 2004, when the Government of Chile proposed our nation a financial compensation of the 50% derived from its use of the spring waters of this groundwater resource, for a five-year term, in order to—meanwhile—carry out technical surveys that would demonstrate that the right [Chile claims over this resource] is based on the fact that this is a shared aquifer, and that natural and permanent waterbodies within Chilean territory recharge said aquifer. By 2006, earlier diagnosis surveys began to be carried out to address the issue.

In face of the above, and given that there are dissimilar opinions concerning the origin of the waters of the Silala Springs, it was decided that a scientific research ought to be performed regarding the following research topic: "CHARACTERIZATION OF THE SILALA SPRINGS," in the understanding that characterization means "defining, analyzing and determining relations," in order to DEFINE in clear terms the meaning of *Aquifer*, *High Andean Wetland* [hereinafter *Bofedal*], *Springs*, *Fossil waters* and *international course river*; ANALYZE, quantitatively, the surface waters by means of a water balance; MODEL the possible water scenarios derived from climate change and guarantee the availability of water for future generations; and DETERMINE the RELATION between surface water and groundwater resources, quantitatively and qualitatively.

In order to achieve this goal, a detailed structural geological mapping was prepared for the area where the springs well up, defining the area's rock types and the influence of primary and secondary porosity of colluvial-alluvial material and ignimbrite rocks.

Fifteen Vertical Electrical Soundings (VES) were preformed to define the thickness of the different formations of the area, up to a depth of 90 meters. In the areas close to where these profiles were carried out, permeability tests—with the falling head method—and infiltration speed tests—with the Kostiakov-equation double ring method—were also completed and yielded real values for these variables.

The surveys described above are contained in this report and, by having completed them, we believe we have complied with the bearing that the people deserve from the University. Thank you.

English translation prepared by DIREMAR. The original language text remains the authoritative one.

[Logo of the Tomas Frias Autonomous University]

CHAPTER I

GEOLOGY

[Logo of the Faculty of Geological Engineering]

[Letterhead on all pages: "Tomas Frias Autonomous University, Faculty of Geological Engineering"
"Hydrogeological characterization of the Silala Springs"]

CHAPTER I. GEOLOGICAL DESCRIPTION OF THE SILALA SPRINGS

1.1. DESCRIPTION OF THE AREA

1.1.1. Location

The surveyed area of the Silala Springs is located in Canton Quetena Grande, South Lipez Province, of Potosi Department. It is geographically located in the Western Cordillera of the Andes, at reference coordinates 7566000 North and 602000 East, UTM WGS84 ZONE 19 SUD. The area borders the international border with the Republic of Chile to the west, passing through boundary landmarks LXXIII, LXXIV and LXXV; the North Lipez province to the north; the San Antonio de Lipez and San Antonio de Esmoruco Cantons to the east; and the International border with the Republic of Argentina to the south (See Annex A.2, Map 1/8).

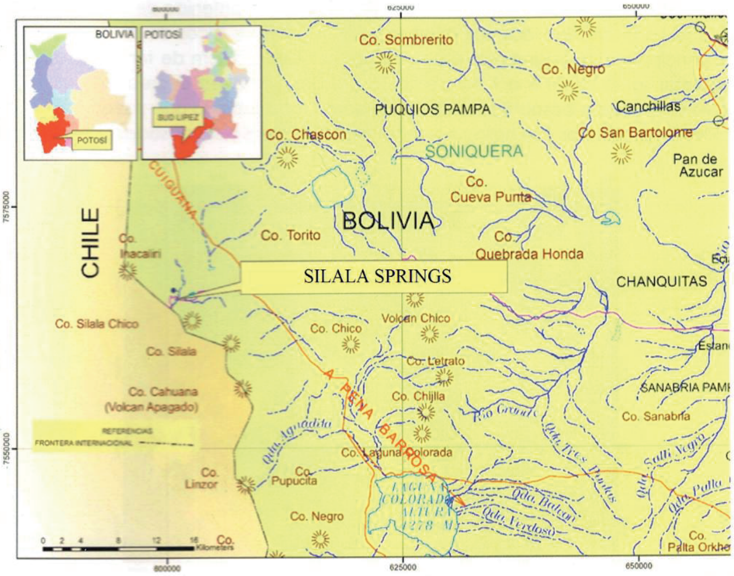

Figure 1.1. Location of the Silala Springs

The main access route to the area surveyed is the First Order Potosi – Uyuni paved road, with a distance of 220 Km; the second section comprises the Uyuni – San Cristobal second order road, with a distance of 90 km; and, finally, the third section the third order San Cristobal – Alota – Silala road, with a distance of 160 km. The total length comprises 470 Km, from Potosi city to the area where the Silala Springs well up.

1.1.2. Flora

The flora or vegetation cover present in the Silala region is poor, typical of the region's ecosystem and is represented by high altitude bofedals and a community of Puna desert thickets. The typical flora of the Mountain Range includes several types of thola (Parastrephia, Adesmia and Baccharis spp.) and yareta (Azorella compacta) plants, the latter of which grows sporadically on the slopes of the Inacaliri and Silala volcanoes. The yareta presents features of having been over-exploited and is considered an endangered species.

1.1.3. Wildlife

The wildlife of the area surveyed comprises varieties of species that are characteristic of the Bolivian High Plateau and Western Mountain Range habitats, with no endangered species having been recorded. The following can be mentioned:

- Vicuna (Vicugna vicugna) – Huari – Sawalla
- Viscacha, or Andean chinchillon (Lagidum viscaccia cuvieri)

Among the bird species, the following have been observed:

- Cordillerano Ostrich (Pterocnemia pennata) – Suri
- Andean partridge (Nothoprocta ornata) – Pisaka
- Andean seagull (Larus serranus)
- Blue billed Puna teal (Ana puna) – Chirokankana
- Andean swallow (Petrochelin andecola)

1.1.4. Climate

The Silala area presents a climate characteristic of high mountain desert areas, with extreme temperature variations. The mean monthly temperatures are also unimodal. The maximum temperatures are recorded from December to March, with the highest mean temperature recorded in December—3.9° C. The lowest temperatures are observed from April to August, with mean temperatures that fluctuate between 0° to -4.0° C. The highest mean annual temperature is of 14.2° C and the lowest mean annual temperature is of -15° C. These two extremes provide an approximate variation range of 29° C.

1.2. GEOLOGY

1.2.1. Regional geology

The area of the Silala Springs is located in the southern block of the Western Mountain Range and forms part of the Andes' Central Volcanic Zone. Its regional geology is dominated by the outcropping of materials formed from volcanic activity dating back from the Miocene to the Recent ages. This landscape was modelled by glacial Pleistocene–Holocene processes. The weathering, erosion and deposition processes are represented by unconsolidated Quaternary and Recent sediments that cover large parts of the area. The deposited materials form glacial, fluvioglacial, colluvial and alluvial deposits that comprise polygenic blocks or boulders, clasts of different rocks and sizes, and fine sediments as sand and lime.

By the late Pleistocene, other volcanic centers, as the Cerro Negro Volcano began to form and their effusive volcanism gave rise to andesitic lava deposits, which have covered the preexisting reliefs (Urquidi Barrau, F. Coordinator of the Study on the Geology, Hydrology, Hydrogeology and Environment of the Silala Springs, Final Edition, La Paz - Bolivia. June, 2003, pp. 9-10).

In the Silala ignimbrites, the regional basement is formed by layers of consolidated tuffs that bear the same name. These ignimbrites have a light pink to violet color, a dacitic composition and are made up of plagioclase, quartz, biotite and hornblende. They correspond to the calcalkaline series and are rich in K2O. Their SiO2 content varies between 63 to 66%. The volcanic glass matrix includes lithic fragments of different rock types—mainly pumice rock fragments of up to 10 cm in size—and its flattening index varies from 3 to 1. Data on their total thickness in the area is unavailable, given that their basal contact cannot be observed and that the rock type on which they rest is unknown. These are partially welded tuffs and are strongly fractured and jointed.

These ignimbrite mantles have an inclination to the west. According to radiometric data extrapolated from surrounding areas, these ignimbrites have an age of 7.8 +/- 0.3 million years (Mys), namely, they date back to the Upper Miocene (Choque, 1996; Lema & Ramos, 1996; Richter, et. al., 1992).

The Silala Chico hill Volcanic Dome. This volcanic body of reduced dimensions emerges to the northeast of the Silala volcano, intruding the Silala ignimbrites. It has an approximate basal diameter of 3 km and reaches an altitude of 4849 m.a.s.l. It is covered by dark gray porphyric andesitic-dacitic lavas, comprising 88 to 90% of plagioclase (andesite-labradorite) and 4 to 10% of Pyroxene. The dating completed with samples collected by the Regional Integration Project (RIP, hereinafter) show an age of 6.04 +/- 0.07 Myr for the Silala Chico hill volcanic dome (RIP, in preparation).

The Cerro Negro Volcanic Dome. This volcanic body is found on the margins of the surveyed area, in the northeast. It has a basal diameter of 2 km and an approximate 5200 m.a.s.l. and is composed of light gray andesitic rocks.

The Torito volcanic Dome. This volcanic dome is located in the western sector of the area surveyed. It has a dacitic and andesitic composition and an approximate altitude of 4900 m.a.s.l. Its basal diameter is of 1.6 Km, approximately (see Figure 1.2., p. 5).

1.2.2. Local geology

Locally, the area surveyed has developed in an effusive volcanic environment. The materials, formed as a result of volcanic activity, rest on the ―Silala Ignimbrites‖ and have an age of 7.8 +/- 0.3 million years, i.e. from the Upper Miocene (Choeque, 1996; Lema & Ramos, 1996; Richter, et. al., 1992). The ―Silala Ignimbrites‖ are divided in three horizons; the oldest ones correspond to ignimbrites that have a higher content of violet to whitish plagioclase, over which dacite composition ignimbrites, with consolidated Andesite fragments, rest. Ignimbrites rich in plagioclase–Na rest on top of the latter (See Figure 1.3, p. 11).

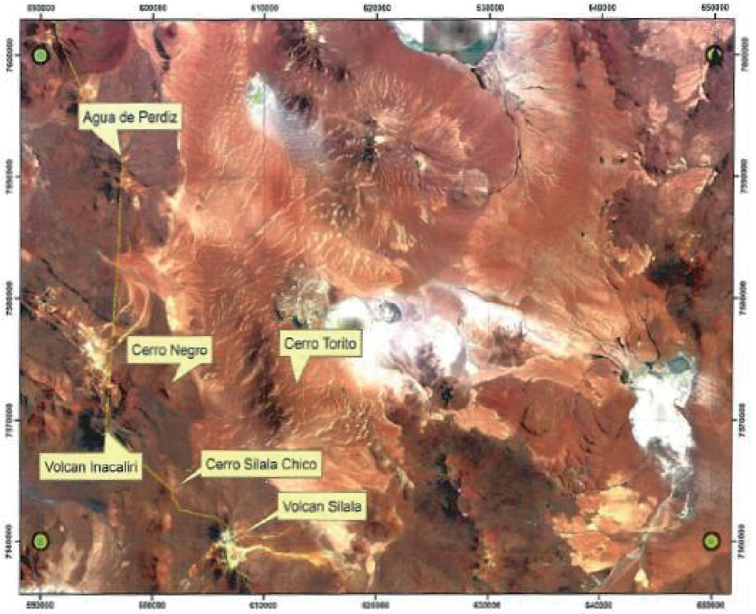

Figure 1.2. Silala Volcanic Domes

The ignimbrites rich in plagioclase outcrop in lower areas, clearly exposed on the flanks of the structural canyon [ravine] where the canals were installed (see Annex A. 4, photograph 3). The presence of the dacite composition ignimbrite, by contrast, is restricted to a guiding horizon of an approximate thickness of 20 cm and is clearly identifiable on the northeast flank of the main canal. In higher parts, the ignimbrites that have a higher content of plagioclase-Na are much more exposed in the central part of the area surveyed. Reduced tuff outcrops of a whitish color and a massive texture can be observed to the east, between the Andesite lava and the Silala ignimbrite. In the central northeastern part, it is possible to observe a horizon that is clearly delimited by its coloration and composition, and which corresponds to gray–blackish Andesite Lava. Silala Chico dome outcrops to the southwest, presenting a composition that corresponds to light gray trachyandesite of a medium granulometry and intermediate composition. This sequence of exposed materials prolongs with the presence of glacial sediments to the northwest of the area surveyed, on the south flank of Inacaliri Volcano.

Colluvial sediments cover 30 to 40% of the area, mainly due to the extreme action of temperature changes, the low gradient and the absence of hydric activities as material transport agents. Alluvial sediments are restricted to water runoff from the springs, in the canalized areas or in their vicinities (see Annex A.2. Map 2/8).

1.3. STRUCTURAL GEOLOGY

The tectonism of the area surveyed is influenced by the uplift and faulting of the Lipez regional block, known as the Cuña Occidental [Western Wedge].

The major representation of this tectonism in the area are the Khenayani fault system, which crosses the area with a regional ENE direction, adjustment faults that follow the same course, and transversal adjustment faults with EW and WNW directions. The latter have a limited but deep extent, and facilitated volcano effusion—with the resulting deposition of igneous and effusive pyroclastic rocks—and the fracturing of basal ignimbrite rocks.

1.3.1. Local Structural Geology

Using the structural mapping and data processing as a basis, 4 domains were identified. These represent the structural zones that govern the geological behavior, which in turn determined the upwelling of the Silala Springs (see Annex A. 1 – Structural Interpretation).

Joints: 1,500 fractures were mapped throughout the study area. Following their interpretation, it was concluded that the maximum stress axis has a preferred EW direction, which gave rise to four structural domains (see Annex A. 2, Map 3/8), each with particular characteristics. For example, fault mirrors were mapped in the 4th domain. These determined the current position of the structural canyon, as well as the secondary porosity of the whole ignimbrite complex that allows the springs to well up (see Annex A. 4, Photographs 4 and 5).

Faults: The position of the fault mirrors (striae) shows that the fractures of the 4th domain were activated by the action of shear stresses, which formed the current geomorphology of the canyon (tectonic pit/structural gully).

The fault mirrors mapped have an average dipping direction of 140/48° (azimuth of the dipping direction), a trend with an azimuth of 225, and a plunge (subsidence) of 110; with a raque of 110 SW, conditioning a structural control for the upwelling of the springs of the NWW sector.

1st Domain

From the structural interpretation, it can be perceived that fractures "b" and "c" respond to shear fractures with respect to the main stress axis of a NE trend of 81°; fractures "a" and "d" respond to shears of a second order in relation to the shear stresses.

There are fractures of angle strike extension, which fluctuate from 81° N – 85° E and concur with the direction of the topographic depression of the area in which the springs flow, with a preferential Rb [no explanation on what the acronym means is provided in the source text, but Direction is inferred as the possible meaning] of N 81° E.

From an interpretation of the Rose diagram, it can be perceived that the ruling fracture direction is 80° N – 85° W. The latter is the reason why the flow of the SEE sector springs has a higher rate, inasmuch as water always flows to areas where there is less resistance. These extension fractures are open fractures that enable the upwelling of the springs because of their high secondary permeability rate (See Annexes A.1, p. 1-4).

2nd Domain

The 2nd domain is characterized for having a 1st δ (maximum effort axis) of an 85° NE direction and a Plunge of 12° NE, a 2nd δ of an 85° NE direction and a Plunge of 78° SW, and a 3rd δ of an 5° NW direction and a Horizontal Plunge. These caused fractures "b" and "e" to be shear fractures, fractures "a" to be compression fractures, and "c" to be second order shear fractures.

From an interpretation of the Rose diagram (see Rose Diagram, Annex A. l., p. 29), it is possible to perceive a predominant Rb [Direction] in a range of 0° N – 10° W, which matches the compression fractures, and a fracture frequency in a range of 60° - N 68 ° W matching the shear fractures.

The above provides an explanation as to why the 2nd domain section does not comprise any springs, i.e. this domain presents closed fractures, unlike the 1st Domain. (see Annex A. 1, pp. 5-9).

3rd Domain

The 3rd domain is characterized for presenting a 1st δ of a 75° NE direction and a Plunge of 10° SW, a2nd δofa75°NEdirectionandaPlungeof80°NE,anda3 rd δofa15°NWdirectionanda Horizontal Plunge. These caused fractures "a" and "d" to be first order shear fractures, fractures "b" and "c" to be second order shear fractures, and fracture "e" to be compression fractures.

From an interpretation of the Rose diagram, it can be perceived that there is a predominant NS fracture Rb [direction], which corresponds to compression fractures, and NW fractures that correspond to shear fractures, to a lesser degree. This is why springs do not well up in this domain (see Annex A. 1, pp. 10-14).

4th Domain

Fractures "a", "b" and "c" are first order shear fractures, with respect to the 1st δ. Fractures "e" and "d" are second order shear fractures activated by shear stresses. These have activated the predominant faults in the 4th Domain, as a result of the action of shear stresses, where a fault mirror was mapped with a dipping direction of 140°/148°, a 225° trend, a 11° plunge, and a SW 11° raque. This structural control predetermines the emergence of the NWW sector springs (see Annex A. 1, pp. 15-19; see Annex A. 4, photograph 5).

1.4. LITHOLOGY

1.4.1. Inacaliri Volcano

Inacaliri volcano has an approximate diameter of 10 Km, in its basal part, and culminates in a crater of a diameter of 380 m, at an altitude of 5570 m.a.s.l. Two effusive events can be observed in this volcano.

The first volcanic event is represented by the effusion and deposition of dark gray andesitic lava, similar, or subsequent to, the rocks of the Silala Chico hill dome, but falling within the same volcanic event.
The second effusive event superposes new material over the volcanic cone of the first event. This last volcanic activity discharged a flow of andesitic lava that is more basic than that of the Silala Volcano, which covers the preexisting reliefs.

1.4.2. Silala volcano

The Silala volcano is located in the southeast margin of the area surveyed. It has an approximate basal diameter of 4 Km and an altitude of 5700 m.a.s.l. The rocks that this volcano presents comprise dark-gray to gray-light-blue porphyric andesitic-dacitic lavas, with 70 % of plagioclase (andesite-labradorite) and 28 % of pyroxene, which rest on the Silala pyroclastic flows.

1.4.3. Quaternary and Recent Deposits

The unconsolidated deposits, or Quaternary and recent soils cover approximately 30 to 40 % of the area's surface. These are the result of weathering and erosion events that conditioned the colluvial- alluvial material present in the area.

1.4.3.1. Colluvial processes

The colluvial sediments or deposits are found in different parts of the area surveyed, covering soft slopes. These deposits present a primary sedimentary structure.

1.4.3.2. Alluvial activity

The alluvial activity is represented by the runoff of fluvio-glacial waters that gave rise to forms of erosion and material accumulation dating back to 10.000 BP, approximately. The area comprises large alluvial fans that reflect the climatic conditions, and amounts of water runoff that are different from the current ones. Other forms of alluvial accumulation in the area surveyed are alluvial plains, with red paleosols developed on the ignimbrites that date back to 7.8 Myr and andesitic-dacitic lavas from 1.7 Myr ago. In cases where springs or pooling waters well up, they condition the presence of bofedals developed by the influence of a superficial piezometric level on fine to medium sandy-clayey material, particularly in the upper part of the topographical depressions, where the slope is softer, or inexistent. These are bofedals characteristic of high altitudes.

1.5. PETROGRAPHIC DESCRIPTION

Petrographically, the area surveyed formed as a result of a volcanic activity that began during the Andean Cycle of the Upper Miocene. During this cycle, several calderas, and volcanic centers and domes were formed, including Agua de Perdiz (found outside the area surveyed), which manifests as the eruption and deposition of a regionally large ignimbrite mantle, known as the Silala Ignimbrite. The latter are clearly visible in the area and partially covered by lava flows from stratovolcanoes, intruding the latter. This is the first effusive stage that characterizes the area. The most visible volcanic structures that surround the area are the Silala Chico and Torito volcanic domes and the Inacaliri and Silala stratovolcanoes (see Figure No. 1.2, p. 5), which formed as a result of the accumulation of products derived from extrusive and effusive phases. The first, extrusive, phase is represented by the formation of volcanic domes, while the second, effusive, is represented by andesite and andesitic-dacitic lava.

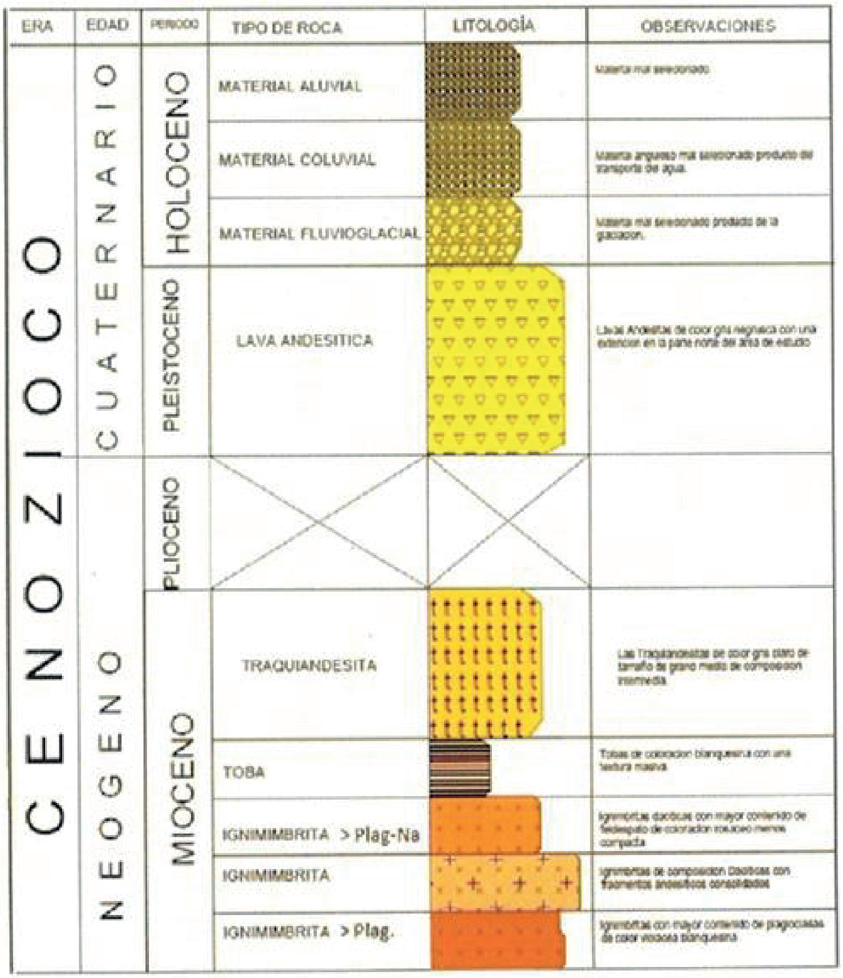

Figure 1.3. Lithological column of the Silala springs

By the end of the Pleistocene, the formation of other volcanic centers, as the Cerro Negro, began. The effusive volcanism of Cerro Negro developed andesite lava deposits that covered preexisting reliefs.

Six lithological units have been identified through the petrographic description of the Silala. The latter's lower part comprises dacite ignimbrite of an unidentified basement and a higher content of plagioclase; the second unit comprises a thin layer of dacite-ignimbrite, with andesite clasts derived from the first [volcanic] event of the Inacaliri; the third unit comprises dacite ignimbrites with a higher content of plagioclase-Na; the fourth unit contains tuffs; the fifth one trachyandesite; and the sixth andesite lava.

1.5.1.1. Silala Ignimbrite

The inferior layer that outcrops in the area is composed of the Silala ignimbrites, which in turn comprises three units:

1.5.1.2. Dacitic-Hypocrystalline Ignimbrites, > Plag

These are characterized for their whitish color and are mainly composed of plagioclase (> Plagioclase). They are of dacitic composition, and also comprise quartz and biotite. They correspond to the calcalkaline series, rich in K_2O, and their SiO_2 content varies between 63% and 66%. Their matrix is vitreous and includes lithic fragments of different rock types, mainly pumice stone fragments. Their thickness is uncertain, given that their basal contact and the rock on which they rest are unknown also. These are partially welded ignimbrite and are strongly fractured and jointed (see Photograph 1.1., p. 13). According to the surveys performed in the area, and on basis of radiometric data extrapolated from surrounding areas, these ignimbrites have an age of 7.8 +/- 0.3 millions of years, i.e. from the Upper Miocene (Choque, 1996; Lema & Ramos, 1996; Richter, et. al., 1992).

1.5.1.3. Dacitic ignimbrite with andesitic clasts

These have a pinkish color and are composed of dacite, with a predominance of feldspar. This unit is more compacted and has less power. To the west of the area surveyed, these ignimbrites have a thickness of, approximately, 15 cm and are restricted in the eastern part. Their grain size is aphanitic, with phaneritic phenocrysts of andesite composition, which pertain to the first Inacaliri volcanic event. Their color index is lower than the 10% (holo-felsic), they have a quartz content that is higher than the 10% (acid), a silica percentage that surpasses the 66%, and contain quartz, feldspar and plagioclase crystals to a lesser extent (see photograph 1.2., p. 14). The crystal faces do not present defined shapes (granular allotriomorphic) and have a banded massive texture (they do present a preferred flow direction).

Photograph 1.1. Dacitic-Hypocrystalline Ignimbrites, > Plag - Na

1.5.1.4. Dacitic ignimbrite > Plag-Na. Light pinkish color Silala

These ignimbrites present Plagioclase – Na, hence their pinkish coloration, as well as feldspar, plagioclase—in a lesser amount—silica, in a 55 to 60 % size of aphanitic grain, with andesitic composition phenocrystals, a color index lower than the 10 % (holofelsic), a quartz content higher than the 10% (acid), and a silica percentage higher than the 66%, presenting quartz, feldspar and plagioclase in minor quantities (see Photograph 1.3. p. 14). The crystals do not present defined forms (granular allotrimorphic) and have a banded massive texture (they do not show a preferential flow direction).

Photograph 1.2. Dacitic-ignimbrite with andesitic clasts

Photograph 1.3. Dacitic ignimbrite > Plag - Na

1.5.1.5. Tuff

These tuffs are visible only in the northeast of the area surveyed. They have a gray-whitish color, and a dacitic composition. They present feldspar, plagioclase, quartz and biotite minerals. Their grain size is aphanitic. They have a color index lower than the 10% (holofelsic), a quartz content that surpasses the 10% (acid), and a silica content higher than the 66% (see photograph 1.4. p. 15). The crystal faces do not present defined shapes (granular allotriomorphic) and have a banded massive texture (they do present a preferred flow direction).

Photograph 1.4. Tuff

1.5.1.6. Trachyandesite

A trachyandesite (intermediate) volcanic dome is found southwest of the area surveyed. This rock has a light gray color and medium grain sizes. Its mineral composition comprises quartz, feldspar, biotite and plagioclase (< amount). Its color index is lower than the 10% (holofelsic), its quarts content is higher than 10% (acid), and its silica content is higher than 66% (see photograph 1.5. p. 16). The crystal faces do not present defined shapes (granular allotriomorphic), have an aphanitic grain size, and present a subophitic texture.

1.5.1.7. Andesitic lavas

These lavas form a layer that overlaps, north of the area surveyed, the Silala Ignimbrites and, to the northeast, the tuffs. They are andesitic in composition, and comprise quartz, feldspar, pyroxene and plagioclase crystals (< amounts). They do not present a fluidal structure, their grain size is aphanitic, their color index lower than the 10-40% (intermediate), and their silica percentage higher than the 52-66% (see photograph No. 8).

The crystal faces do not present defined shapes (granular allotriomorphic) and present a massive texture.

Photograph 1.5. Trachyandesite

Photograph 1.6. Andesite

CHAPTER I (GEOLOGY) – CONCLUSIONS

Locally, the area surveyed has developed in an effusive volcanic environment. The basement of the materials formed as a result of volcanic activity is found on the ―Silala Ignimbrite‖, with an age of 7.8 +/- Myr, namely, the Upper Miocene (Choque, 1996; Lema & Ramos, 1996; Richter, et. al., 1992). The ―Silala Ignimbrites‖ are divided in three horizons; the oldest ones correspond to ignimbrites that have a higher content of whitish plagioclase, over which the dacitic ignimbrites – with consolidated andesitic fragments – rest. The ignimbrites rich in Plagioclase – Na are found in the latter sequence.

The structural mapping and data processing led to the identification of 4 domains that represent the structural zones that predominate the geological behavior, which in turn defines the occurrence of the Silala springs (see Annex A. 2, Map 3/8).

1st Domain: based on the structural interpretation, it can be perceived that fractures "b" and "c" respond to shear fractures in relation to the main axis of a NE 81° trend; fractures "a" and "b" respond to second order sheers in relation to shear stress.

There are fractures of angle strike extension, which fluctuate from 81° N – 85° E and concur with the direction of the topographic depression of the area in which the springs flow, with a preferential Rb [direction] of N 81° E.

From an interpretation of the Rose diagram, it can be perceived that the ruling fracture direction is 80° N – 85° W. The latter is the reason why the flow of the SEE sector springs has a higher rate, inasmuch as water always flows to areas where there is less resistance. These extension fractures are open fractures that enable the upwelling of the springs because of their high secondary permeability rate (See Annexes A.1, p. 1-4).

2nd Domain: it is characterized for having a 1st δ (maximum effort axis) of an 85° NE direction and a Plungeof12°NE,a2nd δofan85°NEdirectionandaPlunge of78°SW,anda3rd δofan5°NW direction and a Horizontal Plunge. These caused fractures "b" and "e" to be shear fractures, fractures "a" to be compression (closed) fractures, and "e" to be second order shear fractures.

From an interpretation of the Rose diagram (see, Annex A. l., p. 29), it is possible to perceive a predominant Rb [Direction] in a range of 0° N – 10° W, which matches the compression fractures, and a fracture frequency in a range of 60° N – 68 ° W—matching the shear fractures.

The above provides an explanation as to why the 2nd domain section does not comprise any springs, i.e. this domain presents closed fractures, unlike the 1st Domain. (see Annex A. 1, pp. 5-9).

3rd domain: it is characterized for presenting a 1st δ of a 75° NE direction and a Plunge of 10° SW, a 2nd δofa75°NEdirectionandaPlungeof80°NE,anda3rd δofa15°NWdirectionanda Horizontal Plunge. These caused fractures "a" and "d" to be first order shear fractures, fractures "b" and "c" to be second order shear fractures, and fracture "e" to be compression fractures.

From an interpretation of the Rose diagram, it can be perceived that there is a predominant NS fracture Rb [direction], which corresponds to compression fractures, and NW fractures that correspond to shear fractures, to a lesser degree. This is why springs do not well up in this domain (see Annex A. 1, pp. 10-14).

4th Domain: Fractures "a", "b" and "c" are first order shear fractures, with respect to the 1st δ. Fractures "e" and ―d" are second order shear fractures activated by shear stresses. These have activated the predominant faults in the 4th Domain, as a result of the action of shear stresses, where a fault mirror was mapped with a dipping direction of 140°/148°, a 225° trend, a 11° plunge, and a SW 11° raque. This structural control predetermines the emergence of the NWW sector springs (see Annex A. 1, pp. 15-19; see Annex A. 4, photograph 5).

Faults have also been identified in the area. The position of the fault mirrors (striae) shows that the fractures of the 4th domain were activated by the action of shear stresses, which formed the current geomorphology of the canyon (tectonic pit/structural gully).

The mapped data of the fault mirrors have an average Dip/Dir of 140/48° (azimuth of the dipping direction); a trend with an azimuth of 225 and a plunge of 110 (sinking); with a raque of 110 W (see Annex A.4, photograph 5), conditioning a structural control for the emergence of the springs of the NWW sector.

Glossary

Crushing:

The action and effect of crushing [something]. To crush (to deform something by exerting pressure, flattening, or reducing its thickness).

BP:

(Commonly abbreviated as AP, and occasionally as BP, from the English ―Before Present‖. It is a time scale used in archeology, geology and other scientific disciplines as a standard to specify when some event occurred in the past.

Bibliography

SERGEOMIN Report, ―Study of the Geology, Hydrology, Hydrogeology and Environment of the Silala Springs‖, 2015

Suárez, R. (2000), Compendium of Bolivia's Geology. Technical Magazine of the Bolivian Fiscal Oil Fields (YPFB). Vol. 18. Cochabamba-Bolivia.

Cabre, R. and Vega, A. 1989. Seismicity of Bolivia. San Calixto Laboratory, Publication 40, La Paz.

Clapperton, C.M. 1979. Glaciation in Bolivia before 3.27 Myr. Nature, 277 (5695): 375-377.

Lavenu, A. 1995. Plio-Quaternary Geodynamics in the Central Andes: the Northern Altiplano of Bolivia. In Suarez R. (ed.) Fossils and Facies of Bolivia: III YPFB Technical Review, 16 (2): 76-96, Cochabamba.

Sebrier, M., Lavenu, A., Fornari, M. and Soulas, J.P. 1988. Tectonics and elevation in the Andes of southern Peru and central Bolivia from the Oligocene to the present. Géodynamique 3 (1-2): 85- 106.

Normal and reverse faulting and the state of stress in the southern central Andes of south Peru. Tectonics 4: 739-780.

Sanchez Otazo, J., ―Notes on Igneous and Metamorphic Petrography‖ p. 30-53, Edit 2001, Potosi-Bolivia

Calcina, l. ―Notes on Igneous and Metamorphic Petrography‖ p. 2-10

[Logo of the Tomas Frias Autonomous University]

CHAPTER II

GEOPHYSICS

[Logo of the Faculty of Geological Engineering]

ÍNDICE

INDEX

FOTOGRAFÍAS

FIGURAS

GRÁFICOS

IMÁGENES

PHOTOGRAPHS

FIGURES

GRAPHICS

IMAGES

CHAPTER II. GEOPHYSICAL SURVEY IN THE SILALA SPRINGS

2.1. Introduction

One of the specific objectives of importance for the Hydrogeological characterization of the Silala springs project has been the application of detailed geophysical surveys to attain knowledge on the electrical properties of the subsoil in order to correlate the lithological units and determine the thickness of each of the geological units present in area.

Said surveys comprised field works completed to elaborate a geophysical modeling based on the extraction of geoelectrical profiles in the areas of interest, which have been defined with the application and use of a SAS 4000/1000 Terrameter resistivity meter.

2.2. Specific objectives

The specific objectives set for the present report are the following:

- Identification of the different geological units in the subsoil, alluvial material layers and ignimbrite by interpreting the different resistivities of the data taken in the field with the Vertical Electrical Sounding technique.
- Determination of the petrophysical properties of the different layers to complement the surface mapping data and correlate it with the information obtained from the subsoil.
- Production of supplementary base information of the subsoil for the geological survey for the purpose of completing the hydrogeological characterization of the Silala springs.

2.3. Theoretical fundamentals of the geophysical method

2.3.1. Application of electrical methods

These methods use the electrical properties variations, and resistivity particularly, of rocks and minerals. They generally use an artificial electric field created on the surface through the passing of a current in the subsoil.

One of the techniques that are most widely used in hydrogeological surveys are electric methods.

The resistivity method allows not surveying sub-horizontal formations, but also determining sub-vertical formations (faults, seams, contact zones, etc.). It further helps define the latter's characteristics to correlate surface formations with those of the subsoil.

2.3.2. Characteristics of the ABEM 4000/1000 TERRAMETER measurement equipment

The SAS 4000/1000 Terrameter is able to complete measurements in four channels, implying that both the resistivity and IP measurements can be performed at a pace four time faster. It can operate in three ways: the resistivity mode comprises power supply from a battery, deep penetration resistivity measurer, with sufficient output for a separation of 2000-m electrodes in proper survey conditions. Circuiterium, namely, electric discrimination and programming network, of separated continuous current tensions, spontaneous powers and noise from the input signal. The relation between tension and intensity (V/I) is calculated automatically and presented digitally in kiloohms, ohms, microohms, or microohms. It provides geometric data on distribution; it can show apparent resistivity. The total range is thus extended from 0.5 milliohms to 1999 kiloohms (see photograph 2.1).

Photograph 2.1. SAS 4000/1000 TERRAMETER Equipment

The most important of all methods that use continuous current produced by artificial generators is the Vertical Electrical Sounding (VES). It is mainly applied in regions where the geological structure is formed by horizontal strata.

The purpose of the VES is to determine the depths of the subsoil layers and their electrical resistivities or conductivities through measurements carried out from the surface.

The graph shown in **Figure 2.1.** presents an outline of the electrode deposition with the Schlumberger configuration applied in the present report.

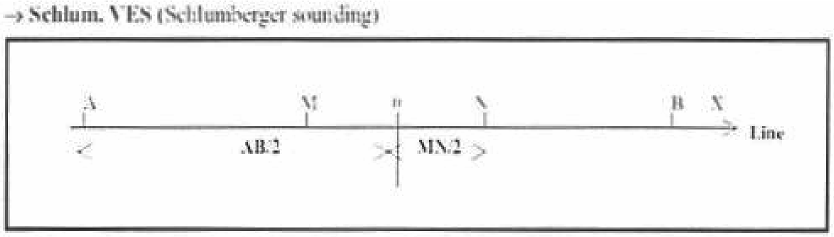

Figure 2.1. Schlumberger configuration for the VES

Where:

A and **B** are current electrodes (through which electric current is injected)

M and **N** are power electrodes (through which the potential difference – created by the injection of electric current of electrodes A and B – between these points is measured).

O is the point in which the VES is performed.

2.4. Geoelectrical survey methodology

The methodology used for the present report was the application of the indirect Vertical Electrical Sounding (VES) geoelectric method based on the collection of surface geological data.

2.4.1. Field activities

In order to determine the subsoil characteristics, 15 vertical electrical soundings (VES) have been performed with their respective locations in UTM WGs 1984 coordinates and at average distances of 250 m, with an estimated depth between 70 to 90 m and a southeast – northeast direction (see **Annexes B. 1** and **B. 2**).

The satellite images show the completion of nine vertical electrical soundings in the NWW area and six in the SEE area, reflecting their respective location (**see Image 2.1** and **2.2**).

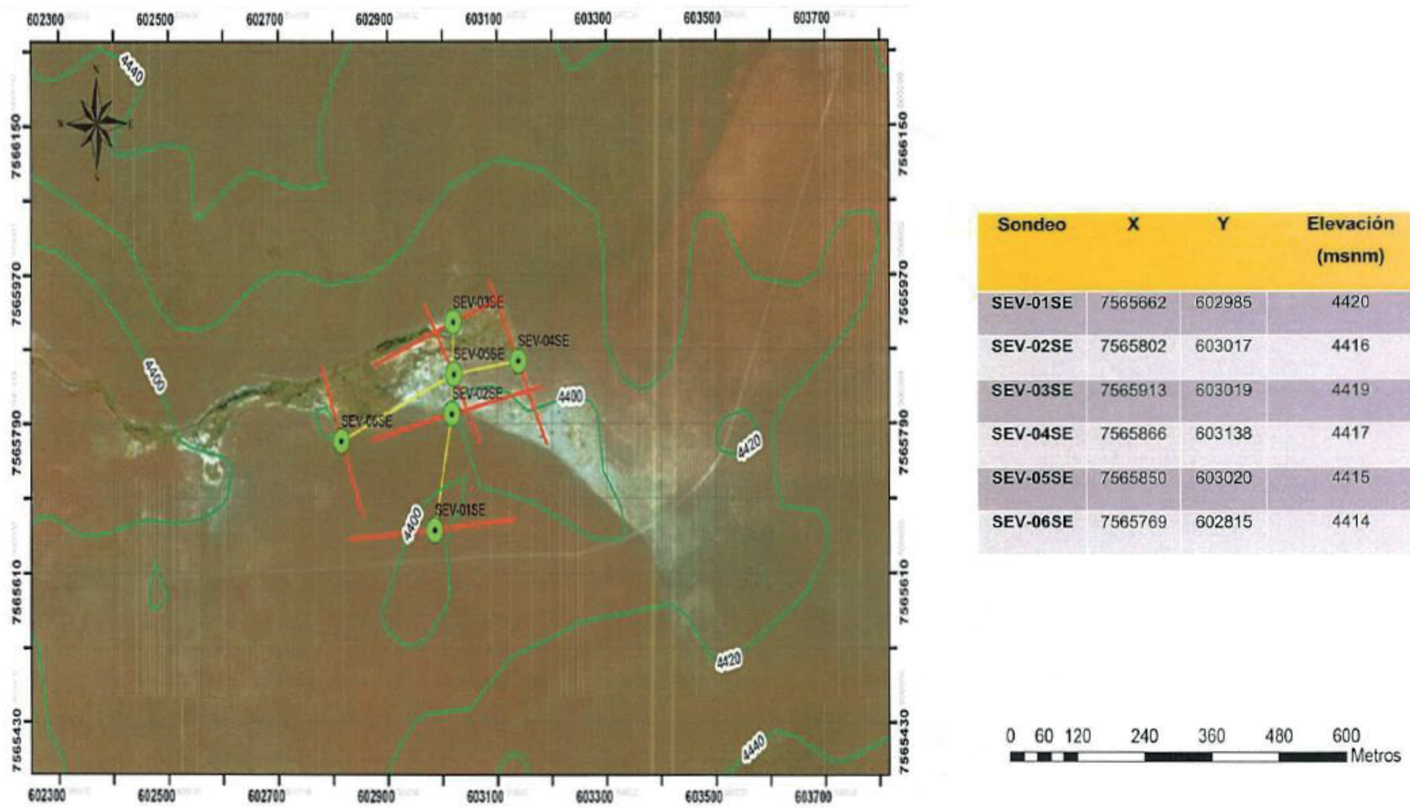

Sondeo	X	Y	Elevación (msnm)
SEV-01SE	7565662	602985	4420
SEV-02SE	7565802	603017	4416
SEV-03SE	7565913	603019	4419
SEV-04SE	7565866	603138	4417
SEV-05SE	7565850	603020	4415
SEV-06SE	7565769	602815	4414

Image 2.1. Location of the VES in the SEE sector (see Annex B. 5)

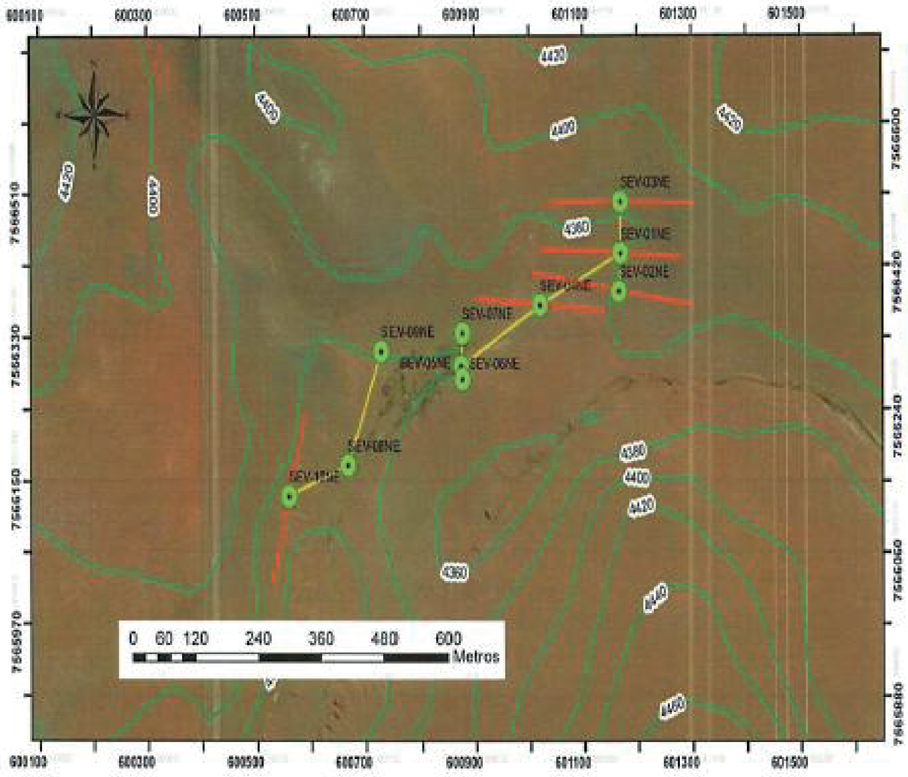

Sondeo	X	Y	Elevación (msnm)
SEV-01NE	7566435	601168	4394
SEV-02NE	7566387	601165	4392
SEV-03NE	7566500	601168	4401
SEV-04NE	7566370	601020	4383
SEV-05NE	7566293	600873	4373
SEV-06NE	7566277	600875	4374
SEV-07NE	7566335	600875	4377
SEV-08NE	7566170	600668	4362
SEV-09NE	7566312	600730	4376
SEV-10NE	7566131	600559	4376

Image 2.2. Location of the VES in the NWW sector (see Annex B. 5)

2.4.2. Desk work

It consisted in processing, analyzing and interpreting all the data generated in the field and desk, with the support of programs that served to integrate the present report.

2.4.2.1. Data processing

The results obtained in the field comprise 6 VES with a SEE direction and 9 VES with a NWW direction, aligned longitudinal and transversally to the springs, with the following characteristics:

VES-01SE Geophysical line

Location

North coordinate	East coordinate	Altitude	Emplacement distance
7565662	602985	4420	250 m

APPARENT RESISTIVITY CALCULATION									
Silala area Sounding No. 1: SEV-01SE									
	MN/2 = 1.5			MN/2 = 5.0			MN/2 = 25		
AB/2	RESIST. V/I Ω	FACTOR K	RESIST. AP	RESIST. V/I Ω	FACTOR K	RESIST. AP	RESIST. V/I Ω	FACTOR K	RESIST. AP
3	79.851	7.0686	564.43						
5	16.51	23.8238	393.24						
7	6.29	48.9566	307.94						
10	2.38	102.364	243.63						
15	835.8	233.264	194.96						
20	380.86	416.524	158.64						
25	208.24	652.144	317.67	845	652.1438	317.67			
30				507.06	940.1238	476.70			
40				244.35	1673.1638	408.84			
50				157.87	2615.6438	412.93			
60				103	1123.122	115.55			
75				75.04	1759.296	132.02			
100				42.86	3133.746	134.31			
125				25.34	4900.896	150.92	177.88	942.48	150.92
150							121.88	1374.45	167.52
175							95.02	1884.96	179.11
200							70.15	2474.01	173.55
250							47.69	3887.73	185.41

Photograph 2.2. Location of the transversal line with respect to the springs

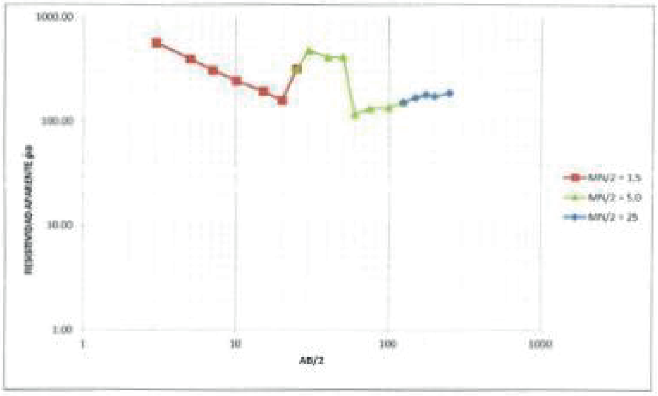

Graph 2.1. Apparent Resistivity Values vs. AB/2

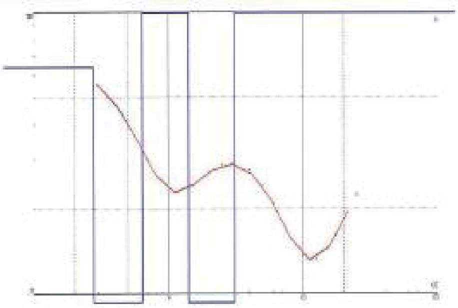

Graph 2.2. Interpretation of the Resistivity Model – Layers

Nº OF LAYERS	sp. h (m)	DEPTH Aprox.(m)	Resist. Ωm	CHARACTERISTICS	LITHOLOGICAL DESCRIPTION
1	2.772	-2.772	**640.2**	The first layer with a resistivity of 640.2 Ohm, with a depth of 2.77 m, corresponds to alluvial material saturated with weathered ignimbrite	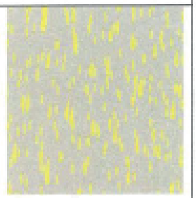
2	3.66	-6.432	**88.74**	The second layer with resistivity of 88.74 Ohm corresponds to welded ignimbrite	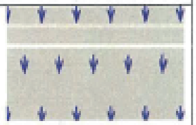
3	7.651	-14.08	**1148**	The third layer has a resistivity of 1148 Ohm, which is an indication of the presence of medium to highly fractured ignimbrite and has a depth of - 14.08 m	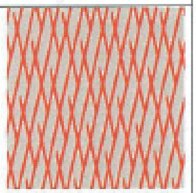
4	17.01	-31.09	**16.5**	The last detected layer is found from -31.09 m and is an indication of the existence of fractures ignimbrite	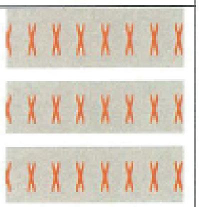

VES-01SE Analysis:

The first layer has a depth of 3.6 meters, with a resistivity of 640.2 Ohm-m, and is an indication of the presence of alluvial material saturated with weathered ignimbrite. The second layer, with 6.43 meters of depth, a thickness of 3.66 m and a resistivity of 88.74 Ohm-m, corresponds to welded material.
The third layer has a depth of 14.08 meters; the resistance increases at more than 1000 Ohm-m; this high resistivity corresponds to medium to highly welded ignimbrite, which is an indication of the rock's fracturing. The last layer, with a depth of 31.09 m, thickness of 17.01 m, and a resistivity of 16.5 Ohm-m, corresponds to fractured ignimbrite material.

Note: Prolongation of the following VES in SEE direction **(see Annex B. 1)**.

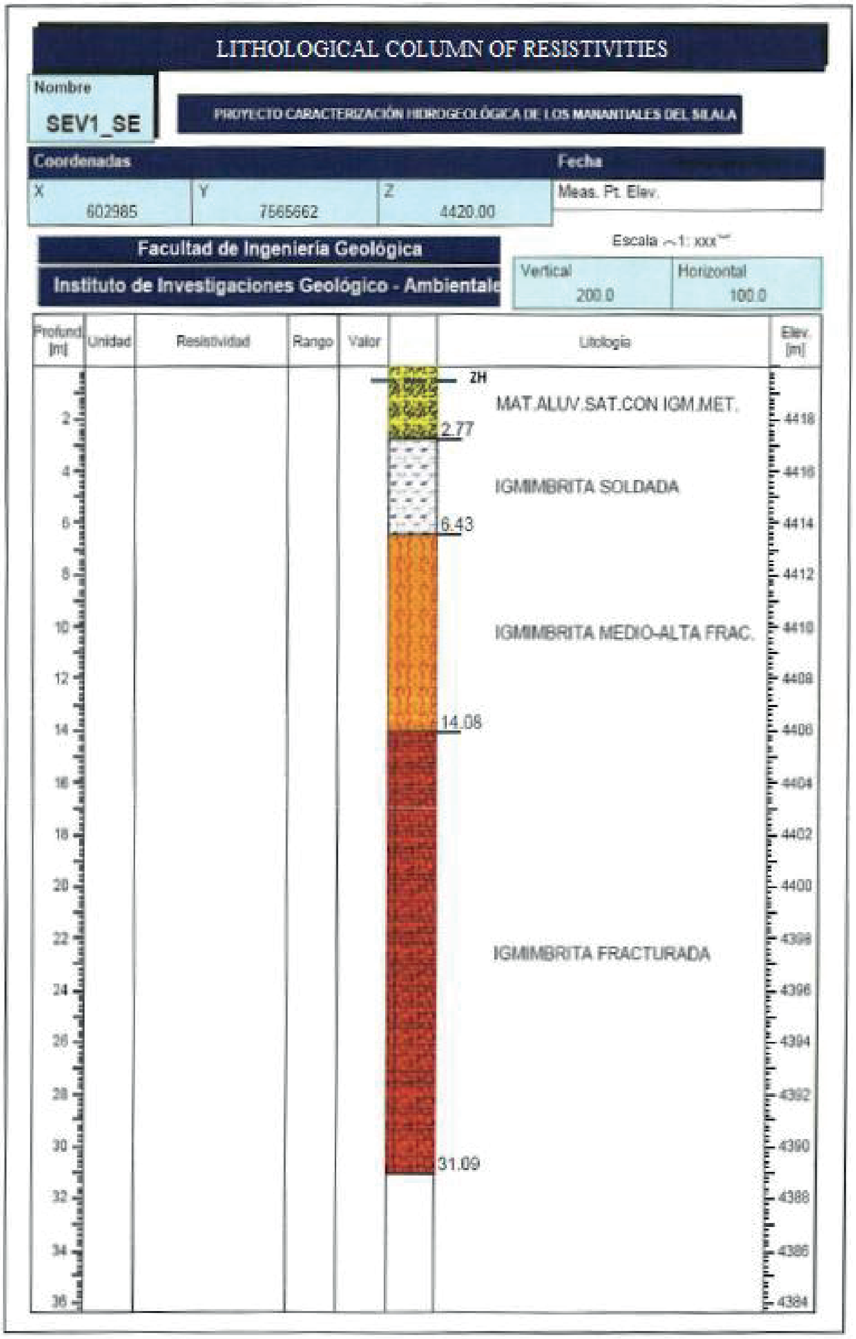
LITHOLOGICAL COLUMN OF RESISTIVITIES
Nombre
SEV1_SE
PROYECTO CARACTERIZACIÓN HIDROGEOLÓGICA DE LOS MANANTIALES DEL SILALA
Coordenadas
Fecha
X 602985
Y 7565662
Z 4420.00
Meas. Pt. Elev.
Facultad de Ingeniería Geológica
Instituto de Investigaciones Geológico - Ambientale
Escala
Vertical 200.0
Horizontal 100.0
Profund [m]
Unidad
Resistividad
Rango
Valor
Litologia
Elev. [m]
ZH
MAT.ALUV.SAT.CON IGM.MET.
2.77
IGMIMBRITA SOLDADA
6.43
IGMIMBRITA MEDIO-ALTA FRAC.
14.08
IGMIMBRITA FRACTURADA
31.09

VES-01 NE Geophysical line

Location:

North coordinate	East Coordinate	Altitude	Emplacement distance
7566435	601168	4394	150 m

APPARENT RESISITIVITY CALCULATION									
SILALA AREA									
SOUNDING No. 1: SEV-01NE									
	MN/2 = 1.5			MN/2 = 5,0			MN/2 = 25		
	RESIST.	FACTOR	RESIST.	RESIST.	FACTOR	RESIST.	RESIST.	FACTOR	RESIST.
AB/2	V/I Ω	K	AP	V/I Ω	K	AP	V/I Ω	K	AP
3	110	7.0686	779.03						
5	42.541	23.8238	1013.49						
7	17.133	48.9566	838.77						
10	8.574	102.3638	877.67						
15	3.9767	233.2638	927.62						
20	2.2502	416.5238	937.26						
25	1.41	652.1438	606.08	5.2375	188.496	606.08			
30				31	274.89	854.27			
40				5.153	494.802	2549.71			
50				332.02	777.546	258.16			
60				332.02	1123.122	372.90			
75				166.2	1759.296	292.39			
100				98.058	3133.746	307.29			
125				43.629	4900.896	353.26	297.16	942.48	353.26
150							290.46	1374.45	399.22

32

Photograph 2.3. Location of the longitudinal line with respect to the springs

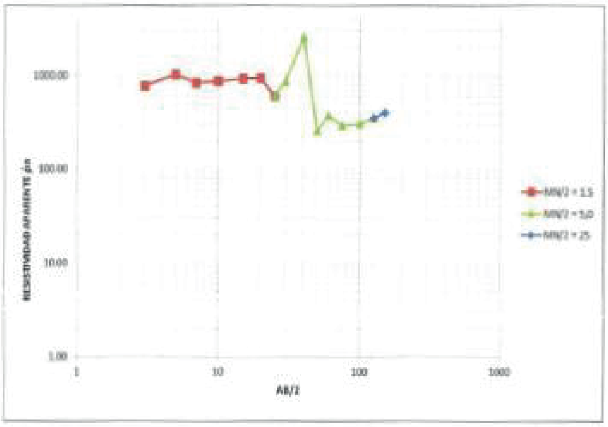

Graph 2.3. Apparent resistivity values vs. AB/2

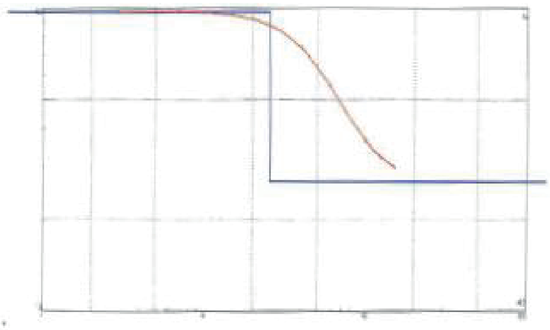

Graph. 2.4. Interpretation of the Resistivity Model – Layers

N° OF LAYERS	sp. h (m)	DEPTH Aprox. (m)	Resist. Ωm	CHARACTERISTICS	LITHOLOGICAL DESCRIPTION
1	7.159	-16.28	**866.9**	The first layer with a resistivity of 866.9 Ohm, a depth of 16.28 m, corresponds to alluvial material saturated with clayey materials and weathered ignimbrite	
2	16.04	-32.32	**44.42**	The second layer, with a resistivity of 44.42 Ohm, corresponds to fractured ignimbrite with a thickness of 16.04 and begins at -32.32 m	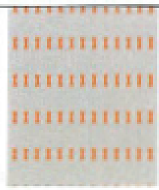

VES-01 NE Analysis:

The 1st layer with resistivity of 866.9 Ohm-m and a depth of 16.28 meters, indicating the presence of alluvial material saturated with clay sediments and weathered Ignimbrite.

The last layer with 32.32 meters of depth and resistivity of 44.42 Ohm-m corresponds to fractured Ignimbrite.

NOTE: Continuation of the Vertical Electrical Sounding (VES) in a northwest-west direction **(see Annex B.2)**.

LITHOLOGICAL COLUMN OF RESISTIVITIES

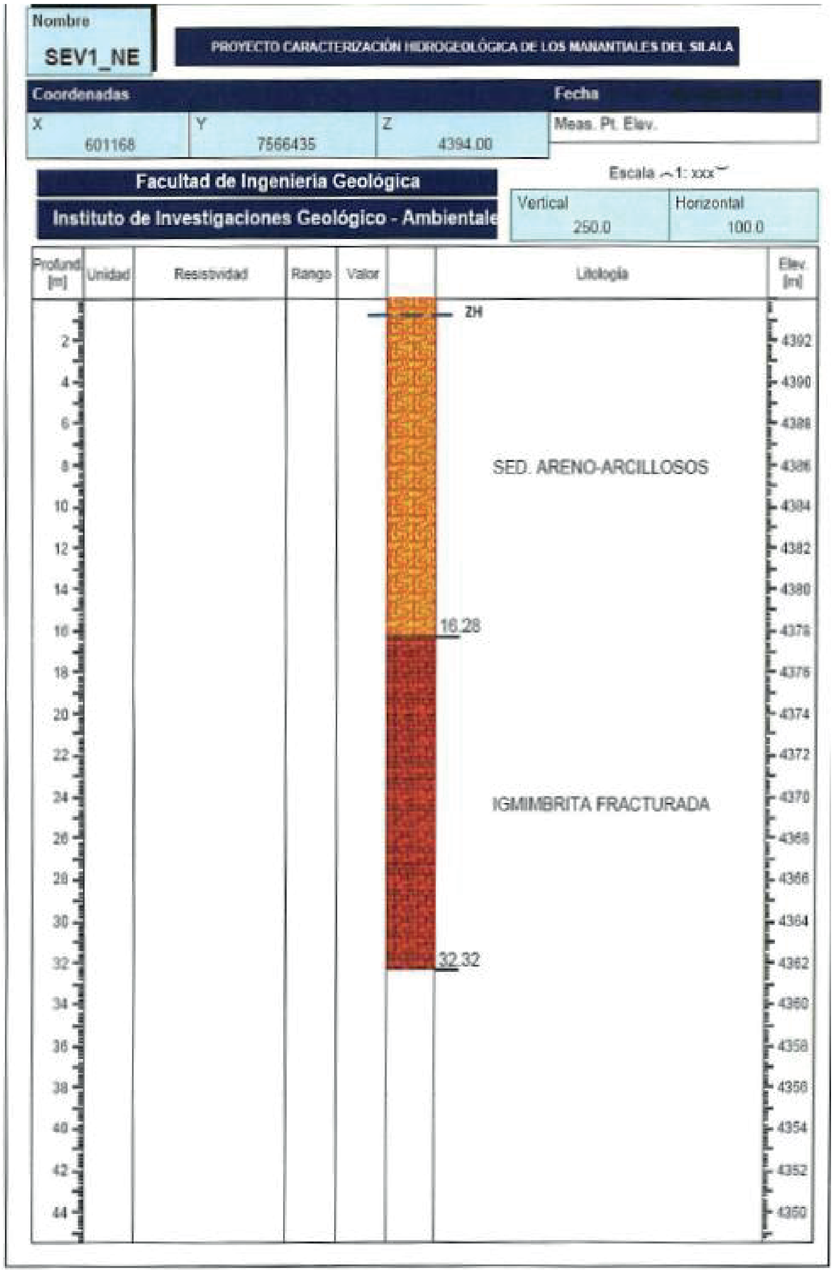

2.5. Interpretation of Profiles – Geo-electric Sections

The methodology for the interpretation of the Vertical Electrical Sounding (VES), mentioned in this chapter, involved the generation of six profiles of resistivity, shown in Annex 8.3, and six geo- electric sections applying the one-dimensional model of interpretation shown in Annex 8.4.

2.5.1. Resistivity Profiles

Six resistivity profiles were integrated with an average research depth of 70 to 90 meters; which are shown below.

Resistivity Profile 1

Integrated by three Vertical Electrical Sounding (VES) (VES-01SE, VES-02SE and VES-03SE) carried out in the Silala springs with an AB length of 300 meters, with preferential southeast-east direction and a depth of investigation of up to 70 meters (see Image 2.3). Resistivity values from 30 to more than 1,000 Ohm-m are identified.

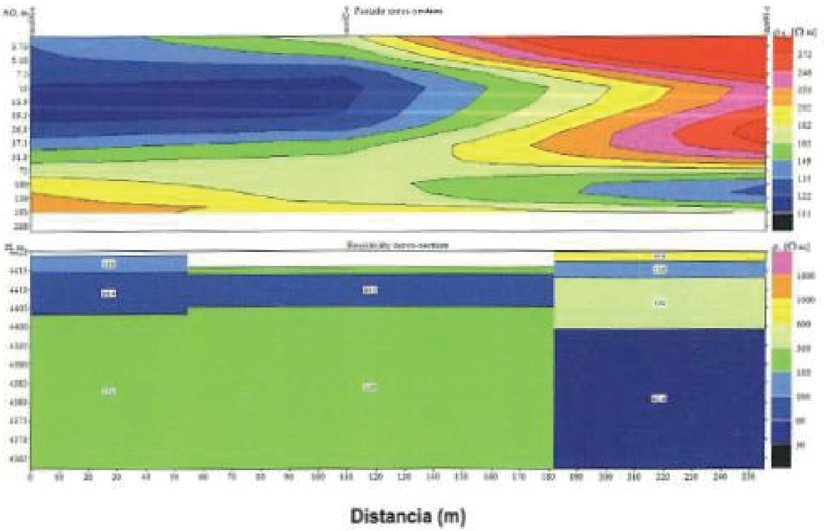

Image 2.3: Resistivity Profile 1 (see Annex B.3)

The values between 60 to 180 Ohm-m are located in the superficial part of the north flank up to a variable depth of 0 to 18 meters. The values of 200 to 600 Ohm-m are located at depth below 20 meters up to a distance of 180 meters. A body of resistivity higher than 800 Ohm-m is located in the sounding VES-02SE and VES-01SE at a depth of 70 meters, registering volcanic rock. In the VES- 01SE sounding at the depth of 6 meters there is a resistivity of 300 to 600 Ohm-m identified by the light green color.

Resistivity Profile 2

Integrated by three VES (VES-04SE, VES-05SE and VES-06SE) carried out in the Silala springs with an AB length of 200 meters, with preferential southeast-east direction and a depth of investigation of up to 70 meters (see Image 2.4).

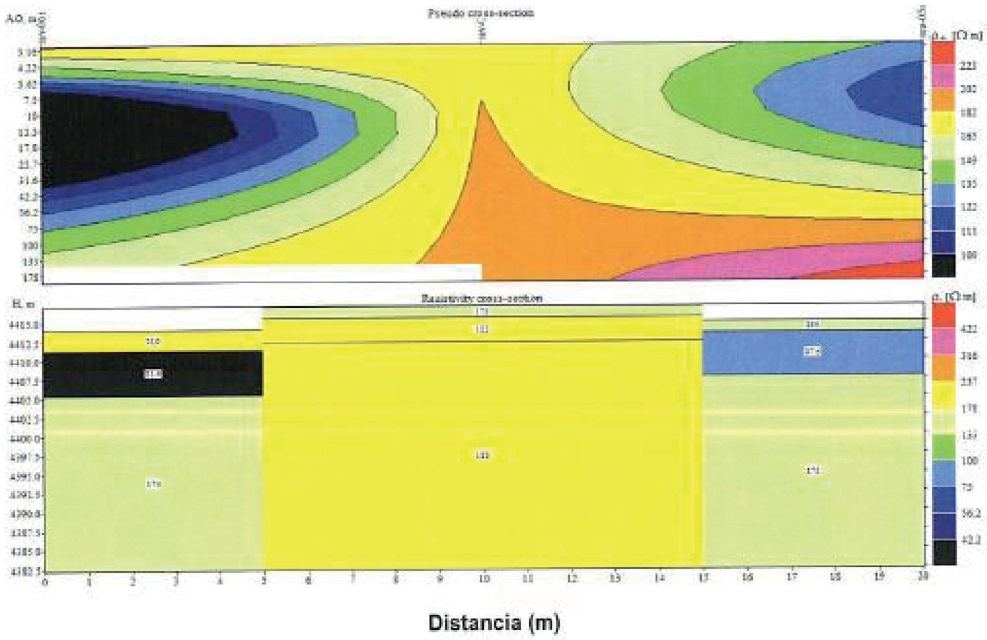

Figure 2.4: Resistivity Profile 2 (see Annex B.3).

Resistivity values from 40 to more than 500 Ohm-m are identified. The values between 150 to 250 Ohm-m are located in the VES-06SE and VES-05SE up to a variable depth of 1 to 5 meters and 30 meters. The values of 100 to 200 Ohm-m are located at depth, below 10 meters. A body of resistivity lower than 80 Ohm-m is located in the VES-04SE sounding at a depth of 3 to 5 meters, recording the presence of groundwater.

Resistivity Profile 3
Integrated by three VES (VES-01NE, VES-02NE - VES-03NE), carried out with an AB length of 300 meters, with preferential northwest-west direction and a depth of investigation of up to 70 meters (see Image 2.5).

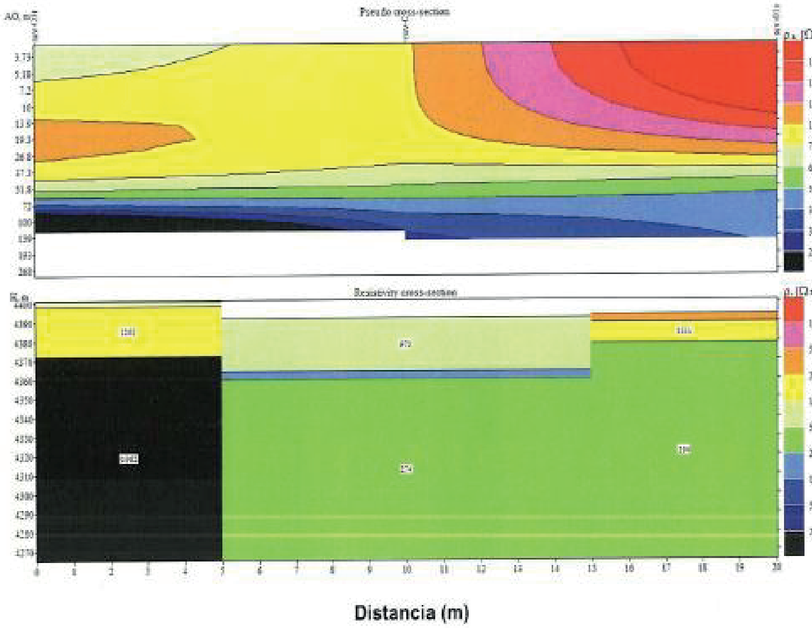

Image 2.5: Resistivity Profile 3 (see Annex B.3).

Resistivity values from 20 to more than 1,000 Ohm-m are identified. Values above 1,000 Ohm-m are located in the VES-03NE and VES-01NE, up to a variable depth of 3 to 25 meters. The values of 200 to 500 Ohm-m are located at depth below 20 meters. A body of resistivity lower than 40 Ohm-m is located in the VES-03NE sounding at a depth of 30 meters from 5 meters away, recording the presence of groundwater due to the low resistivity.

Resistivity Profile 4

Integrated by three VES (VES-01NE, VES-04NE, VES-05NE), with an AB/2 length of 300 meters, with preferential northwest-west direction and a depth of investigation of 70 meters (see Image 2.6).

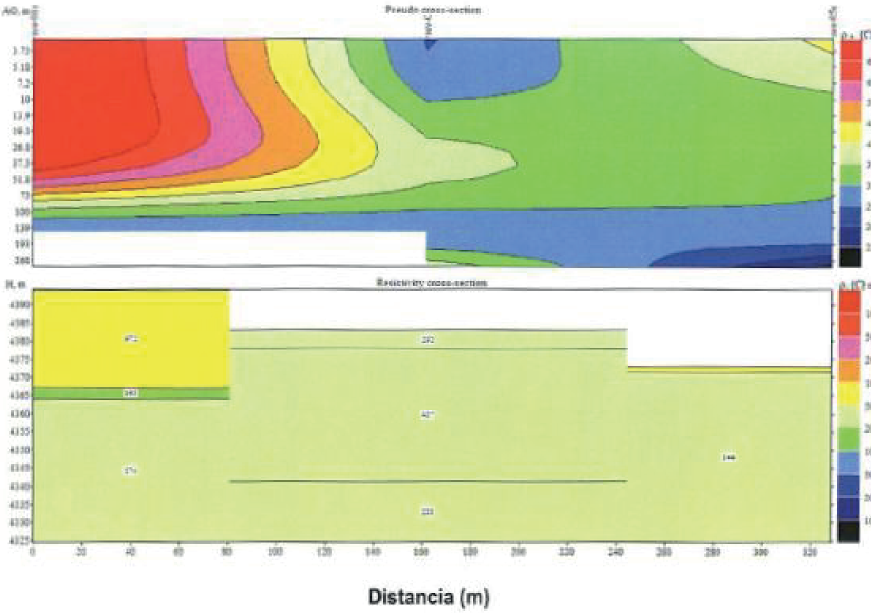

Figure 2.6: Resistivity Profile 4 (see Annex B.3).

Resistivity values from 50 to more than 1,000 Ohm-m are identified. Values between 500 to 1000 Ohm-m are located in VES-01NE - VES-04NE to a variable depth of 0 to 20 meters. The values of 100 to 200 Ohm-m are located in VES-01NE at a depth below 25 meters. A body of resistivity higher than 200 Ohm-m is located in sounding VES-04NE and VES-05NE at a depth of 8 to 30 meters, respectively, recording the presence of confined groundwater; this is due to the low resistivity value verified in the profiles.

Resistivity Profile 5
Integrated by three VES (VES-05NE, VES-06NE and VES-07NE), with an AB/2 length of 300 meters, with preferential northwest-west direction and a depth of investigation of up to 70 meters (see Image 2.7).

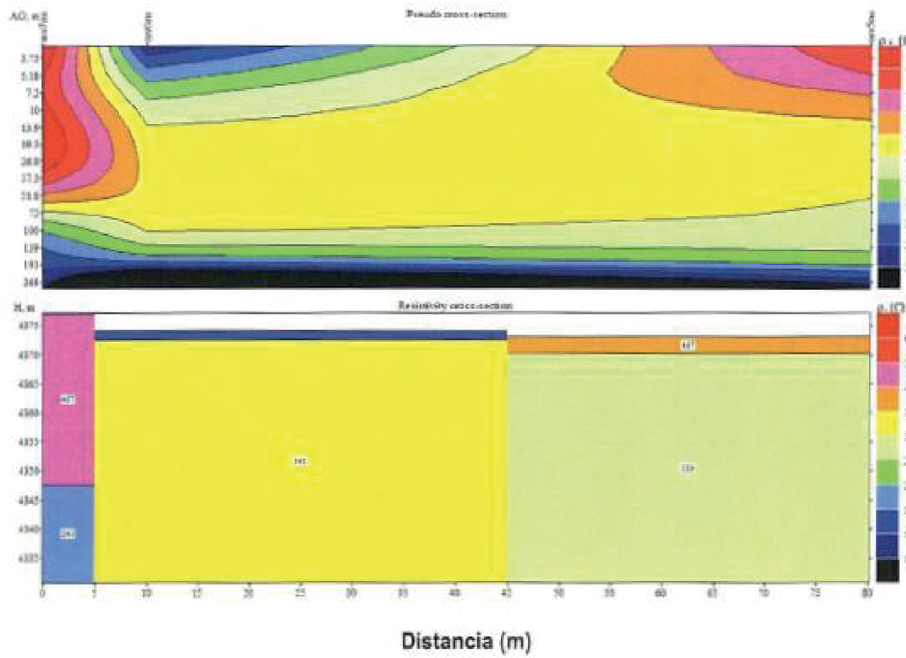

Figure 2.7: Resistivity Profile 5 (see Annex B.3).

Resistivity values from 150 to more than 650 Ohm-m are identified. Values higher than 450 Ohm-m are located in VES-05NE up to a variable depth of 30 meters and values of 200 to 250 Ohm-m, with a depth of 30 meters at a distance of 5 meters, registering the presence of underground water. Values of 300 to 400 Ohm-m are located at a depth below 8 meters, and comprise a distance of 40 meters. A body of resistivity lower than 300 Ohm-m is located in the VES-07NE sounding at a depth of 5 meters.

Resistivity Profile 6
Integrated by two VES (VES-08NE - VES-09NE), with an AB/2 length of 250 meters, with preferential northwest-west direction and a depth of investigation of up to 70 meters (see Image 2.8).

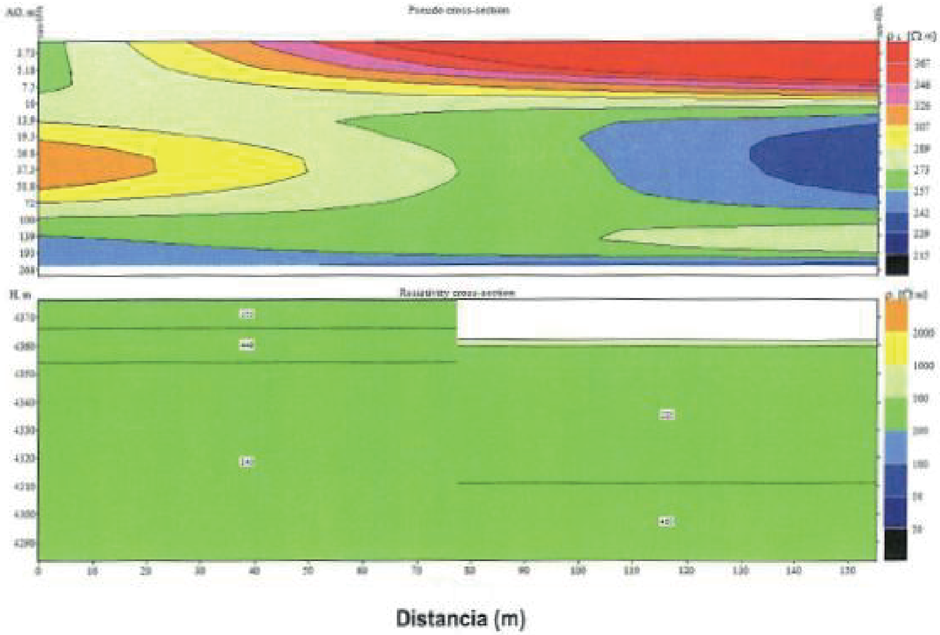

Distance (m)

Figure 2.8: Resistivity Profile 6 (see Annex B.3).

Resistivity values from 20 to more than 1,000 Ohm-m are identified. The values between 200 to 500 Ohm-m are located in both VES of the survey (VES-08NE and VES-09NE) up to a depth of 70 meters, recording the presence of groundwater in fractured ignimbrites, and this is due to low resistivity.

2.5.2. Geo-electric Sections

In order to identify the geo-electric units present in the sub-soil and correlate them with the geological units, six geo-electric sections were elaborated, taking as a basis the resistivity profiles and the results of the one-dimensional models of each VES.

Geo-electric Section 1. Figure 2.2.

This section identified the last contact at a depth of 70 meters. It has a north-south preferred direction and is integrated by three VES (VES-01SE, VES-02SE and VES-03SE) with a total AB length of approximately 300 meters. The analysis indicates the presence of four geo-electric units with variable thicknesses (see Image 2.9).

The resistivity values presented in this section range from 50 to more than 1,000 Ohm-m. Unit A is the first geo-electric unit that is presented; it has resistivity values of 130 to 600 Ohm-m with a thickness of 1 to 6 meters. Then Unit B is presented, with resistivity values of 70 to 90 Ohm-m with a thickness of 3 to 5 meters. Unit C has resistivity values from 100 to greater than 1,000 Ohm-m with a thickness of 7.5 to 20.5 meters. Unit D corresponds to the last geo-electric layer; it has resistivity values of 20 to 400 Ohm-m with a thickness of 20 to 200 meters. The characteristics of each geo-electric unit are described in the tables of each respective VES.

Image 2.9: Geo-electric Section 1

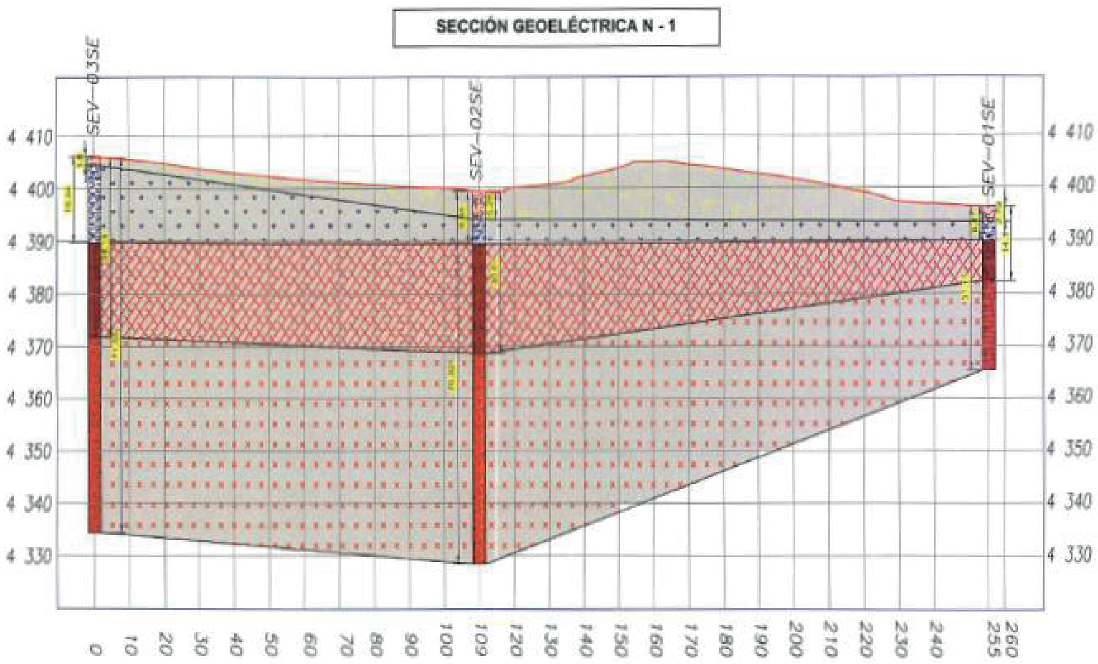

Figure 2.2: Geo-electric Section of Resistivities 1 (see Annex B.4).

Geo-electric Section 2. Figure 2.3.

The last contact was identified at a depth between 35 and 50 meters, depending on the location of the soundings, the largest depth is located in the central part of the profile. It has a preferential east-west direction and is composed of three soundings, VES-04SE, VES-05SE and VES-06SE, with a total AB length of approximately 200 meters. The analysis identifies three geo-electric units with variable thicknesses **(see Image 2.10)**.

The resistivity values presented in this section vary from 10 to more than 600 Ohm-m. Unit **A** has resistivity values of 150 to 207 Ohm-m with a thickness of 1.5 to 3.5 meters. Unit **B** presents the values of resistivity from 13 to 98 Ohm-m with a thickness of 1.6 to 5.9 meters. Unit **C** with resistivity values greater than 600 Ohm-m is presented as the last layer with a thickness greater than 45 meters. The characteristics of each geo-electric unit are described in the tables of each respective VES.

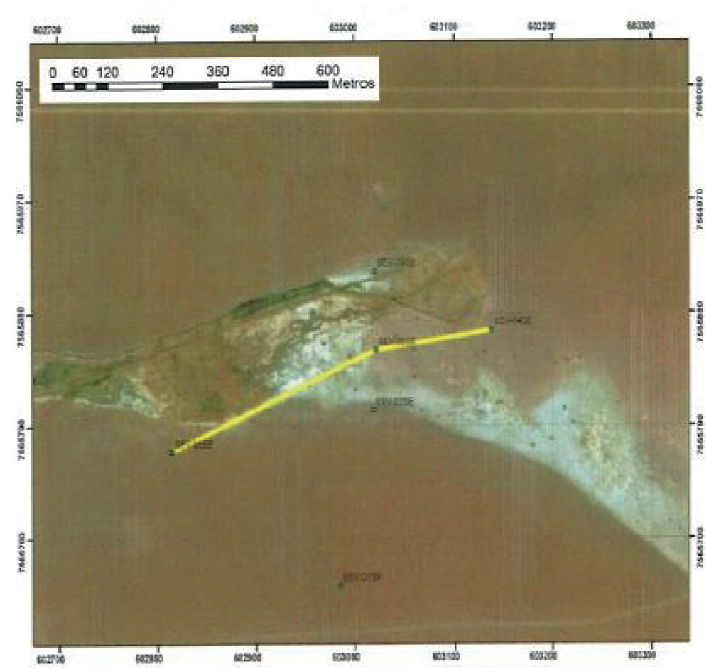

Image 2.10: Geo-electric Section 2

GEO-ELECTRIC SECTION N – 2

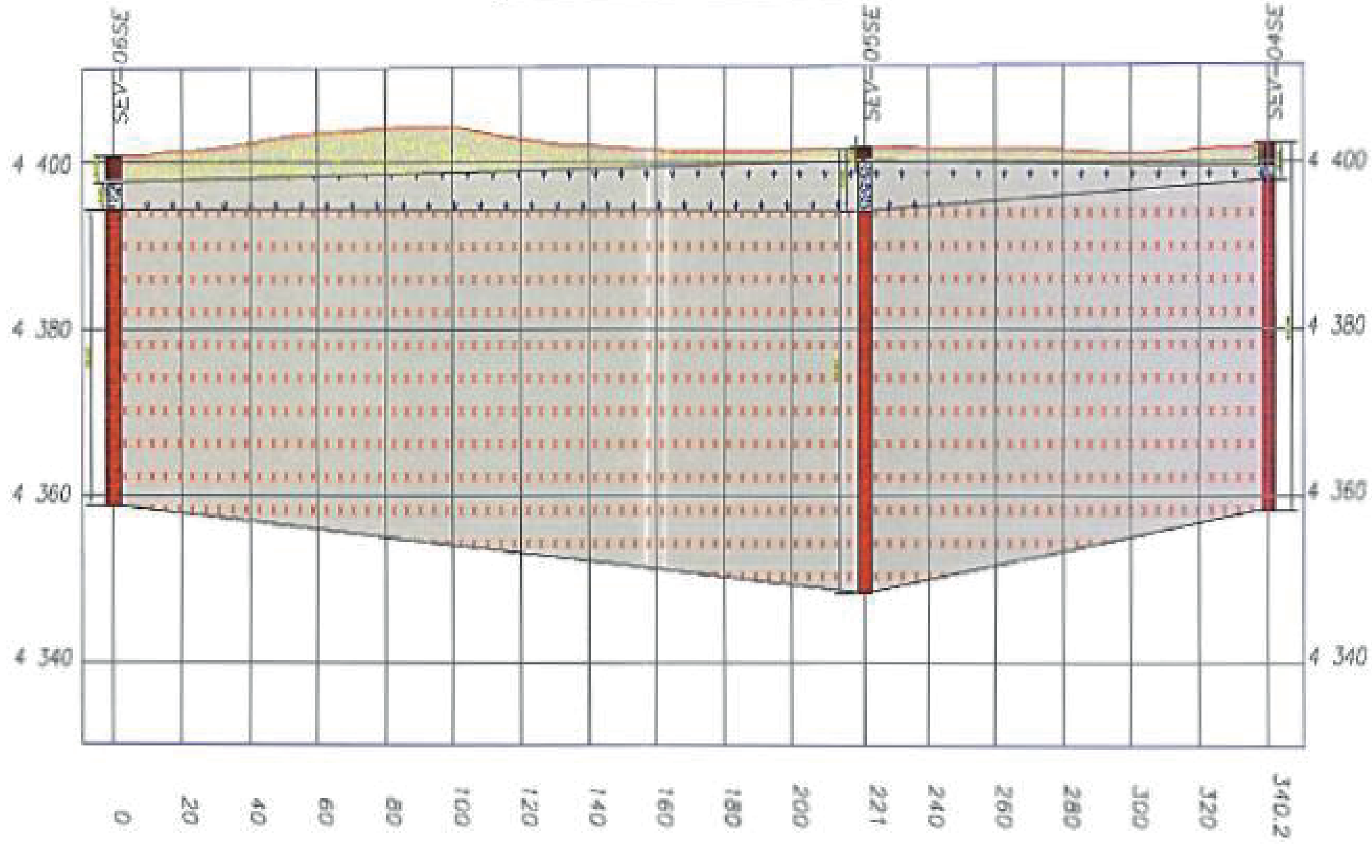

Figure 2.3: Geo-electric Section of Resistivities 2 (see Annex B.4).

Geo-electric Section 3. Figure 2.4.

The last contact was identified at a depth of 70 meters. It has a north-south preferred direction and is integrated by three VES (VES-01NE, VES-02NE and VES-03NE) with a total AB length of approximately 300 meters. The analysis indicates the presence of two geo-electric units with variable thicknesses (see Image 2.11).

The resistivity values presented in this section range from 31 to more than 1,000 Ohm-m. Unit A is the first geo-electric unit that is presented; it has resistivity values of 200 to 1,167 Ohm-m with thicknesses of 7.7 to 15.6 meters. Unit B is the last geo-electric unit that is presented, with values of resistivity from 31 to more than 900 Ohm-m with a thickness of 16 to 30.5 meters. The characteristics of each geo-electric unit are described in the tables of each respective VES.

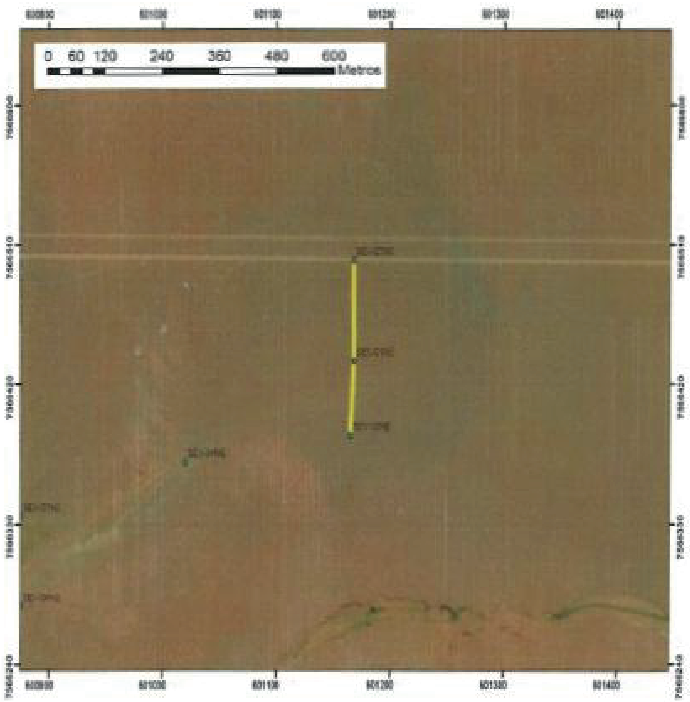

Image 2.11: Geo-electric Section 3

GEO-ELECTRIC SECTION N – 3

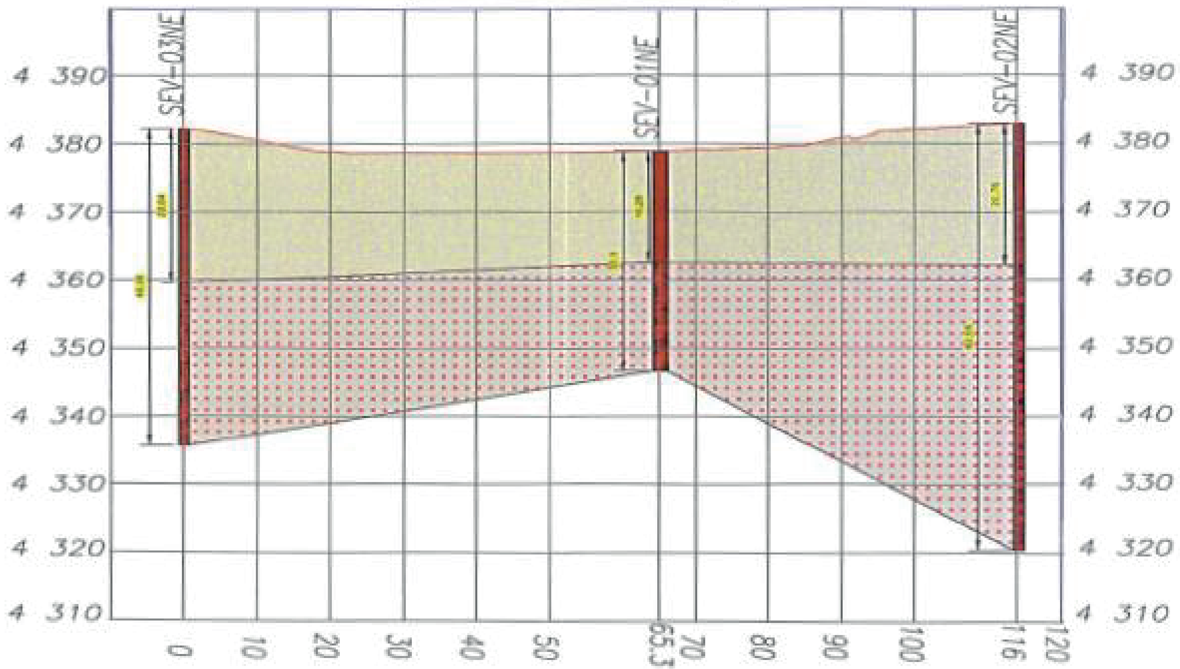

Figure 2.4: Geo-electric Section of Resistivities 3 (see Annex B.4).

Geo-electric Section 4. Figure [2].5.

The last contact was identified at a depth of 70 meters. It has a north-south preferred direction and is composed of three VES (VES-01NE, VES-04NE and VES-05NE) with a total AB length of approximately 300 meters. The analysis indicates the presence of three geo-electric units with variable thicknesses **(see Image 2.12)**.

The resistivity values presented in this section range from 40 to more than 800 Ohm-m. Unit **A** is the first geo-electric unit that is presented only in VES-04NE and VES-05NE; it has resistivity values of 200 to 300 Ohm-m with a thickness of 4 to 11.5 meters. Unit **B** has the largest depth that is located in the central part of the profile, with resistivity values of 430 to 867 Ohm-m with a thickness of 7 to 41.6 meters. Unit **C** has resistivity values from 44 to greater than 200 Ohm-m with a thickness of 16 to 123.5 meters. The characteristics of each geo-electric unit are described in the tables of each respective VES.

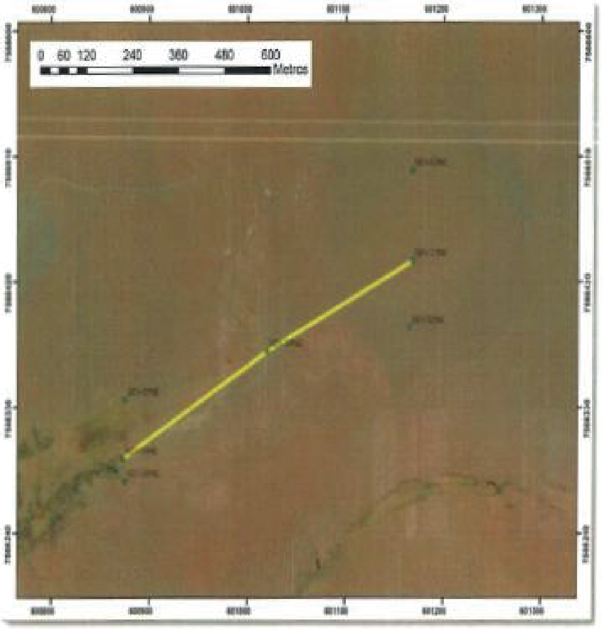

Image 2.12: Geo-electric Section 4

GEO-ELECTRIC SECTION N – 4

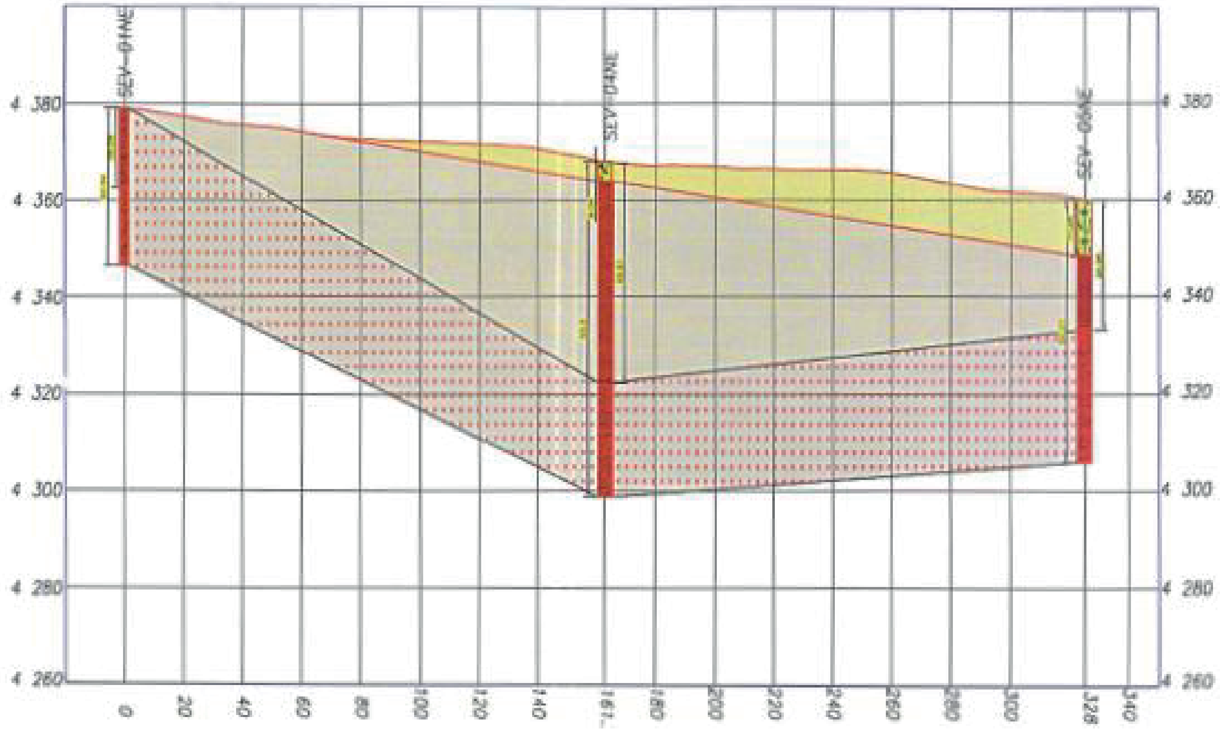

Figure 2.5: Geo-electric Section of Resistivities 4 (see Annex B.4).

Geo-electric Section 5. Figure 2.6.

The geo-electric section 5 identified the last contact at a depth of 70 meters. It has a preferential east-west direction and is integrated by three VES (VES-05NE, VES-06NE and VES-07NE) with a total AB length of approximately 300 meters. The analysis indicates the presence of three geo- electric units with variable thicknesses (see Image 2.13).

The resistivity values presented in this section range from 141 to more than 1,000 Ohm-m. Unit A is the first geo-electric unit that is presented; it has resistivity values of 230 to 393 Ohm-m with a thickness of 3.6 to 11.5 meters. Unit B has resistivity values from 342 to more than 1,000 Ohm-m with a thickness of 7.3 to 59.6 meters. Unit C has the largest depth located on the right side of the profile, with resistivity values from 141 to greater than 700 Ohm-m with a thickness of 25.3 to 40 meters. The characteristics of each geo-electric unit are described in the tables of each respective VES.

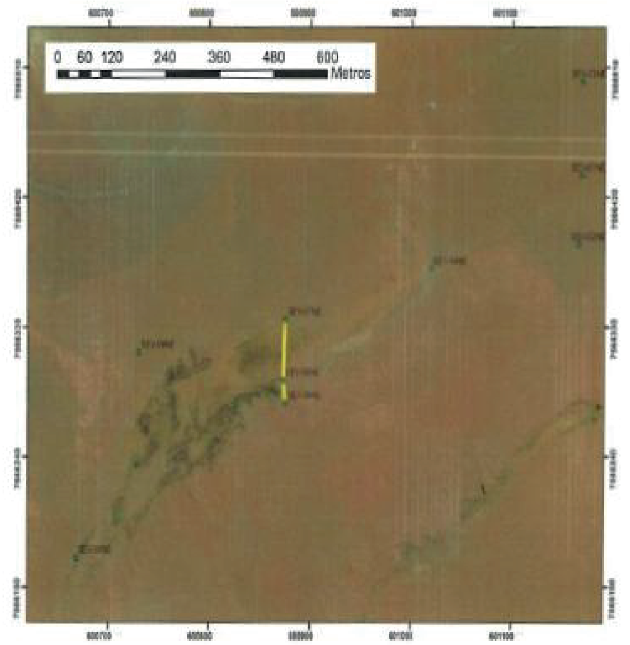

Image 2.13: Geo-electric Section 5

GEO-ELECTRIC SECTION N – 5

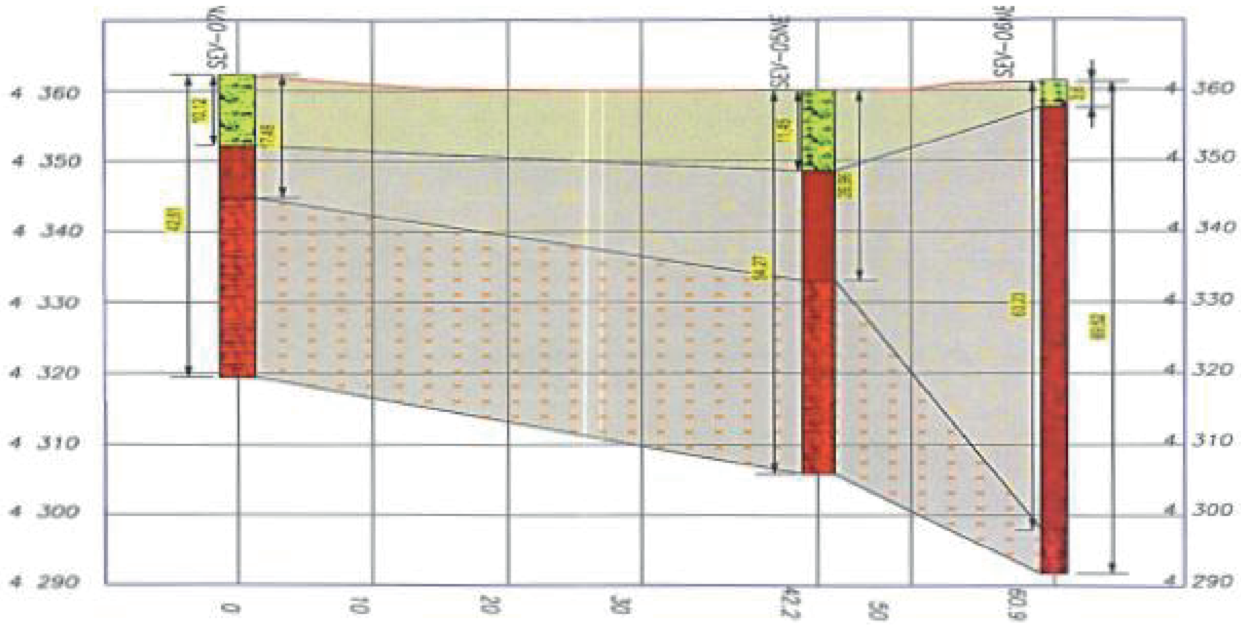

Figure 2.6: Geo-electric Section of Resistivities 5 (see Annex B.4).

Geo-electric Section 6. Figure 2.7.

The last contact was identified at a depth of 70 meters. It has a preferential east-west direction and is integrated by two VES (VES-08NE and VES-09NE), with a total AB length of approximately 250 meters. The analysis indicates the presence of two geo-electric units with variable thicknesses (see Image 2.14).

The resistivity values presented in this section range from 161 to more than 600 Ohm-m. Unit A is the first geo-electric unit that is presented; it has resistivity values of 161 to 695 Ohm-m with a thickness of 1.8 to 2.4 meters. Unit B is presented in greater depth with respect to Unit A as shown in the profile, with resistivity values of 223.6 to 330 Ohm-m and with a thickness of 60 to 65.8 meters. The characteristics of each geo-electric unit are described in the tables of each respective VES.

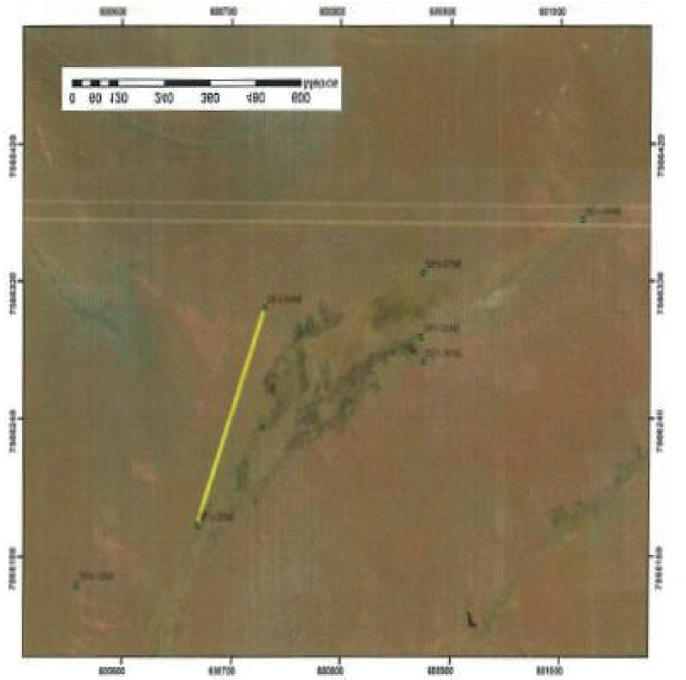

Image 2.14: Geo-electric Section 6

GEO-ELECTRIC SECTION N – 6

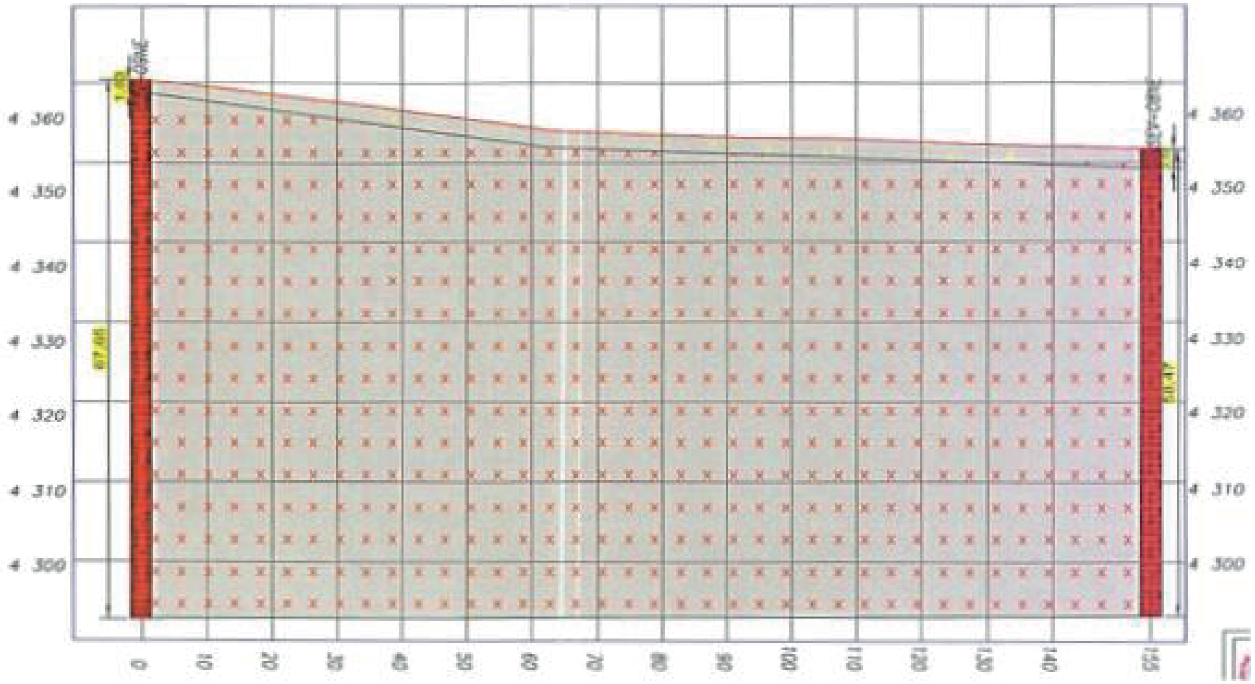

Figure 2.7: Geo-electric Section of Resistivities 6 (see Annex B.4).

Conclusions CHAPTER 11 (GEOPHYSICS)

In the study area, 15 Vertical Electrical Soundings (VES) were made; in south-east-east and north- west direction, where the following aspects are concluded:

VES-01SE Analysis:

The 1st layer has a depth of 3.6 meters, with a resistivity of 640.2 Ohm-m; it indicates the presence of alluvial material saturated with weathered Ignimbrite. The 2nd layer with 6.43 meters of depth, has a thickness of 3.66 meters and a resistivity of 88.74 Ohm-m, corresponding to welded ignimbrite material.

The 3rd layer is 14.08 meters deep and the resistance increases to more than 1000 Ohm-m. This high resistivity corresponds to a medium-high saturated ignimbrite, which indicates the fracturing of the rock. The last layer has a depth of 31.09 meters, a thickness of 17.01 meters and a resistivity of 16.5 Ohm-m; it corresponds to fractured ignimbrite material. The presence of the water table is found from 0.28 meters, being a level considered as almost emerging.

VES-02SE Analysis:

The 1st layer has a depth of 5,255 meters, a resistivity of 137.8 Ohm-m, which indicates the presence of alluvial material saturated with weathered ignimbrite. The 2nd layer has 9.92 meters of depth, a thickness of 4,664 meters and a resistivity of 75.83 Ohm-m, corresponding to welded ignimbrite.

The 3rd layer has a depth of 30.71 meters and a resistivity of 158.4 Ohm-m. This resistivity corresponds to medium-high saturated ignimbrite, which indicates the fracturing of the rock.
Finally, the last layer has a resistivity of 249.4 Ohm-m with a depth of 70.92 meters, indicating the presence of fractured ignimbrite.

VES-03SE Analysis:

The 1st layer has a depth of 5,255 meters, has a resistivity of 135.8 Ohm-m, which indicates the presence of alluvial material saturated with weathered ignimbrite. The 2nd layer has a depth of 16.44 meters, a thickness of 1,962 meters and a resistivity of 75.27 Ohm-m, corresponding to welded ignimbrite.

The 3rd layer has a depth of 34.35 meters and a resistivity of 145.2 Ohm-m. This resistivity corresponds to medium-high saturated ignimbrite, which indicates the fracturing of the rock.

The last layer has a depth of 71.78 meters, a thickness of 17.91 meters and a resistivity of 368.6 Ohm-m, indicating the presence of fractured ignimbrite.

VES-04SE Analysis:

The 1st layer has a depth of 2,697 meters, a resistivity of 202.2 Ohm-m, which indicates the presence of alluvial material saturated with mixture of medium-high fractured ignimbrite. The 2nd layer has a depth of 4,324 meters and a thickness of 1,628 meters, a resistivity of 37.88 Ohm-m and corresponds to welded material.

The 3rd layer has a depth of 43.88 meters, a thickness of 39.55 meters, a resistivity of 206.1 Ohm-m, resistivity that responds to fractured ignimbrite, which indicates the fracturing of the rock.

VES-05SE Analysis:

The 1st layer has a depth of 1.5 meters with a resistivity of 155.3 Ohm-m; it indicates the presence of alluvial material saturated with fractured medium-high ignimbrite mixture. The 2nd layer has a depth of 4,324 meters, a thickness of 1,628 meters, with a resistivity of 37.88 Ohm-m, corresponding to welded ignimbrite.

The 3rd layer has a depth of 43.88 meters, a thickness of 45.55 meters and a resistivity of 206.1 Ohm-m; it responds to fractured ignimbrite, which indicates the fracturing of the rock.

VES-06SE Analysis:

The 1st layer has a depth of 3,174 meters with a resistivity of 207.3 Ohm-m; it indicates the presence of alluvial material saturated with fractured medium-high ignimbrite mixture. The 2nd layer has a depth of 3.31 meters, a thickness of 3.301 meters, with a resistivity of 13.22 Ohm-m, corresponding to welded material.

The last layer has a depth of 35.43 meters and a resistivity of 604.2 Ohm-m; it belongs to fractured ignimbrite, which indicates the fracturing of the rock.

VES-01NE Analysis:

The 1st layer has a resistivity of 866.9 Ohm-m and a depth of 16.28 meters. It indicates the presence of alluvial material saturated with clay sediments and weathered ignimbrite.

The last layer has a depth of 32.32 meters and a resistivity of 44.42 Ohm-m, corresponding to fractured ignimbrite. The presence of the water table is found from 0.40 meters.

VES-02NE Analysis:

The 1st layer has a resistivity of 200.4 Ohm-m and a depth of 20.76 meters. It indicates the presence of alluvial material with clay sediments and weathered ignimbrite.

The last layer has a depth of 62.55 meters and a resistivity of 901 Ohm-m, corresponding to fractured ignimbrite.

VES-03NE Analysis:

The 1st layer has a resistivity of 1167 Ohm-m and a depth of 22.7 meters. It indicates the presence of alluvial material saturated with clay sediments and weathered ignimbrite.

The last layer has a depth of 46.59 meters and a resistivity of 31.23 Ohm-m, corresponding to fractured ignimbrite.

VES-04NE Analysis:

The 1st layer has a depth of 4,044 meters and a resistivity of 257.4 Ohm-m. It indicates the presence of alluvial material saturated with sandy sediments. The 2nd layer has a depth of 45.69 meters, a thickness of 41.65 meters and a resistivity of 429.6 Ohm-m, corresponding to sandy-clayey sediments.

The 3rd layer has a depth of 69.3 meters and a resistivity of 200.8 Ohm-m, corresponding to fractured ignimbrite that indicates the fracturing of the rock.

VES-05NE Analysis:

The 1st layer has a depth of 11.45 meters and a resistivity of 295.6 Ohm-m, indicating the presence of alluvial material saturated with sandy sediments. The 2nd layer has a depth of 26.96 meters, a thickness of 15.5 meters and a resistivity of 600.9 Ohm-m, corresponding to sandy-clayey sediments.

The last layer has a depth of 54.27 meters and a resistivity of 141.9 Ohm-m, corresponding to fractured ignimbrite that indicates the fracturing of the rock.

VES-06NE Analysis:

The 1st layer has a depth of 3.622 meters and a resistivity of 239 Ohm-m, indicating the presence of alluvial material saturated with sandy sediments. The 2nd layer has a depth of 63.25 meters, a thickness of 59.63 meters and a resistivity of 342.4 Ohm-m, corresponding to sandy-clayey sediments.
The 3rd layer has a depth of 59.52 meters and a resistivity of 780.1 Ohm-m, corresponding to fractured ignimbrite that indicates the fracturing of the rock.

VES-07NE Analysis:

The 1st layer has a depth of 10.12 meters and a resistivity of 392.9 Ohm-m, indicating the presence of alluvial material with sandy sediments. The 2nd layer has a depth of 17.48 meters, a thickness of 7.363 meters and a resistivity of 1,112 Ohm-m, corresponding to sandy-clayey sediments.
The last layer has a depth of 42.81 meters and a resistivity of 154.4 Ohm-m, corresponding to fractured ignimbrite that indicates the fracturing of the rock.

VES-08NE Analysis:

The 1st layer has a depth of 2.368 meters and a resistivity of 694.9 Ohm-m, indicating the presence of alluvial material with sandy-clayey sediments. The 2nd layer has a depth of 58.47 meters, a thickness of 60.36 meters and a resistivity of 223.6 Ohm-m, corresponding to fractured ignimbrite.

VES-09NE Analysis:

The 1st layer has a depth of 1.831 meters and a resistivity of 161.3 Ohm-m, indicating the presence of alluvial material with sandy-clayey sediments. The 2nd layer has a depth of 67.65 meters, a thickness of 65.82 meters and a resistivity of 330.4 Ohm-m, corresponding to fractured ignimbrite material.

Recommendations

 It is recommended to take into account the VES geophysical tests carried out in the south- east and north-east directions in the springs, which show lithological correlation of alluvial sediments and fractured ignimbrite volcanic material.

 Seismic refraction methods must be designed at a great depth in order to pass the ignimbrite packages and detect the underground water storage package.

 Drilling is recommended in the southeast - northeast sectors, in the head and at the end of the spring system, where the capacity of groundwater flow can be defined through hydraulic tests (Lefrang Method).

CHAPTER 3

MODELLING

TABLE OF CONTENTS

FIGURES

TABLES

MAPS

CHAPTER III. SIMULATION OF THE WATER SUPPLY OF THE SILALA SPRINGS

3.1. Background

According to Hydraulic Dams and Desertification in Bolivia (1995), to determine the relationships between water supply, captured water, water dedicated to consumptive use of crops, and water which returns, and requires a series of hydrological analysis data.

In the study area, the hydrological regime is variable during the seasons of the year, with very little contribution of rain, according to historical precipitation data is 80 mm; therefore, the problem of establishing a water balance becomes more complicated.

According to water balance calculation methods, knowledge of the structure of the water balance of lagoons, surface basins and subterranean basins is fundamental for to achieve a more rational use of water resources in space and time, as well as to improve their control and redistribution.

On the other hand, the effects of climate change are becoming increasingly evident in the world and therefore in Bolivia. In the highlands of our country, the surface water regime has emerged from the historically known hydrological regimes. Periods of drought and intense precipitation are less and less predictable. It is therefore necessary to clarify the relationship between soil-water-plant-air.

The present research consists of carrying out a water balance to establish the movement of water and the water supply or runoff. In the study area, the numerical simulation value of the water balance is intended to quantify the contribution of rainwater to the volume of water anthropically channeled to the neighboring country of Chile.

In the study area there is no meteorological information or hydrological studies, the station closest to 40 km is Laguna Colorada, whose data are very consistent, the same that served to calibrate the modeling. For this reason, a classical water balance was not undertaken, which is why it was decided to carry out a "numerical simulation" of the water supply from the Silala springs.

3.2. Justification

During the last few decades, there has been a lack of information on the origin of the water resources drained by the aforementioned artificial channels; therefore it is necessary to quantify the origin of these water resources and determine whether the source is surface water, groundwater or a percentage of both.

3.3. Objective

Numerically simulate the surface water supply of the Silala zone, which will make it possible to quantify the amount of rainwater that reaches the drainage channels.

3.4. Meteorological Information

In spite of having a very significant advance in the application of remote sensors with multi- resolution and multi-temporal images, the greatest difficulty consists in obtaining meteorological data. This occurs in Bolivian territory as in most of the countries of the region; however through specialized software it is possible to access data, including timetables, from automatic stations located in various parts of our planet and our country.

In this respect, in 2002, the LOCLIM software was developed to provide an estimate of the climatic conditions around the globe, and to obtain a database of more than 30000 stations located all over the world. This software has incorporated several methods of interpolation of specific data and it was considered that, for the purposes of estimating the water supply of the study area, this information is appropriate because it was validated with historical data from the weather station of Colorada Lagoon.

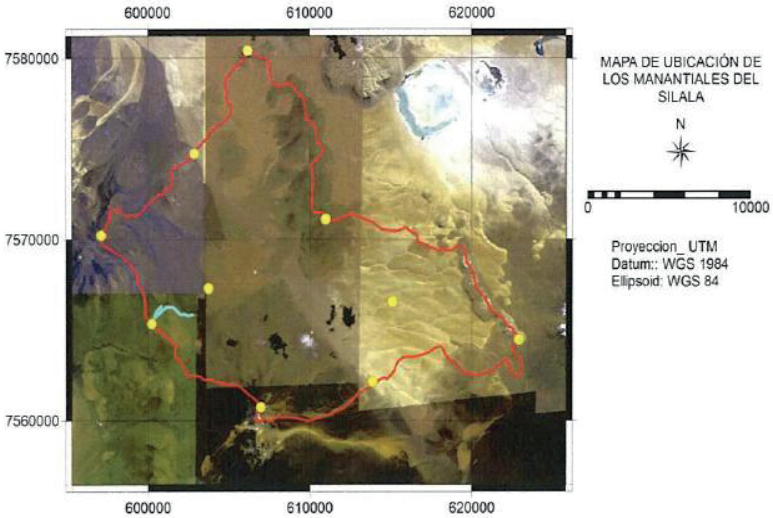

Figure 3.1. Location of simulated stations

N°	NAME	COUNTRY	Longitude	Latitude	Elevation (m.a.s.l.)
1	Alto D Comete	Argentina	-65,26	-24,21	1.253,0
2	Jujuy	Argentina	-65,28	-24,16	1.303,0
3	La Quiaca	Argentina	-65,60	-22,10	3.459,0
4	S. Salvador D	Argentina	-65,30	-24,18	1.303,0
5	Salta-Aereo	Argentina	-65,48	-24,85	1.221,0
6	Challapata	Bolivia	-66,76	-18,86	3.720,0
7	Chuquina	Bolivia	-67,40	-17,83	3.824,0
8	Oploca	Bolivia	-65,76	-21,31	3.120,0
9	Oruro	Bolivia	-67,06	-18,05	3.702,0
10	Pazña	Bolivia	-66,90	-18,60	3.710,0
11	Pocoata	Bolivia	-66,16	-18,65	3.423,0
12	Potosi	Bolivia	-65,71	-19,53	3.934,0
13	Puna	Bolivia	-65,46	-19,75	3.420,0
14	Salinas de G	Bolivia	-67,70	-19,60	3.630,0
15	Sucre	Bolivia	-65,26	-19,01	2.903,0
16	Tacagua	Bolivia	-66,76	-18,88	3.720,0
17	Tarija	Bolivia	-64,71	-21,53	1.875,0
18	Calama	Chile	-68,90	-22,50	2.312,0
19	Parincota	Chile	-69,26	-18,16	4.420,0
20	Refresco	Chile	-69,86	-25,31	1.850,0

Table 3.1. Stations taken into account for numerical simulation (Source LOCCLIM)

The LocClim software, based on information from a point expressed in latitude, longitude and elevation, provides data on the monthly total precipitation average and monthly average temperature for a year (January to December). The consistency of the simulated information through ten points located in the study area was verified with data from the Laguna Colorada station.

Station	Jan	Feb	Mar	Apr	May	Jun	Jul	Aug	Sep	Oct	Nov	Dec
EstSim1	82,7	69,0	24,8	0,0	0,0	1,3	1,3	0,5	0,0	0,0	0,0	7,3
EstSim2	23,5	0,0	0,0	0,4	0,0	0,0	0,0	0,0	0,0	0,0	0,0	0,0
EstSim3	9,8	0,0	0,0	0,0	0,0	0,0	0,0	0,0	0,0	0,0	0,0	0,0
EstSim4	29,2	12,2	0,0	0,0	0,0	0,0	0,0	0,0	0,0	0,0	0,0	0,0
EstSim5	41,7	26,0	1,0	0,0	0,0	0,0	0,0	0,0	0,0	0,0	0,0	0,0
EstSim6	32,6	15,3	0,0	0,0	0,0	0,0	0,0	0,0	0,0	0,0	0,0	0,0
EstSim7	25,1	8,0	0,0	0,0	0,0	0,0	0,0	0,0	0,0	0,0	0,0	0,0
EstSim8	18,4	1,0	0,0	0,0	0,0	0,0	0,0	0,0	0,0	0,0	0,0	0,0
EstSim9	39,1	23,1	0,0	0,0	0,0	0,0	0,0	0,0	0,0	0,0	0,0	0,0
EstSim10	48,4	32,9	4,9	0,0	0,0	0,0	0,0	0,0	0,0	0,0	0,0	0,0

Table 3.2. Total monthly precipitation data of stations simulated from the LOCCLIM satellite

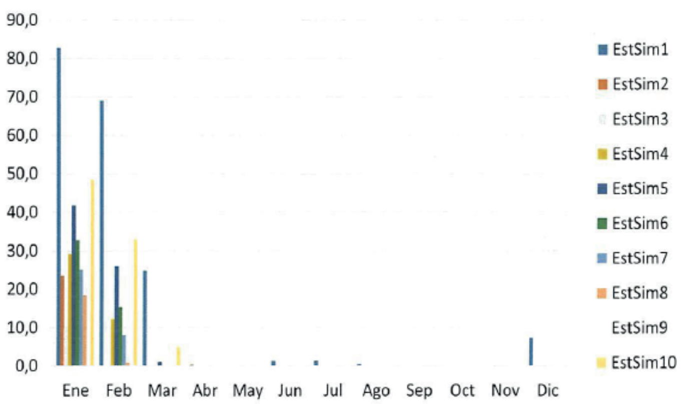

Figure 3.2. Monthly precipitation graph for simulated stations

Figure 3.1 shows the location of the simulated stations (points), with precipitation and temperature data. The simulation of the water supply or surface runoff was carried out with information from the stations shown in Table 3. 1. 20 stations were taken into account, of which 5 are from Argentina, 12 from Bolivia and 3 from Chile Table 3.1.

Station	Jan	Feb	Mar	Apr	May	Jun	Jul	Aug	Sep	Oct	Nov	Dec	Elevation
EstSim1	9,50	9,34	9,24	7,55	4,60	1,19	1,52	2,36	5,33	6,92	8,19	9,21	4281,00
EstSim2	5,27	5,44	5,68	4,43	1,37	-2,16	-1,76	-1,22	1,67	3,18	4,30	5,08	5345,00
EstSim3	5,42	5,59	5,86	4,46	1,48	-1,97	-1,51	-1,08	1,84	3,27	4,36	5,17	5636,00
EstSim4	7,09	7,11	7,22	5,81	2,77	-0,76	-0,40	0,31	3,26	4,84	6,03	6,89	4897,00
EstSim5	10,05	10,06	10,30	6,97	1,33	-4,89	-4,03	-3,14	2,00	4,58	6,74	9,97	4591,00
EstSim6	7,20	7,21	7,31	5,90	2,86	-0,68	-0,32	0,40	3,36	4,94	6,13	7,00	4876,00
EstSim7	7,90	7,92	8,26	6,78	3,70	0,19	0,68	1,33	4,42	5,98	7,07	7,79	4978,00
EstSim8	7,60	7,65	8,07	6,62	3,49	-0,06	0,45	1,11	4,22	5,80	6,88	7,51	5117,00
EstSim9	9,13	9,05	9,27	7,69	4,61	1,10	1,54	2,33	5,44	7,05	8,21	8,99	4650,00
EstSim10	8,85	8,75	8,71	7,07	4,11	0,68	1,03	1,81	4,78	6,35	7,59	8,57	4455,00

Table 3.3. Average monthly temperature data for simulated stations from the LOCCLIM satellite

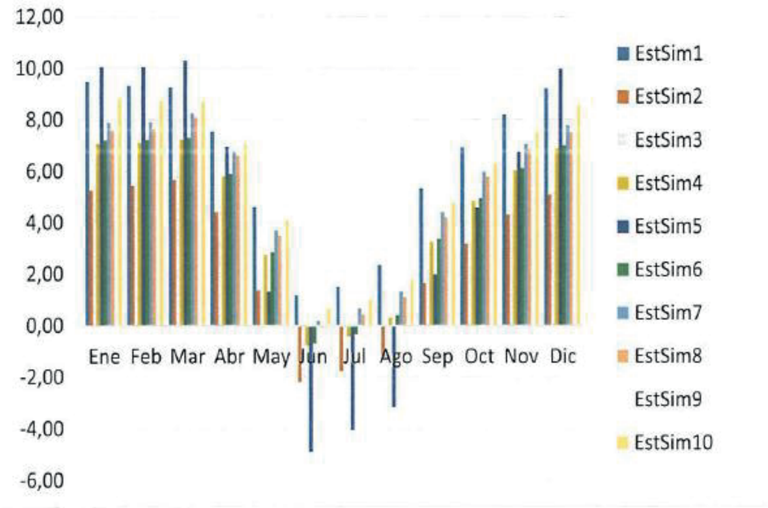

Figure 3.3. Monthly average temperature graph for simulated stations

Table 3.2 shows the average monthly precipitation of the ten simulated stations. Figure 3.2 details the relationship of precipitation vs. months of the ten stations simulated in the Silala.

On the other hand, Table 3.3 shows the information on the average monthly temperature of the ten simulated stations, and Figure 3.3 shows the graph representing the average monthly temperature of the ten simulated stations.

From these data, interpolated and rasterized precipitation maps are obtained for the twelve months.

For temperature, the Thornthwaite-Mather formula uses the average temperature per month. In flat terrain it is correct to interpolate the linear temperature between the seasons of the climate. In regions where there is a large difference in altitude, this method will not work. With the empirical knowledge that temperature decreases by 0.46 C for every 100 meters of altitude increase it is possible to optimize the interpolation method (Agricultural Compendium, 1981). If the actual altitude is greater than the theoretical altitude, the temperature correction is subtracted (the temperature decreases as the altitude increases). If the actual altitude is lower than the theoretical altitude, the temperature correction is added (the temperature increases as the altitude decreases). This form of interpolation was used by Orstom/Unesco/II 11I/Scnamhi (1990).

Under this principle, the interpolated temperatures were corrected, obtaining corrected temperature maps for the months January to December.

3.5. Water Balance Calculation Methodology

The water balance model is based on equilibrium calculations by C.W. Thorntwaite and J.R. Mather Thorntwaite and Mather, 1995. The model calculates the water balance for a point. With the use of GIS, the water balance is modeled taking into account the spatial distribution of precipitation, evapotranspiration, temperature and characteristics of geology, soil, vegetation, etc.

The general formula of the water balance can be expressed by the following equation:

$$\mathbf{P = ETR + O + R +} \Delta \mathbf{S}$$

Where:

P= Precipitation

ETR= Real Evapotranspiration

D= Surface Runoff (Supply)

R= Deep Infiltration or Percolation

ΔS = variation in retention of water storage in the soil

These are the main elements that have to be estimated to calculate the moisture content in the soil, deficit and supply or runoff of water for the area of the Silala springs.

It is then possible to visualize how the deficit and supply act, in spatial and temporal variation, during the hydrological year, to estimate how much of the water flow, coming from rain, feeds the flow of the artificial channels, without taking into account the great contribution of the underground aquifers of the Silala springs.

In a simple way, the work methodology is exemplified in the flow chart represented in Figure 3. 4. This flow diagram conceptualizes the GIS platform with the relationships and links of the elements considered in the calculation of the water supply, as they are presented below where each of the formulas used is specified.

One of the great advantages of the Geographic Information System is that it allows the introduction and execution of mathematical and statistical formulas that even facilitate the elaboration of a model for the calculations as if they were matrices in raster format for spatial-temporal analysis. All the formulas used are described in this report according to their application.

In the flow diagram it can be observed that the initial maps are the GEOLOGICAL, the TOPOGRAPHIC, the HISTORICAL MONTHLY ACCUMULATED PRECIPITATION information and the HISTORICAL MONTHLY MEDIUM TEMPERATURE of the ten points strategically chosen according to their geographical location and elevation (see Figure 3.1).

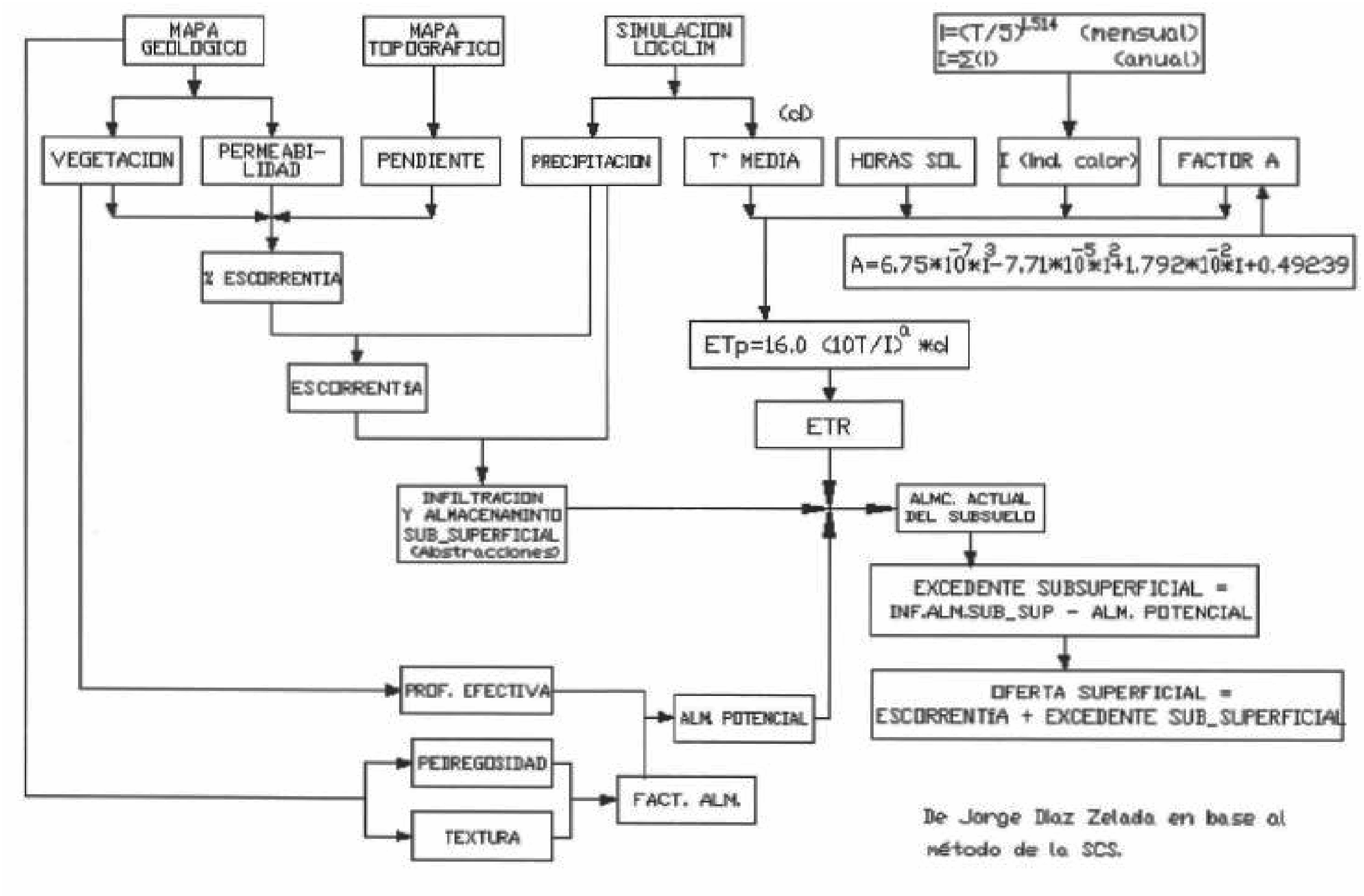

Figure 3.4. Flowchart of the numerical simulation of water supply

3.6. Simulation of the percentage of runoff from precipitation

The biophysical maps required for the calculation of the “monthly supply” of water in the Silala study area by the Thornthwaite & Mather method are (see Figure 3.4):

- Geological
- Vegetation
- Infiltration
- Digital Elevation Model

3.6.1. Geology of the Silala zone

The interpretation of the geology of the study area was carried out using the interpretation of remote sensors and based on geological reports from institutions such as SERGEOMIN, corroborated by the survey of geological information from field to detail carried out by the brigade of the Tomas Frias Autonomous University.

The unit that occupies the largest area are the Mio-Pliocenic volcanic lava, occupying 105, 16 km2, representing 42.2% of the study area. This unit is preferably located on the southern and northern flanks with small outcrops to the east and west of the study area (see Table 3. 4 and Map 3. 1).

The second most important geological unit are the Rhyolitic Ignimbrites (Welded tuff’s) with a total of 87 km2, representing 34.9% of the total area. This unit is preferably located to the north and east; however, there are also smaller outcrops to the west and south of the study area (see Table 3.4 and Map 3.1).

On the other hand, with an area of 57.2 km2 and 22.9% of the study area, there are the Pleistocene Non- Consolidated Deposits, which are located in the central part of the study area (see Table 3. 4 and Map 3. 1).

GEOLOGICAL UNIT	Area (m2)	Area (km2)	% Area
Mio-pliocenic volcanic lavas	105162500	105,2	42,2
Rhyolite Ignimbrites (Welded Tuff’s)	86996875	87,0	34,9
Pleistocenic non-consolidated deposits	57160000	57,2	22,9
SUM	**249319375**	**249,3**	**100,0**

Table 3.4. Geological units of the Silala springs

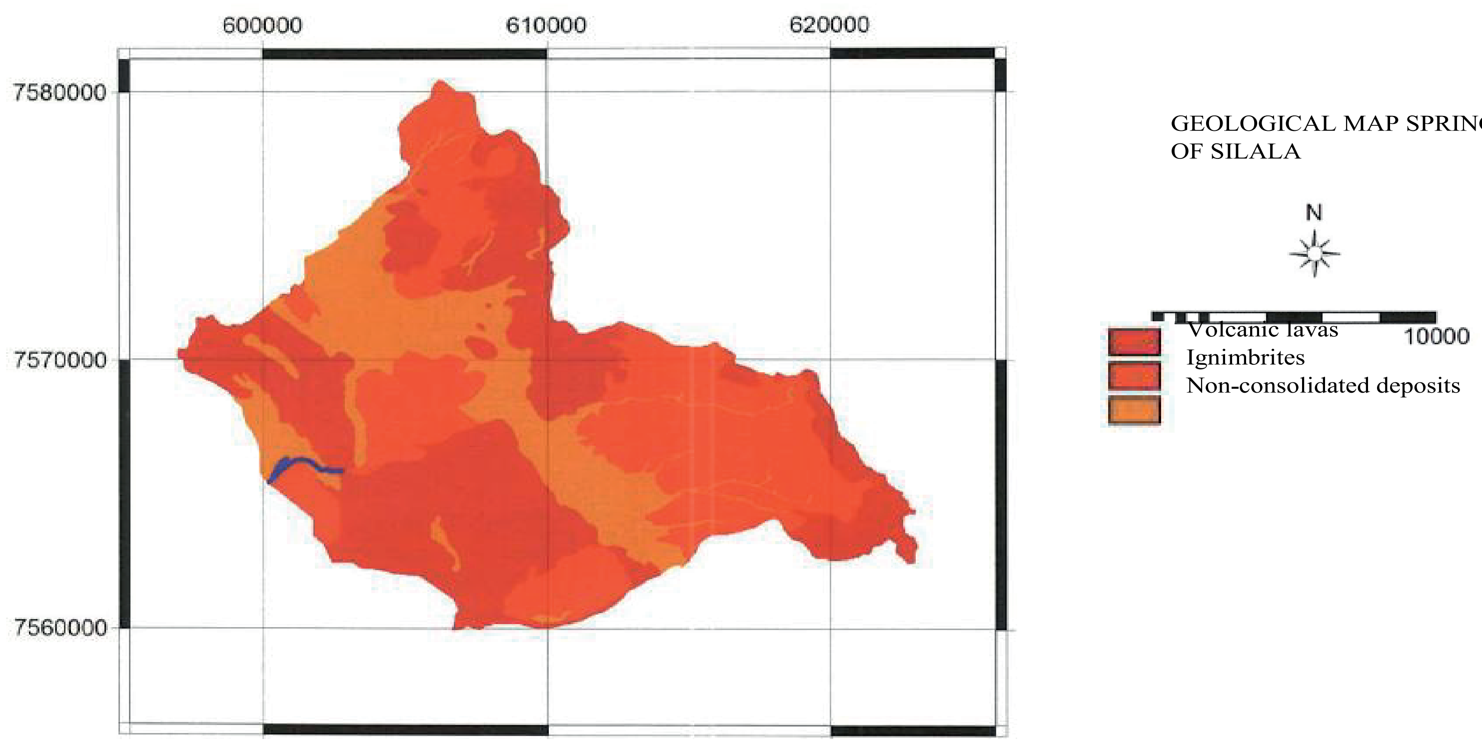

GEOLOGICAL MAP SPRINGS
OF SILALA

3.6.2. Description of the vegetation map

The vegetation has a very important influence on the amount of surface runoff. Dense and high vegetation can intercept rainfall, while incipient vegetation can favor soil erosion and the amount of supply water in the study area. The vegetation also protects the soil against the direct impact of raindrops on soil aggregates (Margan, 1981). According to the Soil Conservation Service (1964), five classes are defined:

No vegetation
Crops (permanent and temporary)
Grass, open vegetation
Shrubs and
Forest, dense vegetation

Due to the characteristics of the area of the Silala springs, only two units were identified: "Grass, open vegetation" and 'no vegetation' (see Table 3.5).

VEGETATION UNITS	**Area (m2)**	**Area (Km2)**	**% Area**
No vegetation	192159375	192,2	77,1
Grass and open vegetation	57160000	57,2	22,9
SUM	**249319375**	**249,3**	**100,0**

Table 3.5. Vegetation units of the Silala springs

The predominant unit is "No vegetation", with an area of 192.2 km2, occupying 77.1% of the total area of the study area. This unit is found throughout the entire study area (see Table 3.5 and Map 3.2).

A second unit is "Grass and open vegetation", whose area is 57.2 km2, which represents 22.9% of the total area. Like the previous unit, it is found along the whole basin, with intercalations of the unit of Pasture and Open Vegetation (see Table 3. 5 and Map 3. 2).

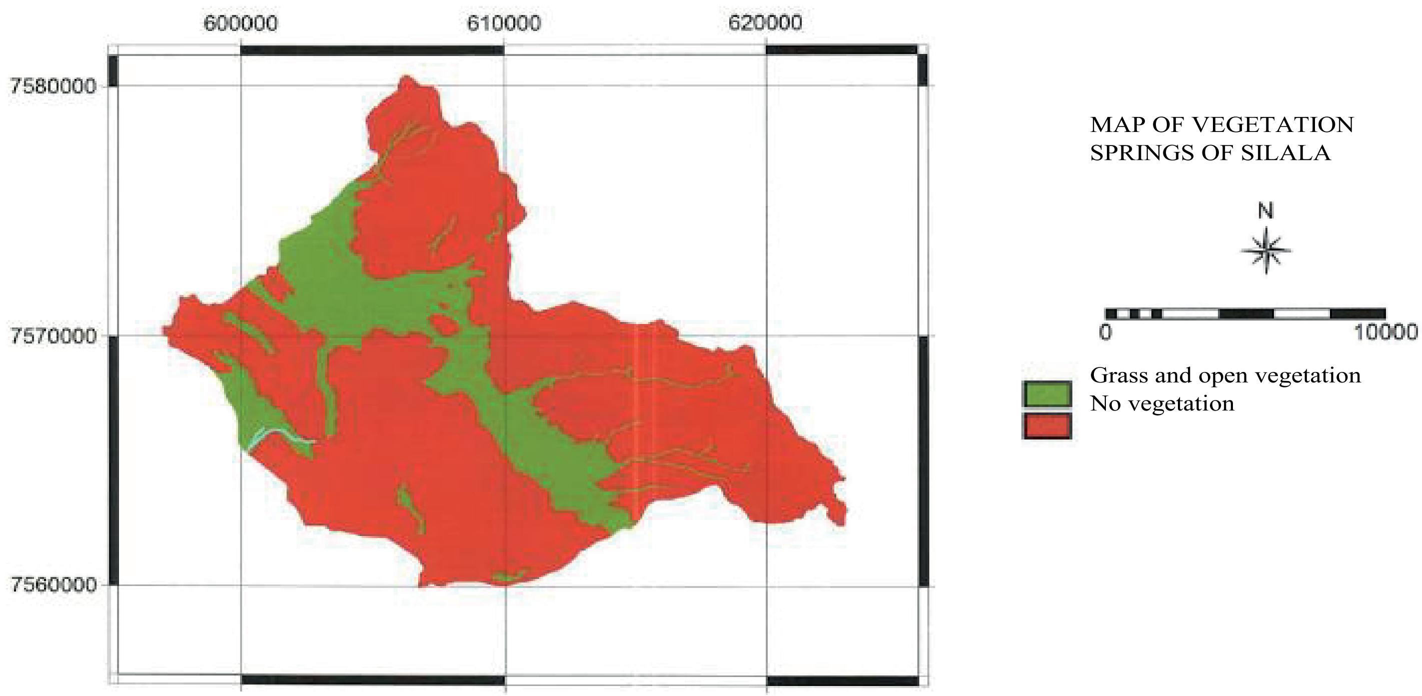
600000
610000
620000
7580000
7570000
7560000
MAP OF VEGETATION
SPRINGS OF SILALA
N
0
10000
Grass and open vegetation
No vegetation

3.6.3. Description of the infiltration map

Infiltration is the passage of water through the surface of the soil to the interior of the earth; percolation is the movement of water within the ground and both phenomena are closely linked, because the first cannot continue until the second takes place.

The water that infiltrates in excess of the subsurface runoff may become part of the groundwater, which may eventually reach the watercourses.

Therefore, infiltration is the process by which water penetrates the soil, through the surface of the land, and is retained by it or reaches an aquifer level increasing the previously accumulated volume. Surpassed by the field capacity of the soil, the water descends by the combined action of capillary forces and gravity. This part of the process is called infiltration - storage.

In the present research work, this parameter is fundamental to define the degree of infiltration, which in turn is defined as the volume of water infiltrated by a horizontal unit of the surface soil area at any given moment (Hess & Lovelace, 1994). In the US Soil Conservation classification, 3 classes are assigned to infiltration velocity: low, moderate and high.

For this purpose, several infiltration tests were carried out in the area of the Silala springs (see photographs 5, 6 and 7 in Annex C.1). After evaluating the infiltration tests, the geology map was reclassified according to these three levels of infiltration; however, in the study zone only Moderate and Low infiltration are presented (see Table 3. 6). This information is used for its application in the crossing of two-dimensional maps and tables for the estimation of runoff.

INFILTRATION UNITS	Area (m2)	Area (Km2)	% Area
Moderate	162322500	162,3	65,1
Low	86996875	87,0	34,9
SUM	**249319375**	**249,3**	**100,0**

Table 3.6. Infiltration units of the Silala springs

The moderate infiltration coincides with the outcrops of quaternary rock, whose porosity is high. The geological formations of this group are characterized by the fact that they are made up of loose material from non-consolidated materials. Moderate porosity formations occupy 162.3 km2, representing 65.1% of the study area and are located throughout the study area (Table 3. 6 and Map 3. 3).

The low permeability formations occupy 87.0 km2, representing 34.9% of the total area of the study zone. Their location is adjacent to the least permeable geological formations of the area, such as outcrops of volcanic igneous rock (Table 3. 6 and Map 3. 3).

3.6.4. Percent Slope Map

For the calculation of the slope, it is required the digital elevation model of the terrain that was obtained from the delimitation of the study area. The highest elevation of the study basin is 5689 and the minimum elevation is 4301 meters above sea level. (see Map 3. 4)

From the digital elevation model, gradients in the "x" and "y" directions were extracted. From the gradient maps dfdx and dfdy and applying the following equation, the percentage slope map is obtained in raster format.

*Slope:= (((HYP(dfdx, dfdy)/20)*100))*

However, this map of percentage slopes must still be reclassified in the ranges that allow the application of the runoff classification method. The ranks are as follows:

0-1%
1-5%
5-20%
20-50%
>50

This reclassified map is intended to perform a multi-criteria analysis in combination with vegetation and infiltration maps.

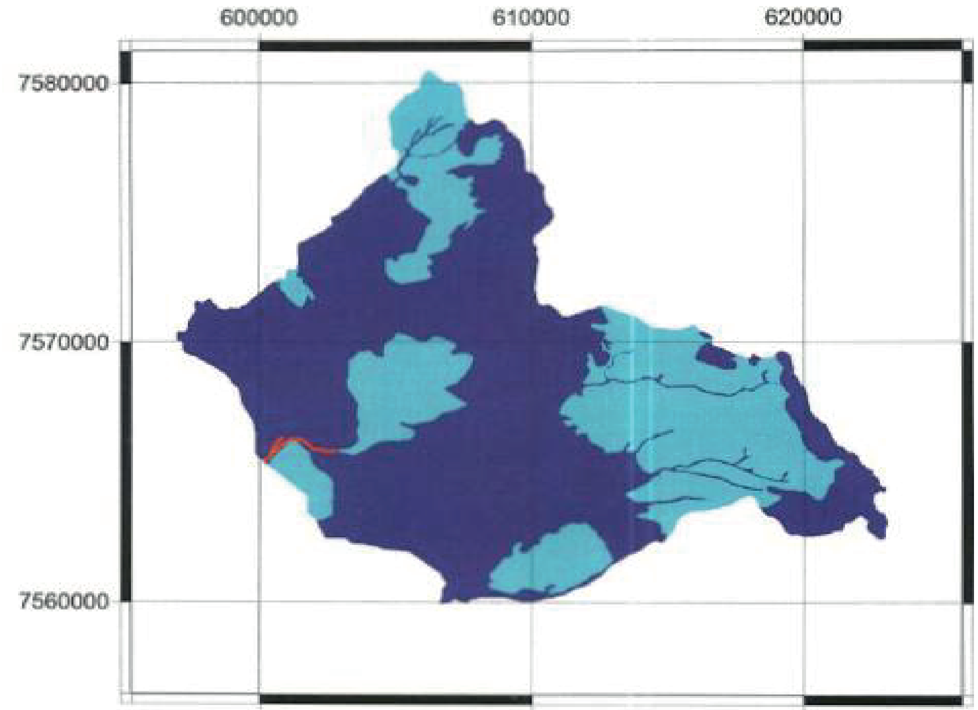

MAPA DE VEGETACION MANANTIALES DEL SILALA

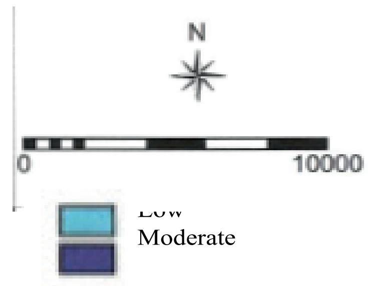

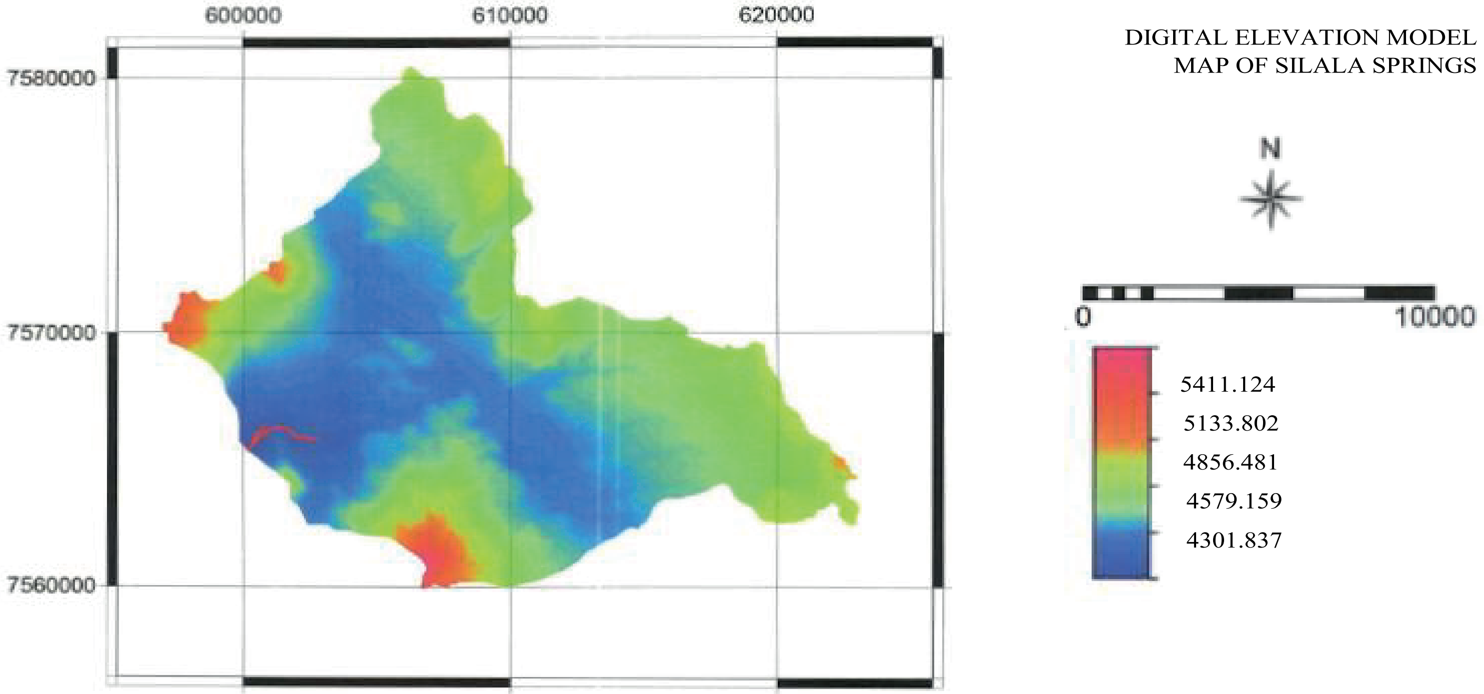

DIGITAL ELEVATION MODEL
MAP OF SILALA SPRINGS

3.6.5. Map of Surface Runoff, Infiltration and Storage

From the maps of VEGETATION (Map 3. 2), INFILTRATION VELOCITY (Map 3. 3) and SLOPE (Classified in ranges), the reclassification is carried out according to Table 3. 7. Thus, for each vegetation unit, it was reclassified with the values of infiltration speed and slope range. From the crossing and algebra of maps, we obtain the map of the percentage of rainwater that will become runoff from the Silala springs (see Map 3.5).

VEGETATION	INFLITRATION VELOCITY	SLOPE				
		>50%	50-20%	20-5%	5-1%	< 1%
No vegetation	Low	0.80	0.75	0.70	0.65	0.60
	Moderate	0.70	0.65	0.60	0.55	0.50
	High	0.50	0.45	0.40	0.35	0.30
Crops	Low	0.70	0.65	0.60	0.55	0.50
	Moderate	0.60	0.55	0.50	0.45	0.40
	High	0.40	0.35	0.30	0.30	0.25
Grass, open vegetation	Low	0.65	0.60	0.55	0.50	0.45
	Moderate	0.55	0.50	0.45	0.40	0.35
	High	0.35	0.30	0.25	0.20	0.15
Shrubs	Low	0.60	0.55	0.50	0.45	0.40
	Moderate	0.50	0.45	0.40	0.35	0.30
	High	0.30	0.25	0.20	0.15	0.10
Forest, dense vegetation	Low	0.55	0.50	0.45	0.40	0.35
	Moderate	0.45	0.40	0.35	0.30	0.25
	High	0.25	0.20	0.15	0.10	0.05

Table 3.7. Factors for the estimation of the SCS USA Surface Runoff

On the map of the percentage of runoff from the Silala springs (see Map 3.5), it can be seen that the more runoff, the more impermeable formations are present, and conversely, the more permeable formations, the less runoff.

Map 3.5, therefore, reflects the percentage of precipitation, which will become surface runoff, and then become part of the volume of water drained by artificial channels. Map 3.5, multiplied by the monthly precipitation maps, provides maps of monthly surface runoff in mm (see Annex C.2).

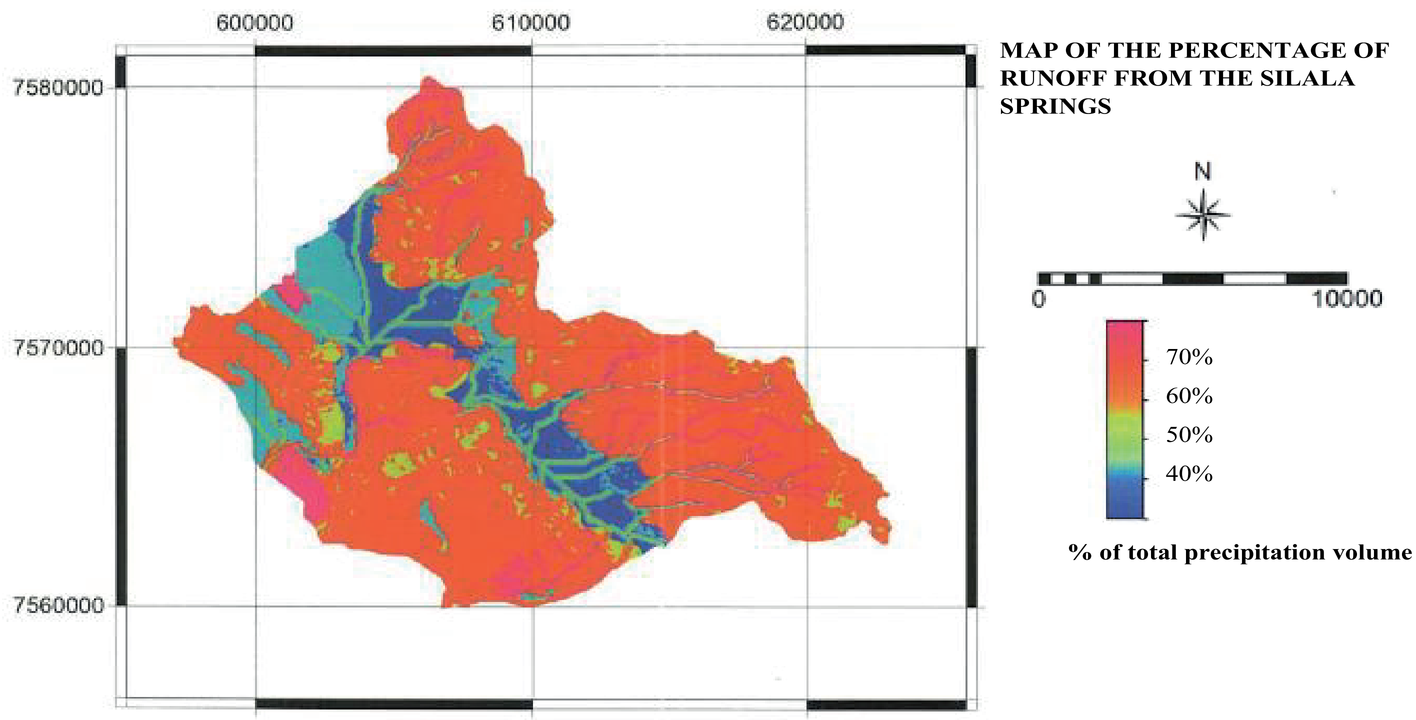

MAP OF THE PERCENTAGE OF RUNOFF FROM THE SILALA SPRINGS

On the other hand, the concept taken from "Infiltration and storage": in this calculation method, it is the water infiltrated into the soil up to one meter deep in direct relation between precipitation and surface runoff. As seen in the formula below.

Infiltration and storage = precipitation – runoff

To obtain the "Infiltration and Storage" maps, each runoff map (mm/month) is subtracted from the precipitation map of the same month (mm/month) from which twelve new "Infiltration and Storage" maps were obtained.

3.7. Potential Evapotranspiration

The simulation of Potential Evapotranspiration was carried out using the Thorntwaite equation, which in 1948 developed an empirical method to estimate potential evapotranspiration. It is mainly based on the average monthly temperature. The method was optimized with Mather in 1957 adding the factor "hours of sun".

The Thorntwaite-Mather formula is as follows:

$$\mathbf{ETp = 16.0\ (10T/I)^{a} * d}$$

Where:

ETp = Potential Evapotranspiration

T = average monthly temperature

I= heat index in a year (12 months = Σi monthly)

a = change factor

d = hours of brightness (in units of 30 days with 12 hours of sun each)

The temperatures of ten strategically chosen points were simulated taking into account the Colorada lagoon station as an index station (see Table 3. 3).

3.7.1. Temperature Adjustment with Digital Terrain Elevation Model

The Thorntwaite-Mather formula uses the average temperature per month. In flat terrain it is correct to interpolate the linear temperature between the seasons of the climate. Since there is a great difference of altitude in the zone of the springs of the Silala, with elevations that oscillate between 4301 and 5689 m.a.s.l., this method is not correct reason why it is required to include a factor of correction to the maps of monthly temperatures. With the theoretical knowledge that temperature decreases by 0.46 degrees for every 100 m of altitude increase it is possible to optimize the interpolation method (Agricultural Compendium, 1981). Thus, the interpolated temperature maps were adjusted with the digital elevation model to obtain a better adjustment for the temperature maps from January to December.

3. 7.2. Heat index (I)

To obtain this annual parameter, we start by calculating the monthly heat indexes applying the relationship:

$$\mathbf{i=(T/5)^{1.514}}$$

Where:

i = Monthly heat index

T = Average monthly temperature

The annual heat index (1) is the sum of the heat indexes per month (i) (Thorntwaite and Mather, 1957). In the geographic information system, an “i” factor map was created for each month. The sum of these twelve maps generated the annual heat index map.

$$\mathbf{I = \Sigma(i)}$$

I = Annual heat index or correction factor based on latitude

3.7.3. Hours of brightness (d)

The average number of hours of brightness depends on the latitude of the basin and the month of the year. Thornwaite and Mather created a table to express the average duration of hours of brightness (d) in units of 30 days with 12 hours of sun each. The Silala springs are found at 22 degrees latitude in the southern hemisphere. For each month, a map was created with a value for the whole basin. The values were extracted by interpolation for the required latitude of 22o, from the table created by Thorntwaite and Mather (1957), in which the relationship between latitude and hours of brightness is expressed (see Table 3. 8).

LAT SUR	JAN	FEB	MAR	APR	MAY	JUN	JUL	AUG	SEP	OCT	NOV	DIC
5	1.04	0.95	1.04	1.00	1.02	0.99	1.02	1.03	1.00	1.05	1.03	1.06
10	1.08	0.97	1.05	0.99	1.01	0.96	1.00	1.01	1.00	1.06	1.05	1.10
15	1.12	0.98	1.05	0.98	0.98	0.94	0.97	1.00	1.00	1.07	1.07	1.12
20	1.14	1.00	1.05	0.97	0.96	0.91	0.95	0.99	1.00	1.08	1.09	1.15
25	1.17	1.01	1.05	0.96	0.94	0.88	0.93	0.98	1.00	1.10	1.11	1.18
30	1.20	1.03	1.06	0.95	0.92	0.85	0.90	0.96	1.00	1.12	1.14	1.21
35	1.23	1.04	1.06	0.94	0.89	0.82	0.87	0.94	1.00	1.13	1.17	1.25
40	1.27	1.06	1.07	0.93	0.86	0.78	0.84	0.92	1.00	1.15	1.20	1.29
45	1.31	1.10	1.07	0.91	0.81	0.71	0.78	0.90	0.99	1.17	1.26	1.36
50	1.37	1.12	1.08	0.89	0.77	0.67	0.74	0.88	0.99	1.19	1.29	1.41

Table 3.8. Possible duration of hours of brightness Thornthwaite (1948)

3.7.4. Modification factor (a)

The modification factor “a” is directly related to the temperature by means of the annual heat index (1) and is calculated according to the following formula:

$$\mathbf{a = 6.75 * 10^{-7} * I^3 - 7.71 * 10^{-5} * I^2 + 1.792 * 10^{-2} * I + 0.49239}$$

Where:

a = Modification factor

I = Annual heat index

3.7.5. Calculation of Potential Evapotranspiration (Combination of T, I, d, a)

Twelve maps were created, from January to December, to visualize the ETp distribution. Combining all factors “T”, “I”, “d” and “a” using the equation of Thorntwaite and Mather. The ETp is calculated in each pixel per month with a pixel size of (25*25) m2 (See Annex C3).

The Etp, annual total, is equal to the sum of the monthly Etp. Figure 3. 5 shows the potential annual evapotranspiration of the study area ranging from 430 to 530 mm per year.

On the other hand, taking into account the ETp, and the real availability of water, twelve maps of the real evapotranspiration ETr were obtained. In turn, the sum of these 12 maps resulted in the annual ETr map shown in Figure 3. 6. Due to the low levels of precipitation in the study area, the annual ETr ranges from O to 91 mm.

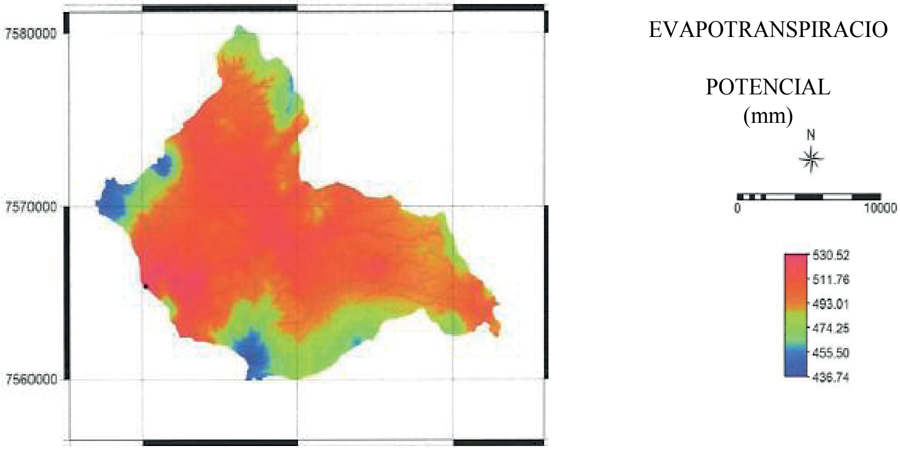

Figure 3.5. Potential annual evapotranspiration in the zone of the Silala springs

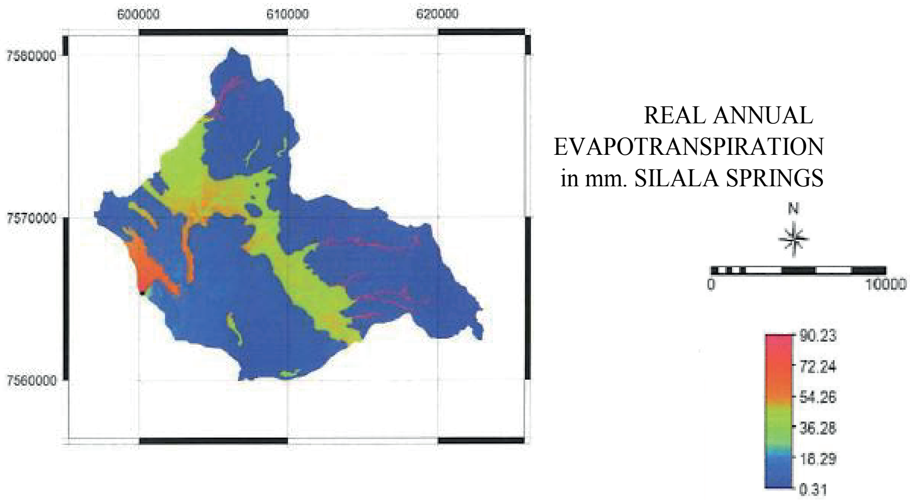

Figure 3.6. Actual annual evapotranspiration in the zone of the Silala springs

3.8. Soil Water Retention Capacity

Soil retains water in two ways: as free moisture in the pores in interstices between solid clay particles and organic particles (Agricultural compendium, 1981).

The second type of moisture is not available for plants and is called Hygroscopic Moisture.

The amount of water retained in the soil, available to the plants, is a factor in the water balance. If effective precipitation and the actual amount of water stopped are not sufficient to comply with evapotranspiration requirements, a deficit will occur. This means that the vegetation will not be able to absorb moisture from the soil and will fall under stress. On the other hand, when the retention capacity of the soil is saturated and there is effective precipitation, the water will percolate to the subsoil. In this case it is a surplus of water.

It is important to calculate the maximum amount of water that can be retained in the soil. This is called potential retention capacity. Booker in 1984 expressed the potential retention capacity as a relationship between soil texture and stoniness by means of a table from which we extracted only the data that were applied in this balance and which is shown in Table 3.11.

3.9. Soil texture map

The soil textural classification was carried out in the Soil Laboratory of the Agronomy Major from samples that were obtained in the surveyed area. This classification is based on the system applied by the USDA according to the size of the particles, in which the following classification is used:

- Silt, all particles whose size varies from 0.002 to 0.05 mm;
- Clay, all particles less than 0.002 mm.

In the description of the texture map, we have that the unit that occupies the largest area of the basin is the ―Rocky Outcrop‖: with 192.2 km2, which represent 77.1% of the area of the basin. This unit is characterized by being formed by outcrops of volcanic rock and is located along the entire basin (see Table 3. 9 and Map 3.6).

Soil Texture	Area (m2)	Area (km2)	% Area
Rocky outcrop	192159375	192,2	77,1
Loamy Silty	57160000	57,2	22,9
TOTAL	**249319375**	**249,3**	**100,0**

Table 3. 9: Units of soil texture of the Silala basin

3.10. Map of stoniness and gravel in percentage (%)

The stoniness map refers to the area occupied by rocks between boulders and angles. This value is important, because the higher this percentage is, the lower the possibility of impact of raindrops.

In Figure 3.7 and Table 3.10. Percentage of stoniness. Silala Springs – Table 3.10, it can be observed that the predominant unit is the unit with a content of 80 to 100% of stoniness. This unit occupies an area of 105.2 km^2, which represents 42.2% of the surveyed area; while the unit with 0 to 5% of stoniness occupies 22.9% of the total area with 57.2 km^2.

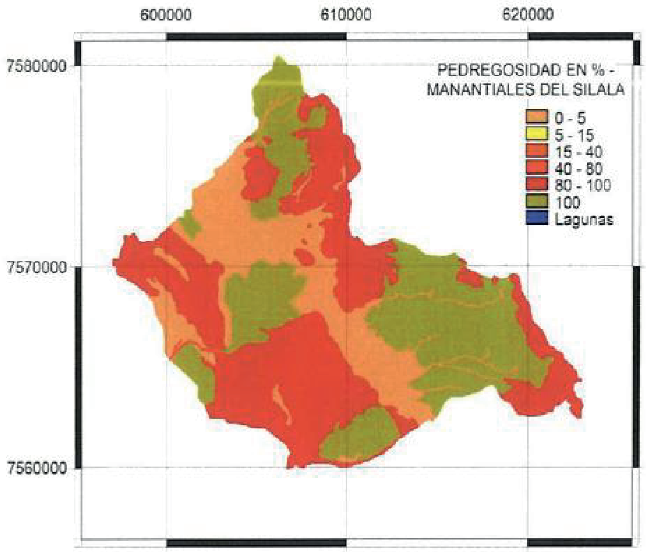

Figure 3.7: Percentage of stoniness – Silala Springs.

Stoniness Percentage	Area (m2)	Area (km2)	% Area
80 – 100	105162500	105,2	42,2
100	86996875	87,0	34,9
0 – 5	57160000	57,2	22,9
TOTAL	**249319375**	**249,3**	**100,0**

Table 3.10: Percentage of stoniness – Silala Springs.

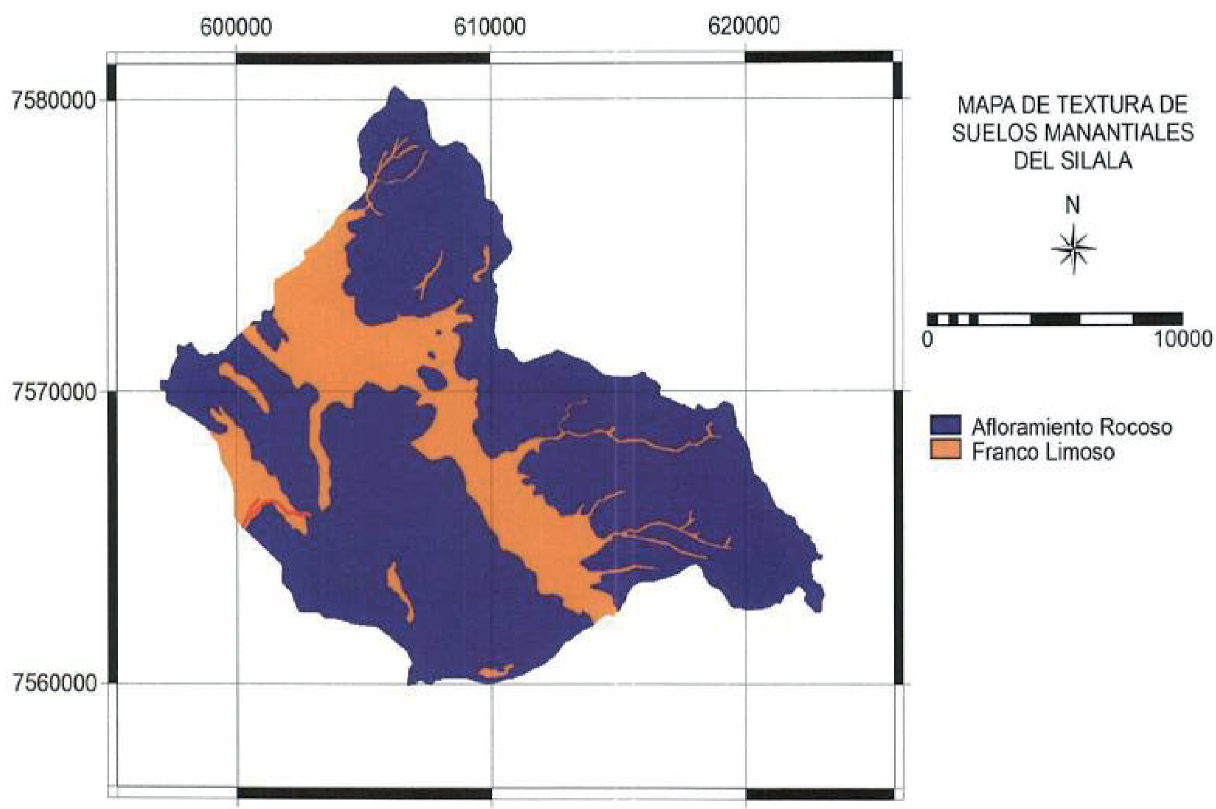

Map 3.6: Map of soil texture of the Silala Springs.

TEXTURE	WATER RETENTION CAPACITY IN THE SOIL (mm/m). STONYNESS AND GRAVEL IN%					
	0%	0-5%	5-15%	15-40%	40-80%	80%
Clay	140	130	120	90	50	10
Loam	170	160	140	110	40	20
Sand	90	80	70	60	30	10
Sandy-Loamy	110	100	90	70	40	10
Clay-Sandy	110	100	90	70	40	10
Clay-Loamy	150	140	130	100	55	10
Sandy						
Loamy-Sandy	150	130	120	100	55	10
Clay-Silty	160	140	130	110	55	10
Clay-Loamy	170	150	140	110	65	20
Silty						
Loamy-Silty	190	170	150	130	70	20
Loamy-Clay	150	130	120	100	55	10

Table 3. 11: Retention capacity of soil moisture. (Drainage Analysis and Extraction of Hydrologic Properties from a Digital Elevation Model, 1996).

3.11. Potential retention capacity

The potential retention capacity is calculated by multiplying the effective soil depth and the water retention capacity. It is assumed that there are no variations in stoniness and texture in a unit of land, so all the pixels located in a unit of land are classified with a value of texture and stoniness (see table 3.11). The potential retention capacity is used in the first month as a maximum of retained water to start the water balance. The water balance begins in December as this is the first month with storage that also uses the rain of the previous month (first month with rains). The maps used for Texture (see Map 3.6) and percentage of stoniness (see Figure 3.7) were constituted in important elements and were derived from the geological map with the change of attribute according to the parameters of Table 3.12.

GEOLOGICAL UNITS	Infiltration	Soil Texture	Vegetation (SCS)	Stoniness (&)	Effective Depth (cm)
Unconsolidated deposits	Moderate	Loamy-Silty	Grass and open vegetation	0 – 5	0.20
Ignimbrites	Low	Rocky outcrop	Without vegetation	100	0.09
Volcanic lavas	Moderate	Rocky outcrop	Without vegetation	80 – 100	0.09

Table 3. 12: Table of attributes of the map of the geological units of the Silala springs area.

3.12. Actual retention of moisture in the soil

Water retention will vary over time as evapotranspiration reduces water and effective precipitation adds water. The effective precipitation is added to the maximum retention capacity and the potential evapotranspiration is subtracted.

For the next month the rest of the water retained is added again to the effective precipitation and the potential evapotranspiration is subtracted. The actual retention can be calculated with the following equation:

$$S_{(a)} = P_{(ef)} + S_{(a)mes-1} - ETp$$

$$0 <= S_{(a)} <= S_{(p)}$$

Where:

S(a) = Potential storage

P(ef) = Potential evapotranspiration

S(a)mes-1 = Actual storage of the previous month

ETp = Effective precipitation

S(p) = Actual storage

The water balance calculations begin after the dry season, when P > Etr. In our case, it started in December and showed the maximum humidity retention in the months of February to March, with insignificant volumes for the volume of water drained to the drainage canals. In the rest of the months, there is no moisture retention, showing still much less significant values.

3.13. Actual Evapotranspiration

Potential evapotranspiration is the amount of water that evaporates when there is enough available water retained in the soil and subsoil and that month's precipitation.

The actual evapotranspiration depends on the effective precipitation, the potential evapotranspiration and the water storage of the previous month. When the effective precipitation and storage of the previous month is equal to or greater than the potential evapotranspiration, the actual evapotranspiration is equal to the potential evapotranspiration. If the effective precipitation and storage of the previous month is less than the potential evapotranspiration, the actual evapotranspiration is equal to the effective precipitation plus the storage of the previous month's humidity. The following equation expresses the aforementioned:

If:

$$P_{(ef)} + S_{(a)mes-1} >= ET_p \text{ entonces } ET_a = ET_p$$

$$\text{Dónde: } ETa = P(ef) + S(a)mes\text{-}1$$

Therefore, the actual evapotranspiration is the amount of water that really evaporates from the plants and the bare soil. In case there is enough water to evaporate (or in situations of excess), the potential evapotranspiration is equal to the actual evapotranspiration (ETp = ETr). If there is not enough water available then ETr < ETp. Due to the high water deficit of the survey area, the actual evapotranspiration is much lower than the potential evapotranspiration.

The calculations begin in December (generally the first month with precipitation). The actual retention for November is then used for the following calculations that begin in December.

3.14. Water deficit

The amount of soil moisture will be reduced when the effective precipitation is less than the potential evapotranspiration. At a certain moment the amount of water retained is zero and the vegetation still requires evaporation. Then there is a deficit. The deficit in this survey does not refer to the stress situation of the plants or to the point of permanent wilting, but to a moment of water stress suffered by the plants. This can also be expressed in an equation:

$$\text{Déficit de agua} = ET_p - (P_{(ef)} + S_{(a)mes-1})$$

The deficit only occurs when positive values are calculated. When negative values are calculated for the water deficit in this equation (ó: P(ef) + S(a)mes-1 > ETp and Eta = ETp) then these values are reclassified as zero (for calculation purposes).

It should be understood as the water deficit the amount of water that the plants in the survey area require, according to their spatial and temporal presence, for their normal development. However, deficit levels do not mean that plants reach the point of permanent wilting, but that they suffer water stress, which is reflected in plant development and production.

Month	Superficial runoff (hm3)	Inf_Alm (hm3)	ETP (hm3)	Deficit (hm3)	Supply (hm3)	Supply (l/sec)
January	5,81	3,14	16,74	11,57	7,86	2,93
February	3,22	1,75	14,56	12,81	1,55	0,64
March	0,46	0,25	15,93	15,68	0,21	0,08
April	0,00	0,00	12,19	12,19	0,00	0,00
May	0,00	0,00	1,39	7,39	0,00	0,00
June	0,02	0,01	0,78	0,78	0,01	0,00
July	0,02	0,01	1,60	1,59	0,01	0,00
August	0,01	0,00	3,11	3,10	0,00	0,00
September	0,00	0,00	8,75	8,75	0,00	0,00
October	0,00	0,00	12,18	12,18	0,00	0,00
November	0,00	0,00	14,19	14,19	0,00	0,00
December	16,62	0,05	16,62	16,56	0,05	0,02

Table 3.13: Statistical analysis of the area of the Silala springs (in hm3 and in l / sec)

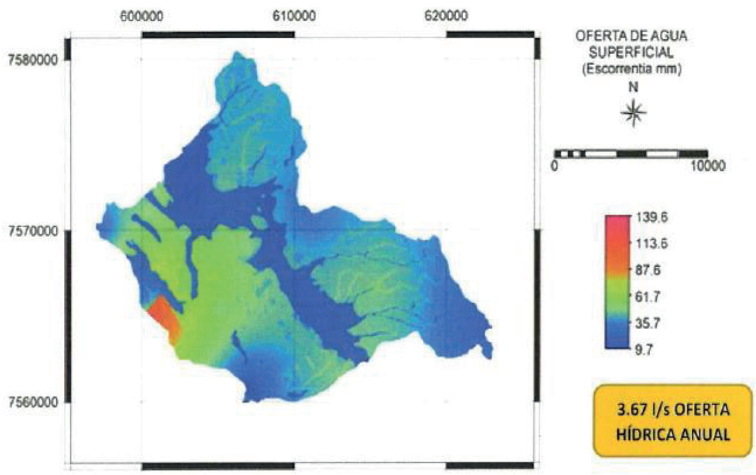

Figure 3.8: Map of Annual Water Supply (m/year)

3.15. Water surplus

When the effective precipitation is greater than the potential evapotranspiration, the amount of moisture retained will increase. Water will be retained up to the maximum amount of potential storage capacity (S(a) = S(p)). If more water enters the soil, it will percolate as surplus. The following equation expresses this relation:

Subsurface Water Surplus = P(ef) - ETr + S(a)mes-1

Where: **ETr = ETp and S(a) = S(p)**

When negative values are calculated with the equation (P(ef) - ETp + S(a)mes-1 < S(p) there is no surplus. Negative values must be reclassified as zero. In the survey area, due to the incipient amount of this factor, it can be considered 0.

3.16. Water supply

The water supply of the survey area will be equal to the sum of the surface runoff plus the surplus of the subsurface water and is expressed as:

WATER SUPPLY = SURFACE RUNOFF + SUB-SUPERFICIAL SURPLUS

The calculation was made in each of the 625 m2 area pixels, which allows us to establish the supply of surface water at the exit of artificial canals. For this, it is sufficient to make the summation of all the pixels that contribute with their ―SUPPLY‖ when leaving the survey area (see Figure 3.8 and Annex C2).

Once the water supply of the survey area has been calculated, this volume is 2.93 l/sec for the month of January and 0.64 l/sec for the month of February, making a total of 3.67 l/sec per year. The rest of the months are considered 0 l/sec, since the supply values obtained are insignificant (see Table 3.13 and Annex C4).

Conclusions CHAPTER III (WATER MODELING)

The georeferencing of the satellite image has allowed the interpretation of the image with the reallocation of values and indexes for several parameters that have to do with the water balance and the estimate of water supply. These indexes and parameters were corroborated with the fieldwork.

The study basin area was rasterized in pixels of 25*25 m, which allowed a detailed analysis of the water supply.

The ratio Monthly Precipitation versus Potential Evapotranspiration is from 1 to 5. This means that for every millimeter of rain, 5mm evaporates; this leads to a superficial water deficit in the survey area.

The water supply or surface runoff generated by the precipitation of the survey area only has a maximum flow of 2.93 l/sec for the month of January and 0.64 l/sec for the month of February, 0.08 l/sec for the month of March and 0.02 l/sec in the month of December. The rest of the months have a contribution of 0 l/sec.

In total the contribution of rainwater precipitation does not exceed 3.67 l/sec, throughout the year, a volume that is insignificant compared to the average 200 l/sec, evacuated through the artificial canals into Chilean territory.

Recommendations

 Install a digital meteorological station and digital piezometers in order to obtain up-to-date information on the surface water-groundwater ratio, in order to obtain updated information.

Chapter IV

Hydrochemistry

INDEX

PHOTOGRAPHS

FIGURES

Tables

CHAPTER IV: HYDROCHEMISTRY OF THE WATERS OF THE SILALA SPRINGS

4.1. Introduction

Hydro-geochemistry is an interdisciplinary science that studies the chemical properties of surface and underground water, and its relation with regional geology. Analyzes the ions dissolved in water and the water–solid interaction processes.

It is the compilation of several sciences, such as the chemistry of water, which concerns the study of chemical processes and reactions that affect the distribution and circulation of dissolved species in natural waters, combined with geology and biology, because during the hydrological cycle water interacts directly with the biosphere.

The chemical quality of surface and groundwater is determined by the amount and concentration of dissolved substances in them.

The aquifer systems are conditioned by the constant interaction between a solid phase formed by rocks and minerals, a gas phase and a liquid phase. As a result of this relation, groundwater acquires a defined chemical composition and is characteristic of the system in which it is immersed. In this context, the study of the chemical composition of water can contribute to the knowledge and determination of its origin, directions of flow, extension of aquifer systems and the possible underground connection between hydrographically independent basins.

The information will allow a classification of waters affected mainly by evaporation processes, flows between basins and their concordance with numerical flow models, which are based on meteorological, hydrological, piezometric and geophysical information.

4.1.1. Spring Water

Water that spontaneously emerges to the surface of the earth with a flow determined by the hydrological cycle, after being captured through works carried out for its exploitation. It does not have the properties of mineral water and is of good quality.

4.2. Theoretical basis

4.2.1. Water chemical analysis

The determination of the chemical-physical properties of natural water is an essential tool for the analysis of water quality.

For the application of hydro-geochemical methods, the water solution, water balance and geochemical parameters that characterize each system must be taken into account, relating the volume of infiltration, circulation of the water with the chemical composition of the same in the discharge area of the aquifers.

The second phase of the work will consist of selecting points or stations of systematic observation, where the necessary registration or measurement equipment is installed for the control of the flows and the chemical composition of the waters. The chemical composition of meteoric waters is controlled by the chemical balances of carbonates and other minerals and varies over time. For this reason, chemical analyzes and pH measurements, as well as electrical conductivity, must be done ―in situ‖.

 Anions

a) Chloride Ion, comes from:

Washing of land of marine origin: The waters and fossils can provide important amounts. Rainwater and its concentration in the terrain.

Mixture with seawater in coastal regions.

More rarely it can come from gases and liquids associated with volcanic emanations.

It is the most abundant anion in seawater, but may be the least important of the fundamentals in inland waters. It almost never saturates and is very difficult to alter by ionic or other type of action.

b) Sulfate Ion, comes from:

Washing of lands formed in conditions of great aridity or in a marine environment.

Oxidation of igneous rock sulfides, metamorphic sedimentary rocks.

Concentration of rainwater in the soil.

c) Bicarbonate and Carbonate Ions, come from:

Dissolution of atmospheric CO2 or soil.

d) Ion Nitrate, comes from:

Processes of natural nitrification, decomposition of organic matter and urban, industrial and livestock pollution.

In small proportion of rainwater, volcanic emanations and washing of old soils.

It is often an indicator of pollution, in which case it is usually stratified, dominating the higher concentrations in the upper part of the free aquifer.

- **Cations**

a) Sodium, comes from:

Attack of feldspars, feldspatoids and other silicates. Locally of the solution of germ salt or natural sodium sulfate. Rarely of emanations and phenomena related to magmatic processes.
Concentration of rainwater, is the most abundant cation in seawater, is very affected by the change of bases.

b) Potassium, comes from:

Attack of the orthoclase and other silicates (micas, clays, etc.). Locally of the dissolution of natural potassium salts (silvinite, carnallite, etc.). In small amount of rainwater contributions.

c) Calcium, comes from:

Dissolution of limestones, dolomites, gypsum and anhydrite. Attack of feldspars and other calcium silicates. Dissolution of calcareous cement of many rocks. Concentration of rainwater. It is frequently in a saturated state and its stability in solution depends on the equilibrium C02- C03HC03. It can precipitate easily and is very affected by the ionic change.

d) Magnesium, comes from:

Dissolution of dolomites and dolomite limestones; attack of magnesium and ferromagnetic silicates. Locally washed magnesium evaporite rocks (carnallite, kaiserite, etc.).

It dissolves more slowly than calcium and tends to remain in solution when it precipitates. It is affected by the ionic change.

e) Iron, comes from:

Attack of ferric silicates, attack of sulfides and iron oxides, attack of most sedimentary rocks. Its stability depends fundamentally on the redox potential; it solubilizes and precipitates easily. Only minimal amounts of dissolved iron are present in oxidizing media.

- **Sodic Bicarbonated Waters.**

The main action of these waters is of digestive type. They are used mainly in drinks, in doses of 100 to 200 ml before breakfast, lunch and dinner, until reaching a total dose of 1000 to 1500 ml per day. In general, these waters behave as antacids, acting as neutralizers of gastric acidity and because of their buffering capacity they also favor the action of pancreatic enzymes and the saponifying power of bile. They also have a cholecystokinetic action. They are favorable for the treatment of hepatopancreatic disorders.

4.2.2. Water classification by its use

The chemical composition of natural water, according to the use that is given to it, is called water quality, and there are a series of norms that regulate the permissible concentrations that each element or indicator of quality must have according to the different uses.

In addition to the chemical-physical quality of the waters, it is necessary to control the bacteriological quality. The contamination of water by pathogenic organisms is mainly due to dumping or percolation of urban or agro-industrial waste, since this type of microorganism does not originate in natural conditions.

4.2.3. Groundwater geochemical composition

In natural groundwater, most dissolved substances are in the ionic state, most of the hydro- geochemical aspects will be about these ions.

In groundwater, the elements to be analyzed in the field are the following:

- PH
- Temperature
- Total dissolved solids
- Conductivity
- Hardness
- Taste
- Odor

4.3. Laboratory chemical analysis

Six samples were analyzed in the Laboratories dependent on the Tomas Frias Autonomous University – JICA; where 10 important ions were programmed with different analysis methods: Potentiometric, Gravimetric, Colorimetric, Volumetric, Atomic Absorption and chemical physical parameters in situ with the HATCH portable equipment (see Photograph 4.1).

As a comparison parameter to those reported by the laboratory, it shows a good relation within the permissible ranges.

Cations.- Sodium, Potassium, Manganese, Cadmium, Copper, Calcium, Iron, Magnesium.

Anions.- Bicarbonate, Carbonate, Chlorine, Nitrate, Nitrite, Sulphate.

Photograph 4.1: Atomic adsorption equipment.

4.4. Sampling Methodology - Monitoring

The sampling methodology is defined from a monitoring scheme and respecting international standards in order to minimize errors in the reading of elements (See Photograph 4.2). The analyzes were carried out before 72 hours in compliance with the indicated norms, due to the distance effect, preservatives had to be used and transferred to specialized laboratories of the UATF; for the Chemical Analysis (see Annex 0.1).

The values of the chemical analyzes, reported by laboratory, were subjected to an ionic balance in order to verify the quality of the same; with the analyzes that report an error of less than 10%, the water quality was determined, using as comparison parameters the permissible limits established in the Regulation of the Environment Law, with respect to Water Contamination (RMCH).

Photograph 4.2: Portable equipment for measuring physical-chemical parameters *in situ*.

In the evaluation of the cations the following elements were considered: calcium, magnesium, sodium, potassium and iron. For the evaluation of the anions, sulfates, chlorides, carbonates, nitrates, bicarbonates were considered and to determine the physical-chemical parameters the pH, TOS, conductivity, salinity and temperature were analyzed.

The classification of the waters, were made according to the rules of the Ministry of Sustainable Development and Environment (MDSMA) such as:

CLASS A: Natural waters of the highest quality, which enables them as drinking water for human consumption without any previous treatment, or with simple bacteriological disinfection in the necessary cases verified by laboratory.

CLASS B: Waters of general utility, for human consumption, require physical treatment and bacteriological disinfection.

CLASS C: Waters of general utility, which in order to be qualified for human consumption requires complete physical-chemical treatment and bacteriological disinfection.

CLASS D: Waters of minimum quality, which for human consumption, in extreme cases of public necessity, require an initial process of pre-sedimentation, since they can have a high turbidity due to high TOS content and then complete physical-chemical treatment and special bacteriological disinfection against eggs and intestinal parasites.

4.5. Field Methodology

In the field phase, a detailed inventory of water from the Silala springs was made of six samples in surface water in waterbodies, such as the Inacaliri Volcano Sector and the SES sector, samples that were obtained in order to know and differentiate the quality of them.

Photograph 4.3: Water sampling.

4.6. Procedure – Hydro-chemical Interpretation

Techniques that helped classify the type of groundwater proposed by international organizations such as WHO were used. For the global interpretation of the hydro-geochemical behavior of the analyzes of surface waters and waters coming from the springs of the survey area, Collective Diagrams were applied, such as the PIPER, SITFF, WILCOX, which allowed to see the behavior and the comparison of the samples of the different samples in the springs, which allowed defining its genesis and the behavior of the elements in a panoramic way.

At the same time, specialized software such as Excel, GWW, which served in the interpretation and generation of thematic graphs and maps, etc., was used as tools.

For the global interpretation of the hydro-geochemical behavior of the analysis of surface waters and those coming from the springs of the survey area, they were carried out with the application of collective diagrams.

4.6.1. Collective Diagrams

Collective diagrams were made such as: Piper, Schoeller and Wilcox Diagrams and the logarithmic classification, where the content of the ions is seen in relation to the permissible limits established by the WHO, which allowed to see the behavior and the comparison of the samples of the different samples in the springs, which allowed defining its genesis and the behavior of the elements in a panoramic way.

4.7. Interpretation and evaluation of results

The tasks of water reconnaissance and sampling carried out during the field stage, complemented by the laboratory analyzes, compatible with the parameters of permissible limits, allow an evaluation of the characteristics and conditions of the hydro-geochemical behavior.

In order to analyze the geochemical behavior in the springs, the contents of the calcium, magnesium, sodium and potassium cations, and the anions of sulfates, chlorides, carbonates, bicarbonates were taken into account, which allowed us to make the geochemical classification in springs. Likewise, the chemical-physical parameters were determined by measuring the pH, TOS, conductivity, salinity, with the portable equipment shown in the figure.

4.7.1. Chemical-Physical Analysis

a) pH: The behavior of the pH in the samples in the Silala Springs, is considered as Alkaline pH between 8.0-8.40, which according to the permissible limit is below the value, which indicates a type of alkaline water allowed (see Figure 4.1).

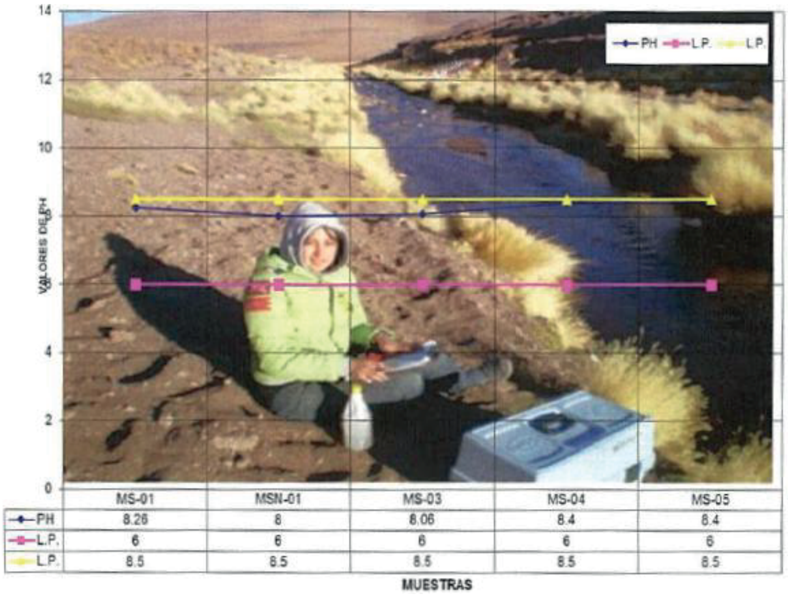

Figure 4.1: Concentrations of pH in the Silala Springs.

4.7.2. Behavior of Anions

a) Sulfates (S04 Permissible limit 300 mg/l). The behavior of contents of S04 in all the samples obtained in the different points does not exceed the limit between 5.4 - 15 < 300 mg/l, values that are in the established range with the exception of sample MS-04 that results in a value of 400 > 300 mg/l that exceeds 33.33% more than indicated (see Figure 4.2).

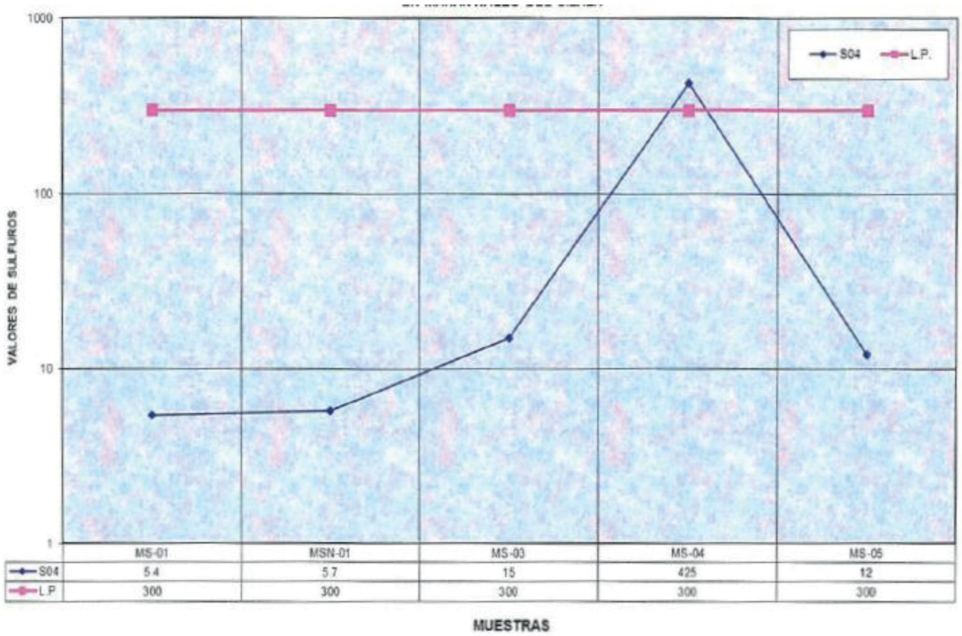

Figure 4.2: Sulphate Concentrations mg/l (see Annex D.3.4).

c) Chlorides (CI, Permissible limit 30 mg/l). The Chloride values in the water samples taken are below the permissible limit, comprised between 1.9 – 55.67 < 30 mg/l, values obtained in the ranges described.

d) Bicarbonate - Carbonates (HC03-C03 Allowable limit 500 (mg / l). The values of the samples report values that do not exceed the limits between 3.43 – 7.43 mg/l < 500 mg/l. The contents of anions are lower because salts and borates are not present in the vicinity of the lagoons. Sample MS-04 exceeds the value with respect to the permissible limit 2215.35 > 500 mg/l (see Figure 4.3 and Figure 4.4).

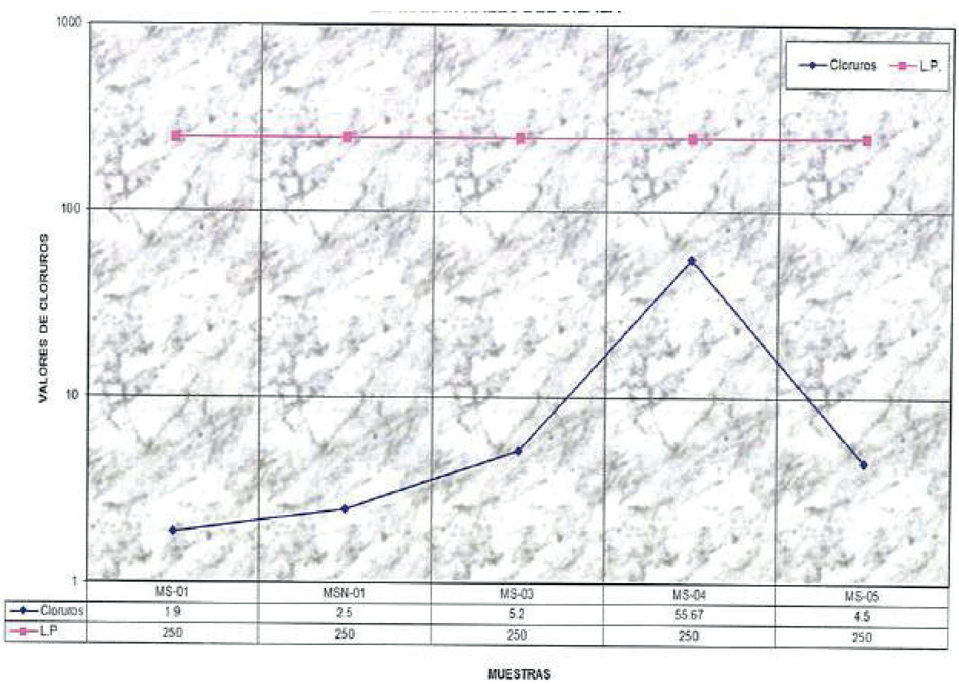

Figure 4.3. Chloride Concentrations mg/l.

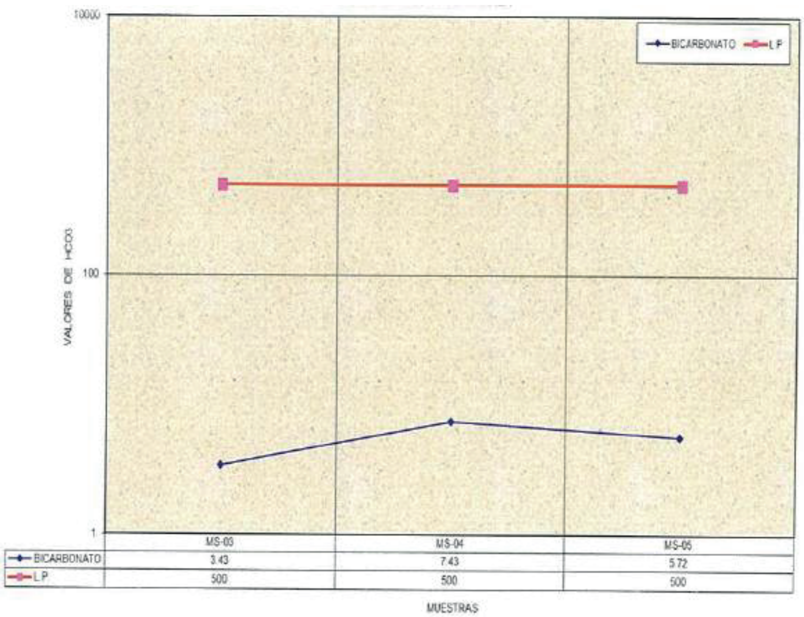

Figure 4.4: Bicarbonate Concentrations mg/l (see Annex D.3.1).

102

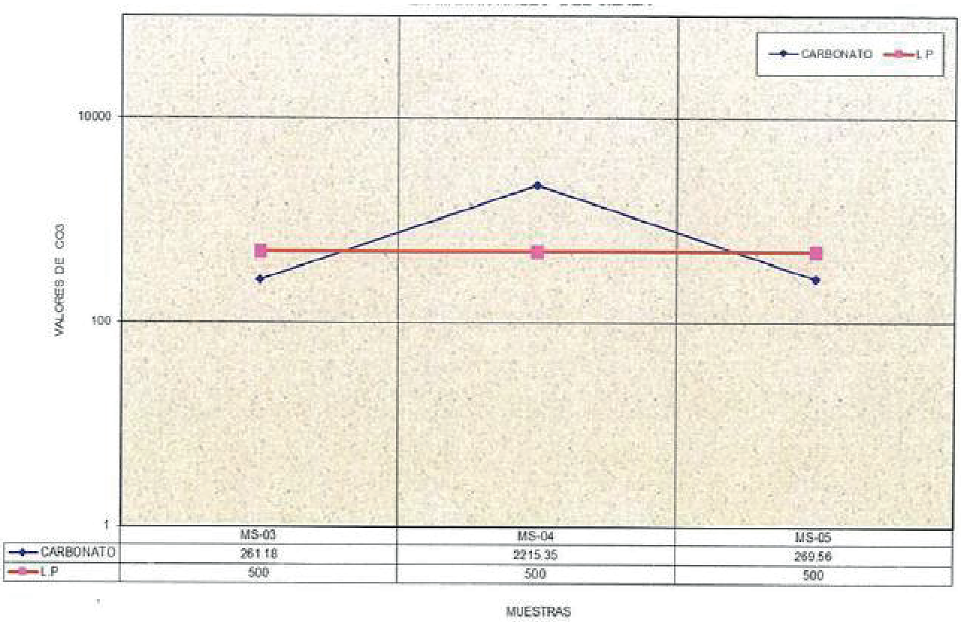

Figure 4.4: Carbonate Concentrations mg/l.

4.7.3. Behavior of Cations

Sodium – Na (Permissible Limit 100 mg/l): The Na content exceeds the permissible limit established in two samples M-1 and MS-04 between 343.3 - 1986.6 mg/l, obtaining a high performance of this cation by the migration and chemical exchange of salts present and the evaporation present in the surveyed site. The other samples are below the permissible limit of 20.6 94.7 mg/l < 100 mg/l (see Figure 4.6).

Calcium (Ca) (Permissible Limit 200 mg/l): According to the analysis obtained in these samples, the concentrations obtained are between the ranges of 4.6 - 197.68 mg/l < 200 mg/l, values that do not exceed the established permissible limit (see Figure 4.7).

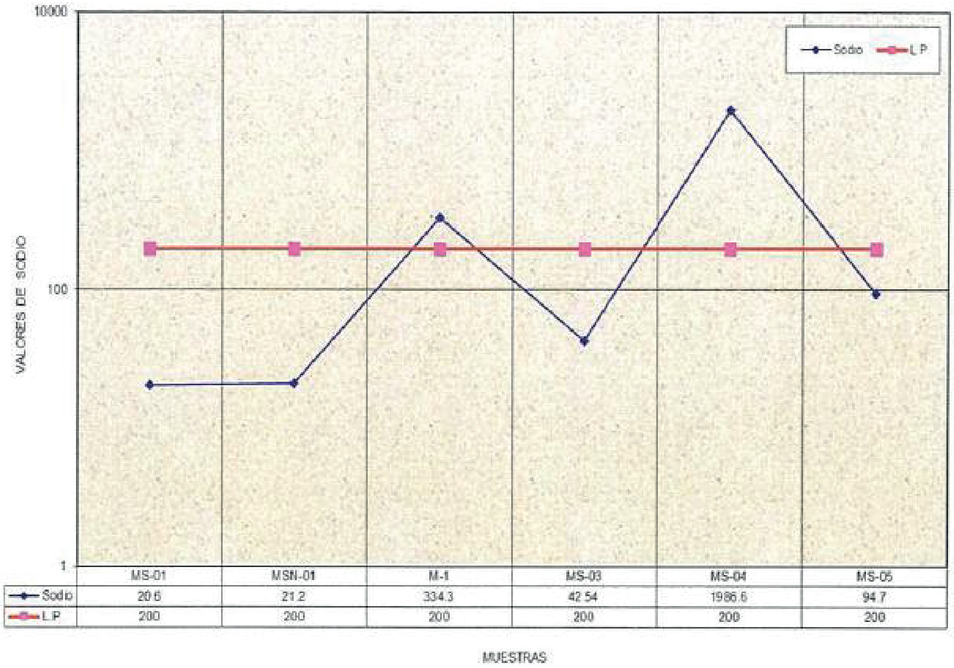

Figure 4.6. Sodium concentrations mg/l (see Annex D.3.2).

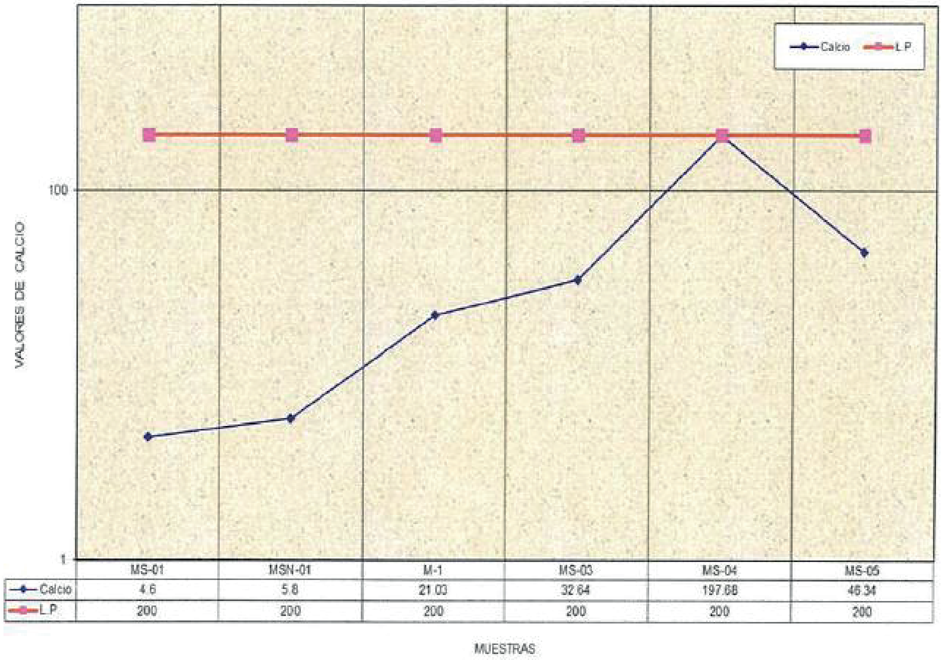

Figure 4.7: Calcium Concentrations mg/l.

Potassium (K) (Permissible Limit 100 mg/l). The concentrations due to this cation do not exceed their established limit, they are between values in mg/l of 1.2 - 128.34, except for sample MS-04 that exceeds the permissible limit and governs the concentration as it is one of the major ions 485.62 mg/l > 100 mg/l (see Figure 4.8).

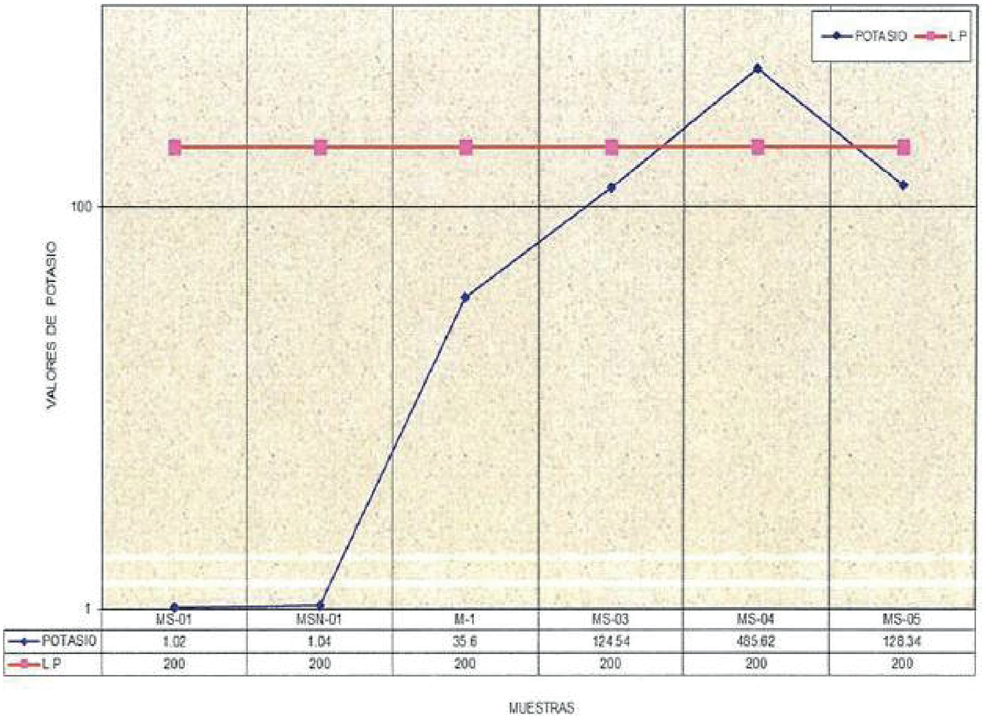

Figure 4.8: Potassium Concentrations mg/l (see Annex D.3.3).

4.8. Interpretation Techniques – Hydro-chemical Diagrams

For the hydro-chemical and hydro-geochemical evaluation and interpretation of the composition of natural waters, individual diagrams have been used (Stiff Diagrams) that allow us to represent the chemical characteristics of a single sample. In order to compare the chemical characteristics of a group of samples, the classic Piper triangular diagrams and the columnar Schoeller diagrams have been used, and to determine the suitability of water for irrigation purposes, the Wilcox diagram has been used. The classification of waters according to the sampling in the Silala springs includes a methodology of analysis of cations and anions based on the majority presence of each element.

4.8.1. Stiff Diagram

The Stiff diagram is a variety of horizontal diagrams, where the results are represented in four horizontal lines, equally spaced and divided by a vertical median. The cations are represented on the left and the anions on the right. The concentration of the different ions is expressed in milliliters equivalent per liter. On a horizontal axis, the scale is normal, which allows us to compare the composition of the samples with each other by size.

According to the Stiff diagrams shown in Figure 4.9, in the upwelling waters that contribute to the Silala springs, Samples MS_01, MSN_01 for the predominant ion are classified as Bicarbonated – Sodic – Potassium (see Figure 4.9).

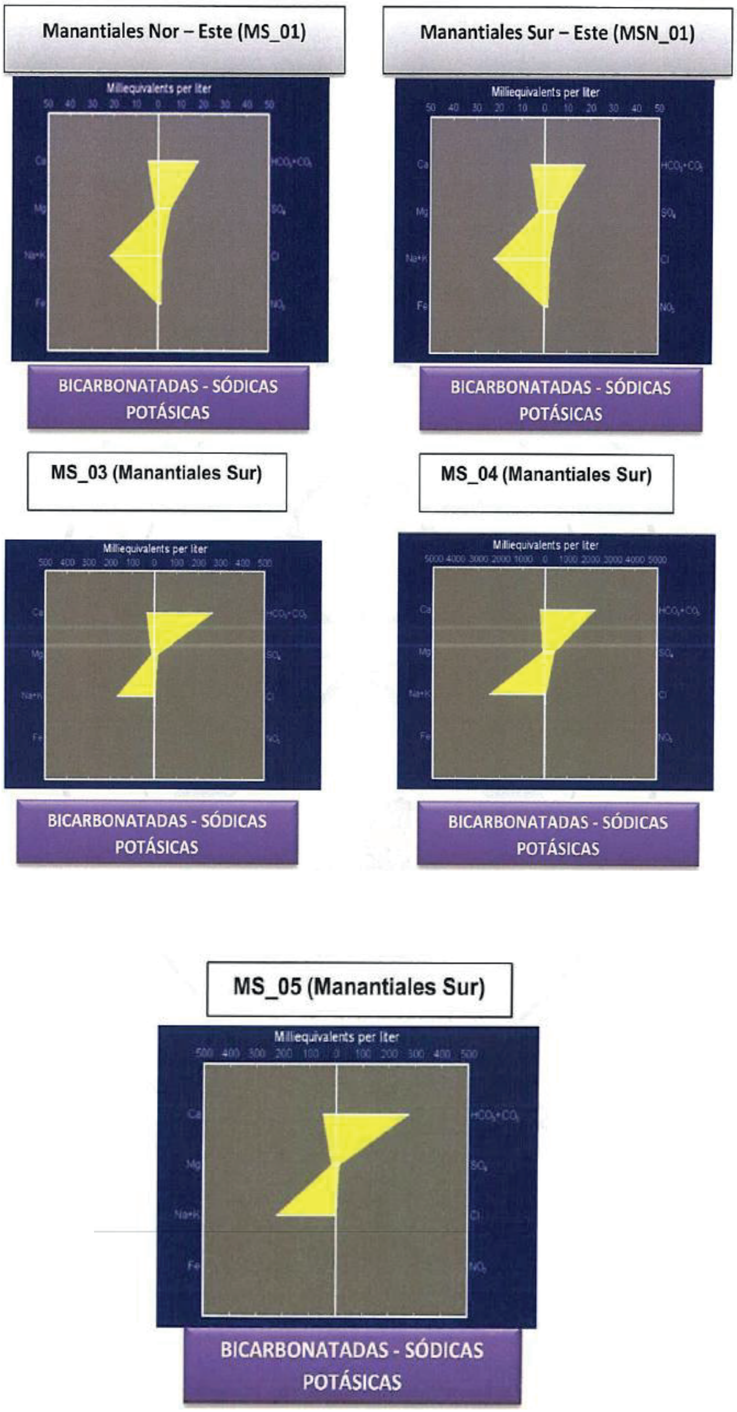

Figure 4.9: Stiff diagrams of the survey area.

4.8.2. Piper Diagram

In order to represent the chemical characteristics of the waters of the Silala springs, Piper's triangular diagrams have been used. The anions and cations have been represented in two different triangles, with a central rhomboidal field, where a third point deducted from those representing cations and anions is represented, the concentration is represented in % of meq/l.

According to the Piper diagram, the waters of the Silala springs correspond to BICARBONATE – SODIUM POTASSIUM hydro-chemical facies, as shown in Figure 4.10.

Code	Name	Piper Diagram	Stiff Diagram	Water Type
MS-01	NORTH-EAST SPRINGS	BICARBONATE – SODIUM POTASSIUM	BICARBONATE – SODIUM POTASSIUM	SPRINGS
MSN-01	SOUTH-EAST SPRINGS	BICARBONATE – SODIUM POTASSIUM	BICARBONATE – SODIUM POTASSIUM	SPRINGS
M-1	INACALIRI VOLCANO	SULPHATE – MAGNESIUM	SULPHATE – MAGNESIUM	LAGOON – CRATER
MS-03	SOUTH SPRINGS	BICARBONATE – SODIUM POTASSIUM	BICARBONATE – SODIUM POTASSIUM	SPRINGS
MS-04	SOUTH SPRINGS	BICARBONATE – SODIUM POTASSIUM	BICARBONATE – SODIUM POTASSIUM	SPRINGS
MS-05	SOUTH SPRINGS	BICARBONATE – SODIUM POTASSIUM	BICARBONATE – SODIUM POTASSIUM	SPRINGS

Table 4.1: Behavior of the Hydro-chemical Areas in the Silala Springs.

BICARBONATE – SODIUM POTASSIUM

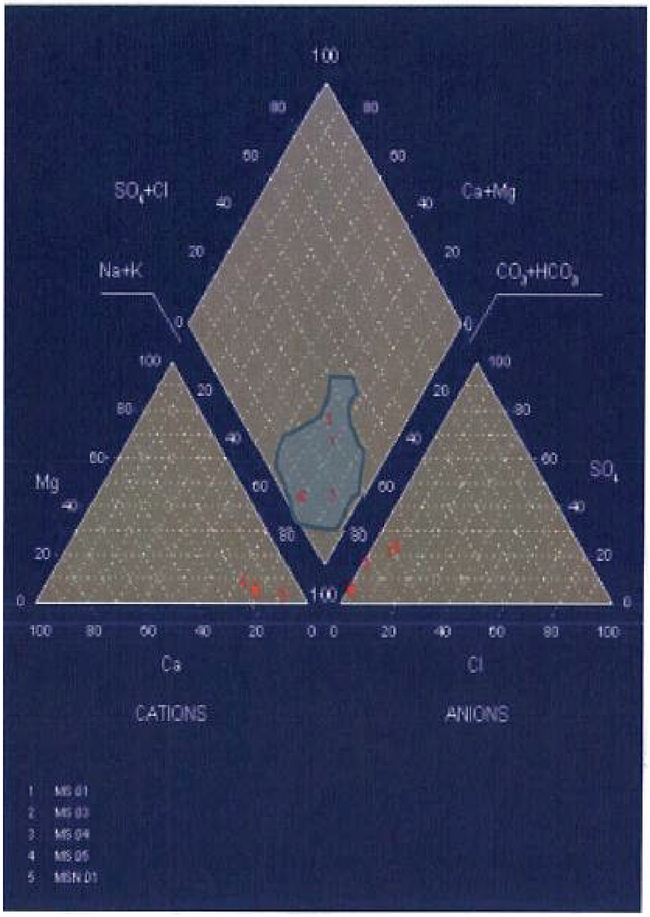

Figure 4.10: Piper Diagram of the survey area.

Both the PIPER diagram and the STIFF diagram give the same type of water with its predominant concentrations coming from the springs belonging to the Silala as shown in Table 4.1.

From the analysis of the table, it is concluded that there is no difference between the classifications of Piper and Stiff.

4.8.3. Wilcox Diagram

The classification established by the SAR index Wilcox diagram, and the salt coefficient is based on the following characteristics:

 The total concentration of soluble salts expressed by the electrical conductivity in micromhos per cm at 25 °C.
 The relative concentratxion of sodium with respect to calcium and magnesium called the SAR index (Sodium Absorption Radius), based on the following formula:

$$SAR = \frac{Na}{\sqrt{\frac{Ca + Mg}{2}}}$$

For the index to be representative, precipitation of calcium or magnesium salts should not occur as a consequence of evapotranspiration.

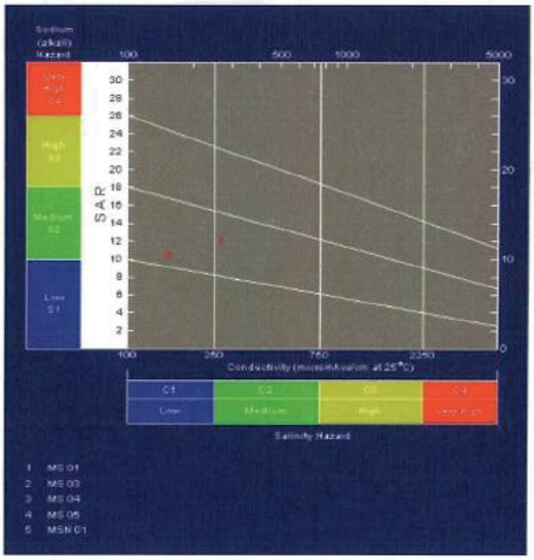

Figure 4.11: SAR Wilcox Diagram

To the waters of a constant SAR are attributed a greater danger of alkalizing of the soil the greater the total concentration (According to Custodian, page 1980).

What is shown in the following graph is the Wilcox diagram. Classifying these waters according to the norms as:

SAMPLE MSN 01 (Springs South – East) According to the diagram, it is classified as CI-S2 with a SAR index of 11.32 what corresponds to be a type of water of low salinity with medium sodium content, with some danger of sodium accumulation in highly textured soils with low permeability.

SAMPLE MS-01 (Springs North - East) With a SAR index of 12.82 classified as water according to the graph type C2-S4 medium salinity waters and high sodium content, for this reason it is not advisable to use for irrigation in general.

4.9. Anomalies maps

- **Water anomalies**

An anomalous distribution of elements in subterranean and meteoric waters is called hydro- geochemical anomaly. As the elements are generally transported in dissolved form in natural waters, the most suitable elements for geochemical exploration of waters are the relatively mobile elements.

A very successful application of geochemical water exploration consists of the determination of U in groundwater and meteoric waters.

- **Abnormalities in Drainage Sediments**

Sediment from springs, lakes, floodplains, active sediments of water currents and sediments, which act as filters for water, belongs to drainage sediments.

Drainage systems often start from springs. The sediments located in the vicinity of the springs and the filtration sediments tend to exhibit appreciable anomalies and therefore these sediments are useful for a geochemical exploration. The active sediments of water currents include elastic and hydromorphic material from the filtration sectors, the elastic material eroded from the banks of detrital material located in riverbeds and hydromorphic material absorbed or precipitated by the upwelling waters. The anomalies developed in these active sediments can extend several ten kilometers with respect to their source. Studies of these anomalies are used frequently and preferably to achieve general recognition. In the case of lakes, the elastic components and the material absorbed or precipitated from the sediments are studied. In areas with a high number of lakes such as in the Precambrian shield area of Canada modeled by glaciers, the geochemical survey of lake sediments may be the most economical and effective method for a general survey.

4.10. Analysis of Volcanic Soils

4.10.1. Physical and Chemical Properties of the Soil

Soil is a normal constituent of nature, with mineral and organic components and a biological component formed by organisms that live in it and the physical, chemical and biochemical alteration of the rocks causes the formation of new highly reactive mineral constituents.

The soil is the surface covering of most of the continental surface of the Earth. It is an aggregate of unconsolidated minerals and organic particles produced by the combined action of wind, water and the processes of organic disintegration.

4.10.2. Textures Triangle

The texture indicates the relative content of different sized particles, such as sand, silt and clay, in the soil. The texture has to do with the ease with which the soil can be worked, the amount of water and air that it retains and the velocity with which the water penetrates the soil and passes through it.

The textural triangle method is based on the system applied by the USDA according to the size of the particles, in which the following classification is used:

- Silt, all particles whose size varies from 0.002 to 0.05 mm;
- Clay, all particles less than 0.002 mm.

In the field phase, 4 soil samples were obtained from the Silala springs.

The 1st sample Ssee-SUE01, taken on 23 October 2016 at 09:25 am, indicates SILT-LOAMY as type of soil, with a higher percentage of 55.8% silt, 40.3% sand and 3.9% clay.

Photographs 4.4 - 4.5: Sampling of volcanic soils.

The 2nd sample Ssee-SUE02, taken on 23 October 2016 at 10:50 am, indicates **SILT-LOAMY** as type of soil, with a higher percentage of 54.2% silt, 44.4% sand and 1.4% clay.

The 3rd sample SnWW-SUE01, was taken on 24 October, 2016 at 12:43 pm, indicates **SILT-LOAMY** as type of soil, with a higher percentage of 73.7% silt, 24.6% sand and 1.7% clay.

The 4th sample SnWW-SUE02, was taken on 24 October 2016 at 14:42 pm, indicates **SILT-LOAMY** as type of soil, with a higher percentage of 60.3% silt, 20.1% sand and 19.6% clay.

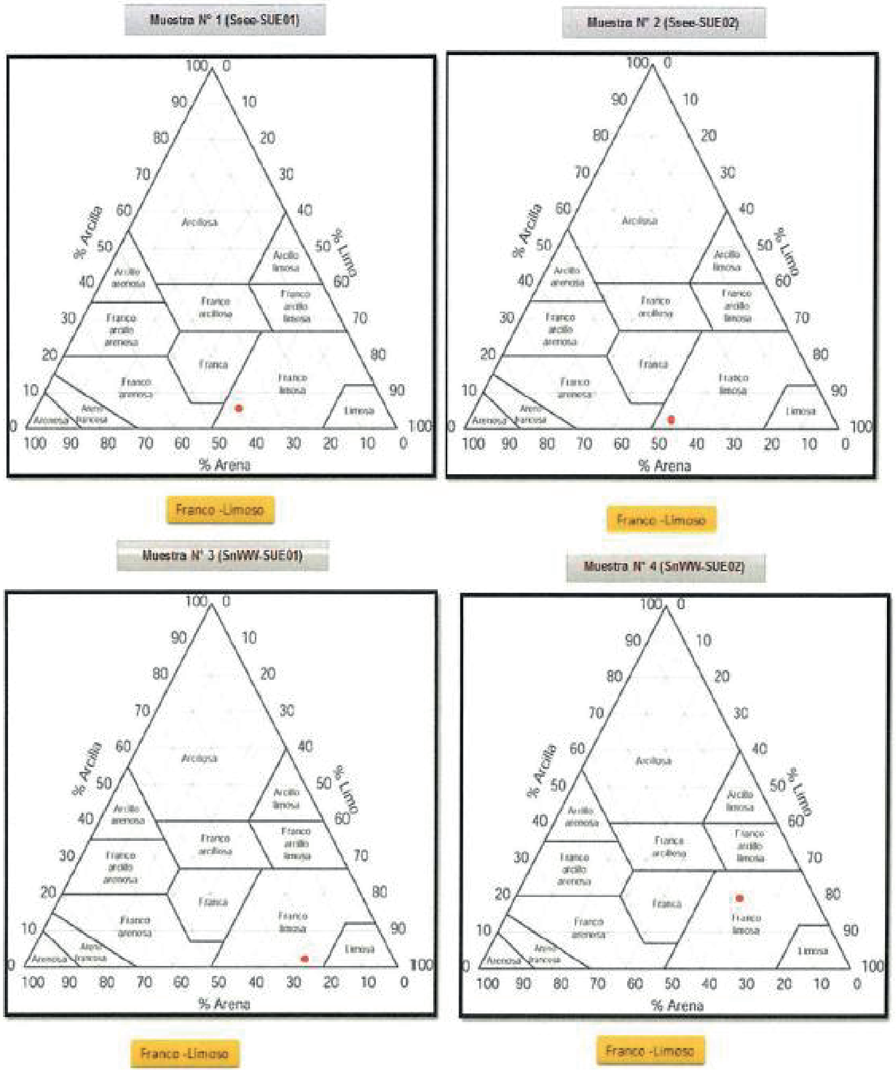

Figure 4.12. Classification of Soils by the Textural Triangle (USDA)

Conclusions CHAPTER IV (HYDROCHEMISTRY)

- The presence of older and recent volcanic deposits in the area is evidenced, which alter the composition, hydro-chemical migration in the waterbody.
- The geo-morphological features reflect units of volcanic origin - denudational, alluvial, lacustrine and fluvial–lacustrine.
- The soils determined in the area are deep and very susceptible to wind erosion and due to their chemical characteristics present limitations in their agricultural use.
- It is evidenced by the results of the hydrogeological survey that most of the contributions of the springs are of underground origin because they are found as means of discharge to depths and located in ignimbrite rocks due to the effect of fracturing and secondary permeability.
- The hydro-chemical facie of the waterbody in the North-northeast and South-East springs; they are classified as SODIUM BICARBONATED POTASSIUM waters, reflecting low conductivities between 110 - 140 ms/cm and almost neutral pH; showing a type A cationic stability, classified as suitable for human consumption and used for irrigation.
- For the samplings carried out in the Inacaliri volcano, in the center of the volcano, they are classified as SULPHATED – MAGNESIAN waters. This behavior is due to the effects of migration and disintegration of volcanic activity.

Recommendations

- Due to the monitoring and control established for this period, a periodic control over these canals is recommended in order to evaluate the isotopic behavior.
- Expand the research to the other sub-basins in order to obtain information on the quality of hydro-chemical profiles in water resources.
- Recommend, at the request of the Governorate, the preservation of natural resources (Water - Soil), as it is an important reserve for future generations.

CHAPTER V

HYDROGEOLOGY

INDEX

FIGURES

TABLES

MAPS

CHAPTER V: HYDROGEOLOGICAL CHARACTERIZATION OF THE SILALA SPRINGS

5.1. Introduction

Hydrogeology is that part of hydrology that corresponds to the storage, circulation and distribution of terrestrial waters in the saturated area of geological formations, taking into account the physical and chemical properties, their interactions with the physical and biological environment and their reactions to the action of men.

The HYDROGEOLOGICAL CHARACTERIZATION has allowed defining different variables such as: geological, geo-morphological, geophysical, hydro-geochemical, hydrological, hydrogeological, which have allowed quantifying the volume of surface water and the volume of groundwater, as well as the quality and the hydraulic-genetic relation in the Silala springs.

For the hydrogeological characterization of the Silala springs, field mapping was carried out in detail, which allowed determining the lithology, the structural interpretation from the mapping of 1,500 fractures present in the survey area, which allowed determining the type of fracture, the frequency of them, which condition the secondary permeability in the area.

Geophysical profiles (SEV) were also carried out; the same ones that allowed determining the thicknesses of the different geological structures and the depth of them, with their petro-physical characteristics, that allowed elaborating the stratovolcanic columns.

Due to the lack of meteorological information in the survey area, water modeling was carried out through a Geographical Information System (ILWIS - LOCCLIM), which allowed determining the water supply and the volume of runoff.

The hydro-geochemical analysis of the waters of the Silala springs, both in the southeast-east sector and in the northwest-west sector, which allowed determining the quality of the same classifying them as SODIC-POTASSIC BI-CARBONATED waters, which allowed us differentiating from the waterbodies present at higher altitudes such as the Inacaliri Volcano (5,570 m.a.s.l.), which has a classification of MAGNESIUM-SULFATED water, which does not corresponds to the quality of the spring water.

5.2. Definition of fundamental concepts

Spring: It is a point or area of the surface of the terrain in which an appreciable amount of water from an aquifer flows naturally to the surface.

Slope: Inclined plane that allows the runoff of water.

Bofedals: Ever-green physiognomy associations that generally have high groundwater levels and permanent surface runoff.

River: More or less abundant water current that continues flowing naturally and that ends in another basin or in the sea.

International Course River: It is defined as a watercourse that crosses or separates the territories of two or more States.

Fossil water: Groundwater that remains for millennia, millions of years under the subsoil in aquifers and that was sealed by geological processes preventing its recharge.

Permafrost soils: It is the soil layer permanently frozen but not permanently covered with ice or snow from very cold or periglacial regions such as the tundra.

The hydrological cycle

The hydrological cycle is fundamental in hydrology; it is a continuous process without beginning or end. The concept of a hydrological cycle involves the movement or transfer of water masses from one place to another and from one state to another.

The hydrological cycle aims to characterize quantitatively important factors within the water balance of the survey area, such as precipitation (P), evapotranspiration (Evt), runoff and variations of the water reserve in the soil (ΔR or infiltration – storage).

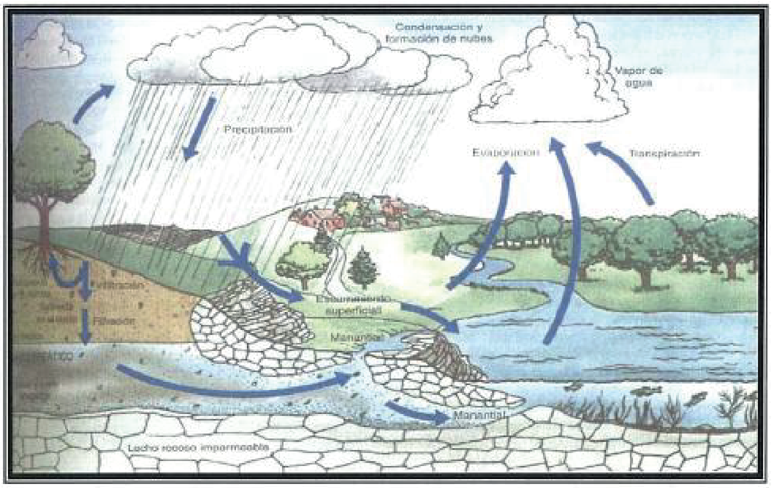

Figure 5.1: Hydrological Cycle (Environmental Sciences – Mcgraw Hill).

To calculate the water balance through modeling, the following equation was applied (see Figure 5.):

$$P = Ev + ETP + Ese + \Delta \quad + I$$

Where:

P = Precipitation

Ev = Evaporation

ETP = Potential Evapotranspiration

Esc = Surface runoff (supply)

Δ = Surface storage

I = Infiltration

Also for the underground water balance the following equation was used (see Figure 5).

$$I = EscSub + EVT + Cc + Im + R$$

Where:

I = Infiltration

EscSub = Sub-surface runoff

EVT = Evapotranspiration

Cc = Field capacity

Im = Wilting Index

R = Recharge to the aquifer

However, the recharge factor R, is the most important parameter in the variation of the piezometric and phreatic levels, and can be expressed as:

$$R = I - EscSub - EVT - Cc - Im$$

Where:

R = Recharge to the aquifer

I = Infiltration

EscSub = Sub-surface runoff

EVT = Evapotranspiration

Cc = Field capacity

Im = Wilting Index

Variables that allowed operationalizing the thematic maps of the modeling, which allowed obtaining the water balance of whose results it was defined that there is a **WATER DEFICIT** (see Figure 5.2).

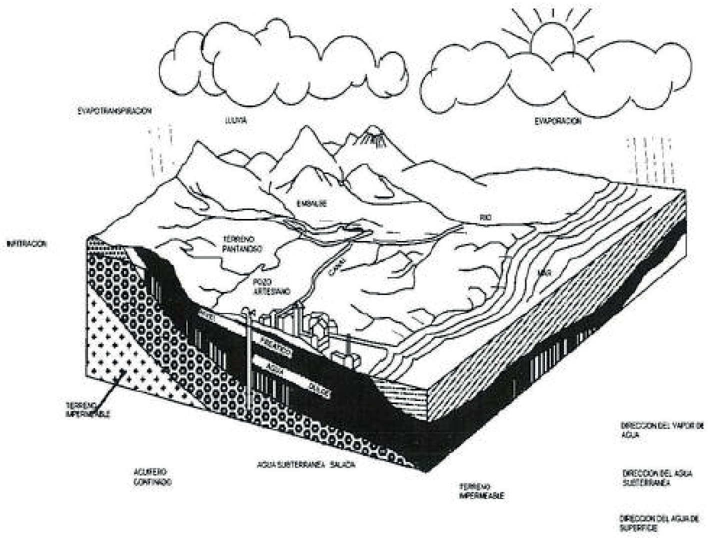

Figure 5.2: Diagram of the Hydrological Cycle in relation to Precipitation, Infiltration and Recharge.

5.3. Survey Objective

The objective of this survey was the hydrogeological characterization of the Silala springs, understanding methodologically as a characterization to define, analyze and establish hydrological relations.

5.4. Survey Scope

The physical characterization of the survey area, allowed defining –from the topographic highs– the survey area surrounding the Silala springs (see Figure 5.3), in order to define the type of recharge.

5.5. Hydro-morphological Parameters of the Survey Area

The physical characteristics of an area are elements that have a great importance in the superficial hydrological behavior of the same and have their direct impact on the hydrogeology of the survey area. These physical characteristics are classified into two types according to their impact in the survey area: those that condition the volume of runoff and infiltration, as well as the area and type of soil, and those that determine the velocity of response,

as well as the length of the canal, the average inclination of the slope and the hypsometric curve that allows determining the average elevation of the survey area. However, in the absence of a river, the survey of the length of the canal and the slope of the canal has no relevance.
There is a close correspondence between the hydrological regime and the physical characterization of the survey area, for which the knowledge of these has great practical utility, since in establishing relations and comparisons between them with known, modeled and calculated hydrological data, hydrological values could be determined indirectly in sections of practical interest where data are lacking or where, for reasons of physiographic or economic nature, the installation of hydrometric stations is not feasible (see Chapter III).

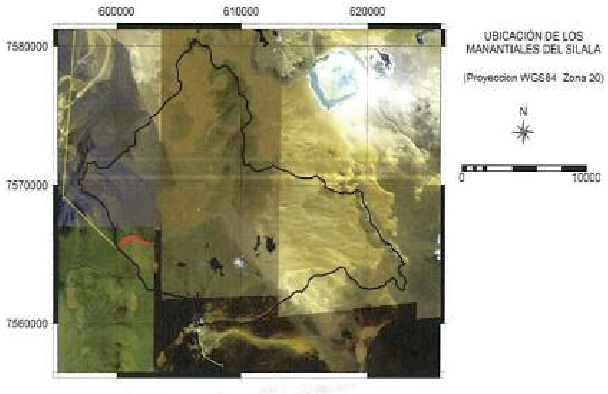

Figure 5.3: Location of the Survey Area, Silala Springs.

Area of the Survey Area

The area of the survey area is of great importance because it serves as a basis for determining other elements such as: parameters, coefficients, relations, and classification of the type of the survey area. On the other hand, in general, runoff and supply flows decrease as the area of the survey area decreases. The growth of the area acts as a compensation factor so that it is more common to detect instantaneous increases and immediate response in the survey areas.

The systematization of all the information indicated through a GIS has allowed us obtaining the area of the Silala area of 249319375 m2, equivalent to 249.31 km2 (see Figure 5.4). The area was obtained from the processing of ASTER satellite information.

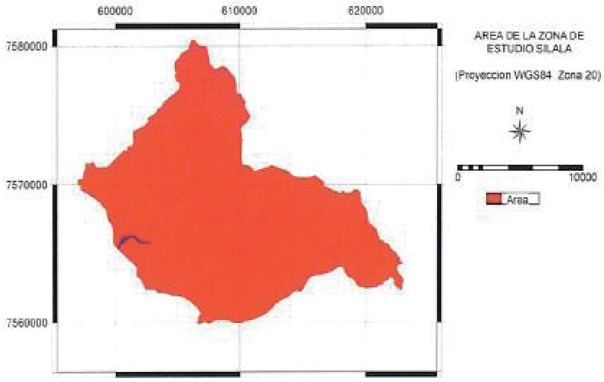

Figure 5.4: Area of the Survey Area – Silala Springs.

Average slope steepness

The average slope inclination of the survey area was calculated according to the following equation:

$$S_m = \frac{1}{DA} * \sum (S_i * DA_i)$$

Where:

Sm = Average inclination of the slope
DA = Total drainage area
Si = Average slope of each sub-area in which the basin is reclassified
DAi = Each of the reclassified sub-areas

123

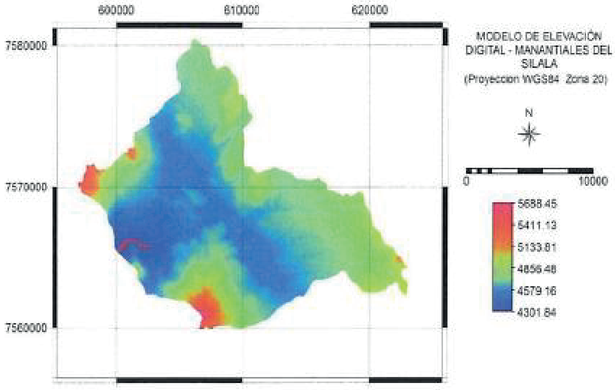

Figure 5.5: Digital Elevation Model of the Silala Springs.

Elevation Ranges	Average Slope	Area (m^2)	Average Slope with Area Product	Accumulated Area	Percentage of Accumulated Area	Average Elevation (m)
4400	13,8	1577500	21769500	1577500	0,6	4.300
4400 – 4600	26,2	65798125	1723910875	67375625	27,4	4.500
4600 – 4800	29,6	120144375	3556273500	187520000	76,4	4.700
4800 – 5000	30,2	46436875	1402393625	233956875	95,3	4.900
5000 – 5200	32,6	7070000	230482000	241026875	98,2	5.100
5200 – 5400	32,8	3253750	106723000	244280625	99,5	5.300
5400 – 5600	47,8	1037500	49592500	245318125	99,9	5.500
5600 – 5800	37	237500	8787500	245555625	100	5.700
Summation		245555625	7099932500			
Average inclination of the slope (%)			**28,9**			

Table 5.1: Calculation of the average slope inclination of the Silala area

The Digital Elevation Model (DEM) of the survey area (see Figure 5.5) was reclassified into sub- areas of level ranges or topographic heights. In the case of the Silala area, it was divided into 200- meter ranges (see Figure 5).

Once all the calculations have been made, the ―average inclination of the slope‖ is 28.9% (see Figure 5.6).

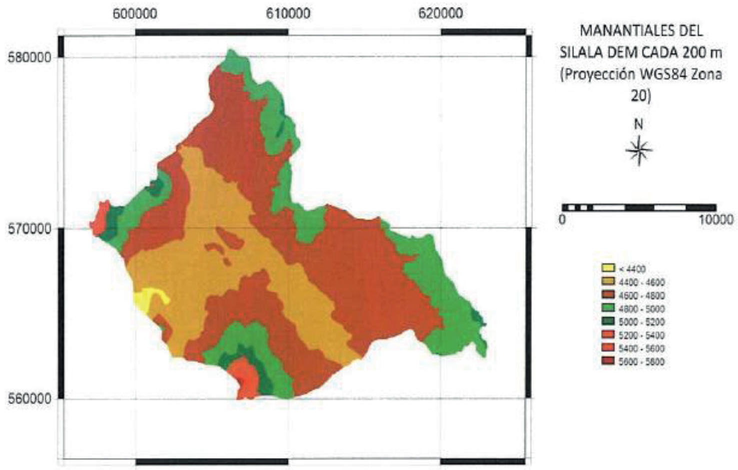

Figure 5.6: Reclassification of the **Digital Elevation Model (DEM)** in ranges of 200 meters from the Silala springs.

Hypotometric curve

From Table 5.1, and taking into account the columns ―Percentage of accumulated area‖ and ―Average height‖, the hypsometric curve is obtained. The distribution of the area of the survey area is obtained at different topographic levels, in order to compare storage and flow characteristics in the basin (see Figure 5).

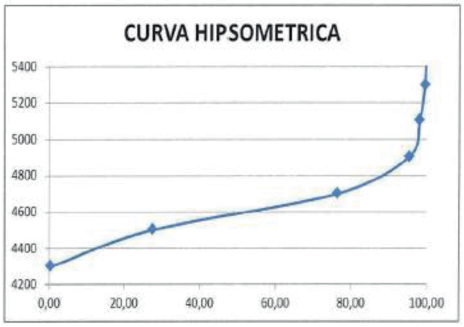

Figure 5.7: Hypsometric Curve of the Silala Area.

It is interesting to know how the area of the survey area is distributed at different topographic levels, in order to compare storage characteristics. This is achieved from the hypsometric curve.

From Figure 5.7, it can be deduced that it is a curve that reflects a basin with a minimum erosive potential. This aspect corroborates the existence of minimum volumes of surface runoff.

5.6. Hydrogeological Survey

Geological units of the Silala area

From the interpretation of the geology of the survey area, which was carried out in Chapters I, II and III of this report, the presence of three geological units was defined: Mio-Pliocene Volcanic Lavas, Rhyolitic Ignimbrites (Welded Tuffs) and Pleistocene Unconsolidated Deposits.

The unit that occupies the largest area is the Mio-Pliocene Volcanic Lavas, occupying 105.16 km2, representing 42.2% of the survey area. The second unit in importance is the Rhyolitic Ignimbrites (Welded Tuffs), with a total of 87 km2, representing 34.9% of the total area. Finally, the third unit has an area of 57.2 km2, representing 22.9% of the survey area; we have the Pleistocene Unconsolidated Deposits (see Chapter III, Map 3.1, p. 68).

5.7. Obtaining Hydrogeological Parameters

In order to obtain the parameters of permeability, it was necessary to resort to different direct and indirect methods, applied mainly to the Ignimbrite formations considered as Aquifers.

Unconsolidated deposit formations, because they have more or less favorable levels of effective porosity for the storage of groundwater, are considered as Aquitards.

The compact volcanic lava formations do not have expected levels of porosity, they are classified as Aquifuges.

5.7.1. Hydrogeological Parameters of Unconsolidated Deposits

For the hydrogeological characterization of the unconsolidated deposits of the Silala springs, we proceeded to obtain the soil texture, perform infiltration velocity tests, through the infiltration test by the Double Ring Method based on the Kostiakov Equation and the permeability tests at greater depth through the Descending Level Method (see Annex E.1 – Infiltration Test Tables).

5.7.1.1. Soil Texture

The texture of the soil indicates the relative content of different sized particles, such as sand, silt and clay. As it also has to do with the amount of water and air it retains and the velocity with which water penetrates the ground and passes through it.

In the survey area, soil samples were taken at four points that after having been analyzed in laboratories resulted in a SILTY- LOAMY texture (see Figure 5.8, Table 5.2).

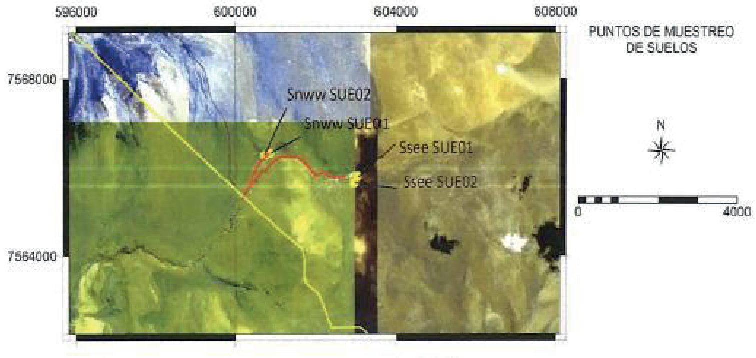

Figure 5.8: Soil sampling points from the Silala springs.

SAMPLE	TEXTURE
Ssee-SUE01	Silt-Loamy
Ssee-SUE02	Silt-Loamy
Snww-SUE01	Silt-Loamy
Snww-SUE02	Silt-Loamy

Table 5.2: Textural Classification of Soils

Geological formations that are composed of silt contents are classified as Aquitards (See Annex D.1., Soil Certificate).

5.7.1.2. Infiltration Velocity Tests

It is called ―infiltration‖ to the process of vertical migration through which water penetrates the surface, a process that allows saturating the geological formations.

The infiltration test by the double ring method consists of saturating a portion of the soil limited by two concentric rings so that the variation of the water level in the inner cylinder can then be measured. Through the Kostiakov Equation, the infiltration velocity was obtained. This information defined the soil type for a range of 30–50 cm, on average, from which results average values of infiltration velocity were obtained with a permeability calculated in the southeast-east sector of 1.08 m/day and in the northwest-west sector of 2.44 m/day (see Annex E.1., Infiltration Tests).

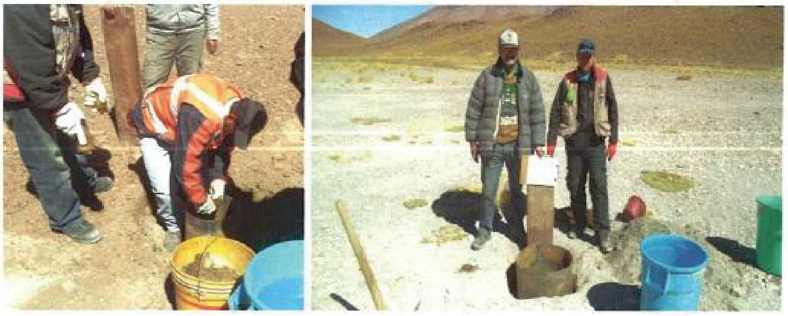

Photograph 5.1: Infiltration Tests by the Double Ring Method.

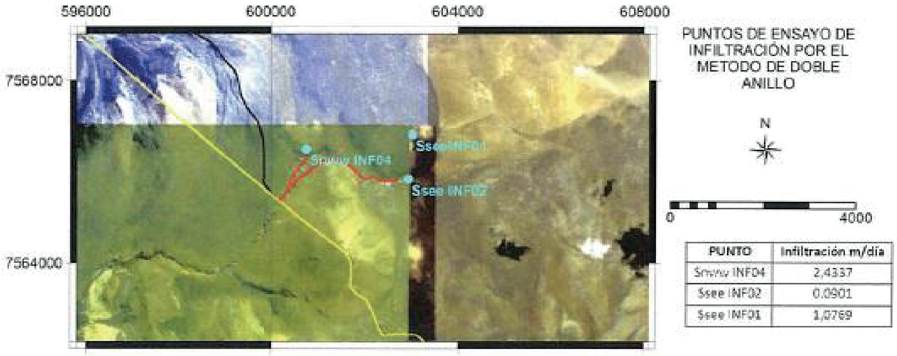

Figure 5.9: Location of Infiltration Test Points

As shown in Figure 5.9, three infiltration tests were carried out on the points coded as: Snww INF04, Ssee INF02 and Ssee INF01.

The results of these soil tests shown in Table 5.3, classify them as Aquitards.

POINT	Infiltration m/day
Snww INF04	2,4337
Ssee INF02	0,0901
Ssee INF01	1,0769

Table 5.3: Results of the Infiltration Test.

5.7.1.3. Permeability Tests

Permeability is the ability of a material to allow a flow to pass through it without altering its internal structure. It is stated that a material is permeable if it allows an appreciable amount of fluid to pass through it in a given time.

The coefficient of permeability can be expressed according to the following equation:

$$k = Q / IA$$

Where:

k: coefficient of permeability or hydraulic conductivity [m/s]

Q: flow rate [m^3/s]

I: gradient

A: section [m^2]

For the calculation of this permeability value of the unconsolidated formations of the colluvial-alluvial material, the Descendant Level Method was applied to a depth of 1.5–2 meters (see Figure 5 and Figure 5.10), with a constant load at four points in the survey area, whose results are shown in Table 5.4 (see Annex E.2., Permeability Tests).

Photograph 5.2: Permeability Tests.

POINT	PERMEABILITY cm/min	PERMEABILITY cm/min	PERMEABILITY cm/sec	PERMEABILITY cm/day
Snww PERM01	0,3348	3,3480	0,00006	4,8211
Ssee PER02	0,3348	3,3480	0,00006	4,8211
Ssee PER03	0,2259	2,2590	0,000004	3,2530
Ssee PER04	0,4326	4,3260	0,000007	6,2294

Table 5.4: Results of the Permeability Tests.

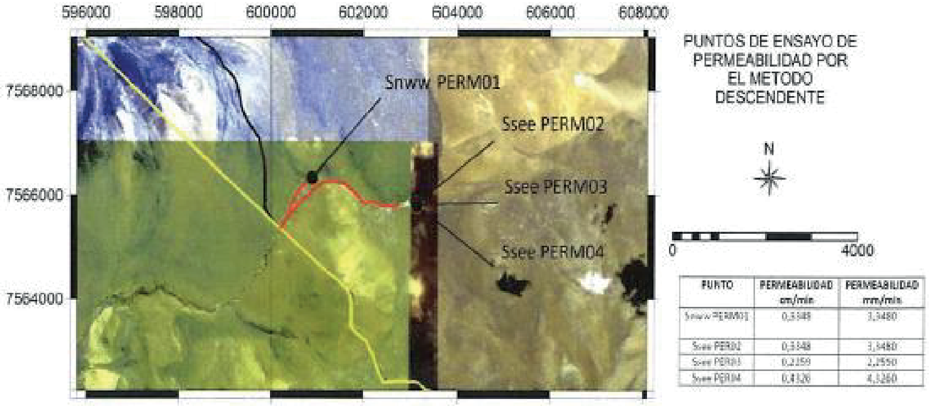

Figure 5.10: Location of Permeability Test points.

The permeability and storage coefficient of volcanic rocks is mainly a function of the degree of fracture or secondary porosity, as an effect of the tectonism of the survey area. However, there are calculated average values that are compatible with Table 5.6 –that according to Custodio (1996)– Ignimbrites are classified as Regular to Good Aquifers, according to Table 5.5.

Permeability m/day	10^{-6} 10^{-5} 10^{-4} 10^{-3} 10^{-2} 10^{-1} 1 4.607 10 10^{2} 10^{3}				
Rating	Impermeable	Low permeability	Somewhat permeable	Permeable	Very permeable
Aquifer rating	Aquiclude	Aquitard	Poor Aquifer	Aquifer from regular to good	Excellent Aquifer
Type of materials	Compact clay Shale Granite	Silt Sandy Silt Clay Silty	Fine sand Silty Sand Fractured limestone	Clean sand Gravel and sand Fine sand	Clean sand

Table 5.5: Classification of terrains by permeability (according to Custodio and Llamas)

5.7.2. Hydrogeological Parameters of the Miocene Ignimbrite Formation

The hydrogeological survey in volcanic rocks is a very special case since they are not part of the typical fissured or porous aquifers. Recent volcanic materials encompass rocks of different nature around the Siloli Chico Hill volcanic dome.

Photograph 5.3: Siloli Chico Hill volcanic dome.

From the interpretation of the structural geology of the survey area, we have a Domain 1, characterized by fractures of extension of courses, which fluctuate from N 81-85° E, coinciding with the direction of the topographic depression through which the springs flow, with a preferred course of N 81° E. These geological structures are located in the Ignimbrites of the survey area, so this formation can be classified as a secondary porosity aquifer. However, as seen in the Chapter on ―Modeling the Water Supply‖, the recharge from meteoric waters is null, so it can be affirmed that the origin of the water from the springs also has another source that is located outside the survey area, in Bolivian territory of higher elevations; consequently they cannot be considered fossil waters.

5.7.3. Hydrogeological Parameters of Volcanic Lava Formation

This formation, correspond to Domain 2, which are characterized by the presence of shear fractures. From the interpretation of the Frequency Rosette it can be perceived predominance of course with a range of N 0-10° W, which coincides with compression fractures, as well as a fracturing frequency in a range of N 60-68° W, which coincides with shear fractures. For all the above, it can be explained in the section of Domain 2 that there are no springs, since there is a preference for closed fractures unlike Domain 1 and 4, which are extension fractures. Consequently, it can be affirmed that this formation behaves like an Aquifuge.

5.8. Hydrogeological Map of the Silala Springs

Once the geological formations have been characterized –from the hydrogeological point of view– based on the type of soil texture, infiltration, permeability and the interpretation of structural geology, we proceeded with obtaining the geological map that served as the basis for developing the hydrogeological map of the survey area. Where three hydrogeological units are presented, which in order of importance for the area they occupy, are: Aquifuge, Aquifer of Secondary Porosity and Aquitard.

The Aquifuge of the Silala area is non-fractured volcanic rock, it occupies an area of 104.98 km2, and representing 42.11% of the total area (see Table 5.5). This hydrogeological unit is located in the north, northeast and south of the survey area (see Map 5.1), these are Mio-Pliocene Volcanic Lavas with very low permeability.

The second hydrogeological unit is a secondary porosity aquifer, which occupies 86.95 km2, representing 34.87% of the total area (see Table 5.5). This hydrogeological unit is located mostly in the eastern sector of the survey area. Another important sector of emplacement of this unit is the North, Center and South (See Map 5.1). Lithologically it is formed by Ignimbrites that have been affected by an intense jointing, having identified a ―Domain 1‖ of open jointing, which gives a secondary porosity. Since it is a cracked aquifer, the water content depends on the degree and distribution of the fracture. However, the recharge conditions, due to the effect of meteoric waters, are incipient (WATER DEFICIT), so they are not likely to contribute any amount of water to the artificial drainage canals to Chile.

The third unit, in order of importance for the area it occupies, is an Aquitard, which occupies 57.39 km2, and representing 23.02% of the total area (see Table 5.5). This hydrogeological unit is formed by river deposits (in the ravines), morrhenic deposits, colluvial, colluvial-fluvial deposits and alluvial deposits. The survey area is mainly located in the central part (see Map 5.1).

For all the above we can point out that the surface hydrogeological map does not contribute to the upwelling of the Silala springs. Due to the volumes that have been gauged in a range of 160 to 250 l/s, consequently the recharge to the aquifers comes from Bolivian territory with higher elevations than those of the survey area.

Hydrological Unit	Area (m^2)	Area (km^2)	% Area
Aquifuge	104977500	104,98	42,11
Aquifer of secondary porosity	86949375	86,95	34,87
Aquitard	57392500	57,39	23,02
TOTAL	**249319375**	**249,32**	**100,0**

Table 5.5: Hydrogeological Units of the Silala Area.

The detailed geological mapping in the survey area has allowed the elaboration of the structural geological map (see Annex A.2 – Map 2/8 – Chapter 1), which has allowed the strato-volcanic column to be elaborated (see Table 5.6).

These thematic maps allowed validating the hypothesis of the geological and hydrogeological history and its relation with the geomorphology and the materials present in the survey area. This has allowed classifying correspondingly the permeability of all the formations present in the survey area classified as: Aquifuges, Aquitards and regular to good Aquifers.

ERA	AGE	PERIOD	ROCK TYPE	LITHOLOGY	STORAGE (%)	PERMEABILITY (m/day)
CENOZOICO	CUATERNARIO	HOLOCENO	MATERIAL ALUVIAL		DE 1 - 40	DE 0.2 a 8.64
			MATERIAL COLUVIAL		DE 1 – 40	DE 0.2 a 8.64
			MATERIAL FLUVIOGLACIAL		DE 1 - 40	DE 0.2 a 8.64
		PLEISTOCENO	LAVA ANDESITICA		DE 1 - 10	De 1.5 a 19.87
	NEOGENO	PLIOCENO				
		MIOCENO	TRAQUIANDESITA		DE 1 - 10	De 1.5 a 19.87
			TOBA		DE 1 - 20	DE 0.2 a 8.64
			IGNMIMBRITA> Plag-Na		DE 1 – 50	10x10-5 a 1
			IGNMIMBRITA		DE 1 – 50	10x10-5 a 1
			IGNMIMBRITA >Plag		DE 1 – 50	10x10-5 a 1

Table 5.6: Storage and permeability of volcanic rocks (Source: Custodio (1996), Sanders & Smith (1998), Morris & Johnson (1982)).

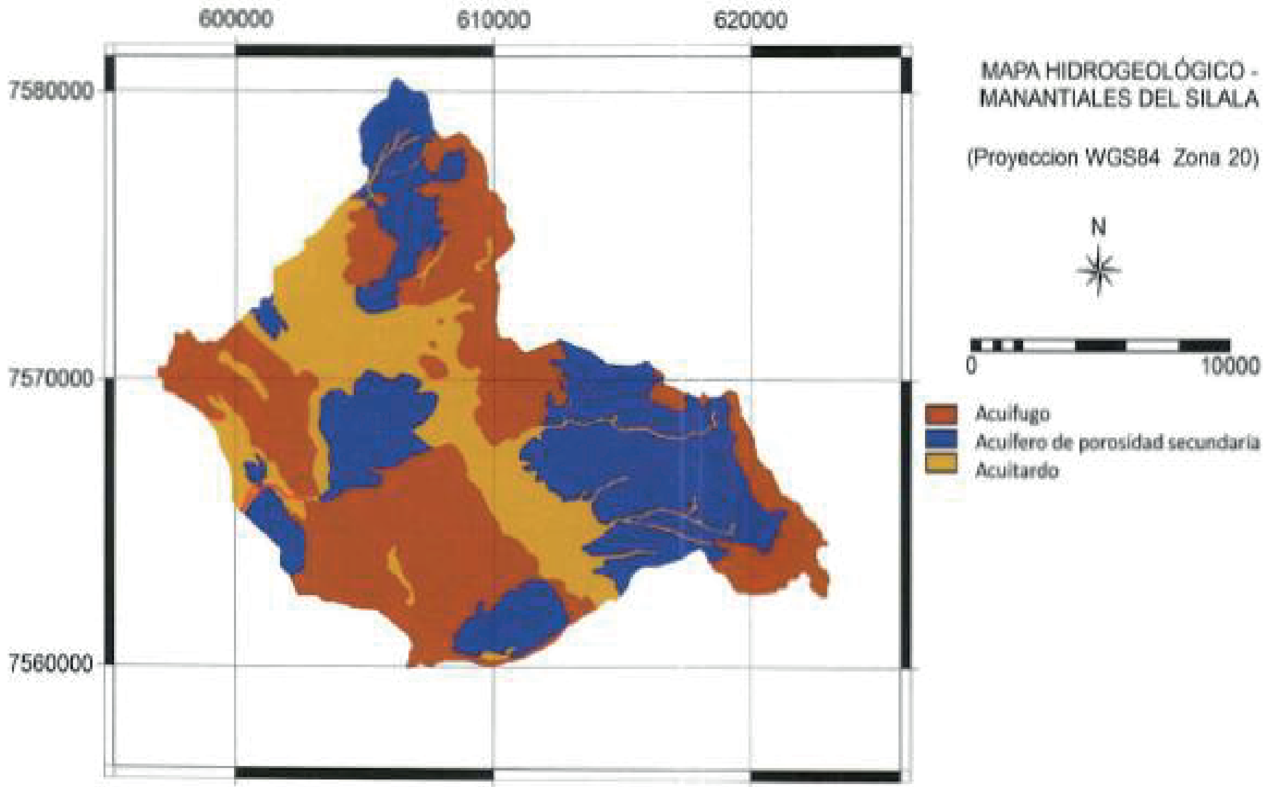

Map 5.1: Hydrogeological Map of the Silala Springs.

Conclusions CHAPTER V (HYDROGEOLOGY)

The recharge of the Ignimbrite aquifer is not possible under the hydrological regime of the survey area, since the meteoric water volumes are minuscule, there is a Water Deficit, therefore the volumes of permanent variable flow that are evacuated towards the artificial canals are validated according to the results of the survey of the superficial hydrological modeling and the gauges carried out in the sector.

The ignimbrite volcanic rock formation is a secondary permeability aquifer due to the degree of fracturing it presents, which come from geological formations that are below the ignimbrite layer, whose recharge is in Bolivian territory at higher elevations than in the survey area.

The piezometric levels of the bofedals present in the area were depressed in anthropogenic form in order to increase the upwelling of the groundwater towards the canals.

Considering an average flow of 200 l/sec, flowing through artificial canals, the surface water supply of the survey area only represents 1.4% of these flows. The remaining 98.6% comes from deep underground aquifers, which migrate their waters through two spring systems structurally controlled by extension fractures in Domain 1, southeast-east springs, and by the shear fractures product of efforts of cupola Domain 4 and faults present in the northwest-west springs, which also conditioned the topographic depression.

The chemical analyzes carried out in the Silala springs define them as SODIC-POTASSIC BICARBONATED waters, and the chemical analyzes carried out in natural and permanent waterbodies with higher elevations classify them as MAGNESIUM-SULFATED waters, consequently, there is no hydro-geochemical relations.

Due to the geological, hydrogeological and topographic characteristics of the survey area, it can be concluded that it is a confined aquifer with secondary permeability.

Due to all the hydrological and hydrogeological characteristics, we can conclude that it is not a shared aquifer, that there is a water deficit, that the recharge is in Bolivian territory and that there is no international course river.

Recommendations

 It is recommended to carry out geophysical surveys by the seismic method in order to determine the thickness of the Ignimbrite layer and, in turn, to define the geological formations that lie below the plate.

 An exploration stage should be planned based on the geophysical drilling results that allow samples of the deep geological formations to be correlated stratigraphically with the aquifers present in Bolivian territory.

Conclusions and Recommendations

GENERAL CONCLUSIONS

CHAPTER I: GEOLOGY

- From the structural mapping of 1,500 fractures and the processing of these data, 4 domains were identified, which represent the dominant structural areas of geological behavior, which defines the upwelling of the Silala springs.

- There are extension fractures whose courses fluctuate between N 81°-85° E, coinciding with the direction of the topographic depression; where the springs flow.

- The directions frequency rosette of Domain 1 shows a preferential fracturing in a range of N 80°-85° W, that respond to fractures of extension, which is why they facilitate the migration of the springs because they are open fractures.

- The frequency rosette of Domain 4 shows a fracture preference of N 50-60° W, fractures that respond to decuple shear stress, that conditioned faults of a N 50° E direction, with a dip of 48° SE and a striation of S 45° W direction, and a trend of 11°; efforts that conditioned the current geomorphology of topographic depression (see Annex A.3, planes 6/8, 7/8 and 8/8), where are the outcrops of the Silala Sector north-northwest springs (see Annex A.2 planes 2/8, 3/8 and 4/8).

CHAPTER II: GEOPHYSICS

- In the study area, 15 Vertical Electrical Probes (SEV) were carried out; in the southeast- east sector and in the northwest-west sector, where the upwelling of the springs are located, an average horizontal linear laying of 250 meters and a depth investigated AB/2 of 90 meters, with an average range of 100 to 1000 Ohm-m, having been determined 2 to 4 lithological layers.

- In the 6 geo-electric profiles executed in the southeast-east sector, four lithological units (A, B, C and D) of variable thickness were determined. Unit A presents saturated alluvial material and weathered Ignimbrite with a thickness of 5.25 meters. Unit B presents consolidated Ignimbrite material with a thickness of 4.66 meters at a depth of 9.92 meters. Unit C reflects Ignimbrite materials with a thickness of 20.79 meters at a depth of 30.71 meters. Unit D corresponds to the last geo-electric layer, with a thickness of 40.21 meters and a depth of less than 70.91 meters (SEV3), having as maximum depth of the profiles executed up to 90 meters, whose resistivities are similar to the final layer with fractured Ignimbrite material.

- The wet zone detected from the interpretation of the 6 profiles, has a depth range of 0.28 to 0.50 meters, average thickness of the bofedals.

- In the 9 geo-electrical profiles executed from the northwest-west sector, three lithological units (A, B and C) were determined. Unit A presents alluvial material saturated with clay sediments and weathered ignimbrite with a thickness of 4.04 meters. Unit B with sandy- clayey sediments with a thickness of 41.65 meters at a depth of 45.69 meters. Unit C presents fractured ignimbrite material with a thickness of 23.61 meters at a depth of 69.3 meters.

- The wet zone detected from the interpretation of the 9 profiles is found at 0.40 meters.

- The calibration of the equipment was carried out in the outcropping horizons in the survey area, which in turn allowed reconstructing the strato-volcanic column (see Annex A.3, planes 6/8, 7/8 and 8/8).

CHAPTER III: MODELING

- The georeferencing of the satellite image through a Geographic Information System (ILWIS) has allowed the generation of thematic maps such as: Geological, Topographic Map, Vegetation, Permeability, Slope, Soil Texture, Stoniness, Effective Depth of Plant Roots. The same ones that were verified through a detailed field mapping in the survey area.

- The ratio of Monthly Precipitation versus Potential Evapotranspiration is from 1 to 5, this means that for every millimeter of rain, 5mm evaporates; this leads to a superficial water deficit in the survey area. Values that ratify the annual reports of SENAMHI (Colorada Lagoon Station), where they report average values of 80 mm of precipitation and a potential evaporation of 580 mm.

- The water supply or surface runoff generated by the precipitation in the survey area only has a maximum flow of 2.83 l/sec for the month of January and 0.64 l/sec for the month of February. The rest of the months have 0 l/sec of surface water supply to the artificial drainage canals. The total annual flow is 3.67 l/sec.

CHAPTER IV: HYDROCHEMISTRY CAPÍTULO IV: HIDROQUÍMICA

 The hydro-chemical quality of the springs' water in the southeast-east and northwest-west sectors, reflect SODIUM BICARBONATED POTASSIUM facies, classified as type A, (suitable for human consumption, according to Law N° 1333).

 There are several waterbodies such as Blanca and Chica lagoons with (4,600 m.a.s.l.) and Kara with (4,509 m.a.s.l.) which, due to their quality of BRACKISH WATER, cannot be recharge areas. At the same time samplings were carried out in the INACALIRI Volcano, which are classified as SULPHATED – MAGNESIAN waters, which do not show quality relation with the spring waters.

CHAPTER V: HYDROGEOLOGY

 The recharge of the Ignimbrite aquifer is not possible under the hydrological regime of the survey area, since the volumes of meteoric water are minimal –there is a water deficit– therefore the volumes of permanent variable flow of the springs that are evacuated towards the artificial canals; they are validated according to the historical data reported by the Meteorological Station of the Colorada Lagoon and the results of the surveyy of the superficial hydrological modeling, as well as the results of the gauging by the windlass method executed in the sector.

 The formation of Ignimbrite volcanic rock behaves as a permeable medium, due to the secondary porosity that results from fracturing. Consequently, the outcrops of the Silala springs come from deep aquifers of the geological formations that are below the igneous layer, whose recharge is found in natural and permanent bodies in Bolivian territory with higher elevations than in the survey area.

 The piezometric levels of the bofedals present in the area were depressed in an anthropic form in order to increase the outcrop of the underground water of the canals towards lower elevations.

 Considering an average flow of 200 l/sec, flowing through artificial canals, the surface water supply of the survey area only represents 1.4% of these flows. The remaining 98.6% comes from deep underground aquifers, which migrate their waters through two spring systems, structurally controlled by extension fractures in the southeast-east springs of Domain 1, and by the shear fractures product of efforts of coupe Domain 4 and faults present in the northwest-west springs that also conditioned the topographic depression present in the area.

 The chemical analyzes carried out in the Silala springs define them as SODIC-POTASSIC BICARBONATED waters, and the chemical analyzes carried out in natural and permanent waterbodies with higher elevations classify them as MAGNESIUM-SULFATED waters, consequently, there is no hydraulic relation with surface waters of the springs.

 Throughout the hydrological and hydrogeological characterization we can conclude that it is not a shared aquifer, that there is a water deficit, that the recharge is located in Bolivian territory, that they cannot be considered fossil waters and that there is no international course river.

RECOMENDACIONES

 It is recommended to carry out geophysical surveys by the seismic method in order to determine the thickness of the Ignimbrite layer and, in turn, to define the geological formations that lie below.

 An exploration stage must be planned based on the geophysical results by the seismic method, drillings that will allow obtaining samples of deep geological formations (aquifers) to correlate stratigraphically with the aquifers present in Bolivian territory.

ANNEX A.

GEOLOGY

ANNEX A. 1.

STRUCTURAL

INTERPRETATION

1ST DOMAIN JOINTS SILALA PROJECT

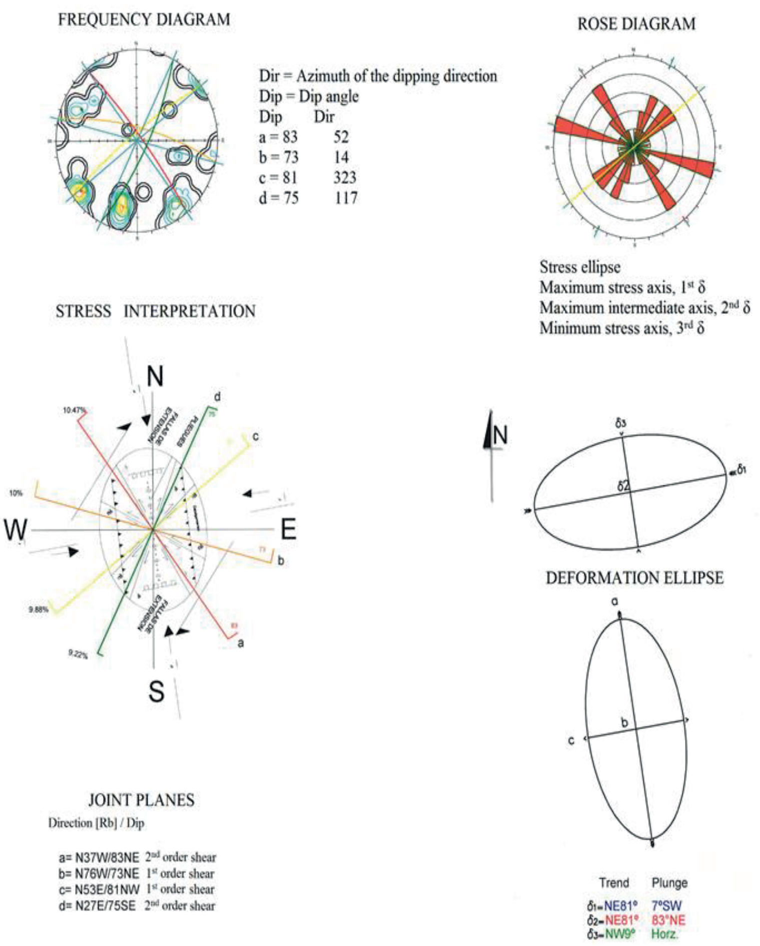

INTERPRETATION

Based on the structural interpretation, it can be perceived that fractures —b‖ and —c‖ respond to shear fractures in relation to the main axis of a NE 81° trend; fractures —a‖ and —b‖ respond to second order sheers in relation to shear stress.

There are fractures of angle strike extension, which fluctuate from 81° N – 85° E and concur with the direction of the topographic depression of the area in which the springs flow, with a preferential Rb [direction] of N 81° E.

From an interpretation of the Rose diagram, it can be perceived that the ruling fracture direction is 80° N – 85° W. The latter is the reason why the flow of the SEE sector springs has a higher rate, inasmuch as water always flows to areas where there is less resistance. These extension fractures are open fractures that enable the upwelling of the springs because of their high secondary permeability rate.

1ST DOMAIN JOINTS

SILALA PROJECT

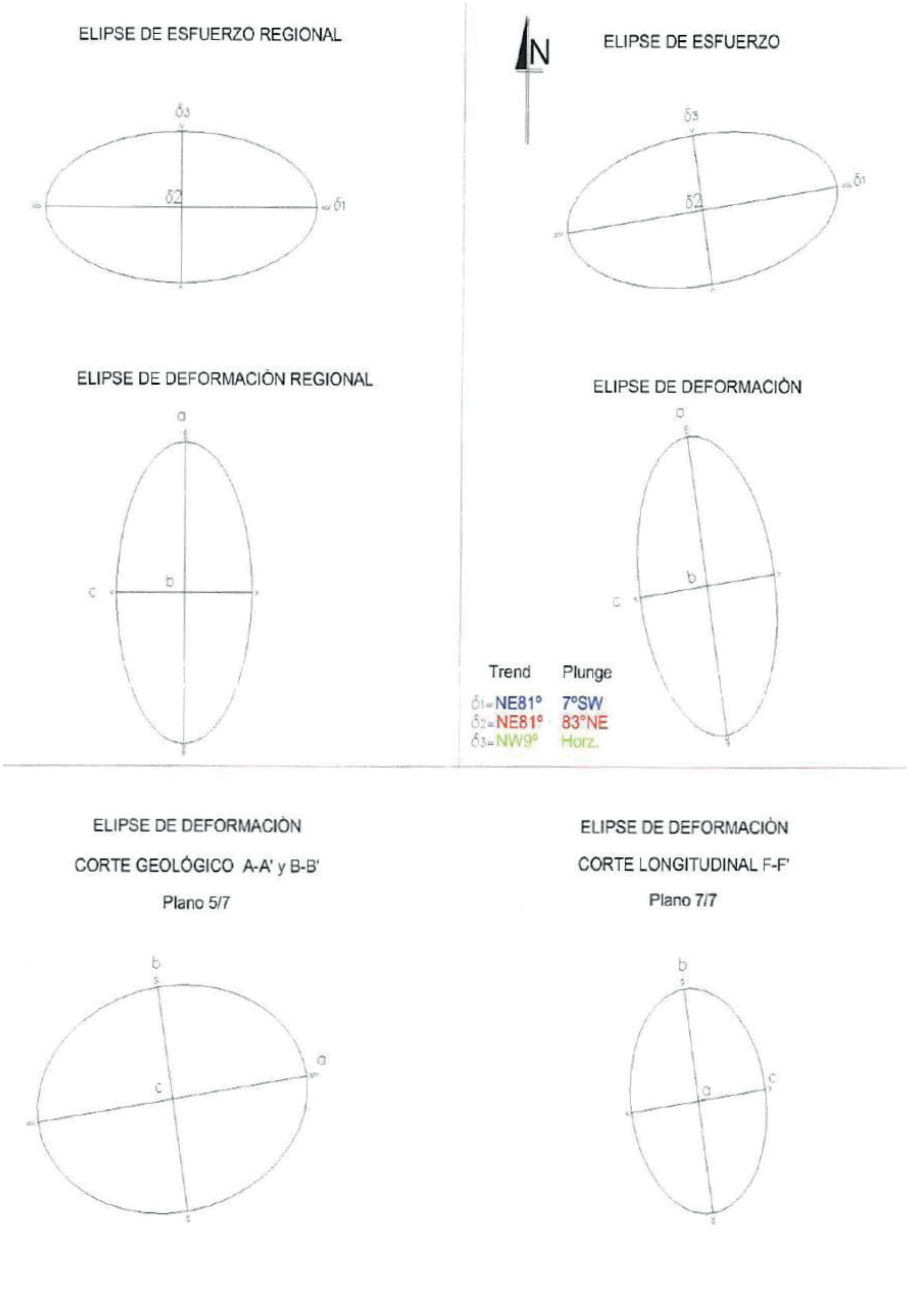

1ST DOMAIN JOINTS

CUTTINGS

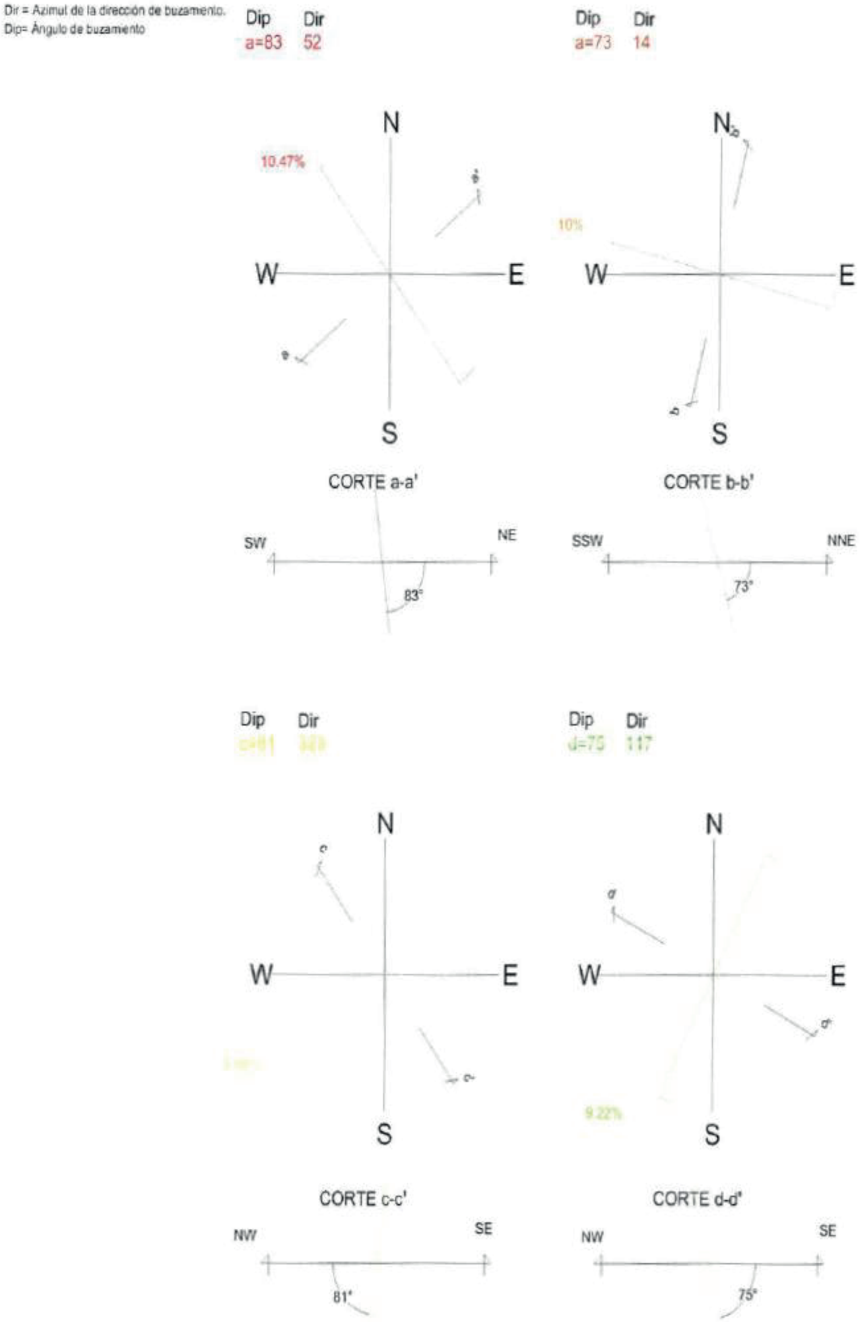

FREQUENCY DIAGRAM

1ST DOMAIN

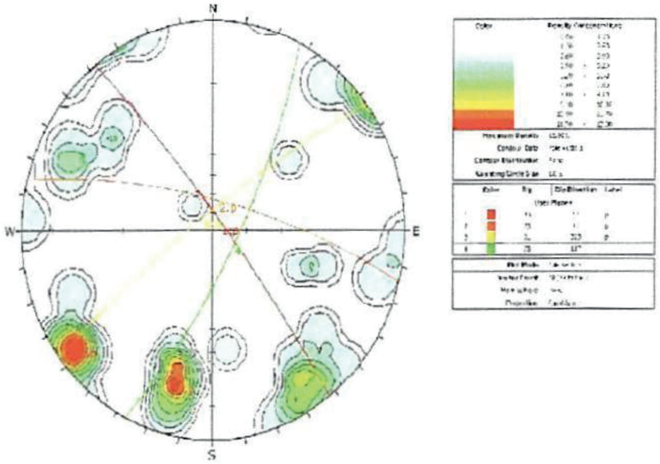

ROSE DIAGRAM

1ST DOMAIN

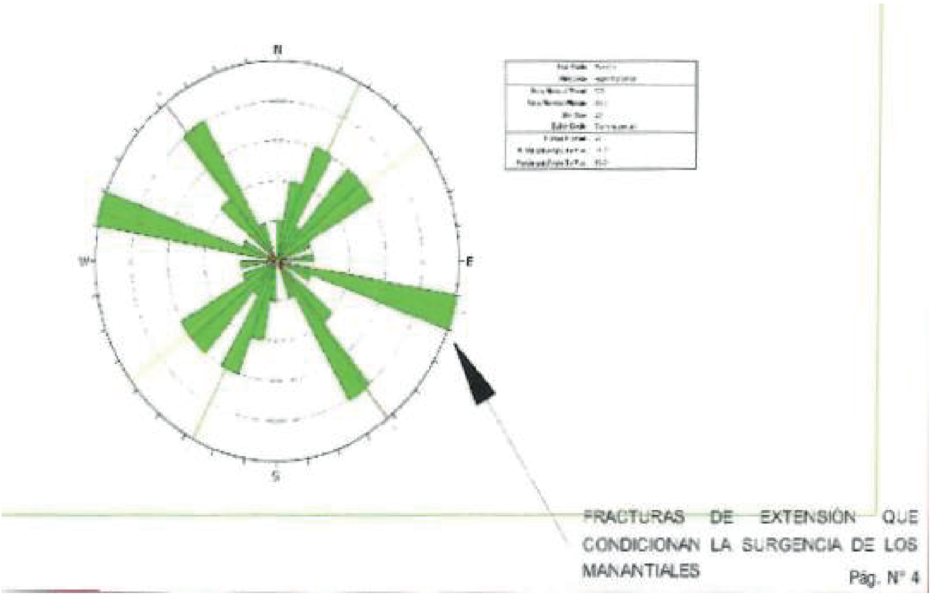

2ND DOMAIN JOINTS

SILALA PROJECT

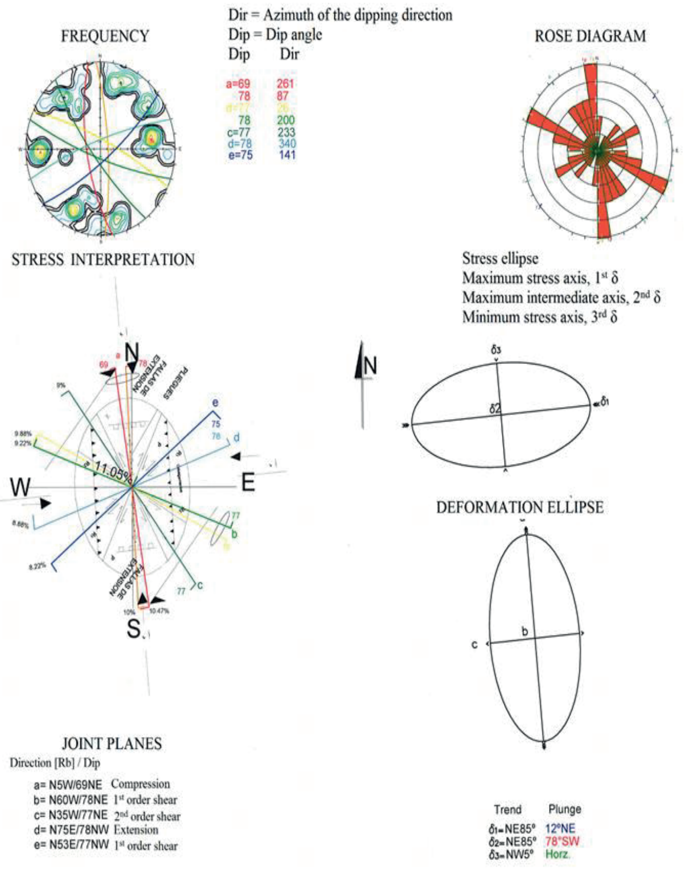

INTERPRETATION

2nd Domain: it is characterized for having a 1st δ (maximum effort axis) of an 85° NE direction and a Plungeof12°NE,a2nd δofan85°NEdirectionandaPlungeof78°SW, anda3rd δofan5°NW direction and a Horizontal Plunge. These caused fractures ―b‖ and ―e‖ to be shear fractures, fractures ―a‖ to be compression (closed) fractures, and ―e‖ to be second order shear fractures.

From an interpretation of the Rose diagram (see, Annex A. l., p. 29), it is possible to perceive a predominant Rb [Direction] in a range of 0° N – 10° W, which matches the compression fractures, and a fracture frequency in a range of 60° N – 68 ° W— matching the shear fractures.
The above provides an explanation as to why the 2nd domain section does not comprise any springs, i.e. this domain presents closed fractures, unlike the 1st Domain.

2ND DOMAIN JOINTS

SILALA PROJECT

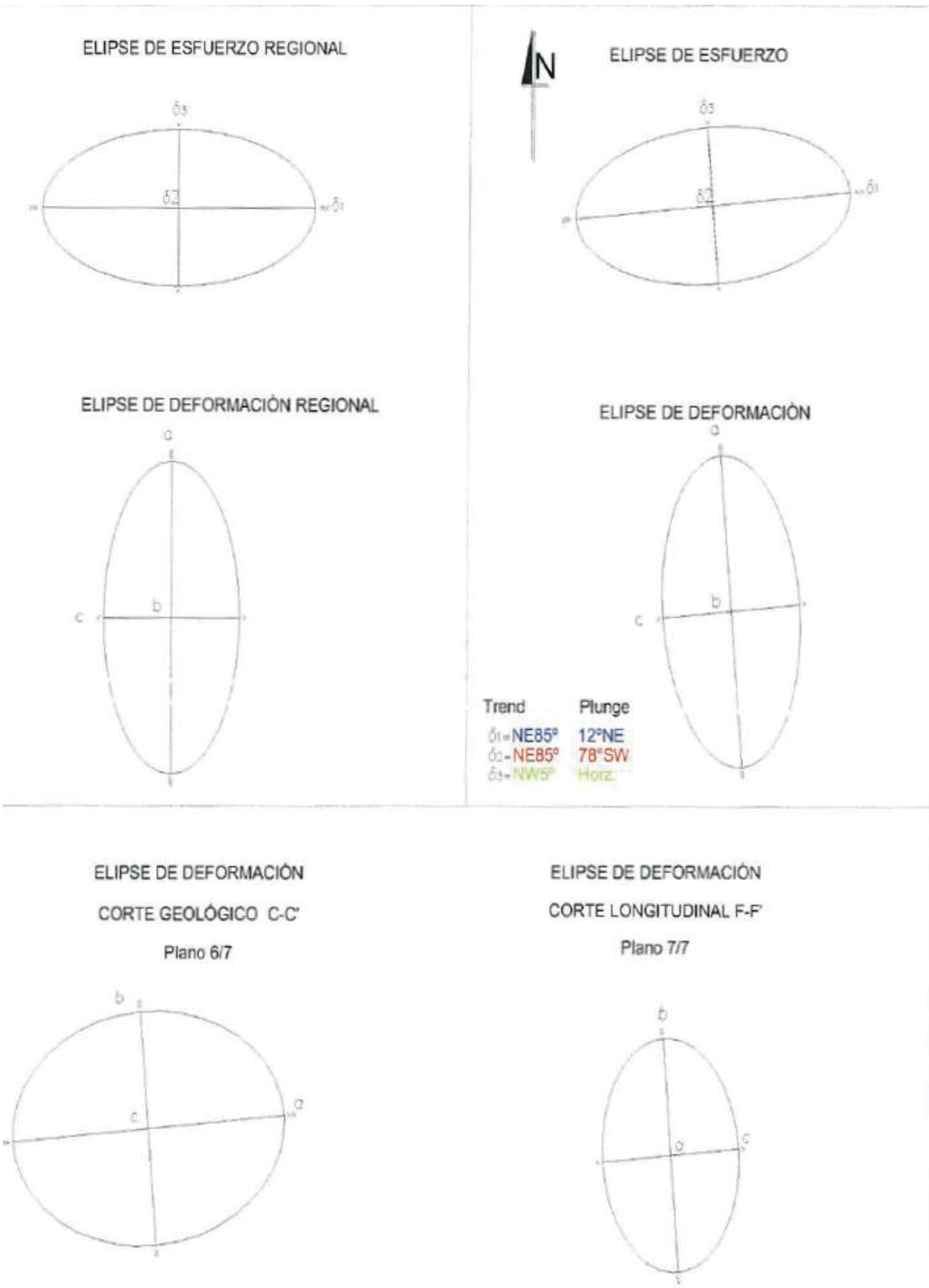

2ND DOMAIN JOINTS

CUTTINGS

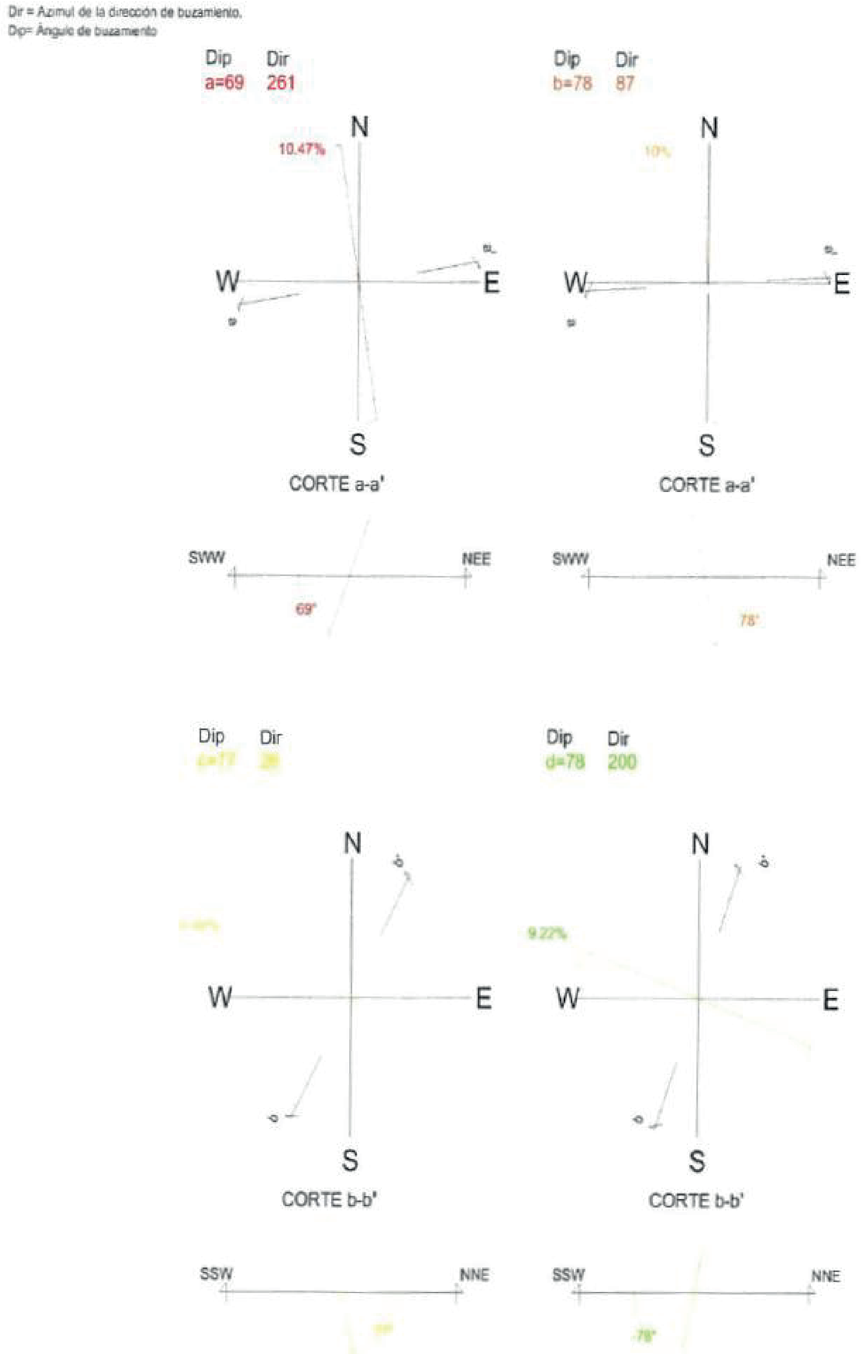

2ND DOMAIN JOINTS

CUTTINGS

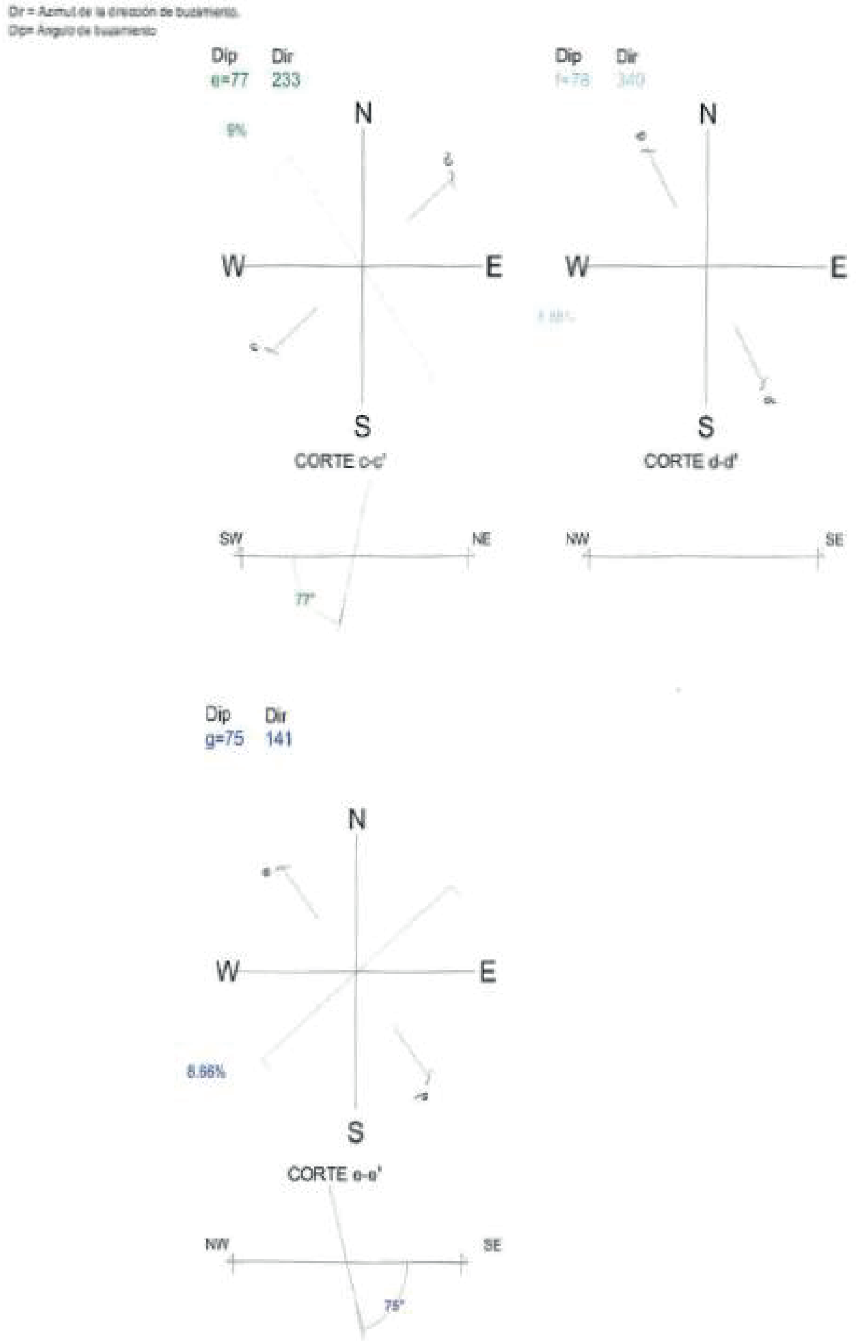

2ND DOMAIN

FREQUENCY DIAGRAM

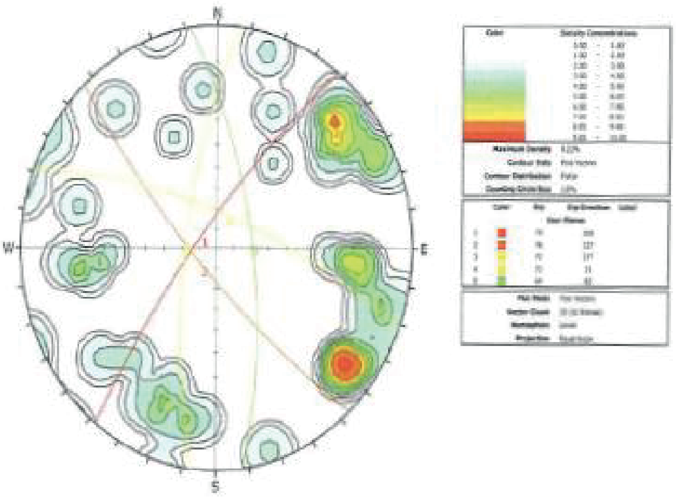

2ND DOMAIN

ROSE DIAGRAM

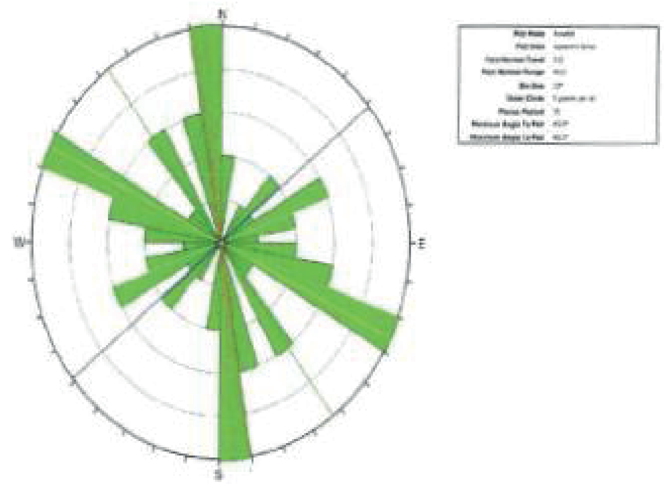

3RD DOMAIN JOINTS

SILALA PROJECT

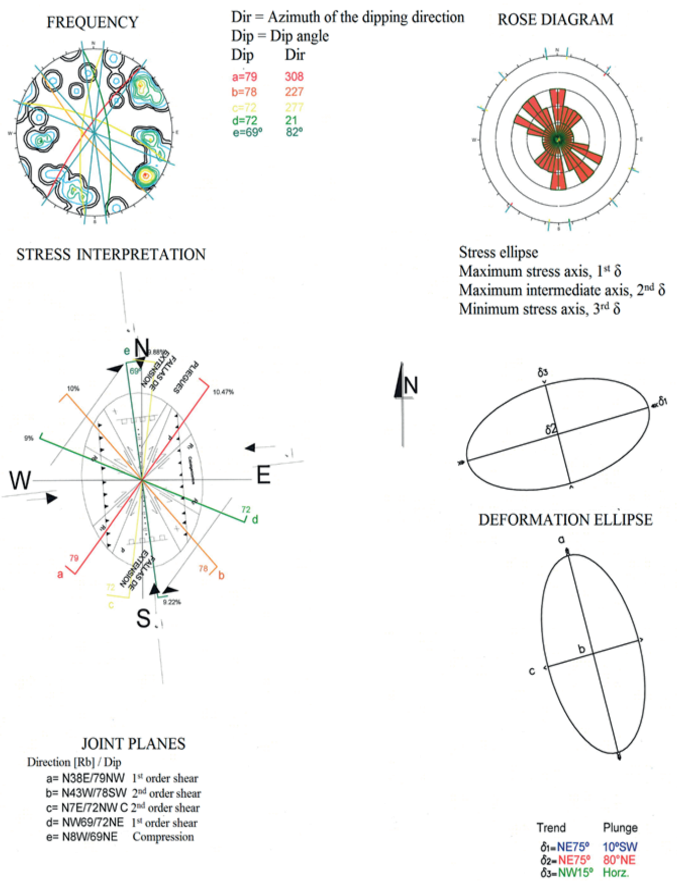

INTERPRETATION

3rd domain: it is characterized for presenting a 1st δ of a 75° NE direction and a Plunge of 10° SW, a 2nd δofa75°NEdirectionandaPlungeof80°NE,anda3rd δofa15°NWdirectionanda Horizontal Plunge. These caused fractures ―a‖ and ―d‖ to be first order shear fractures, fractures ―b‖ and ―c‖ to be second order shear fractures, and fracture ―e‖ to be compression fractures.

From an interpretation of the Rose diagram, it can be perceived that there is a predominant NS fracture Rb [direction], which corresponds to compression fractures, and NW fractures that correspond to shear fractures, to a lesser degree. This is why springs do not well up in this domain.

3RD DOMAIN JOINTS

SILALA PROJECT

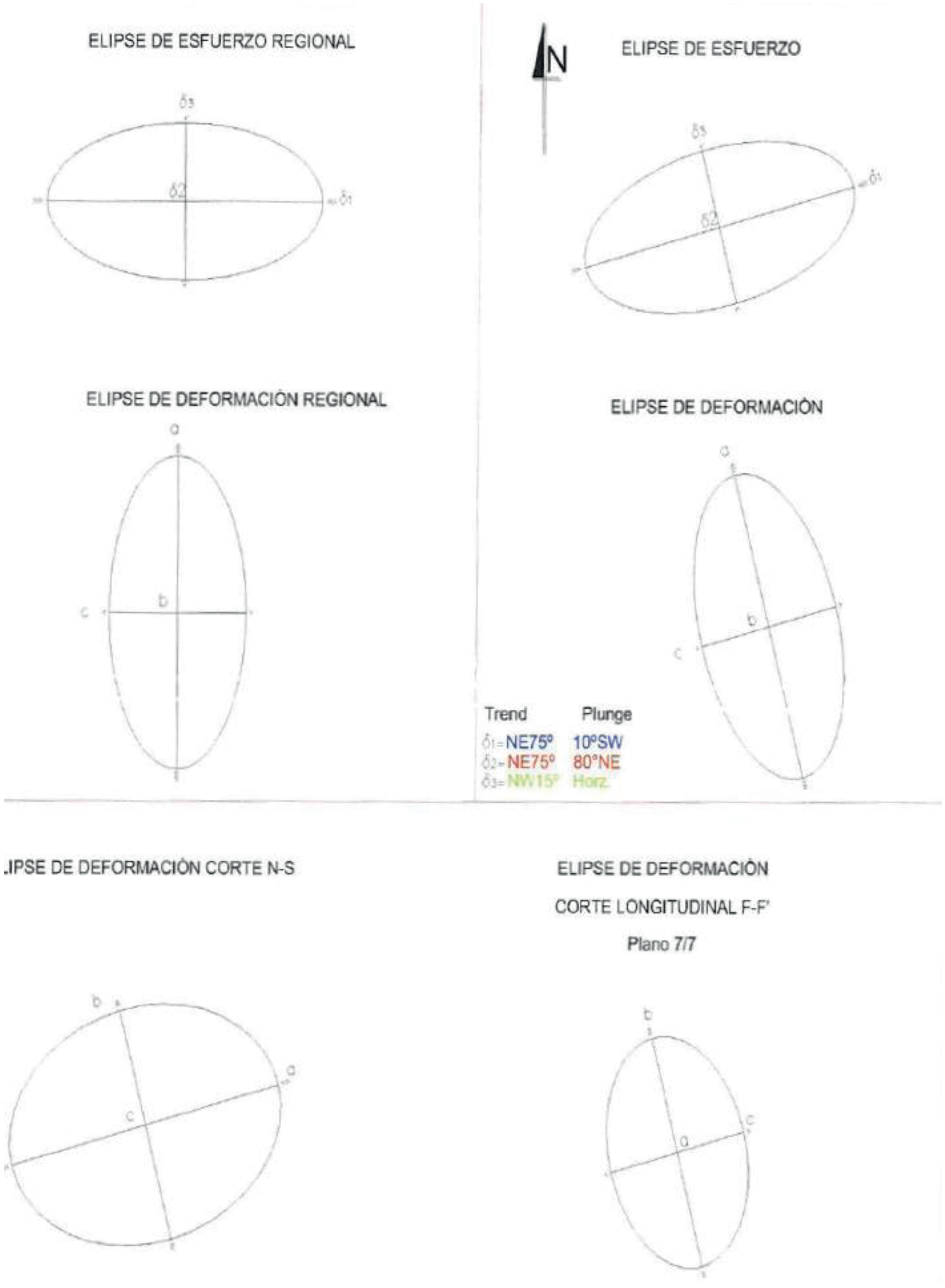

3RD DOMAIN JOINTS

SILALA PROJECT

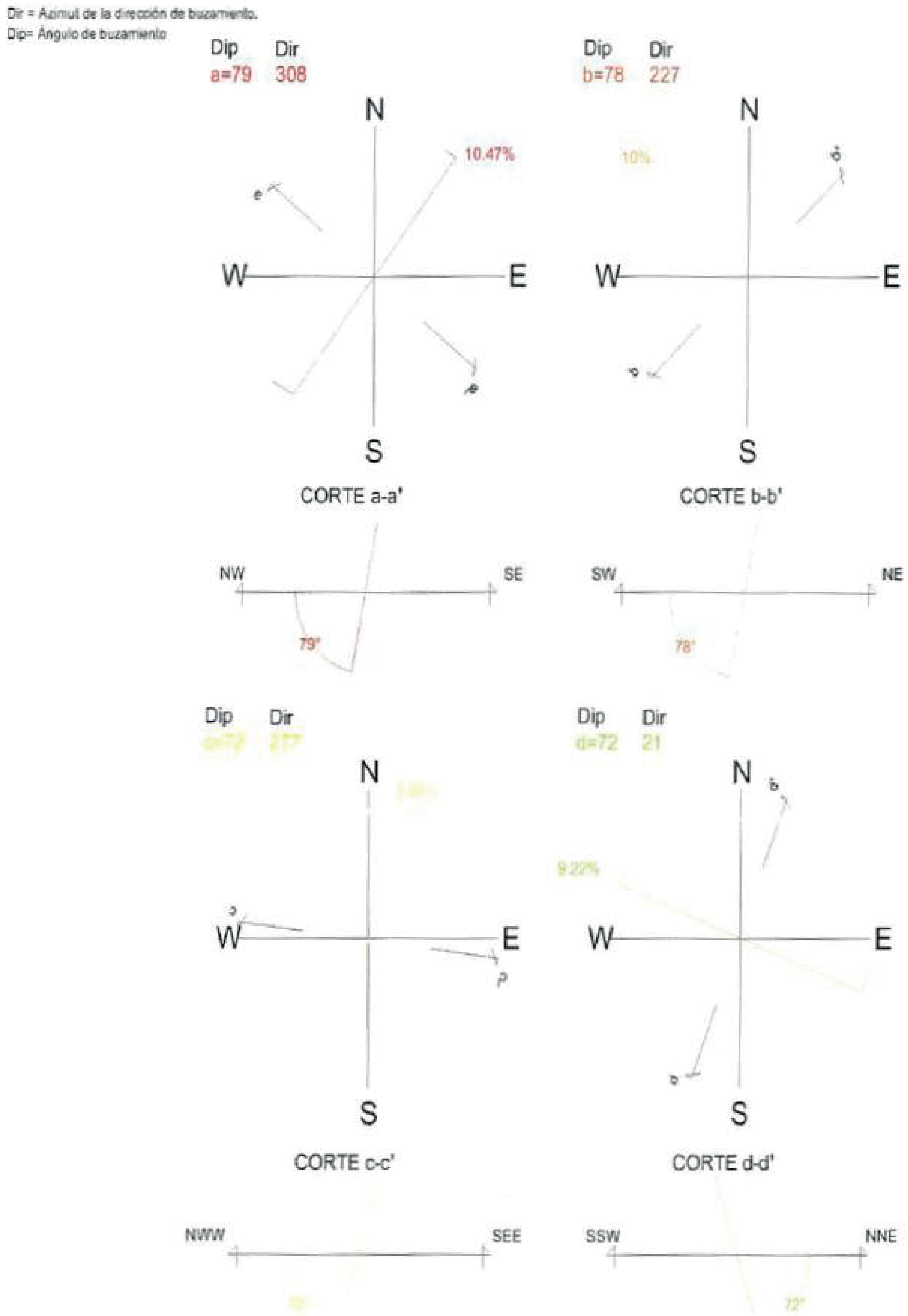

3RD DOMAIN JOINTS

SILALA PROJECT

Dir = Azimut de la dirección de buzamiento.
Dip= Ángulo de buzamiento

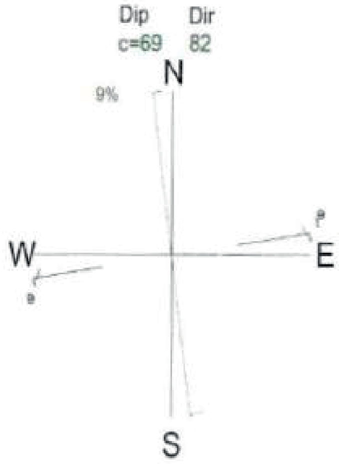

FREQUENCY DIAGRAM

3RD DOMAIN

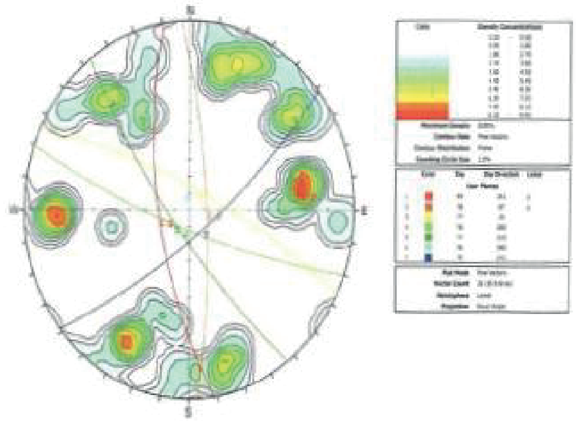

ROSE DIAGRAM

3RD DOMAIN

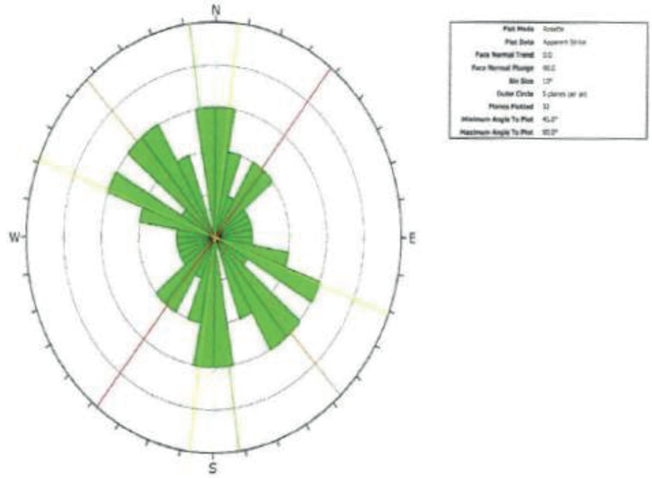

4TH DOMAIN JOINTS

SILALA PROJECT

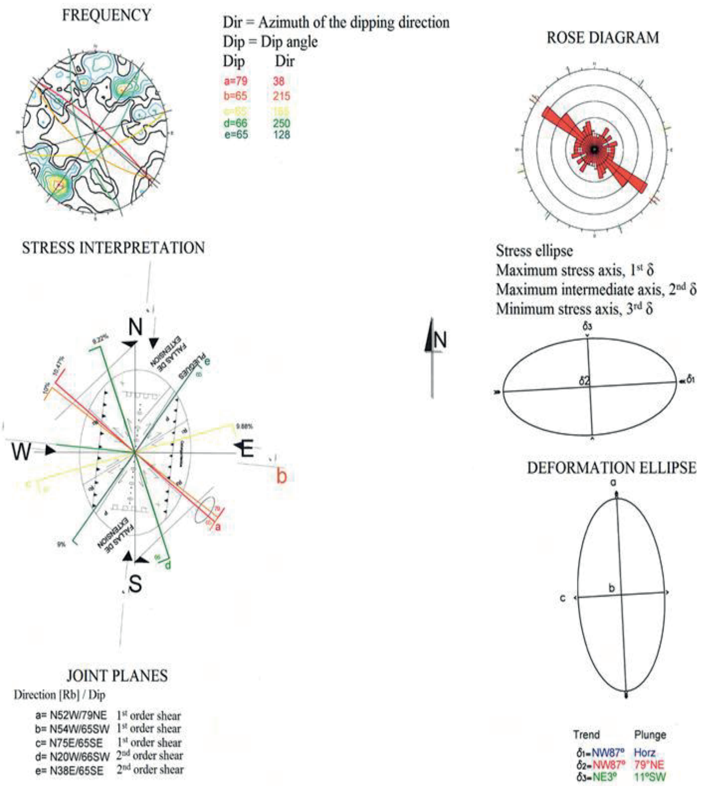

INTERPRETATION

Fractures ―a‖, ―b‖ and ―c‖ are first order shear fractures, with respect to the 1st δ.

Fractures ―e‖ and ―d‖ are second order shear fractures activated by shear stresses.

These have activated the predominant faults in the 4th Domain, as a result of the action of shear stresses, where a fault mirror was mapped with a dipping direction of 140°/148°, a 225° trend, a 11° plunge, and a SW 11° raque. This structural control predetermines the emergence of the NWW sector springs.

4TH DOMAIN JOINTS

SILALA PROJECT

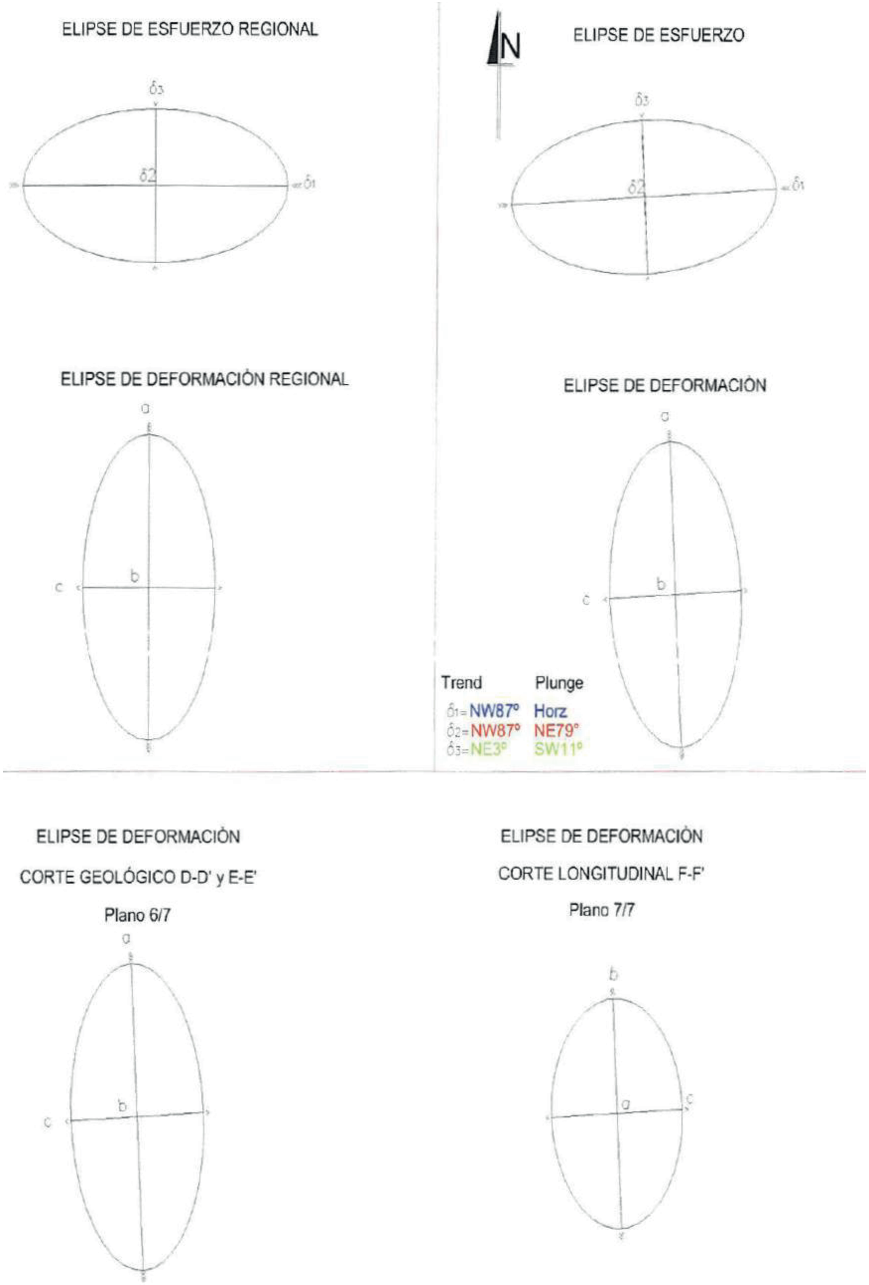

4TH DOMAIN JOINTS

CUTTINGS

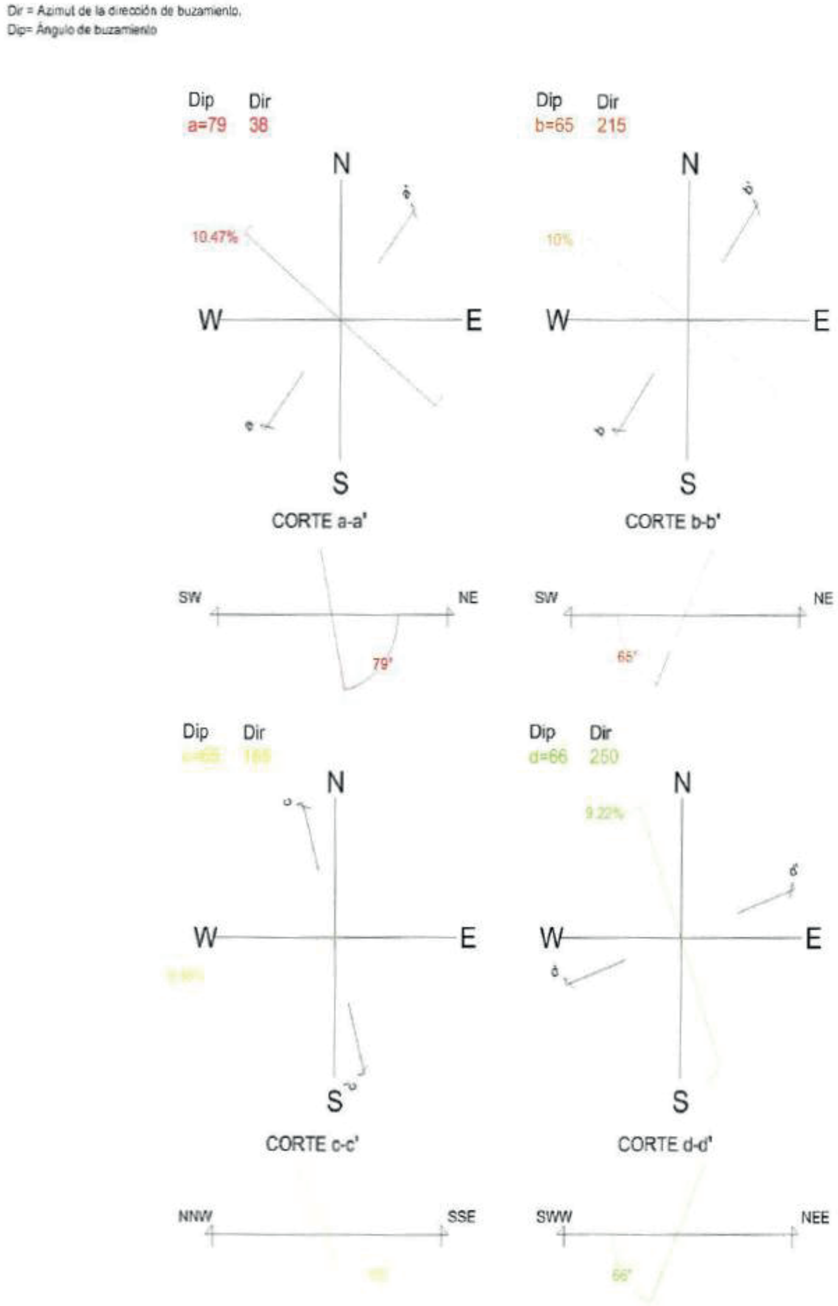

4TH DOMAIN JOINTS

CUTINGS

Dr = Azimut de la dirección de buzamiento.
Dp= Ángulo de buzamiento

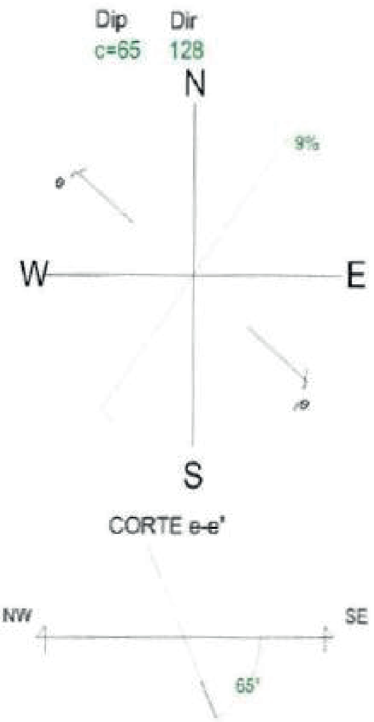

FREQUENCY DIAGRAM

4TH DOMAIN

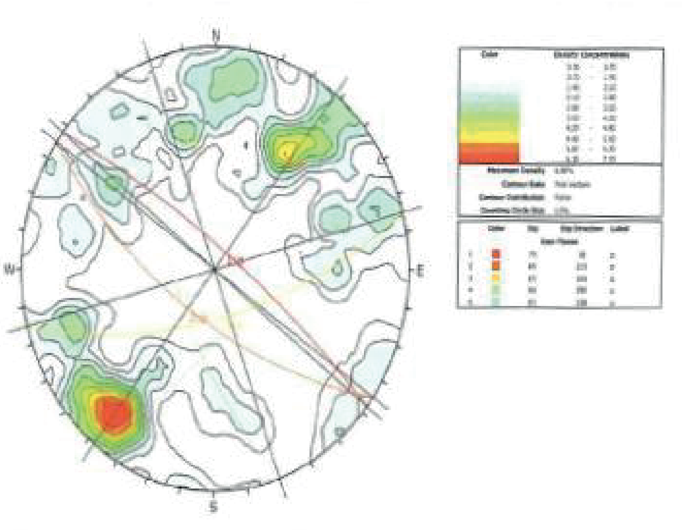

ROSE DIAGRAM

4TH DOMAIN

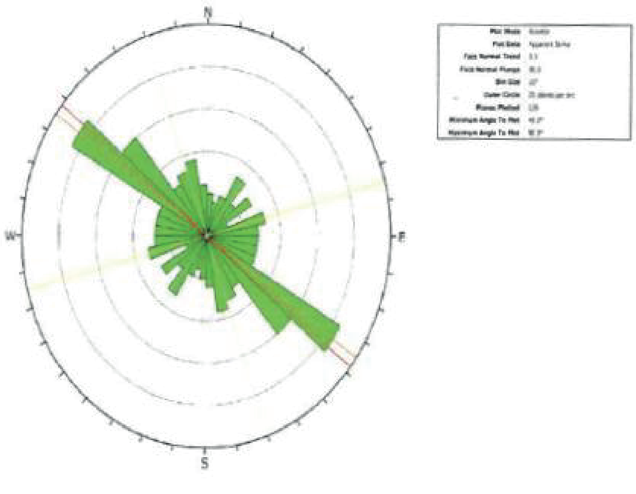

STRUCTURAL FAULT

SILALA PROJECT

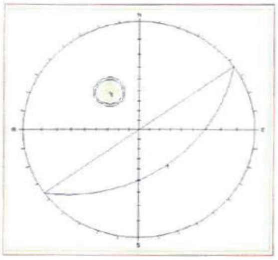

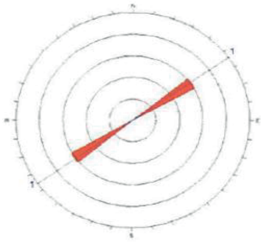

Dip	Dir
48	140
Trend	225
Plunge	11
Raque	11

Dir = Azimut de la dirección de buzamiento.
Dip= Ángulo de buzamiento

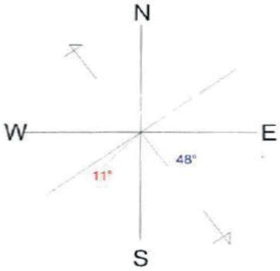

CUTTINGS

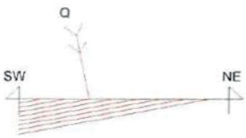

INTERPRETATION

The position of the fault mirrors (striae) shows that the fractures of the 4th domain were activated by the action of shear stresses, which formed the current geomorphology of the canyon (tectonic pit/structural gully).

Fault mirror, Dip/Dir of 140/48, trend 225, plunge 110, raque of 11 SW. This structural control conditions the emergence of the springs of the NWW sector.

ANNEX A. 2.

GEOLOGICAL AND

STRUCTURAL MAPS

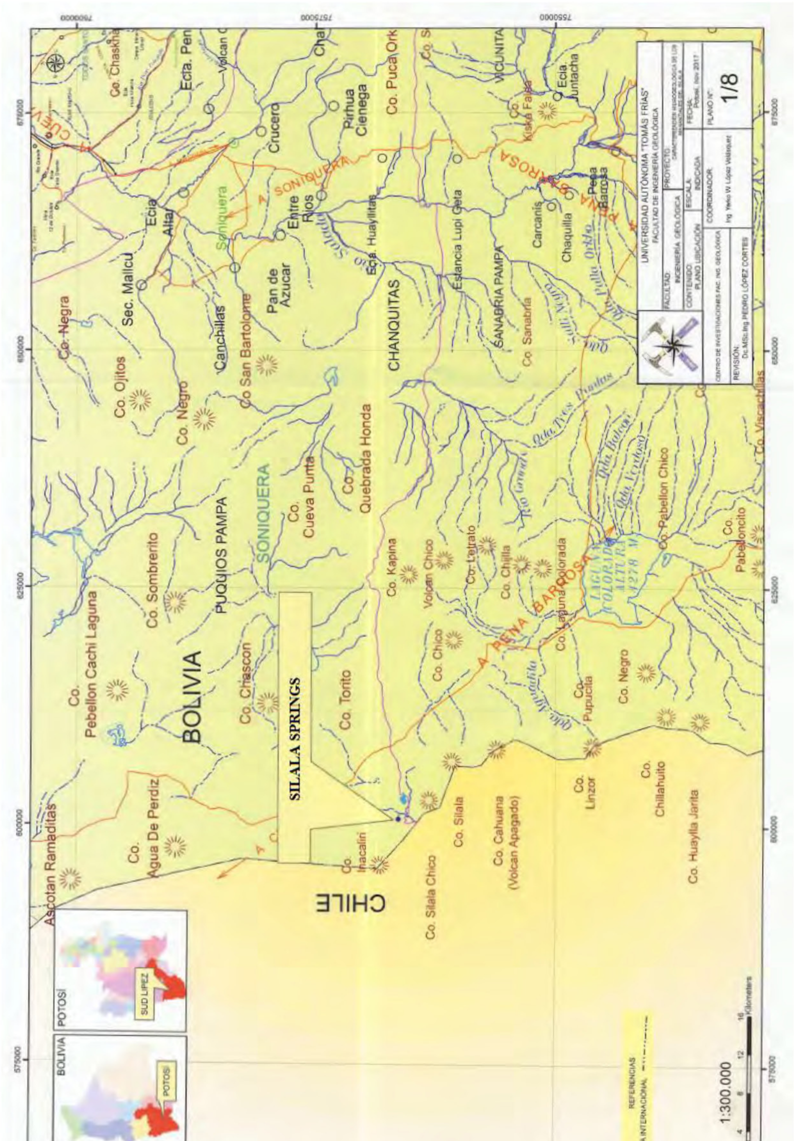
SILALA SPRINGS
BOLIVIA
CHILE
SONIQUERA
PUQUIOS PAMPA
CHANQUITAS
SANABRIA PAMPA
Co. Silala
Co. Silala Chico
Co. Inacaliri
Co. Cahuana (Volcan Apagado)
Co. Linzor
Co. Chillahuito
Co. Huaylla Jarita
Co. Torito
Co. Chascon
Co. Pebellon Cachi Laguna
Co. Agua De Perdiz
Ascotan Ramaditas
Co. Sombrerito
Co. Kapina
Volcan Chico
Co. Chico
Co. Negro
Co. Pupucila
Co. Cueva Punta
Co. Quebrada Honda
Co. San Bartolome
Canchillas
Co. Ojitos
Co. Negra
Sec. Mallcu
Pan de Azucar
Entre Rios
Crucero
Pirhua Cienega
Estancia Lupi Ceta
Co. Sanabria
Carcanis
Chaquilla
Kiska Falla
Ecia. Juntacha
Co. Pabellon Chico
Co. Pabelloncito
Co. Viscachillas
BOLIVIA
POTOSÍ
SUD LIPEZ
REFERENCIAS
FRONTERA INTERNACIONAL
1:300.000
Kilometers
UNIVERSIDAD AUTÓNOMA "TOMÁS FRÍAS"
FACULTAD DE INGENIERÍA GEOLÓGICA
1/8

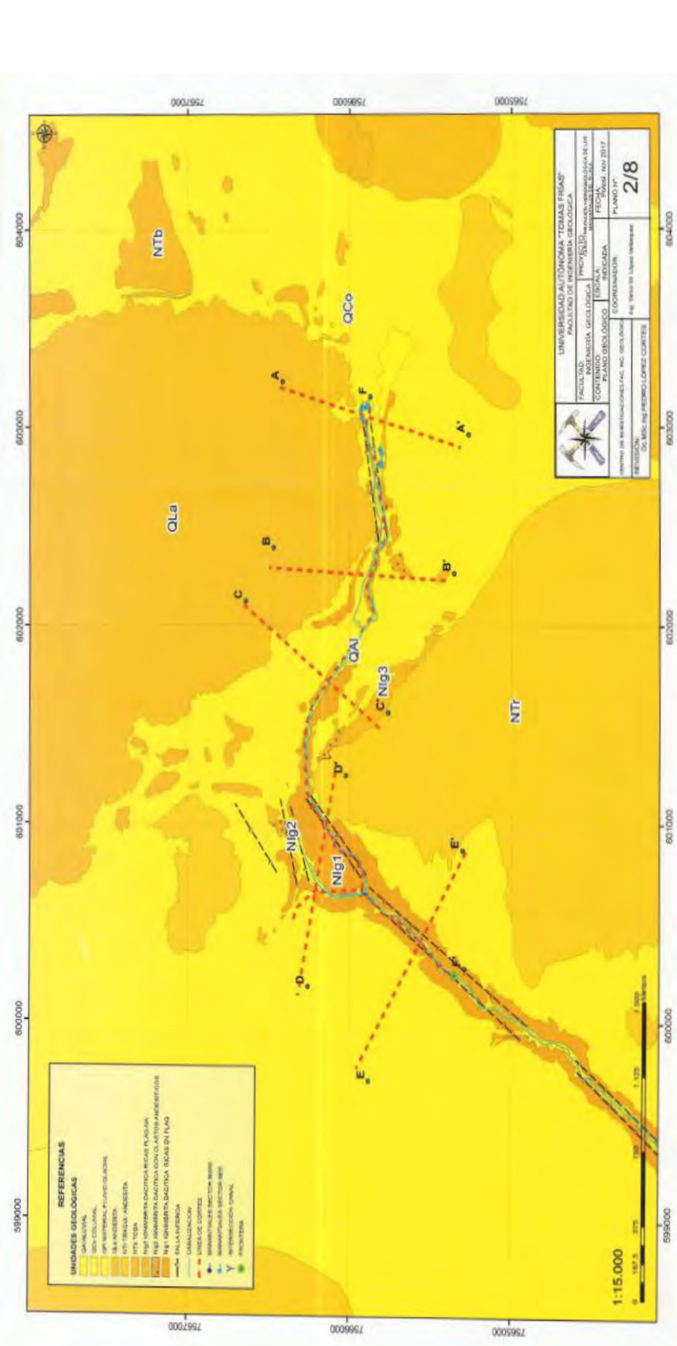

REFERENCIAS
UNIDADES GEOLÓGICAS
1:15.000
QLa
NTb
QCo
QAl
NIg1
NIg2
NIg3
NTr
UNIVERSIDAD AUTÓNOMA "TOMÁS FRÍAS"
FACULTAD DE INGENIERÍA GEOLÓGICA
2/8

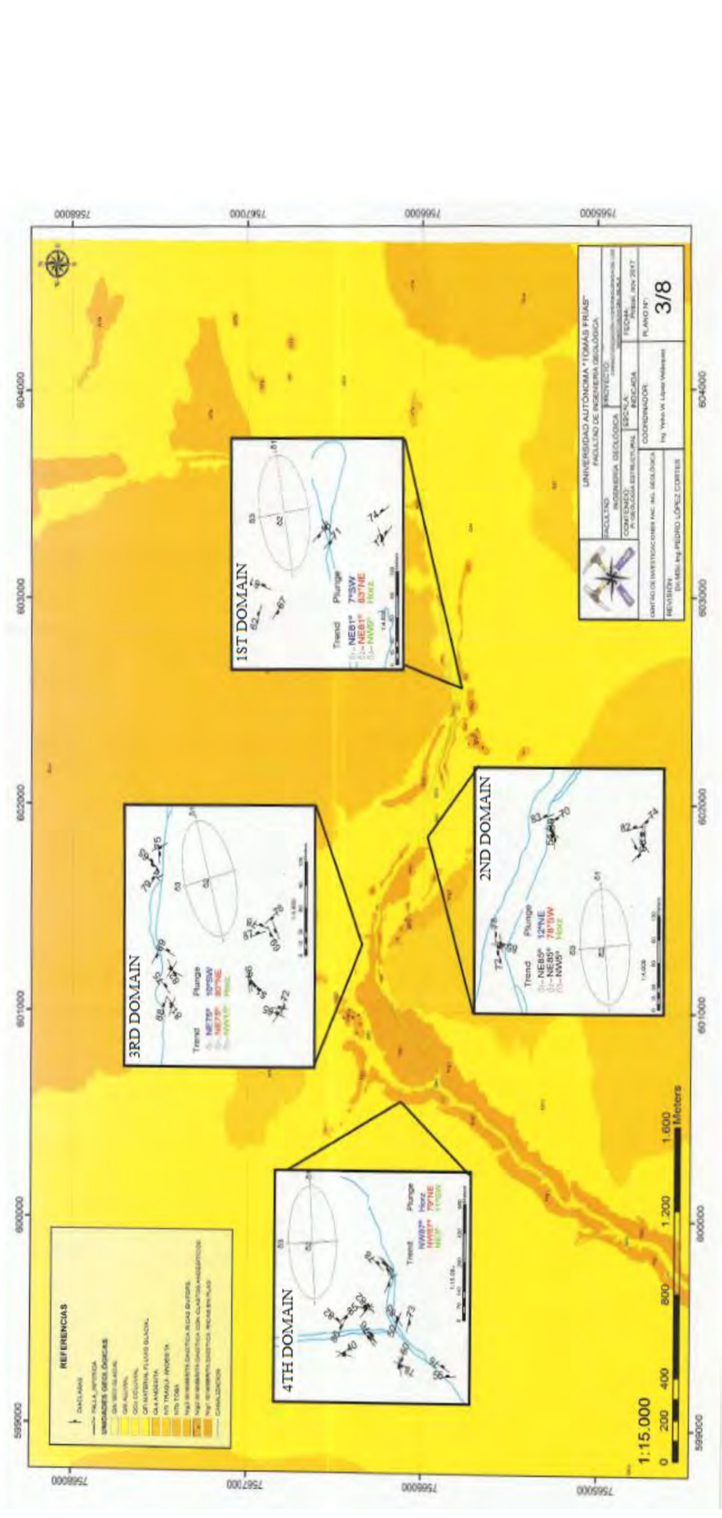
1ST DOMAIN
2ND DOMAIN
3RD DOMAIN
4TH DOMAIN
REFERENCIAS
1:15,000
UNIVERSIDAD AUTÓNOMA "TOMÁS FRÍAS"
FACULTAD DE INGENIERÍA GEOLÓGICA
3/8

54

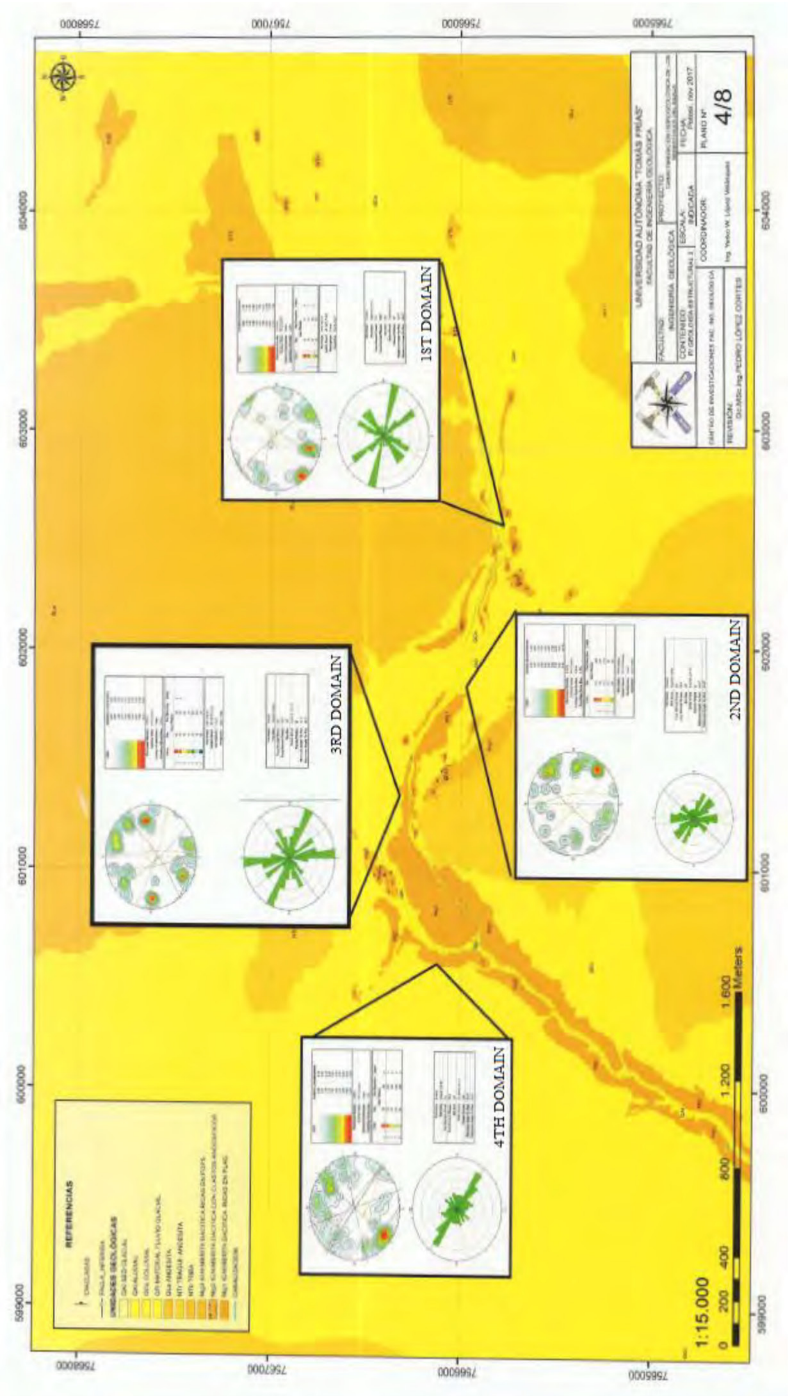
1ST DOMAIN
2ND DOMAIN
3RD DOMAIN
4TH DOMAIN
REFERENCIAS
UNIDADES GEOLÓGICAS
1:15.000
Meters
UNIVERSIDAD AUTÓNOMA "TOMAS FRIAS"
FACULTAD DE INGENIERIA GEOLOGICA
PLANO N°
4/8

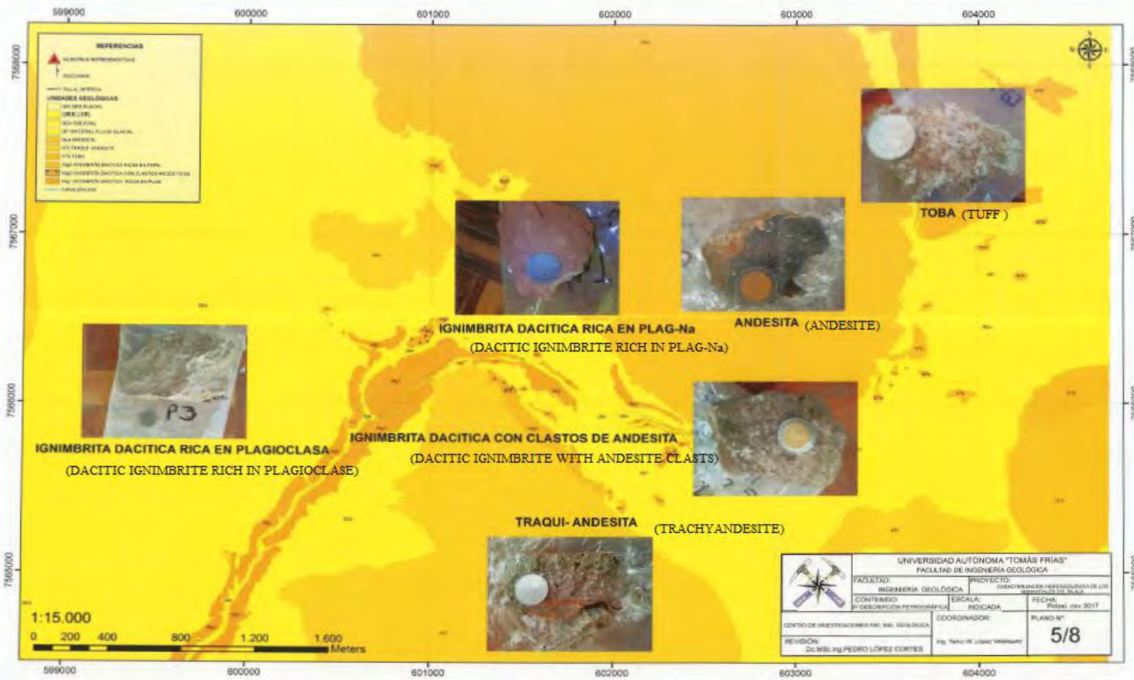
TOBA (TUFF)
IGNIMBRITA DACITICA RICA EN PLAG-Na
(DACITIC IGNIMBRITE RICH IN PLAG-Na)
ANDESITA (ANDESITE)
IGNIMBRITA DACITICA RICA EN PLAGIOCLASA
(DACITIC IGNIMBRITE RICH IN PLAGIOCLASE)
IGNIMBRITA DACITICA CON CLASTOS DE ANDESITA
(DACITIC IGNIMBRITE WITH ANDESITE CLASTS)
TRAQUI- ANDESITA
(TRACHYANDESITE)
1:15.000
0 200 400 800 1.200 1.600 Meters
UNIVERSIDAD AUTÓNOMA "TOMÁS FRÍAS"
FACULTAD DE INGENIERÍA GEOLÓGICA
5/8

ANNEX A. 3.

GEOLOGICAL

CROSS-CUTTINGS

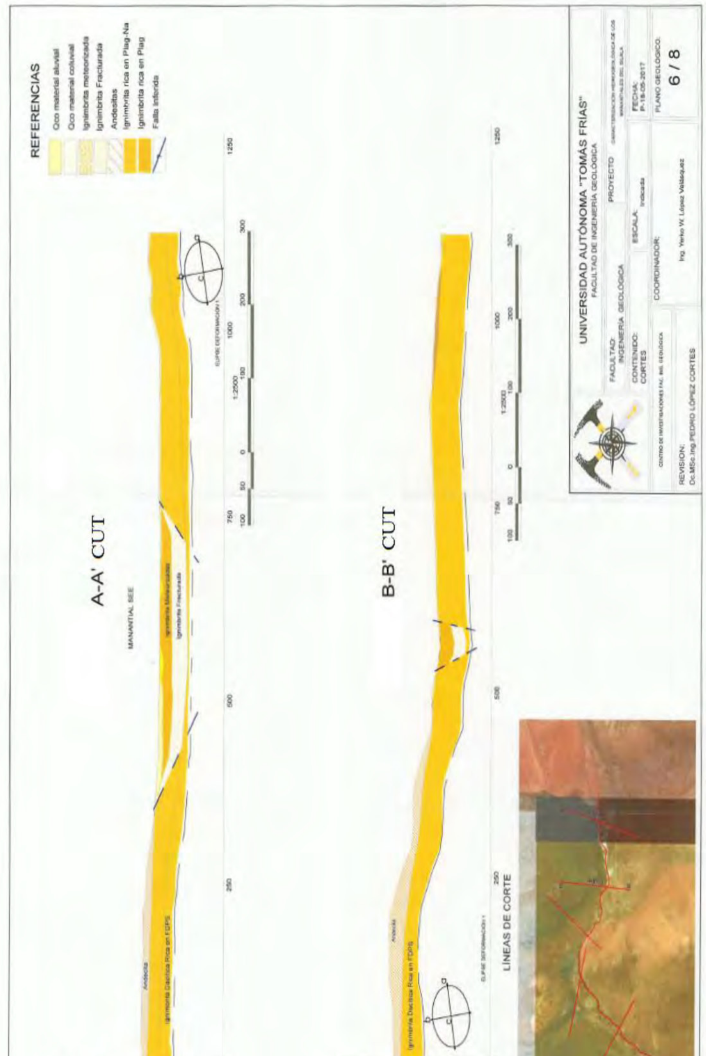
A-A' CUT
B-B' CUT
REFERENCIAS
Qco material aluvial
Qco material coluvial
Ignimbrita meteorizada
Ignimbrita Fracturada
Andesitas
Ignimbrita rica en Plag-Na
Ignimbrita rica en Plag
Falla Inferida
LÍNEAS DE CORTE
UNIVERSIDAD AUTÓNOMA "TOMÁS FRÍAS"
FACULTAD DE INGENIERIA GEOLOGICA
6 / 8

59

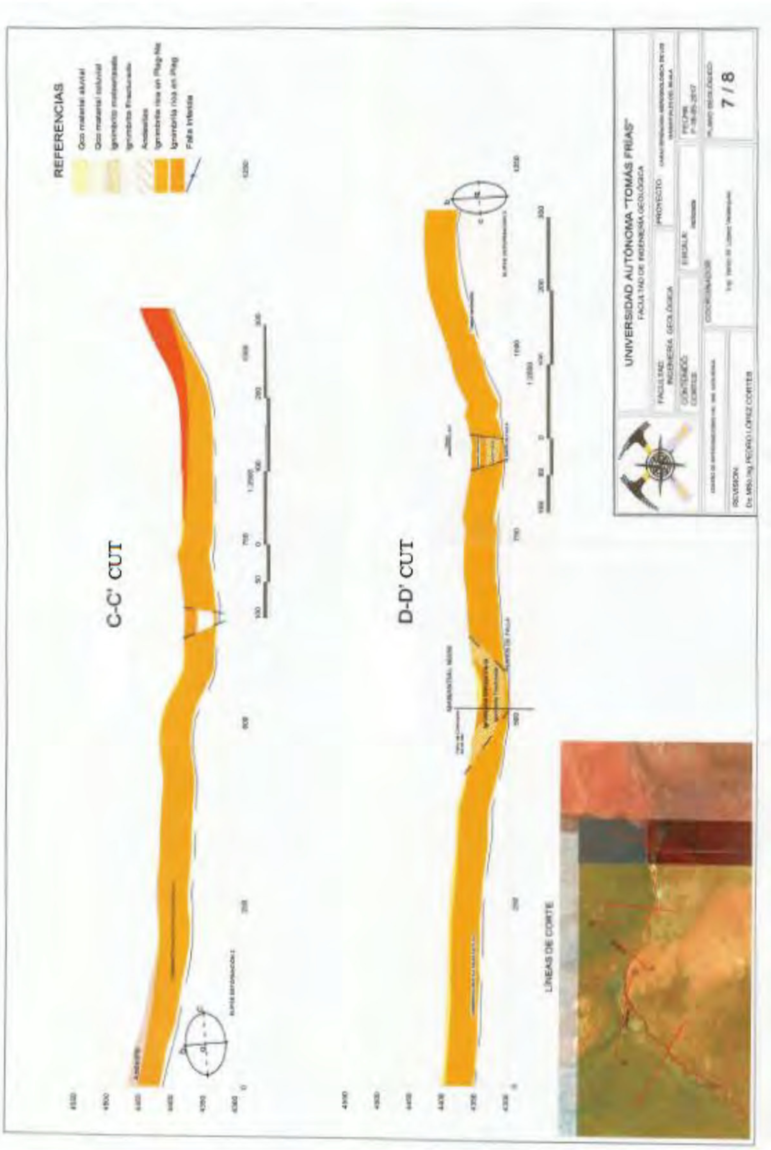

C-C' CUT
D-D' CUT
REFERENCIAS
LÍNEAS DE CORTE
UNIVERSIDAD AUTÓNOMA "TOMÁS FRÍAS"
FACULTAD DE INGENIERÍA GEOLÓGICA
7 / 8

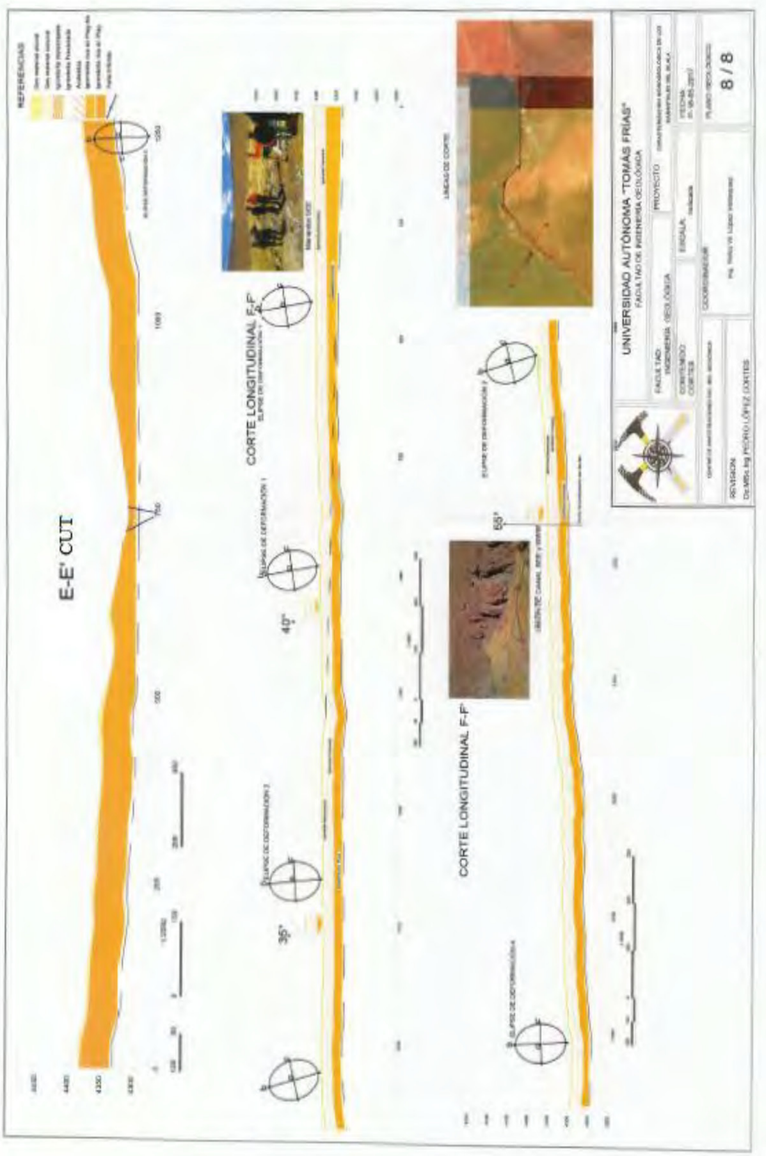
E-E' CUT
CORTE LONGITUDINAL F-F'
CORTE LONGITUDINAL F-F'
35°
40°
68°
REFERENCIAS
UNIVERSIDAD AUTÓNOMA "TOMÁS FRÍAS"
FACULTAD DE INGENIERÍA GEOLÓGICA
8 / 8

ANNEX B.

GEOPHYSICS

ANNEX B.1.

GEOPHYSICAL SURVEYS

SEE SECTOR – SILALA SPRINGS

Geophysical Line SEV-02SE

Location:

North Coordinate	East Coordinate	Height	Wing
7565802	603017	4416	300 m

CALCULATION OF APPARENT RESISTIVITY									
Silala Zone									
No. of Survey 2: SEV-02SE									
AB/2	M/N2= 1.5			MN/2= 5,0			MN/2= 25		
	RESIST. V/IΩ	FACTOR K	RESIST. AP	RESIST. V/IΩ	FACTOR K	RESIST. AP	RESIST. V/IΩ	FACTOR K	RESIST. AP
3	19	7.0686	134.80						
5	5.65	23.8238	134.60						
7	2.61	48.9566	127.78						
10	1.18	102.3638	120.79						
15	496.23	233.2638	115.75						
20	285.7	416.5238	119.00						
25	192.2	652.1438	125.34						
30	140.95	940.1238	132.51						
40	85.69	1673.164	143.37						
50	298.33	2615.644	156.45	210.77	2615.64	156.45			
60				151	1123.12	169.54			
75				101.16	1759.3	177.97			
100				60.94	3133.75	190.97			
125				41.38	4900.9	199.38	223.69	942.48	199.38
150							151.18	1374.45	207.79
175							113.02	1884.96	213.04
200							86.37	2474.01	213.68
250							55.51	3887.73	215.81
300							37.01	5615.61	207.83

Photograph B.1.1. Location of the transversal line with respect to the spring.

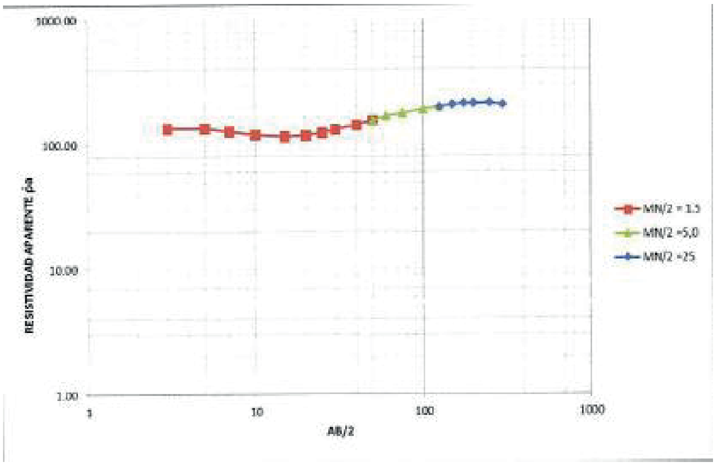

Graph B.1.1. Apparent Resistivity Values vs. AB/2

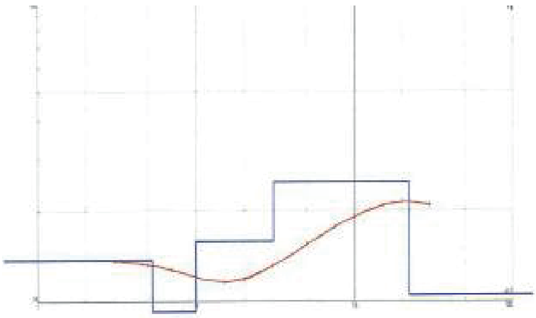

Graph B.1.2. Interpretation of Resistivity Model - Layers.

N° of LAYERS	Layer Thickness (m)	Approx. Depth (m)	Resist. Ωm	Characteristics	Lithological Description
1	5.255	-5. 255	**137.8**	The first layer with resistivity of 137.8 Ohm-m with depth of 5.255 meters corresponds to alluvial material saturated with weathered ignimbrite.	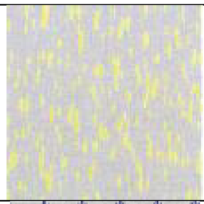
2	4.664	-9.92	**75.83**	The second layer with resistivity of 75.83 Ohm-m corresponds to welded ignimbrita.	
3	20.79	-30.71	**158.4**	The third layer has a resistivity of 158.4 Ohm-m indicating the presence of fractured medium-high ignimbrite and has a depth of -30.71 m.	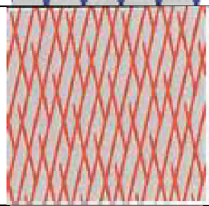
4	191.2	-70.92	**249.4**	The last layer detected is from -70.92 m, indicating the existence of fractured ignimbrite.	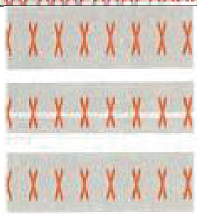

SEV-02SE analysis:

The 1st layer has a depth of 5,255 m, Resistivity of 137.8 Ohm-m indicating the presence of alluvial material saturated with weathered ignimbrite, the 2nd layer with 9.92 meters deep, thickness of 4,664 m has a resistivity of 75.83 Ohm-m corresponding to welded ignimbrite.

The 3rd layer with 30. 71 m of depth has resistance of 158.4 Ohm-m this resistivity corresponds to ignimbrite high medium saturated, which indicates the fracturing of the rock. Finally, the last layer has a resistivity of 249.4 Ohm-m with a depth of 70.92 m indicates the presence of fractured ignimbrite.

LITHOLOGICAL COLUMN OF RESISTIVITIES				
Name **SEV2_SE**	**HYDROGEOLOGICAL CHARACTERIZATION PROJECT OF THE SILALA SPRINGS**			
Coordinates			**Date**	
X 603017	Y 7565802	Z 4416.00	Meas. Pt. Elev.	
Faculty of Geological Engineering			Scale	11: xxx
Geological-Environmental Research Institute			Vertical 500.0	Horizontal 150.0

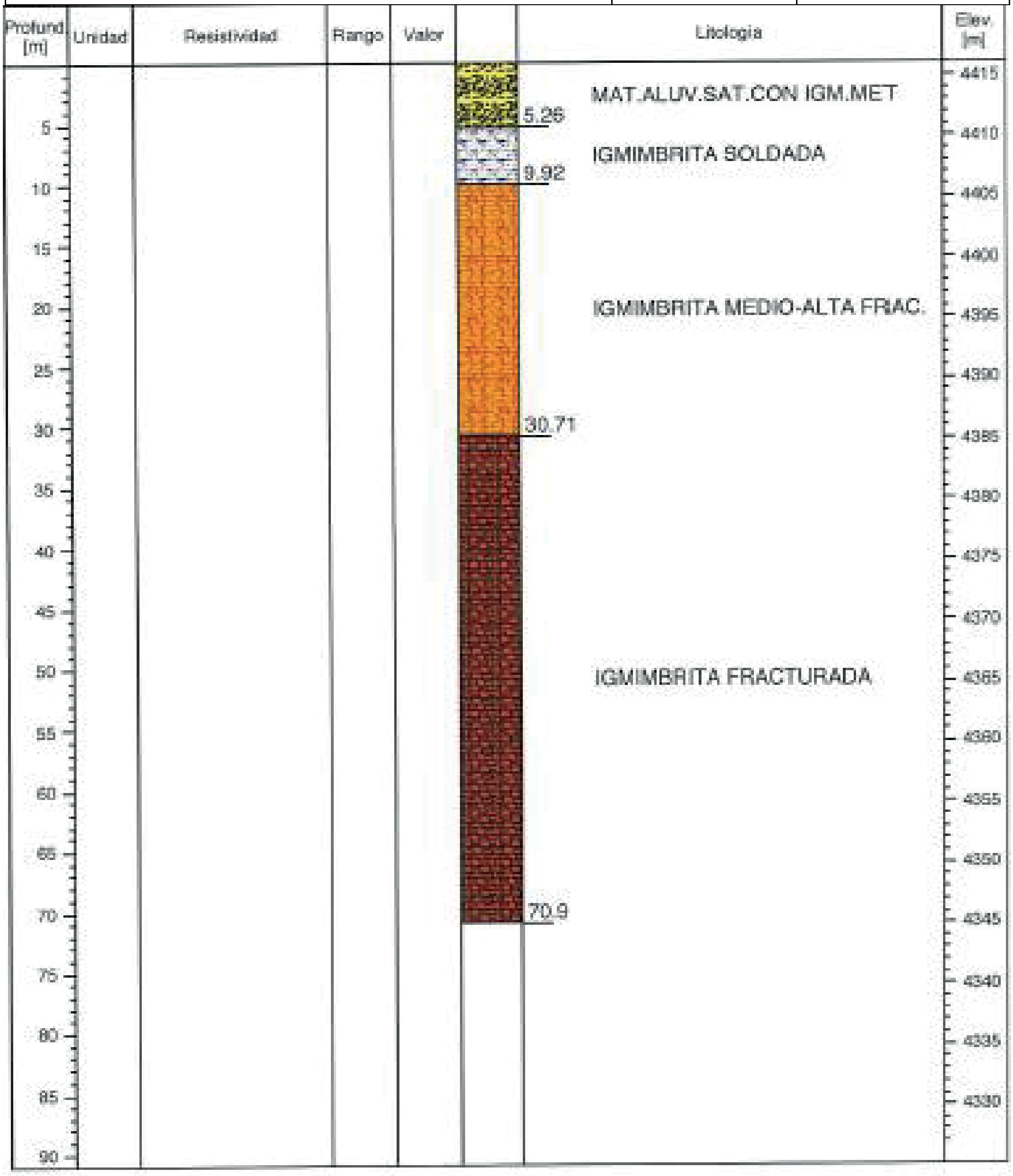

North Coordinate	East Coordinate	Height	Wing
7565913	603019	4419	300 m

CALCULATION OF APPARENT RESISTIVITY									
Silala Area									
N° of Survey 3: SEV-03SE									
AB/2	M/N2= 1.5			MN/2= 5,0			MN/2= 25		
	RESIST. V/IΩ	FACTOR K	RESIST. AP	RESIST. V/IΩ	FACTOR K	RESIST. AP	RESIST. V/IΩ	FACTOR K	RESIST. AP
3	17	7.0686	119.52						
5	4.661	23.8238	111.04						
7	2.2027	48.9566	107.84						
10	1.1527	102.3638	117.99						
15	573.54	233.2638	133.79						
20	342.73	416.5238	142.76						
25	233.32	652.1438	152.16						
30	168.63	940.1238	158.53						
40	104.77	1673.164	175.30						
50	75.122	2615.644	185.12	250.04	777.546	185.12			
60				174	1123.122	194.94			
75				109.52	1759.296	192.68			
100				54.957	3133.746	172.22			
125				33.048	4900.896	184.88	207.43	942.48	184.88
150							143.72	1374.45	197.54
175							110.24	1884.96	207.80
200							81.935	2474.01	202.71
250							49.699	3887.73	193.22
300							32.321	5615.61	181.50

Photography 8.1.2. Location of the longitudinal line with respect to the spring.

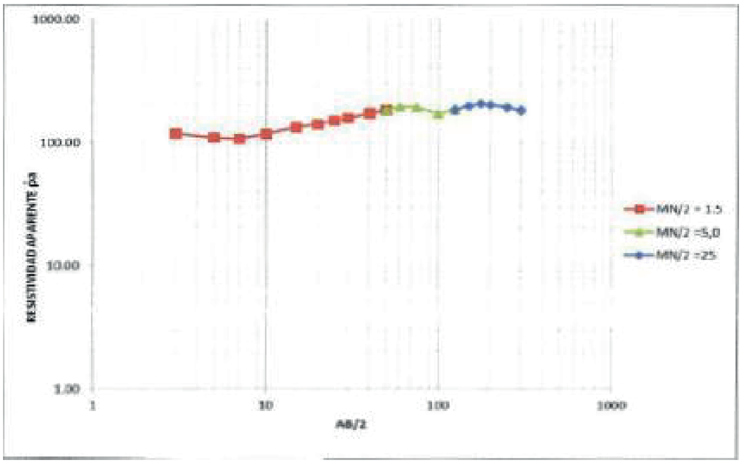

Graph 8.1.3. Apparent Resistivity Values vs. AB/2

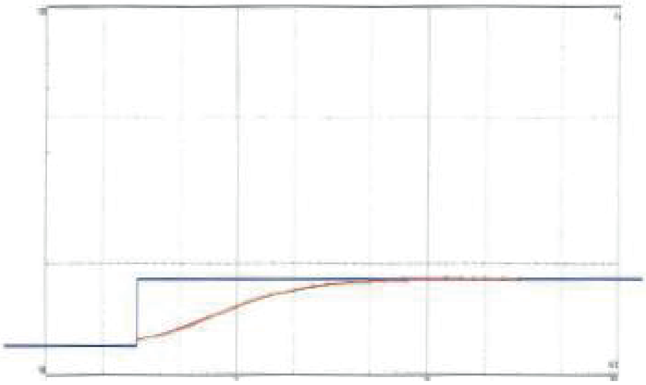

Graph 8.1.4. Interpretation of Resistivity Model - Layers.

N° LAYERS	Layer Thickness. (m)	Approx. Depth. (m)	Resist. Ωm	Characteristics	Lithological Description
1	**1.8**	**-1.8**	135.8	The first layer with a resistivity of 135.8 Ohm-m with a depth of 5,255 m corresponds to alluvial material saturated with weathered ignimbrite.	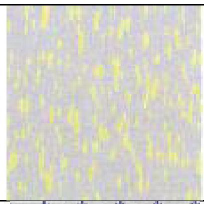
2	1.962	**-16.44**	75.27	The second layer with a resistivity of 75.27 Ohm-m corresponds to welded ignimbrite.	
3	12.68	-34.35	145.2	The third layer has a resistivity of 145.2 Ohm-m indicating the presence of medium high fractured ignimbrite and has a depth of -34.35 m.	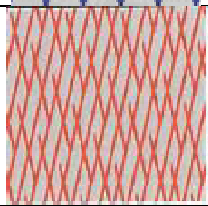
4	17.91	-71.78	368.6	The last layer detected is found from the -71.78 m, indicates the existence of fractured ignimbrite	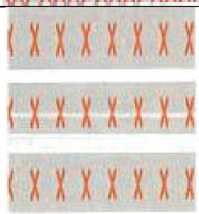

SEV-03SE Analysis:

The 1st layer with a depth of 5,255 m, has a Resistivity of 135.8 Ohm-m indicating the presence of alluvial material saturated with weathered ignimbrite, the 2nd layer has a depth of 16.44 meters, thickness of 1,962 m and resistivity of 75.27 Ohm-m corresponding to welded ignimbrite.

The 3rd layer with 34.35 m depth, the resistance is 145.2 Ohm-m this resistivity corresponds to saturated medium high ignimbrite, which indicates the fracturing of the rock. The last layer has depth of 71.78 m, thickness of 17.91 m and resistivity of 368.6 Ohm-m indicates presence of fractured ignimbrite.

LITHOLOGICAL COLUMN OF RESISTIVITIES				
Name SEV3_SE	**HYDROGEOLOGICAL CHARACTERIZATION PROJECT OF THE SILALA SPRINGS**			
Coordinates			**Date**	
X 603019	Y 7565913	Z 4419.00	Meas. Pt. Elev.	
Faculty of Geological Engineering			Scale	11: xxx
Geological-Environmental Research Institute			Vertical 400.0	Horizontal 100.0

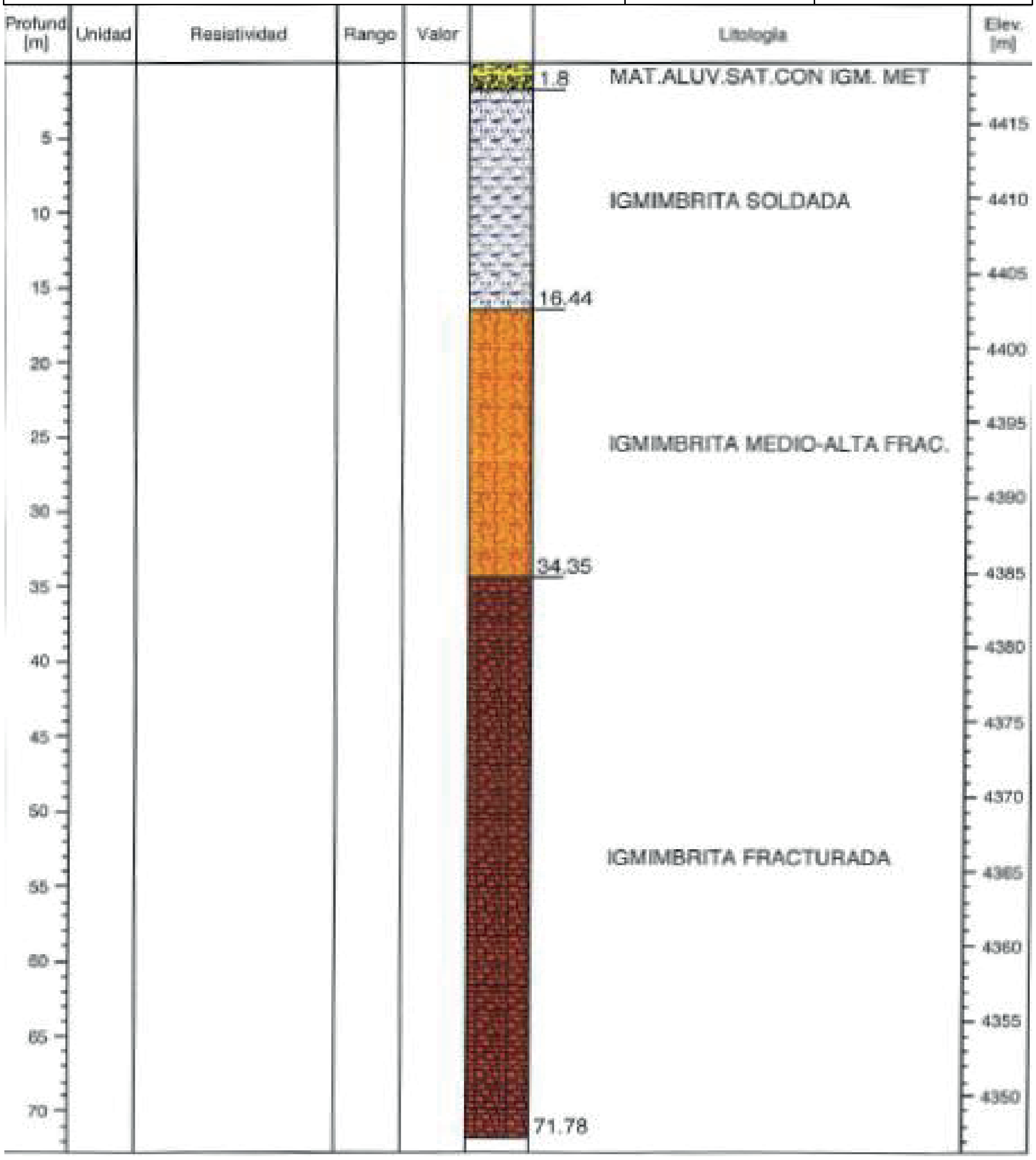

Geophysical Line SEV-04SE

Location:

North Coordinate	East Coordinate	Height	Wing
7565866	603138	4417	200 m

CALCULATION OF APPARENT RESISTIVITY									
Silala Area									
No. of Survey 4: SEV-04SE									
AB/2	**M/N2= 1.5**			**MN/2= 5,0**			**MN/2= 25**		
	RESIST. V/IΩ	FACTOR K	RESIST. AP	RESIST. V/IΩ	FACTOR K	RESIST. AP	RESIST. V/IΩ	FACTOR K	RESIST. AP
3	25	7.0686	176.95						
5	6.2189	23.8238	148.16						
7	2.5414	48.9566	124.42						
10	1.1576	102.3638	118.50						
15	519.92	233.2638	121.28						
20	294.53	416.5238	122.68						
25	196.81	652.1438	128.35						
30	149.72	940.1238	140.76						
40	94.981	1673.164	158.92						
50	67.96	2615.644	165.57	211.58	777.549	165.57			
60				153	1123.122	172.22			
75				97.202	1759.296	171.01			
100				54.579	3133.746	171.04			
125				31.29	4900.896	174.00	196.33	942.48	174.00
150							128.75	1374.45	176.96
175							102.69	1884.96	193.57
200							75.816	2474.01	187.57

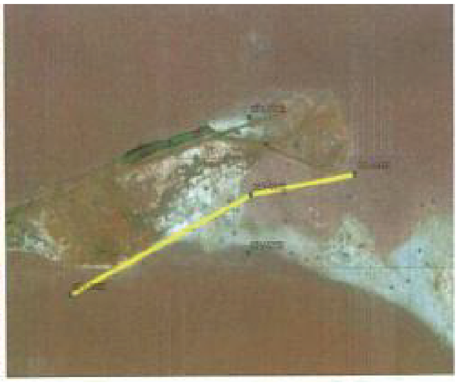

Photograph B.1.3. Location of the longitudinal line with respect to the spring.

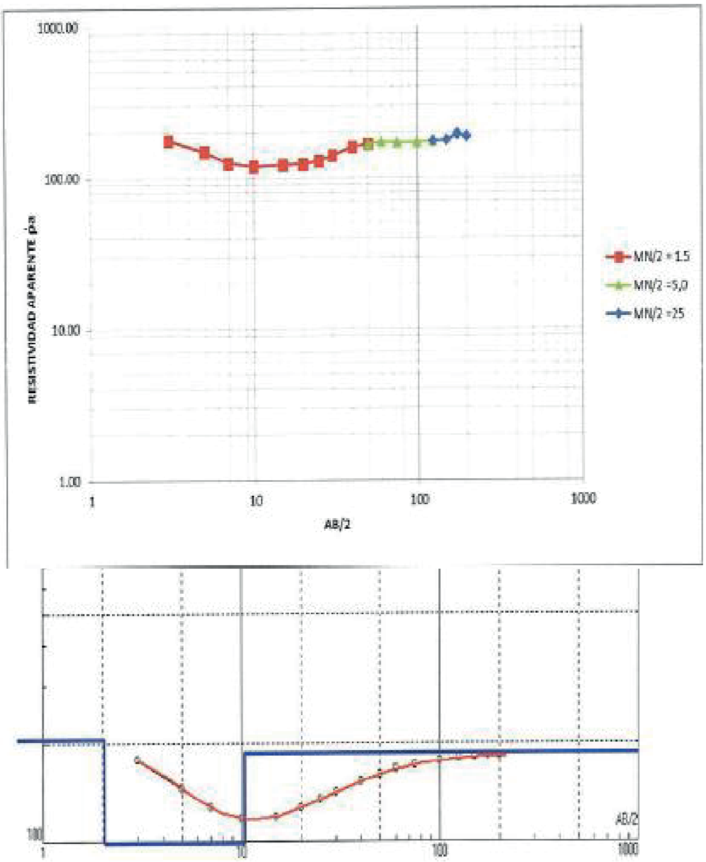

Graph B.1.6. Interpretation of Resistivity Model - Layers.

N° LAYERS	Layer Thickness. (m)	Approx. Depth. (m)	Resist. Ωm	Characteristics	Lithological Description
1	2.697	-2.697	**203.3**	The first layer with a resistivity of 203.3 Ohm-m with a depth of -2697 m corresponds to alluvial material saturated with a medium-high fractured ignimbrite mixture.	
2	1.628	-4.324	**37.88**	The second layer with resistivity of 37.88 ohm corresponds to welded ignimbrite.	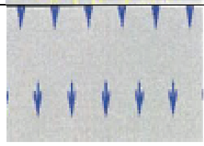
3	39.55	-43.88	**206.1**	The third layer has a resistivity of 206.1 Ohm-m indicating the presence of fractured ignimbrite and starts at a depth of -43.88 m.	

SEV-04SE Analysis:

The 1st layer with a depth of 2,697 m, has a resistivity of 202.2 Ohm-m indicating the presence of saturated alluvial material with a mixture of medium-high fractured ignimbrite, the 2nd layer with a depth of 4,324 m and a thickness of 1,628 m has a resistivity of 37.88 Ohm-m corresponding to welded material.

The 3rd layer with 43.88 m deep, 39.55 m thick resistance of 206.1 Ohm-m resistivity responding to fractured ignimbrite, which indicates rock fracturing.

LITHOLOGICAL COLUMN OF RESISTIVITIES				
Name **SEV4_SE**	**HYDROGEOLOGICAL CHARACTERIZATION PROJECT OF THE SILALA SPRINGS**			
Coordinates			**Date**	
X 603138	Y 7565866	Z 4417.00	Meas. Pt. Elev.	
Faculty of Geological Engineering			Scale 11: xxx	
Geological-Environmental Research Institute			Vertical 300.0	Horizontal 100.0

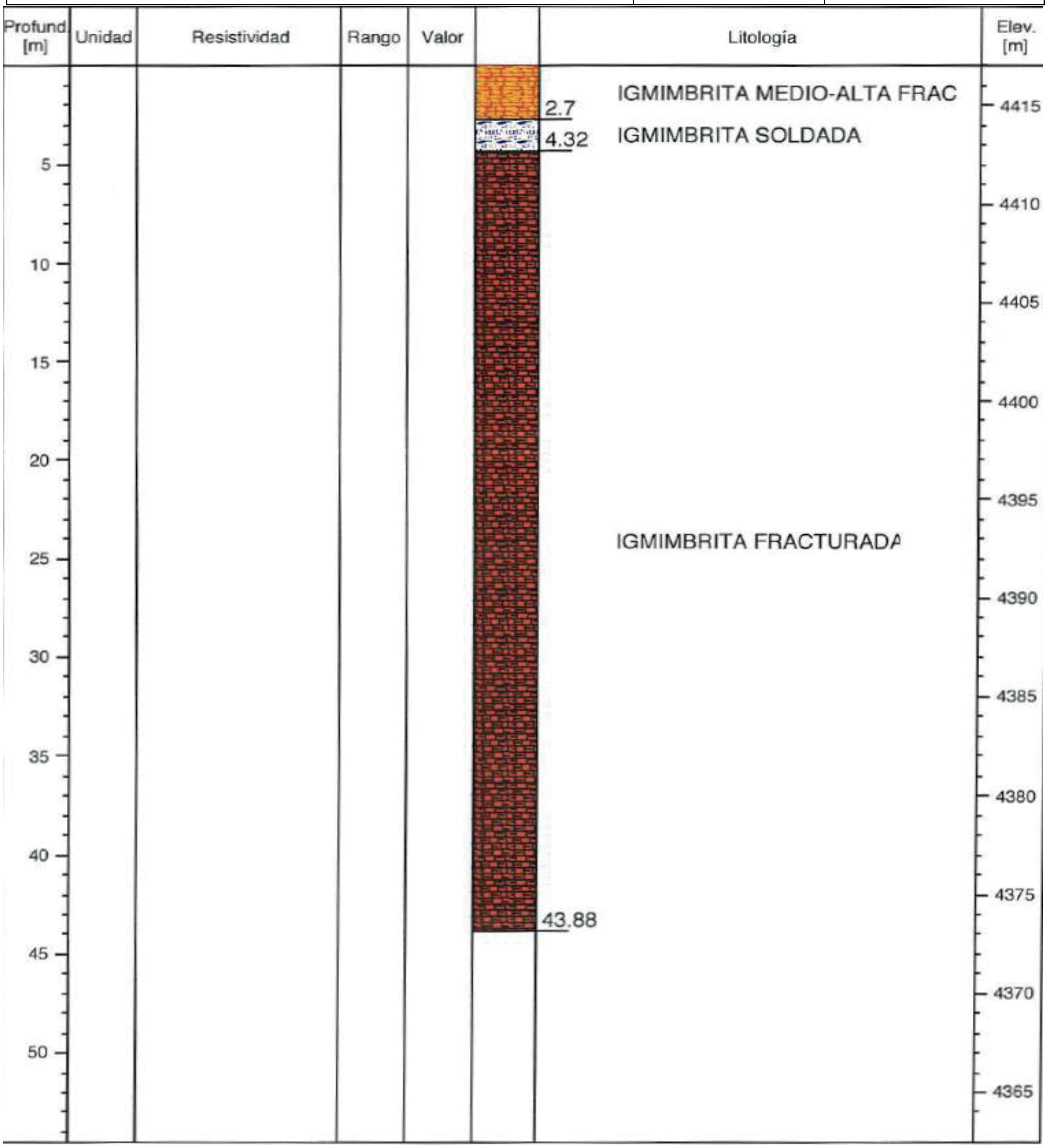

Geophysical Line SEV-05SE

Location:

North Coordinate	East Coordinate	Height	Wing
7565850	603020	4415	200 m

CALCULATION OF APPARENT RESISTIVITY									
Silala Area									
No. of Survey 5: SEV-05SE									
AB/2	**M/N2= 1.5**			**MN/2= 5,0**			**MN/2= 25**		
	RESIST. V/IΩ	FACTOR K	RESIST. AP	RESIST. V/IΩ	FACTOR K	RESIST. AP	RESIST. V/IΩ	FACTOR K	RESIST. AP
3	19	7.0686	134.34						
5	4.8079	23.8238	114.54						
7	2.3482	48.9566	114.96						
10	1.1169	102.364	114.33						
15	530.17	233.264	123.67						
20	320.4	416.524	133.45						
25	218.6	652.144	142.56						
30	162.27	940.124	152.55						
40	95.884	1673.16	160.43						
50	68.746	2615.64	146.55	240.16	777.546	146.55			
60				170	1123.12	190.76			
75				105.56	1759.3	185.71			
100				62.885	3133.75	197.07			
125				44.551	4900.9	199.38	244.92	942.48	199.38
150							167.84	1374.45	230.69
175							129.49	1884.96	244.08
200							97.735	2474.01	241.80

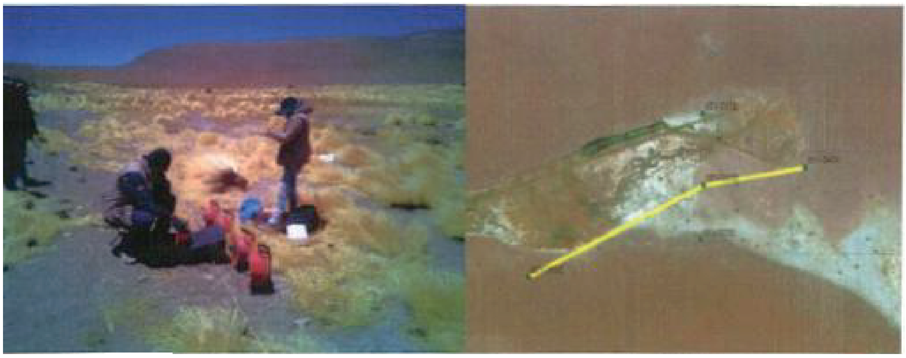

Location of the longitudinal line with respect to the spring.

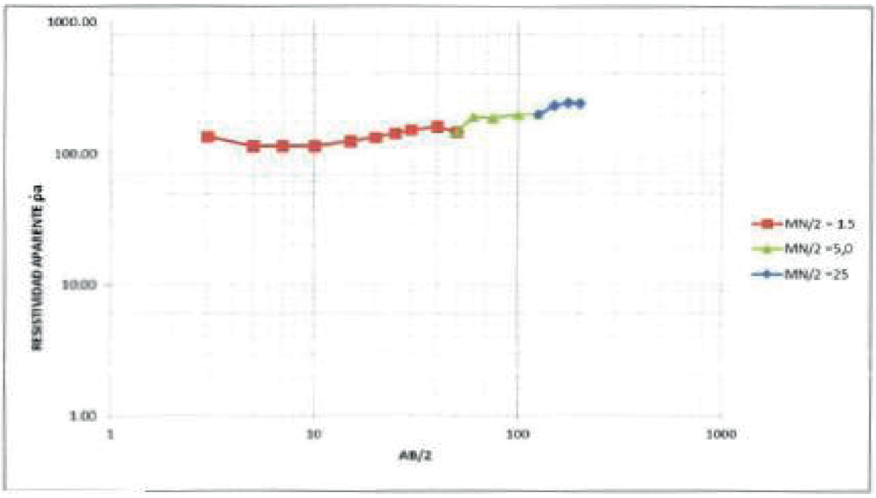

Graph. 8.1. 7. Apparent Resistivity Values vs. AB/2

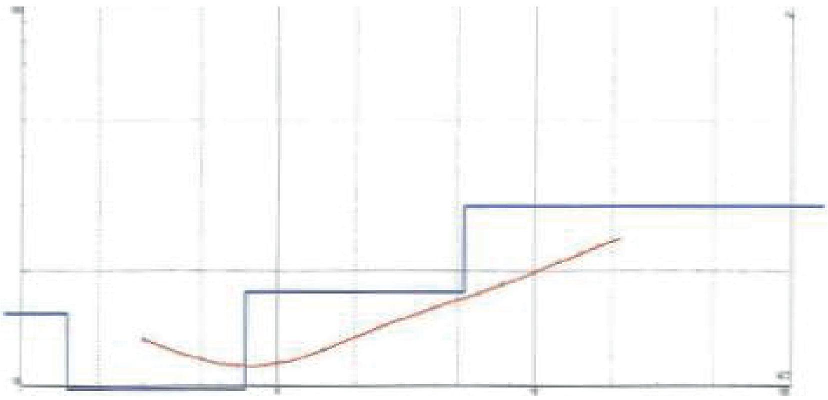

Graph B.1.8. Interpretation of Resistivity Model - Layers.

N° LAYERS	Layer Thickness. (m)	Approx. Depth. (m)	Resist. Ωm	Characteristics	Lithological Description
1	1.5	-1.5	**155.3**	The first layer with a resistivity of 155.3 ohm and a depth of -1.5 m corresponds to alluvial material saturated with a medium-high fractured ignimbrite mixture.	
2	5.944	-7.444	**98.17**	The second layer with resistivity of 98.17 Ohm-m corresponds to welded ignimbrita with thickness of 5.944	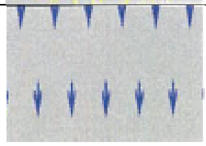
3	45.55	-52.99	**176.4**	The last layer has a resistivity of 176.4 Ohm-m indicating the presence of fractured ignimbrite and starts at a depth of -52.99 m.	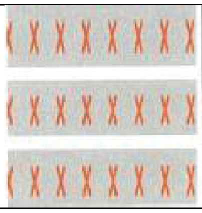

SEV-05SE Analysis:

The 1st layer has a depth of 1.5 m, with resistivity of 155.3 Ohm-m indicates the presence of saturated alluvial material with a mixture of fractured medium-high ignimbrite, the 2nd layer has a depth of 4,324 meters thick of 1,628 m with resistivity of 37.88 Ohm corresponding to welded ignimbrite.

The 3rd with a depth of 43.88 m thickness of 45.55 m and resistivity of 206.1 Ohm-m responds to fractured ignimbrite, which indicates the fracturing of the rock.

LITHOLOGICAL COLUMN OF RESISTIVITIES				
Name **SEV5_SE**	**HYDROGEOLOGICAL CHARACTERIZATION PROJECT OF THE SILALA SPRINGS**			
Coordinates			**Date**	
X 603020	Y 7565850	Z 4415.00	Meas. Pt. Elev.	
Faculty of Geological Engineering			Scale	11: xxx
Geological-Environmental Research Institute			Vertical 350.0	Horizontal 50.0

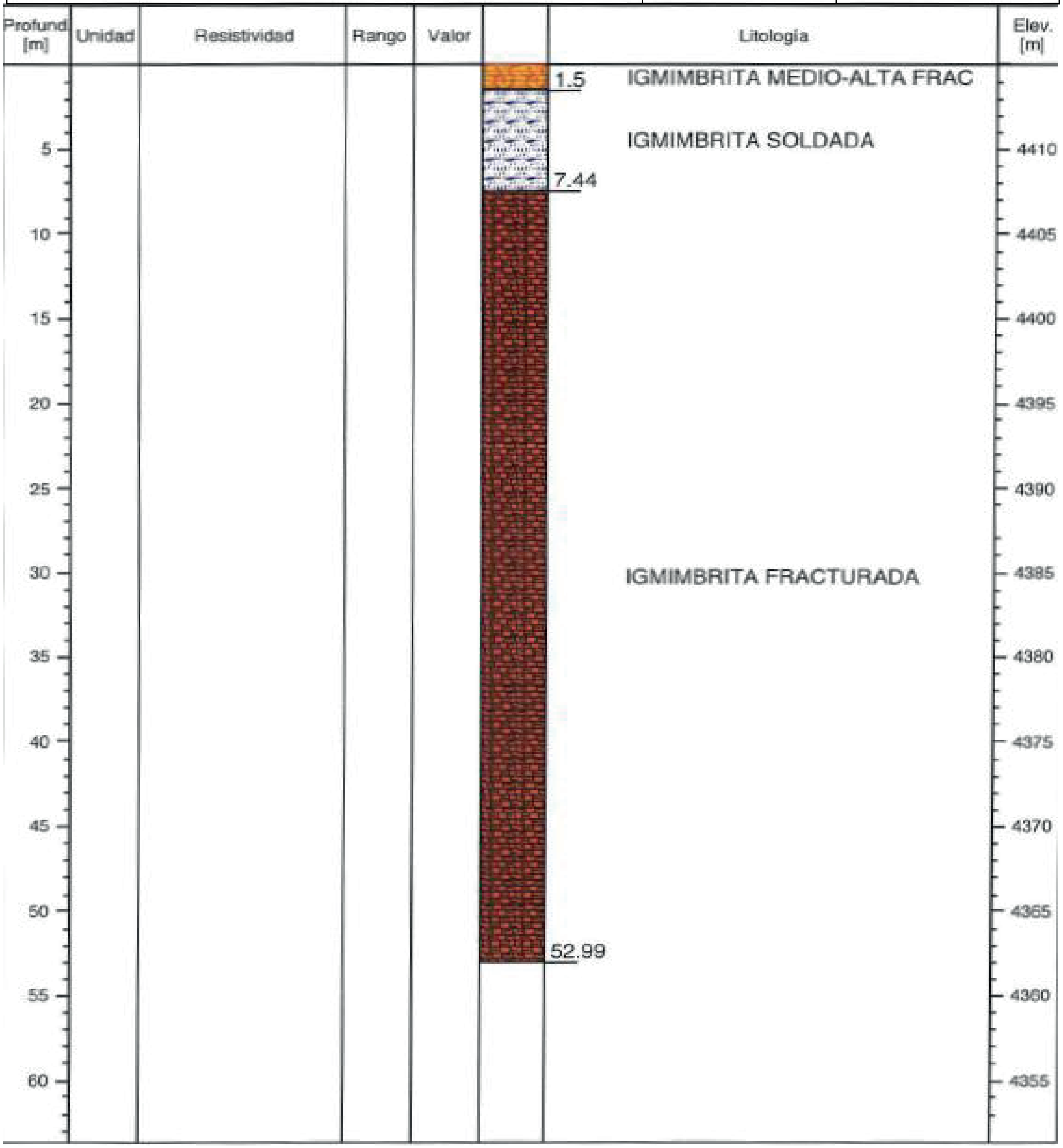

Geophysical Line SEV-06SE

Location:

North Coordinate	East Coordinate	Height	Wing
7565769	602815	4414	150 m

CALCULATION OF APPARENT RESISTIVITY									
Silala Zone									
No. of Survey 6: SEV-06SE									
AB/2	**M/N2= 1.5**			**MN/2= 5,0**			**MN/2= 25**		
	RESIST. V/IΩ	FACTOR K	RESIST. AP	RESIST. V/IΩ	FACTOR K	RESIST. AP	RESIST. V/IΩ	FACTOR K	RESIST. AP
3	24	7.0686	171.05						
5	5.97	23.8238	142.23						
7	2.4681	48.9566	120.83						
10	365.05	102.3638	37.37						
15	255.54	233.2638	59.61						
20	161.92	416.5238	67.44						
25	163.53	652.1438	106.65						
30	102.18	940.1238	96.06						
40	65.535	1673.164	109.65						
50	46.072	2615.644	118.73	171.85	2615.644	118.73			
60				114	1123.122	127.81			
75				73.082	1759.296	128.57			
100				45.266	3133.746	141.85			
125				30.815	4900.896	145.39	166.06	942.48	145.39
150							108.36	1374.45	148.94

Photograph B.1.5. Location of the longitudinal line with respect to the spring.

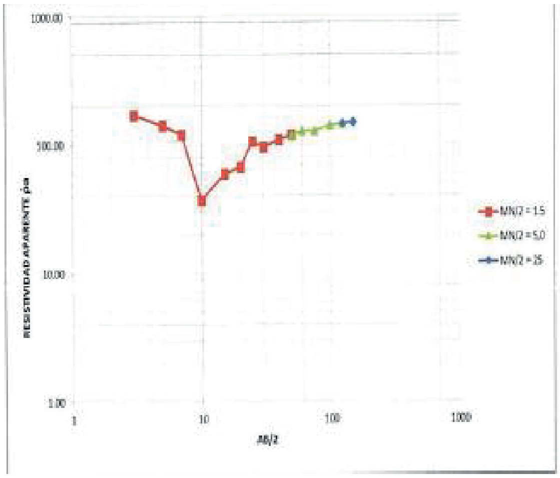

Graph B.1.9. Apparent Resistivity Values vs. AB / 2

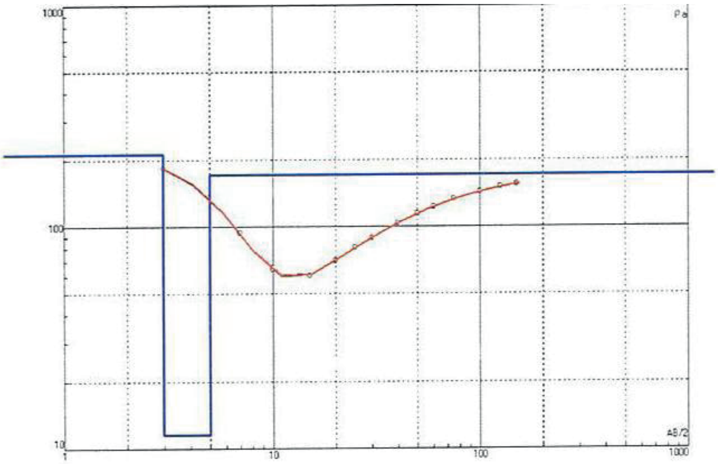

Graph B.1.1 O. Interpretation of Resistivity Model - Layers.

N° LAYERS	Layer Thickness. (m)	Approx. Depth. (m)	Resist. Ωm	Characteristics	Lithological Description
1	3.174	-3.174	**207.3**	The first layer with a resistivity of 207.3 Ohm-m with a depth of -3.174 m corresponds to alluvial material saturated with a medium-high fractured ignimbrite mixture.	
2	3.301	-3.31	**13.22**	The second layer with a resistivity of 13.22 Ohm-m corresponds to welded ignimbrite with a thickness of 3.301.	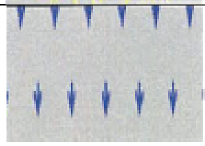
3	35.44	-35.43	**604.2**	The last layer has a resistivity of 604.2 Ohm-m that indicates the presence of fractured ignimbrite and starts at a depth of 35.43 m.	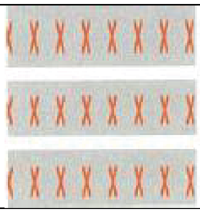

SEV-06SE Analysis:

The 1st with depth of 3.174 m, has resistivity of 207.3 Ohm-m indicates presence of saturated alluvial material with mixture of ignimbrite medium high fractured, the 2nd layer has 3.31 meters deep thickness of 3.301 m and resistivity of 13.22 Ohm responds to welded material.

The last layer with 35.43 m depth and resistivity of 604.2 Ohm-m belongs to fractured ignimbrite that indicates the fracturing of the rock.

LITHOLOGICAL COLUMN OF RESISTIVITIES				
Name SEV6_SE	**HYDROGEOLOGICAL CHARACTERIZATION PROJECT OF THE SILALA SPRINGS**			
Coordinates			**Date**	
X 602815	Y 7565769	Z 4414.00	Meas. Pt. Elev.	
Faculty of Geological Engineering			Scale	11: xxx
Geological-Environmental Research Institute			Vertical 300.0	Horizontal 50.0

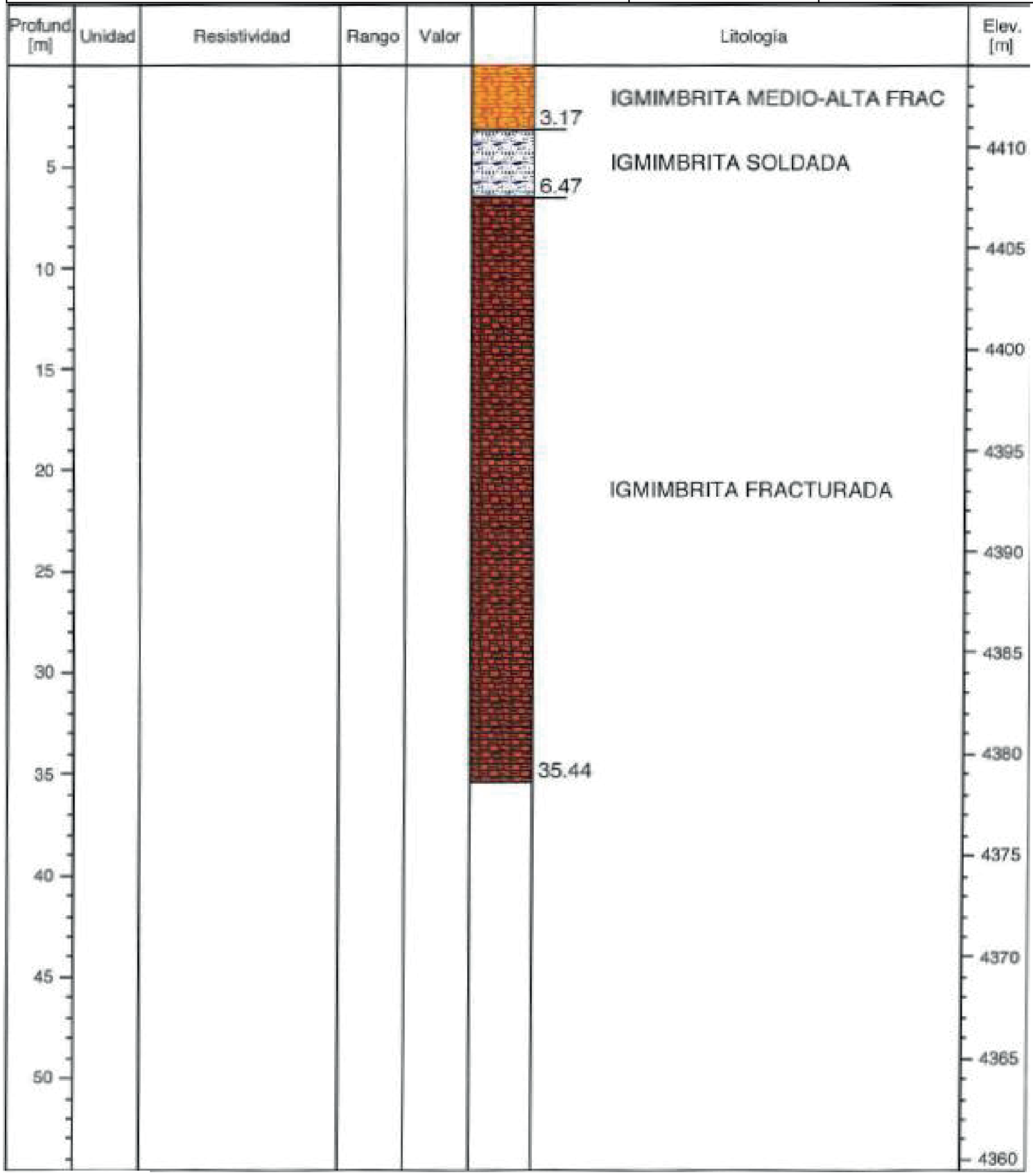

ANNEX B.2.

GEOPHYSICAL SURVEYS

NWW SECTOR - SILALA SPRINGS

Geophysical Line SEV-02NE

Location:

North Coordinate	East Coordinate	Height	Wing
7566387	601165	4392	300 m

CALCULATION OF APPARENT RESISTIVITY									
Silala Zone									
No. of Survey 2: SEV-02NE									
	M/N2= 1.5			**MN/2= 5,0**			**MN/2= 25**		
AB/2	RESIST. V/IΩ	FACTOR K	RESIST. AP	RESIST. V/IΩ	FACTOR K	RESIST. AP	RESIST. V/IΩ	FACTOR K	RESIST. AP
3	470	7.0686	3323.16						
5	134.01	23.8238	3192.63						
7	59.018	48.9566	2889.32						
10	23.157	102.3638	2370.44						
15	7.5104	233.2638	1751.90						
20	3.37	416.5238	1403.69						
25	1.7533	652.1438	1211.56	6.4623	188.496	1211.56			
30				4	274.89	1019.43			
40				1.446	494.802	715.48			
50				757.81	777.546	589.23			
60				420.73	1123.122	472.53			
75				250.08	1759.296	439.96			
100				154.14	3133.746	483.04			
125				86.14	4900.896	427.41	397.69	942.48	427.41
150							270.5	1374.45	371.79
175							217.2	1884.96	409.41
200							167.71	2474.01	414.92
250							104.63	3887.73	406.77
300							83.75	5615.61	470.31

Photograph B.2.1. Location of the longitudinal line with respect to the spring.

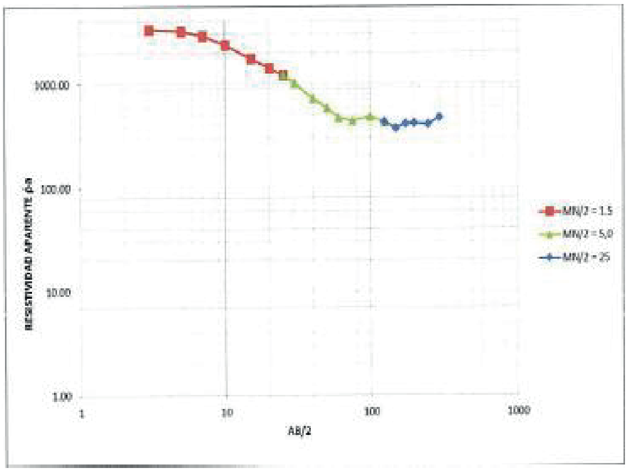

Graph 8.2.1. Apparent Resistivity Values vs. AB/2

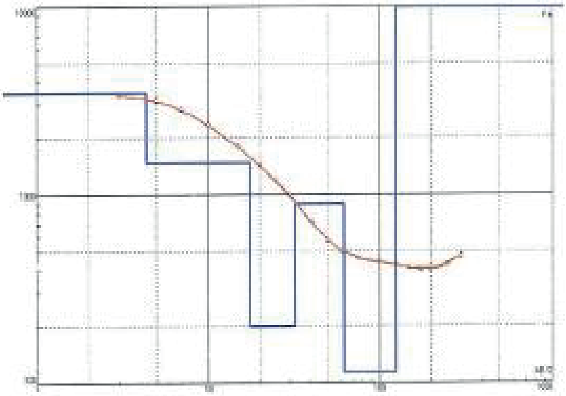

Graph B.2.2. Interpretation of Resistivity Model - Layers.

N° LAYERS	Layer Thickness. (m)	Approx. Depth. (m)	Resist. Ωm	Characteristics	Lithological Description
1	14.39	-20.76	**200.4**	The first layer with a resistivity of 200.4 Ohm-m with a depth of -20.76 m corresponds to alluvial material saturated with clay sediments and weathered ignimbrite.	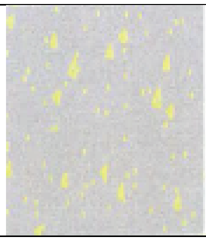
2	30.48	-62.55	**901**	The second layer with resistivity of 901 Ohm-m corresponds to fractured ignimbrite with thickness of 16.04 and starts from -62.55 m.	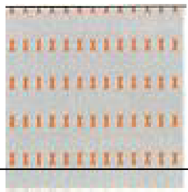

SEV-02NE Analysis:

The 1st layer with resistivity of 200.4 Ohm-m and a depth of 20.76 m indicates the presence of alluvial material saturated with clay sediments and weathered ignimbrites.

The last layer with 62.55 m depth and resistivity of 901 Ohm-m responds to fractured ignimbrite.

LITHOLOGICAL COLUMN OF RESISTIVITIES				
Name **SEV2_NE**	**HYDROGEOLOGICAL CHARACTERIZATION PROJECT OF THE SILALA SPRINGS**			
Coordinates			**Date**	
X 601165	Y 7566387	Z 4392.00	Meas. Pt. Elev.	
Faculty of Geological Engineering			Scale	11: xxx
Geological-Environmental Research Institute			Vertical 500.0	Horizontal 100.0

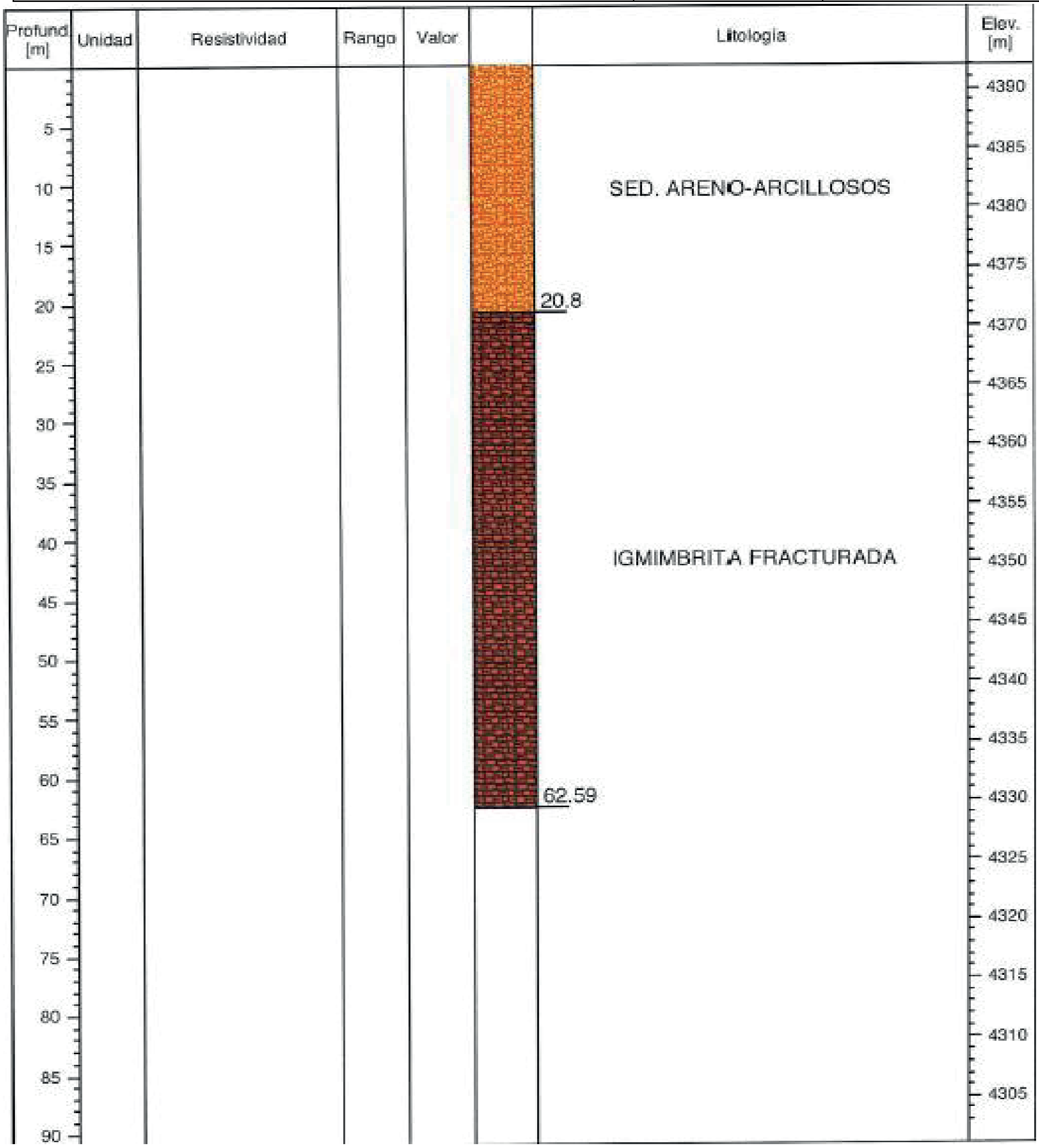

Geophysical Line SEV-03NE

Location:

North Coordinate	East Coordinate	Height	Wing
7566500	601168	4401	125 m

CALCULATION OF APPARENT RESISTIVITY						
Silala Zone						
No. of Survey 3: SEV-03NE						
AB/2	**M/N2= 1.5**			**MN/2= 5,0**		
	RESIST. V/IΩ	FACTOR K	RESIST. AP	RESIST. V/IΩ	FACTOR K	RESIST. AP
3	246	7.0686	1739.16			
5	5.977	23.8238	142.39			
7	35.619	48.9566	1743.79			
10	16.156	102.364	1653.79			
15	6.1773	233.264	1440.94			
20	2.8114	416.524	1171.02			
25	1.4821	652.144	1039.75	5.976	188.496	1039.75
30				3	274.89	908.48
40				1.2962	494.802	641.36
50				681.95	777.546	530.25
60				258.3	1123.122	290.10
75				145.95	1,759.30	525.46
100				44.663	3133.746	139.96
125				26.176	4900.896	128.29

Photograph 8.2.2. Location of the longitudinal line with respect to the spring.

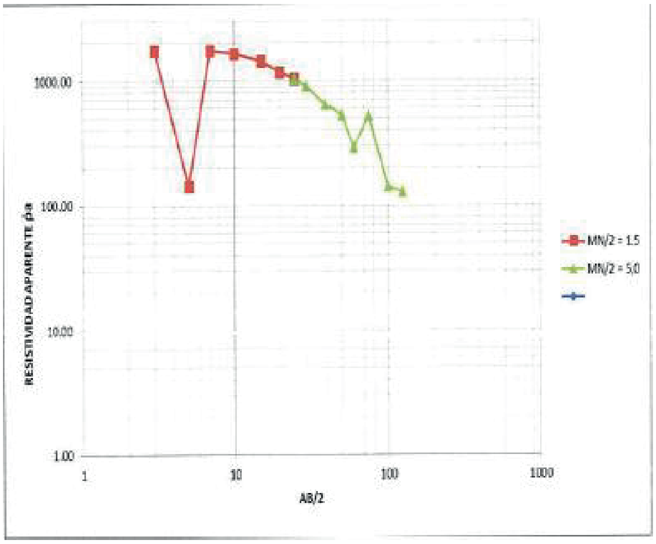

Figure 8.2.3. Apparent Resistivity Values vs. A8 / 2

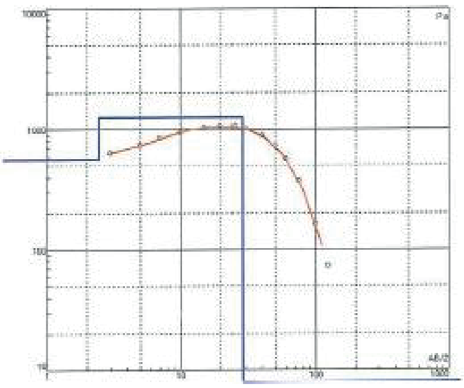

Graph B.2.4. Interpretation of Resistivity Model - Layers.

N° LAYERS	Layer Thickness. (m)	Approx. Depth. (m)	Resist. Ωm	Characteristics	Lithological Description
1	15.87	-22.7	**1167**	The first layer with a resistivity of 1167 Ohm-m with a depth of -22.7 m corresponds to alluvial material saturated with clay sediments and weathered ignimbrite.	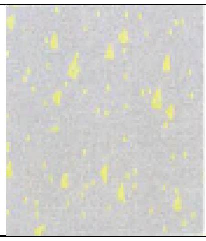
2	23.89	-46.59	**31.23**	The second layer with resistivity of 31.23 Ohm-m corresponds to fractured ignimbrite with thickness of 23.89 and starts from -46.59 m.	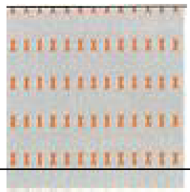

SEV-03NE Analysis:

The 1st layer with resistivity of 1167 Ohm-m and depth of 22. 7 m indicates the presence of alluvial material saturated with clay sediments and weathered ignimbrite.

The last layer with 46.59 m depth and resistivity of 31.23 Ohm-m responds to fractured ignimbrite.

LITHOLOGICAL COLUMN OF RESISTIVITIES				
Name SEV3_NE	**HYDROGEOLOGICAL CHARACTERIZATION PROJECT OF THE SILALA SPRINGS**			
Coordinates			**Date**	
X 601168	Y 7566500	Z 4401.00	Meas. Pt. Elev.	
Faculty of Geological Engineering			Scale	11: xxx
Geological-Environmental Research Institute			Vertical 300.0	Horizontal 80.0

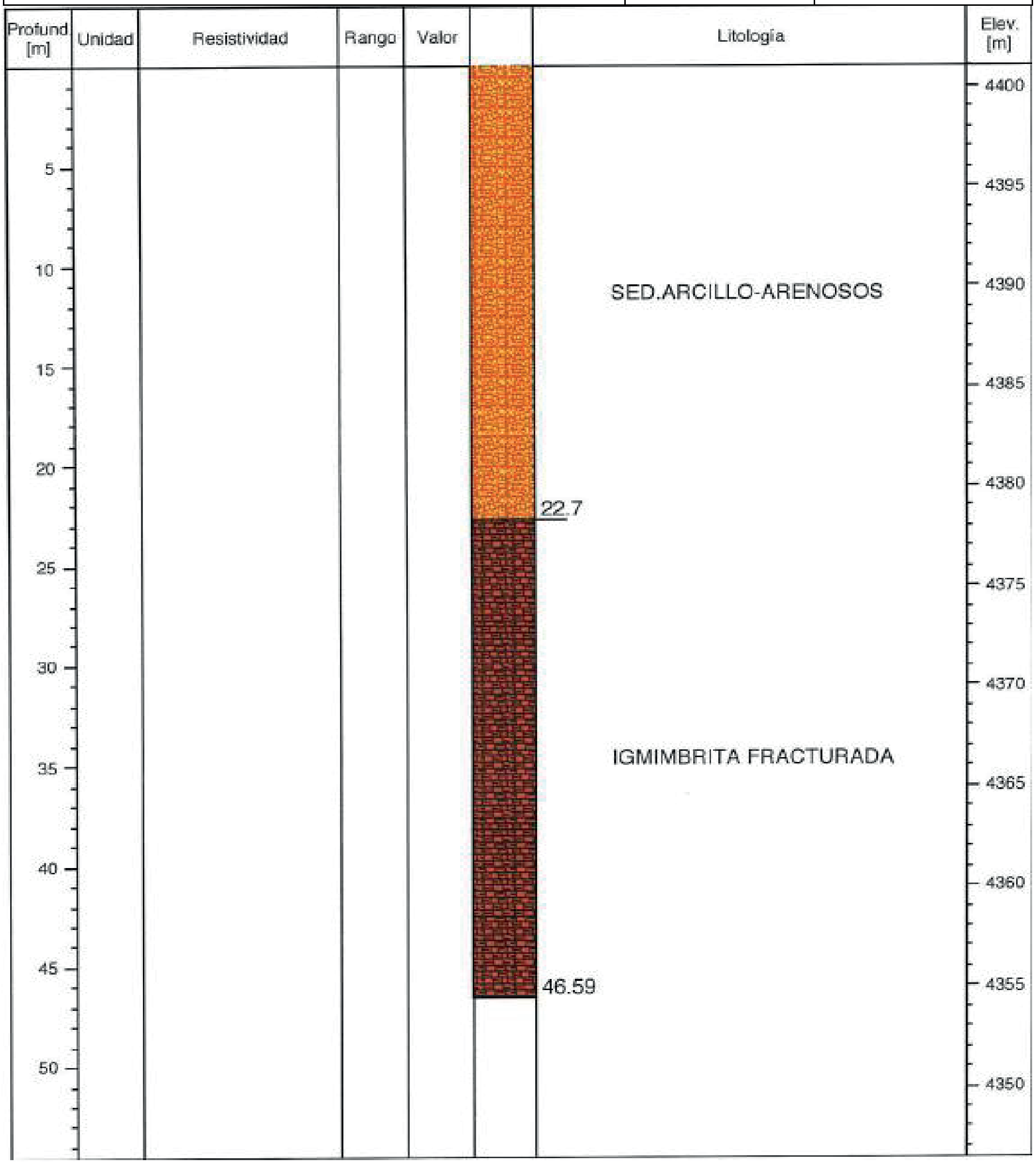

Geophysical Line SEV-04NE

Location:

North Coordinate	East Coordinate	Height	Wing
7566370	601020	4383	300 m

CALCULATION OF APPARENT RESISTIVITY									
Silala Zone									
No. of Survey 4: SEV-04NE									
AB/2	M/N2= 1.5			MN/2= 5,0			MN/2= 25		
	RESIST. V/IΩ	FACTOR K	RESIST. AP	RESIST. V/IΩ	FACTOR K	RESIST. AP	RESIST. V/IΩ	FACTOR K	RESIST. AP
3	43	7.0686	305.99						
5	12.072	23.8238	287.60						
7	6.4835	48.9566	317.41						
10	3.3325	102.364	341.13						
15	1.5365	233.264	358.41						
20	857.88	416.524	357.33						
25	557.45	652.144	374.92	2.113	188.496	374.92			
30				1	274.89	392.52			
40				802.35	494.802	397.00			
50				499.57	777.546	388.44			
60				352.93	1123.12	396.38			
75				191.95	1759.3	337.70			
100				108.7	3133.75	340.64			
125				81.807	4900.9	324.22	356.87	942.48	324.22
150							223.94	1374.45	307.79
175							163	1884.96	307.25
200							131.24	8474.01	324.69
250							89.775	3887.73	348.94
300							73.135	5615.61	410.70

Photograph 8.2.3. Location of the longitudinal line with respect to the spring.

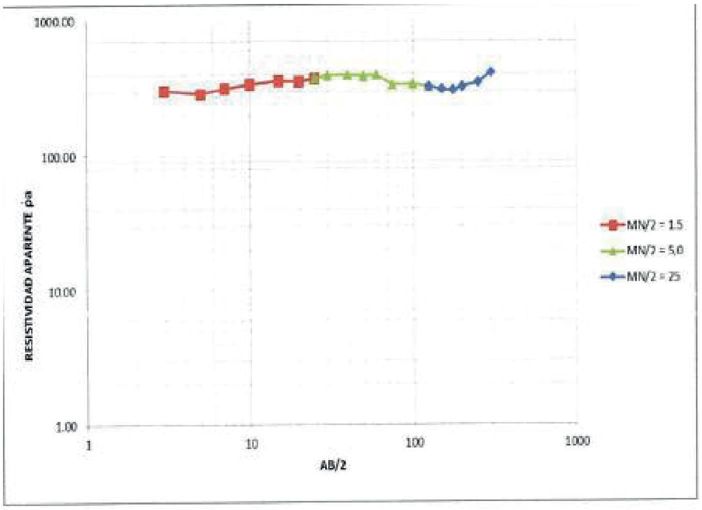

Graph 8.2.5. Apparent Resistivity Values vs. AB/2

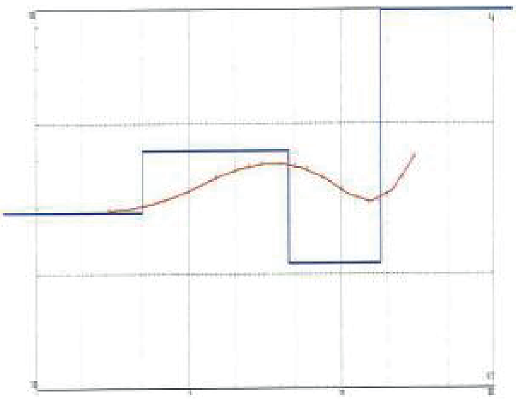

Graph 8.2.6. Interpretation of Resistivity Model - Layers.

N° LAYERS	Layer Thickness. (m)	Approx. Depth. (m)	Resist. Ωm	Characteristics	Lithological Description
1	4.044	-4.044	**257.4**	The first layer with a resistivity of 257.4 Ohm-m with a depth of -4.044 m corresponds to alluvial material saturated with sandy sediments.	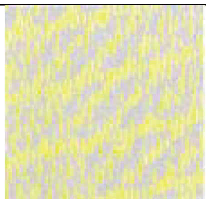
2	41.65	-45.69	**429.6**	The second layer with resistivity of 429.6 Ohm-m corresponds to sand-clay sediments with a thickness of 41.65 m.	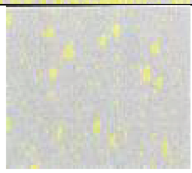
3	123.5	-69.3	**200.8**	The last layer has a resistivity of 200.8 Ohm-m indicating the presence of fractured ignimbrite and starts at a depth of -35.43 m.	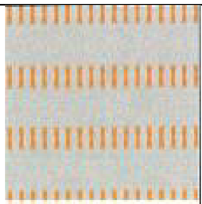

SEV-04NE Analysis:

The 1st layer with a depth of 4,044 m and resistivity of 257.4 Ohm-m indicates the presence of alluvial material saturated with sandy sediments. The 2nd layer with a depth of 45.69 m, thickness of 41.65 m and resistivity of 429.6 Ohm-m corresponding to sand-clay sediments.

The 3rd layer with 69.3 m depth and resistance of 200.8 Ohm-m responds to fractured ignimbrite, which indicates rock fracturing.

LITHOLOGICAL COLUMN OF RESISTIVITIES				
Name SEV4_NE	**HYDROGEOLOGICAL CHARACTERIZATION PROJECT OF THE SILALA SPRINGS**			
Coordinates			**Date**	
X 601020	Y 7566370	Z 4383.00	Meas. Pt. Elev.	
Faculty of Geological Engineering			Scale	11: xxx
Geological-Environmental Research Institute			Vertical 500.0	Horizontal 100.0

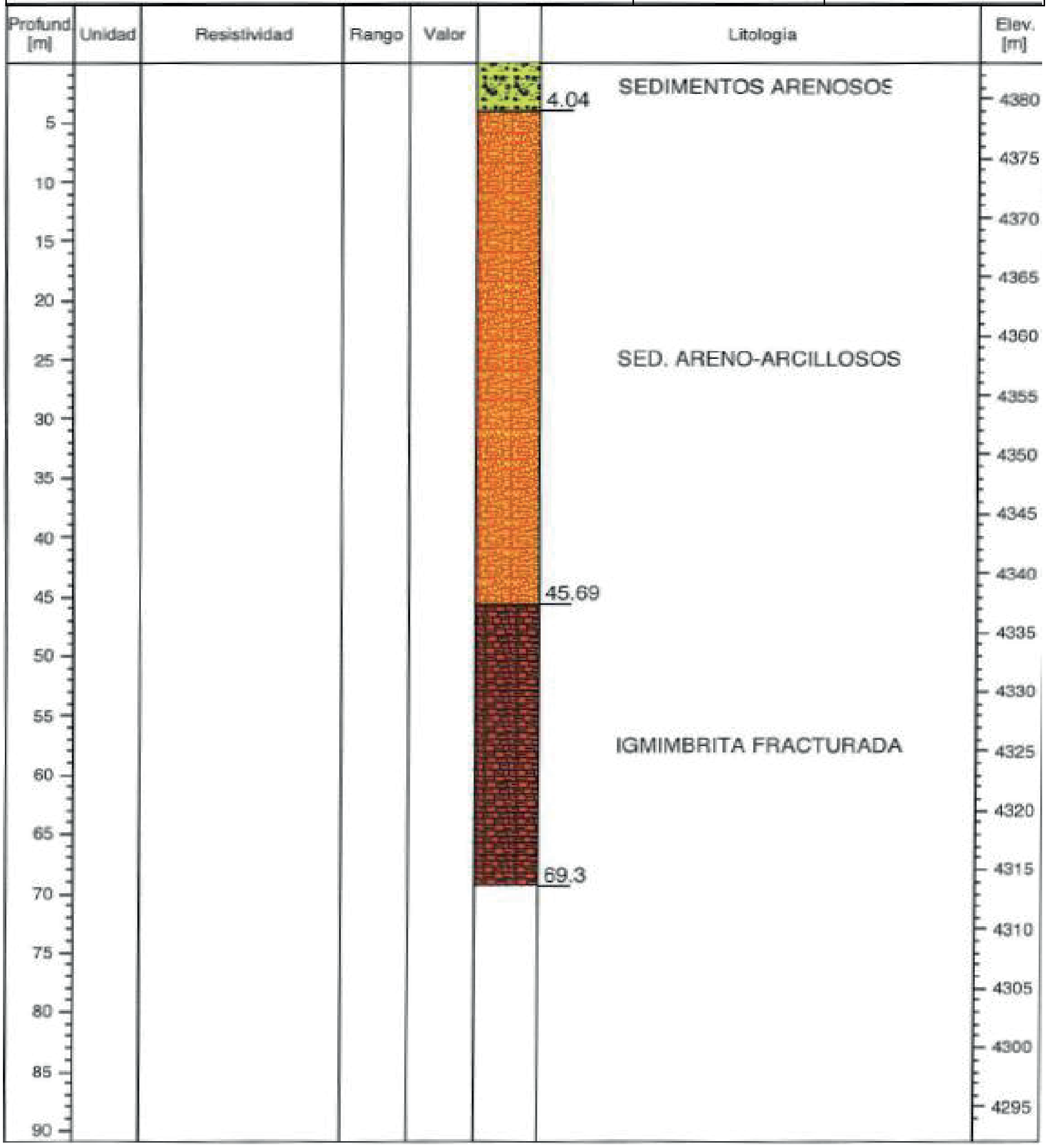

Geophysical Line SEV-05NE

Location:

North Coordinate	East Coordinate	Height	Wing
7566293	600873	4373	300 m

CALCULATION OF APPARENT RESISTIVITY									
Silala Zone									
No. of Survey 5: SEV-05NE									
AB/2	**M/N2= 1.5**			**MN/2= 5,0**			**MN/2= 25**		
	RESIST. V/IΩ	FACTOR K	RESIST. AP	RESIST. V/IΩ	FACTOR K	RESIST. AP	RESIST. V/IΩ	FACTOR K	RESIST. AP
3	42.81	7.0686	302.61						
5	29.223	23.824	696.20						
7	6.4503	48.957	315.78						
10	3.1399	102.36	321.41						
15	1.4431	233.26	336.62						
20	812.75	416.52	338.53						
25	503.2	652.14	347.26	1.8405	188.496	347.26			
30				1.295	274.89	355.98			
40				749.95	494.802	371.08			
50				468.05	777.546	363.93			
60				346.44	1123.122	389.09			
75				172.5	1759.296	303.48			
100				100.98	3133.746	316.45			
125				66.809	4900.896	312.62	361.12	942.48	312.62
150							224.67	1374.45	308.80
175							162.89	1884.96	307.04
200							118.38	2474.01	292.87
250							73.551	3887.73	285.95
300							40.48	5615.61	227.32

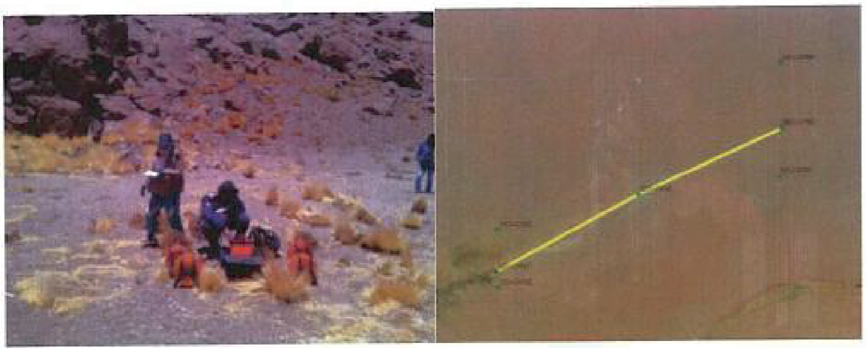

Photograph B.2.4. Location of the longitudinal line with respect to the spring.

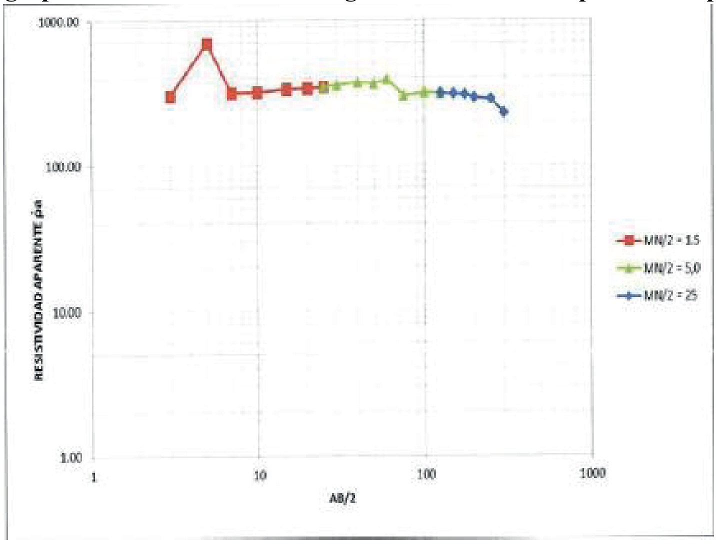

Graph B.2.7. Apparent Resistivity Values vs. AB/2

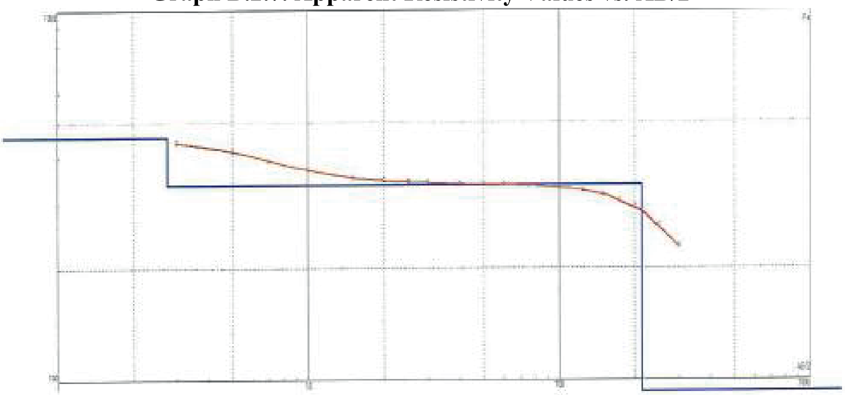

Graph B.2.8. Interpretation of Resistivity Model - Layers.

N° LAYERS	Layer Thickness. (m)	Approx. Depth. (m)	Resist. Ωm	Characteristics	Lithological Description
1	11.45	-11.45	**295.6**	The first layer with a resistivity of 295.6 Ohm-m with a depth of 11.45 m corresponds to alluvial material saturated with sandy sediments.	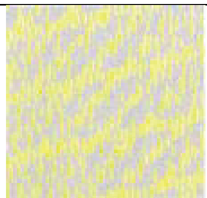
2	15.5	-26.96	**600.9**	The second layer with resistivity of 600.9 Ohm-m corresponds to sand-clay sediments with a thickness of 15.5 m and a depth of -26.96 m.	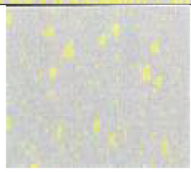
3	27.32	-54.27	**141.9**	The last layer has a resistivity of 141.9 Ohm-m which indicates the presence of fractured ignimbrite and starts at a depth of -54.27 m.	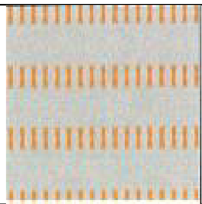

SEV-05NE Analysis:

The 1st layer has a depth of 11.45 m and resistivity of 295.6 Ohm-m indicating the presence of alluvial material saturated with sandy sediments, the 2nd layer with a depth of 26.96 m thick of 15.5 m and resistivity of 600.9 Ohm-m corresponding to sand-clay sediments.

The last layer is 54.27 m deep and has a resistance of 141.9 Ohm-m responds to fractured ignimbrite, which indicates rock fracturing.

LITHOLOGICAL COLUMN OF RESISTIVITIES				
Name **SEV5_NE**	**HYDROGEOLOGICAL CHARACTERIZATION PROJECT OF THE SILALA SPRINGS**			
Coordinates			**Date**	
X 600873	Y 7566293	Z 4373.00	Meas. Pt. Elev.	
Faculty of Geological Engineering			Scale 11: xxx	
Geological-Environmental Research Institute			Vertical 400.0	Horizontal 50.0

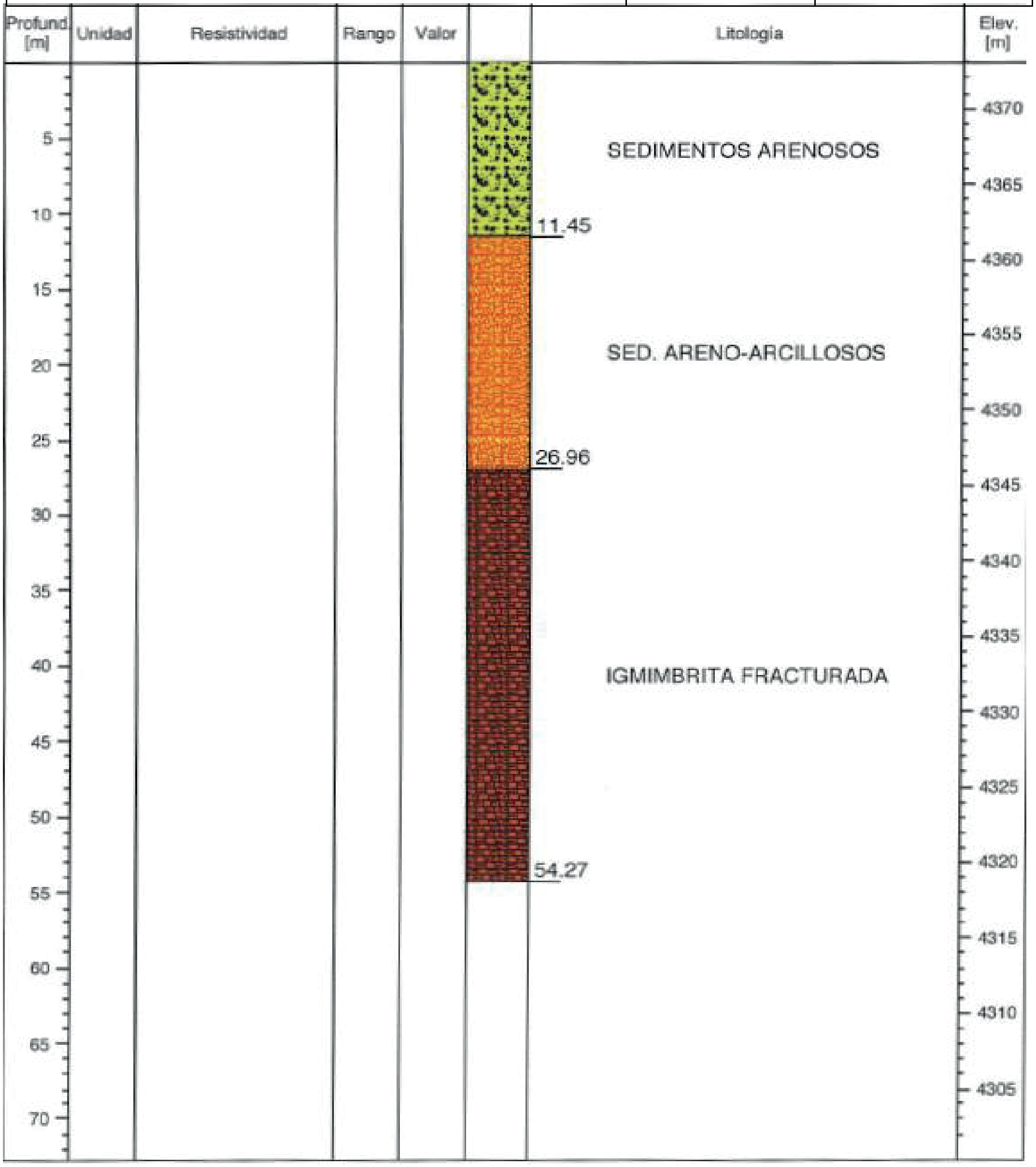

Geophysical Line SEV-06NE

Location:

North Coordinate	East Coordinate	Height	Wing
7566277	600875	4374	300 m

CALCULATION OF APPARENT RESISTIVITY									
Silala Zone									
No. of Survey 5: SEV-05NE									
	M/N2= 1.5			MN/2= 5,0			MN/2= 25		
AB/2	RESIST. V/IΩ	FACTOR K	RESIST. AP	RESIST. V/IΩ	FACTOR K	RESIST. AP	RESIST. V/IΩ	FACTOR K	RESIST. AP
3	33.057	7.0686	233.67						
5	12.823	23.8238	305.49						
7	6.0706	48.9566	297.20						
10	3.105	102.3638	317.84						
15	1.4663	233.2638	342.03						
20	839.91	416.5238	349.84						
25	537.72	652.1438	356.16	1.8742	188.5	356.16			
30				1.3186	274.89	362.47			
40				723.82	494.8	358.15			
50				461.33	777.55	358.71			
60				298.74	1123.1	335.52			
75				178.52	1759.3	314.07			
100				103.65	3133.7	324.81			
125				66.622	4900.9	323.06	371.06	942.48	323.06
150							233.77	1374.45	321.31
175							170.43	1884.96	321.25
200							121.39	2474.01	300.32
250							66.35	3887.73	257.95
300							24.879	5615.61	139.71

Photograph B.2.5. Location of the longitudinal line with respect to the spring.

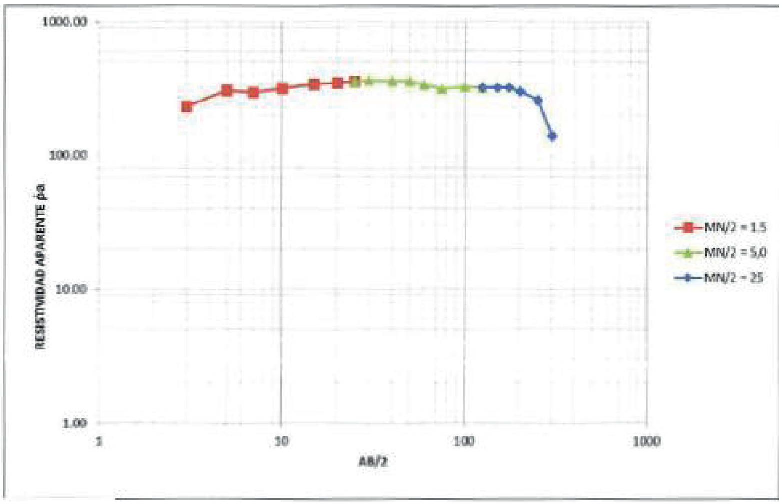

Graph B.2.9. Apparent Resistivity Values vs. AB/2

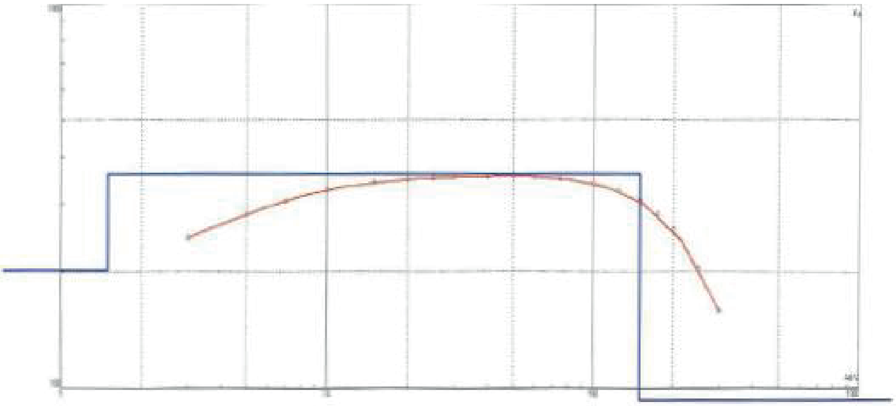

Graph B.2.1 O. Interpretation of Resistivity Model - Layers.

N° LAYERS	Layer Thickness. (m)	Approx. Depth. (m)	Resist. Ωm	Characteristics	Lithological Description
1	3.622	-3.622	**239**	The first layer with resistivity of 239 Ohm-m corresponds to alluvial material saturated with sandy sediments.	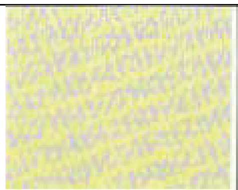
2	59.63	-63.25	**342.4**	The second layer with resistivity of 342.4 Ohm-m corresponds to sand-clay sediments with a thickness of 59.63 m and a depth of -63.25 m.	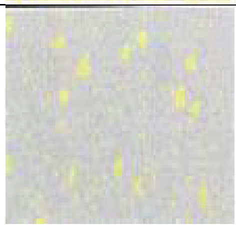
3	40.11	-69.52	**780.1**	The last layer has a resistivity of 780.1 Ohm-m indicating the presence of ignimbrite and starts at a depth of -69.52m.	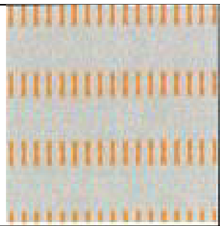

SEV-06NE Analysis:

The 1st layer with a depth of 3,622 m and resistivity of 239 Ohm-m indicates the presence of alluvial matter saturated with sandy sediments, the 2nd layer has a depth of 63.25 meters thick of 59.63 m and resistivity of 780.1 Ohm-m corresponding to sand-clay sediments.

The 3rd layer with 59.52 m depth and resistivity of 780.01 Ohm-m responds to fractured ignimbrite, which indicates rock fracturing.

<table>
<tr><th colspan="5">LITHOLOGICAL COLUMN OF RESISTIVITIES</th></tr>
<tr><td>Name
SEV6_NE</td><td colspan="4">HYDROGEOLOGICAL CHARACTERIZATION PROJECT OF THE SILALA SPRINGS</td></tr>
<tr><td colspan="3">Coordinates</td><td colspan="2">Date</td></tr>
<tr><td>X
600875</td><td>Y
7566277</td><td>Z
4374.00</td><td colspan="2">Meas. Pt. Elev.</td></tr>
<tr><td colspan="3">Faculty of Geological Engineering</td><td colspan="2">Scale 11: xxx</td></tr>
<tr><td colspan="3">Geological-Environmental Research Institute</td><td>Vertical
500.0</td><td>Horizontal
100.0</td></tr>
</table>

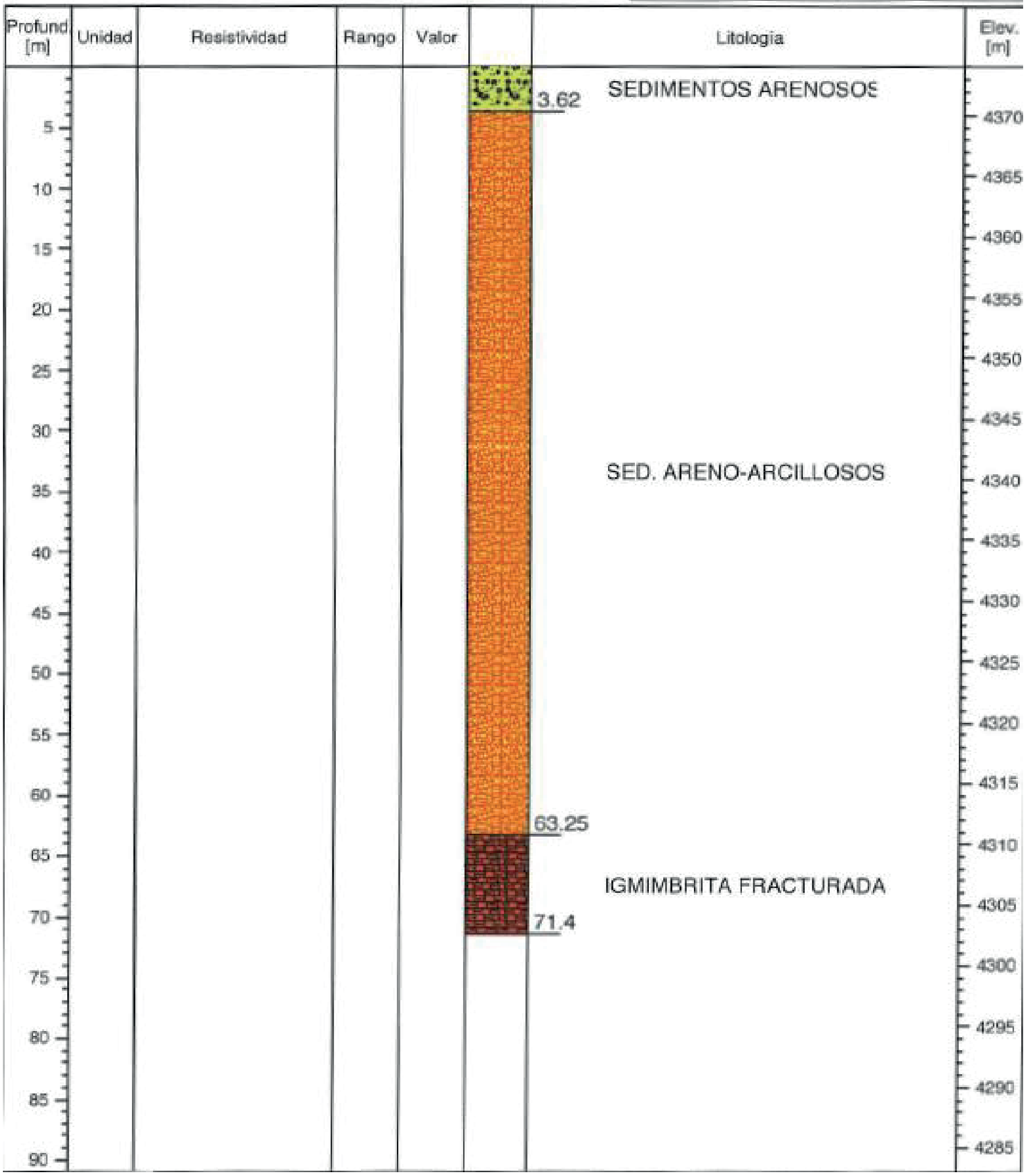

Geophysical Line SEV-07NE

Location:

North Coordinate	East Coordinate	Height	Wing
7566335	600875	4377	300 m

CALCULATION OF APPARENT RESISTIVITY									
Silala Area									
No. of Survey 7: SEV-07NE									
	M/N2= 1.5			**MN/2= 5,0**			**MN/2= 25**		
AB/2	RESIST. V/IΩ	FACTOR K	RESIST. AP	RESIST. V/IΩ	FACTOR K	RESIST. AP	RESIST. V/IΩ	FACTOR K	RESIST. AP
3	68.702	7.0686	485.63						
5	18.855	23.8238	449.20						
7	9.0481	48.9566	442.96						
10	4.3893	102.364	449.31						
15	2.0722	233.264	483.37						
20	1.1291	416.524	470.30						
25	650.32	652.144	470.03	2.4771	188.496	470.03			
30				1.7089	274.89	469.76			
40				813.36	494.802	402.45			
50				496.31	777.546	385.90			
60				345.16	1123.122	387.66			
75				178.25	1759.296	313.59			
100				97.212	3133.746	304.64			
125				63.757	4900.896	284.86	297.92	942.48	284.86
150							192.87	1374.45	265.09
175							140.57	1884.96	264.97
200							103.66	2474.01	256.46
250							70.583	3887.73	274.41
300							42.48	5615.61	238.55

Photograph B.2.6. Location of the longitudinal line with respect to the spring

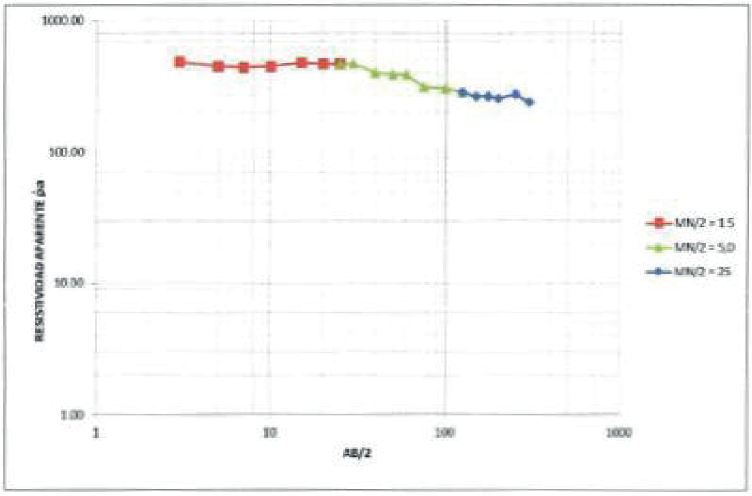

Graph B.2.11. Apparent Resistivity Values vs. AB/2

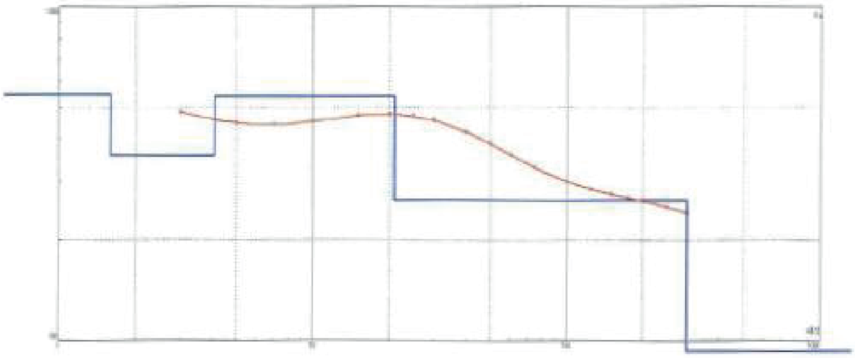

Graph B.2.12. Interpretation of Resistivity Model - Layers.

N° LAYERS	Layer Thickness. (m)	Approx. Depth. (m)	Resist. Ωm	Characteristics	Lithological Description
1	10.12	-10.12	**392.9**	The first layer with resistivity of 239.9 m corresponds to alluvial material saturated with sandy sediments.	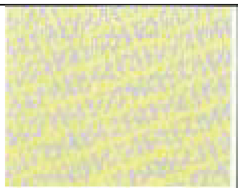
2	7.363	-17.48	**1112**	The second layer with a resistivity of 1112 Ohm-m corresponds to sand-clay sediments with a thickness of 7.363 m and a depth of -17.48 m.	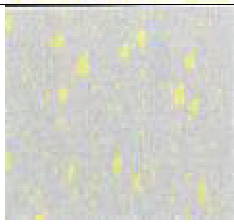
3	25.33	-42.81	**154.4**	The last layer has a resistivity of 154.4 Ohm-m which indicates the presence of fractured ignimbrite with a thickness of 25.33 m.	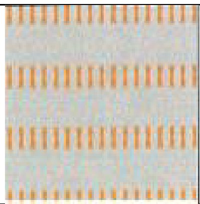

SEV-07NE Analysis:

The 1st layer with a depth of 10.12 m and resistivity of 392.9 Ohm-m indicates the presence of alluvial material saturated with sandy sediments, the 2nd layer is 17.48 m deep and 7.363 m thick and resistivity of 112 Ohm-m corresponding to sand-clay sediments.

The last layer has a depth of 42.81 m and resistivity of 154.4 Ohm-m responds to fractured ignimbrite, which indicates rock fracturing.

LITHOLOGICAL COLUMN OF RESISTIVITIES				
Name **SEV7_NE**	**HYDROGEOLOGICAL CHARACTERIZATION PROJECT OF THE SILALA SPRINGS**			
Coordinates			**Date**	
X 600857	Y 7566335	Z 4377.00	Meas. Pt. Elev.	
Faculty of Geological Engineering			Scale 11: xxx	
Geological-Environmental Research Institute			Vertical 300.0	Horizontal 50.0

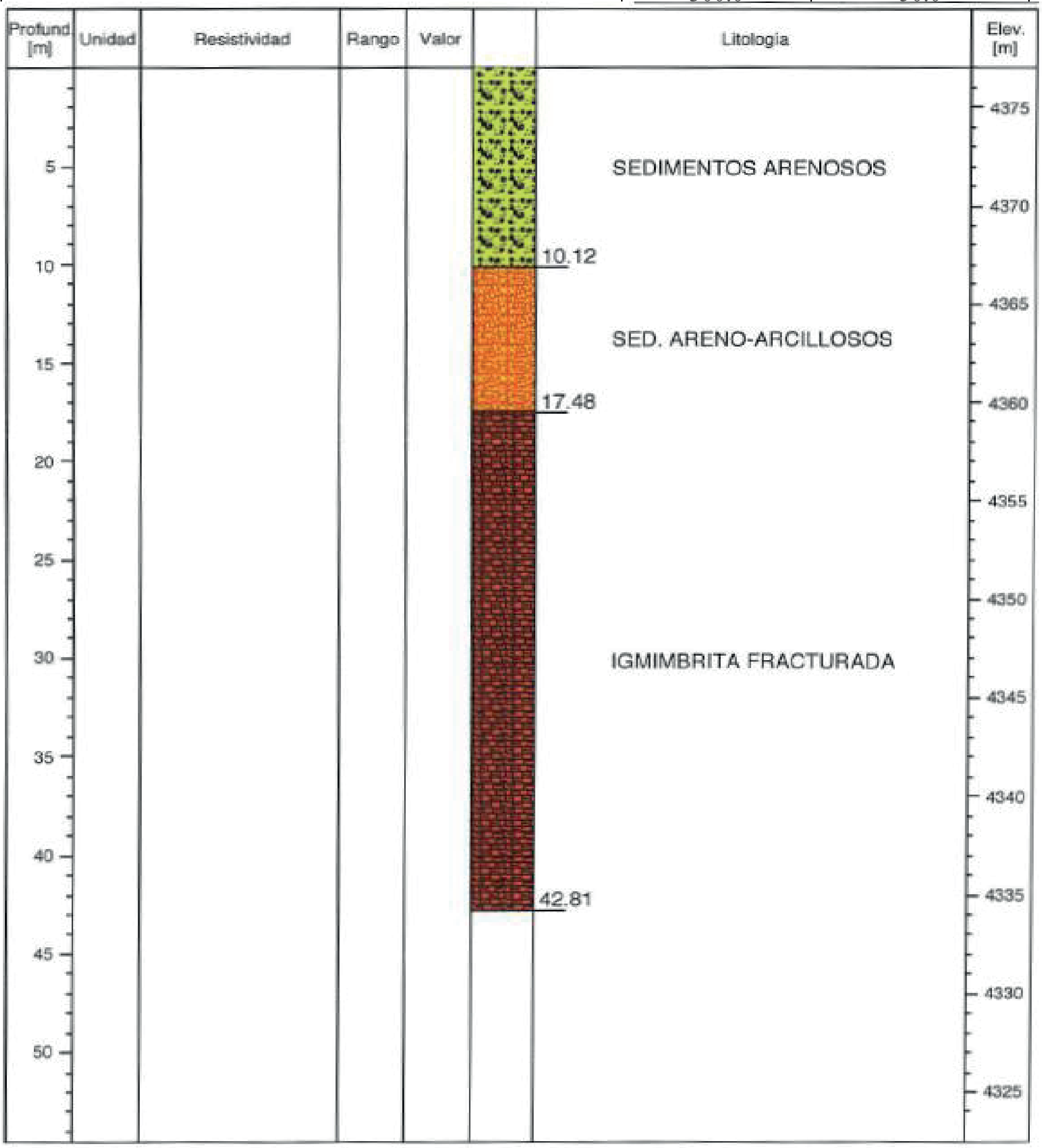

Location:

North Coordinate	East Coordinate	Height	Wing
7566170	600668	4362	250 m

CALCULATION OF APPARENT RESISTIVITY									
Silala Zone									
No. of Survey 8: SEV-08NE									
AB/2	**M/N2= 1.5**			**MN/2= 5,0**			**MN/2= 25**		
	RESIST. V/IΩ	FACTOR K	RESIST. AP	RESIST. V/IΩ	FACTOR K	RESIST. AP	RESIST. V/IΩ	FACTOR K	RESIST. AP
3	87.347	7.0686	617.42						
5	18.258	23.8238	434.97						
7	7.3165	23.9566	434.97						
10	2.7933	102.3638	285.93						
15	1.0777	233.2638	251.39						
20	539.72	416.5238	224.81						
25	338.57	652.1438	220.80						
30	241.66	940.1238	227.19						
40	134.65	1673.164	238.64	490.44	494.802	238.64			
50				321.65	777.546	250.10			
60				219.89	1123.122	246.96			
75				131.17	1759.296	230.77			
100				83.435	3133.746	261.46			
125				63.238	4900.896	266.99	285.95	942.48	266.99
150							198.27	1374.45	272.51
175							159.7	1884.96	301.03
200							126.48	2474.01	312.91
250							46.413	3887.73	180.44

Photograph B.2.7. Location of the longitudinal line with respect to the spring.

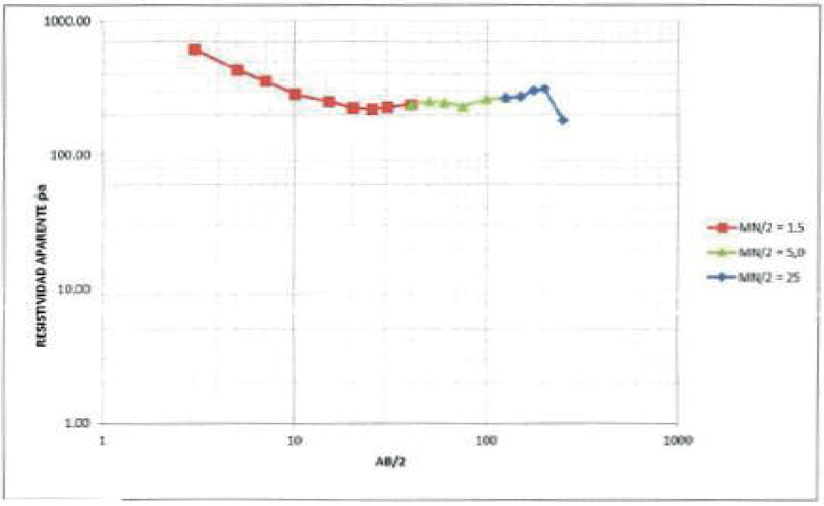

Graph B.2.13. Apparent Resistivity Values vs. AB/2

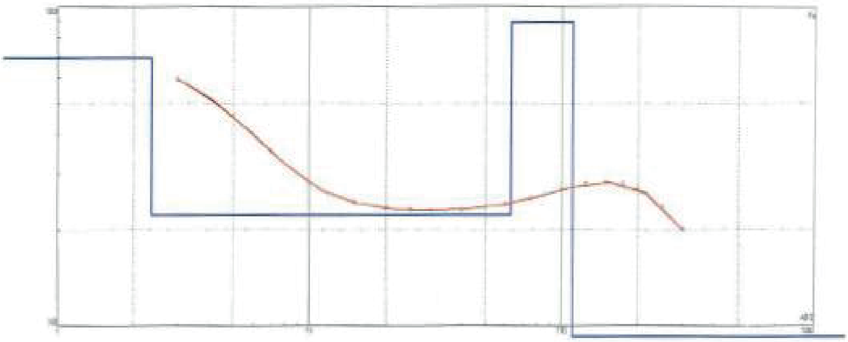

Graphic B.2.14. Interpretation of Resistivity Model - Layers

N° LAYERS	Layer Thickness. (m)	Approx. Depth. (m)	Resist. Ωm	Characteristics	Lithological Description
1	2.368	-2.368	**694.9**	The first layer with resistivity of 694.9 m corresponds to alluvial material saturated with sand-clay sediments.	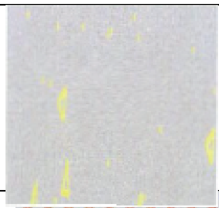
2	60.36	-58.47	**223.6**	The last layer has a resistivity of 223.6 Ohm-m corresponds to fractured ignimbrite with a thickness of 60.36 m from a depth of -58.47 m.	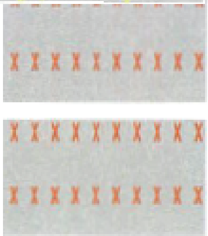

SEV-08NE Analysis:

The 1st layer with a depth of 2,368 m and resistivity of 694.9 Ohm-m indicates the presence of alluvial material saturated with sand-clay sediments, the 2nd layer has a depth of 58.47 m thick of 60.36 m and resistivity of 223.6 Ohm-m corresponding to the fractured ignimbrite.

<table>
<tr><td colspan="4">LITHOLOGICAL COLUMN OF RESISTIVITIES</td></tr>
<tr><td>Name
SEV8_NE</td><td colspan="3">HYDROGEOLOGICAL CHARACTERIZATION PROJECT OF THE SILALA SPRINGS</td></tr>
<tr><td colspan="3">Coordinates</td><td>Date</td></tr>
<tr><td>X
600668</td><td>Y
7566170</td><td>Z
4362.00</td><td>Meas. Pt. Elev.</td></tr>
<tr><td colspan="3">Faculty of Geological Engineering</td><td>Scale 11: xxx</td></tr>
<tr><td colspan="3">Geological-Environmental Research Institute</td><td>Vertical 400.0 | Horizontal 100.0</td></tr>
</table>

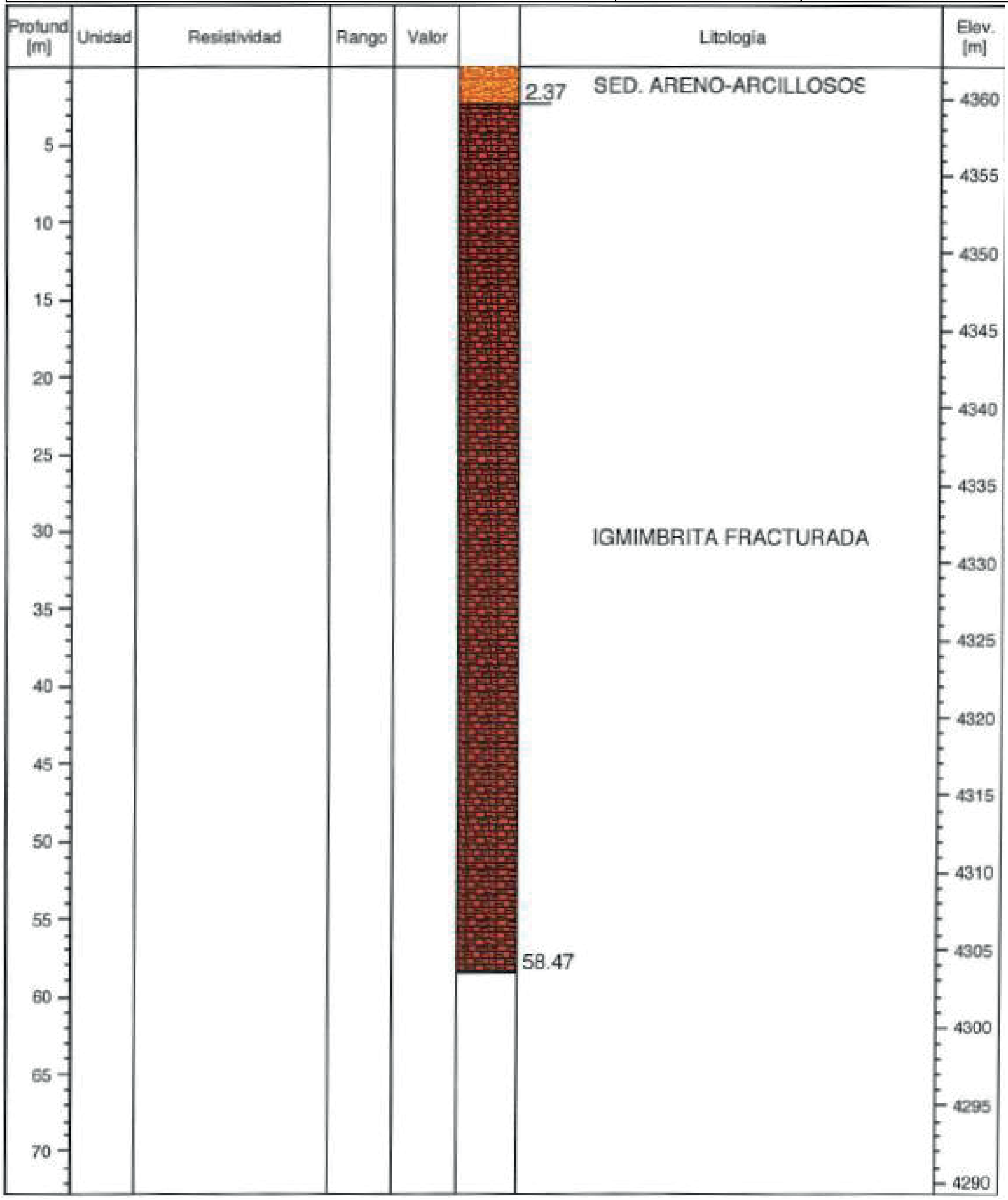

Geophysical Line SEV-09NE

Location:

North Coordinate	East Coordinate	Height	Wing
7566312	600730	4376	250 m

CALCULATION OF APPARENT RESISTIVITY									
Silala Zone									
No. of Survey 9: SEV-09NE									
AB/2	**M/N2= 1.5**			**MN/2= 5,0**			**MN/2= 25**		
	RESIST. V/IΩ	FACTOR K	RESIST. AP	RESIST. V/IΩ	FACTOR K	RESIST. AP	RESIST. V/IΩ	FACTOR K	RESIST. AP
3	39.305	7.0686	277.831						
5	10.916	23.8238	260.061						
7	5.3234	48.9566	260.616						
10	2.7383	102.364	280.303						
15	1.2611	233.264	294.169						
20	717.74	416.524	298.956						
25	470.13	652.144	306.592						
30	334.03	940.124	314.030						
40	196.76	1673.16	330.007	728.16	494.802	330.077			
50				445.15	777.546	346.124			
60				275.78	1123.122	309.735			
75				146.39	1759.296	257.543			
100				71.558	3133.746	267.001	431.83	589.05	267.001
125							293.33	942.48	276.001
150							191.09	1374.45	262.6436
175							132.24	1884.96	249.2671
200							103.2	2474.01	255.3178
250							57.475	3887.73	223.4473

Photograph B.2.8. Location of the longitudinal line with respect to the spring

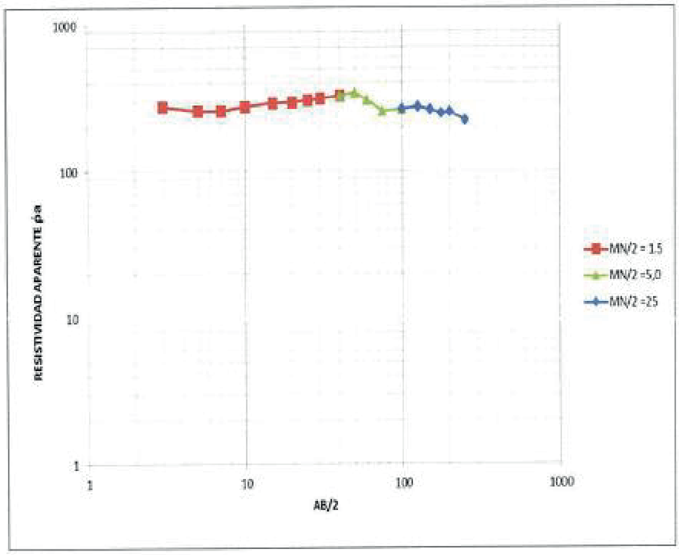

Graph B.2.15. Apparent Resistivity Values vs AB/2 values.

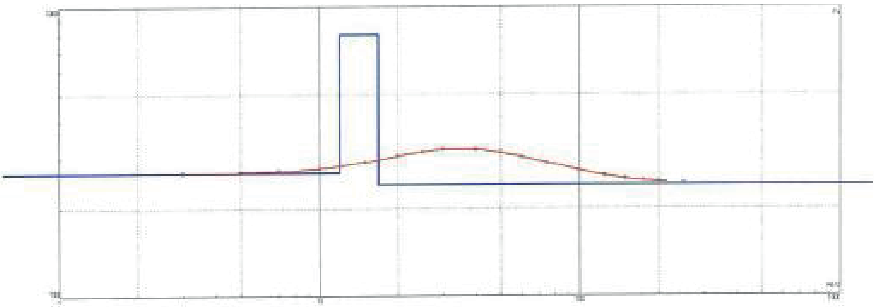

Graph B.2.16. Interpretation of Resistivity Model – Layers

N° LAYERS	Layer Thickness. (m)	Approx. Depth. (m)	Resist. Ωm	Characteristics	Lithological Description
1	2.181	-1.831	**161.3**	The first layer with resistivity of 161.3 m corresponds to alluvial material saturated with sand-clay sediments.	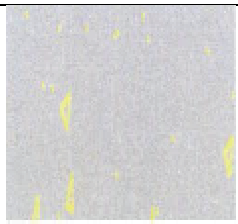
2	65.82	-67.65	**330.4**	The last layer has a resistivity of 330.4 Ohm-m corresponds to fractured ignimbrite with thickness of 65.82 m from a depth of -67.65 m.	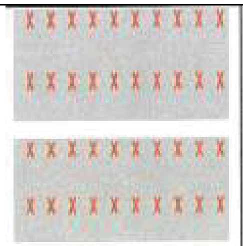

SEV-09NE Analysis:

The 1st with a depth of 1,831 m and resistivity of 161.3 Ohm-m indicates the presence of alluvial material saturated with sand-clay sediments, the 2nd layer has a depth of 67.65 m thick of 65.82 m and resistivity of 330.4 Ohm-m corresponding to fractured ignimbrite material.

LITHOLOGICAL COLUMN OF RESISTIVITIES				
Name **SEV9_NE**	**HYDROGEOLOGICAL CHARACTERIZATION PROJECT OF THE SILALA SPRINGS**			
Coordinates			**Date**	
X 600730	Y 7566312	Z 4376.00	Meas. Pt. Elev.	
Faculty of Geological Engineering			Scale 1: xxx	
Geological-Environmental Research Institute			Vertical 450.0	Horizontal 50.0

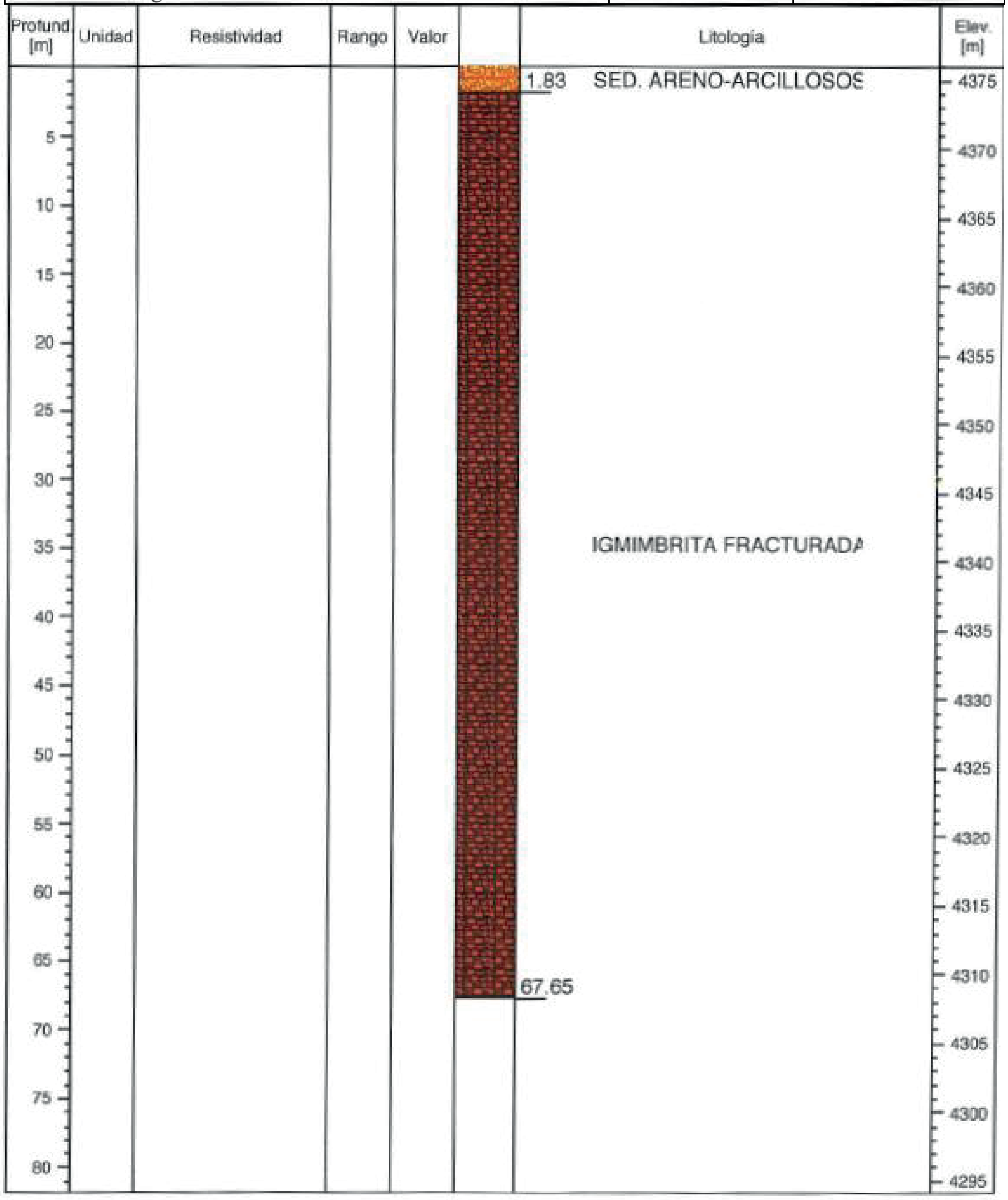

ANNEX B.3.

RESISTIVITY PROFILES - SILALA SPRINGS

Annex B.3.1.

Resistivity Profile 1

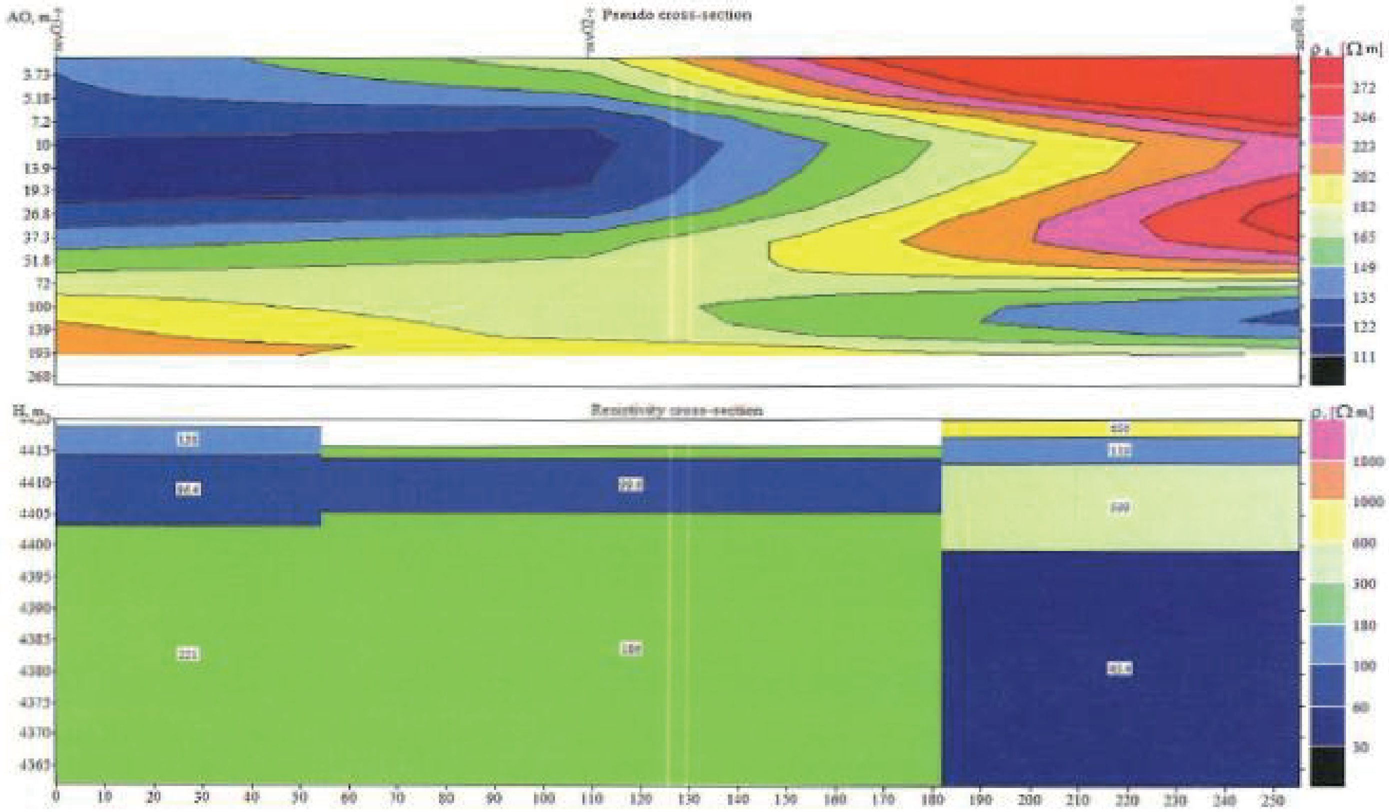

Annex B.3.2

Resistivity Profile 2

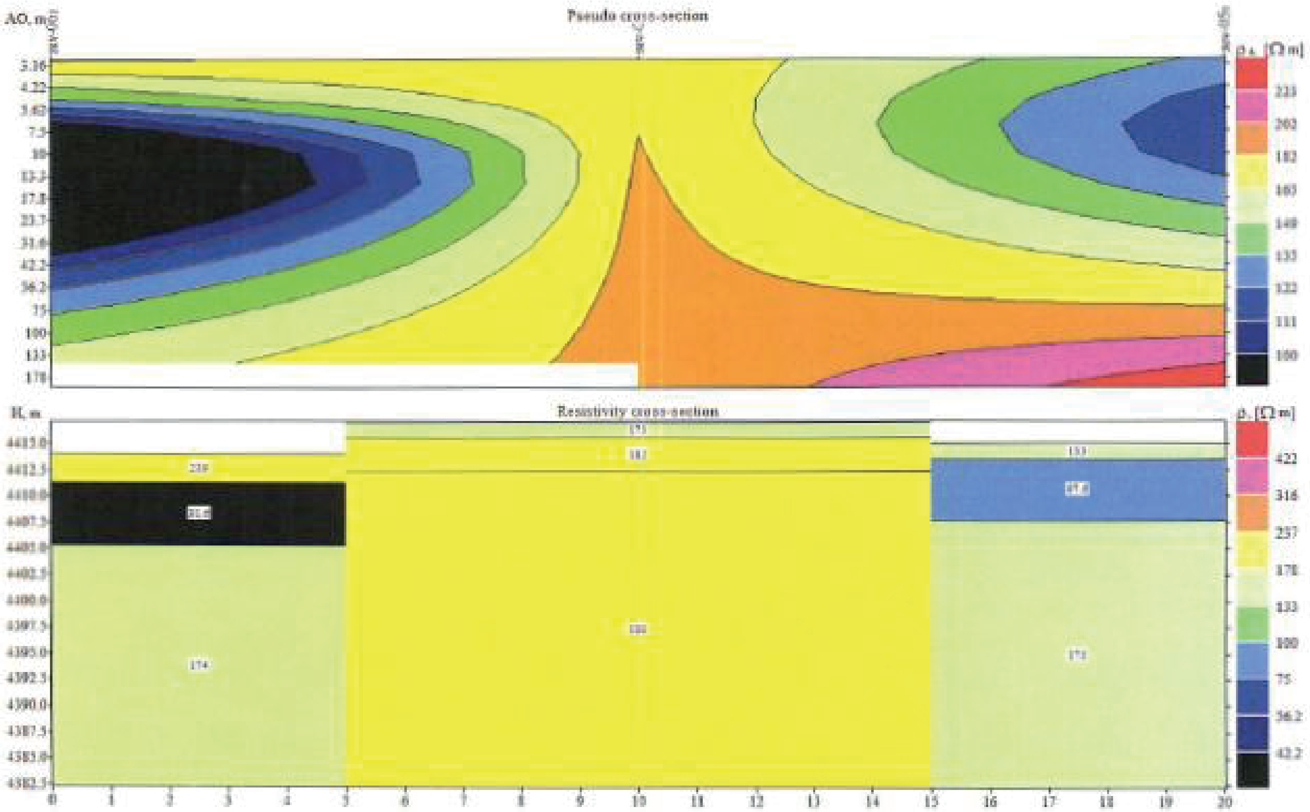

Annex B.3.3

Resistivity Profile 3

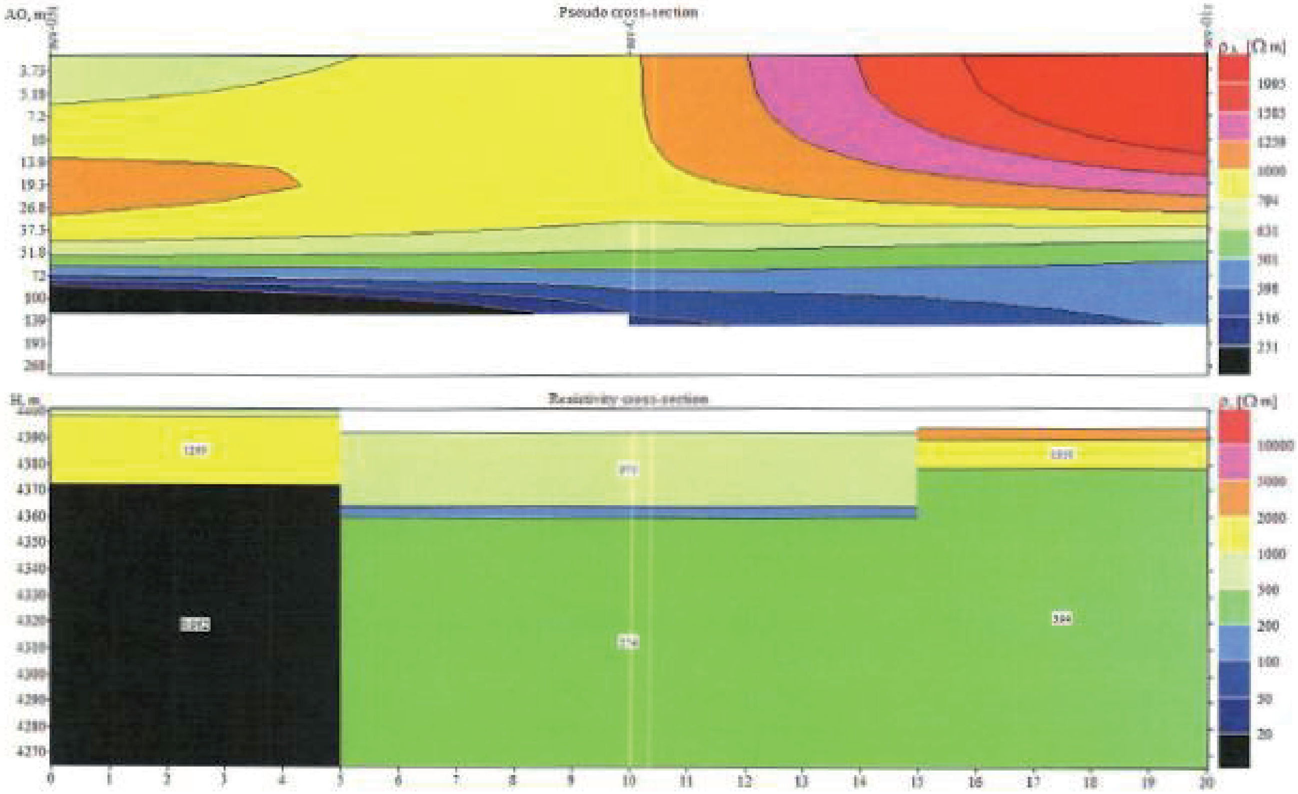

Annex B.3.4.

Resistivity Profile 4

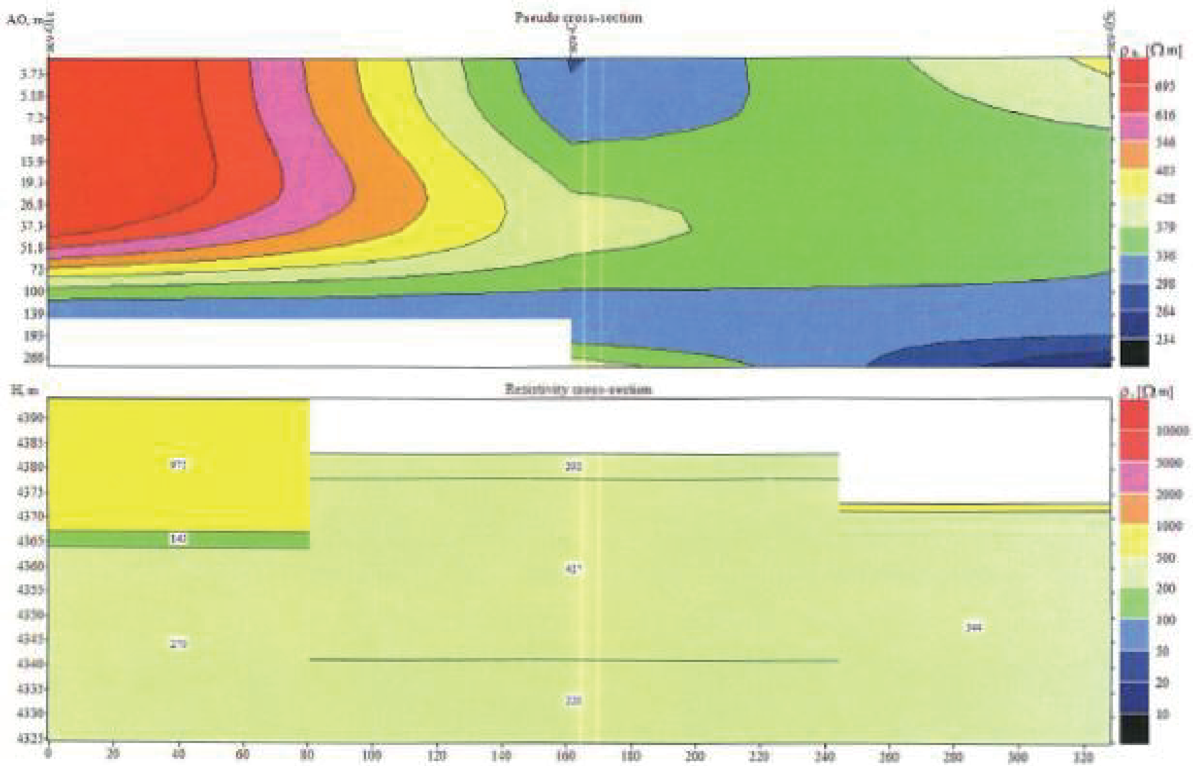

Resistivity Profile 5

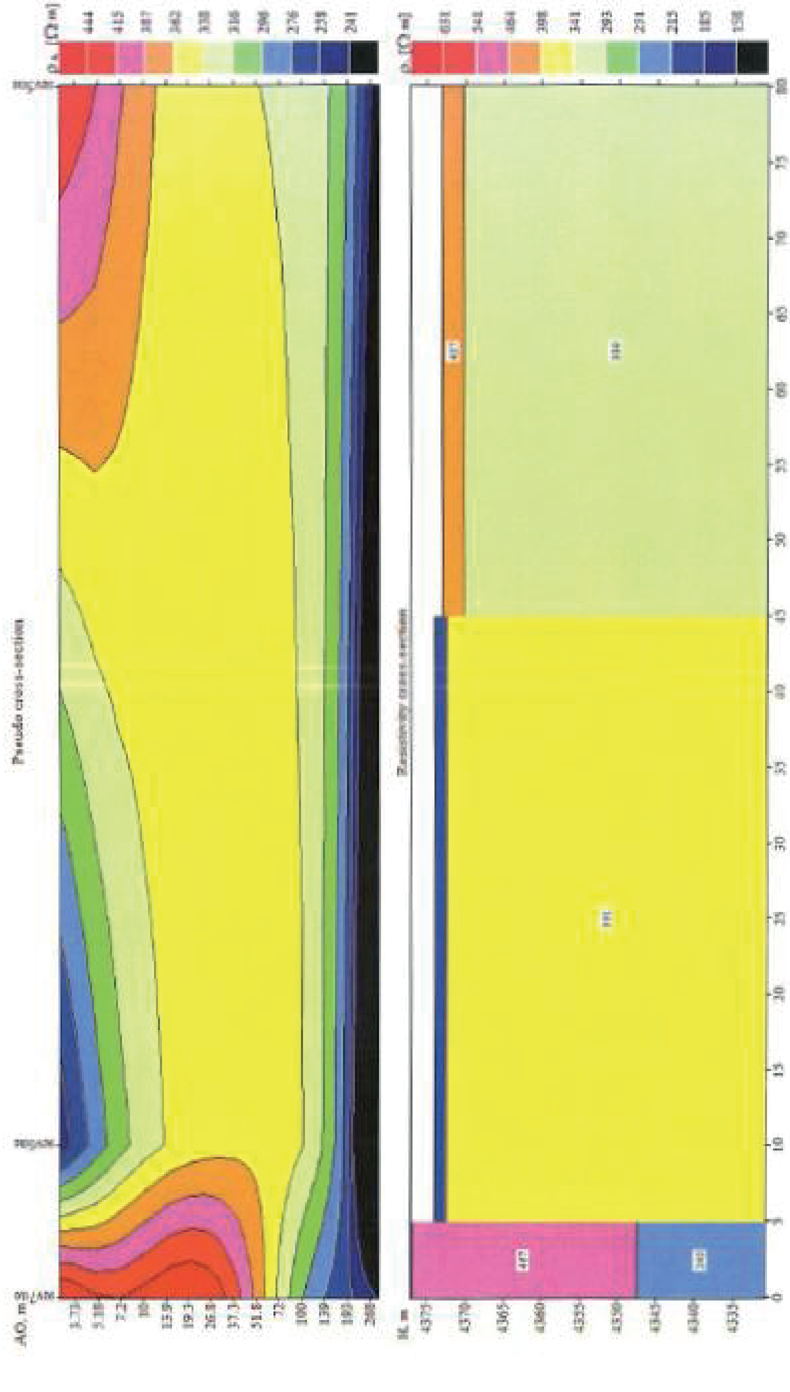

Annex B.3.6.

Resistivity Profile 6

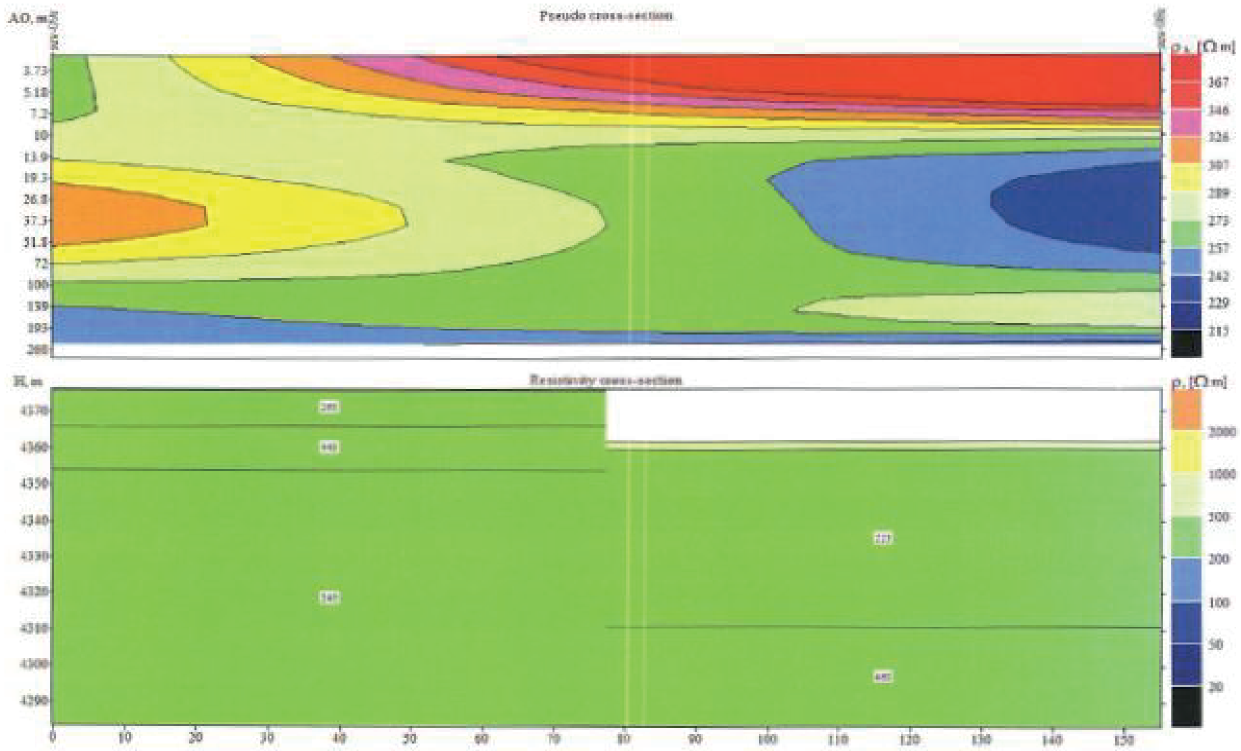

ANNEX B.4.

GEOELECTRICAL SECTIONS - SILALA SPRINGS

GEOELECTRIC SECTION N -1

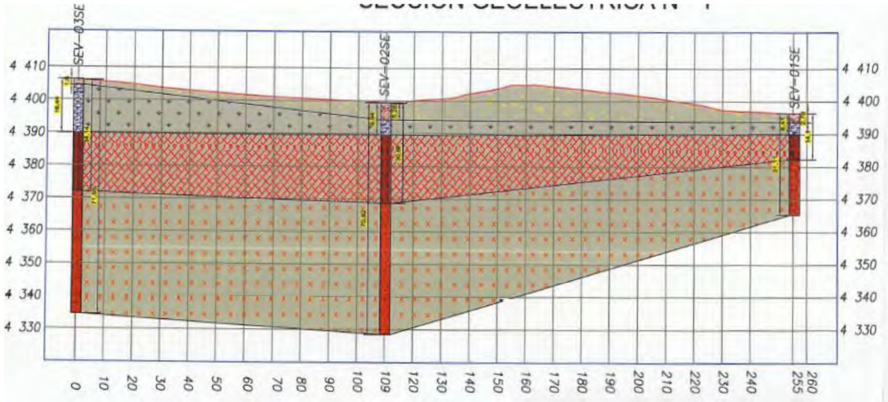

REFERENCES	
DESCRIPTION	SYMBOLOGY
ALLUVIAL MATERIAL WITH METORIZED IGNIMBRITE	
WELDED IGNIMBRITE	
MEDIUM HIGH FRACTURED IGNIMBRITE	
FRACTURED INGNIMBRITE	
SECTION LINE	
SEV LOCATION	

horizontal scale

1:1100

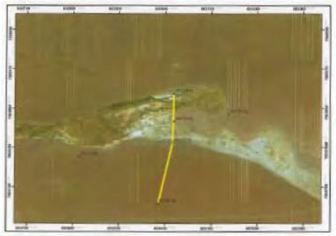

vertical scale

1:1000

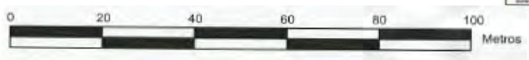

GEOELECTRIC SECTION N -2

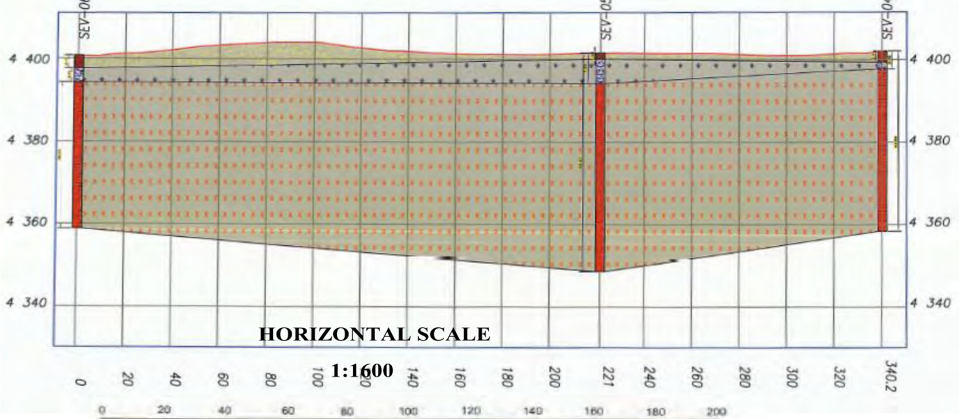

HORIZONTAL SCALE

1:1600

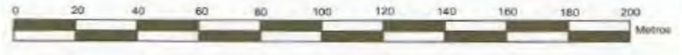

VERTICAL SCALE

1:800

REFERENCES	
DESCRIPTION	**SYMBOLOGY**
ALLUVIAL MATERIAL WITH METORIZED IGNIMBRITE	
WELDED IGNIMBRITE	
FRACTURED INGNIMBRITE	
SECTION LINE	
SEV LOCATION	

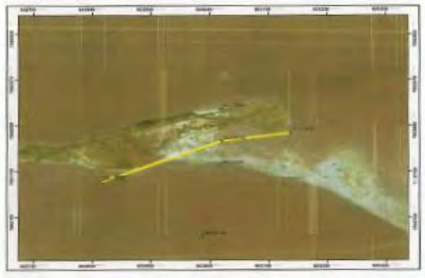

GEOELECTRIC SECTION N -3

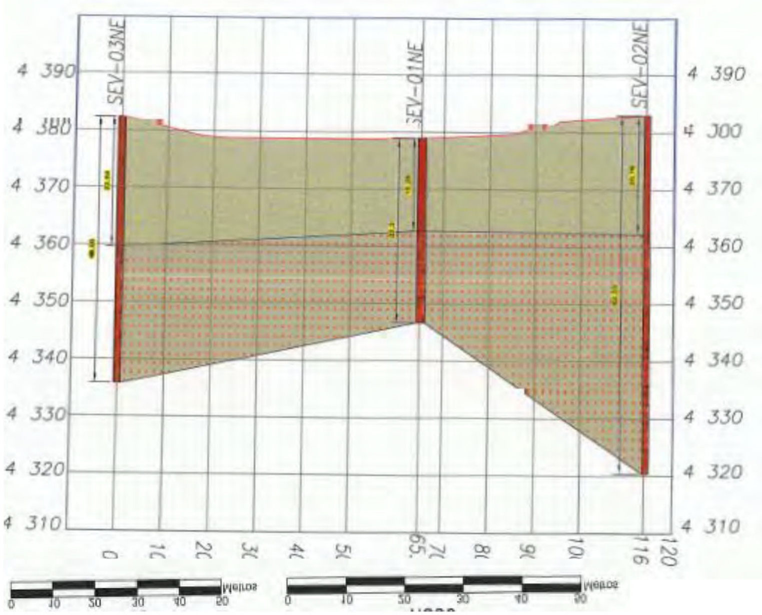

REFERENCES	
DESCRIPTION	**SYMBOLOGY**
ALLUVIAL MATERIAL SATURATED WITH CLAY SEDIMENTS AND WEATHERED IGNIMBRITE	
FRACTURED INGNIMBRITE	
SECTION LINE	
SEV LOCATION	

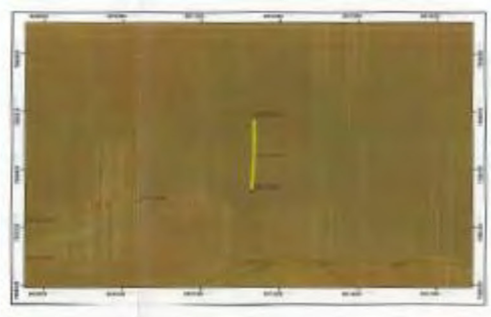

GEOELECTRIC SECTION N -4

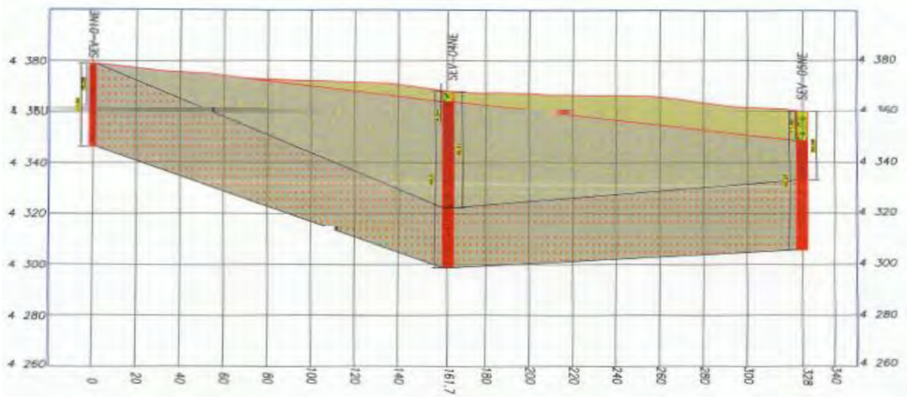

REFERENCES	
DESCRIPTION	**SYMBOLOGY**
ALLUVIAL MATERIAL SATURATED WITH SANDY SEDIMENTS	
ALLUVIAL MATERIAL SATURATED WITH CLAY SANDY SEDIMENTS	
WELDED IGNIMBRITE	
SECTION LINE	
SEV LOCATION	

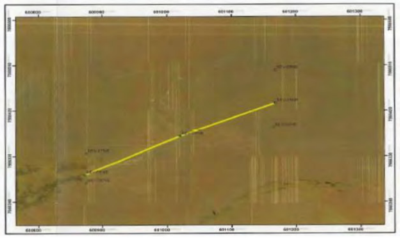

Horizontal Scale

1:1500

Vertical Scale

1: 1000

English translation prepared by DIREMAR. The original language text remains the authoritative one.

GEOELECTRIC SECTION N - 5

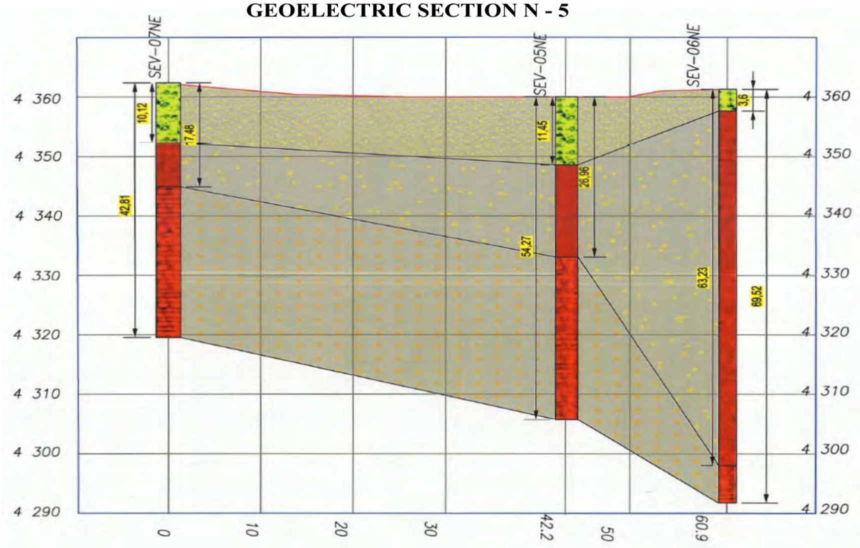

HORIZONTAL SCALE

1: 400

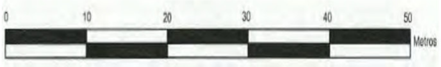

VERTICAL SCALE

1: 500

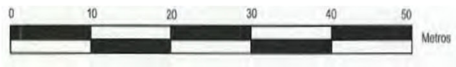

REFERENCES	
DESCRIPTION	**SYMBOLOGY**
SATURATED ALLUVIAL MATERIAL WITH SANDY SEDIMENTS	
ALLUVIAL MATERIAL SATURATED WITH CLAY SANDY SEDIMENTS	
WELDED IGNIMBRITE	
SECTION LINE	
SEV LOCATION	

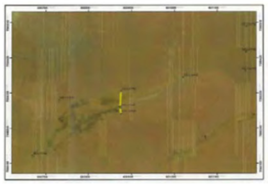

GEOELECTRIC SECTION N - 6

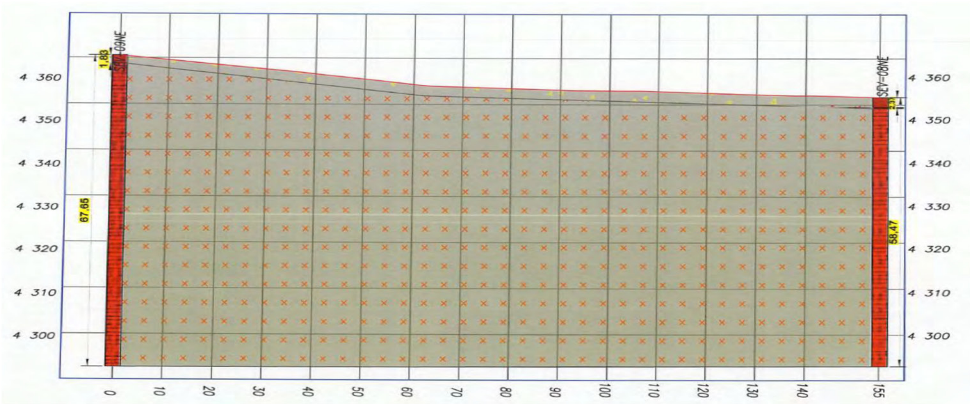

Horizontal Scale

1:800

Vertical Scale

1:500

REFERENCES	
DESCRIPTION	**SYMBOLOGY**
ALLUVIAL MATERIAL SATURATED WITH CLAY SANDY SEDIMENTS	
WELDED IGNIMBRITE	
SECTION LINE	
SEV LOCATION	

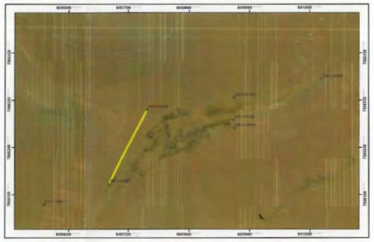

ANNEX B.5.

NWW LONGITUDINAL AND TRANSVERSAL CUTS - SEE

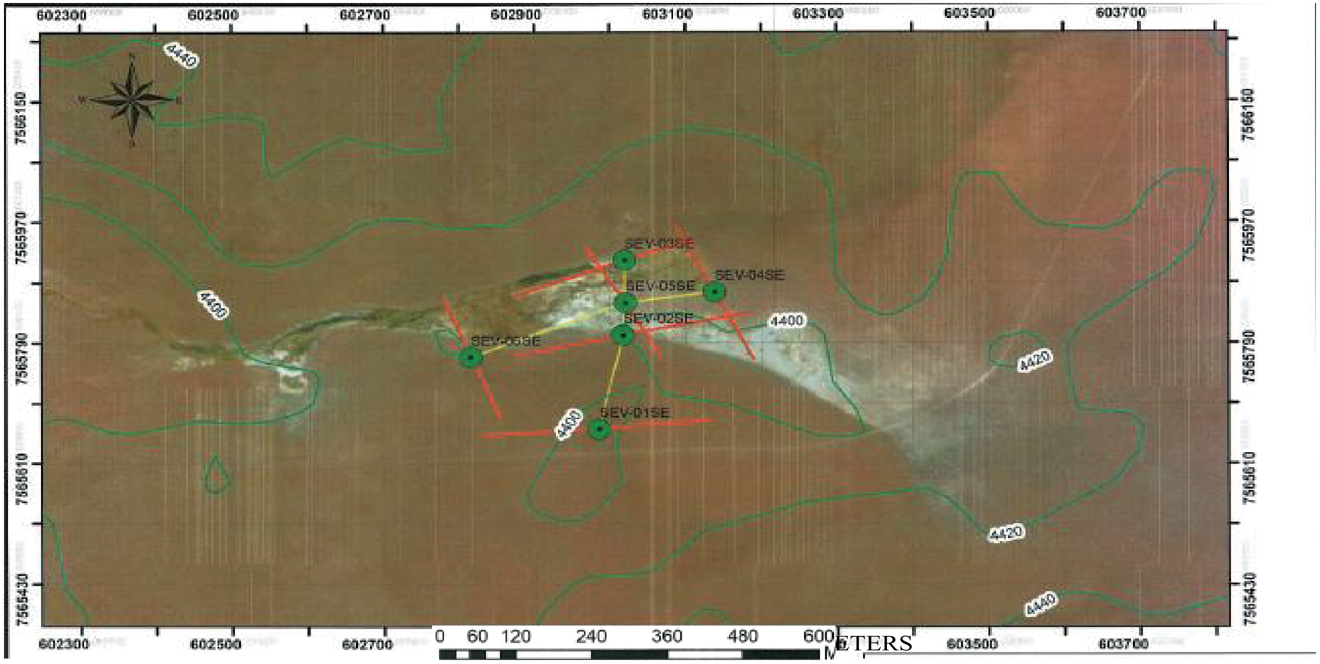

References

SEV SE Locations

Cable Distance SEV

Contour Lines

Cuts

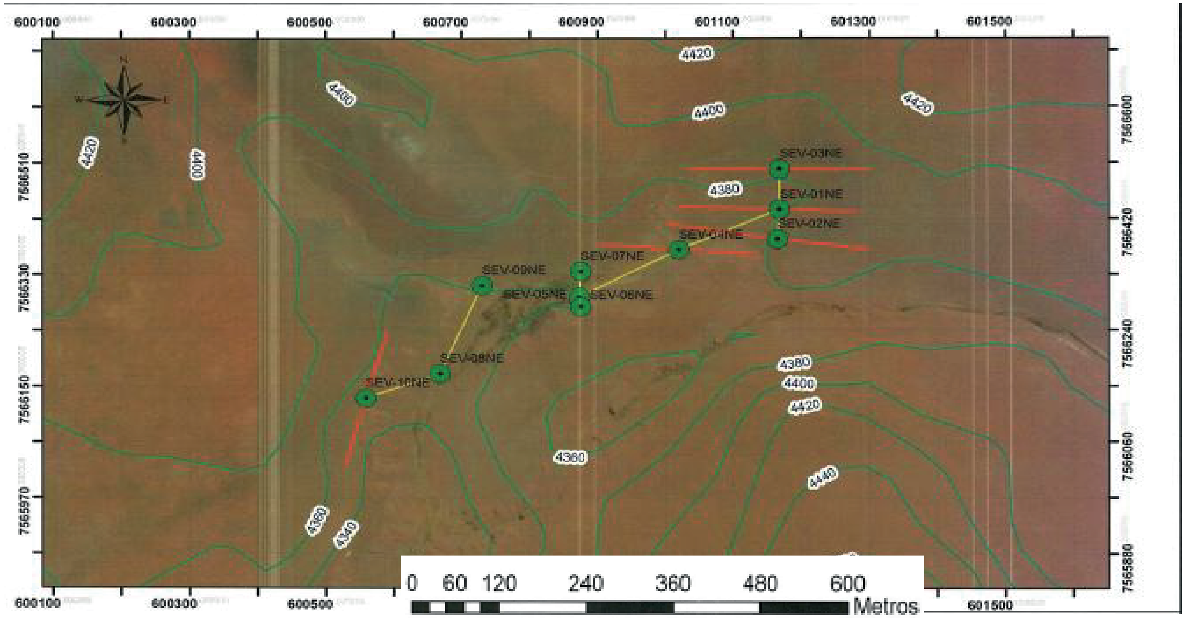

References

SEV SE Locations

Cable Distance SEV

Contour Lines

Cuts

Annex C.

Modeling

Annex C.1.

Photographs

Photograph 1: In the Silala Springs.

Photograph 2: Artificial canals that drain the waters of the Silala springs towards Chile.

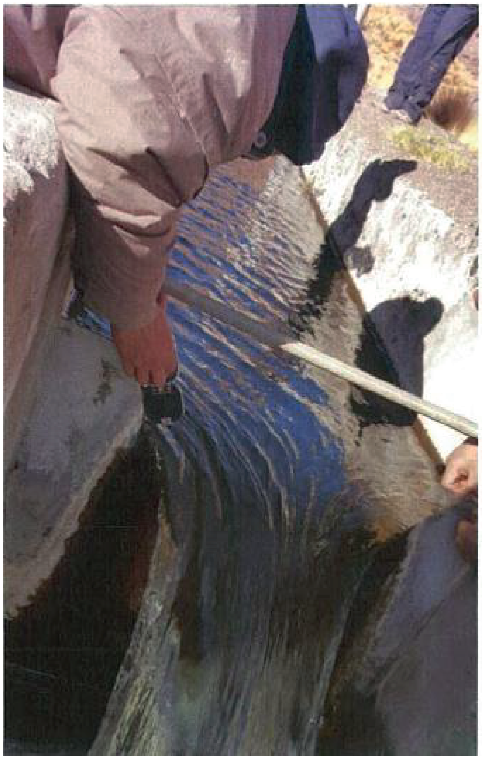

Photograph 3: Water of very good quality and quantity that is poured into the Republic of Chile.

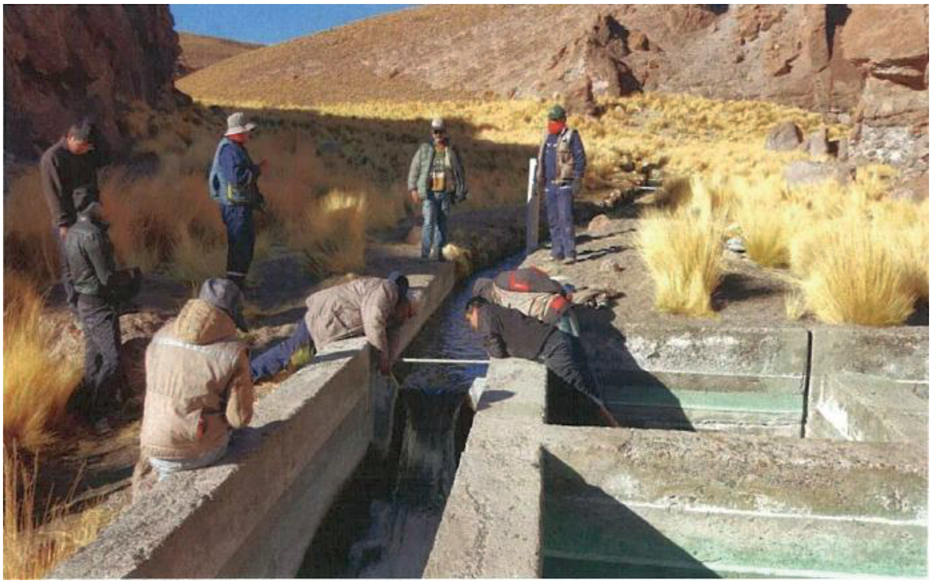

Photograph 4: Weir for the Measurement of Flows.

Photograph 5: Performing Infiltration Tests.

Photograph 6: Performing Infiltration Tests.

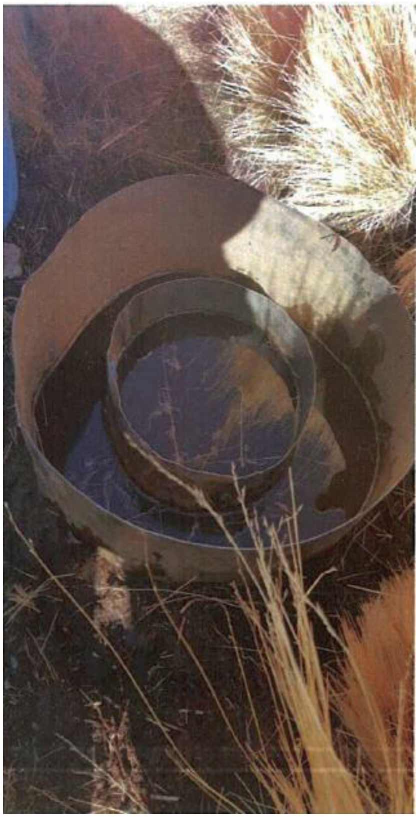

Photograph 7: Infiltration Tests by the Double Ring Method.

Photograph 8: Performance of Permeability Tests on the substrate.

Photograph 9: Taking soil samples.

Photograph 10: Measurement of the root depth of plants.

ANNEX C.2.

Monthly maps of surface runoff (in mm)

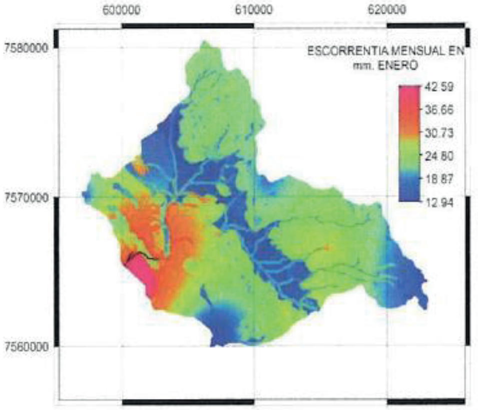
ESCORRENTIA MENSUAL EN mm. ENERO
42.59
36.66
30.73
24.80
18.87
12.94
600000
610000
620000
7580000
7570000
7560000

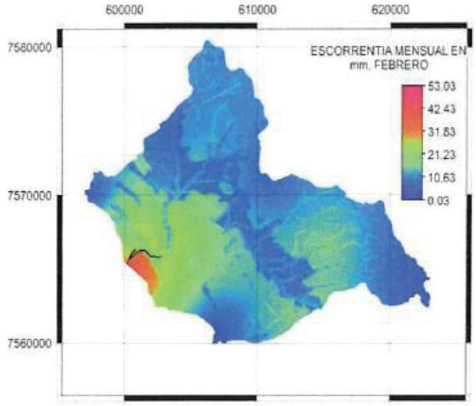
ESCORRENTIA MENSUAL EN mm. FEBRERO
53.03
42.43
31.83
21.23
10.63
0.03
600000
610000
620000
7580000
7570000
7560000

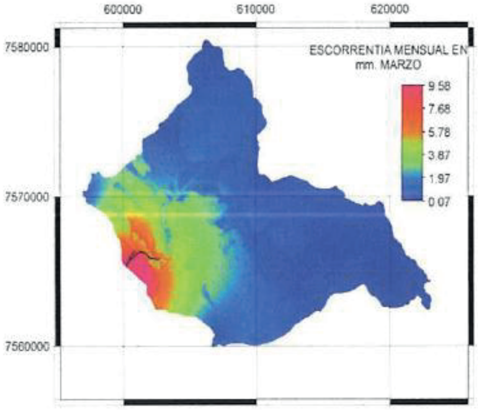
ESCORRENTIA MENSUAL EN mm. MARZO
9.58
7.68
5.78
3.87
1.97
0.07
600000
610000
620000
7580000
7570000
7560000

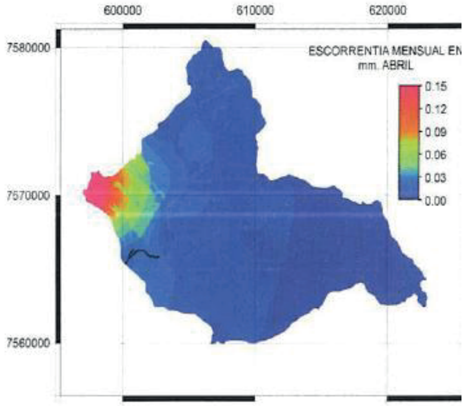
ESCORRENTIA MENSUAL EN mm. ABRIL
0.15
0.12
0.09
0.06
0.03
0.00
600000
610000
620000
7580000
7570000
7560000

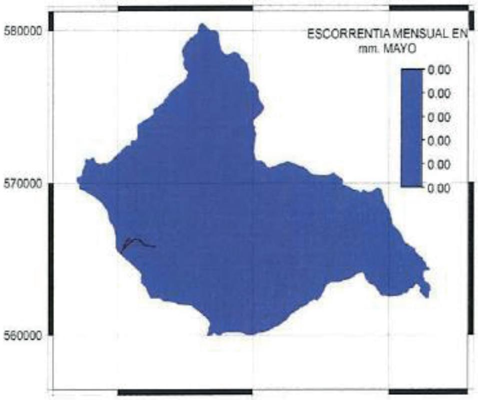
ESCORRENTIA MENSUAL EN mm. MAYO
0.00
0.00
0.00
0.00
0.00
0.00
600000
610000
620000
580000
570000
560000

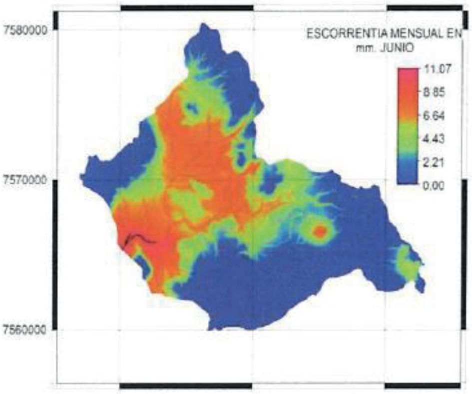
ESCORRENTIA MENSUAL EN mm. JUNIO
11.07
8.85
6.64
4.43
2.21
0.00
600000
610000
620000
7580000
7570000
7560000

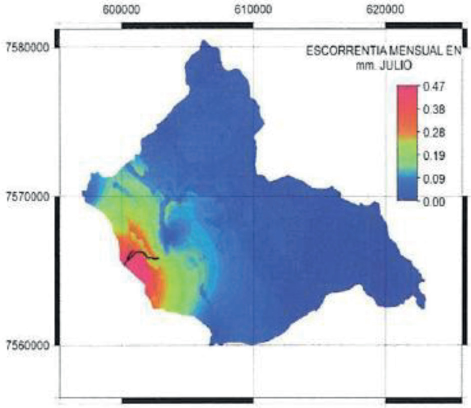
600000
610000
620000
7580000
7570000
7560000
ESCORRENTIA MENSUAL EN
mm. JULIO
0.47
0.38
0.28
0.19
0.09
0.00

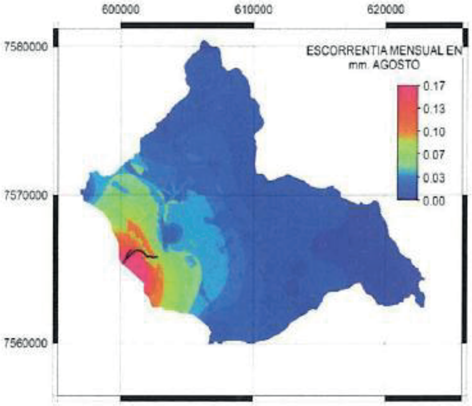
600000
610000
620000
7580000
7570000
7560000
ESCORRENTIA MENSUAL EN
mm. AGOSTO
0.17
0.13
0.10
0.07
0.03
0.00

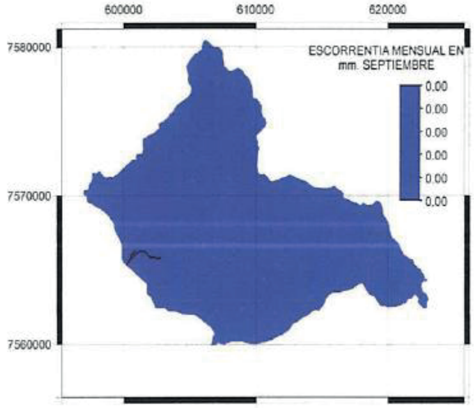
600000
610000
620000
7580000
7570000
7560000
ESCORRENTIA MENSUAL EN
mm. SEPTIEMBRE
0,00
0,00
0,00
0,00
0,00
0,00

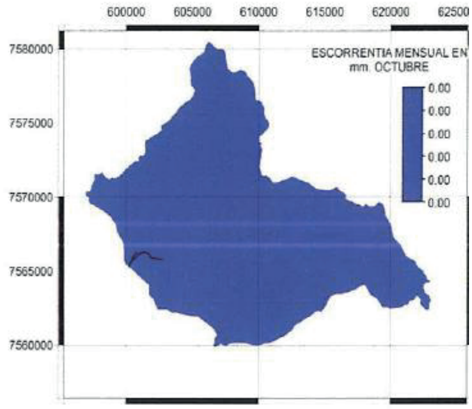
600000
605000
610000
615000
620000
62500
7580000
7575000
7570000
7565000
7560000
ESCORRENTIA MENSUAL EN
mm. OCTUBRE
0.00
0.00
0.00
0.00
0.00
0.00

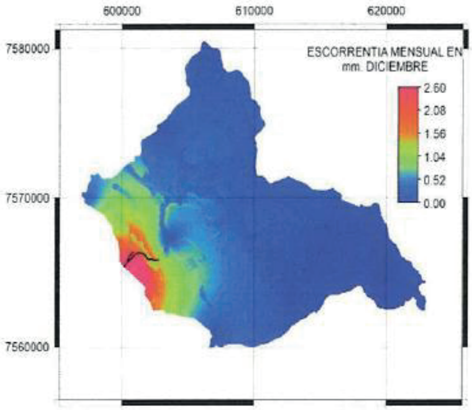
600000
610000
620000
7580000
7570000
7560000
ESCORRENTIA MENSUAL EN
mm. DICIEMBRE
2.60
2.08
1.56
1.04
0.52
0.00

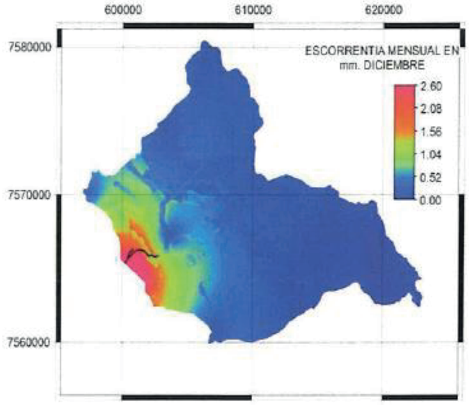
600000
610000
620000
7580000
7570000
7560000
ESCORRENTIA MENSUAL EN
mm. DICIEMBRE
2.60
2.08
1.56
1.04
0.52
0.00

ANNEX C.3.

Monthly maps of potential evaporation (in mm)

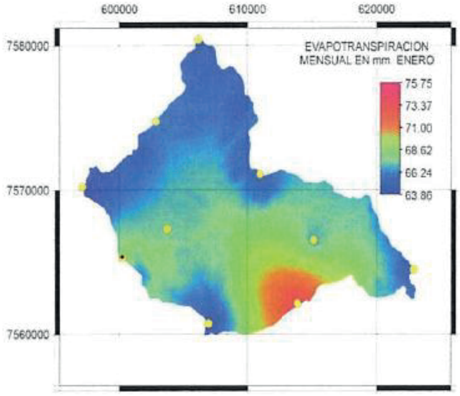
600000
610000
620000
7580000
7570000
7560000
EVAPOTRANSPIRACION
MENSUAL EN mm. ENERO
75.75
73.37
71.00
68.62
66.24
63.86

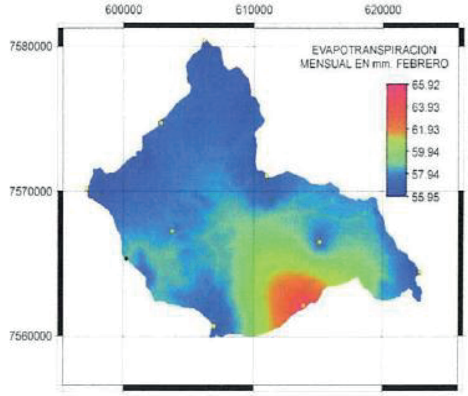
600000
610000
620000
7580000
7570000
7560000
EVAPOTRANSPIRACION
MENSUAL EN mm. FEBRERO
65.92
63.93
61.93
59.94
57.94
55.95

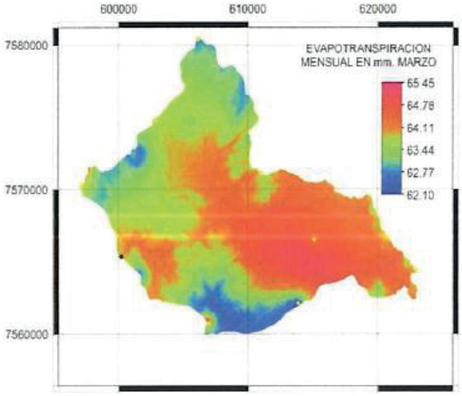
600000
610000
620000
7580000
7570000
7560000
EVAPOTRANSPIRACION
MENSUAL EN mm. MARZO
65.45
64.78
64.11
63.44
62.77
62.10

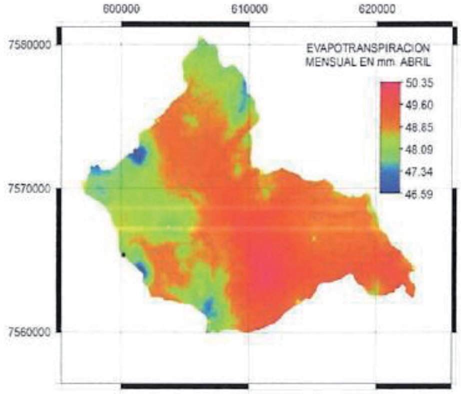
600000
610000
620000
7580000
7570000
7560000
EVAPOTRANSPIRACION
MENSUAL EN mm. ABRIL
50.35
49.60
48.85
48.09
47.34
46.59

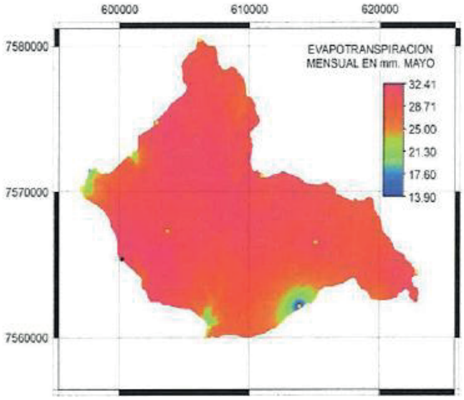
600000
610000
620000
7580000
7570000
7560000
EVAPOTRANSPIRACION
MENSUAL EN mm. MAYO
32.41
28.71
25.00
21.30
17.60
13.90

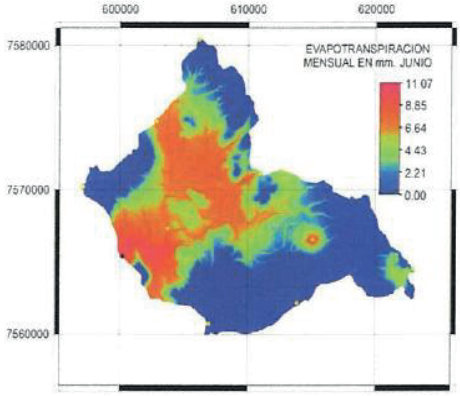
600000
610000
620000
7580000
7570000
7560000
EVAPOTRANSPIRACION
MENSUAL EN mm. JUNIO
11.07
8.85
6.64
4.43
2.21
0.00

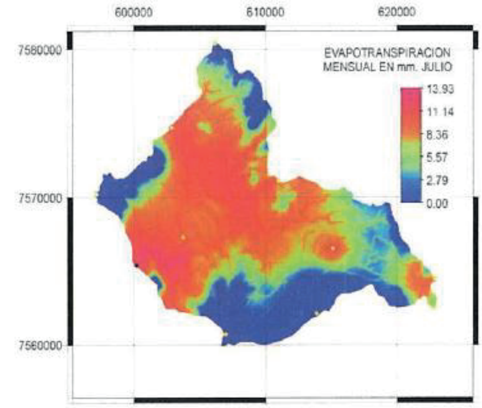
EVAPOTRANSPIRACION
MENSUAL EN mm. JULIO
13.93
11.14
8.36
5.57
2.79
0.00
600000
610000
620000
7580000
7570000
7560000

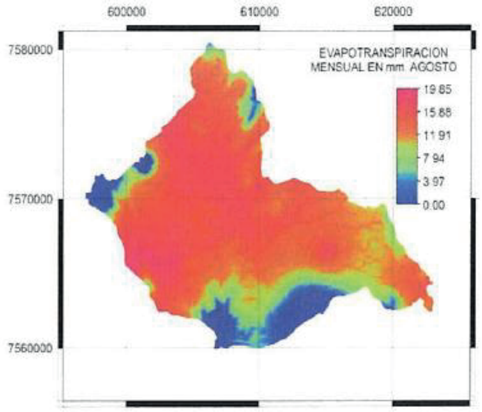
EVAPOTRANSPIRACION
MENSUAL EN mm. AGOSTO
19.85
15.88
11.91
7.94
3.97
0.00
600000
610000
620000
7580000
7570000
7560000

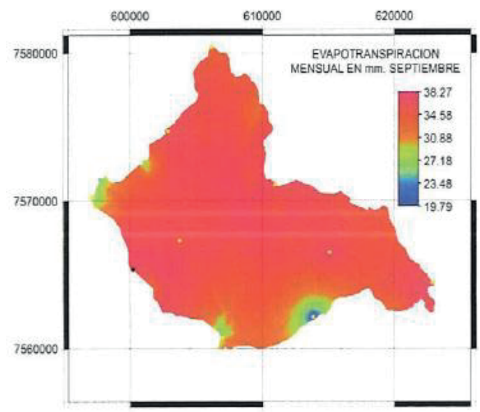
EVAPOTRANSPIRACION
MENSUAL EN mm. SEPTIEMBRE
38.27
34.58
30.88
27.18
23.48
19.79
600000
610000
620000
7580000
7570000
7560000

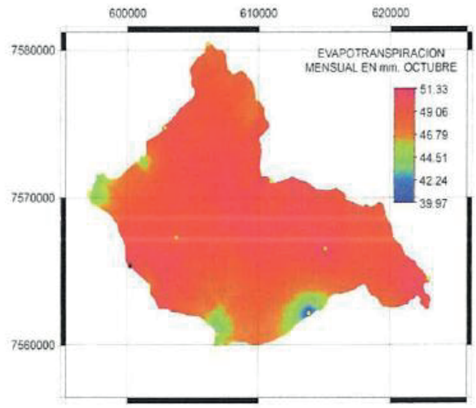
EVAPOTRANSPIRACION
MENSUAL EN mm. OCTUBRE
51.33
49.06
46.79
44.51
42.24
39.97
600000
610000
620000
7580000
7570000
7560000

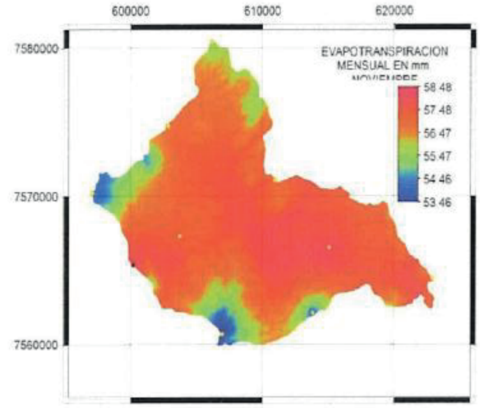
EVAPOTRANSPIRACION
MENSUAL EN mm
58.48
57.48
56.47
55.47
54.46
53.46
600000
610000
620000
7580000
7570000
7560000

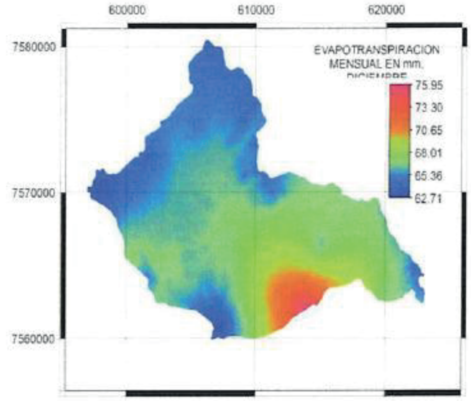
EVAPOTRANSPIRACION
MENSUAL EN mm.
75.95
73.30
70.65
68.01
65.36
62.71
600000
610000
620000
7580000
7570000
7560000

ANNEX C.4.

Map of annual water supply (mm / year)

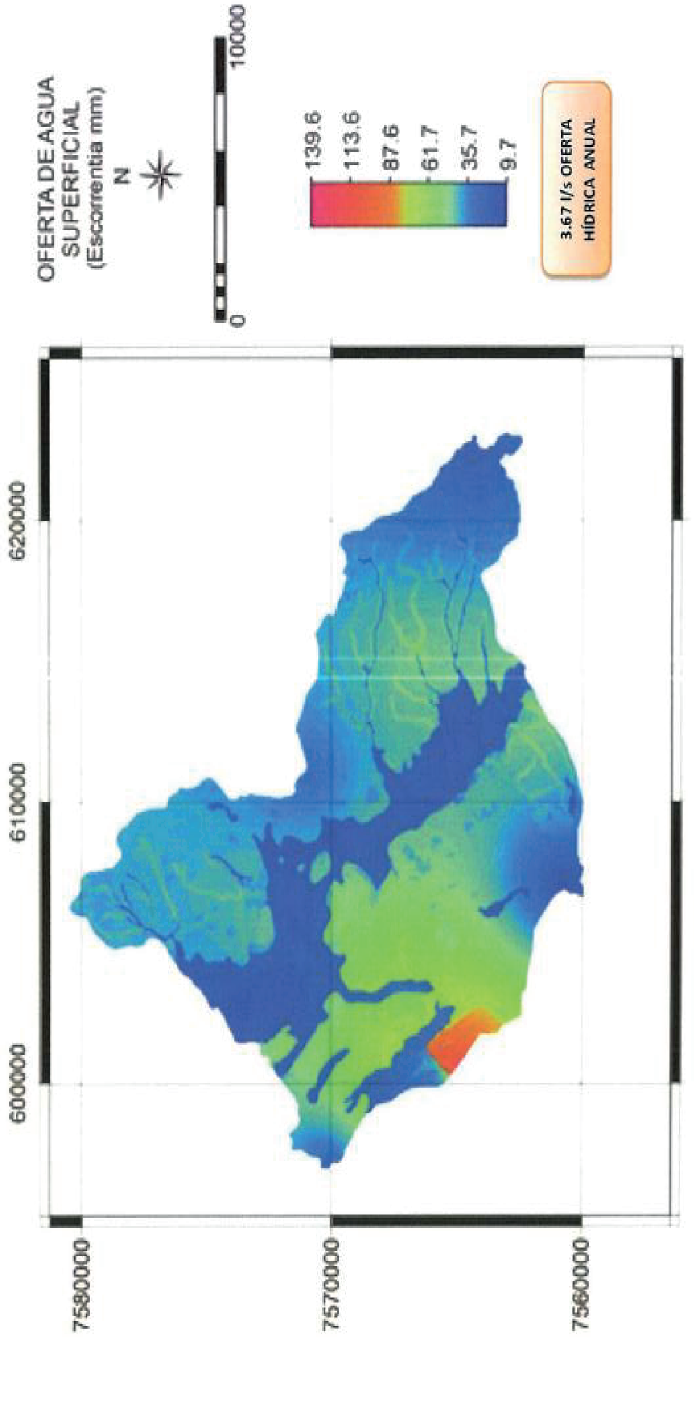

OFERTA DE AGUA SUPERFICIAL (Escorrentia mm)
N
0
10000
139.6
113.6
87.6
61.7
35.7
9.7
3.67 l/s OFERTA HÍDRICA ANUAL
600000
6100000
6200000
7580000
7570000
7560000

ANNEX D.

HYDROCHEMISTRY

ANNEX D.1.

LABORATORY CERTIFICATES

TOMAS FRIAS AUTONOMOUS UNIVERSITY

GEOLOGICAL ENGINEERING FACULTY

POTOSI – BOLIVIA

N° 001132

GEOCHEMICAL LABORATORY

ANALYSIS CERTIFICATE

Requested by: Project: Silala Springs (Research Institute)

N°	**ORIGIN AND DETAIL**				**LAWS**
PARAMETER	**UNIT**	**SI – N° 01**	**SI – N° 02**	**SI – N° 03**	
Bicarbonate	mg/l				
Carbonate	mg/l				
Chloride	mg/l				
Nitrite	mg/l				
Nitrate	mg/l				
Sulfate	mg/l				
pH					
Conductivity	uS/cm				
Temperature	°C				
Suspended Sol.	mg/l				
Dissolved Sol.	mg/l				
Total Sol.	mg/l				
Calcium	mg/l				
Magnesium	mg/l				
Sodium	mg/l				
Potassium	mg/l				
**					
SI – N° 01	Silala; 16:30; 22/09/17				
SI – N° 02	Silala; 17:30; 22/09/17				
SI – N° 03	Silala; 18:30; 22/09/17				

Note.- Water sampling carried out by Eng. Juan Carlos Erquicia. Reception in the laboratory on 11/26/17 at 4:30 p.m.

Potosi, 29 January 2018

CENTRO DE INVESTIGACION MINERO Y AMBIENTAL "CIMA-JICA-UATF"
Departamento de Análisis Químico "D A Q"
ANALISIS QUIMICO - BACTERIOLOGICO: AGUAS, SUELOS, SEDIMENTOS y MINERALES

1-1

INFORME DE RESULTADOS

Nº:	255	Fecha Recepción:	2016-12-07		Fecha de Entrega	2017-01-13

ATOS DEL CLIENTE:

mbre/Razón social	Ing. Juan C. Erquicia		
rección	-------	Teléfono/Fax	
rsona de contacto	Ing. Juan Carlos ERQUICIA		

ATOS DE LA MUESTRA:

ocedencia:	SILALA				
po de Muestra:	agua	Fecha de Muestreo		Hora	
uestreado por :	Cliente:				

RESULTADOS: DE AGUA

Parámetros		Manganeso	Hierro	Sodio	Potasio	Calcio	Magnesio
Límite de detección del método		0,02	0,07	0,05	0,01	0,1	0,05
Unidad		mg/L	mg/L	mg/L	mg/L	mg/L	mg/L
Método Estándar Aplicado		JISK0102 56.2	JISK0102 57.2	JISK0102 48.3	JISK0102 49.3	JISK0102 50	JISK0102 51
Método ó técnica de ensayo		A.A. Llama Normal	A.A. Llama Normal	Cromatografía Iónica	Cromatografía Iónica	Cromatografía Iónica	Cromatografía Iónica
Fecha Ensayo		2017-01-12	2017-01-12	2017-01-12	2017-01-12	2017-01-12	2017-01-12
Cod. Laboratorio	Cod. Original						
UAQ_1_255_1	M-1	<0,02	<0,07	334,3	35,6	21,03	26,15

ERVACIONES Y CONCLUSIONES:

El presente informe, es el resultado del análisis químico de la muestra de agua

Lic. Elena UÑO UÑO
RESPONSABLE DAQ

DIRECTOR "CIMA-UATF"
Ing. Franz T. ...
DIRECTOR CIMA -UATF
Universidad Autónoma Tomás Frías

JICA
C.I.M.A.
U.A.T.F.
Potosí - Bolivia

Si el laboratorio no realizó el muestreo, no es responsable de la preservación, transporte y representatividad de la muestra. El almacenamiento de las muestras es de 3 meses

esq. Villazon s/n. Edificio Facultad de Ingeniería Minera bloque 1. Segundo piso Teléfono/fax 62-29711 E-Mail: cima_uatf@yahoo.es

TOMAS FRIAS AUTONOMOUS UNIVERSITY
FACULTY OF AGRICULTURAL SCIENCES AND LIVESTOCK
AGRONOMIC ENGINEERING MAJOR
CHEMICAL ANALYSIS LABORATORY: SOILS, WATER AND BROMATOLOGICAL

RESULTS REPORT

RECEPTION DATE	2 December 2016
DELIVERY DATE	28 March 2017

CLIENT INFORMATION:

Name	Eng. Jorge Diaz
Survey Title	CHARACTERIZATION OF THE SILALA SPRINGS
Telephone	

SAMPLE INFORMATION:

Analysis Type	Soil
Sample N°	1
Department	Potosi
Province	South Lipez
Municipality	San Pablo de Lipez
Community	Quetena
Sampling Date	23 October 2016
Sampling Time	09:25 am

Physical Analysis of the Soil

ORIGINAL CODE	PARAMETER	UNIT	HUMIDITY	METHOD
Ssee-SUE01	Humidity	%	3.788	Gravimetry
	Bulk density	g/cc	1.455	Gravimetry
	Sand	%	40.3	Gravimetry
	Silt		55.8	
	Clay		3.9	
	Texture	%	Silt-Loamy	

Lic. Roxana Careaga Tapia
Head of the Soil Chemical Laboratory

TOMAS FRIAS AUTONOMOUS UNIVERSITY
FACULTY OF AGRICULTURAL SCIENCES AND LIVESTOCK
AGRONOMIC ENGINEERING MAJOR
CHEMICAL ANALYSIS LABORATORY: SOILS, WATER AND BROMATOLOGICAL

RESULTS REPORT

RECEPTION DATE	2 December 2016
DELIVERY DATE	28 March 2017

CLIENT INFORMATION:

Name	Eng. Jorge Diaz
Survey Title	CHARACTERIZATION OF THE SILALA SPRINGS
Telephone	

SAMPLE INFORMATION:

Analysis Type	Soil
Sample N°	2
Department	Potosi
Province	South Lipez
Municipality	San Pablo de Lipez
Community	Quetena
Sampling Date	23 October 2016
Sampling Time	10:50 am

Physical Analysis of the Soil

ORIGINAL CODE	PARAMETER	UNIT	HUMIDITY	METHOD
Ssee-SUE02	Humidity	%	0.423	Gravimetry
	Bulk density	g/cc	1.454	Gravimetry
	Sand	%	44.4	Gravimetry
	Silt		54.2	
	Clay		1.4	
	Texture	%	Silt-Loamy	Gravimetry

Lic. Roxana Careaga Tapia
Head of the Soil Chemical Laboratory

TOMAS FRIAS AUTONOMOUS UNIVERSITY
FACULTY OF AGRICULTURAL SCIENCES AND LIVESTOCK
AGRONOMIC ENGINEERING MAJOR
CHEMICAL ANALYSIS LABORATORY: SOILS, WATER AND BROMATOLOGICAL

RESULTS REPORT

RECEPTION DATE	2 December 2016
DELIVERY DATE	28 March 2017

CLIENT INFORMATION:

Name	Eng. Jorge Diaz
Survey Title	CHARACTERIZATION OF THE SILALA SPRINGS
Telephone	

SAMPLE INFORMATION:

Analysis Type	Soil
Sample N°	3
Department	Potosi
Province	South Lipez
Municipality	San Pablo de Lipez
Community	Quetena
Sampling Date	24 October 2016
Sampling Time	12:43

Physical Analysis of the Soil

ORIGINAL CODE	PARAMETER	UNIT	HUMIDITY	METHOD
Ssee-SUE02	Humidity	%	0.447	Gravimetry
	Bulk density	g/cc	1.463	Gravimetry
	Sand	%	24.6	Gravimetry
	Silt		73.7	
	Clay		1.7	
	Texture	%	Silt-Loamy	Gravimetry

Lic. Roxana Careaga Tapia
Head of the Soil Chemical Laboratory

TOMAS FRIAS AUTONOMOUS UNIVERSITY
FACULTY OF AGRICULTURAL SCIENCES AND LIVESTOCK
AGRONOMIC ENGINEERING MAJOR
CHEMICAL ANALYSIS LABORATORY: SOILS, WATER AND BROMATOLOGICAL

RESULTS REPORT

RECEPTION DATE	2 December 2016
DELIVERY DATE	28 March 2017

CLIENT INFORMATION:

Name	Eng. Jorge Diaz
Survey Title	CHARACTERIZATION OF THE SILALA SPRINGS
Telephone	

SAMPLE INFORMATION:

Analysis Type	Soil
Sample N°	4
Department	Potosi
Province	South Lipez
Municipality	San Pablo de Lipez
Community	Quetena
Sampling Date	24 October 2016
Sampling Time	14:42

Physical Analysis of the Soil

ORIGINAL CODE	PARAMETER	UNIT	HUMIDITY	METHOD
Ssee-SUE02	Humidity	%	57.504	Gravimetry
	Bulk density	g/cc	0.596	Gravimetry
	Sand	%	20.1	Gravimetry
	Silt		60.3	
	Clay		19.6	
	Texture	%	Silt-Loamy	Gravimetry

Lic. Roxana Careaga Tapia
Head of the Soil Chemical Laboratory

ANNEX D.2

Sampling Points

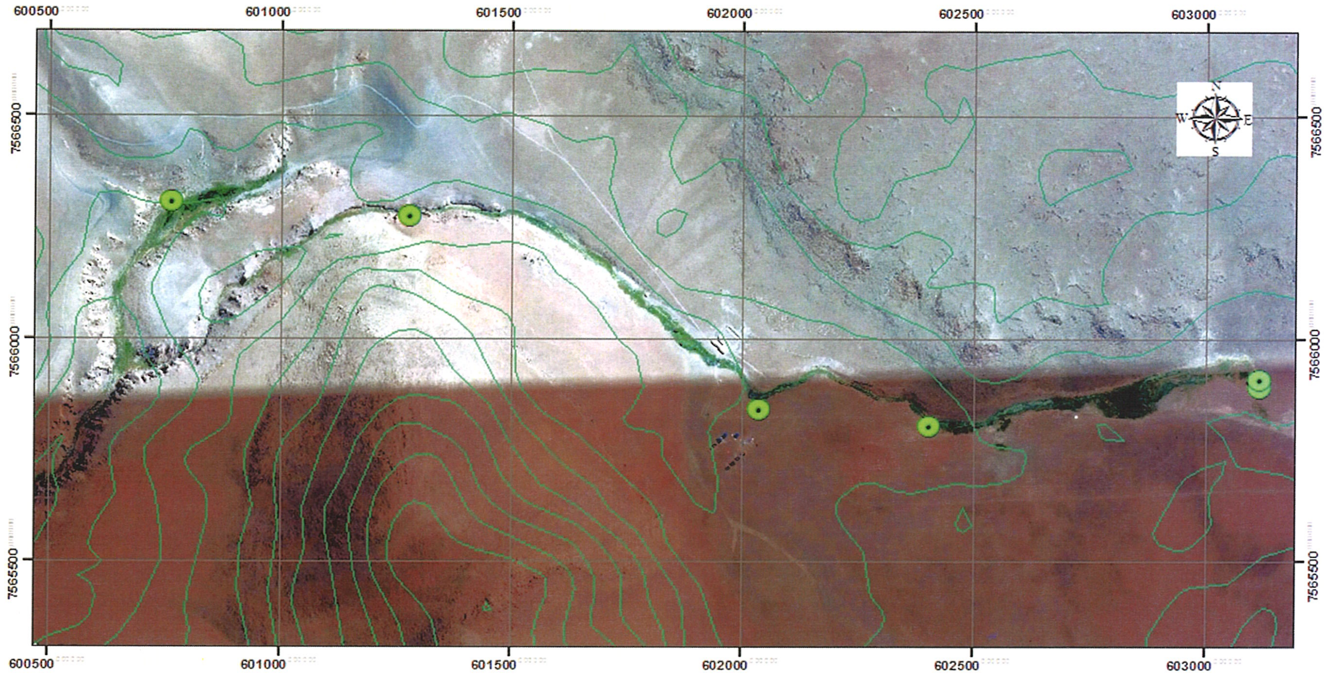

Referencias

- Puntos de muestreo de Agua
- Curvas de nivel

1:11.000

0 130 260 520 780 1.040 m

UNIVERSIDAD AUTÓNOMA TOMÁS FRÍAS
FACULTAD DE INGENIERÍA GEOLÓGICA
INSTITUTO DE INVESTIGACIÓN GEOLÓGICO - AMBIENTAL

PROYECTO CARACTERIZACIÓN HIDROGEOLÓGICA DE LOS MANANTIALES DEL SILALA

PUNTOS DE MUESTREO DE AGUAS

Realizado:	Inv. Mauricio Jh. Casanova V.	Escala: 1:11000	D1/1
Director I.G.M.A.:	Ing. Juan Carlos Erquicia L.		
Vo. Bo. Vicerrector U.A.T.F.:	Dr. Ing. Pedro López Cortés	Fecha: Julio/2017	

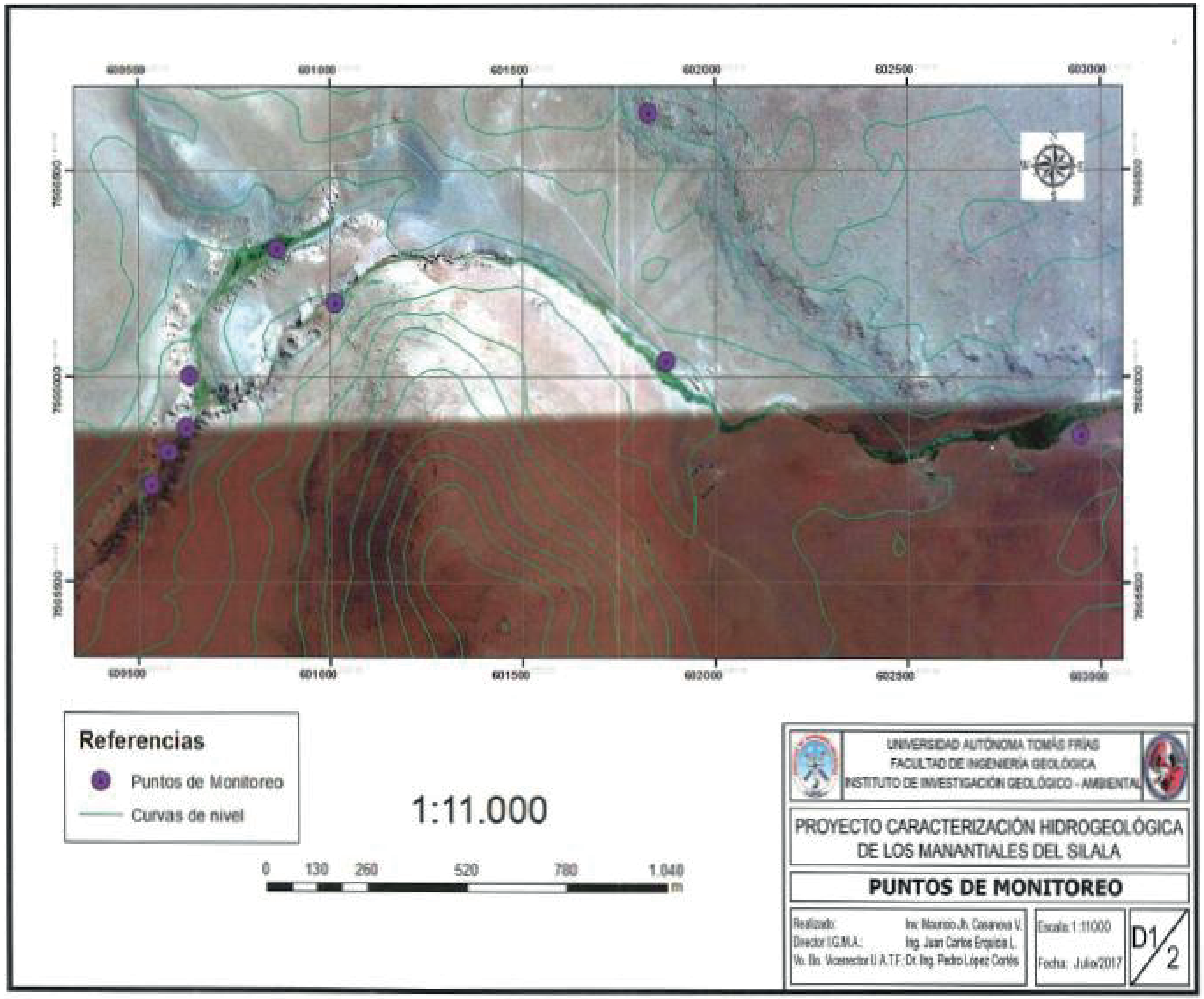
600500
601000
601500
602000
602500
603000
7566500
7566000
7565500
Referencias
Puntos de Monitoreo
Curvas de nivel
1:11.000
0 130 260 520 780 1.040 m
UNIVERSIDAD AUTÓNOMA TOMÁS FRÍAS
FACULTAD DE INGENIERÍA GEOLÓGICA
INSTITUTO DE INVESTIGACIÓN GEOLÓGICO - AMBIENTAL
PROYECTO CARACTERIZACIÓN HIDROGEOLÓGICA DE LOS MANANTIALES DEL SILALA
PUNTOS DE MONITOREO
Realizado: Inv. Mauricio Jh. Casanova V.
Director I.G.M.A.: Ing. Juan Carlos Enquica L.
Vo. Bo. Vicerector U.A.T.F.: Dr. Ing. Pedro López Cortés
Escala: 1:11000
Fecha: Julio/2017
D1/2

ANNEX D.3.

ANOMALIES MAPS

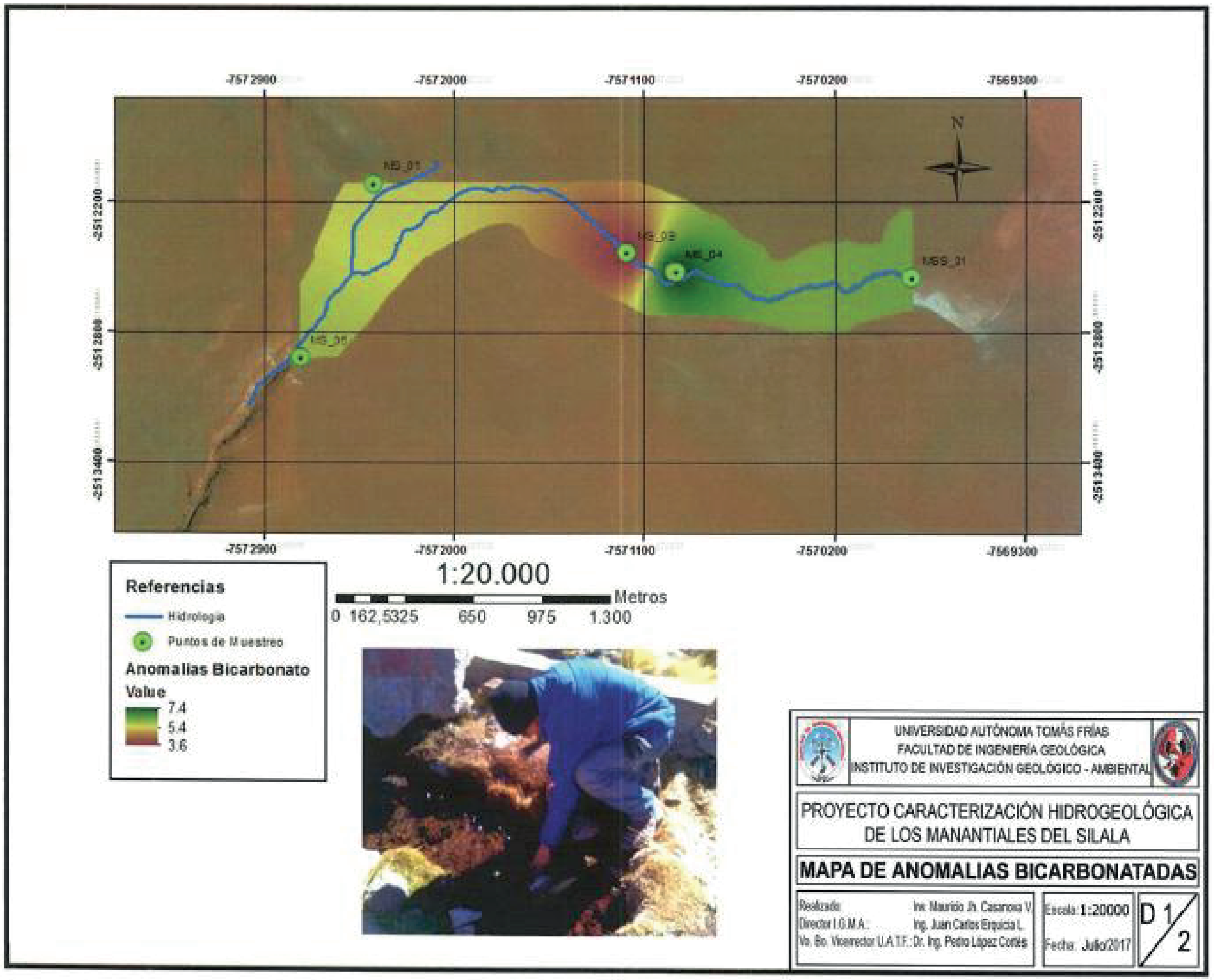
-757 2900
-757 2000
-757 1100
-7570200
-7569300
-2512200
-2512800
-2513400
N
MS_01
MS_03
MS_04
MSS_01
MS_05
Referencias
Hidrología
Puntos de Muestreo
Anomalías Bicarbonato
Value
7.4
5.4
3.6
1:20.000
Metros
0 162,5325 650 975 1.300
UNIVERSIDAD AUTÓNOMA TOMÁS FRÍAS
FACULTAD DE INGENIERÍA GEOLÓGICA
INSTITUTO DE INVESTIGACIÓN GEOLÓGICO - AMBIENTAL
PROYECTO CARACTERIZACIÓN HIDROGEOLÓGICA DE LOS MANANTIALES DEL SILALA
MAPA DE ANOMALIAS BICARBONATADAS
Realizado: Inv. Mauricio Jh. Casanova V.
Director I.G.M.A.: Ing. Juan Carlos Ezquicia L.
Vo. Bo. Vicerrector U.A.T.F.: Dr. Ing. Pedro López Cortés
Escala: 1:20000
Fecha: Julio/2017
D 1/2

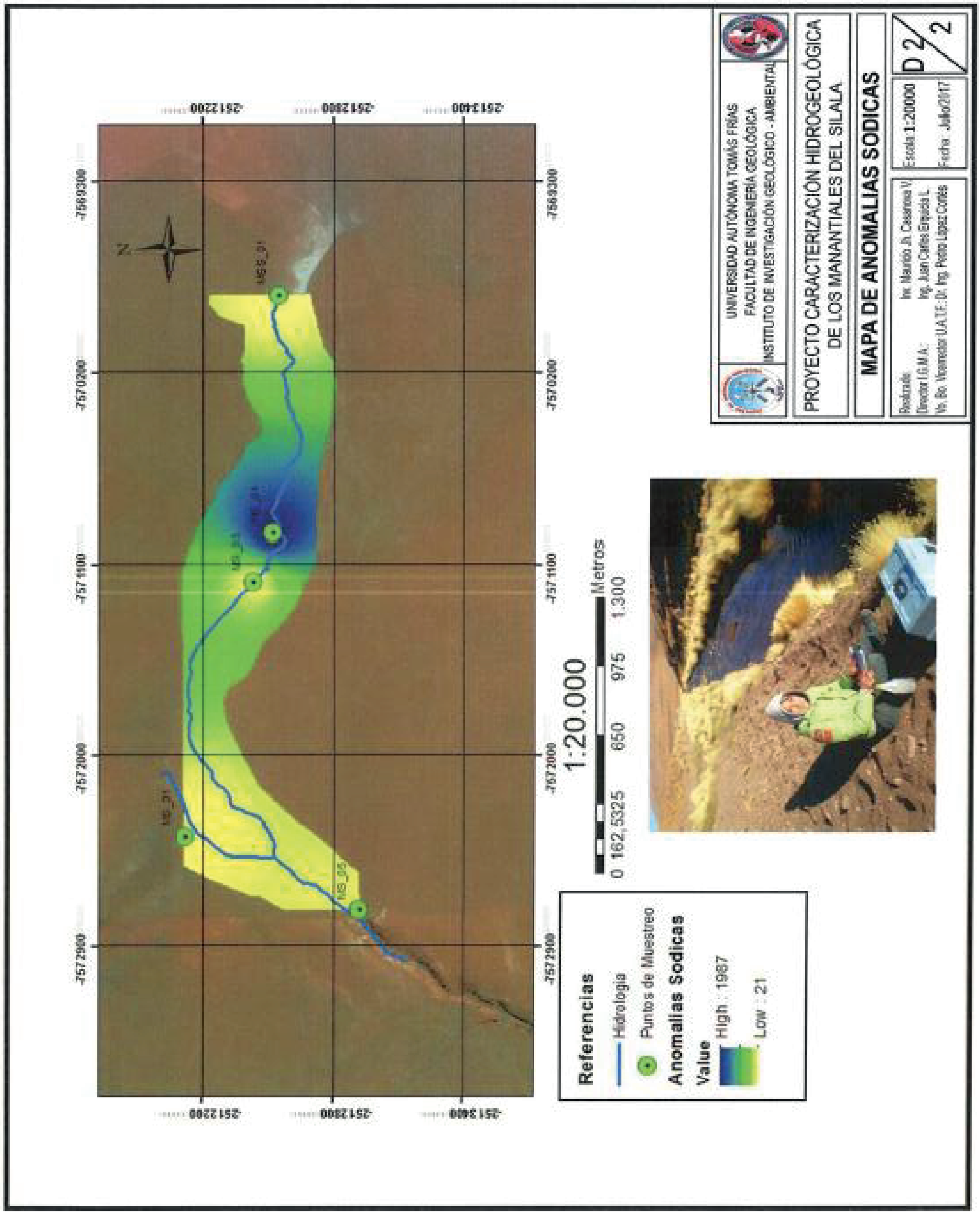
UNIVERSIDAD AUTÓNOMA TOMÁS FRÍAS
FACULTAD DE INGENIERÍA GEOLÓGICA
INSTITUTO DE INVESTIGACIÓN GEOLÓGICO - AMBIENTAL
PROYECTO CARACTERIZACIÓN HIDROGEOLÓGICA DE LOS MANANTIALES DEL SILALA
MAPA DE ANOMALIAS SODICAS
Realizado: Inv. Mauricio Jh. Casanova V.
Director I.G.M.A.: Ing. Juan Carlos Enríquez L.
Vo. Bo. Vicerrector U.A.T.F.: Dr. Ing. Pedro López Cortés
Escala: 1:20000
Fecha: Julio/2017
D 2/2
Referencias
Hidrología
Puntos de Muestreo
Anomalías Sodicas
Value
High : 1987
Low : 21
1:20.000
0 162,5325 650 975 1.300
Metros
-7572900
-7572000
-7571100
-7570200
-7569300
-2512200
-2512800
-2513400

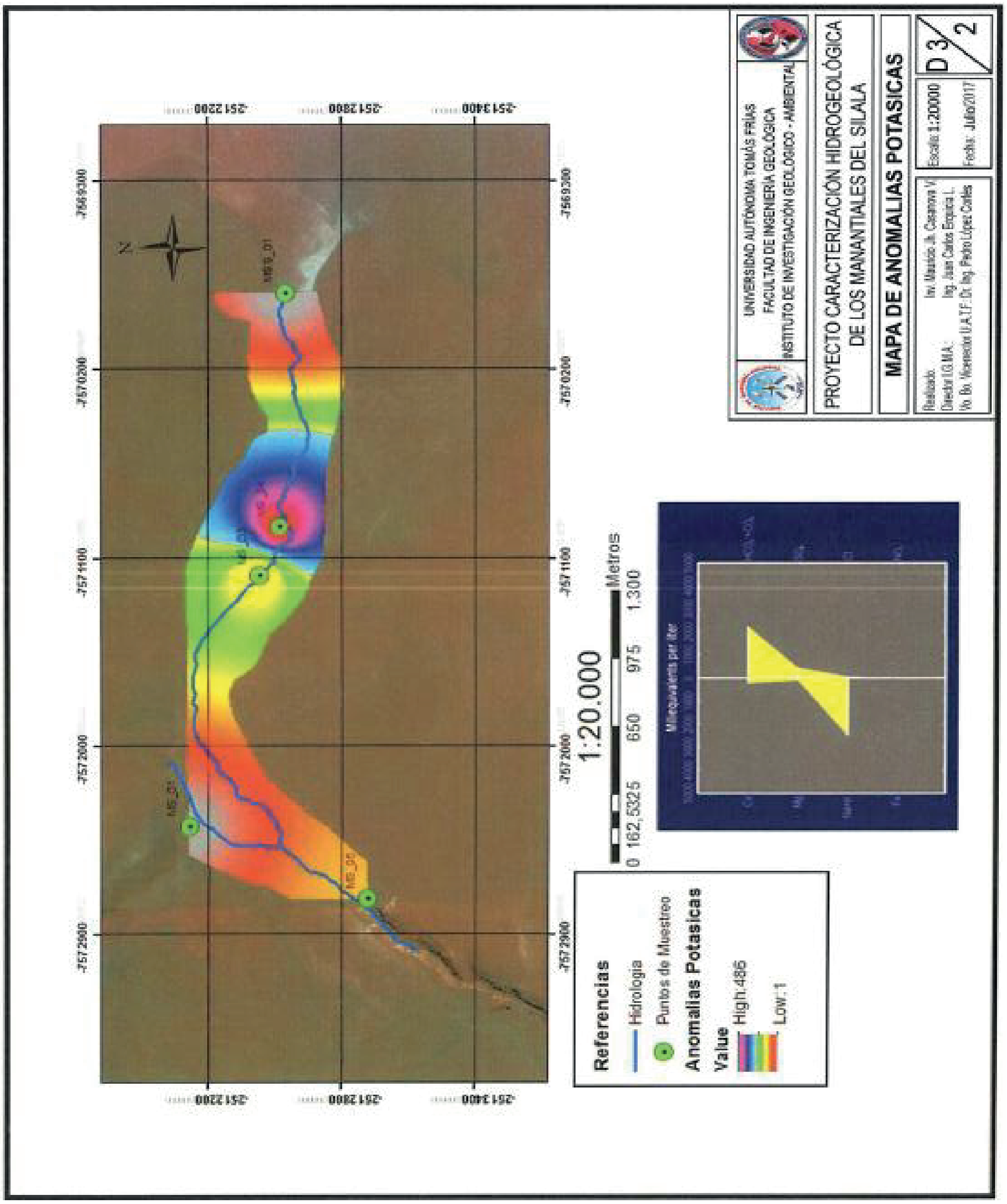
UNIVERSIDAD AUTÓNOMA TOMÁS FRÍAS
FACULTAD DE INGENIERÍA GEOLÓGICA
INSTITUTO DE INVESTIGACIÓN GEOLÓGICO - AMBIENTAL
PROYECTO CARACTERIZACIÓN HIDROGEOLÓGICA DE LOS MANANTIALES DEL SILALA
MAPA DE ANOMALIAS POTASICAS
Realizado: Inv. Mauricio Jh. Casanova V.
Director I.G.M.A.: Ing. Juan Carlos Enriquez L.
Vo. Bo. Vicerector U.A.T.F.: Dr. Ing. Pedro López Cortés
Escala: 1:20000
Fecha: Julio/2017
D 3 / 2
Referencias
Hidrologia
Puntos de Muestreo
Anomalias Potasicas
Value
High:486
Low:1
1:20,000
0 162,5325 650 975 1.300 Metros
N
-7572900
-7572000
-7571100
-7570200
-7569300
-2512200
-2512800
-2513400

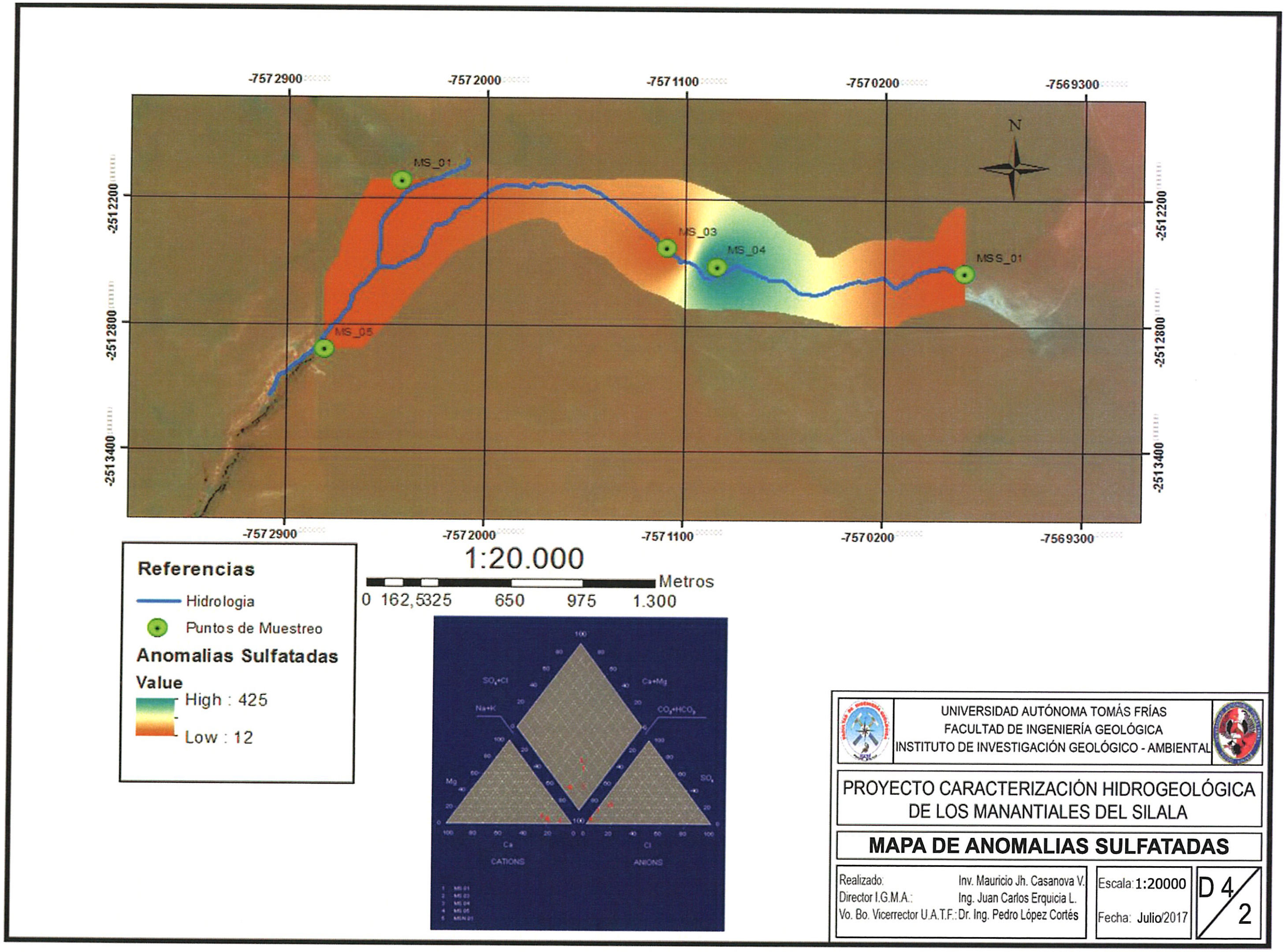
-7572900
-7572000
-7571100
-7570200
-7569300
-2512200
-2512800
-2513400
N
MS_01
MS_03
MS_04
MSS_01
MS_05
Referencias
Hidrologia
Puntos de Muestreo
Anomalias Sulfatadas
Value
High : 425
Low : 12
1:20.000
0 162,5325 650 975 1.300 Metros
SO4+Cl
Ca+Mg
Na+K
CO3+HCO3
Mg
SO4
Ca
Cl
CATIONS
ANIONS
UNIVERSIDAD AUTÓNOMA TOMÁS FRÍAS
FACULTAD DE INGENIERÍA GEOLÓGICA
INSTITUTO DE INVESTIGACIÓN GEOLÓGICO - AMBIENTAL
PROYECTO CARACTERIZACIÓN HIDROGEOLÓGICA
DE LOS MANANTIALES DEL SILALA
MAPA DE ANOMALIAS SULFATADAS
Realizado: Inv. Mauricio Jh. Casanova V.
Director I.G.M.A.: Ing. Juan Carlos Erquicia L.
Vo. Bo. Vicerrector U.A.T.F.: Dr. Ing. Pedro López Cortés
Escala: 1:20000
Fecha: Julio/2017
D 4/2

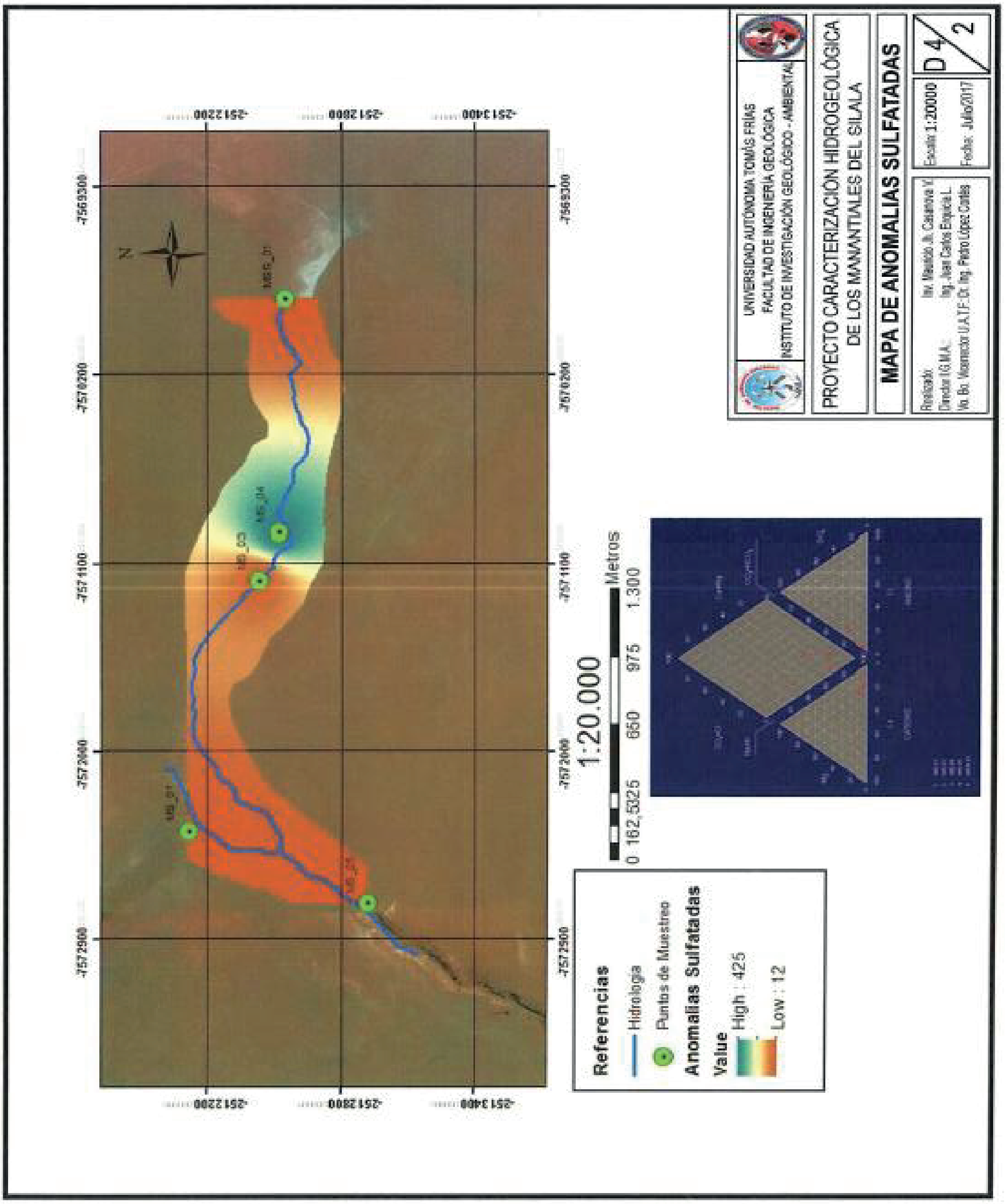
UNIVERSIDAD AUTÓNOMA TOMÁS FRÍAS
FACULTAD DE INGENIERÍA GEOLÓGICA
INSTITUTO DE INVESTIGACIÓN GEOLÓGICO - AMBIENTAL
PROYECTO CARACTERIZACIÓN HIDROGEOLÓGICA DE LOS MANANTIALES DEL SILALA
MAPA DE ANOMALIAS SULFATADAS
Escala: 1:20000
Fecha: Julio/2017
D 4
2
Referencias
Hidrología
Puntos de Muestreo
Anomalias Sulfatadas
Value
High : 425
Low : 12
1:20.000
0 162,5325 650 975 1.300
Metros
N
MS_01
MS_02
MS_03
MS_04
-7572900
-7572000
-7571100
-7570200
-7569300
-2512200
-2512800
-2513400

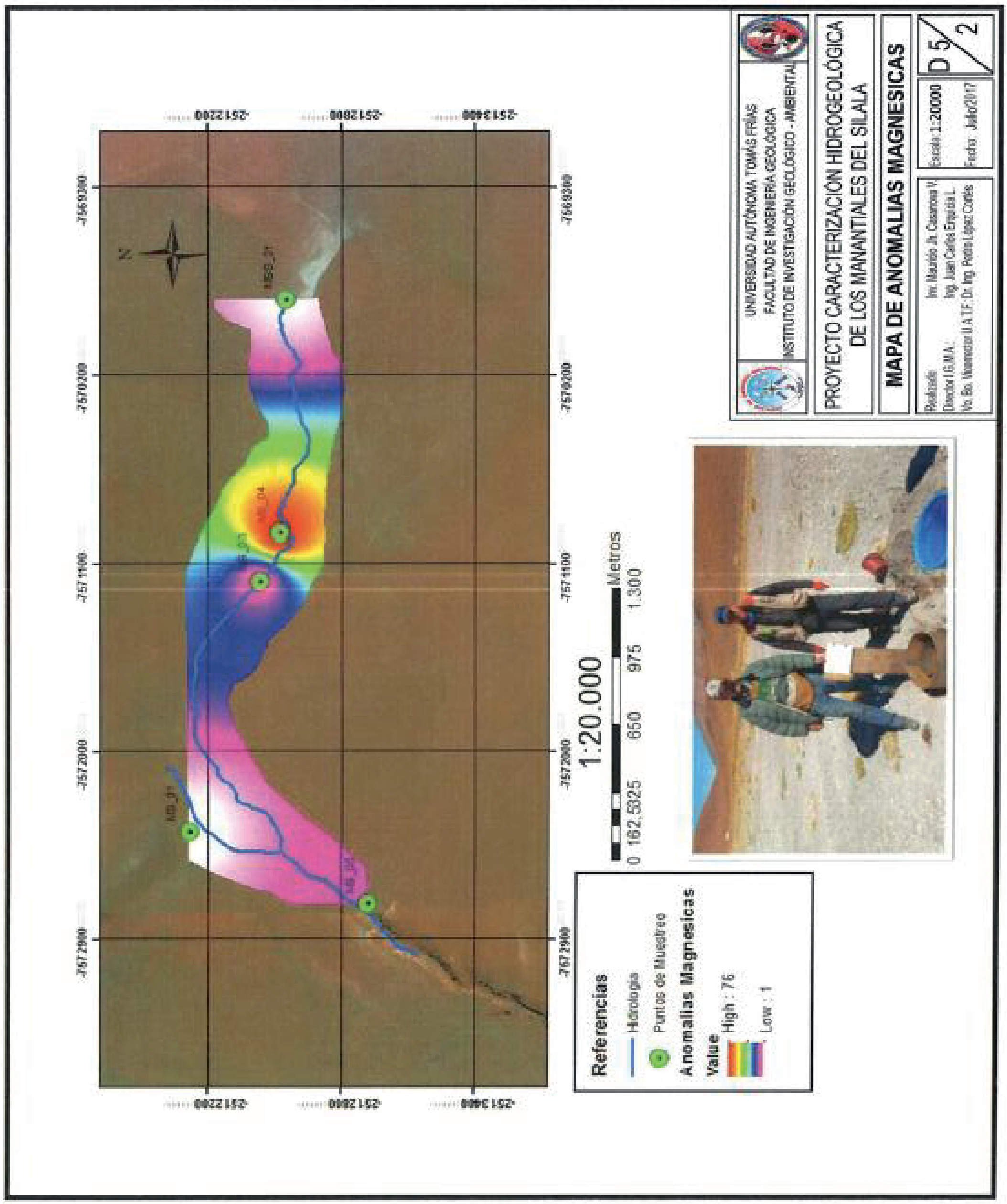

UNIVERSIDAD AUTÓNOMA TOMÁS FRÍAS
FACULTAD DE INGENIERÍA GEOLÓGICA
INSTITUTO DE INVESTIGACIÓN GEOLÓGICO - AMBIENTAL
PROYECTO CARACTERIZACIÓN HIDROGEOLÓGICA DE LOS MANANTIALES DEL SILALA
MAPA DE ANOMALIAS MAGNESICAS
Escala: 1:20000
Fecha: Julio/2017
D 5
2
Referencias
Hidrologia
Puntos de Muestreo
Anomalias Magnesicas
Value
High : 76
Low : 1
1:20.000
0 162.5325 650 975 1.300
Metros
N

ANNEX D.4.

PHOTOGRAPHIC REPORT

Photograph N° 1

Obtaining Infiltration Test Data

Photograph N° 2

Base point for obtaining Infiltration Data

Photograph N° 3

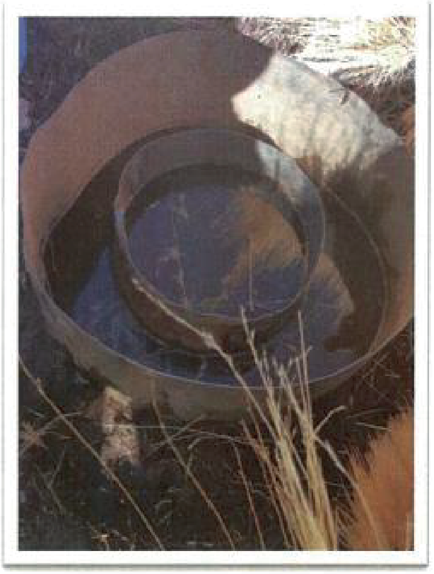

Infiltration Tests by the Double Ring Method

Photograph N° 4

Infiltration Velocity Test.

Photograph N° 5

Performance of Permeability Tests on the Substrate

Photograph N° 6

Settling of the PVC Tube for the Permeability Test

Photograph N° 7

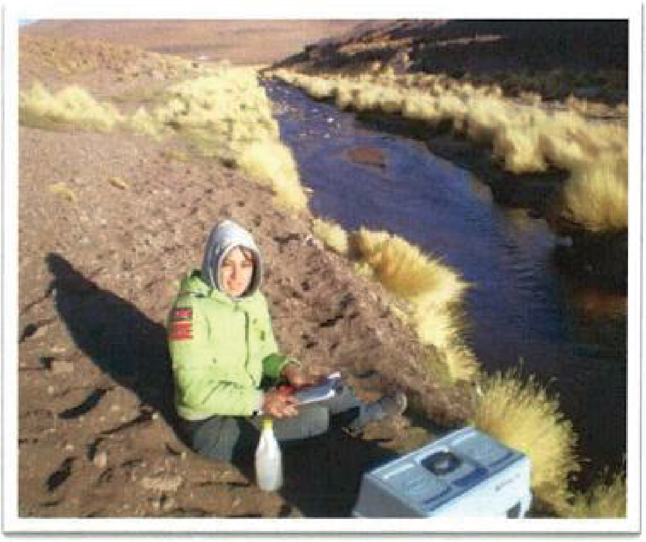

Obtaining water parameters through the Multi-parameter Team

Photograph N° 8

Runoff from the springs from SEE - Measurement of Physicochemical Parameters

Photograph N° 9

Soil Sampling

Photograph N° 10

Measurement of the root depth of plants

Photograph N° 11

UATF-FAC Working Brigade of Geological Engineering in the Silala Springs

ANNEX E.

HYDROGEOLOGY

ANNEX E.1.

INFILTRATION TESTS

INFILTRATION TEST OF INFILTROMETER RINGS

SILALA WELL: Snww INF04
Coordinates: E: 600767,571
N: 7566500,704
Height: 4394.67 m.a.s.l.

TIME (min)	Partial Sheet (mm)	Infiltration Velocity (mm/min)	Accumulated Time (min)	Accumulated Sheet (mm)
0	0		0	0
0,5	2	4	0,5	2
0,5	1,4	2,8	1	3,4
0,5	1,1	2,2	1,5	4,5
0,5	1	2	2	5,5
0,5	1	2	2,5	6,5
0,5	1	2	3	7,5
0,5	0,9	1,8	3,5	8,4
0,5	0,9	1,8	4	9,3
0,5	0,8	1,6	4,5	10,1
0,5	0,7	1,4	5	10,8

Accumulated Time	Infiltration Velocity (mm/min)			
0		m=	-0,417	
0,5	4	b=	3,3067	
1	2,8	t=	5	
1,5	2,2	KOSTIAKOV MODEL		
2	2	Instant infiltration velocity	I=	b*T (m)
2,5	2		I=	3.3067*(5-0.417)
3	2		I=	1.6901 mm/min
3,5	1,8			
4	1,8			
4,5	1,6			
5	1,4			

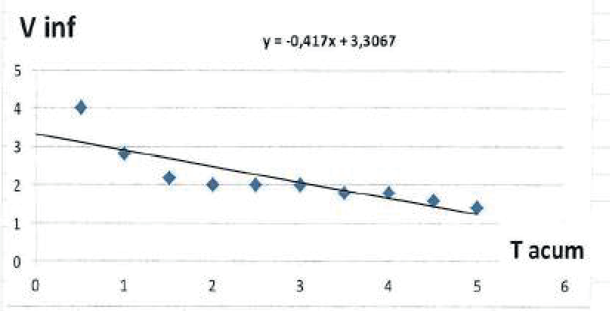

INFILTRATION TEST OF INFILTROMETER RINGS

SILALA WELL: Ssee INF01
Coordinates: E: 603064
N: 7566812
Height: 4416

TIME (min)	Partial Sheet (mm)	Infiltration Velocity (mm/min)	Accumulated Time (min)	Accumulated Sheet (mm)
0	0		0	0
0,5	0,7	1,4	0,5	1,7
0,5	0,3	0,6	1	1
0,5	1	2	1,5	2
0,5	0,5	1	2	2,5
0,5	0,5	1	2,5	3
0,5	0,7	1,4	3	3,7
0,5	0,3	0,6	3,5	4
0,5	1,4	2,8	4	5,4
0,5	0,8	1,6	4,5	6,2

Accumulated Time	Infiltration Velocity (mm/min)			
0		m=	-0,417	
0,5	1,4	b=	3,3067	
1	0,6	t=	5	
1,5	2	KOSTIAKOV MODEL		
2	1	Instant infiltration velocity	I=	b*T (m)
2,5	1		I=	3.3067*(5-0.417)
3	1,4		I=	1.6901 mm/min
3,5	0,6			
4	2,8			
4,5	1,6			

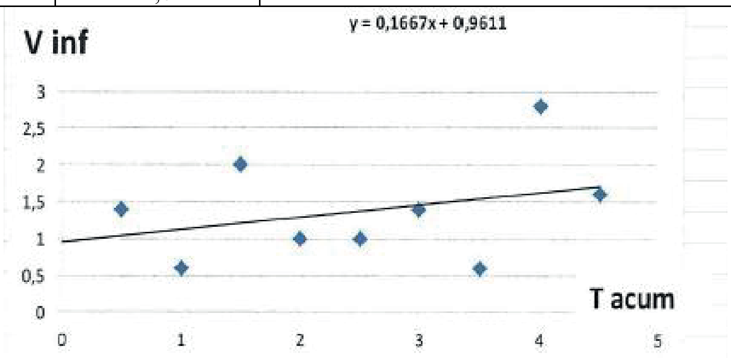

INFILTRATION TEST OF INFILTROMETER RINGS

SILALA WELL: Ssee INF02
Coordinates: E: 602988 602973
N: 7565669 7565834
Height: 442

TIME (min)	Partial Sheet (mm)	Infiltration Velocity (mm/min)	Accumulated Time (min)	Accumulated Sheet (mm)
0	0		0	0
0,5	0,4	0,8	0,5	0,4
0,5	0,3	0,6	1	0,7
0,5	0,2	0,4	1,5	0,9
0,5	0,3	0,6	2	1,2
0,5	0,3	0,6	2,5	1,5
0,5	0,2	0,4	3	1,7
0,5	0,3	0,6	3,5	2
0,5	0,3	0,6	4	2,3
0,5	0,2	0,4	4,5	2,5
0,5	0,2	0,4	5	2,7

Accumulated Time	Infiltration Velocity (mm/min)			
0		m=	-0,0509	
0,5	0,8	b=	0,068	
1	0,6	t=	5	
1,5	0,4	**KOSTIAKOV MODEL**		
2	0,6	Instant infiltration velocity	I=	b*T (m)
2,5	0,6		I=	3.3067*(5-0.417)
3	0,4		I=	**0.06265 mm/min**
3,5	0,6			
4	0,6			
4,5	0,4			
5	0,4			

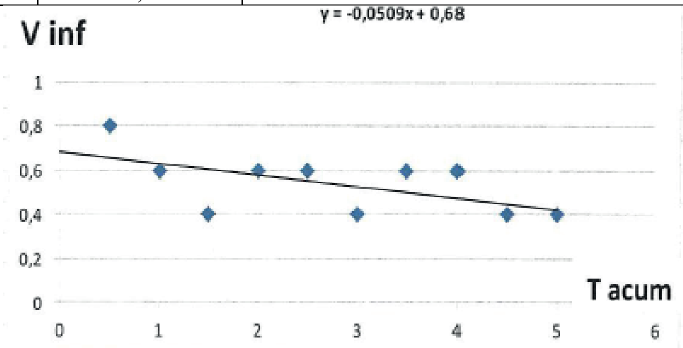

ANNEX E.2.

PERMEABILITY TESTS

PERMEABILITY TEST BY DESCENDING LEVEL

SILALA WELL: Ssee PERM03 Date: 26/Oct/2016

Coordinates: E: 603130,159

N: 7565778,9

Height: 4411,6 m.a.s.l.

$$k = \frac{\pi * D}{11(t2 - t1)} * \ln\left(\frac{h1}{h2}\right)$$

TIME (min)	Partial Sheet (mm)	Accumulated Time	Accumulated Sheet	(h1/h2)	Permeability (cm/min)
0	0,1	0	0,1	1,000	0,000
3	0,5	3	0,5	0,200	0,965
3	0,6	6	1,1	0,455	0,473
3	0,4	9	1,5	0,733	0,186
3	0,3	12	1,8	0,833	0,109
3	0,4	15	2,2	0,818	0,120
3	0,3	18	2,5	0,880	0,077
3	0,5	21	3	0,833	0,109
3	0,3	24	3,3	0,909	0,057
3	0,6	27	3,9	0,846	0,100
3	0,4	30	4,3	0,907	0,059
				Average=	**0,226**

Accumulated Time	Infiltration Velocity (mm/min)			
0	0,000	m=	-0,0139	
3	0,965	b=	0,4142	
6	0,473	t=	30	
9	0,186	**KOSTIAKOV MODEL**		
12	0,109	Instant infiltration velocity	I=	b*T (m)
15	0,120		I=	0.4142*(30-0.0139)
18	0,077		I=	**0.350 cm/min**
21	0,109			
24	0,057			
27	0,100			
30	0,059			

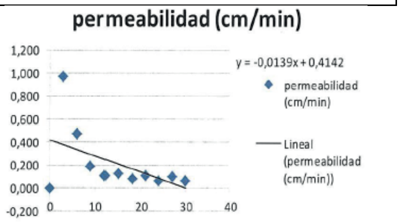

PERMEABILITY TEST BY DESCENDING LEVEL

SILALA WELL: Ssee PERM04 Date: 26/Oct/2016
Coordinates: E: 603115.502
N: 7565860.414
Height: 4410,2 m.a.s.l.

$$k = \frac{\pi * D}{11(t2 - t1)} * \ln\left(\frac{h1}{h2}\right)$$

TIME (min)	Partial Sheet (mm)	Accumulated Time	Accumulated Sheet	(h1/h2)	Permeability (cm/min)
0	0,1	0	0,1	1,000	0,000
2	5	2	5	0,020	3,519
2	2,5	4	7,5	0,667	0,365
2	2	6	9,5	0,789	0,213
2	2,2	8	11,7	0,812	0,187
2	1,3	10	13	0,900	0,095
2	1	12	14	0,929	0,067
2	2	14	16	0,875	0,120
2	1	16	17	0,941	0,055
2	1,5	18	18,5	0,919	0,076
2	1,3	20	19,8	0,934	0,061
				Average =	**0,4325**

Accumulated Time	Infiltration Velocity (mm/min)			
0	0,000	m=	-0,0668	
2	3,519	b=	1,1009	
4	0,365	t=	20	
6	0,213	**KOSTIAKOV MODEL**		
8	0,187	Instant infiltration velocity	I=	b*T (m)
10	0,095		I=	1.1009*(30-0.0668)
12	0,067		I=	**0.90123 cm/min**
14	0,120			
16	0,055			
18	0,076			
20	0,061			

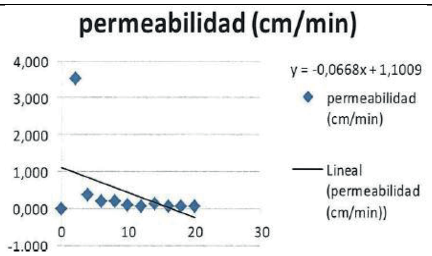

PERMEABILITY TEST BY DESCENDING LEVEL

SILALA WELL: Ssee PERM01 Date: 26/Oct/2016
Coordinates: 603139
N: 7565802
Height: 4,426 m.a.s.l.

$$k = \frac{\pi * D}{11(t2 - t1)} * \ln\left(\frac{h1}{h2}\right)$$

TIME (min)	Partial Sheet (mm)	Accumulated Time	Accumulated Sheet	(h1/h2)	Permeability (cm/min)
0	0,1	0	0,1	1,000	0,000
3	1,6	3	1,6	0,063	2,494
3	0,7	6	2,3	0,696	0,326
3	0,4	9	2,7	0,852	0,144
3	0,4	12	3,1	0,871	0,124
3	0,3	15	3,4	0,912	0,083
3	0,3	18	3,7	0,919	0,076
3	0,5	21	4,2	0,881	0,114
3	0,3	24	4,5	0,933	0,062
3	0,1	27	4,6	0,978	0,020
3	0,4	30	5	0,920	0,075
				Average =	**0,3199**

Accumulated Time	Infiltration Velocity (mm/min)			
0	0,000	m=	-0,0316	
3	2,494	b=	0,7938	
6	0,326	t=	20	
9	0,144	**KOSTIAKOV MODEL**		
12	0,124	Instant infiltration velocity	I=	b*T (m)
15	0,083		I=	0.7938*(30-0.0316)
18	0,076		I=	**0.7221 cm/min**
21	0,114			
24	0,062			
27	0,020			
30	0,075			

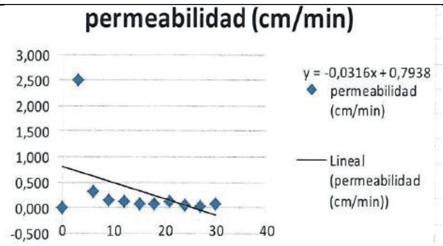

PERMEABILITY TEST BY DESCENDING LEVEL

SILALA WELL: Snww PERM01 Date: 26/Oct/2016

Coordinates: E: 603139 600877

N: 7565802 7566333

Height: 4,426 m.a.s.l.

$$k = \frac{\pi * D}{11(t2 - t1)} * \ln\left(\frac{h1}{h2}\right)$$

TIME (min)	Partial Sheet (mm)	Accumulated Time	Accumulated Sheet	(h1/h2)	Permeability (cm/min)
0	0,1	0	0,1	1,000	0,000
0,5	0,8	0,5	0,8	0,125	1,871
0,5	0,8	1	1,6	0,500	0,624
0,5	0,5	1,5	2,1	0,762	0,245
0,5	1	2	3,1	0,677	0,350
0,5	0,3	2,5	3,4	0,912	0,083
0,5	0,6	3	4	0,850	0,146
0,5	0,4	3,5	4,4	0,909	0,086
0,5	0,6	4	5	0,880	0,115
0,5	0,5	4,5	5,5	0,909	0,086
0,5	0,5	5	6	0,917	0,078
				Average =	**0,3349**

Accumulated Time	Infiltration Velocity (mm/min)			
0	0,000	m=	-0,1599	
0,5	1,871	b=	0,7347	0,56799529
1	0,624	t=	20	
1,5	0,245	**KOSTIAKOV MODEL**		
2	0,350	Instant infiltration velocity	I=	b*T (m)
2,5	0,083		I=	0.7938*(30-0.0316)
3	0,146		I=	**0.5679 cm/min**
3,5	0,086			
4	0,115			
4,5	0,086			
5	0,078			

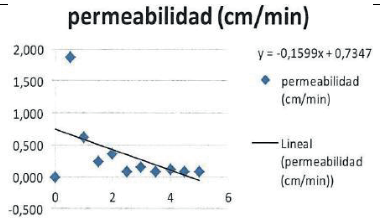

PERMEABILITY TEST BY DESCENDING LEVEL

SILALA WELL: Ssee PERM02 Date: 26/Oct/2016

Coordinates: E: 603138

N: 7565808

Height: 4,426 m.a.s.l.

$$k = \frac{\pi * D}{11(t2 - t1)} * \ln\left(\frac{h1}{h2}\right)$$

TIME (min)	Partial Sheet (mm)	Accumulated Time	Accumulated Sheet	(h1/h2)	Permeability (cm/min)
0	0,1	0	0,1	1,000	0,000
3	1,4	3	1,4	0,071	2,374
3	0,6	6	2	0,700	0,321
3	0,4	9	2,4	0,833	0,164
3	0,6	12	3	0,800	0,201
3	0,5	15	3,5	0,857	0,139
3	0,5	18	4	0,875	0,120
3	0,3	21	4,3	0,930	0,065
3	0,7	24	5	0,860	0,136
3	0,6	27	5,6	0,893	0,102
3	0,4	30	6	0,933	0,062
				Average =	**0,3349**

Accumulated Time	Infiltration Velocity (mm/min)			
0	0,000	m=	-0,0291	
3	2,374	b=	0,7718	0,73648643
6	0,321	t=	5	
9	0,164	**KOSTIAKOV MODEL**		
12	0,201	Instant infiltration velocity	I=	b*T (m)
15	0,139		I=	0.7718*(30-0.0291)
18	0,120		I=	**0.73643 cm/min**
21	0,065			
24	0,136			
27	0,102			
30	0,062			

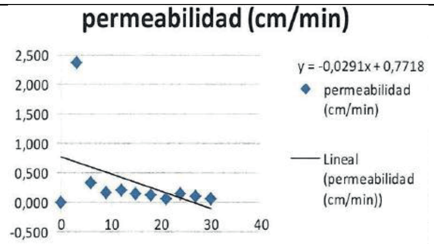

Annex E.3.

Photographic Report

Photograph 1: Measurement of Flows.

Photograph 2: Determination of the Infiltration Capacity.

Photograph 3: Permeability Measurement (K)

Photograph 4: Permeability Measurement (K)